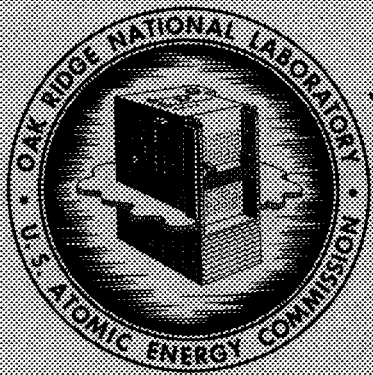


ORNL
MASTER COPY

74

ORNL-3605
Volume 2
UC-33 -- Propulsion Systems and
Energy Conversion
TID-4500 (34th ed.)

PROCEEDINGS OF 1963
HIGH-TEMPERATURE LIQUID-METAL HEAT TRANSFER
TECHNOLOGY MEETING



OAK RIDGE NATIONAL LABORATORY
operated by
UNION CARBIDE CORPORATION
for the
U.S. ATOMIC ENERGY COMMISSION

Printed in USA. Price \$7.00. Available from the Clearinghouse for Federal
Scientific and Technical Information, National Bureau of Standards,
U.S. Department of Commerce, Springfield, Virginia

LEGAL NOTICE

This report was prepared as an account of Government sponsored work. Neither the United States, nor the Commission, nor any person acting on behalf of the Commission:

- A. Makes any warranty or representation, expressed or implied, with respect to the accuracy, completeness, or usefulness of the information contained in this report, or that the use of any information, apparatus, method, or process disclosed in this report may not infringe privately owned rights, or
- B. Assumes any liabilities with respect to the use of, or for damages resulting from the use of any information, apparatus, method, or process disclosed in this report.

As used in the above, "person acting on behalf of the Commission" includes any employee or contractor of the Commission, or employee of such contractor, to the extent that such employee or contractor of the Commission, or employee of such contractor prepares, disseminates, or provides access to, any information pursuant to his employment or contract with the Commission, or his employment with such contractor.

ORNL-3605
Volume 2

Contract No. W-7405-eng-26

PROCEEDINGS OF 1963
HIGH-TEMPERATURE LIQUID-METAL HEAT TRANSFER
TECHNOLOGY MEETING

SPONSORED BY THE
ENGINEERING DEVELOPMENT BRANCH, DIVISION OF REACTOR DEVELOPMENT
UNITED STATES ATOMIC ENERGY COMMISSION

AT
OAK RIDGE NATIONAL LABORATORY

SEPTEMBER 4-6, 1963

DECEMBER 1964

OAK RIDGE NATIONAL LABORATORY
Oak Ridge, Tennessee
operated by
UNION CARBIDE CORPORATION
for the
U.S. ATOMIC ENERGY COMMISSION

This report was printed from the best available material.

CONTENTS

Volume 1

Preface		v
The MPRE — A Boiling Potassium Reactor System	A. P. FRAAS	1
The Determination of the Latent Heat of Vaporization, Vapor Pressure, Enthalpy, and Density of Liquid Rubidium and Cesium up to 1800°F	P. Y. ACHENER	3
Thermophysical Properties of Rubidium and Cesium	F. TEPPER, A. MURCHISON, J. ZELENAK, and F. ROEHLICH	26
Thermophysical Property Measurements of Alkali Liquid Metals	J. W. COOKE	66
The Thermodynamic and Transport Properties of Potassium	A. W. LEMMON, JR., H. W. DEEM, E. H. HALL, and J. F. WALLING	88
Thermoelectric Potentials of Molten and Refractory Metals	C. F. BONILLA, R. R. KYI, H. T. DRUE, and D-I. LEE	116
Report on High Temperature Liquid Metal Heat Transfer Research at Geoscience, Ltd.	H. F. POPPENDIEK and N. D. GREENE	139
Lithium-Boiling Potassium Refractory Metal Loop Facility.	J. P. DAVIS, G. M. KIKIN, W. M. PHILLIPS, and L. S. WOLFSON	171
Heat Transfer Coefficients in Liquid Metal Co-Current Flow Double Pipe Heat Exchangers	R. P. STEIN	194
Natural Convection Heat Transfer Coefficients for Liquid Tin at High Heat Fluxes	A. F. BRINSMADE and L. G. DESMON	240
The Effect of Surface Conditions on Pool Boiling Heat Transfer of Sodium	P. J. MARTO and W. M. ROHSENOW	263
Pool Boiling of Potassium	C. F. BONILLA, M. M. WIENER, and H. BILFINGER	286
Superheat Requirements with Boiling Liquid Metals	A. I. KRAKOVIK	310
Recent Experimental Results in ORNL Studies with Boiling Potassium	H. W. HOFFMAN	334
Boiling Studies with Potassium	R. E. BALZHISER	351

CONTENTS

Volume 2

An Experimental Investigation of Forced-Convection Vaporization of Potassium	P. J. BERENSON and J. J. KILLACKEY	1
Summary of Recent Results of Sodium Boiling Studies	R. C. NOYES	24
A Proposed Mechanism and Method of Correlation for Convective Boiling Heat Transfer with Liquid Metals	J. C. CHEN	47
Heat Transfer and Pressure Drop Characteristics for Boiling Rubidium in Forced Convection	C. R. FISHER	64
Alkali Metals Boiling and Condensing Investigations	R. D. BROOKS and J. LONGO, JR.	86
Potassium-Mercury Amalgam Boiling Heat Transfer, Two-Phase Flow, and Properties Investigation	Y. S. TANG, C. R. SMITH, and P. T. ROSS	110
Heat Transfer During Film Condensation of a Liquid Metal Vapor	S. P. SUKHATME and W. M. ROHSENOW	132
Liquid Metal Jet Condensers	L. HAYS	153
Fog-Flow Mercury Condensing Pressure Drop Correlation	A. KOESTEL, M. GUTSTEIN, and R. T. WAINWRIGHT	198
Heat Transfer from a Hot Sodium Spray Impinging on a Vertical Plate	W. H. NURICK, J. D. SEADER, and T. A. COULTAS	235
Measurement of the Pressure Drop of Superheated Cesium Vapor Across a Laminar Flow Device	W. A. SAMUEL	250
Selected Parameters for Two-Phase Flow of Sodium	K. GOLDMANN	270
Stability of Parallel-Path Two-Phase Flow	T. J. VILD and D. E. SILL	293
The Application of Alkali Metal Vapor Systems to MHD Space Power Generators	B. HOFFMAN and F. SHAIR	316
Analysis of the Acceleration of Lithium in a Two-Phase Nozzle	B. G. ELLIOTT	353
Meeting Summation	R. N. LYON	371
List of Attendees		381

AN EXPERIMENTAL INVESTIGATION OF
FORCED-CONVECTION VAPORIZATION OF POTASSIUM

by

P. J. Berenson

J. J. Killackey

AiResearch Manufacturing Company
A Division of The Garrett Corporation
Los Angeles, California

Work Performed for the
Aeronautical Systems Division
United States Air Force
Under Contract AF 33(657)-10922

Presented at the
HIGH TEMPERATURE LIQUID METAL HEAT TRANSFER CONFERENCE
Oak Ridge National Laboratory
September 4-6, 1963

AN EXPERIMENTAL INVESTIGATION OF FORCED-CONVECTION VAPORIZATION OF POTASSIUM

by

P. J. Berenson
J. J. Killackey

INTRODUCTION

The test program described here is being conducted by the AiResearch Manufacturing Company in support of the SNAP-50/SPUR boiler design, which is now under development at AiResearch. The boiler is a shell-and-tube design with lithium flowing outside the tubes and potassium vaporizing inside the tubes. System design requirements call for a boiler that will produce dry vapor at the outlet and be of a reasonable weight and size. Boiling potassium test results obtained thus far show that, at up to approximately 50 percent vapor quality, the boiling heat-transfer coefficient is extremely high (20,000 to 30,000 Btu per hr ft² °F) and that the lithium side controls the boiler heat-transfer rate, and hence the size. The present experimental program is therefore directed towards obtaining data in the high-vapor-quality region, where a substantial drop in the boiling heat-transfer coefficient is normally observed and the magnitude of the potassium coefficient becomes significant. Additional test objectives include determining two-phase pressure drop in swirl flow and investigations of boiling flow stability.

The first test series described here was conducted using a "whirler" or twisted ribbon as the tube insert. No tests have been made with a plain tube because the available data for plain tubes indicated very low coefficients and a severe penalty in boiler size and weight. It was considered essential at high vapor qualities to exert a positive means to drive the remaining liquid droplets in the high-velocity vapor core to the tube wall, where vaporization would occur.

TEST EQUIPMENT

Details of the test rig are shown schematically in Figure 1. A motorized throttle valve located upstream of the boiler is used to promote stable flow during boiling operation. The condenser is a single-tube, air-cooled unit; no attempt has been made to measure condensing heat-transfer coefficients. A metal bellows assembly is used to absorb the potassium displaced when boiling is initiated. By regulating the accumulator head pressure, it is possible to control the potassium saturation temperature.

The preheater and boiler can be considered as one long tube, with the instrumentation concentrated in the boiler section. The test units are located inside a vacuum chamber to reduce heat losses and minimize surface oxidation. The preheater is fabricated from a stainless-steel billet 3 inches in diameter and 12 inches long. Five 0.250-inch-diameter holes drilled through the billet and interconnected with crossover tubes serve as five potassium tube passes. "Thermocoax" sheath-type resistance-heating wire is placed in a

spiral groove cut on the outside diameter of the unit and brazed in place. A single electrical power input control is used on the preheater.

Basic construction of the boiler test section is shown in Figure 2. The unit is fabricated from nickel and is designed for a maximum heat flux at the inner wall of 600,000 Btu per hr ft² at a potassium saturation temperature of 1600°F. Criteria for selection of nickel were as follows:

1. Compatibility with potassium at temperatures up to 1600°F
2. High thermal conductivity, which tends to minimize the heater surface temperature
3. Effectiveness of stainless-steel-to-nickel welded or brazed joints
4. Machinability
5. Availability

A 0.180-inch-diameter hole drilled through the boiler serves as the flow passage. A twisted ribbon (whirler) with a twist ratio, γ , of 3.0 internal diameters per 180 degrees of twist is inserted in the drilled hole over the full length of the boiler. The test boiler is slotted to divide the unit into six thermally isolated 2-inch-long sections. "Thermocoax" heating wire is brazed in a spiral groove cut on the outer diameter of each element, and the electrical power input to each section is independently controlled. Thus, it is possible to determine a series of heat-transfer coefficients down the boiler length. The test section is mounted horizontally and is surrounded by 3 inches of Microquartz insulation.

INSTRUMENTATION

Sheath-type Geminal N and P thermocouples, 1/16 inches OD, are used to measure all temperatures. As shown in Figure 2, a series of thermocouples is used to measure the radial temperature gradient through each of the boiler elements. Temperature-measuring sections with three thermocouples per section are located at the preheater inlet and the boiler inlet and outlet. Mixing sections are located immediately upstream of the temperature-measuring sections, at the preheater and boiler inlets. There is no mixing section at the boiler outlet because the fluid would be at saturation conditions and the pressure loss due to mixing would be excessive.

Pressure measurements are made with Wiancko pressure transducers. Each transducer is located in an oven maintained at 195°F to prevent freezing the potassium and to temperature-stabilize the transducer elements. Pressure transducers were determined to be accurate within ± 0.1 psi, which is the level of sensitivity required to obtain an accurate value of saturation temperature based on the measured saturation pressure and a vapor pressure curve.

Heat input to each boiler element and the preheater is determined by use of a precision wattmeter, accurate to one percent of full-scale. Before the loop is filled with potassium, the test units are calibrated for heat loss

by measuring the power input necessary to maintain a given temperature level without any deliberate removal of heat. The EM flowmeter was checked by use of a heat balance across the test elements and was found to be accurate to within ± 5 percent.

All data are recorded using a digital voltmeter equipped with a tape printout unit. A complete set of data consisting of about 130 temperature, pressure, and flow points can be recorded in approximately one minute, which is of great value since it eliminates the need to maintain steady-state conditions over an extended period of time. Conventional strip-chart recorders are employed, however, to examine various points in the loop to ensure that a reasonably steady boiling condition has been achieved before data are taken.

TEST OPERATION

Stable flow during two-phase boiling operation is achieved by controlling the degree of throttling across the flow control valve; however, no detailed studies were made during this series of runs to determine the degree of orificing required to promote stability. The valve located downstream of the condenser was full-open during testing and was used only to facilitate draining of the loop. Control of the potassium saturation temperature was achieved by regulating the condenser air flow and adjusting the accumulator head pressure.

Large amounts of liquid superheating, in the range of 200°F to 500°F, have been observed in the operation of forced-convection boiling potassium loops. The resulting instabilities have produced audible noise, which has been termed "explosive boiling." Test data obtained from the heat-transfer loop described here were carefully reviewed, but no evidence of explosive boiling could be detected; measured saturation temperatures and pressures were in close agreement.

DATA PROCESSING

A computer program has been developed to process the more than 100 measurements obtained in each run. The measured temperatures at the four radial locations in each boiler section are extrapolated to the inner and outer wall of the boiler using a least-squares-fit straight line on semilog graph paper. The net heat input is determined from the electrical power input and the calibrated heat loss. Based on the measured flow and the net heat input to each section, the potassium quality at the boundaries of each boiler section is calculated from a heat balance. The potassium physical properties used in the analysis are those given by Weatherford, et al.*

* Weatherford, W. D., Tyler, John C., and Ku, P. M., "Properties of Inorganic Energy-Conversion and Heat Transfer Fluids for Space Applications," WADD Technical Report 61-96, November 1961.

The saturation temperature distribution of the potassium is determined by using the Martinelli two-phase pressure drop correlation.* This is done as follows. The pressure drop for each section is calculated based upon the appropriate average quality of the section. The two-phase pressure drop is based upon the largest of either the superficial liquid pressure drop or the superficial gas pressure drop. As a result, the Martinelli multiplying parameter is always less than 4.2. Each of the predicted pressure drops is normalized by multiplying it by the ratio of the total measured pressure drop to the total predicted pressure drop. Finally, the potassium saturation temperature at the boundary of each section is determined from the calculated saturation pressure.

The friction factor used to predict the pressure drop is based upon test data obtained at isothermal liquid conditions and at temperatures less than 1000°F. Basing the friction factor on the resultant velocity, total path length, and equivalent diameter gives the following correlation:

$$f = \frac{0.72}{Re^{0.25}}$$

It is postulated that the measured friction factor is more than double the standard correlation as a result of wall roughness. The passage is a drilled hole and thus is considerably rougher than drawn tubing. The ratio of the roughness height to the diameter will be measured to verify this possibility.

The heat-transfer coefficient for each boiler section is calculated from the heat flux and the difference between the extrapolated inside wall temperature and the arithmetic average potassium saturation temperature. It was not clear how to choose the potassium saturation temperature for each section; the use of the arithmetic average was the simplest choice that seemed reasonable.

A typical computer printout for one run is presented in Figure 3. In addition to the numerical printout, the measured radial wall temperatures, extrapolated inner wall temperature, and calculated potassium saturation temperature for each section are automatically plotted on semilog graph paper as shown in Figure 4.

DISCUSSION OF RESULTS

The results of the first test series are presented as a series of tables in the appendix. With the exception of run B-3-7, the potassium entered the boiler partially vaporized. All the data reported are for vaporization of two-phase potassium.

* Lockhart, R. W., and Martinelli, R. C., "Proposed Correlation of Data for Isothermal Two-Phase, Two-Component Flow in Pipes," Chemical Engineering Progress, Vol 45, No. 1, pp. 39-48, January 1949.

Test results were deleted if the measured temperature at the boiler boundaries differed by more than 20°F from the saturation temperature (as defined by the measured saturation pressure). The largest difference generally occurred at the boiler exit in runs with high pressure drop; the measured temperature was the larger. The maximum deviation observed was 45°F. Several plausible explanations for the temperature discrepancies exist. The measured temperature is close to a stagnation value, whereas the saturation temperature is based on static conditions. Velocity effects could account for a difference of about 10°F. There is a gradual expansion between the outlet pressure tap and the temperature measurement section necessary to accommodate the three thermocouples, and a recovery of static pressure could occur. Complete pressure recovery could account for about 10°F, although it is difficult to state the exact amount because of the presence of two-phase flow.

Another possibility is that thermodynamic equilibrium did not exist. That is, if large pressure drops occur in a forced-convection vaporizer, the residence time of the fluid in the passage may not be great enough to allow the expanding fluid to reach thermodynamic equilibrium. As a result, the actual fluid temperature is greater than the saturation temperature corresponding to the fluid pressure. The heat-transfer coefficients reported are based upon the equilibrium saturation temperature, because heat exchangers are designed assuming thermodynamic equilibrium properties. Until the discrepancy can be fully explained, however, the data points will not be considered.

The computer results are reported without modification for all boiler sections in which the maximum deviation of any of the four radial thermocouples from the least-squares-fit straight line was less than 2.5°F. Sections with a maximum deviation of greater than 10°F are not reported. All sections with maximum deviations between 2.5 and 10°F were critically examined to deduce which thermocouple was inaccurate and the best straight line was drawn through the remaining three points. In runs B-2-0 to B-3-5, it was concluded that the inner thermocouple in section 2 was consistently inaccurate. A straight line was drawn through the remaining three points as shown by the dashed line in Figure 4. This changed the inside wall temperature from a value less than the average saturation temperature to a value that gave a heat-transfer coefficient consistent with the other measurements.

The outer thermocouple in section 4 was eliminated in runs B-1-5 to B-1-15. The deviation of the thermocouple eliminated in the two sets of runs was approximately the same in each run. The reprocessed data are denoted with an asterisk after the value of the heat-transfer coefficient. Since the uncertainty in the extrapolated inner wall temperature is probably $\pm 5^\circ\text{F}$ to 10°F , the value of the heat-transfer coefficient for low values of $T_w - T_{\text{sat}}$ can be very uncertain.

The ratio between the measured pressure drop and the predicted pressure drop using the Martinelli correlation and Equation (1) was always within 30 percent of 0.56. One possible reason for this discrepancy may be the use of the measured rough-tube friction factor, which is more than double the smooth-tube value. One of the factors that the Martinelli multiplication factor

accounts for is the increased pressure drop produced in going from a smooth tube to a wall that is roughened because of either waves on the liquid film or drops adhering to the wall. Therefore, if the surface is initially mechanically roughened, the Martinelli multiplier should be less in going from single-phase to two-phase flow. An alternative and simpler approach is to use the Martinelli method as proposed, but always use a friction factor correlation for smooth tubes.

The data from five runs of approximately equal flow rate are plotted in Figure 5. Here, it is assumed that the heat-transfer coefficient is a function of total flow rate and quality. The fact that the heat-transfer coefficient decreases as the quality increases indicates that a larger fraction of the wall is becoming dry as the quality increases; the flow pattern is changing from annular to mist flow. The relatively gradual decrease in heat-transfer coefficient is due to the twisted tape centrifuging the liquid droplets to the wall. It appears that all the data were in this transition flow regime. Consistent with other investigations, the heat-transfer coefficient tends to decrease with increased flow at constant quality in this flow regime. No attempt was made to correlate the data.

Testing has been interrupted because of accumulated failures of the resistance-heating-wire-to-conductor joint in the individual boiler heater elements. Inactive sections are indicated in the tabulated data by a small, negative net heat input. The reason for the negative heat input is that the section is hot, and therefore is still subject to a heat loss, even though there is no electrical power input. The boiler test section is now being modified to provide more reliable heating elements, and a new test series will be run to more completely define boiling heat-transfer performance in swirl flow.

APPENDIX
TEST RESULTS

Run No.: B-1-5 Date: 4/8/63 Flow Rate: 0.370 lb/min
 Preheater Inlet Temperature: 799 °F Pressure Drop Ratio: 0.422

Section	P	1	2	3	4	5	6
Net Heat Input, watts	1779	-43.9	-44.8	606	607	-44.5	-43.3
Heat Flux, Btu/hr ft ²				263,500	263,820		
Exit Quality, percent	14.41	13.65	12.68	24.22	35.57	34.79	34.04
Average Quality, percent				18.55	29.89		
Exit Sat. Temp., °F	1633.6	1632.3	1631.1	1628.9	1625.1	1621.3	1617.5
Average $T_w - T_{sat}$, °F				8.1	7		
h , Btu/hr ft ² °F				32,716	37,700*		

Run No.: B-1-7 Date: 4/8/63 Flow Rate: 0.233 lb/min
 Preheater Inlet Temperature: 798 °F Pressure Drop Ratio: 0.455

Section	P	1	2	3	4	5	6
Net Heat Input, watts	1760	-43.8	-44.6	607	597	-44.4	-43.2
Heat Flux, Btu/hr ft ²				263,660	259,620		
Exit Quality, percent	33.48	32.23	30.96	48.99	66.73	65.45	64.21
Average Quality, percent				39.97	57.86		
Exit Sat. Temp., °F	1631.9	1630.3	1628.7	1626.1	1622.2	1618.6	1615
Average $T_w - T_{sat}$, °F				7.3	7		
h , Btu/hr ft ² °F				35,980	37,000*		

Run No.: B-1-6 Date: 4/8/63 Flow Rate: 0.262 lb/min
 Preheater Inlet Temperature: 804 °F Pressure Drop Ratio: 0.434

Section	P	1	2	3	4	5	6
Net Heat Input, watts	1758	-44.2	-45	606	597	-44.7	-43.6
Heat Flux, Btu/hr ft ²				263,500	259,460		
Exit Quality, percent	27.61	26.50	25.36	41.38	57.14	56.0	54.9
Average Quality, percent				33.37	49.26		
Exit Sat. Temp., °F	1637.1	1635.7	1634.3	1631.9	1628.2	1624.7	1621.1
Average $T_w - T_{sat}$, °F				7.4	7		
h , Btu/hr ft ² °F				35,715	37,000*		

Run No.: B-1-8 Date: 4/8/63 Flow Rate: 0.207 lb/min
 Preheater Inlet Temperature: 782 °F Pressure Drop Ratio: 0.536

Section	P	1	2	3	4	5	6
Net Heat Input, watts	1759	-43.9	-44.7	597	592	-44.5	-43.3
Heat Flux, Btu/hr ft ²				259,250	257,340		
Exit Quality, percent	39.49	38.09	36.65	56.55	76.29	74.86	73.46
Average Quality, percent				46.6	66.42		
Exit Sat. Temp., °F	1633.1	1631.2	1629.4	1626.4	1622.1	1618.3	1614.4
Average $T_w - T_{sat}$, °F				7.8	11		
h , Btu/hr ft ² °F				33,308	23,400*		

*Based on revised fit of wall-temperature gradient obtained by elimination of erroneous thermocouple reading.

P = Preheater

Run No.: B-1-9 Date: 4/8/63 Flow Rate: 0.165 lb/min
 Preheater Inlet Temperature: 787°F Pressure Drop Ratio: 0.614

Section	P	1	2	3	4	5	6
Net Heat Input, watts	1730	-43.9	-44.7	597	597	-44.5	-43.4
Heat Flux, Btu/hr ft ²				259,260	259,400		
Exit Quality, percent	53.25	51.45	49.63	74.58	99.53	97.70	95.92
Average Quality, percent				62.11	87.06		
Exit Sat. Temp., °F	1633.6	1631.7	1629.8	1626.6	1622.3	1619.7	1616.9
Average $T_w - T_{sat}$, °F				8.1	15		
h, Btu/hr ft ² °F				32,111	17,300*		

Run No.: B-1-14 Date: 4/9/63 Flow Rate: 0.3315 lb/min
 Preheater Inlet Temperature: 773°F Pressure Drop Ratio: 0.545

Section	P	1	2	3	4	5	6
Net Heat Input, watts	1656	-43.7	-44.6	572	578	-44.5	-43.2
Heat Flux, Btu/hr ft ²				248,570	251,030		
Exit Quality, percent	15.25	14.40	13.54	25.50	37.55	36.69	35.85
Average Quality, percent				19.52	31.52		
Exit Sat. Temp., °F	1628.9	1627.4	1626	1623.4	1619.0	1616.5	1610
Average $T_w - T_{sat}$, °F				11.9	11		
h, Btu/hr ft ² °F				20,842	22,800*		

Run No.: B-1-13 Date: 4/9/63 Flow Rate: 0.335 lb/min
 Preheater Inlet Temperature: 782°F Pressure Drop Ratio: 0.413

Section	P	1	2	3	4	5	6
Net Heat Input, watts	1751	-43.8	-44.7	607	607	-44.5	-43.3
Heat Flux, Btu/hr ft ²				263,620	263,960		
Exit Quality, percent	17.01	16.16	15.29	27.83	40.38	39.51	38.67
Average Quality, percent				21.56	34.10		
Exit Sat. Temp., °F	1631.9	1630.6	1629.4	1627.2	1623.5	1619.9	1616.3
Average $T_w - T_{sat}$, °F				8.7	7		
h, Btu/hr ft ² °F				30,447	37,700*		

Run No.: B-1-15 Date: 4/9/63 Flow Rate: 0.204 lb/min
 Preheater Inlet Temperature: 747°F Pressure Drop Ratio: 0.584

Section	P	1	2	3	4	5	6
Net Heat Input, watts	1641	-44.2	-45	577	572	-44.8	-43.7
Heat Flux, Btu/hr ft ²				250,590	248,660		
Exit Quality, percent	35.7	34.26	32.79	52.38	71.81	70.33	68.89
Average Quality, percent				42.58	62.09		
Exit Sat. Temp., °F	1637.1	1635.4	1633.8	1631.0	1626.8	1623.1	1619.3
Average $T_w - T_{sat}$, °F				10.3	11		
h, Btu/hr ft ² °F				24,263	22,600*		

*Based on revised fit of wall-temperature gradient obtained by elimination of erroneous thermocouple reading.

P = Preheater

Run No.: B-2-0 Date: 4/6/63 Flow Rate: 0.808 lb/min
 Preheater Inlet Temperature: 894°F Pressure Drop Ratio: 0.585

Section	P	1	2	3	4	5	6
Net Heat Input, watts	2785	-44.8	937	907	925	926	-39.5
Heat Flux, Btu/hr ft ²			407,170	394,070	400,980	402,800	
Exit Quality, percent	7.38	7.47	15.92	24.10	32.40	40.71	40.95
Average Quality, percent			11.70	20.01	28.25	36.56	
Exit Sat. Temp., °F	1623	1619	1610.4	1594.2	1566.9	1521.3	1463.3
Average $T_w - T_{sat}$, °F			10	17	16.6	31.6	
h, Btu/hr ft ² °F			40,720*	23,200*	24,193	12,740	

Run No.: B-2-2 Date: 4/6/63 Flow Rate: 0.563 lb/min
 Preheater Inlet Temperature: 889°F Pressure Drop Ratio: 0.590

Section	P	1	2	3	4	5	6
Net Heat Input, watts	2812	-43.9	953	962	963	957	-38.7
Heat Flux, Btu/hr ft ²			414,010	418,190	418,670	415,810	
Exit Quality, percent	18.14	18.11	30.21	42.39	54.53	66.54	66.64
Average Quality, percent			24.16	36.3	48.46	60.54	
Exit Sat. Temp., °F	1613.8	1607.9	1596.9	1577.5	1545.3	1493.0	1426.8
Average $T_w - T_{sat}$, °F			0	15.1	19.8	41.3	
h, Btu/hr ft ² °F			∞*	27,614	21,114	10,080	

Run No.: B-2-1 Date: 4/6/63 Flow Rate: 0.584 lb/min
 Preheater Inlet Temperature: 885°F Pressure Drop Ratio: 0.592

Section	P	1	2	3	4	5	6
Net Heat Input, watts	2782	-44.0	943	952	944	947	-38.1
Heat Flux, Btu/hr ft ²			409,650	413,810	410,010	411,480	
Exit Quality, percent	16.44	16.42	27.98	39.62	51.11	62.60	62.72
Average Quality, percent			22.2	33.80	45.37	56.85	
Exit Sat. Temp., °F	1613.8	1608.1	1597.5	1578.6	1547.1	1495.5	1430.3
Average $T_w - T_{sat}$, °F			10	15.6	19.4	38.4	
h, Btu/hr ft ² °F			40,965*	26,546	21,091	10,716	

Run No.: B-2-3 Date: 4/6/63 Flow Rate: 0.527 lb/min
 Preheater Inlet Temperature: 893°F Pressure Drop Ratio: 0.596

Section	P	1	2	3	4	5	6
Net Heat Input, watts	2773	-43.6	943	948	944	947	-37.6
Heat Flux, Btu/hr ft ²			409,820	411,820	410,050	411,450	
Exit Quality, percent	20.16	20.09	32.85	45.63	58.30	70.95	71.02
Average Quality, percent			26.47	39.24	51.96	64.62	
Exit Sat. Temp., °F	1608.8	1602.7	1591.3	1571.4	1538.4	1485.4	1417.1
Average $T_w - T_{sat}$, °F			3	14.6	23.7	48.1	
h, Btu/hr ft ² °F			136,500*	28,141	17,266	8,553	

*Based on revised fit of wall-temperature gradient obtained by elimination of erroneous thermocouple reading.

P = Preheater

Run No.: B-2-4 Date: 4/7/63 Flow Rate: 0.605 lb/min
 Preheater Inlet Temperature: 890°F Pressure Drop Ratio: 0.667

Section	P	1	2	3	4	5	6
Net Heat Input, watts	2826	-45.2	956	971	962	995	-40.4
Heat Flux, Btu/hr ft ²			415,430	421,770	417,990	432,180	
Exit Quality, percent	15.49	15.51	26.91	38.43	49.81	61.52	61.69
Average Quality, percent			21.20	32.67	44.12	55.67	
Exit Sat. Temp., °F	1633.6	1628	1617.1	1597.3	1564.6	1508.9	1437.2
Average $T_w - T_{sat}$, °F			8	16.6	23.5	49.3	
h, Btu/hr ft ² °F			51,900*	25,440	17,760	8,763	

Run No.: B-3-2 Date: 4/7/63 Flow Rate: 0.483 lb/min
 Preheater Inlet Temperature: 896°F Pressure Drop Ratio: 0.597

Section	P	1	2	3	4	5	6
Net Heat Input, watts	2828	-43.5	963	963	963	966	-37.5
Heat Flux, Btu/hr ft ²			418,550	418,310	418,650	419,980	
Exit Quality, percent	24.29	24.17	38.31	52.39	66.41	80.39	80.39
Average Quality, percent			31.24	45.35	59.40	73.40	
Exit Sat. Temp., °F	1607.5	1601.1	1589.1	1568.2	1534.4	1480	1409.6
Average $T_w - T_{sat}$, °F			8	14.7	27.9	57.2	
h, Btu/hr ft ² °F			52,300*	28,476	15,032	7344	

Run No.: B-2-5 Date: 4/7/63 Flow Rate: 0.874 lb/min
 Preheater Inlet Temperature: 877°F Pressure Drop Ratio: 0.65

Section	P	1	2	3	4	5	6
Net Heat Input, watts	2813	-45.2	842	960	951	955	-40.8
Heat Flux, Btu/hr ft ²			366,050	417,370	413,470	414,830	
Exit Quality, percent	5.20	5.36	12.50	20.57	28.55	36.55	36.86
Average Quality, percent			8.93	16.53	24.56	32.55	
Exit Sat. Temp., °F	1632.5	1628.9	1621.1	1604.9	1576.8	1528	1463.3
Average $T_w - T_{sat}$, °F			8	15.6	18.7	34.3	
h, Btu/hr ft ² °F			45,750*	26,765	22,115	12,096	

Run No.: B-3-3 Date: 4/7/63 Flow Rate: 0.488 lb/min
 Preheater Inlet Temperature: 882°F Pressure Drop Ratio: 0.584

Section	P	1	2	3	4	5	6
Net Heat Input, watts	2844	-43.3	963	973	963	966	-36.3
Heat Flux, Btu/hr ft ²			418,640	422,710	418,640	419,390	
Exit Quality, percent	23.85	23.73	37.74	51.81	65.68	79.53	79.56
Average Quality, percent			30.74	44.77	58.74	72.60	
Exit Sat. Temp., °F	1605	1598.6	1586.7	1565.8	1531.9	1477.2	1405.8
Average $T_w - T_{sat}$, °F			9	13.2	29.3	64.6	
h, Btu/hr ft ² °F			52,300*	32,143	14,281	6499	

*Based on revised fit of wall-temperature gradient obtained by elimination of erroneous thermocouple reading.

P = Preheater

Run No.: B-3-4 Date: 4/7/63 Flow Rate: 0.484 lb/min
 Preheater Inlet Temperature: 884°F Pressure Drop Ratio: 0.611

Section	P	1	2	3	4	5	6
Net Heat Input, watts	2842	-43.8	963	972	963	967	-38.7
Heat Flux, Btu/hr ft ²			418,340	422,480	418,620	420,040	
Exit Quality, percent	24.06	23.93	38.04	52.23	66.22	80.18	80.15
Average Quality, percent			30.98	45.13	59.22	73.20	
Exit Sat. Temp., °F	1611.9	1605.5	1593.5	1573.0	1539.8	1486.8	1419.6
Average $T_w - T_{sat}$, °F			11	15.1	23.1	46.0	
h , Btu/hr ft ² °F			38,100*	28,006	18,101	9138	

Run No.: B-3-7 Date: 4/7/63 Flow Rate: 1.18 lb/min
 Preheater Inlet Temperature: 864°F Pressure Drop Ratio: 0.725

Section	P	1	2	3	4	5	6
Net Heat Input, watts	2830	-42.1	842	960	951	949	-41.8
Heat Flux, Btu/hr ft ²				417,100	415,160	412,420	
Exit Quality, percent	0	0	4.79	10.88	16.92	22.96	23.33
Average Quality, percent				7.84	13.90	19.94	
Exit Sat. Temp., °F	1637.1	1636.8	1631.9	1618.8	1593.0	1547.3	1485.1
Average $T_w - T_{sat}$, °F				16.4	17.9	34.9	
h , Btu/hr ft ² °F				25,504	23,090	11,301	

Run No.: B-3-5 Date: 4/7/63 Flow Rate: 0.550 lb/min
 Preheater Inlet Temperature: 885°F Pressure Drop Ratio: 0.596

Section	P	1	2	3	4	5	6
Net Heat Input, watts	2827	-43.9	962	967	963	966	-36.2
Heat Flux, Btu/hr ft ²			418,240	420,230	418,570	420,000	
Exit Quality, percent	19.01	18.96	31.46	43.96	56.37	68.77	68.86
Average Quality, percent			25.27	37.71	50.17	62.57	
Exit Sat. Temp., °F	1614.4	1608.4	1597.2	1577.5	1544.8	1491.9	1424.4
Average $T_w - T_{sat}$, °F			10	13.4	22.6	43.2	
h , Btu/hr ft ² °F			41,824*	31,406	18,522	9714	

*Based on revised fit of wall-temperature gradient obtained by elimination of erroneous thermocouple reading.

P = Preheater

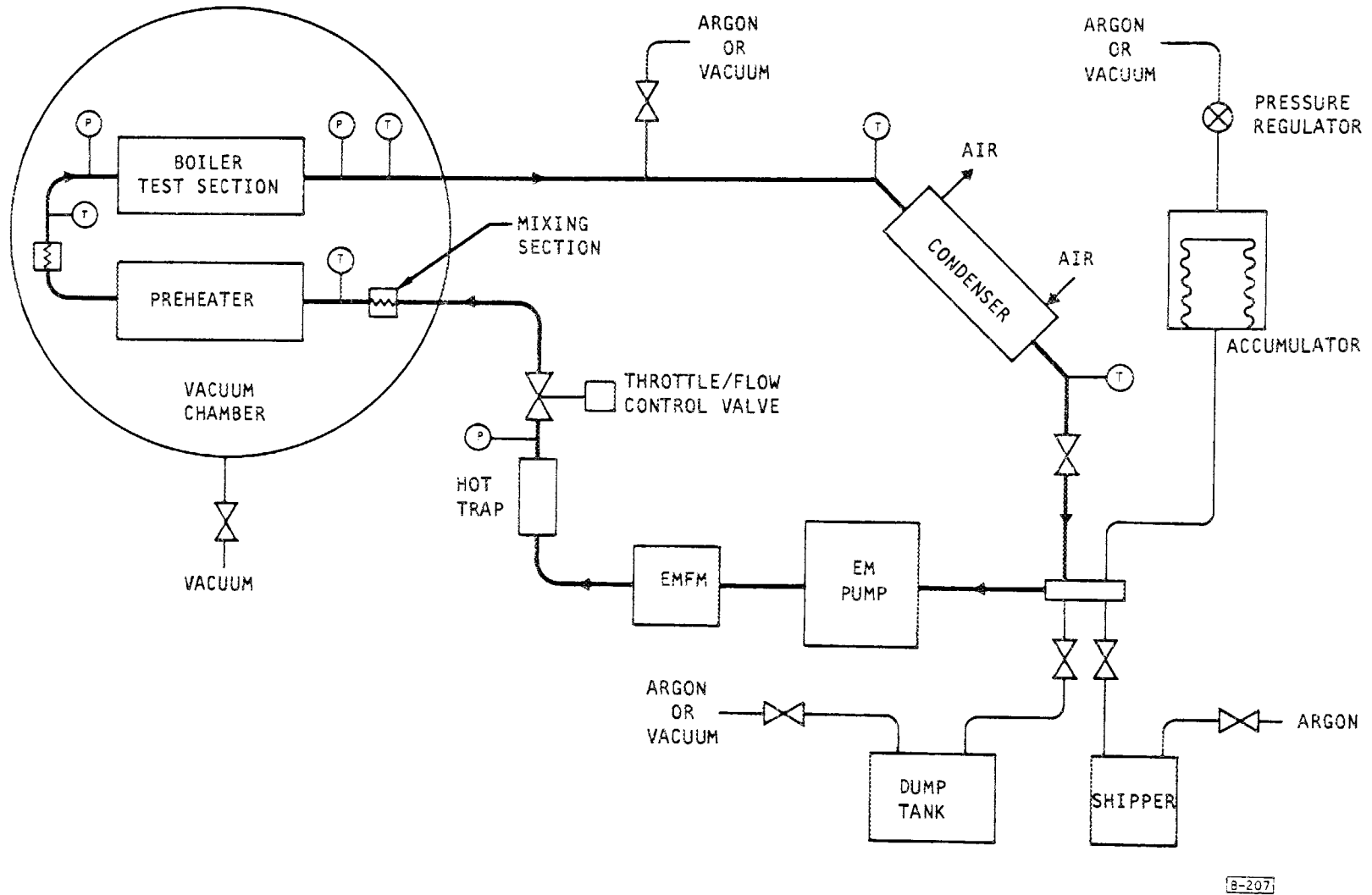
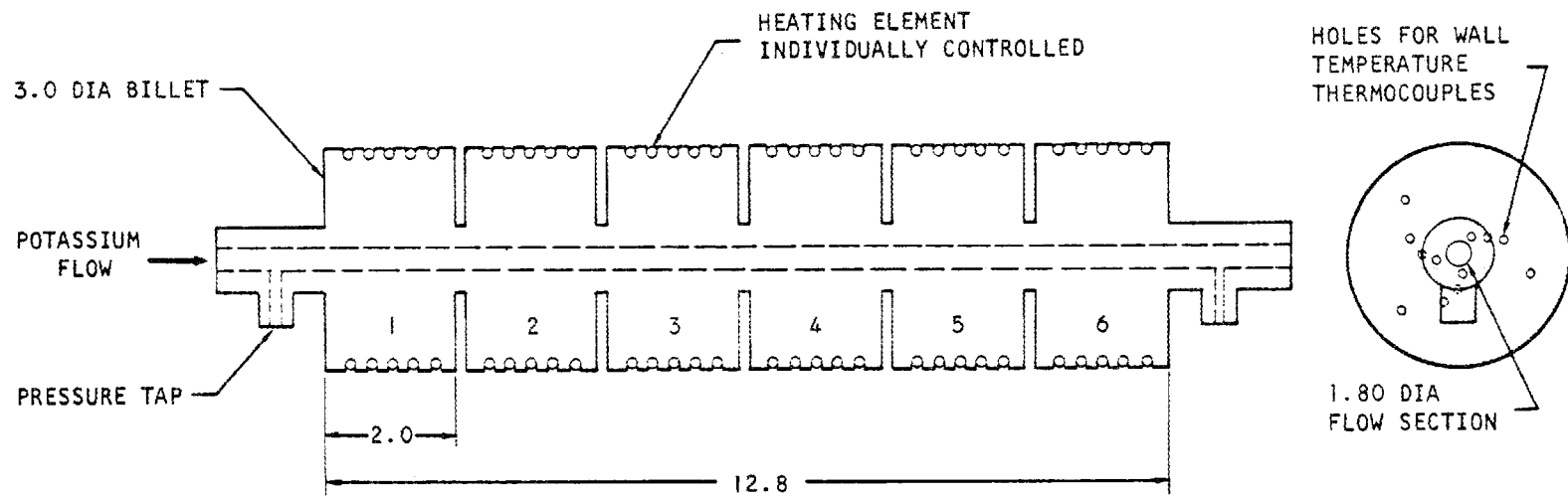


Figure 1. Schematic Diagram of Test Equipment



8-208

Figure 2. Boiler Test Section

POTASSIUM SINGLE-TUBE TEST

POTASSIUM SINGLE-TUBE TEST							
RUN NO. = B-2-1, DATE = 4/6/63, BAROMETER = 28.65, FLOWMETER, TEMP, DEG.F, = 802.00							
FLOWMETER (REC.), MV = 0.4010, FLOW, LB/MIN. = 0.5842, FLOW, CALC. = 1.1741, PERC. = -1.010							
BOILING STARTED IN PREHEATER							
	PREHEATER, BOILER-	SECT.1	SECTION 2	SECTION 3	SECTION 4	SECTION 5	SECTION 6
INPUT -							
BOILER W TEMP, DEG F, POS.1		1610.9	1665.3	1681.9	1661.4	1632.8	1513.0
BOILER W TEMP, DEG F, POS.2		1614.2	1725.0	1726.4	1711.8	1670.9	1515.0
BOILER W TEMP, DEG F, POS.3		1614.7	1750.5	1758.6	1741.4	1697.3	1516.4
BOILER W TEMP, DEG F, POS.4		1613.3	1770.0	1781.4	1760.5	1718.2	1517.8
K PREHTR INLET TEMP-1, DEG F =	885.6						
-2, DEG F =	886.7						
-3, DEG F =	884.4						
K BOILER INLET TEMP-1, DEG F =	1617.7						
-2, DEG F =	1616.2						
-3, DEG F =	1617.2						
K BOILER EXIT TEMP-1, DEG F =	1443.8						
-2, DEG F =	1445.2						
-3, DEG F =	1444.3						
PREHEATER TEMP, I/C 95, DEG F,	1671.9						
POTASSIUM PRESSURE, PSIA		39.60					17.40
ELEC. INPUT, WATTS, 1	990.0	0.0	1000.0	1010.0	1000.0	1000.0	0.0
2	1005.0						
3	1020.0						
ANSWERS -							
WALL TEMP INSIDE, DEG F		1609.3	1587.5	1603.6	1582.3	1559.7	1508.9
WALL TEMP OUTSIDE, DEG F		1615.7	1814.7	1820.6	1802.7	1753.7	1519.6
TEMP POS 1, DEG F, CALC.		1611.7	1668.6	1682.7	1662.6	1632.9	1512.9
AV. DEV, 4 THERM, DEG F		0.001	0.000	0.000	0.000	0.001	0.000
MAX. DEV (DEG F) AT THERM.		1.173 2	5.202 2	0.352 2	2.026 3	0.798 4	0.191 4
Q-NEI, WATTS	2781.91	-44.04	942.67	952.26	943.52	946.90	-38.12
HEAT FLUX, BTU/HR FT2		-19137.	409645.	413811.	410012.	411480.	-16565.
Q PERC.		229.7	-118.9	-107.5	-111.7	-83.9	342.5
QUALITY AT OUTLET, PERC.	16.44	16.42	27.98	39.62	51.11	62.60	62.72
AV. QUALITY, PERC.		16.43	22.20	33.80	45.37	56.85	62.66
CHANGE IN QUALITY, PERC.		-0.02	11.56	11.64	11.49	11.48	0.13
SUM PRESS. DROPS, MARTINELLI, PSI =	37.50						
RATIO T PRESS DROP TO MART. SUM =	0.592						
PRESS. DROP, MART, NORM, PSI		0.9017	1.6588	2.8440	4.3134	6.1493	6.3327
PRESS. DROP (MOM), NORM, PSI		-0.0005	0.4955	0.8354	1.2445	1.7844	0.0254
K EXIT SAT TEMP, DEG F	1613.8	1608.1	1597.5	1578.6	1547.1	1495.5	1430.3
INPUT K EXIT TEMP AV, DEG F	1617.0						1444.4
TEMP PERC.		-0.2					-1.0
AV. K SAT TEMP, DEG F		1611.0	1602.8	1588.0	1562.9	1521.3	1462.9
CHANGE IN K SAT TEMP, DEG F		-5.64	-10.64	-18.91	-31.48	-51.60	-65.21
TWALL-TSAT(AV), DEG F		-1.7	-15.4	15.6	19.4	38.4	48.0
HT COEF, BTU/HR FT2 DEG F		11319.8	-26681.8	26545.9	21090.8	10715.9	-359.9

Figure 3. Computer Printout of Reduced Data

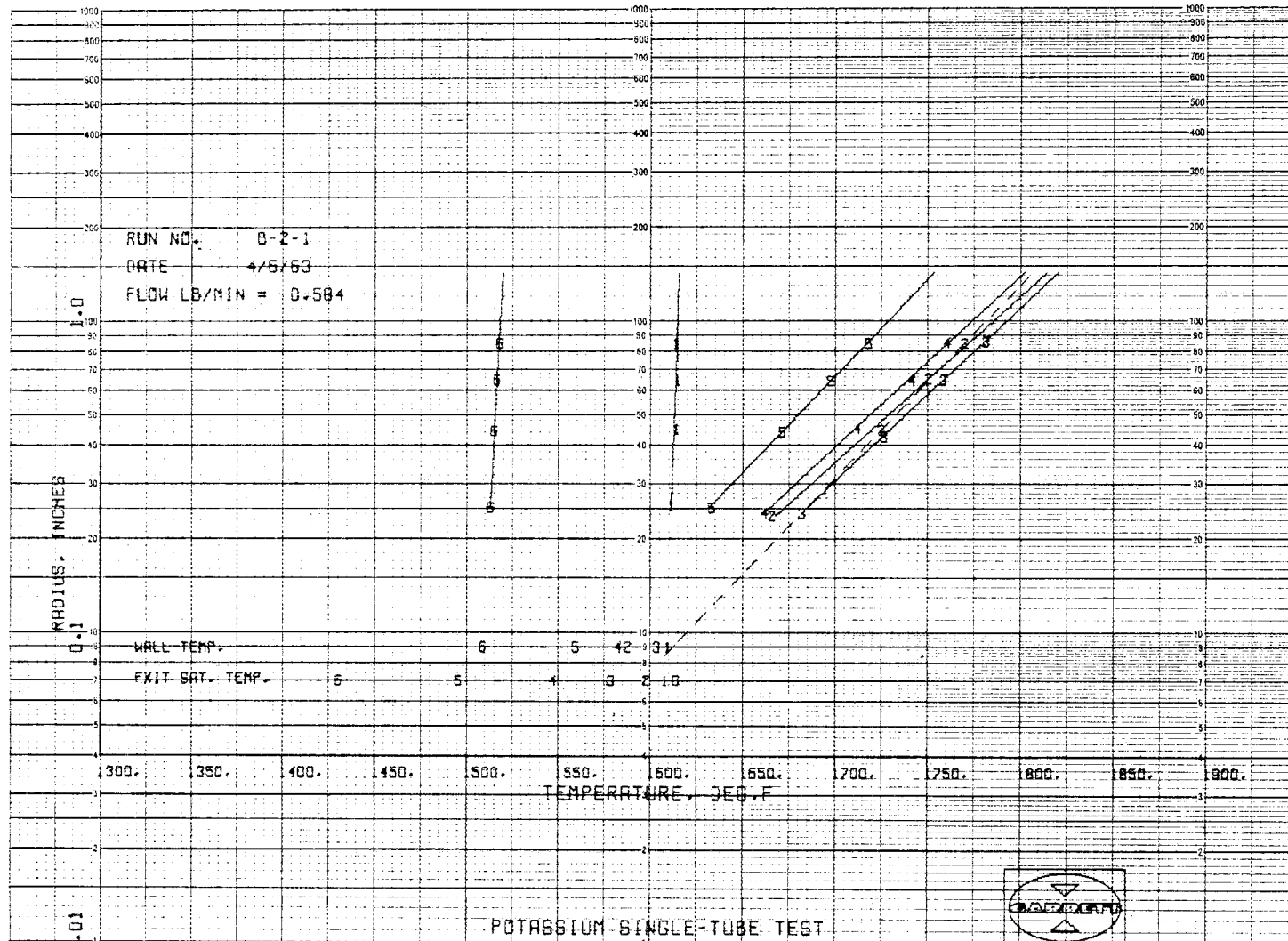


Figure 4. Computer Graphical Output of Reduced Data

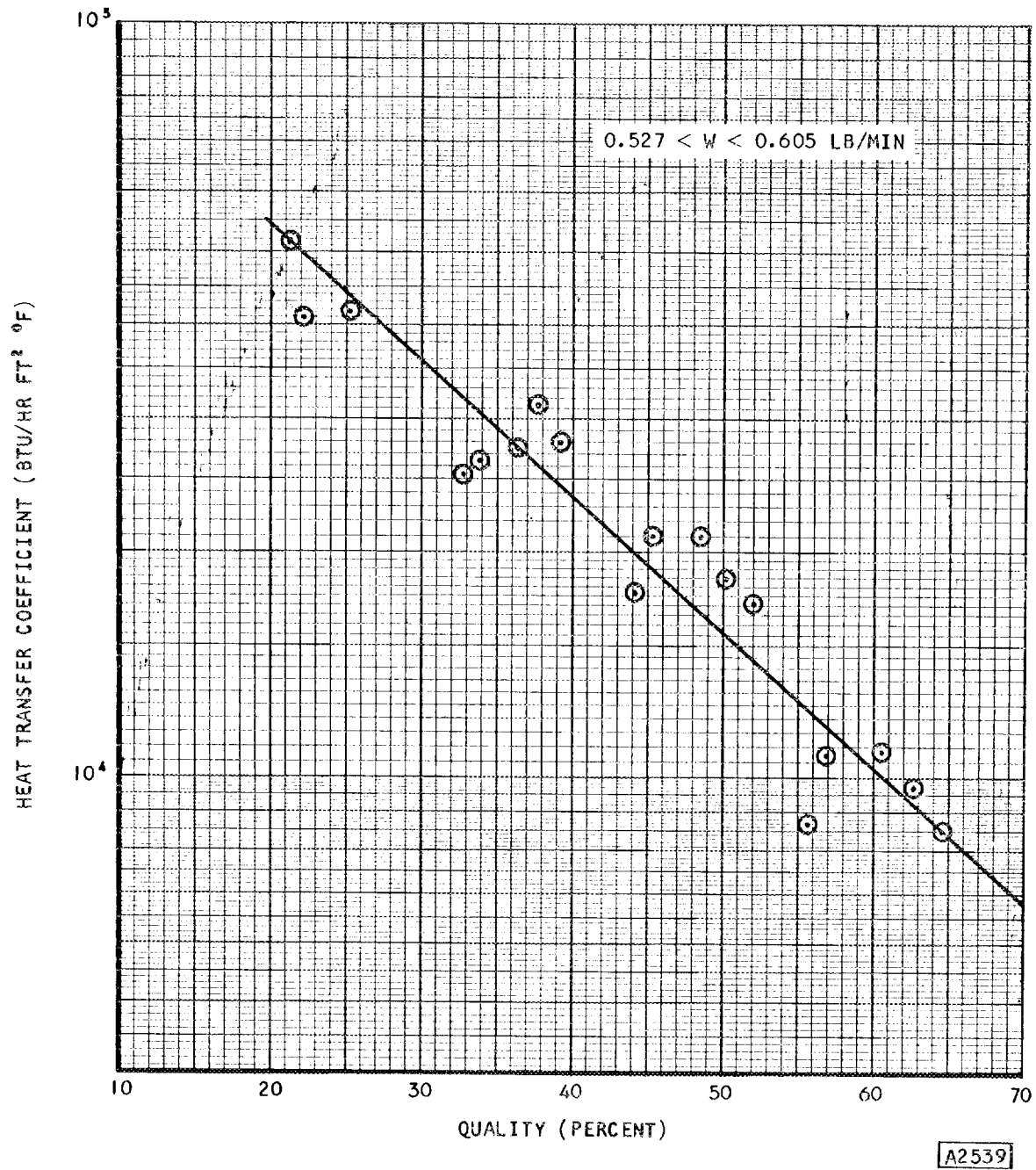


Figure 5. Heat Transfer Results

DISCUSSION

MR. YAROSH: I am curious whether or not there could have been a cavity formed by the approach of the twisted tape to the inside tube surface; and whether or not this may not have accounted for the absence of instabilities.

MR. BERENSON: We have fairly good evidence that there were cavities. The tape was pressed in, but apparently it wasn't a tight fit. We have indication of some cracks between the tape and the tube wall. So this is another source of nucleation sites, in addition to the scratches produced by the drill. By the way, we have cut the boiler open and the inside of the tube is rougher than it was initially.

We are planning on taking roughness measurements, to get the ratio of the roughness height to the tube diameter, so that we can compare this with the single-phase pressure drop results. We want to see if the roughness accounts for the difference between the measurements and the smooth tube predictions.

MR. BROOKS: Paul, is the quality referred to on your plot the average quality for the individual section, rather than a local quality?

MR. BERENSON: Yes. The quality on Fig. 5 is the average quality.

MR. BROOKS: Let's take the lower five points on that plot. Do they refer to five different sections, or do they refer to five different runs?

MR. BERENSON: Five different runs. These are pretty much grouped by runs so you get an idea of the disagreement. I can't remember whether there was a systematic variation with flow rate, or not.

MR. BROOKS: Did you notice any difference radially? We have observed in one of our tests with a twisted ribbon that, if the pressure drop on the two sides of the ribbon are not identical, you can get different performance in the two channels unless you provide some communication.

MR. BERENSON: We didn't notice any difference but, as I mentioned, the tape wasn't brazed in, so there was an opportunity for the pressure to equalize.

MR. BROOKS: Was it a loose tape?

MR. BERENSON: Yes. I think you would describe it as loose, in the same sense that the pressure would tend to equalize. But we had no way to determine whether the performance was circumferentially uniform.

MR. DAVIS: Do you feel that there is a reasonable possibility that the lack of instabilities and so forth was due to the presence of the loose tape, as opposed to the rough condition of the tube, and did you plan to run any additional data with a smooth tube and smooth tape?

MR. BERENSON: This is a very good question. We feel, and we know that Norm Greene does, that using a twisted tape by itself tends to produce stable flow. It appears that one of the major sources of instabilities in a forced convection vaporizer is the plug flow regime, and the twisted tape tends to suppress this regime and give the steady annular flow regime. While we are not planning on running any tests specifically to verify this, we do feel that a twisted tape, or some type of swirler, by itself, can stabilize the flow.

MR. DAVIS: Secondly, was there any significant contribution of the heat transfer due to conducting heat from the walls, and was this taken into account in any way?

MR. BERENSON: I don't know. In our final boiler, we are planning on providing good thermal contact with the wall because, in the high-quality region, where the coefficient is low, we want to use the insert as a fin. Here it was fairly loose, and I would be surprised if there was any contribution. We didn't calculate it.

MR. DAVIS: Does the paper mention why you did not go up to the 100 per cent quality that you had contemplated?

MR. BERENSON: This data was the average quality. Some of the runs achieved 100 per cent exit quality. In our next series of runs we plan to concentrate in the 70 to 100 per cent quality range.

MR. POPPENDINGEK: The gentleman made a comment about the influence of the rotational flow on stability, and I think we both feel this is very important.

In regard to the change of pressure drop, I think we showed last year that, in the case of rotational flow, there is a strong separation of the two phases, and therefore the theoretical pressure drop is lower than the Martinelli correlation. The experimental pressure drop that we measured was lower and was in fair agreement with it. So I think what you got is what you should expect to happen. I think Norman has a comment on the fin effect.

MR. GREENE: I would just like to comment on the fact that, at the high conductances that you had, the fin effect is deleterious rather than helpful. I think you could show that very easily.

MR. BERENSON: Agreed.

MR. FISHER: How was the heat flux distributed in the data plotted in Fig. 5?

MR. BERENSON: It was fairly uniform. In each run the heat flux was uniform, section to section, except in the sections where the heater leads had already failed, in which there was zero heat flux.

MR. FISHER: You show a fairly wide average quality range.

MR. BERENSON: Yes. Unfortunately, we started out operating at a high heat flux. We probably could have run longer if we had started at a lower heat flux and gradually worked up to the failing heat flux.

MR. CHEN: Paul, on this same Fig. 5, heat transfer coefficient is decreasing with quality. I think you have pointed this out in the paper. Some of the other results at least show the opposite effect. You indicated the reason; I wonder if you have some other indications?

MR. BERENSON: The best indication I have is for a different set of flow rates. Some of the data increases with quality and then decreases, which is consistent with what one would expect. When you have annular flow, the heat transfer coefficients would increase until you get to the start of the dry wall transition and then drop off. These runs were at lower flow rates, where you would expect the transition quality to be higher. So this is consistent with previous results. But outside of that, we have no direct evidence. I can't show a photograph of the flow regime.

MR. CHEN: In the model we will talk about after lunch, it appears that, based on the model, you can get heat transfer coefficient decreasing with quality at the lower flow rates, even though you assume an annular type of flow regime.

MR. BERENSON: That's very interesting. I was not aware of it.

MR. HAYS: Were exit qualities of 100 per cent obtained for the test boiler?

MR. BERENSON: Yes.

MR. DWYER: It seemed to me, Jim, two years ago you obtained data where there was considerable fluctuations in pressure and velocity.

MR. KILLACKEY: The fluctuations reported before were pressure. This proves somewhat annoying in trying to determine a saturation temperature. We actually put an R/C filter on the output of the pressure transducer and never did get around to plugging into an oscillograph to see what was happening. So I couldn't really answer whether we had the same effect occur this time.

MR. DWYER: I was wondering if you had the same surface, and so forth.

MR. KILLACKEY: Same boiler.

MR. DWYER: You didn't have the ribbon before.

MR. KILLACKEY: Yes, we had the ribbon before. We had a series of pressure taps down the length of the boiler, about three of them, but one of those failed in the first test so we decided to be a little more conservative this time. We took off the three that were along the boiler and plugged them up. So now it is a little more of a guess-timating procedure.

MR. POPPENDIEK: What did the subcooled tests look like? Where would that fall on that curve?

MR. BERENSON: We have some data which I didn't report. I think, as I recall, the heat transfer coefficient was roughly 5000 in one of the first two sections where we had all liquid flow.

MR. POPPENDIEK: We have been looking at the linear flow data, which is all in essence in the nucleate boiling region; highest quality of about 50 per cent. The curve for water goes the other way than the linear flow. There is really a drastic change here in that annular flow occurs at 20 per cent quality. This is very interesting.

MR. BERENSON: We feel you change over to annular flow at qualities around 1 per cent. By the time you get as high as 50 per cent, you are generally well beyond--into the transition in linear flow.

MR. POPPENDIEK: But the Berkeley data didn't show this at all. This is sort of interesting.

MR. KILLACKY: Well, let's be honest about one thing, though. Below a quality of 40 per cent, we were reporting coefficients greater than 20,000--I think as high as 50,000. The resulting ΔT 's were on the order of about 5 degrees, which is just about the experimental uncertainty involved.

MR. POPPENDIEK: Your points are very good.

MR. KILLACKY: We were clever in selecting the right points! Paul and I had a little bit of an internal dispute here, but we have some other data which shows wet wall qualities beyond 50 per cent. We can also show the high quality coefficient dropping off as the flow increases, which is somewhat the opposite of what you might expect.

MR. KELLY: You mentioned that you take the data rapidly, which makes it unnecessary to run steady-state for a length of time. Were you able to run steady for a length of time?

MR. BERENSON: Before we took a data point, inlet pressures, and temperatures, etc., would be monitored for about 15 minutes to see that they were steady. And then, after we were satisfied that we were at steady-state, the 200 data points were recorded in about two minutes.

MR. DWYER: Thank you very much.

SUMMARY OF RECENT
RESULTS OF SODIUM BOILING STUDIES

by

R. C. Noyes

Prepared for:

High Temperature Liquid Metal
Heat Transfer Technology Conference
Oak Ridge National Laboratory
Sept 4-6, 1963

Work Sponsored by:

U. S. Atomic Energy Commission
Contract: AT(11-1)-GEN-8

Atomics International
Division of North American
Aviation, Inc.
8900 DeSoto Avenue
Canoga Park, California

I. Introduction

Boiling studies are being conducted at Atomics International as part of a larger sodium reactor safety program. The project's objective is to provide basic information on sodium boiling heat transfer and two-phase hydrodynamics. Previous work by Atomics International in this area include a pool boiling study,⁽¹⁾ a condensing study,⁽²⁾ and an analytical study of two-phase flow.⁽³⁾

The current experimental program's objective is to measure void fraction, two-phase pressure drop, boiling heat transfer coefficient and burnout heat flux for sodium in forced convection in a vertical test section. The loop built for this work is described in detail in Reference 4, copies of which have been distributed at this meeting. Calibration of the loop has recently been completed and the first phase of the experimental program is now under way. This report discusses some of the first void fraction and heat transfer data that has been obtained and also presents certain loop performance characteristics not available in Reference 4.

In the process of developing and testing high flux heaters for forced convection studies, considerable new sodium pool boiling data were obtained this year. These data are presented and discussed in detail in Reference 4, and therefore, will be only summarized here. Preliminary results of recent spectral analysis made of surface temperature variations during pool boiling will be presented also.

II. Pool Studies

A. Nucleate Boiling

Recent pool boiling data were obtained from horizontal,

1/4 in. OD by 2 in. long cylindrical high flux heating elements operating about 6" below the free surface of a 1 ft. diameter by about 1 ft. deep sodium pool. The pool was maintained saturated by simultaneously boiling from several additional, uninstrumented immersion heaters. Reflux condensing occurred at a cooled flat plate at the top of the vessel. The apparatus is described in more detail in Reference 4.

The surface temperature of the high flux heater was measured by two 0.025 in. OD, stainless clad, cromel-alumel thermocouples brazed into slots in the outer cladding of the heater. Both stainless and molybdenum clad heaters were tested. The nominal location of the thermocouple junction was .0125 in. from the outer surface of the heater where boiling occurred.

Signals obtained from these thermocouples during boiling were recorded on a Sanborne fast response recording instrument. Figure 1 is a retouched photo of portions of four such recordings. A temperature scale having its zero at pool saturation temperature is superimposed on each recording. The first two traces (A & B) are from runs using a molybdenum clad heater operating at a heat flux of 463,000 Btu/hr ft² in a pool at 3.0 psia (1350°F). Because of a higher chart speed, the first trace (A) most clearly shows the detailed form of the usual surface temperature fluctuations observed. Trace C was recorded with the same heater and under the same conditions as A and B except that the heat flux was 245,000 Btu/hr-ft². Trace D was also recorded at 245,000 Btu/hr ft² with the same heater but at 1.0 psia.

These traces illustrate the form of the raw data obtained from the experiments. These data were reduced by first selecting by eye a value for the mean, minimum and maximum temperature for each

heat flux and pressure. These values were then corrected for the temperature drop between the thermocouple junction and the surface of the cladding. This correction is relatively small for molybdenum heaters; therefore, data obtained from these heaters is most accurate.

The reduced data is summarized in the plots reproduced in Figure 2. The circle symbol indicates the mean value of surface superheat for molybdenum heaters and the triangles indicate the same for stainless heaters. The horizontal bar indicates the range of fluctuation. Stainless heaters had consistently lower surface temperatures than molybdenum heaters.

Mean values of surface superheat obtained from molybdenum heaters are replotted on the single graph shown in Figure 3. The trends are typical of saturated pool boiling data obtained with other liquids. The slope of the boiling-dominated portion of the curves is slightly greater than 2 and the heat transfer coefficient increases with increasing pressure. The experimental curves are parallel to, but slightly to the left of the theoretical prediction of Forster and Zuber⁽⁵⁾. (For instance, the Forster-Zuber prediction for sodium at 3.0 psia lies very near the curve measured at 1.7 psia.)

Since it is not possible to directly observe sodium boiling, a new kind of analysis has recently been performed on some of the surface temperature measurements in an attempt to learn more of the details of the nature of the boiling process. Signals obtained from a heater surface thermocouple during steady state boiling at 1.0 psia were recorded on magnetic tape for about a 15 minute period. The tape was then formed into a continuous loop and played back at higher speed. The resulting signal was fed to an electronic

analyzer which measured relative power spectral density as a function of frequency. Results of the analysis are shown in Figure 4.

A complete interpretation of these results has not been made as yet, however, the following general observations can be made immediately. First, power spectral density for all frequencies is found to be nearly proportional to the square of the heat flux. The amplitude of surface temperature fluctuations (proportional to the square root of the power spectral density); therefore, increases directly in proportion to heat flux. Second, the power spectral density decreases approximately exponentially with increasing frequency. This behavior is believed to be due to a combination of a $1/w$ random noise spectrum and signal attenuation due to thermal inertia which would be expected to follow exponential $\sim \sqrt{w}$. Third, there is a resonance at about 2.4 cps which shifts slightly towards lower frequencies as heat flux increases. This indicates regular, periodic bubble activity at a nucleation site near the thermocouple.

B. Burnout

Several new measurements of burnout heat flux in saturated pool boiling have been obtained with the new 1/4 in. OD heaters. These measurements are plotted as a function of pool pressure in Figure 6 together with measurements made in the old pool boiling apparatus with 3/8 in. OD heaters (circles indicate new measurements). Open symbols indicate burnouts that are considered to be premature based primarily on the fact stable nucleate boiling without burnout has been obtained at the same pressures but significantly higher fluxes on repeated occasions. The scatter of the data is due to the inherent uncertainty of burnout, varia-

tion in size and material of heaters, variation of the method of approach to burnout and perhaps variation of the wetting properties of sodium.

The sodium burnout data has been correlated nondimensionally with water, organic and sulfur data according to the method suggested in the author's discussion of Reference 6. This correlation is shown in Figure 7 and it is also plotted in Figure 6; the dashed lines indicate $\pm 30\%$. The correlating equation is,

$$\frac{(q/A)_c / \lambda \rho_v}{(g \alpha)^{1/3} (Pr/n)^{1/12}} = 1.325 \left[\frac{\rho_L - \rho_v}{\rho_v} \right]^{.545} \quad (1)$$

Colver (7) has recently reported measurements of burnout heat flux for potassium in saturate pool boiling. These data are indicated by the stars connected with a dotted line in Figure 6. The potassium data does not follow the usual trend of increasing approximately as the square root of pressure at low pressure but rather increases about as the 4th root of pressure. Equation (1) predicts the potassium results well at pressures near 1.0 psia, however, it is about 60% high at atmospheric pressure. In view of these results for potassium and the scatter of the sodium data, the pressure dependence for sodium burnout cannot now be regarded as definitely established (the correlation notwithstanding). Additional pool experiments are planned for the near future to attempt to settle this point.

III. Forced Convection Studies

A. Apparatus

A schematic of the working loop built for forced convection studies is shown in Figure 7. The loop has a figure 8 configuration with a counter-flow economizer and subcooler which maintains the

pump temperature at 750°F. The pump is a multipass linear induction EM pump designed for 200 psi at 6 gpm. Performance curves for the pump which have recently been determined are shown in Figure 8. The pump has not been operated at maximum design voltage (230 volts) because of limitation in its power supply.

Figure 9 is a recent photo of the upper half of the working loop showing the preheater, test section, pressure transmitters, void detector (an EM flow meter), high flux heater and the condenser. The test section has an annular flow geometry with dimensions of 1/2 in. outside diameter and 1/4" inside diameter. The 1/4 in. diameter inner element of the annulus is formed in the shorter upper section by a high flux heating element and in the lower section by a 1/4 in. OD tube. These two sections are keyed together to form the continuous inner element.

The hollow lower section contains a 1/16 in. OD thermocouple which can be moved remotely to monitor bulk temperature at any position along the length of the test section. When two-phase flow conditions are established, this thermocouple is used to measure the axial temperature profile which can be converted to a pressure profile using the vapor pressure curve. This method produces more accurate two-phase pressure gradient data than can be obtained from pressure instrumentation directly.

B. Heat Transfer Measurement

A series of forced convection runs have been made in which the heat transfer coefficient at the high flux heater surface was measured at several inlet velocities between 3 and 6 fps. An

attempt was made to maintain the local bulk sodium temperature saturated at 4 psia without significant net vapor being present. This is a difficult condition to achieve perfectly and the actual local sodium temperature was estimated to be sub-cooled about 20°F. The measurements are plotted in the usual manner in Figure 10.

Mean values are plotted; the horizontal bars indicate the range of results obtained during three runs at different flow rates. Variations of heat transfer coefficient with flow rate were not consistent with previous experience; the tendency being for the measured coefficient to decrease slightly with increasing flow. This result is likely to be due to imperfections in the current experimental technique.

C. Void Fraction Measurements

Measurements of void fraction made under adiabatic conditions at 8 psia are shown in Figure 11. For these tests, the vapor was generated to a certain extent in the preheater unit and additional vapor was obtained by flashing between the preheater and the void detector. Mean void fraction is determined by comparing the mean flow signal obtained from the EM flow meter during two-phase flow to the signal obtained at the same temperature and mass flow rate with no voids. Because the flow meter measures only the velocity of the conducting phase (liquid), the signal increases inversely with the flow area for the liquid and thus increases with void fraction. The void area is obtained by subtracting the area occupied by the liquid from the total area of the pipe.

Measured void fractions are significantly lower than is predicted by the correlation of Lockhart and Martinelli (8). This

indicates that low quality, low pressure slip ratios for sodium tend to be higher than for other materials.

IV. Summary

New pool measurements of nucleate boiling heat transfer coefficient for saturated sodium have been accomplished with improved experimental accuracy. Results show sodium to exhibit conventional boiling behavior and to have heat transfer coefficients slightly higher than predicted by Forster and Zuber. Stainless surfaces had slightly higher coefficients than molybdenum surfaces.

A new nondimensional correlation of burnout heat flux in pool boiling has been developed which brings sodium measurements into agreement with measurements on sulfur, water and organic materials. Colver's recent results with potassium, however, do not show the same pressure dependence as the correlation or other data and, therefore, open to question the proper functional dependence of liquid metal burnout on pressure.

A new working loop for experimental study sodium forced convection boiling heat transfer and two-phase flow has been put into operation. Preliminary heat transfer results indicate that, under slightly subcooled conditions, sodium behaves as would be expected from pool boiling results.

Initial measurements of void fraction in two-phase flow at 8 psia and low quality show void fractions somewhat lower than predicted by Lockhart-Martinelli.

References

1. R. C. Noyes, "An Experimental Study of Sodium Pool Boiling Heat Transfer," NAA-SR-6769 (March 1962)
2. G. L. Reed and R. C. Noyes, "Sodium Condensing Heat Transfer, An Experimental Study of One Aspect of Sodium Cooled Reactor Safety", NAA-SR-7325 (July 1962)
3. R. C. Noyes, F. Bergonzoli and J. E. Gingrich, "FUGUE, A Nondimensional Method for Digital Computer Calculation of Steady State Temperature, Pressure and Void Fraction in Pipe Flow With or Without Boiling", NAA-SR-5958 (May 1961)
4. R. C. Noyes, "Boiling Studies For Sodium Reactor Safety, Part I: Experimental Apparatus and Results of Initial Tests and Analysis" NAA-SR-7909 (Sept 1963).
5. H. K. Forster and N. Zuber, "Dynamics of Vapor Bubbles and Boiling Heat Transfer" AICHE Journal, Dec 1955, p. 531
6. R. C. Noyes "An Experimental Study of Sodium Pool Boiling Heat Transfer" Trans. ASME, Journal of Heat Transfer, May 1963.
7. C. P. Colver, "Investigation of Liquid Metal Boiling Heat Transfer" 5th Quarterly Progress Report, Univ. of Michigan, June 1963.
8. R. W. Lockhart and R. C. Martinelli, "Proposed Correlation for Isothermal Two-Phase, Two-Component Flow in Pipes" Chemical Engineering Progress, 45:39-48 (1949).

Nomenclature

$(q/A)_c$	=	critical heat flux (Btu/hr-ft ²)
λ	=	latent heat of vaporization (Btu/#)
ρ_v, ρ_l	=	vapor density, liquid density (#/ft ³)
g	=	local acceleration (ft/hr ²)
α	=	thermal diffusivity of liquid (ft ² /hr)
Pr	=	Prandtl number of liquid
n	=	nondimensional local accelerations (g/gc)
w	=	frequency

FIGURE 1

VARIATION OF SURFACE TEMPERATURE DURING SODIUM BOILING

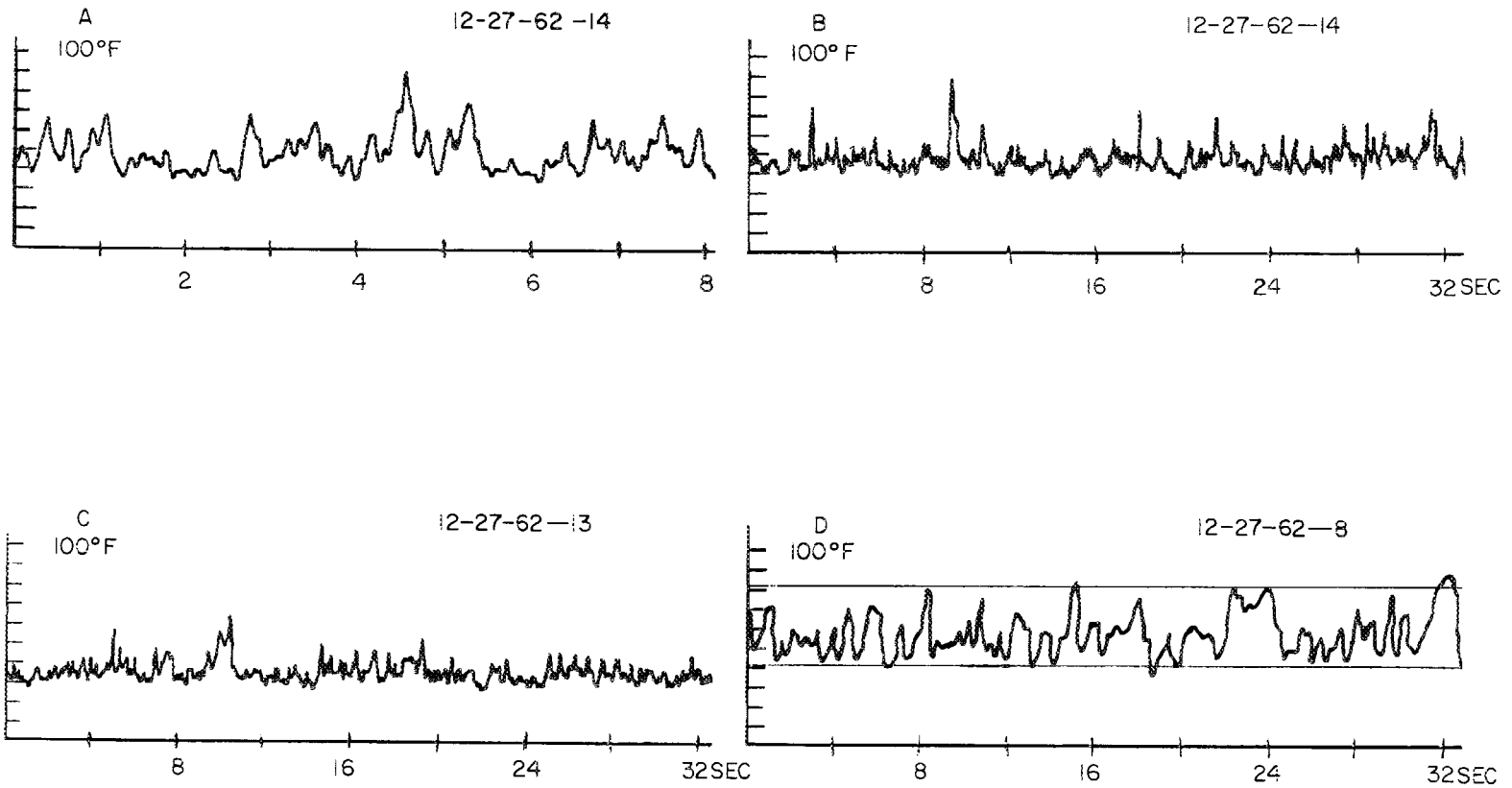


FIGURE 2
SURFACE SUPERHEAT DURING
SATURATED SODIUM POOL BOILING

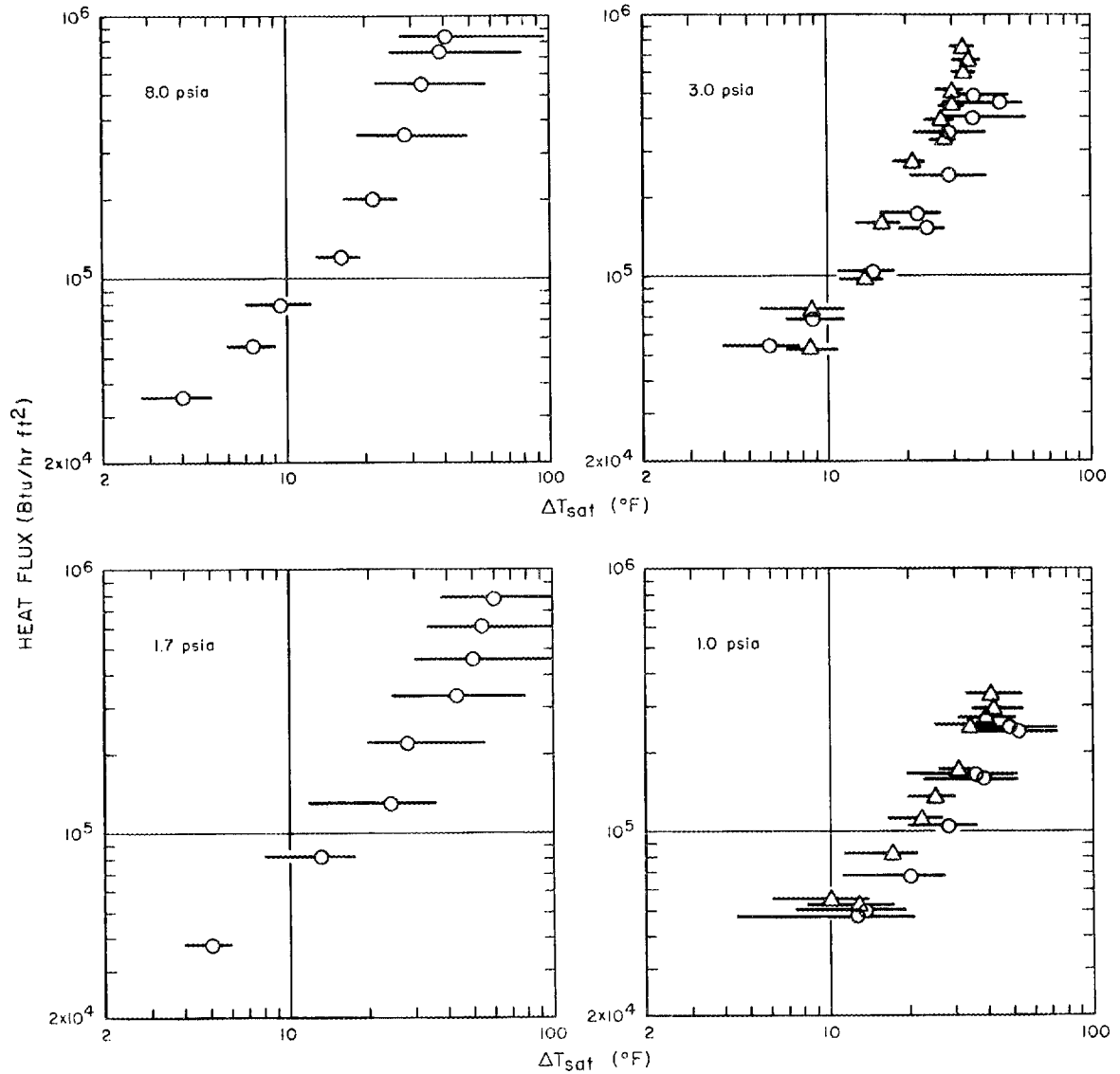


FIGURE 3

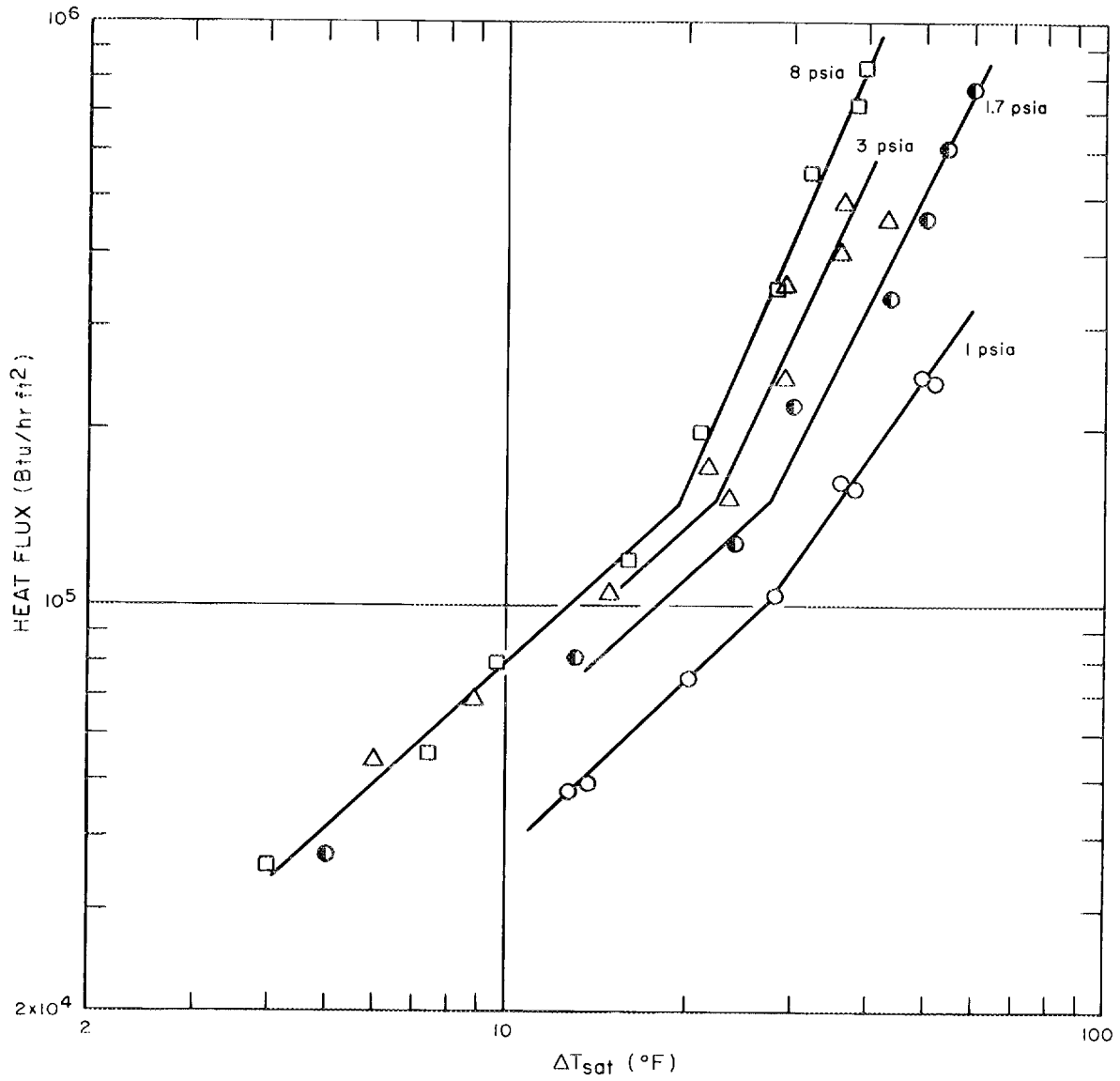
MEAN SURFACE SUPERHEAT DURING SATURATED SODIUM
POOL BOILING FROM MOLYBDENUM HEATER

FIGURE 4
 SPECTRAL ANALYSIS OF SURFACE TEMPERATURE DURING SODIUM BOILING
 POOL PRESSURE = 1 PSIA

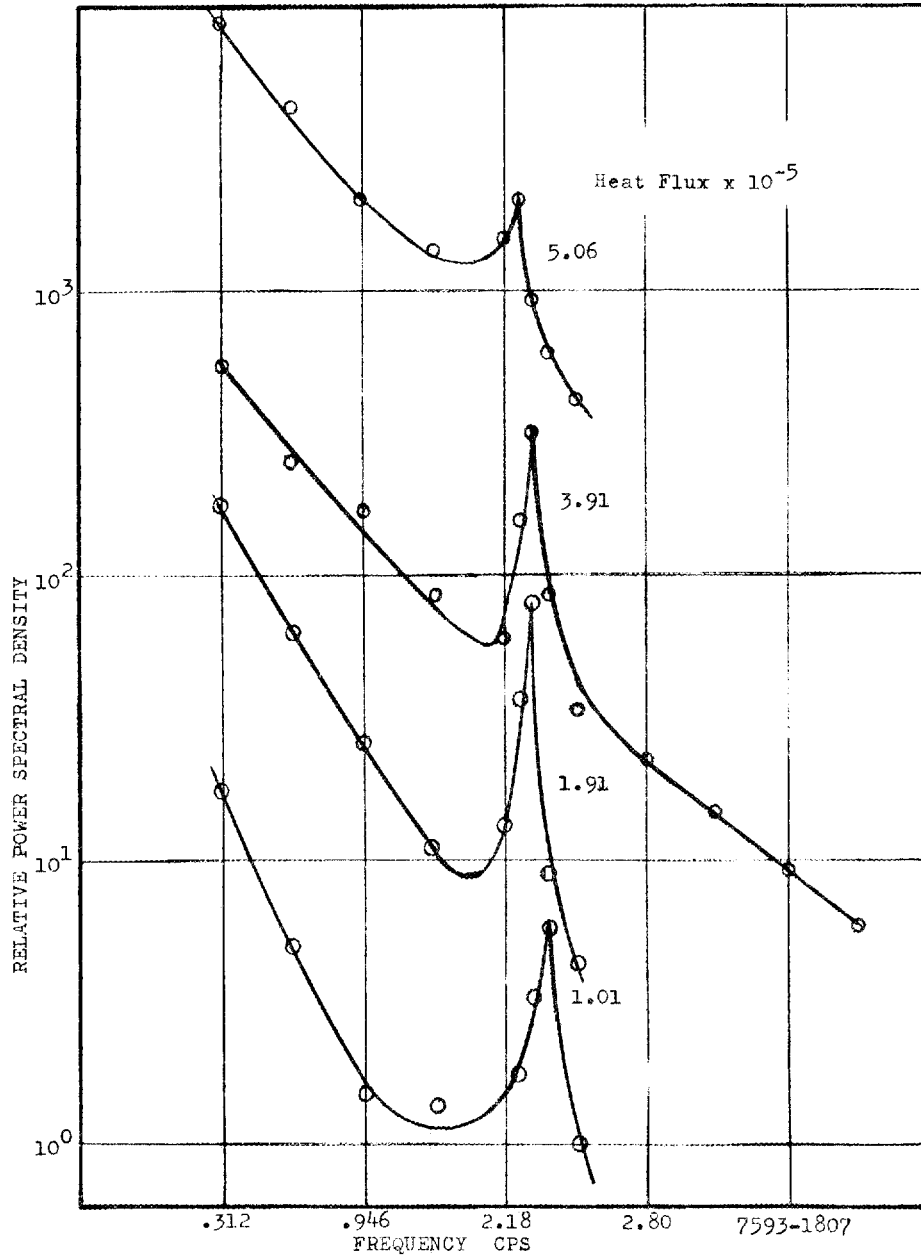


FIGURE 5

BURNOUT HEAT FLUX FOR SODIUM POOL BOILING

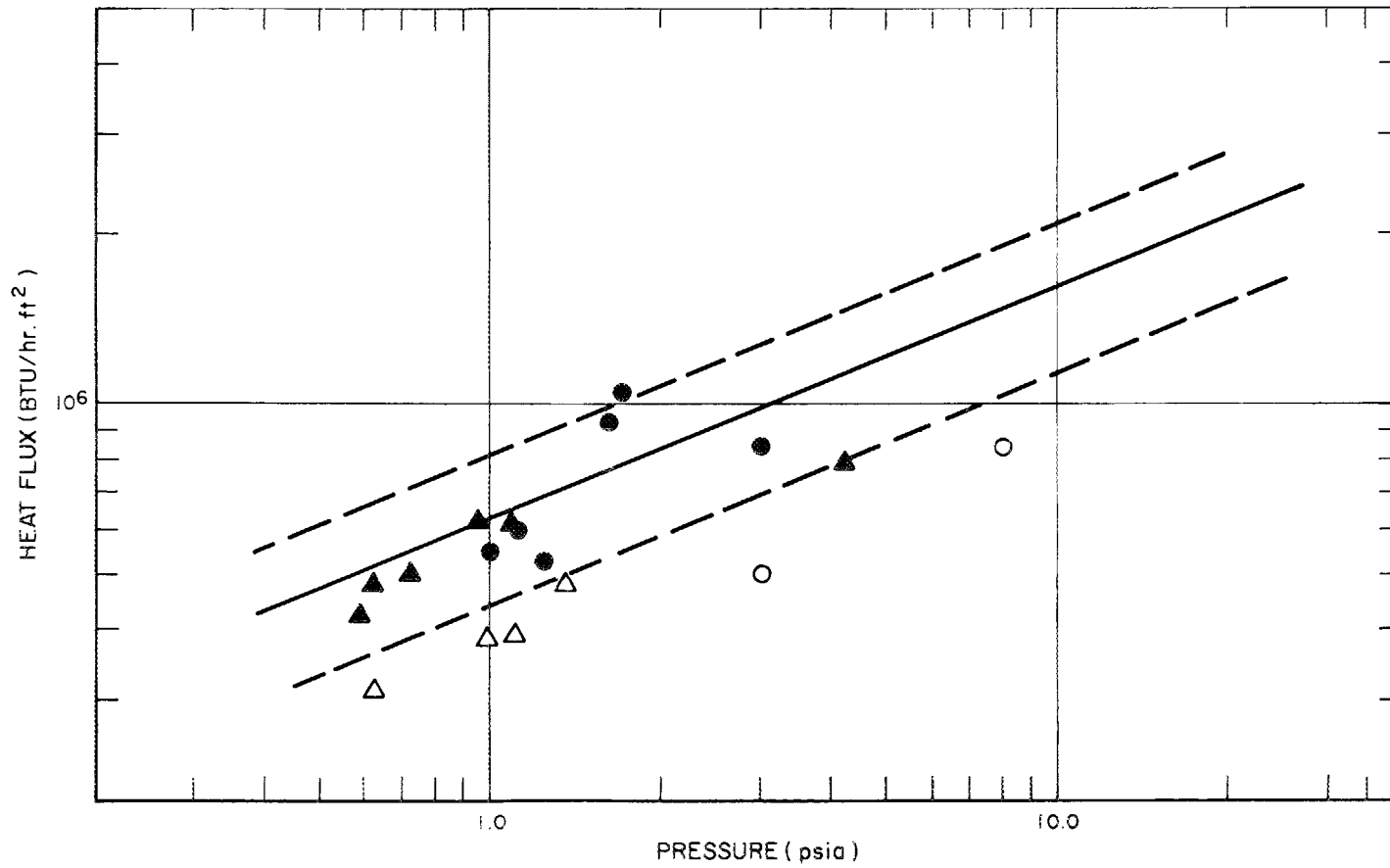


FIGURE 6

CORRELATION OF BURNOUT HEAT FLUX

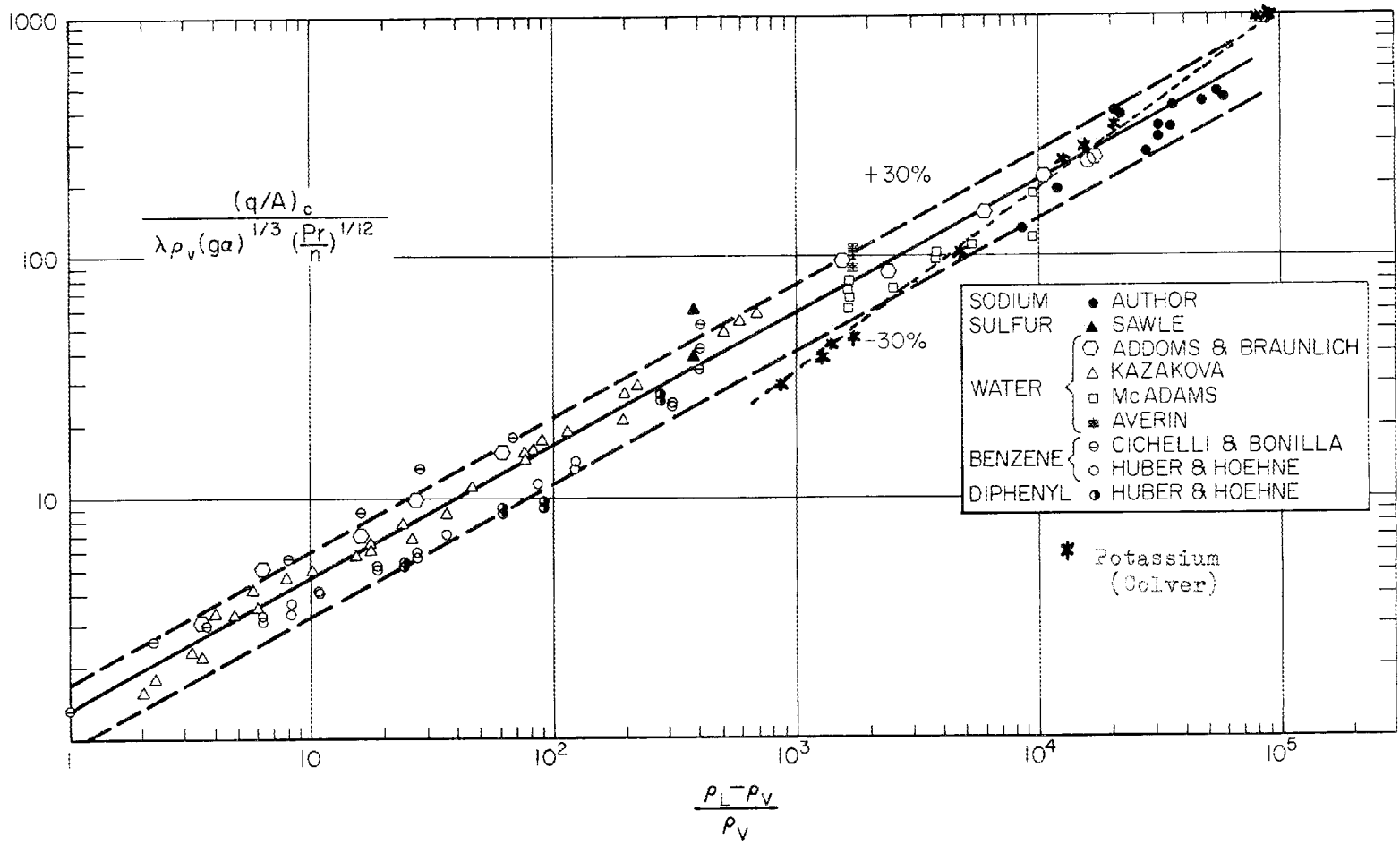


FIGURE 7

WORKING LOOP FOR FORCED CONVECTION BOILING SODIUM STUDIES

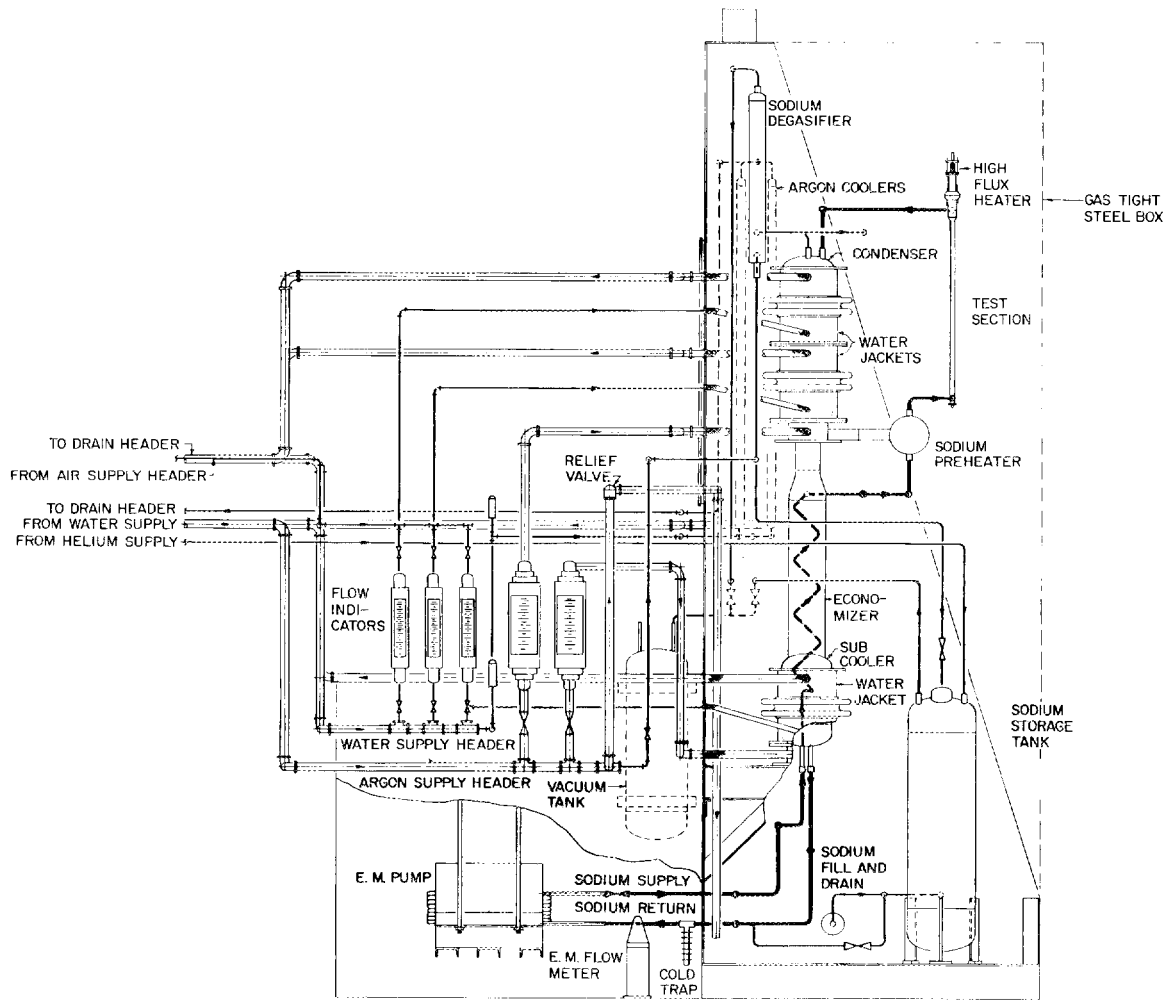


FIGURE 8
PERFORMANCE CURVES FOR
MULTIPASS LINEAR INDUCTION PUMP
SODIUM AT 750°F

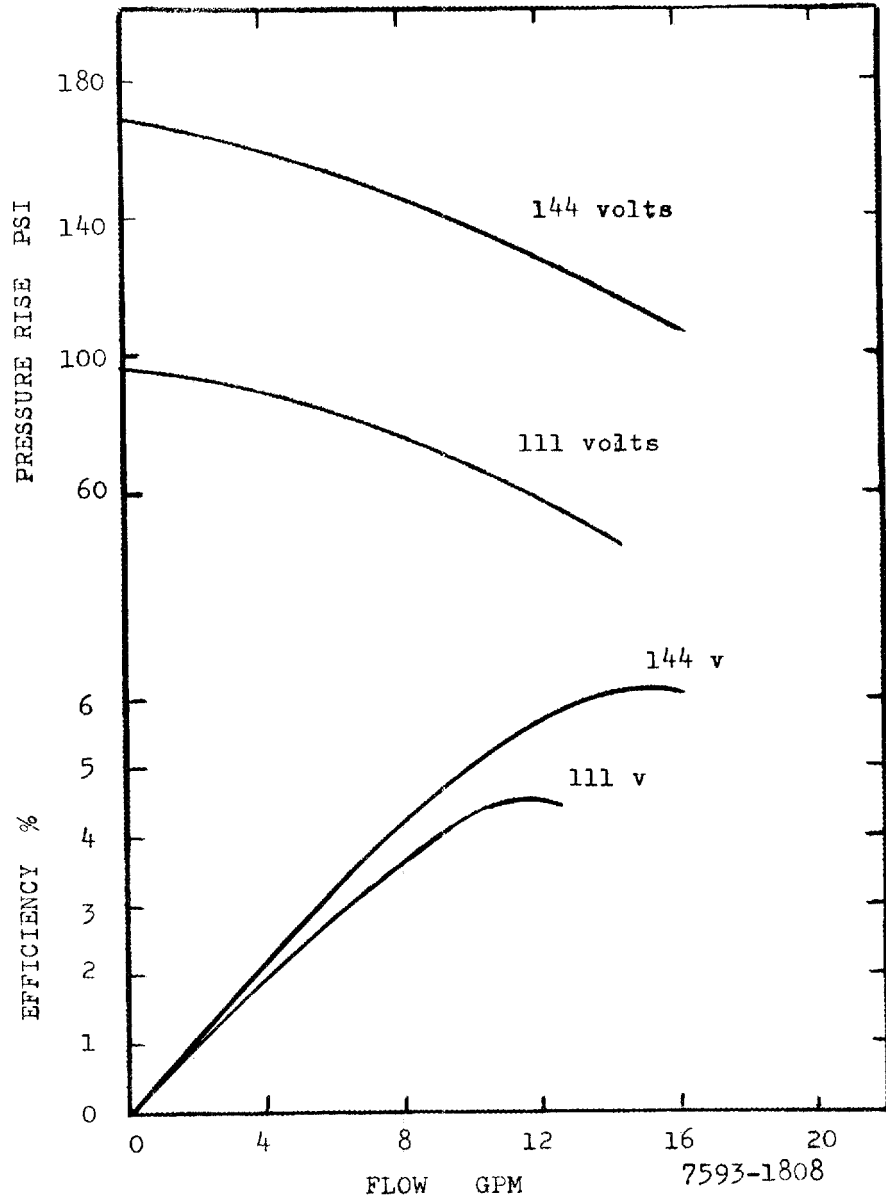


FIGURE 9
LOW PRESSURE BOILING LOOP TEST SECTION

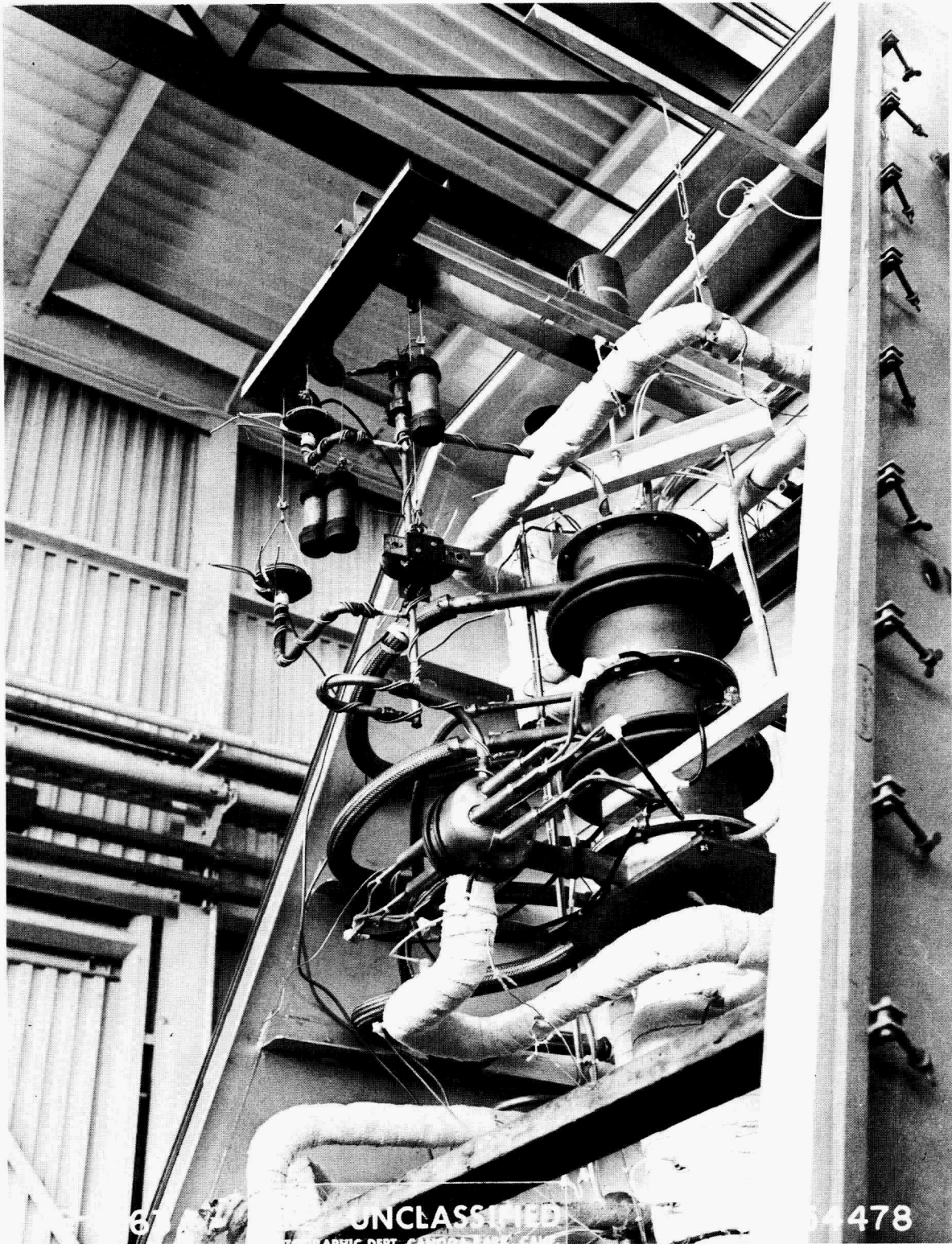


FIGURE 10
HEAT TRANSFER TO BOILING SODIUM
SUBCOOLED FORCED CONVECTION AT 4 PSIA

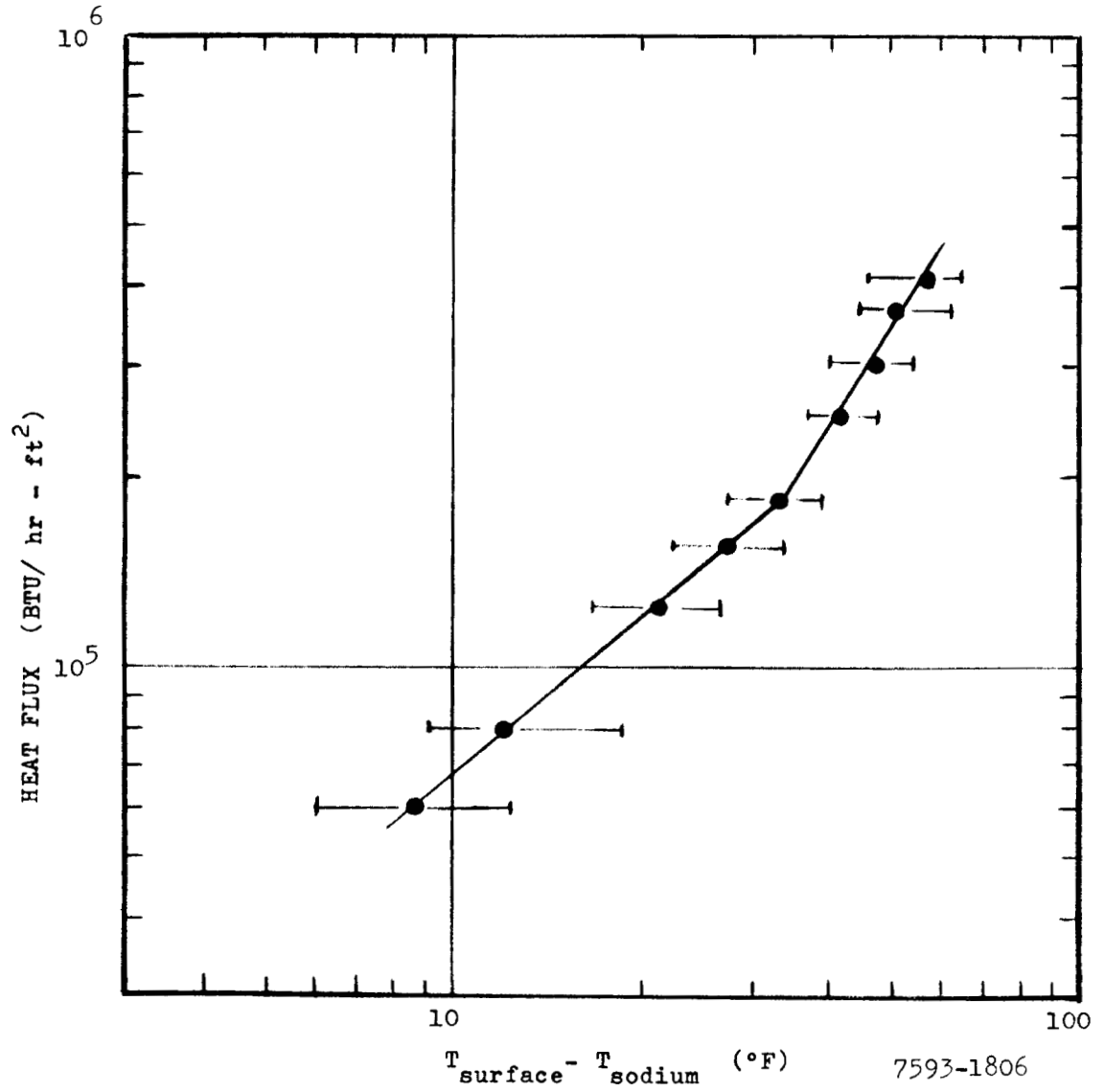
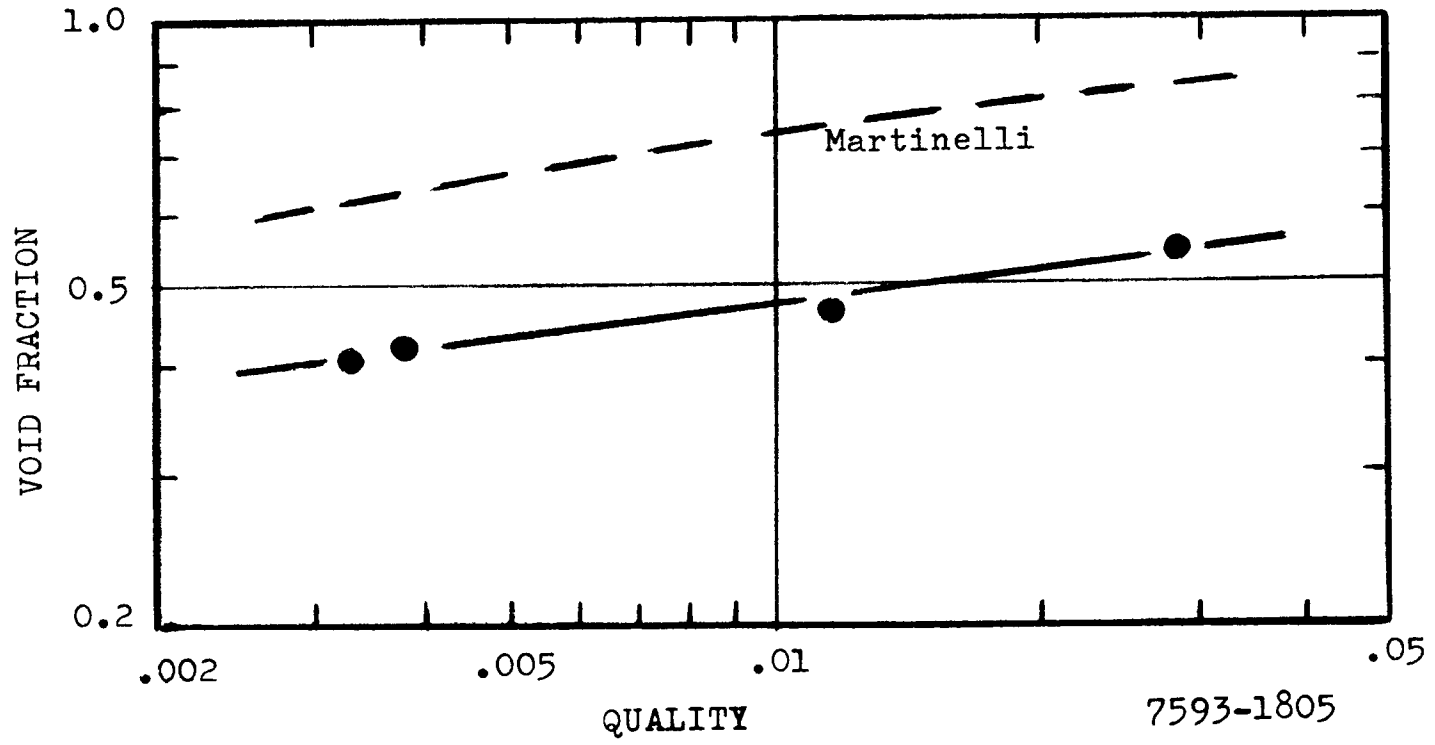


Figure 11

SODIUM VOID FRACTION AT 8 PSIA



DISCUSSION

MR. DWYER: In that second to the last slide you showed there, you had a bend in your plot. This was forced-convection boiling. You say that was all in a sub-cooled, nucleate boiling range? I notice you had a bend in there. It would indicate you probably got into the nucleate boiling.

MR. NOYES: Well, we were boiling. I imagine at the lower surface temperatures it was essentially forced convection heat transfer. As we increase the heat flux, then we get a larger contribution from nucleate boiling. Certainly at the higher heat fluxes we were boiling at the surface. However, the bulk temperatures probably remain slightly sub-cooled at all the points we were making measurements.

MR. DWYER: Up to the bend they were collapsing. Beyond the bend they were collapsing?

MR. NOYES: I believe they were collapsing all the way, really. I think it was all surface type of boiling, although we might have been generating a small amount of net vapor. Can't tell for sure.

MR. BALZHISER: Dick, one comment, perhaps two: With regard to the break in your slope, that curve, we observed a significant change in the fluctuation both as to the amplitude frequencies, somewhere just above 100,000. It seems, if I recall, on the three higher pressure runs, right around 150,000 we observed something that perhaps is significant as to the type of fluctuation.

Second of all, if you can justify throwing away two of those burnout points out here, I think we can agree as to the slope.

MR. NOYES: May I make a comment about the slope of the burnout data? I have been tempted to throw away a lot of those burnout points and pick out those that have a slope that I like! However, I find that is a little dangerous.

In observing some of the data we have obtained, with the same heater at several pressures, even though the pressures were close together, it did appear to me that though the burnout heat flux was increasing roughly

as the square root of the pressure. Although as I say, the data is so scattered, I can't prove it.

MR. KRAKOVIK: You mentioned that the heat transfer coefficient decreases with increase of flow rate. Was this at constant heat flux?

MR. NOYES: Yes, at constant heat flux.

MR. KRAKOVIK: It is good to hear analogous results. In our experiments, at constant flux, a decrease in flow rate resulted in an increase in quality and an increase in the heat transfer coefficient.

MR. NOYES: In all cases, here, we really don't have any quality at all. The average bulk temperature was slightly sub-cooled. I expect, with improved experimental techniques, and if we work hard enough at it, we can eliminate this sort of result.

A PROPOSED MECHANISM AND METHOD OF CORRELATION
FOR CONVECTIVE BOILING HEAT TRANSFER WITH LIQUID METALS *

John C. Chen

Brookhaven National Laboratory

August 1963

ABSTRACT

An additive, interacting mechanism of micro and macro-convective heat transfer is proposed to represent boiling heat transfer with net vapor generation to saturated liquid metals in convective flow. Based on this mechanism, a method for calculating boiling coefficients is developed. The correlating is shown to be in fair agreement with early experimental results for convective boiling of potassium and sodium.

*This work was performed under the auspices of the U. S. Atomic Energy Commission

Introduction

Recently, a new correlation was proposed for the calculation of convective-boiling heat transfer coefficients for ordinary fluids.⁽¹⁾ In tests against experimental results for water and organic fluids, this correlation showed an average deviation of 11%, as compared to deviations of 32% to 43% for previous correlations. This present paper proposes an extension of the new correlation to the case of liquid metals. Specifically, the area of interest is defined by the following conditions:

- (1) boiling heat transfer
- (2) saturated liquid metals
- (3) vertical, axial, convective flow
- (4) stable flow
- (5) no slug flow
- (6) no liquid deficiency
- (7) heat flux less than critical flux

These conditions would normally be satisfied by convective boiling of liquid metals with net vapor generation in annular or mist-annular two-phase flow.

Derivation

The proposed model for convective boiling heat transfer is based on the following two postulates:

- (1) There are two mechanisms which contribute to total heat transfer, i.e., the macro-convective mechanism associated with over-all flow and the micro-convective mechanism associated with bubble growth in the annular liquid film.
- (2) These two mechanisms interact with each other, i.e., the presence of vapor strongly influences macro-convective heat transfer, and conversely, the presence of flow modifies bubble motion and consequently effects micro-convective heat transfer.

On the basis of this model, reference (1) obtained the following expression for calculating the modified micro-convective contribution.

$$h_{mic} = 0.00122 \frac{k_L^{0.79} C_{pL}^{0.45} \rho_L^{0.49} \Delta T^{0.24} \Delta P^{0.75} g_c^{0.25}}{\sigma^{0.5} \mu_L^{0.29} \lambda^{0.24} \rho_v^{0.24}} \times S \quad (1)$$

$$S = \left(\frac{\Delta T_e}{\Delta T} \right)^{0.99} \quad (2)$$

where ΔT_e is the effective superheat for bubble growth in the annular liquid film. S , called the suppression function, is a measure of the suppression of bubble growth by the presence of two-phase flow and was empirically correlated against an effective two-phase Reynolds number, as shown in Figure 1. In extending this theory to the case of boiling liquid metals, it is assumed that the micro-convective heat transfer can still be described by equation (1). This assumption is based on indications that Foster-Zuber's pool-boiling theory, from which equation (1) was derived, appears to be applicable for liquid metals as well as for ordinary fluids. (2)

For the macro-convective contribution to total heat transfer, reference (1) utilized a modified form of the conventional Dittus-Boelter equation. In the current analysis for convective boiling of liquid metals, it is proposed that the following modified form of the Lyon-Martinelli equation be used instead.

$$h_{mac} = \left[\delta + 0.024 (F Re_L^{0.8}) (\beta Pr_L)^\alpha \right] \frac{\gamma k_L}{D} \quad (3)$$

The values for the five parameters α , β , γ , δ , F are listed in Table I.

Table I
Parameters in Macro-Convective Equation

	<u>Liquid Metal</u>	<u>Vapor</u>	<u>Two-phase</u>
δ	7	0	$7z^\epsilon$
γ	1	$\frac{k_v}{k_L}$	$z^\epsilon + \frac{k_v}{k_L}(1-z^\epsilon)$
β	1	$\frac{Pr_v}{Pr_L}$	$z^\epsilon + \frac{Pr_v}{Pr_L}(1-z^\epsilon)$
α	0.8	0.4	$0.4(1+z^\epsilon)$
F	1	$\left(\frac{Re_v}{Re_L}\right)^{0.8}$	$\left(\frac{Re}{Re_L}\right)^{0.8} = f\left(\frac{1}{x_{tt}}\right)$

It is seen that at the limit of 0% quality, equation (3) reduces to the conventional Lyon-Martinelli equation descriptive of single-phase liquid-metal heat transfer. At the other limit of 100% quality, equation (3) becomes the Dittus-Boelter equation for vapor phase heat transfer. In the region of mixed quality where both liquid and vapor are present, it is proposed that the four parameters denoted by Greek letters assume values intermediate between the single-phase values, as shown in Table I. The exponential parameter, ϵ , is a measure of the non-uniformity of phase distribution in the flow pattern. Should the distribution be uniform in such a way that the two-phase values for the parameters are simple arithmetic proportions of the single-phase values, then ϵ is unity. In the case of interest, where liquid is concentrated on the channel wall as an annular film, it is expected that liquid properties would dominate, and ϵ

approaches zero. The exact value for ϵ will have to await empirical determination. The function F is a measure of the effectiveness of two-phase momentum transfer as compared to the corresponding liquid-phase momentum transfer. As shown in reference (1), F can be correlated against the Martinelli parameter. The recommended correlation is reproduced in Figure (2).

Equations (1) and (3), with values of the parameters obtained from Table I and Figures (1) and (2) represent the proposed correlations for the micro- and macro-convective contributions. Total convective boiling heat transfer is then obtained as the sum of the two interacting contributions,

$$h = h_{mic} + h_{mac} \quad (4)$$

Discussion

The one unknown in the above correlation is the exponential parameter, ϵ . As a first approximation, we may treat it as a constant. Moreover, we can expect that for annular flow, ϵ would have a value equal to or close to zero. Figure 3 shows a plot of the ratio h/h_L calculated for several values of ϵ . It is seen that a small change in ϵ , from 0 to 0.05, can strongly influence the two-phase boiling coefficients predicted by this correlation. At the present time, there are not enough experimental results available to determine the correct value or function for ϵ . As a temporary solution, we can assume liquid properties to be entirely dominant and use zero for the value of ϵ .

Figures 4 and 5 show comparisons of the correlation against experimental results for the convective boiling of potassium and sodium, respectively. (3,4) The experimental data are represented by the plotted points while the regions predicted by this correlation for corresponding conditions are represented by the shaded areas. Dengler and Addoms' correlation for convective boiling of ordinary fluids is also shown on these figures for a

reference. It is immediately evident that correlations for ordinary fluids can not be used for the case of liquid metals. The correlation proposed here is seen to come much closer to representing the experimental results.

It should be noted that there still appears to be a consistent deviation, even for this correlation. The calculated values tend to be slightly higher than the ones measured experimentally. This discrepancy may be due to the correlation, the experimental data, or both, since both are just preliminary results at the present time. One possible cause for the discrepancy is that the suppression function, S , was obtained from data with water and organic fluids. It is possible that a secondary effect of Prandtl number should be taken into account. Another possible explanation is that the fluid temperatures were not measured directly in the experimental studies. For the potassium results, fluid temperatures were obtained by interpolation between inlet and exit conditions. For the sodium results, fluid temperatures were obtained from measurements in a downstream mixing box. Both treatments would tend to give saturation fluid temperatures which are lower than the actual temperatures and result in seemingly lower boiling coefficients. An error in fluid temperature corresponding to less than 0.5 psi of saturation pressure could account for the discrepancies between calculated and measured coefficients shown in Figures 4 and 5.

Figures 6 and 7 show samples of the parametric behavior for convective boiling heat transfer of liquid metals, as predicted by the equations proposed here. Figure 6 shows the effects of flow rate on the boiling curve for potassium at 50% quality. Figure 7 shows the combined effects of quality and flow rate on the convective boiling coefficient. One interesting result for the conditions represented in this figure is that at

low flow rates h decreases with increasing quality, at high flow rates h increases with increasing quality, while at intermediate flow rates h passes through a minimum. This serves to point out one useful result of a preliminary model and correlation such as this. It can provide an over-all view and grasp of the phenomenon which can explain seemingly contradicting trends that may be exhibited by experimental results.

Summary

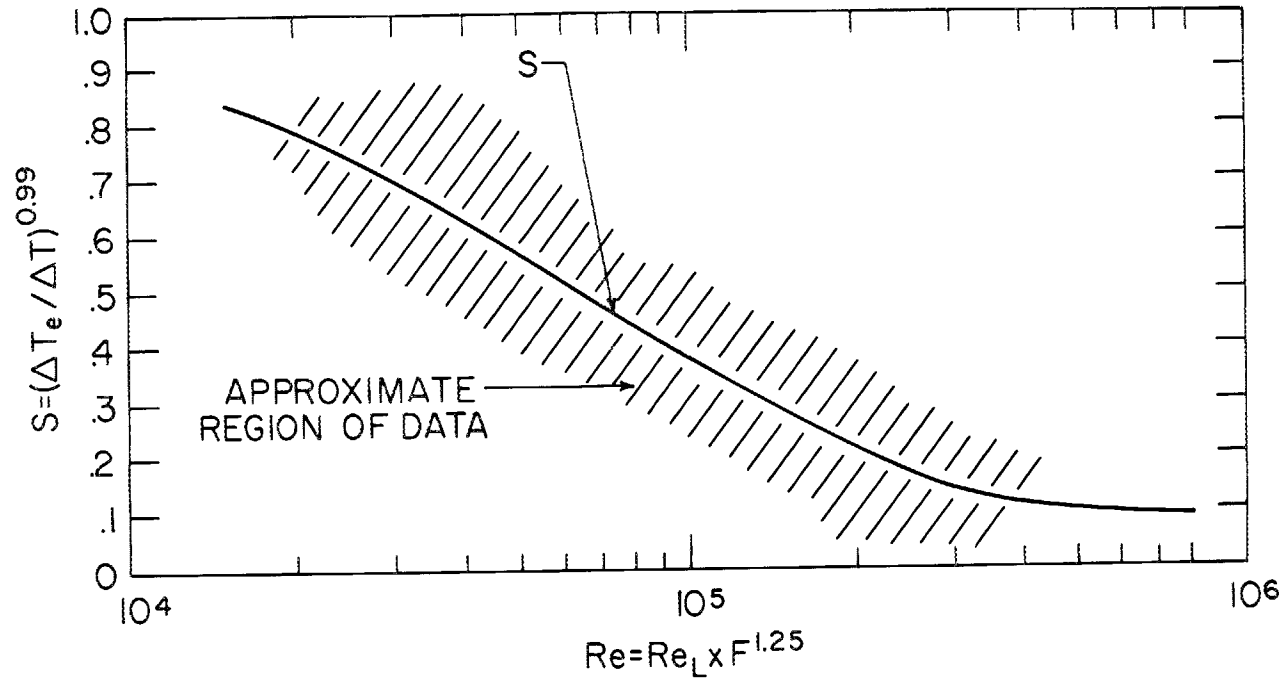
A method is proposed for calculation of convective boiling heat transfer to liquid metals, based on the concept of additive, interacting mechanisms of micro- and macro-convective heat transfer. The resulting correlation is shown to be in reasonable agreement with preliminary experimental results for potassium and sodium. It is anticipated that this work may be useful as a guide for experimental work and future refinements in analysis.

References

1. Chen, J. C., A Correlation for Boiling Heat Transfer to Saturated Fluids in Convective Flow, ASME Paper 63-HT-34, presented at ASME-AIChE Heat Transfer Conference, Boston, August 1963.
2. Camack, W. G., and Forster, H. K., Test of a Heat Transfer Correlation for Boiling Liquid Metals, Jet Propulsion, 27, pp. 1104-1106, Oct. 1957.
3. Hoffman, H. W., and Krakoviak, A. I., Forced-Convection Boiling of Potassium at Near Atmospheric Pressure, Proceedings of 1962 High-Temperature Liquid-Metal Heat Transfer Technology Meeting, BNL 756 (C-35), May 1962.
4. Longo, J, editor, Alkali Metals Boiling and Condensing Investigations, Quarterly Progress Reports 2 and 3, Space Power and Propulsion Section, General Electric, April 1963.

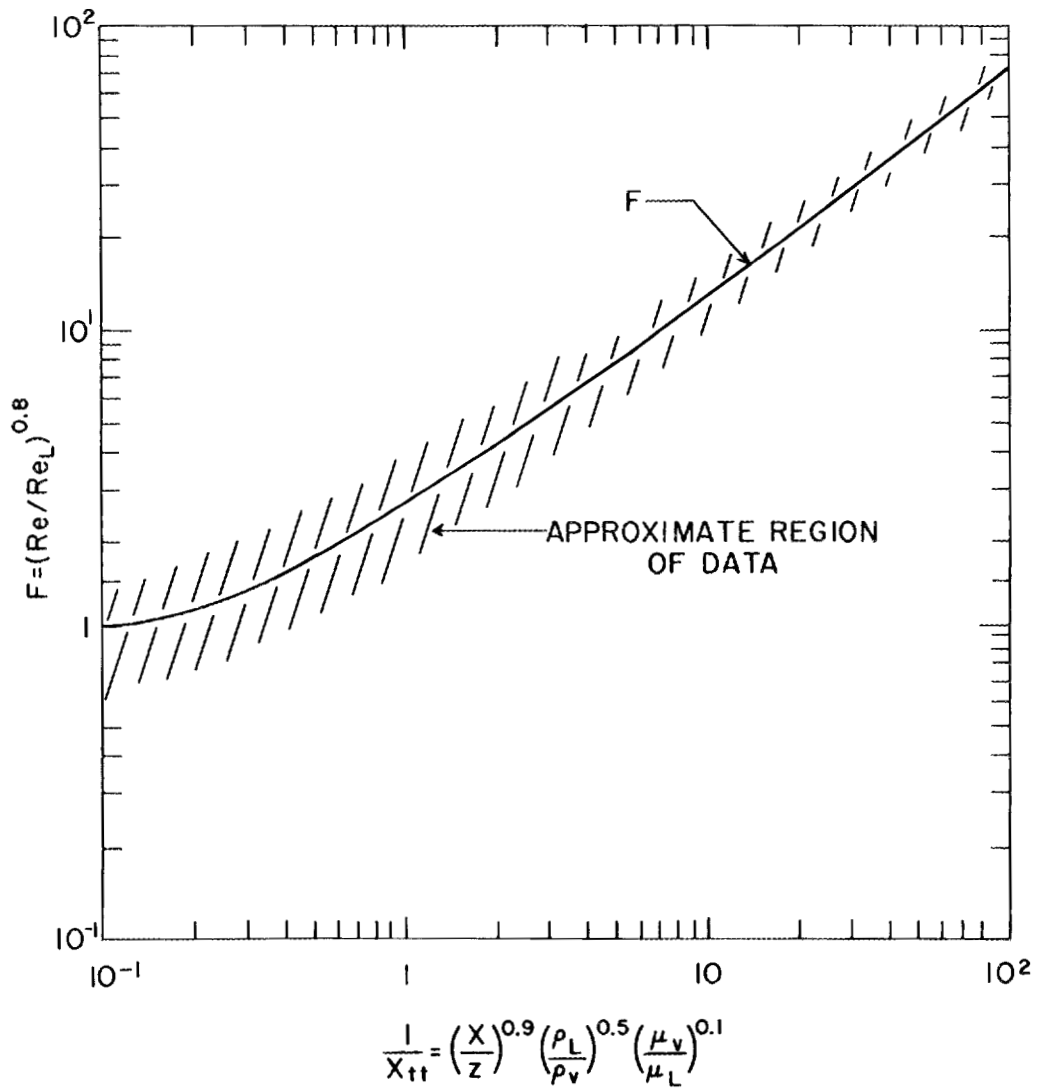
Nomenclature

C_p	heat capacity, (Btu)/(Lb) ($^{\circ}$ F)
D	diameter, (ft)
F	Reynolds number factor, $(Re/Re_L)^{0.8}$
g_c	gravitational constant
h	heat transfer coefficient, (Btu)/(Hr) (Ft ²)
k	thermal conductivity, (Btu)/(Hr) (Ft) ($^{\circ}$ F)
P	pressure, (psf)
Pr	Prandtl number
q/A	heat flux, (Btu)/(Hr) (Ft ²)
Re	Reynolds number
S	suppression function, $(\Delta T_e/\Delta T)^{0.99}$
T	temperature, ($^{\circ}$ R)
X_{tt}	Martinelli parameter, $(\frac{z}{x})^{0.9} (\frac{\rho_v}{\rho_L})^{0.5} (\frac{\mu_L}{\mu_v})^{0.1}$
x	quality, weight fraction of vapor
z	weight fraction liquid
α	parameter defined in Table I
β	parameter defined in Table I
γ	parameter defined in Table I
δ	parameter defined in Table I
ΔP	difference in vapor pressure corresponding to ΔT , (psf)
ΔT	superheat, $T-T_s$
ΔT_e	effective superheat with flow
subscript:	
none	value for two-phase fluid
L	value for liquid
s	value at saturation condition
v	value for vapor
w	value at wall



THE SUPPRESSION FUNCTION

Figure 1



THE REYNOLDS NUMBER FUNCTION

Figure 2

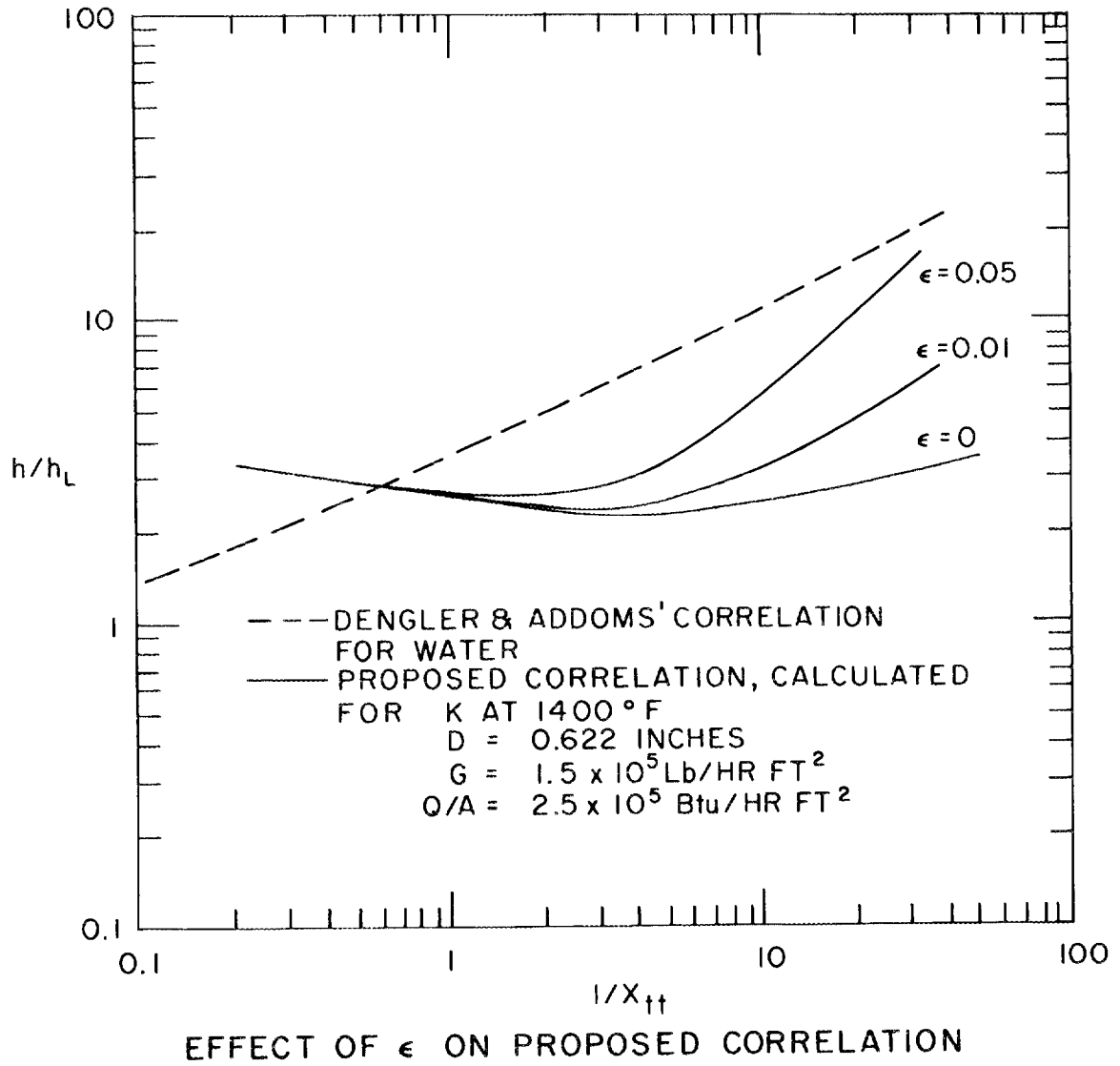
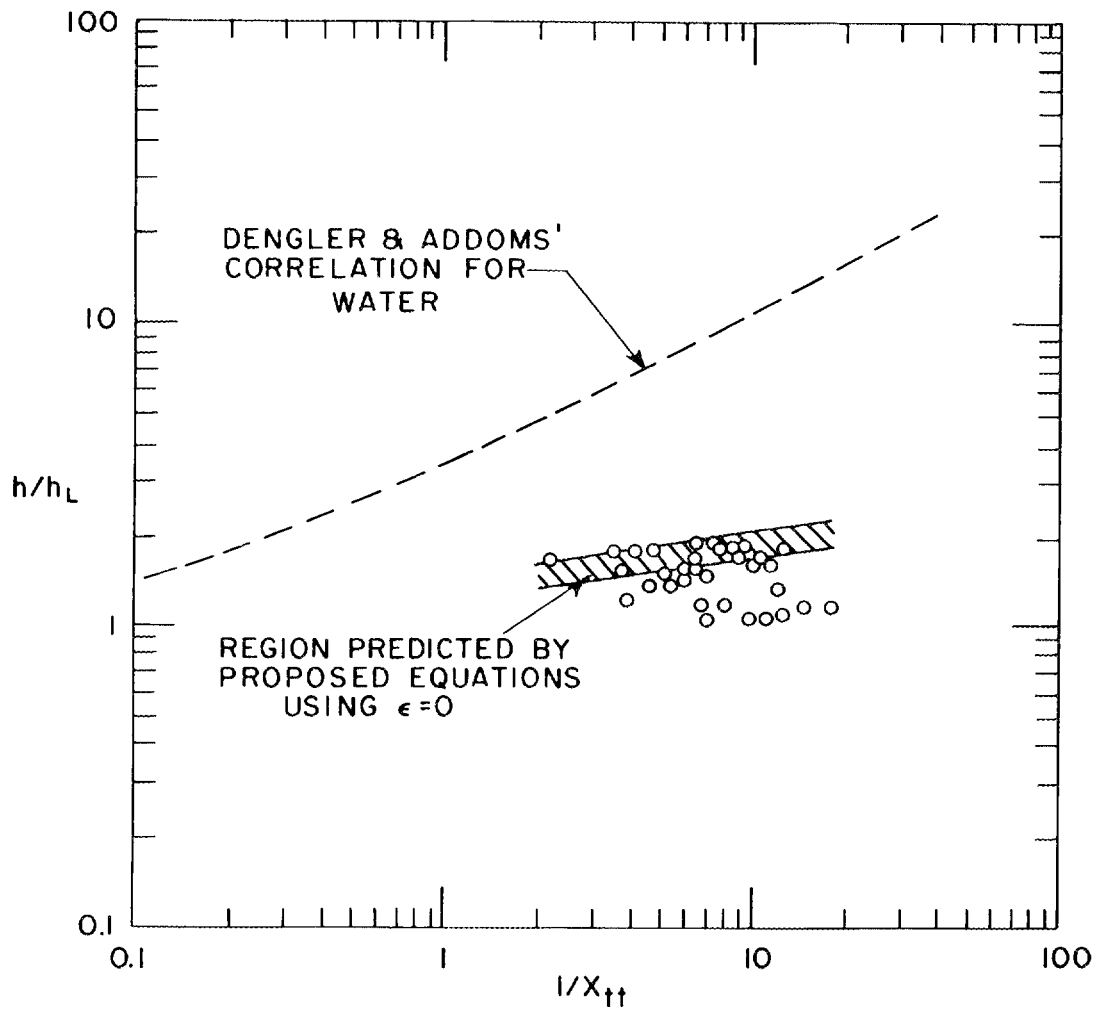
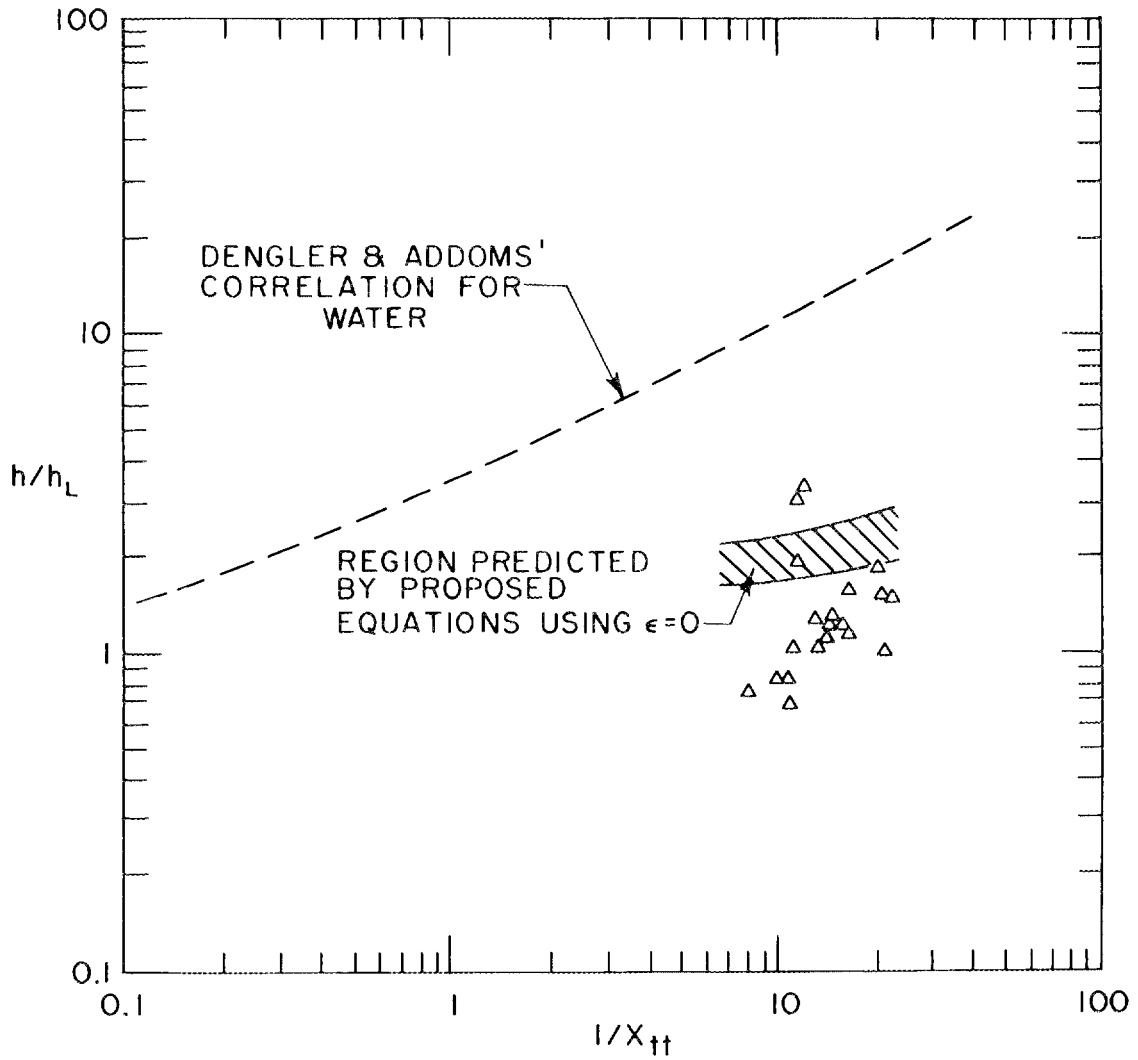


Figure 3



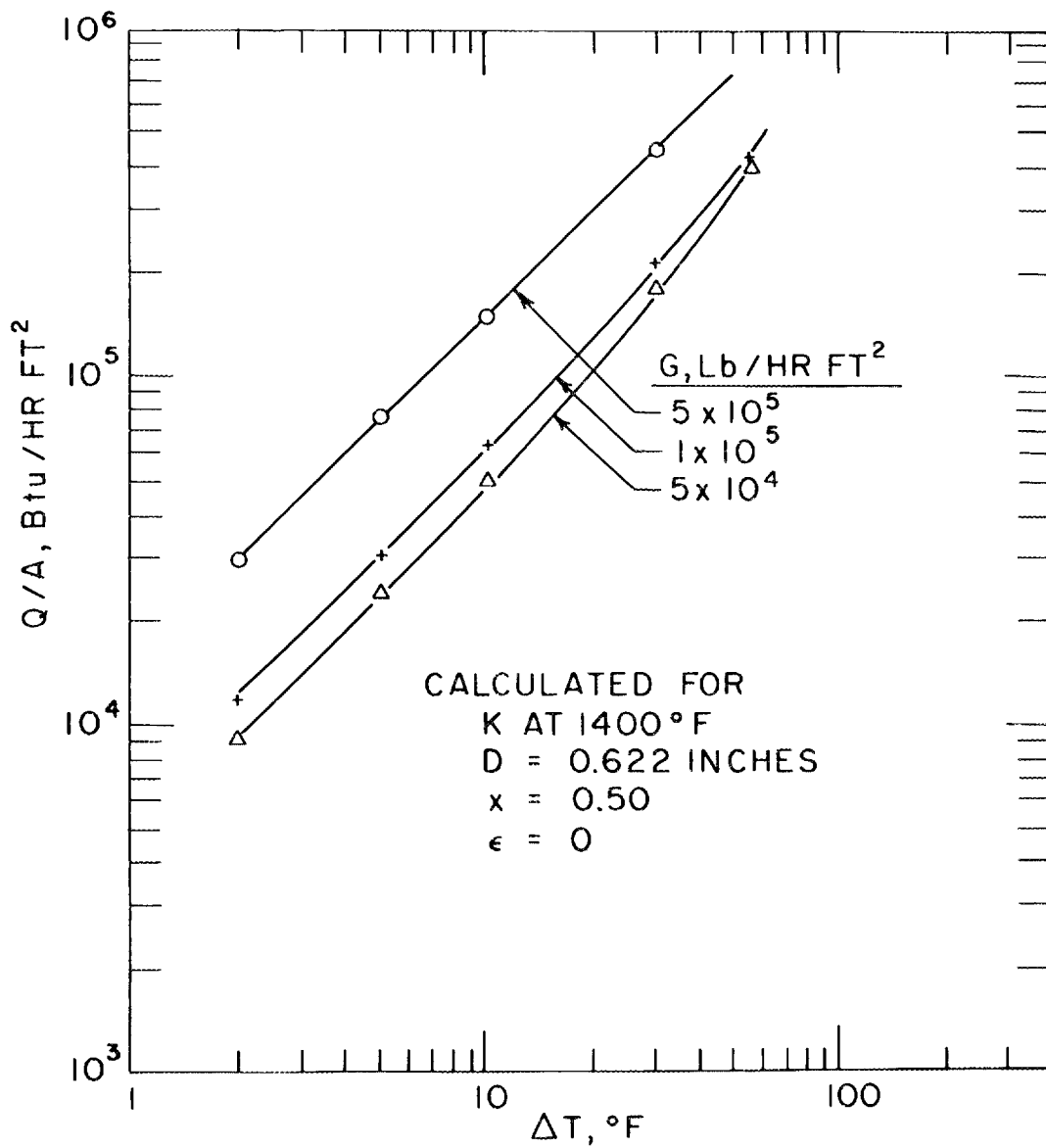
COMPARISON OF PROPOSED CORRELATION WITH ORNL DATA ON CONVECTIVE BOILING OF POTASSIUM

Figure 4



COMPARISON OF PROPOSED CORRELATION WITH GE DATA
ON CONVECTIVE BOILING OF SODIUM

Figure 5



EFFECT OF FLOW RATE ON THE BOILING CURVE
 AS PREDICTED BY THE PROPOSED CORRELATION
 USING $\epsilon = 0$

Figure 6

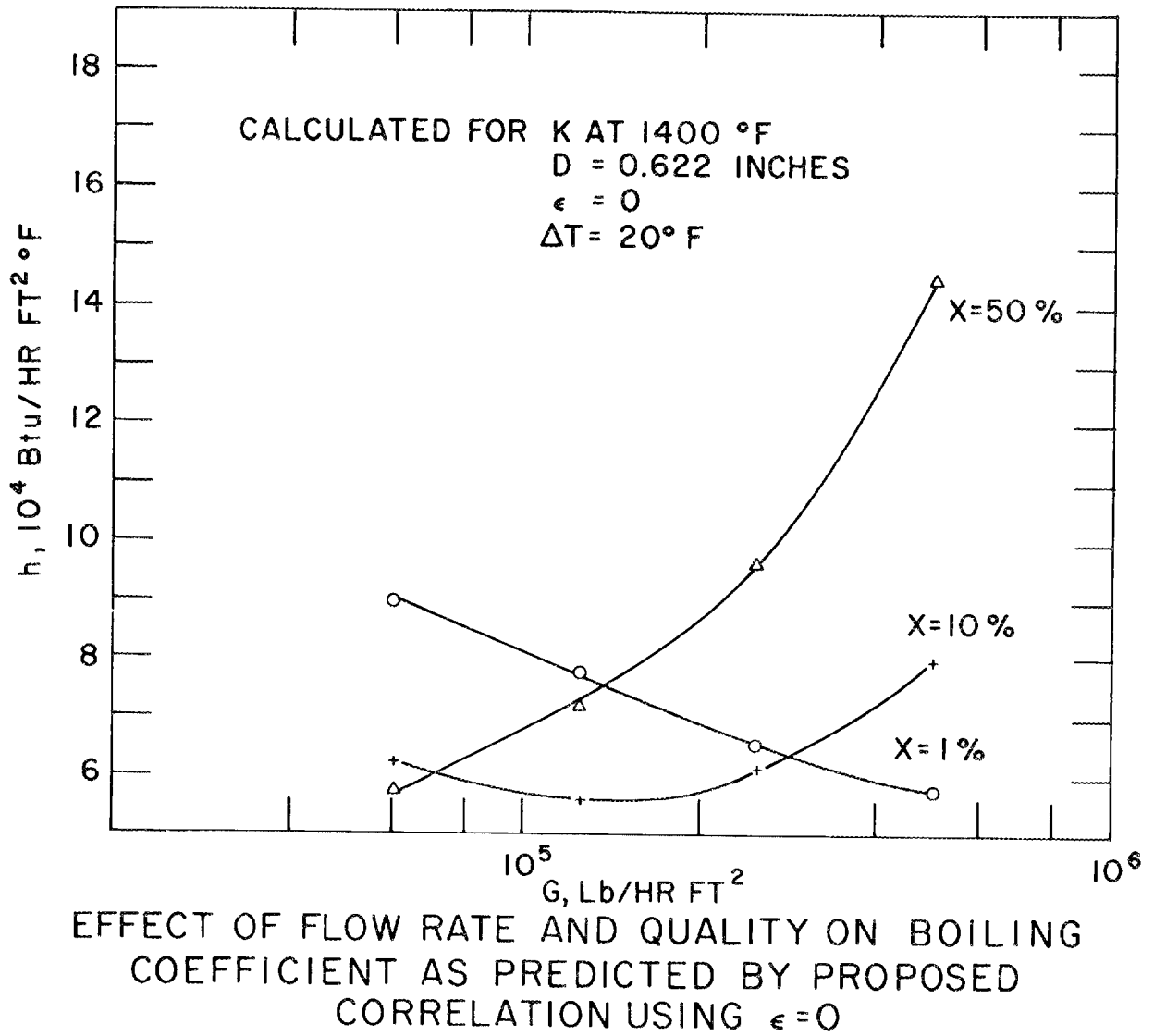


Figure 7

DISCUSSION

MR. BERENSON: When you set $\epsilon =$ to zero in Table 1, all the two-phase parameters reduced to the liquid-metal parameters, with the exception of Alpha; is that right?

MR. CHEN: There is a typographical error in the preprint. The expression for α in Table 1 should be: $\alpha = 0.4(1 + Z^\epsilon)$. Thus, when $\epsilon = 0$, α also reduces to the liquid parameter.

MR. BALZHISER: John, what were the relative magnitudes of the micro- and macroconvective contributions?

MR. CHEN: For most cases, macroconvection contributes more than half of the total heat transfer. However, there are some cases (at high fluxes) when the microconvective contribution predominates.

MR. DAVIS: You would expect, in extending this type of looking at the data which is available into the higher quality regions, that when one starts to talk about dry-wall mechanism, that this would affect only the microconvective contribution. Macroscopic contribution would remain as it.

MR. CHEN: Certainly it is true that the microconvective mechanism would be affected most. However, when you go from, let's say annular flow to fog flow, the momentum transfer may also change, and if so, then you would expect that the macroconvective transfer would also be affected.

MR. STEIN: This kind of analysis always sort of puzzles me, and one of the puzzles is why it works so well, and honestly, John, I can't quite agree with your closing statement, at least for me, that it can explain a lot of the occurrences, and one of the reasons for this, I think, in trying to analyze my own reaction, is that I see a collection of equations and empirical relationships written down which for me, at least, are very difficult to associate with physical laws that we know about, and that we know are verifiable.

For illustration, Newton's laws of motion.

And so, I always worry that somewhere, disguised, within all the juggling is the real reason why it works.

MR. CHEN: In general philosophy I can't but agree with you. I would like to calculate boiling coefficients from the first two laws of thermo; however, as you know, no successful method is yet available for doing so. In view of this, I think that this type of semi-empirical treatment is useful and can give indications of how these various interacting processes do work and what variables are of importance.

MR. DAVIS: At least to some of us, it is comforting that the correlation reduces to the proper limits at zero and 100% quality. Sometimes we see correlations in the literature that are clearly not correct for either the nucleate region or the high-quality region, with no indications whatsoever of which range they are operable, and lead us to believe that only on Friday the 13th should they be employed! So, at least that aspect of this is gratifying.

"HEAT TRANSFER AND PRESSURE DROP CHARACTERISTICS
FOR BOILING RUBIDIUM IN FORCED CONVECTION"

by

C. R. Fisher

AEROJET-GENERAL NUCLEONICS
San Ramon, California

To be presented at the Third Annual Meeting on High
Temperature Liquid-Metal Heat Transfer Technology
Held at Oak Ridge National Laboratory, September
4-6, 1963.

ABSTRACT

This paper describes the results of an experiment performed to determine the heat transfer and pressure drop characteristics of boiling rubidium in forced convection.

The following ranges of operating parameters were included in this investigation:

Mass Flow Rate	117,000-880,000 lb/hr-ft ²
Saturation Temperature	1300-1800°F
Heat Flux	0-325,000 Btu/hr-ft ²
Inlet Subcooling	200-400°F
Outlet Quality	0-0.8
Test Section	0.28 in. ID, smooth, round tube
<u>Pressure Drop</u> Saturation Pressure	0-0.15

This work was performed under contract to the U. S. Atomic Energy Commission on Contract AT(04-3)-368, P. A. No. 1.

1. TEST LOOP

A schematic diagram of the test loop is shown in Figure 1.* Each of the four test section units is a 2 in. OD x 0.28 in. ID x 11.8 in. long bar insulated on the outside by a coating of plasma-sprayed alumina and wrapped with a tantalum resistance heater. The temperature in each bar is determined by means of thermocouples inserted into a pair of holes drilled into the end of each bar.

The two pressure taps shown are dead legs terminating in volumetric pressure transducers manufactured by the Taylor Instrument Company.

The primary flow measuring element is the calorimetric flow meter in which the mass flow of liquid metal is measured by extracting a measured amount of power from the liquid metal and measuring the resulting temperature drop in the liquid metal.

All parts of the test loop exposed to liquid metal at temperatures above 200°F are constructed of columbium-1 zirconium alloy. All other parts are of austenitic stainless steel.

The entire test loop was operated in an environmental chamber containing a high-purity, argon atmosphere.

2. HEAT TRANSFER DATA SUMMARY AND ANALYSIS

Table 1 summarizes the basic parameters which describe the operating conditions at each of the test points. The maximum heat flux column gives the maximum heat flux occurring in the test section regardless of location.

The temperature of the fluid-heating surface interface was not measured directly. The temperature of the heater bar was measured at a point at a larger radius than this interface; therefore, it was necessary to calculate a correction for the geometry effect. This was done by using the well-known equation for radial heat conduction in a long, cylindrical bar. It should be noted that the radial spacing of the innermost thermocouple station from the heat transfer surface was determined by using an analog "field-plotting" technique to assure that the effect of the thermocouple on the angular heat flux distribution would be negligible.

To test the validity of the method of analyzing the heat transfer data, heat transfer coefficients were calculated for sensible heating of the liquid for runs in which no boiling occurred in the first heater block. The points calculated are plotted in Figure 2 in terms of the Nusselt number versus the Peclet number. Also shown in this figure is the Lubarsky-Kaufman^{1**} correlation for forced convection, liquid metal heat transfer. There is a large amount of scatter of the data about the correlating function so that it is difficult to conclude anything from this data.

* Figures appear at the end of the report.

** References are listed at the end of the report.

TABLE 1
SUMMARY OF OPERATING POINTS

<u>Run No.</u>	<u>Weight Flow of Rubidium (lb/hr)</u>	<u>Outlet Quality</u>	<u>Outlet Fluid Temp. (°F)</u>	<u>Max. Heat Flux (Btu/hr-ft²)</u>	<u>Exit Heat Flux (Btu/hr-ft²)</u>
1		Void			
2	58.3	.18	1386	14,900	13,880
3	60.5	.33	1386	27,300	25,200
4	85.6	.22	1414	38,600	4,120
5	99.2	.25	1357	41,100	39,000
6	78.0	.45	1354	53,400	51,800
7	135.7	.14	1375	27,200	27,100
8	161.4	.15	1367	41,000	39,500
9	190.1	.14	1355	47,300	44,100
10	92.5	.15	1487	25,600	22,600
11	74.1	.47	1485	52,800	42,100
12	84.9	.63	1477	76,000	72,800
13	90.1	.78	1466	99,700	97,100
14	212.8	.09	1485	41,600	39,500
15	226.4	.17	1459	67,100	64,100
16	213.9	.31	1420	97,500	97,100
17	318.4	.04	1490	40,500	35,900
18	329.4	.12	1426	57,500	57,500
19	323.0	.18	1408	73,200	70,500
20	103.4	.22	1580	38,750	38,100
21	106.0	.42	1547	65,600	63,400
22	93.6	.69	1537	88,600	84,500
23	96.4	.80	1535	114,700	74,600
24	182.9	.20	1540	60,000	59,400
25	218.9	.24	1507	86,700	82,400
26	203.0	.37	1495	113,100	107,000
27	282.4	.08	1524	60,000	54,000
28	286.5	.17	1495	92,200	87,000
29	299.2	.21	1475	107,100	105,000
30	367.0	.10	1500	84,200	78,500
31	353.0	.27	1475	141,500	140,000
32	106.1	.41	1646	69,600	66,600
33	95.5	.79	1647	105,500	104,200
34	213.6	.22	1647	79,500	76,100
35	222.2	.41	1634	127,800	125,000
36	225.8	.52	1612	164,300	164,000
37	311.3	.10	1646	70,100	65,000
38	296.2	.21	1635	101,200	99,000
39	306.5	.31	1616	141,200	139,200
40	348.6	.04	1653	64,900	55,600
41	366.1	.13	1641	102,600	100,000
42	368.5	.23	1616	145,200	142,300

<u>Run No.</u>	<u>Weight Flow of Rubidium (lb/hr)</u>	<u>Outlet Quality</u>	<u>Outlet Fluid Temp. (°F)</u>	<u>Max. Heat Flux (Btu/hr-ft²)</u>	<u>Exit Heat Flux (Btu/hr-ft²)</u>
43	173.8	.20	1757	67,100	61,100
44	196.8	.51	1749	100,100	94,500
45	199.9	.47	1744	140,000	134,000
46	209.3	.59	1734	174,000	172,000
47	216.5	.64	1731	211,000	134,000
48	298.5	.12	1746	100,000	85,100
49	292.5	.27	1736	138,000	134,000
50	301.3	.41	1719	192,000	191,000
51	357.3	.07	1745	84,500	78,500
52	360.6	.11	1738	95,900	92,800
53	380.5	.22	1722	149,000	143,000
54	389.1	.27	1714	176,000	171,000
55	105.0	.62	1367	241,000	241,000
56	88.1	.74	1352	112,000	112,000
57	93.3	.64	1317	163,000	163,000
58	103.2	.46	1448	206,000	206,000
59	93.4	.73	1444	242,000	242,000
60	213.7	.24	1439	242,000	242,000
61	97.7	.51	1547	191,000	191,000
62	104.7	.63	1638	143,000	143,000
63	206.2	.57	1607	226,000	226,000
64	201.3	.62	1734	228,000	45,100
65	194.6	.33	1537	291,000	291,000
66	289.0	.20	1628	270,000	270,000
67	318.2	.49	1707	288,000	288,000

Most of the heat transfer data taken during the experiment were for the case of nucleate boiling. The nucleate boiling heat transfer coefficients were primarily a function of heat flux; and, to a lesser degree, a function of saturation temperature.

The nucleate boiling data were broken down into nine temperature classes of 50°F per class from 1350 to 1800°F. In each class the following equation was fitted to the data:

$$h = A Q''^n$$

This was done by using a digital computer program after first taking the logarithms of h and Q'' . The results of this analysis are given in Table 2.

TABLE 2

NUCLEATE BOILING HEAT TRANSFER DATA

<u>Temperature Range (°F)</u>	<u>n</u>	<u>log₁₀A</u>	<u>Standard Deviation of log₁₀h</u>	<u>No. of Points</u>
1350-1400	1.126	-2.046	0.1361	57
1400-1450	0.917	-0.918	0.1890	18
1450-1500	1.181	-2.294	0.1061	74
1500-1550	1.325	-3.044	0.1410	58
1550-1600	1.405	-3.414	0.0722	21
1600-1650	1.333	-3.128	0.0861	30
1650-1700	0.958	-1.268	0.1175	15
1700-1750	1.582	-4.427	0.0691	27

The computed values for n and $\log A$ are plotted versus the midpoints of each temperature class in Figures 3 and 4. These quantities show a linear temperature dependence except for two temperature class midpoints: 1425 and 1675°F. No justification has been found for the large deviations at these two points.

Other workers^{2,3} concerned with the nucleate boiling of water have found a dependence of the local heat transfer coefficient upon mass flow rate and quality. Attempts to find such a functional dependence in this data have so far been unsuccessful. The method used in these attempts is to first calculate the constant A for each data point in a temperature class, using the value of n from Figure 3 for that class. This procedure should effectively eliminate the dependence of the constant A upon both heat flux and fluid properties. A should be a function of only mass flow rate and quality. Plots were made of A versus quality for essentially constant mass flow rate and no smooth, functional dependence could be found.

Departure from nucleate boiling (DNB) was obtained at several operating points when the temperature of a heater block rose sharply for a small increase in power to that block. When this phenomenon occurred, the power was reduced until nucleate boiling was obtained just below the heat flux required for DNB to occur. The local conditions for stable nucleate boiling at a heat flux just below DNB are tabulated in Table 3. The number of DNB points obtained is not sufficient to attempt a general correlation of the DNB data.

TABLE 3
DNB POINTS

<u>Mass Flow Rate</u> <u>(lb/hr-ft²)</u>	<u>T_{sat} (°F)</u>	<u>Q''</u> <u>(Btu/hr-ft²)</u>	<u>Quality</u>
187,000	1354	51,800	0.45
216,000	1466	97,100	0.78
231,000	1535	74,600	0.80
540,000	1612	164,000	0.52
518,000	1731	134,000	0.64
252,000	1367	241,000	0.62
211,000	1352	112,000	0.74
223,000	1317	163,000	0.64

3. PRESSURE DROP ANALYSIS

Several correlations for two phase friction factor were tested against the pressure drop data. These included those of Lockhart-Martinelli⁴, Schrock and Grossman⁵ and a modified version of Kutateladze's correlation⁶. The correlations of Lockhart-Martinelli and Schrock and Grossman predict a considerably higher pressure drop across the test section than the measured values for high exit qualities. The modified Kutateladze correlation gives good agreement with the pressure drops measured in this experiment over a wide range of flow rates, qualities and saturation temperatures.

This method may be described as follows:

- 1) Calculate the effective saturation temperature in the test section as follows:

$$T_{\text{effective}} = T_{\text{initial}} - 2/3 (T_{\text{initial}} - T_{\text{exit}})$$

All fluid properties are to be evaluated at $T_{\text{effective}}$.

2) Calculate the mass flow rate:

$$G = \frac{W}{S}$$

3) Calculate the friction factors corresponding to all liquid and all gas flow at this mass flow rate:

$$Re_L = \frac{GD}{\mu_L} ; \quad f_L = \Psi (Re_L)$$

$$Re_G = \frac{GD}{\mu_G} ; \quad f_G = \Psi (Re_G)$$

Where Ψ is the Moody or Blasius friction factor for flow in a smooth, round tube.

4) The frictional pressure gradient is calculated as a function of quality,

$$\left. \frac{dp}{dl} \right|_f = \left[(1 - X) f_L + X f_G \right] \frac{G^2}{2gD} \left[1 + X \left(\frac{\rho_L}{\rho_G} - 1 \right) \right] \frac{1}{\rho_L}$$

The above function is plotted as a function of quality and integrated, numerically, over the length of the test section to give the frictional component of the pressure drop.

5) To evaluate the pressure drop due to momentum change, it is necessary to estimate the volume fraction of vapor, α , at the exit. This is done by using Levy's⁷ momentum exchange model and solving,

$$\frac{(1 - X)^2}{(1 - \alpha)} + \frac{X^2}{\alpha} \left(\frac{\rho_L}{\rho_G} \right) - \frac{1}{2} \frac{(1 - X)^2}{(1 - \alpha)^2} = 0$$

at the exit conditions. The acceleration, or momentum change pressure drop is then calculated from,

$$\Delta P_a = \frac{1}{\rho_L} \left[\frac{(1 - X)^2}{1 - \alpha} + \frac{X^2}{\alpha} \left(\frac{\rho_L}{\rho_G} \right) - 1 \right] \frac{G^2}{g}$$

which may be simplified to,

$$\Delta P_a = \frac{1}{\rho_L} \left[\frac{1}{2} \frac{(1 - X)^2}{(1 - \alpha)^2} - 1 \right] \frac{G^2}{g}$$

when using Levy's equation to calculate α .

The total pressure drop is then the sum of the frictional and acceleration contributions.

The pressure drop data of this experiment have been compared to values calculated by the above procedure for 14 randomly selected runs. Figure 5 is a plot of the measured versus the calculated pressure drops. A statistical analysis was performed to test the agreement between the measured and calculated values. The deviations between the corresponding values were assumed to be representable by a Student's *t* distribution and the analysis showed that the average deviation did not differ from zero at the 95% confidence level. In order to appraise the amount of scatter of the deviations, an *F* test was employed to test the homogeneity of the sample variance and the estimated experimental variance. It was found that the variance of the deviations was larger than can be explained by the limits of error given in the catalog of the manufacturer of the pressure instrumentation. This may be due to the inability of the selected pressure drop correlation to fit the data or it may be due to the experimental error being greater than estimated. Since there was difficulty experienced with a shift in the calibration of the pressure instrumentation, as discussed in a later section, it is likely that the large variance of the deviations is due to experimental error. Another argument for this hypothesis can be made by examining the data points in Figure 5. The least-squares regression line through the data points intersects the horizontal axis at -3.6 psi, suggesting a zero shift in the instrumentation. A comparison of the square of the standard error of estimate of the data, with respect to the regression line, to the estimated experimental variance, using the *F* test as above, shows that these two quantities do not differ at the 95% confidence level. In other words, assuming that a zero shift had taken place in the pressure instrumentation, the amount of scatter in comparing the experimental pressure drop data to the calculated values is no greater than would be expected from the inherent inaccuracies in the pressure instrumentation. For these reasons the above method of calculating two phase pressure drop in forced convection, boiling liquid metal loops is recommended for application in other, similar circumstances.

4. FLOW STABILITY

The design of the test loop included a feature to enhance flow stability. This was in the form of a flow restriction at the entrance to the preheater section. It was a fixed orifice designed to produce a pressure drop equal to that across the test section at the maximum conditions of flow rate, quality and saturation temperature. This design criterion was chosen arbitrarily and was based, in some part, on the experience of other workers with boiling water test loops.

During the experimental runs the flow rate in the loop was considered to be stable when the Speedomax G millivolt recorder connected to the magnetic flow meter output held perfectly steady. When this condition of steady flow was obtained, the pressure recorders drew straight lines on the chart paper. All of the boiling data were taken when these instruments

indicated a steady state situation. However, neither of these instruments are responsive to high frequency variations. It was thought to be desirable to look at the magnetic flow meter output on the screen of an oscilloscope. This was done for Runs 66 and 67. Fluctuations in the flow rate could be detected having an average frequency of about 5 cps and an amplitude variation of about 5% of the total output of the flow meter. Superimposed upon this trace were occasional spikes having a magnitude of 3-4 times the average amplitude of the fluctuations.

5. ERROR ANALYSIS

An error analysis was performed prior to operation of the test loop. The results of this analysis are summarized below in Table 4.

TABLE 4

RESULTS OF ERROR ANALYSIS

<u>Quantity</u>	<u>Estimated Uncertainty (95% Level)</u>
Heat Flux	$\pm 3.9\%$
Wall-to-Fluid Temperature Difference	$\pm 11^{\circ}\text{F}$
Mass Flow Rate	$\pm 3\%$
Pressure	$\pm 2.9\%$
Pressure Difference	$\pm 6.2\%$ (Higher for ΔP less than 4.4 psi)

6. LOOP OPERATION

Prior to filling the loop with liquid metal, the test section heater bars were calibrated for heat loss by applying a measured amount of power to each bar and reading the temperature at a position inside the thermal insulation around each bar for different power settings. The temperature of the argon inside the chamber was maintained at a temperature of $150 \pm 5^{\circ}\text{F}$ during the heat loss calibration. The results of this operation were used later in the analysis of the heat transfer data to correct for heat losses from the test section.

Several unanticipated problems arose in the operation of the test apparatus. At high preheater power levels, the indication from a thermocouple located at the center of the preheater continued to rise rapidly

even when the indicated temperature was 500-600°F above the temperature of the liquid metal in the preheater. This temperature excursion was associated with changes of level in the surge tank and large fluctuations in fluid flow rate as indicated by the magnetic flow meter. These effects can be postulated to be the result of boiling in the preheater due to local hot spots. It was necessary to operate the preheater at a power level low enough to prevent these phenomena from occurring; therefore all runs were performed with 200-400°F inlet subcooling.

The instrumentation used to measure the pressure of the rubidium at the inlet and outlet of the test section indicated liquid metal pressures 10-14 psi higher than that determined by temperature measurements and the vapor pressure curve. This appeared to be the result of a much greater temperature coefficient than listed by the manufacturer in his catalog. The pressure ^{drop} in the boiling rubidium, as determined by the thermocouple readings and the vapor pressure curve, agrees well with that measured by the pressure instrumentation. It is felt that the measurement of pressure drop is more accurate than the measurement of pressure since both pressure pickups operated under similar temperature conditions.

The temperature distribution of the fluid in the test section was measured by means of five thermocouples located at the inlet, outlet and between the four heater bars of the test section. These thermocouples were mounted on the outside of the loop tubing and covered with several inches of thermal insulation. The thermocouples in two positions, i.e., following the first and third heater bars, apparently read low throughout the test runs. In analyzing the data, the fluid temperatures at these two points were estimated.

7. FUTURE WORK IN THIS PROGRAM

The heat transfer test apparatus used in the work reported here for boiling rubidium will soon be filled with cesium and similar data obtained for this metal. The future experimental work will be directed toward obtaining more DNB points for cesium than were obtained for rubidium.

The analysis of the data presented in this report should be regarded as preliminary as more analytical effort will be expended in the generalization of the data in terms of fluid properties and other basic parameters.

The work scope of this program also includes the construction of another heat transfer apparatus containing a swirl, or vortex, generator in the test section. This loop will be operated with both rubidium and cesium to obtain data in a geometry more closely simulating the conditions expected to be found in the boiler of a Rankine cycle, nuclear-electric, space power plant.

NOMENCLATURESYMBOLS

A	=	Constant
D	=	Inside diameter
f	=	Blasius friction factor
g	=	Gravitational constant
G	=	Mass flow rate
h	=	Heat transfer coefficient
n	=	Constant
P	=	Pressure
Q''	=	Heat flux
Re	=	Reynolds number
S	=	Cross-sectional flow area
T	=	Temperature
W	=	Mass flow
X	=	Quality
$\frac{dp}{dl}$	=	Pressure gradient
α	=	Volume fraction of vapor
Δ	=	Difference
μ	=	Viscosity
ρ	=	Density
Ψ	=	Friction factor function

SUBSCRIPTS

a	=	Acceleration
effective	=	Effective or average
Exit	=	Test section exit
f	=	Friction
G	=	Vapor
initial	=	Initiation of boiling
L	=	Liquid
sat	=	Saturation

LIST OF REFERENCES

1. B. Lubarsky and S. J. Kaufman, Review of Experimental Investigations of Liquid-Metal Heat Transfer, NACA TN 3336, 1955.
2. C. E. Dengler, Heat Transfer and Pressure Drop of Water Boiling in a Vertical Tube, PhD Thesis, M.I.T., 1952.
3. J. F. Mumm, ANL-5276, 1954.
4. R. W. Lockhart and R. C. Martinelli, "Proposed Correlation of Data for Isothermal Two-Phase, Two-Component Flow in Pipes," Chem. Engr. Progress, 45, (39-48), 1947.
5. V. E. Schrock and L. M. Grossman, "Local Pressure Gradients in Forced Convection Evaporation," Nuc. Sci. and Engr., 6, (245-250), 1959.
6. S. S. Kutateladze, Heat Transfer in Condensation and Boiling, AEC-tr-3770, p 155, 1959.
7. S. Levy, "Steam Slip - Theoretical Prediction from Momentum Model," J. Heat Transfer, 82, Series C, p 113, 1960.

135-63-2953

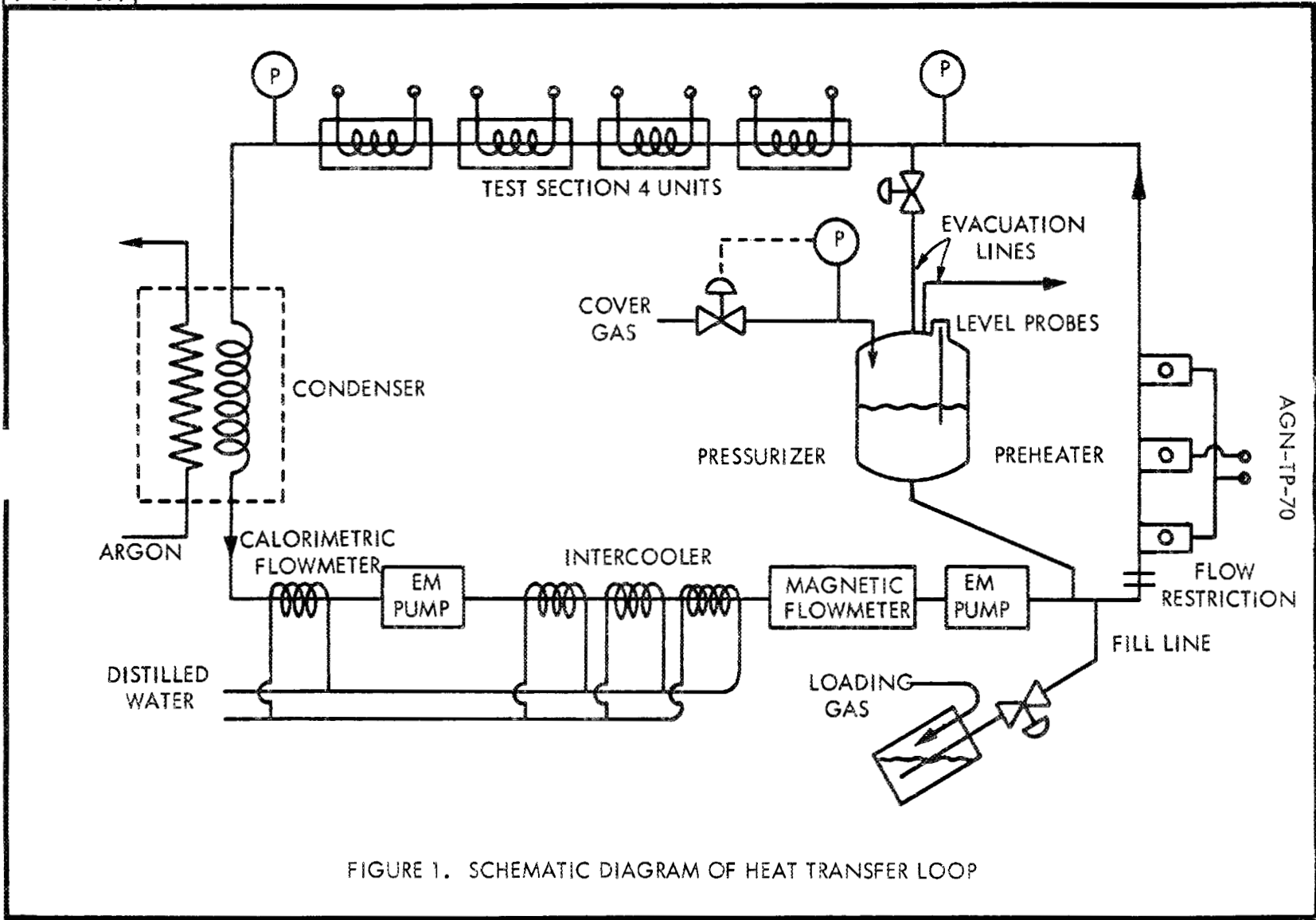
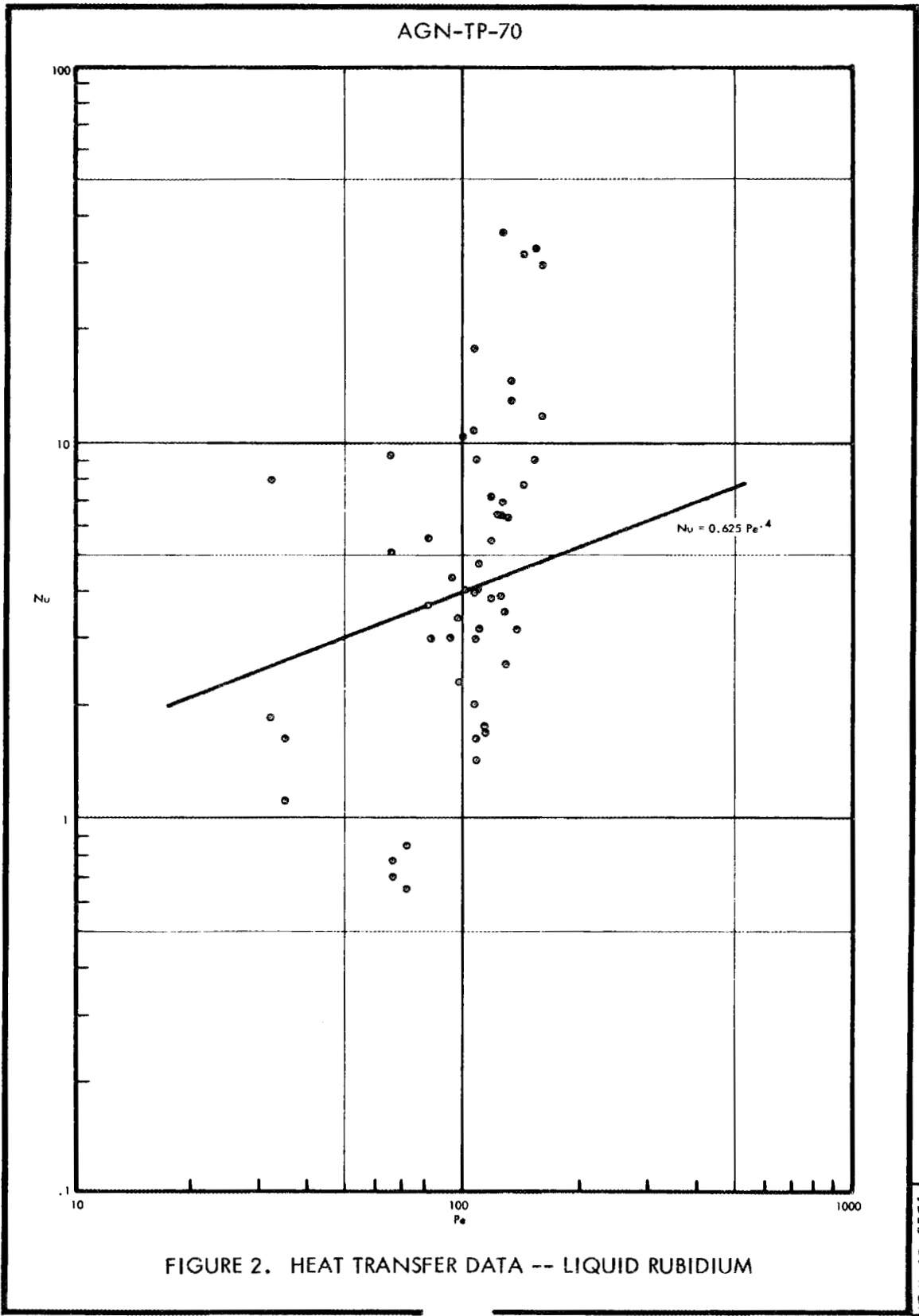


FIGURE 1. SCHEMATIC DIAGRAM OF HEAT TRANSFER LOOP



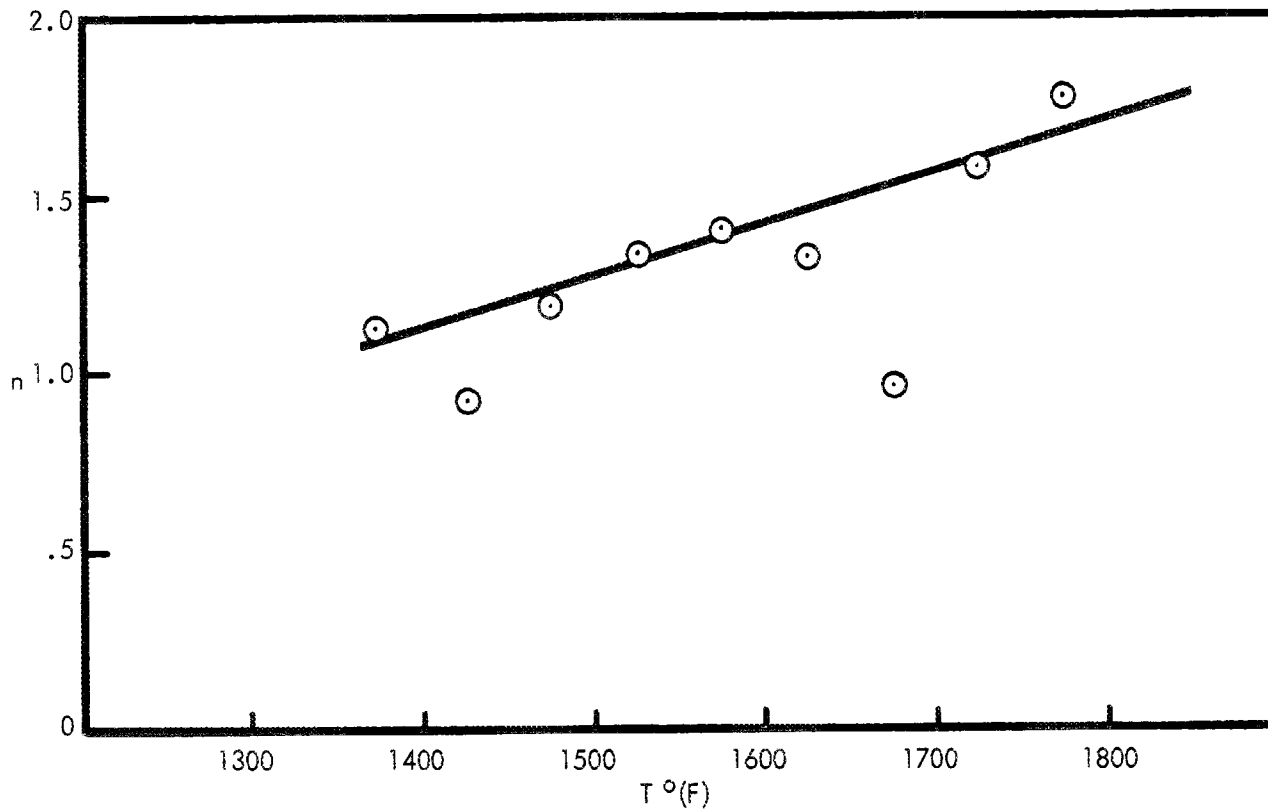


FIGURE 3. n VERSUS TEMPERATURE - NUCLEATE BOILING OF RUBIDIUM

AGN-TP-70

13-5-63-2958

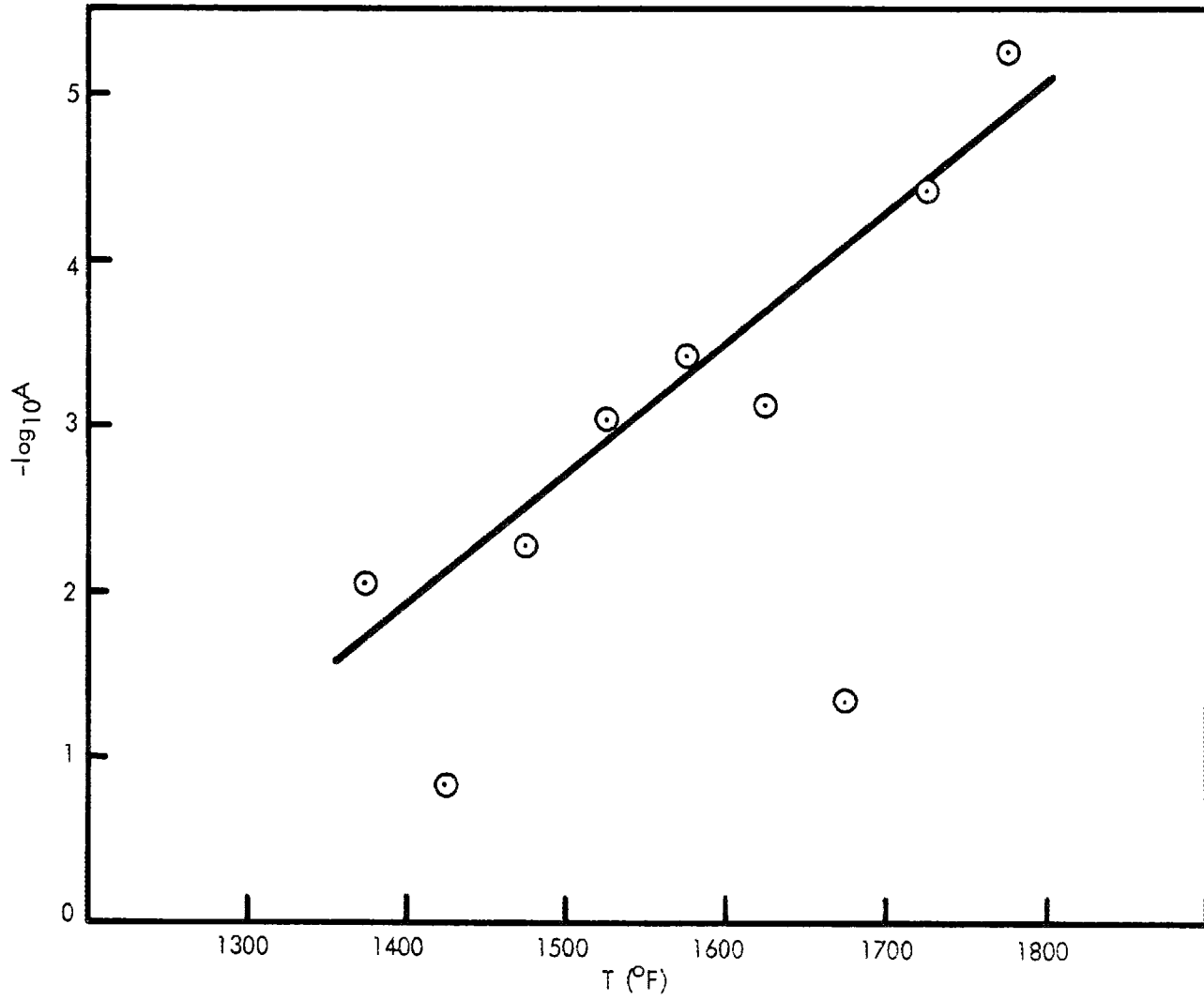
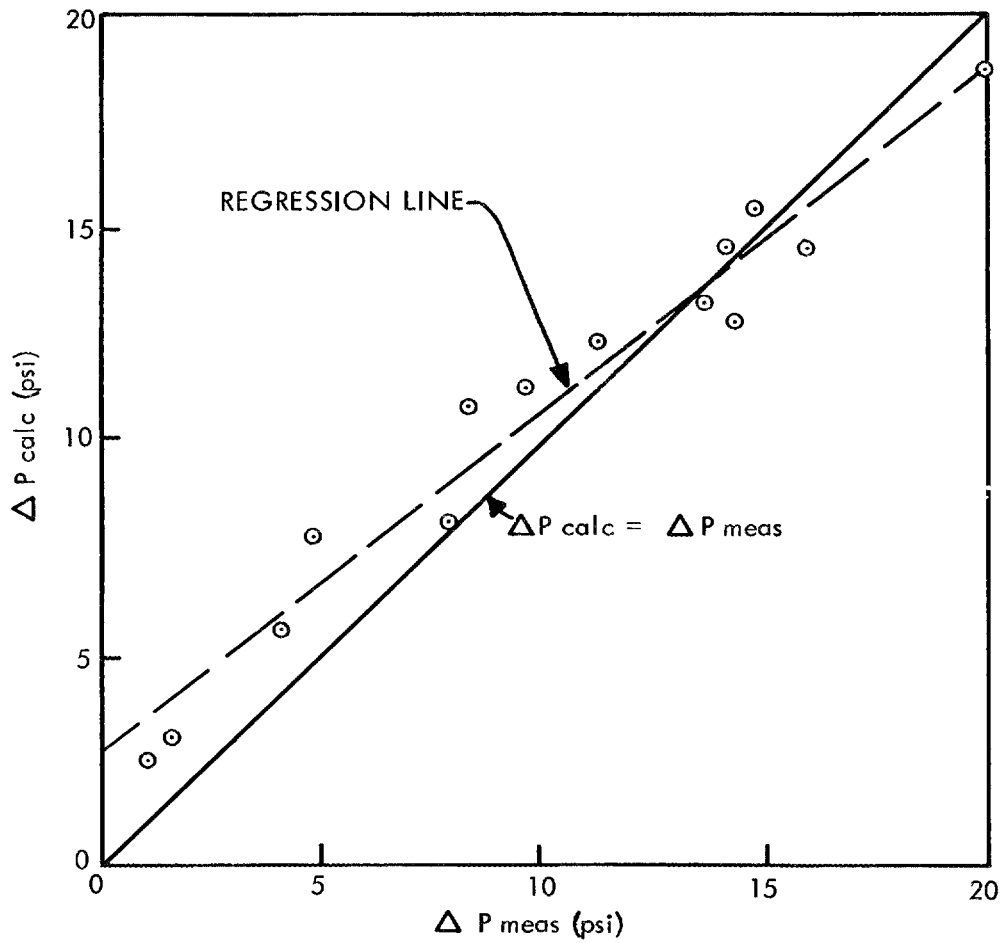


FIGURE 4. $-\log_{10}A$ VERSUS TEMPERATURE - NUCLEATE BOILING OF RUBIDIUM

AGN-TP-70

AGN-TP-70



RANGE OF PARAMETERS

Mass Flow Rate - 177,000 - 931,000 lb/hr-ft²
 Quality - 0 - 0.78
 Saturation Temperature - 1420 - 1734°F

FIGURE 5. MEASURED VERSUS CALCULATED PRESSURE DROP FOR BOILING RUBIDIUM

135-63-2957

DISCUSSION

MR. BROOKS: Would you describe how you made temperature measurements from which to determine the temperature coefficients for us?

MR. FISHER: Yes. Looking at the cross-sectional view, the heater bars look something like this (indicating). The thermocouple is located about 30 mils from the inside diameter of the heater bar, and another thermocouple near the outside. The readings were from the thermocouple closer to the inside surface. A correction was then calculated for the temperature difference between this point and the inside surface, using the heat flux and thermal conductivity of columbium-1 zirconium.

MR. BROOKS: Any reason why you only used two thermocouples at those locations?

MR. FISHER: This was a matter of economics. The thermocouples were platinum-ten-rhodium, tantalum-sheathed thermocouples.

MR. POPPENDIEK: The non-boiling data, conductance data, or Nusselt number data, showed some scatter, but may not be due to experimental error, because I still remember Bill Harrison's data taken here at the Laboratory many years ago. He had, in my opinion, one of the best heat transfer systems you can imagine, the first version of what we have been talking about here, where temperatures were measured very accurately in a copper disc with fluid flowing through. The first data that he obtained were on sodium, with a copper wall, and calculations of error in the system showed it was a wonderful system.

There was a tremendous scatter, the same as yours, or maybe even worse. So this is a big puzzle: Well, why did this happen? Well, it was proved it was not wetting. So upon changing the fluid to mercury, the same test section, same system, a completely different picture developed.

So maybe non-wetting might be a possibility there. Maybe not because of experimental error, but because of this feature. This may not be the answer, but do you have any thoughts about that?

MR. FISHER: We feel, and our magnetic flow meter agreed within approximately 10% of the calorimetric flow meter readings, that the flow meter wet quite well.

MR. POPPENDIEK: Same material?

MR. FISHER: Same material. We think that the test section was also well wet.

MR. POPPENDIEK: What was the order of the magnitude of the conductance again? How high was it?

MR. FISHER: The h value was on the order of 1,000 to 4,000, in that range.

MR. POPPENDIEK: Well then, this may not be it.

MR. FISHER: Also I think I would like to mention, as far as this explosive boiling that we heard about this morning, we did observe that when we were approaching a boiling condition in the test section, starting with all-liquid flow, that in the upstream heater section, where boiling would eventually take place in the steady state, that in the approach to the boiling condition we would note temperature rises of several hundred degrees in this upstream region, which very soon disappeared. These could not be maintained for any length of time. The temperature would rise 100 to 150° and then quickly return to temperatures more consistent with the rest of the apparatus.

Also, I might mention this was rubidium.

We are currently performing cesium heat transfer tests and we observe none of these phenomena for cesium. I don't know what this means.

MR. LEIGHTON: In comparing this type of a test rig to a single, four-foot tube, do you have any indication you believe these results may be optimistic?

MR. FISHER: You mean because of the interruption of the heat?

MR. LEIGHTON: Because of something like 11 diameters in the section?

MR. FISHER: I don't know.

MR. LEIGHTON: Isn't it something to be considered for a rig such as this?

MR. FISHER: Of course we considered this. However, we felt that the advantage of being able to measure the fluid temperature easily between the sections was an advantage; and also the fabrication of this long a test section would have been extremely difficult in one piece. I think you have a good point. I can't really evaluate it.

MR. DWYER: I want to refer again to Fig. 2, the one that Dr. Poppendiek just referred to. I would like to ask first whether it was data taken over a long period of time?

MR. FISHER: Yes, they were.

MR. DWYER: Did you notice any tendency of a fall over the time? That is, over weeks, or months, or days, or what?

MR. FISHER: First, let me say that all this data was taken over an approximately two-week period. We ran the loop 24 hr around the clock. And I don't know whether in that period there had been a tendency to change. This I don't know. I can look into this.

MR. DWYER: This often occurs with metal heat transfer observations, with the single-phase heat transfer. But you have no explanation at all as to the scatter here?

MR. FISHER: No, I don't. The scatter in each temperature range of the nucleate boiling data was considerably less than was shown here. I don't know what this means.

MR. DWYER: I think we will all agree, of course, that the Lubarsky-Kaufman line here is inappropriate, as a matter of fact. I think the line should be simply a horizontal one, the true one, up around the value of 7. In other words, throughout this whole Peclet number range, here, essentially there should be no change in the Nusselt number.

MR. FISHER: This I wonder about, because what you are saying would be for a case of essentially laminar flow which this is not.

MR. DWYER: No, I think it would be true of a more turbulent flow, because you are down in a region where any convection is rather ineffective.

Now because your so-called macro-coefficient is constant, this would tend to make your boiling coefficient also constant.

MR. FISHER: Yes.

MR. DWYER: Wouldn't you say you found it constant, just independent of flow rate?

MR. FISHER: That's right.

MR. DWYER: I think this would tend to back that up. The fact you have a constant single flow coefficient over that whole range. Going back to John Chen's correlations.

MR. FISHER: Yes.

MR. HAYS: Does this data include data from all four sections?

MR. FISHER: Yes. Primarily from the last three sections. The first section was usually used as a pre-heating section.

ALKALI METALS BOILING AND CONDENSING INVESTIGATIONS

Joseph Longo, Jr.,* and Robert D. Brooks*

I. INTRODUCTION

The overall work program of the alkali metal boiling and condensing investigations sponsored by NASA Lewis Research Center at the General Electric Company under contract NAS 3-2528 has three major objectives. The objectives and their current status are:

Phase 1: Design, fabricate and successfully operate three experimental facilities with operating temperatures of 1600, 1850, and 2200^oF respectively. This phase has been completed and reported in Reference 1.

Phase 2: Conduct and correlate boiling and condensing tests on simple geometries. A major portion of this task has been completed. Reference 2.

Phase 3: Conduct and interpret boiling and condensing tests on more advanced geometries. Work has been initiated in this area. Reference 4 will present the status of the work effort in this phase.

The description of the experimental facilities was presented⁽⁵⁾ at the 1962 Liquid Metal Heat Transfer Technology meeting. This paper reviews the operation of these facilities with emphasis on the activities leading up to obtaining stable boiling operation and presents the heat transfer data obtained during Phase 2 testing.

*Space Power and Propulsion Section, General Electric Company, Cincinnati 15, Ohio

II. BOILING STUDIES

A. 300 KW Test Facility

The 300 KW facility is used to obtain potassium boiling and condensing heat transfer data. Both the boiling and condensing test sections are controlled temperature types; i.e., the temperature of the heat rejection fluid (sodium) and the heat sink (air) rather than the heat generation, are controlled. The flow sheet, with the principle components for this facility, is shown in Figure 1. Liquid sodium flows in the primary loop at temperatures up to 1850^oF and flow rates up to 200 gpm. The gas-fired heater has an output of more than 300 KW. Potassium flows in the secondary loop which contains the components for the investigation of potassium two-phase heat transfer characteristics. Temperature measurement for data purposes is accomplished with Pt-Pt 10 Rh thermocouples. Pressure drop measurements are obtained for the boiling tube with diaphragm-type Taylor pressure gages. The design specifications of the potassium loop pump is 30 gpm at 30 psi head and 3.5 gpm at a head of 100 psi. A liquid flow control valve is used to maintain flow and pressure relationships at the boiling test section entrance. An electromagnetic flowmeter measures the liquid potassium flow rate.

The boiling test section is shown in Figure 2. The hot sodium enters at the top left and flows down through the annulus, giving up heat to the center tube, and exits at the bottom. Temperature measuring stations are located to give mixed mean temperatures of the fluid at the inlet and outlet nozzles for both fluids. Outer shell temperatures are measured along the length of the test section. The potassium enters the test section at the bottom right and flows up through the center tube, accepting heat from the

sodium and vaporizing. The potassium vapor is discharged through the outlet at the top left. Pressure measurements of the potassium are made in the inlet plenum and at the exit from the top of the tube. A bellows is provided for accommodating differential thermal expansions between the inner and outer tube. The heat transfer tube (0.929" I.D., 0.093" wall) is of Mo-0.5 Ti alloy, selected for its high thermal conductivity. Thermal shields are provided to control the active length of the test section and to protect the bimetal joints of the center tube. The active heat transfer length is 67.5 inches.

Surveying the independent loop parameters affords the best description of the 300 KW operation. The primary loop pressure is adjusted by controlling the argon pressure in the sodium tank while the pressure in the secondary loop is controlled by the temperature of the sodium and the boiler heat transfer performance. The temperature of the sodium is controlled by the heat input to the furnace which is controlled by regulating the fuel gas flow. The heat removal rate of the potassium condenser is controlled by regulating the coolant air flow to the condenser. The potassium flow rate is established by adjusting the pump voltage and flow control valve. The pressure drop from the boiler to the condenser is regulated by adjusting the vapor throttle valve at the inlet to the vertical condenser. The liquid metal charge to the secondary system is adjusted so that the head tank is maintained approximately one-half full. The free surface area in the head tank then sets the base pressure in the secondary system since the potassium storage tank is isolated from the system in the boiling runs.

The maximum operating limits for the facility can be predicted and are

- a) The maximum acceptable temperature set by facility material requirements.
- b) Maximum sodium flow rate.
- c) Boiler and condenser heat transfer performance.
- d) Furnace output.

The operating region for maximum sodium flow rate can be constructed as shown in Figure 3. The cross-hatched region defines where the facility may be able to operate, subject to any limitations in the performance of the boiler. The y-axis is heat transferred to vapor and not total heat transferred. Curve A-B is the limitation imposed by sonic velocity of the potassium vapor, limiting operation to the right of this curve. Curve B-C is imposed by the furnace design point characteristic; operation must be below this curve. Curve C-D is the limitation imposed on heat transfer in the boiler due to sodium flow rate and boiler resistance; operation must be left of this curve. Curve E-F is the limitation imposed by the projected condenser capacity; operation must be to the right of this line. It should also be noted that curves A-B and C-D are a function of the test boiler, whereas curves B-C and E-F are independent of the boiler being tested.

It has been found that the boiling thermal resistance is indeed small with respect to the overall thermal resistance when the boiler is in nucleate boiling along its entire length at potassium temperatures above 1600°F. A typical run presented in Reference 3 shows that at a heat flux of 215,000 BTU/hr ft², the temperature drop between the inside wall and potassium was 64°F out of an overall temperature differential between the sodium and potassium of 226°F, thus the resistance of the potassium side was ~28% of the total resistance.

At this time, the data have not been reduced sufficiently to determine how close to the Mach 1.0 limitation it will be possible to operate. Depending on the boiler performance, it may be possible to operate very close to the curve on the right.

Overall heat transfer performance data are obtained from the measurements described for the boiling test section of Figure 2. Using the mixed mean fluid temperature at the inlet and outlet, overall heat transfer coefficients can be obtained. For test runs in which the entire boiler is in the nucleate boiling region, average values for nucleate boiling heat transfer coefficients can be obtained. From the sodium temperature distribution along the length, variation in heat transfer can be established. The problems of relating the shell wall thermocouples to the bulk sodium temperature restrict the accuracy with which local heat transfer coefficients can be obtained. However, local values of the heat transfer coefficient at the boiler exit can be obtained with more confidence since the sodium temperature as well as the saturation temperature of the potassium can be measured at this point. The heat input at the exit must be inferred from the outside thermocouples. Local value of other points along the length of the boiler must consider pressure drop in the boiling fluid and its effect on saturation temperature in addition to the problem of relating the wall thermocouples to the bulk sodium temperature. In the film boiling region where a large change of heat transfer coefficient occurs, a good estimate of the film boiling heat flux can be obtained.

One method of correlation, which illustrates the average boiling heat flux versus $(T_{\text{wall}} - T_{\text{saturation}})$ is shown in Figure 4. In this figure the potassium boiling heat flux is established from the sodium bulk temperature drop and flow rate. The thermal resistance of the sodium film and the

resistance of the molybdenum tube are subtracted from the overall resistance and calculated assuming that the potassium temperature is constant with length at the measured outlet temperature. The resistance of the sodium is obtained from a Wilson plot while the resistance of the tube wall is calculated. The potassium resistance obtained in this manner is then used to calculate the temperature difference between the inside boiler tube wall and the potassium. The exit quality is obtained thermodynamically from heat balances after heat loss correction.

In Figure 4 a representative portion of the data are shown for the pressure range 0-30 psia and 30-80 psia at several mass flow rates and several exit quality ranges. At exit qualities up to 65% the heat transfer coefficient was approximately constant over the entire boiling length. At high qualities film boiling lowered the average potassium heat transfer coefficient and therefore average heat flux considerably. The effect of mass flow rate is similar to that observed in other fluids in the nucleate boiling region. Higher pressure appears to give higher heat fluxes as seen in the 35-45% quality data. The ORNL results reported by Hoffman for nucleate boiling in an electrically heated stainless steel tube is shown also.

The pressure drop across the boiling test section was in general so small that measurements accurate enough to correlate it were not possible by means of the diaphragm pressure gages. Two-phase pressure drop data were obtained, however, by measuring the change in saturation temperature across an adiabatic pipe section. These measurements were made for a 1.28-inch diameter tube. By using the vapor pressure relationship, the change in saturation temperature was converted to pressure drop. These results are shown graphically in Figure 5 representing the frictional losses over the range of quality from 10-90% and pressure from 20-70 psia. In this figure,

$\frac{\Delta P_{TP}}{\rho v}$ is plotted as a function of the vapor velocity. The points agree reasonably well in spite of the wide ranges of the variables. The K factor of the line drawn through the data is found to be 2.0. Liquid pressure drop data on this test section gave a K factor of 0.7. Assuming the single phase K factor of the liquid to be equal to that of all vapor, the ratio of two phase pressure drop to single phase vapor pressure drop is equal to 3, i.e.,

$$\frac{\Delta P_{TPF}}{\Delta P_v} = \frac{2.0}{0.7} = 3.0$$

B. 100 KW Test Facility

The 100 KW facility, used to obtain boiling heat transfer data with sodium and potassium, differs from the 300 KW facility in four major areas:

- (1) The boiling test section has a controlled (electric) rate of heat input, rather than a controlled temperature.
- (2) It is designed to exceed the 1850°F limitation of the 300 KW facility, and has operated successfully up to 2200°F.
- (3) Heat is rejected from the system by radiation to the water-cooled walls of the enclosure, rather than to air by convection.
- (4) Because it is smaller in size and power rating, this loop is operated more easily and is, therefore, particularly attractive for development work.

The loop is constructed of columbium alloy tubing to achieve the high temperatures desired, and thus must be operated under a high vacuum of 10^{-8} torr.

Figure 6 is a view of the loop with the vacuum cover in place. A diagram of the components employed is also shown. Figure 7 is a typical plot of the outer wall temperature of the boiling tube. The effect of heat flux is shown

by the several curves. The low heat flux line has a smooth transition from liquid convection to nucleate boiling. At higher heat fluxes a hump in the curves indicates local conditions of superheat or film boiling in the transition region.

Figure 8 shows typical boiling heat transfer coefficients at the outlet as a function of outlet quality. Stable heat transfer results in the boiling of sodium were found to be limited to operation with an inlet orifice having a diameter ratio of approximately 1/7 of the pipe diameter, across which the liquid was flashed into a two-phase condition. A simple twisted ribbon having a pitch ratio of two diameters was also inserted and tested. With this insert it was found possible to obtain stable operation without flashing across an orifice, even with significant values of inlet subcooling. Differences in flow were observed in the two channels formed by the ribbon, indicating a need for pressure equalization at several points along the length of the ribbon. A subsequent change to potassium in the loop has produced data without an insert which is quite stable at exit qualities up to 60% with values of inlet subcooling as high as 800^oF.

III. CONDENSING STUDIES

A. 50 KW Facility

The 50 KW facility has been modified to obtain condensing data for potassium vapor, using liquid sodium for the cooling of the test section. Figure 9 is a detailed drawing of the facility, showing the potassium and sodium loops. Since the facility is constructed of Type 316 stainless steel, operation is limited to 1600^oF. The test section is a vertical annular configuration with potassium condensing downwards inside a thick-walled nickel tube and sodium flowing upwards in the annulus around it.

In the potassium loop, vapor is generated by five 7.5 KW immersion heaters. The potassium vapor flows vertically up through an 8-foot length of 2-inch pipe to which are strapped clamshell heaters rated at 12 KW. Depending on the boiler exit conditions, the quality can be increased or superheat can be achieved in this vertical pipe. The vapor then passes through a throttle valve for control of test section pressure, and a 10-foot length of horizontal 1-inch pipe. The vapor then passes down through the sodium-cooled test section, where either total or partial condensation can be obtained. Condensation is completed or subcooling obtained in the air-cooled subcooler located directly beneath the test section. The liquid then passes through a two-stage electromagnetic pump and an electromagnetic flowmeter back into the boiler. All lines are wrapped with Inconel-sheathed Chromel "A" heating wire, for preheating.

The all-liquid sodium loop is used for cooling the test condenser. The sodium flow passes upwards through the test condenser annulus, picking up heat, and then into an annular air cooler, where heat is rejected to the air. The sodium then passes through the electromagnetic pump, an 8-foot length of 2-inch pipe, an 8-foot length of 1-inch pipe and back into the test section. During loop down-time the dump tank is used as a sodium reservoir.

Figure 10 is a detailed drawing of the 50 KW condensing test section. The outer shell consists of a 42-inch length of 2-1/2-inch schedule 40 pipe with an I.D. of 2.460 inches \pm .005 inch. The nickel inner tube has an I.D. of 0.625-inch and an O.D. of 1.718 inches. Thermocouple wells are located in the nickel tube at its midpoint at radial distances which are approximately equal logarithmic intervals. In each hole are inserted two 0.0395-inch O.D. sheathed Chromel-alumel thermocouples spaced approximately 1/16-inch from each other. This method allows two thermocouple readings to

be taken at approximately the same axial and radial location. The test section is encased in a heavy structural shell to minimize any type of bowing and to maintain a vertical orientation. The structural casing allows the test section to expand vertically but not to deviate from its vertical orientation more than $\pm 1/16$ inch in the 28-inch length between the stiffeners welded to its outer shell.

During the time that this facility has been in operation, "shake-down" liquid-phase and condensing heat transfer data have been obtained for potassium, using the radial temperature profile in the thick-walled nickel tube to determine the local heat flux and inner wall temperature. Due to the small temperature difference between the inner wall of the nickel tube and the average temperature of the potassium stream, thermocouple standardizations are made before and after each series of runs. Also, each test section thermocouple is calibrated, as a function of temperature, by reference to one of the thermocouples.

The technique of intercalibration of the thermocouples is presented in References 2 and 4 and requires runs with only the sodium flowing at two flow levels per temperature level and then only potassium flowing at two flow levels per temperature level. By runs at the same average temperature level and two or more flow rates, a standardization factor independent of heat loss can be obtained for each thermocouple relative to the thermocouple selected as the reference. With these corrections, the sodium heat loss as a function of temperature level is determined, allowing an accurate test section heat balance to be made. The heat given up by the potassium together with the calculated resistance of the nickel wall is then used to determine the temperature gradient across the tube wall which can then be

compared to that gradient measured by the wall thermocouples. Figure 11 is a semi-log plot of the wall thermocouples in an actual heat transfer run after correction of the thermocouples, showing a linear extrapolation that yields the average values of the inner wall temperature and of the heat flux. The deviations from the straight line in Figure 11 may be due to non-uniform circumferential sodium temperature distribution, to minor conductance irregularities in the nickel wall caused by the slots, and to discrepancies in the exact radius of thermal contact of the thermocouple sheaths. However, the average position and slope of the line is felt to be fairly well determined. Currently the thermocouple leads are being replaced and final results are expected to be substantially more consistent. The run of Figure 11 yielded a condensing heat transfer coefficient of about $9000 \text{ BTU/hr ft}^2 \text{ }^\circ\text{F}$ at a film Reynold's number of 900. Boiler operation to date has been limited to 1250°F for determination of overall system performance. Testing will be eventually carried out up to 1550°F with film Reynold's numbers from 900 to 10,000 and heat fluxes from 30,000 to 300,000 BTU/hr ft^2 .

The preliminary heat transfer coefficients obtained for potassium condensing inside the vertical $5/8$ " diameter tube are not in agreement with the theoretical results of Nusselt⁽⁸⁾ or Seban⁽⁹⁾ as shown in Figure 12. That the results are low compared to theory confirms the trends of the heat transfer coefficient results for alkali metal condensation that have been presented in the literature^(6,7), for varying geometries. Although fair agreement is obtained with the predictions of Dukler⁽¹⁰⁾, Dukler's analysis has been shown by Lee⁽¹¹⁾ to be in error at low Prandtl numbers. The horizontal tube data obtained in the 300 KW test is also shown and appears to give lower values of the condensing ratio, than those predicted by the Nusselt and Seban analyses.

REFERENCES

1. Alkali Metals Boiling and Condensing Investigations, Volume I, Experimental Program. Final Report, Contract NAS 5-681, Jan. 1, 1961 - June 30, 1962. SPPS, MSD, General Electric Company, Cincinnati 15, Ohio.
2. Alkali Metals Boiling and Condensing Investigations, Quarterly Reports 2&3, Contract NAS 3-2528, SPPS, MSD, General Electric Company, March 1963.
3. Alkali Metals Boiling and Condensing Investigations, Quarterly Report 4, Contract NAS 3-2528, SPPS, MSD, General Electric Company, April-June, 1963.
4. Alkali Metals Boiling and Condensing Investigations, Quarterly Report 6, Contract NAS 3-2528, SPPS, MSD, General Electric Company, December 1963.
5. Proceedings of the 1962 High-Temperature Liquid-Metal Heat Transfer Technology Meeting, BNL 756 (C-35) p. 131. Brookhaven National Laboratory (May 1962).
6. Roth, J.A., "Condensation of Sodium and Rubidium at Low Heat Fluxes", Report No. ASD-TDR-62-738 (October 1962).
7. Bonilla, C.F. and Engelbrecht, J.C. in Thompson-Ramo-Wooldridge Final Report for Flight Accessories Laboratory, Aeronautical Systems Division, USAF, under Contract AF 33(616)-7368 (July 31, 1961); also Engelbrecht, J.C., M.S. Design in Chemical Engineering, Columbia University (1961).
8. Nusselt, W., Z. Ver. deut Ing., 60, 541 (1916).
9. Seban, R.A., "Remarks on Film Condensation with Turbulent Flow", Trans. ASME, 76, 1954.
10. Dukler, A.E., "Fluid Mechanics and Heat Transfer in Vertical Falling-Film Systems", C.E.P. Symposium Series, No. 30, 56, 1960.
11. Lee, Jon, "Turbulent Film Condensation; Nonmetallic Materials Division, AF Materials Laboratory, Wright-Patterson Air Force Base (1963).

300 KW TEST

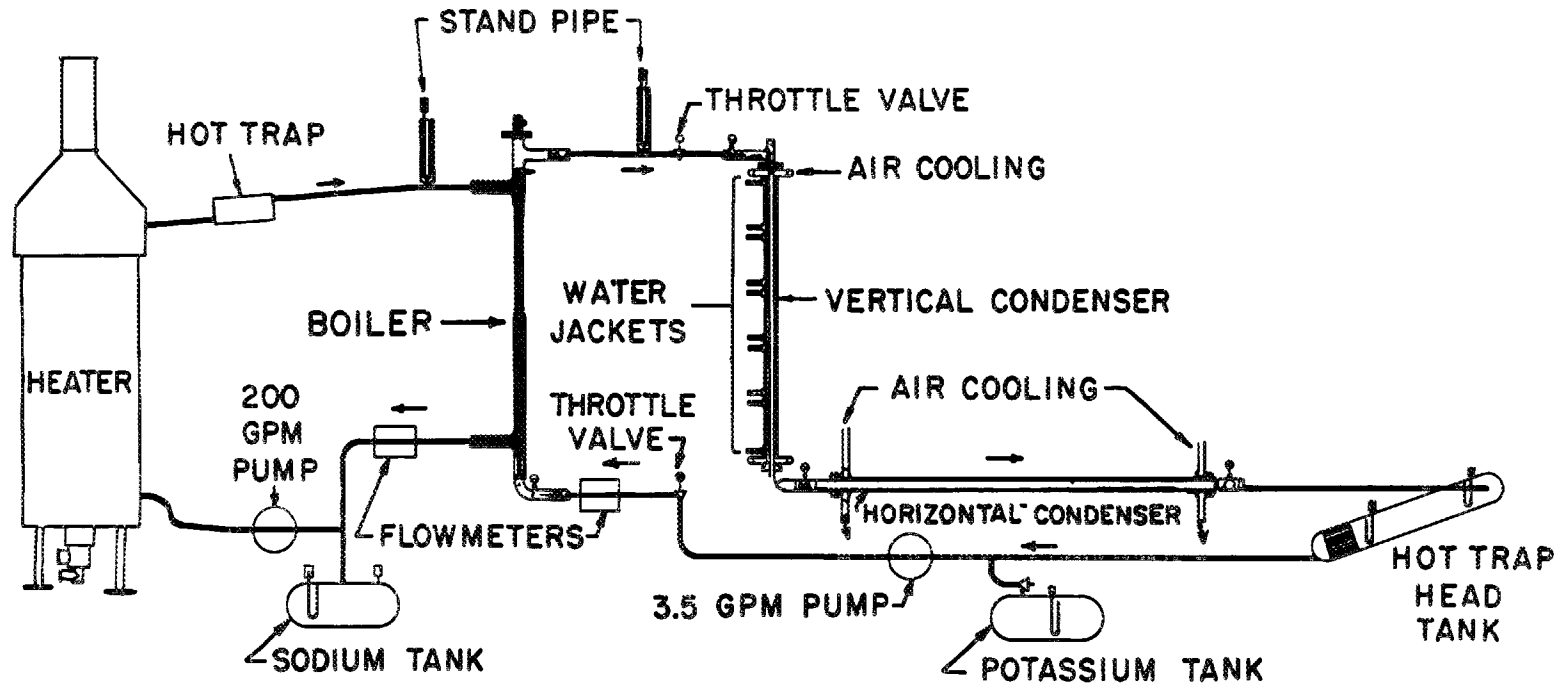
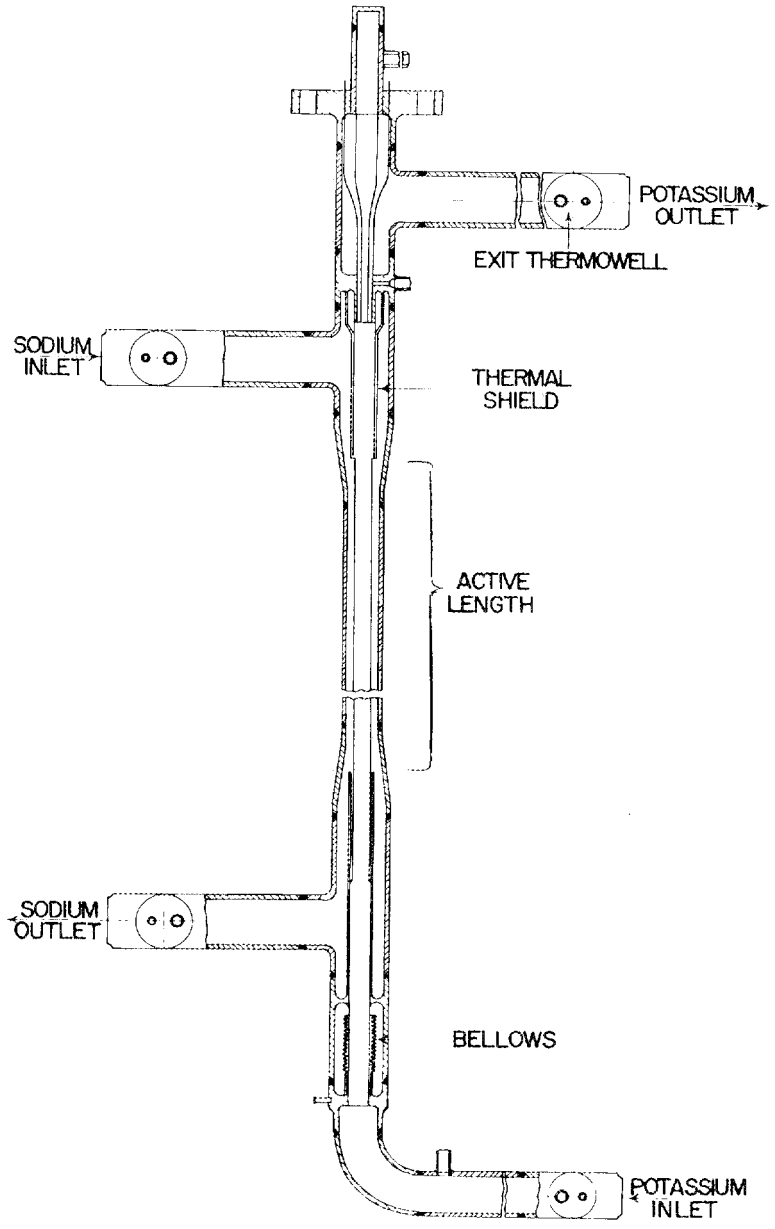


Figure 1. Schematic of 300 KW Boiling and Condensing Facility



BOILER TEST SECTION

Figure 2. 300 KW Boiler Test Section

OPERATING CAPABILITY OF 300 KW FACILITY
WITH PRESENTLY INSTALLED BOILER

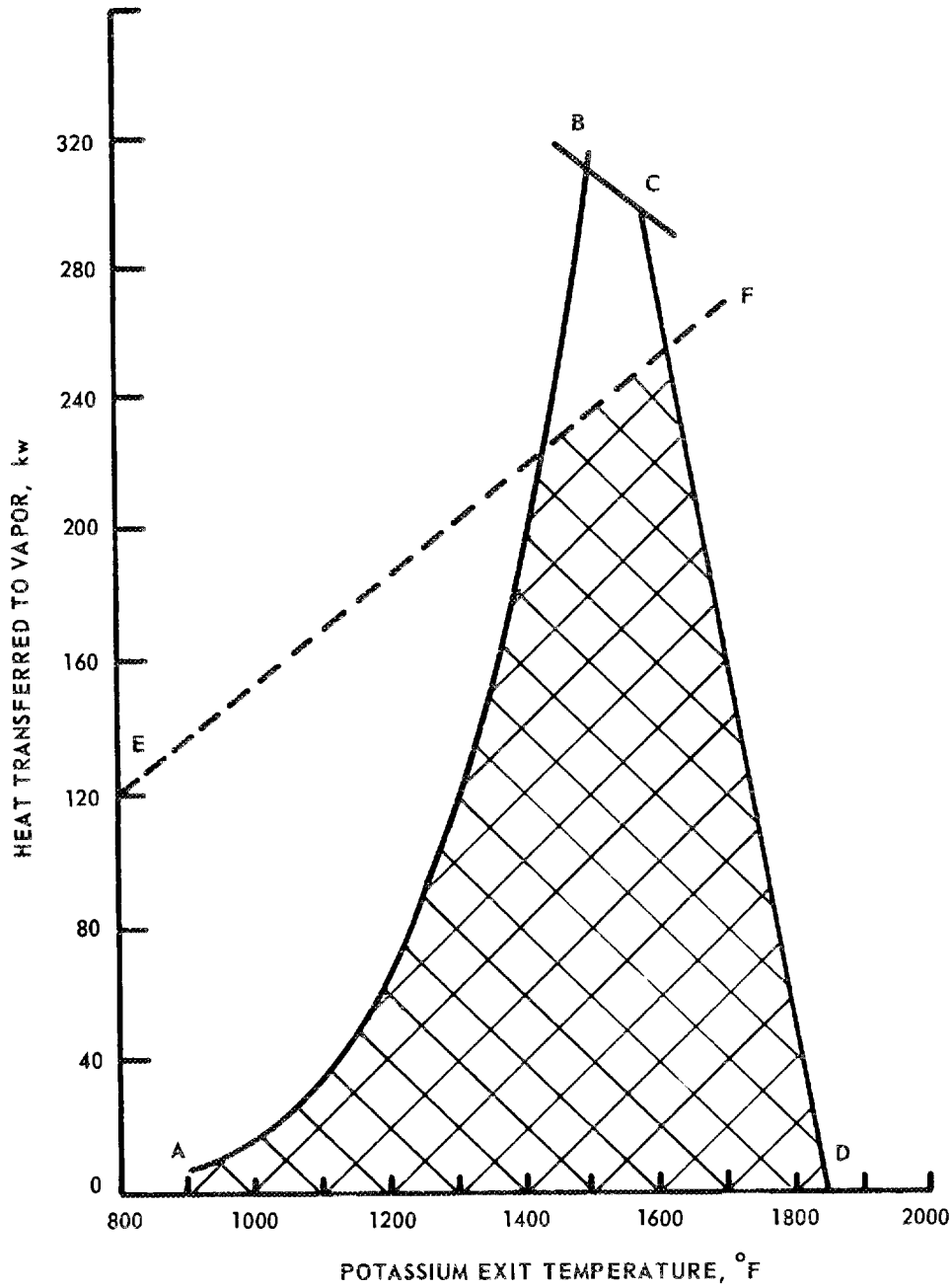


Figure 3. Operating Capability of 300 KW Facility with Presently Installed Boiler

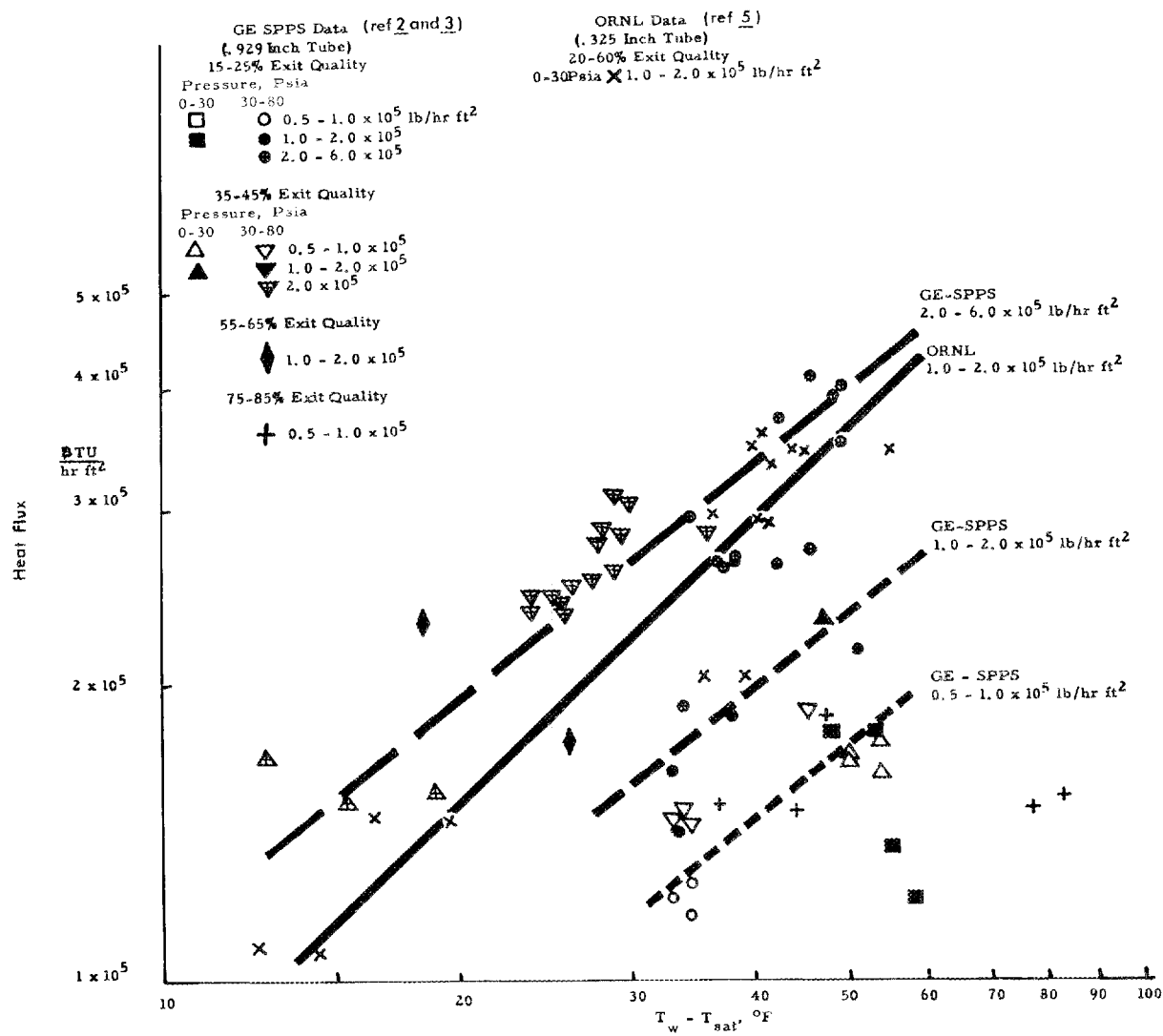


Figure 4. Boiling Potassium Heat Transfer Data

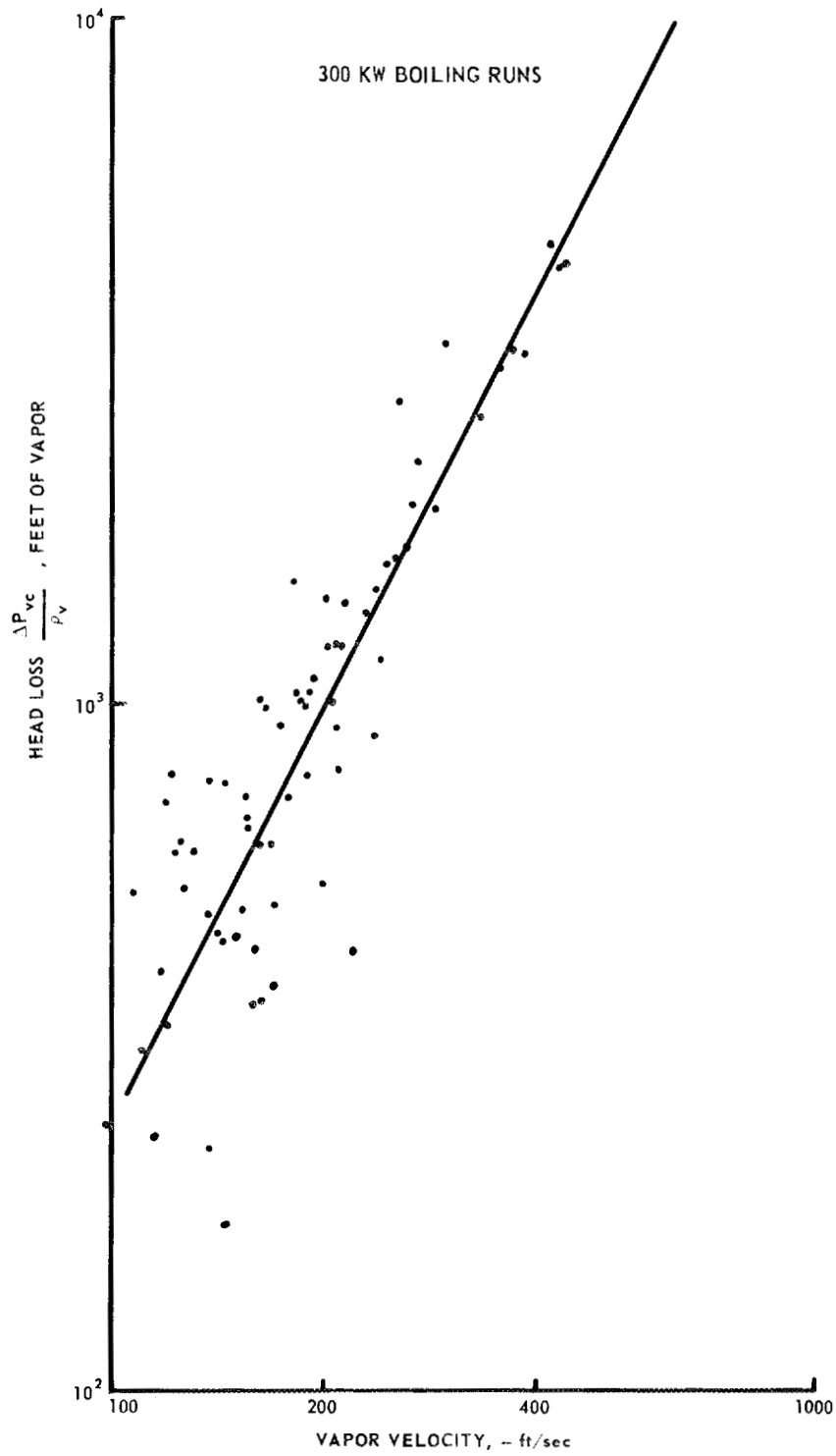


Figure 5. Two Phase Adiabatic Pressure Drop Data - 300 KW System

High Temperature Refractory Alloy Boiling Test Facility

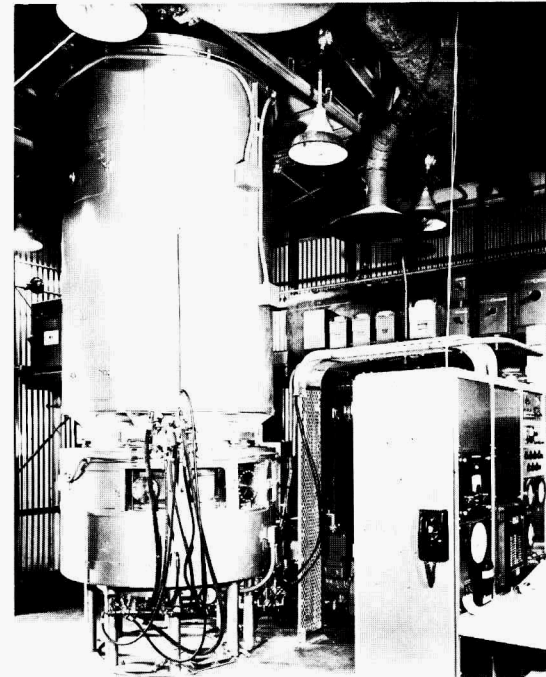
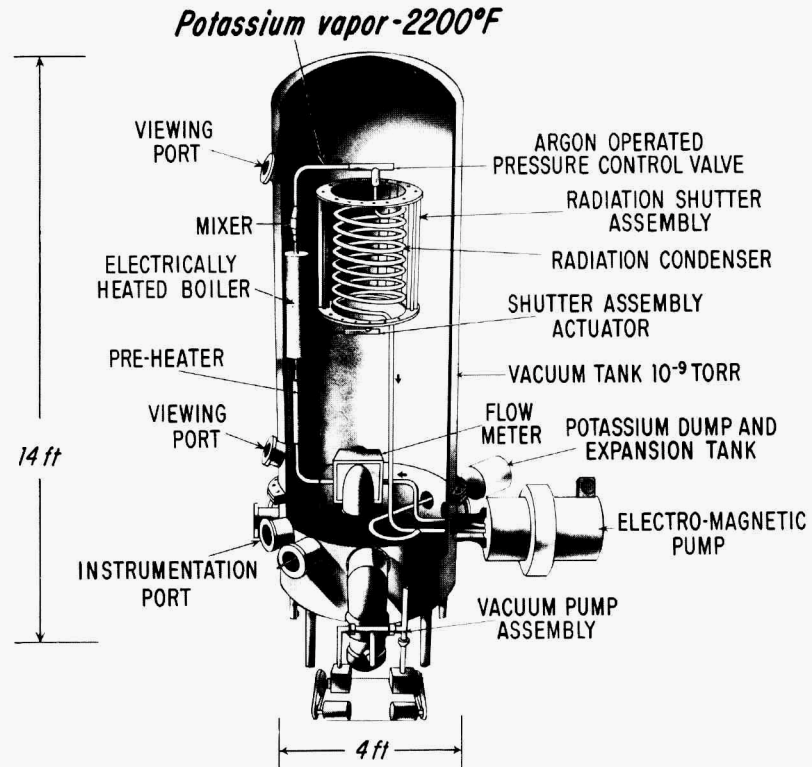


Figure 6. 100 KW Boiling Test Facility

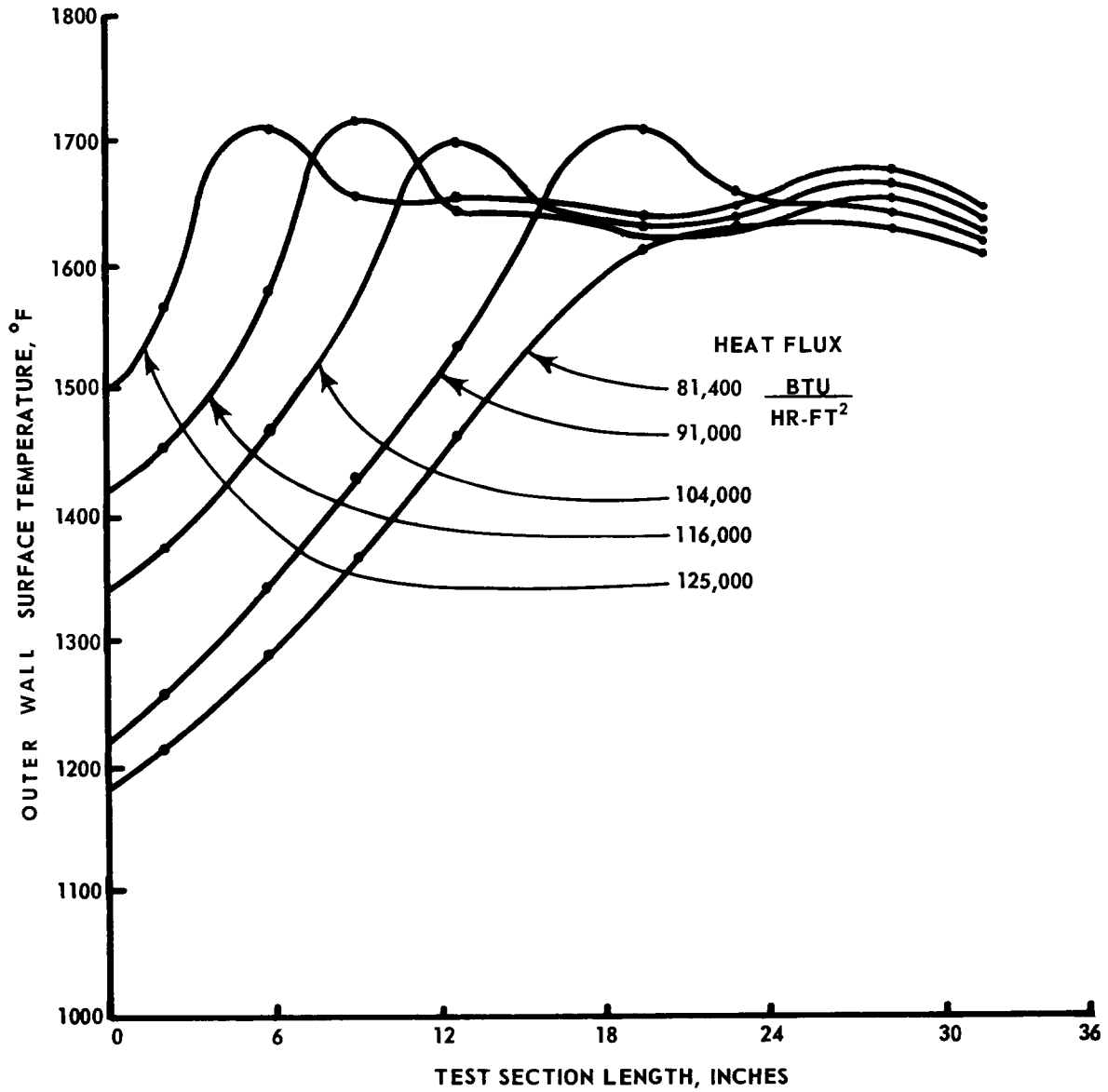
100 KW TEST
POTASSIUM BOILING

Figure 7. Wall Temperature Distribution for Boiling Potassium vs Heat Flux - 100 KW System

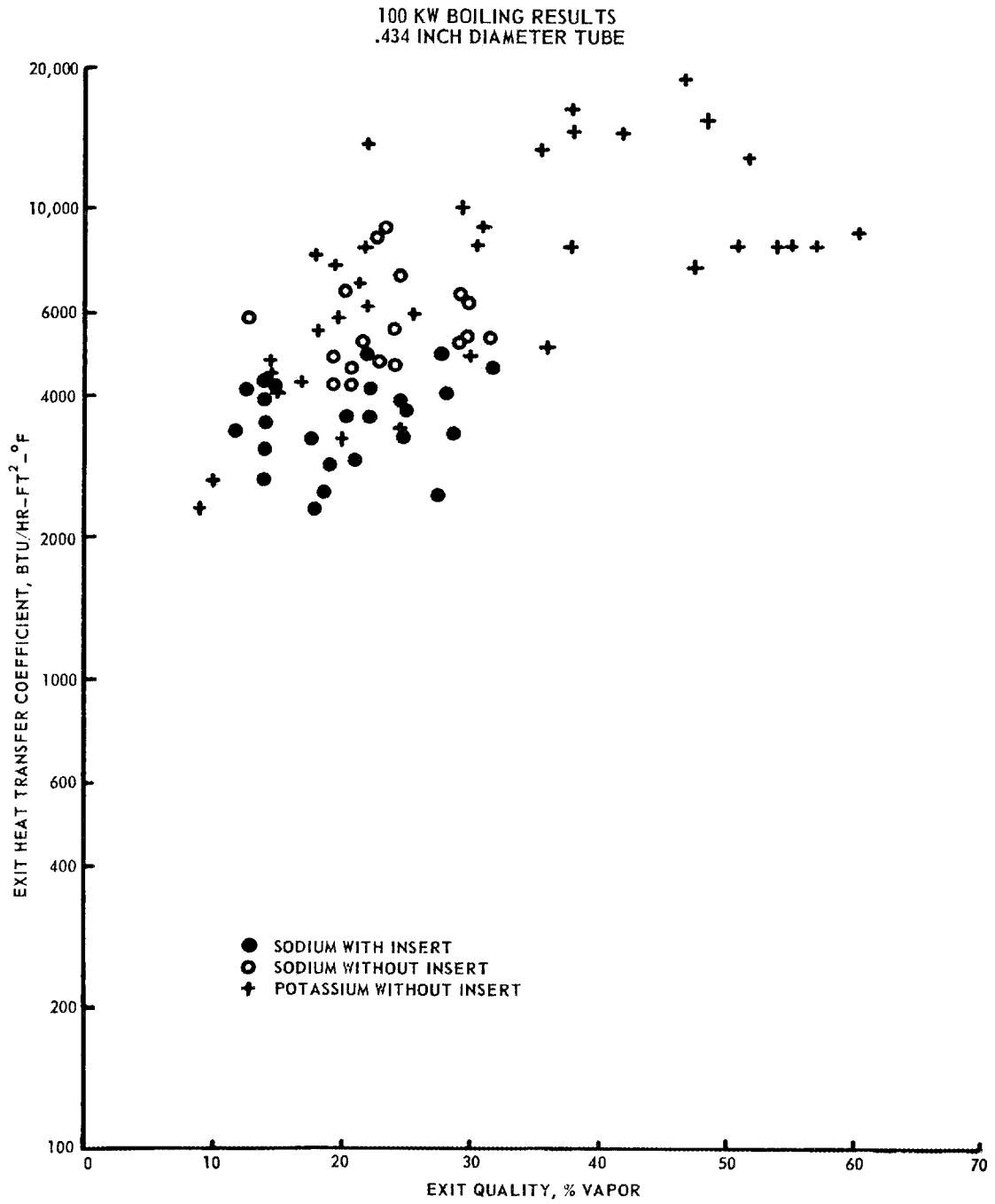


Figure 8. Sodium Nucleate Boiling Heat Transfer Coefficients
- 0.434 in Diameter Tube - 100 KW System

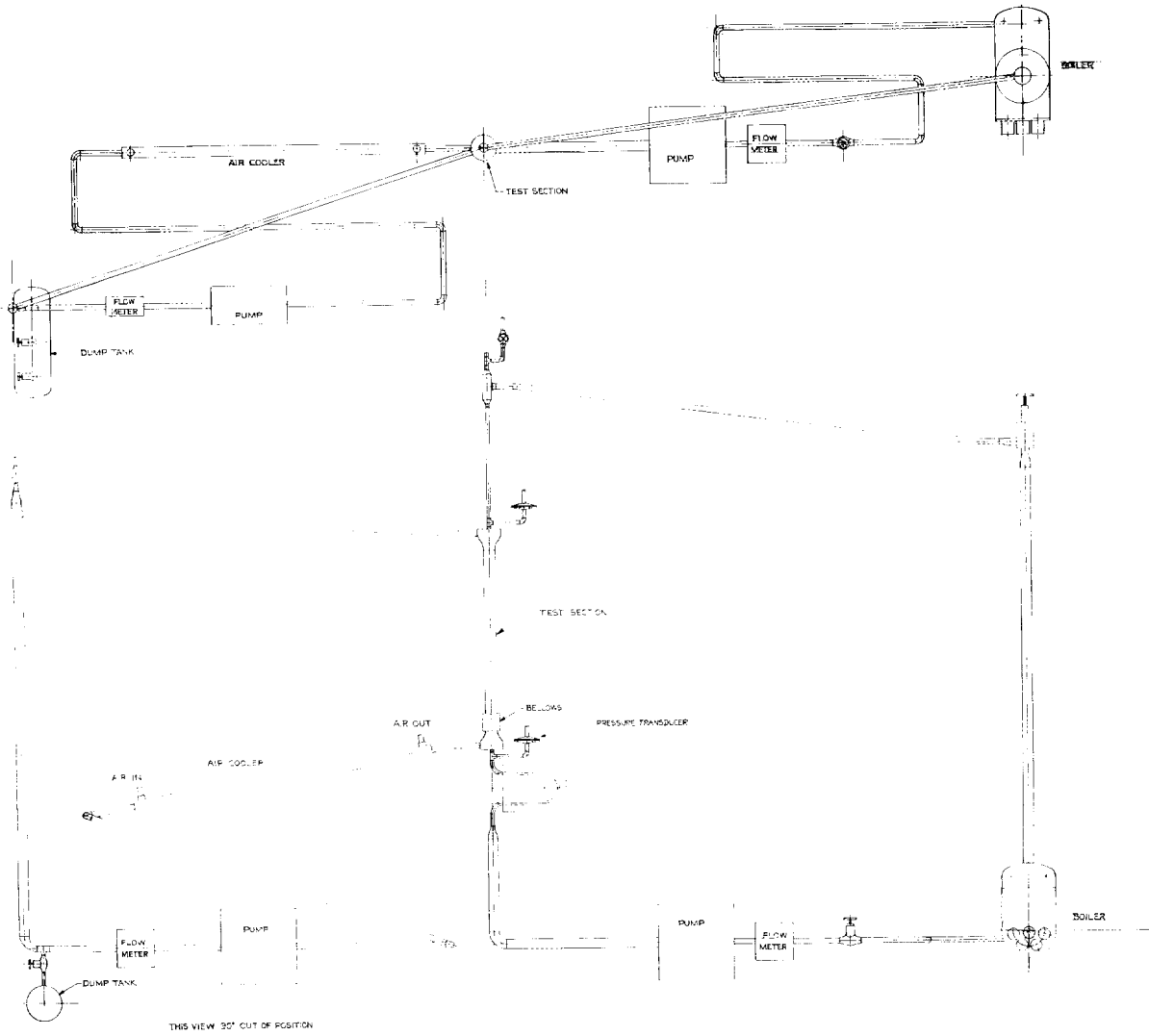


Figure 9. 50 KW Condensing Facility

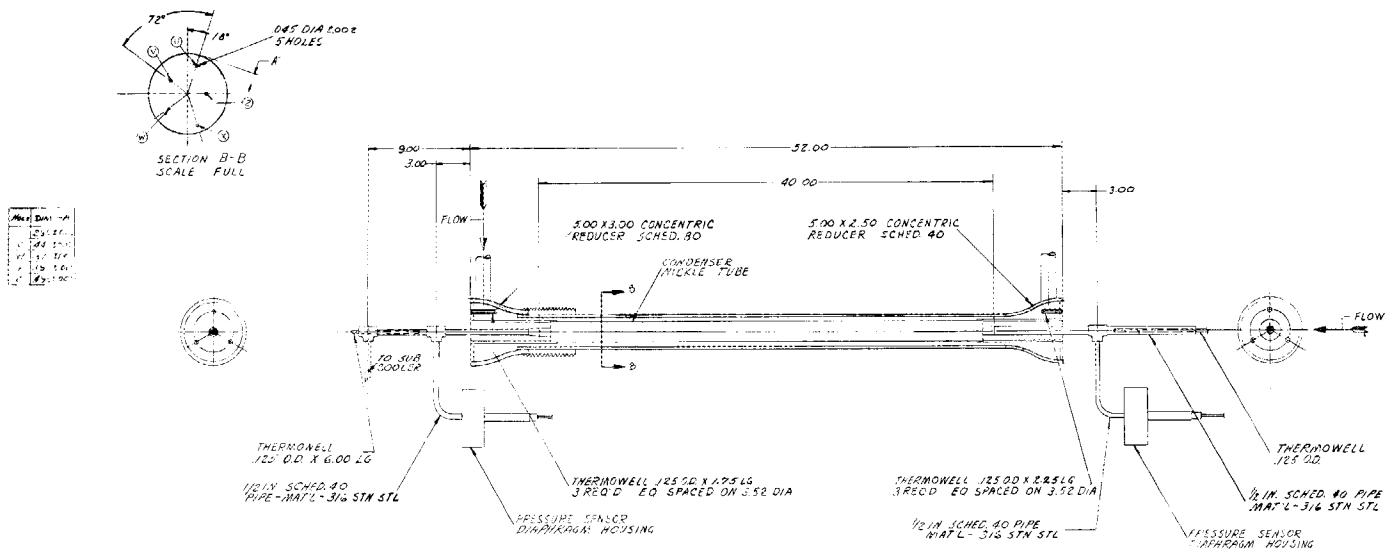


Figure 10. Sketch of 50 KW Condensing Test Section

50 KW CONDENSER
TEST SECTION
SCALE 1/2"
FE 56131-212
Rev. Part April 5, 1963

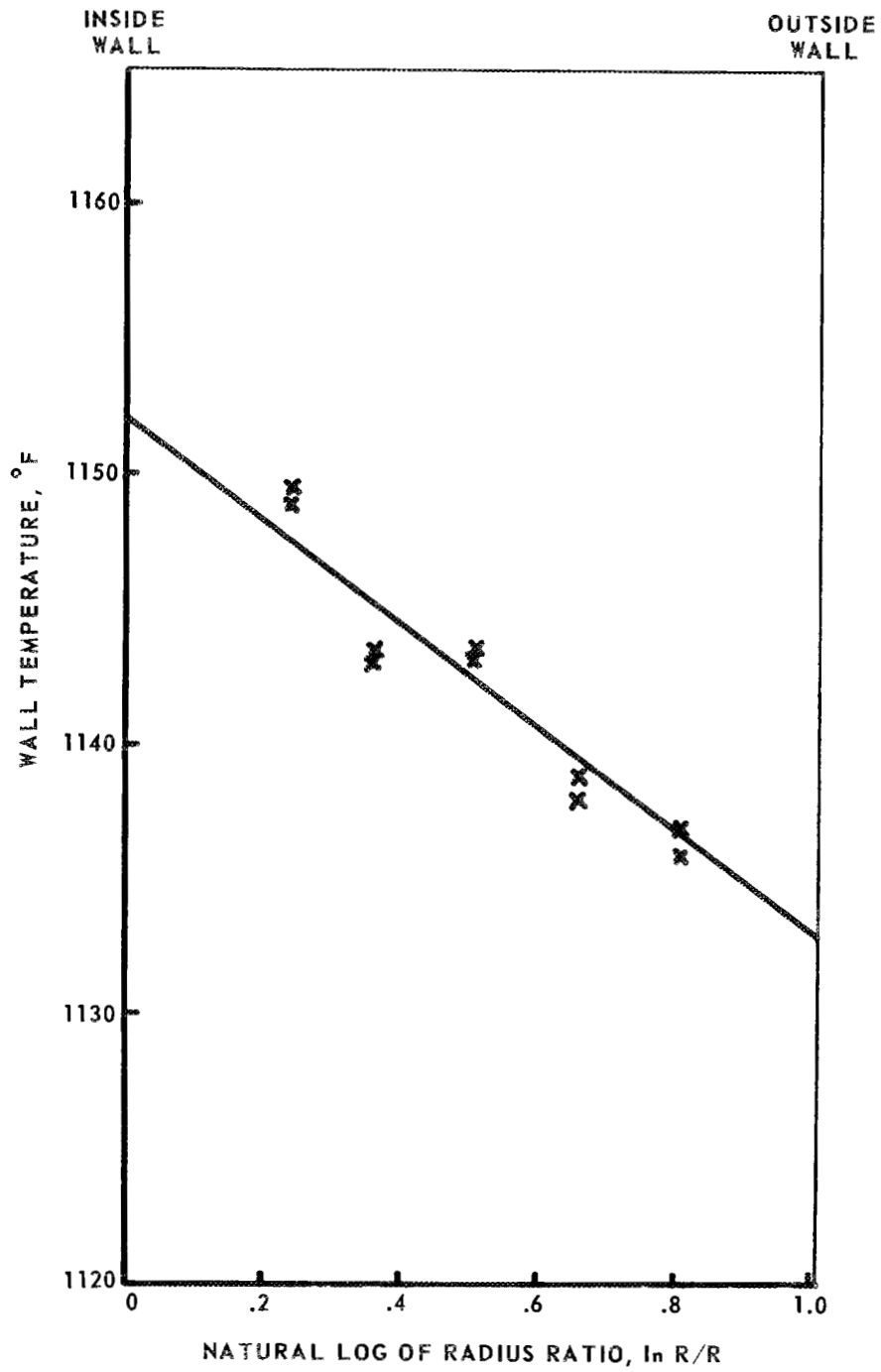


Figure 11. Typical Plot of Wall Radial Temperature Profile for Condensing Run.

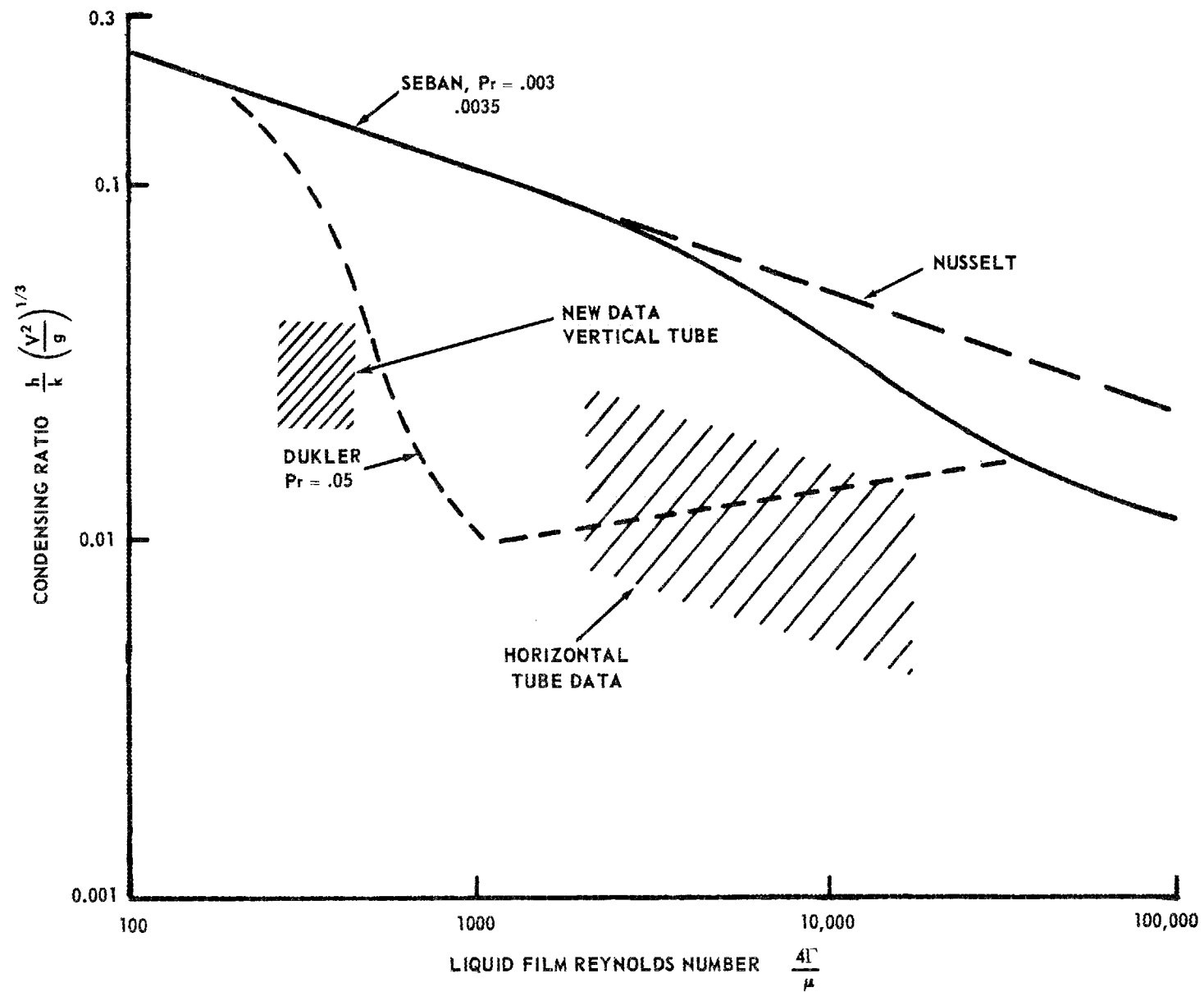


Figure 12. Local Potassium Vapor Condensing Heat Transfer Results

**Potassium-Mercury Amalgam Boiling Heat Transfer,
Two-Phase Flow, and Properties Investigation**

By

Y. S. Tang

C. R. Smith

P. T. Ross

Engineering Dept., Aircraft Engine Operations

ALLISON DIVISION OF GENERAL MOTORS CORPORATION

Indianapolis, Indiana

I. INTRODUCTION

The Allison Research Activity is conducting research directed toward development of a thermally regenerative liquid metal cell.^{1*} This cell, designed to provide power through electrochemical action, employs a potassium-mercury amalgam as the anode and mercury as the cathode. During operation of this cell, the cathode, or mercury stream, receives potassium from the anode, or amalgam stream, by means of the desired ionic reaction. In a closed cycle, therefore, it becomes necessary to purify the "contaminated" mercury stream prior to its reintroduction into the cell. This purification process is presently carried out by a single-stage distillation process accomplished in a boiler-separator unit included as part of the closed system. Thus, to permit system analysis and design and component optimization, information regarding boiling heat transfer and two-phase flow phenomena of the mercury-potassium amalgams is required. In addition, the severe lack of basic property data as determined by an extensive literature survey indicated a need for additional work in this area. To provide such information, the Heat Transfer and Fluid Dynamics Group, Research Activity, is conducting a program on mercury-potassium amalgam liquid metal research. The purpose of the present investigation is to (1) evaluate boiling heat transfer performance of mercury-potassium amalgam over a range of compositions, (2) investigate binary two-phase flow phenomena associated with the boiling of the amalgams, and (3) carry out the required basic property determination studies required for analysis and design of the cell system. The results reported herein represent a continuation of the work reported at the Second Annual Meeting on High-Temperature Liquid Metal Heat Transfer Technology, Brookhaven National Laboratory, May 1962.²

*Superscripts denote references listed in Section V of this report.

II. BINARY LIQUID METAL BOILING HEAT TRANSFER

Studies conducted with boiling binary systems of water and organic liquids^{3,4,5} indicate that the critical heat flux for boiling binary mixtures may be higher than that of either component; in addition, the boiling heat transfer coefficient of certain compositions reaches a minimum value lower than that of either component. It is conceivable, therefore, that the same phenomena may exist in a binary liquid metal system, and the boiling characteristics of pure components could not be used as limits for mixtures of these components.

While many investigations are currently being conducted to obtain forced-convection boiling heat transfer information for liquid metal systems, no information is available regarding a binary metallic system. The present study was initiated, therefore, to obtain boiling heat transfer characteristics of different compositions of potassium-mercury amalgams. Initial results employing a 44.5% (by weight) potassium amalgam have been previously reported in a paper presented at the 50th National AIChE meeting.⁶ In addition to the previously reported data, the results of a second series of experiments employing 44.5% K amalgams and 14.7% K amalgams are reported in the following paragraphs. The latter data will be reported in greater detail in a paper to be presented at the National AIChE annual meeting in December 1963.⁷

EXPERIMENTAL APPARATUS

The experimental liquid metal loop used is shown schematically in Figure 1. The amalgam flows clockwise from the EM pump through the preheater, then into the test section where boiling occurs. From the boiler, the amalgam flows through an enlarged section (where void fraction measurements are taken) into an air-cooled condenser. From the condenser, the amalgam flows through the downcomer and is returned to the pump. This experimental apparatus was employed for both boiling heat transfer studies and the two-phase flow investigation.

The test section consists of a 3/8-in. OD by 0.035-inch wall stainless steel tube. The tube was inserted between the halves of eight 0.828-in. thick copper disks spaced 0.063 in. apart. These copper disks contained, as a heat source, cartridge heaters with a maximum sheath temperature of 1600°F. The boiler (Figure 2) is capable of supplying 12.6 kw to the inner diameter of the tube. Through the use of thermocouples positioned for measuring both radial temperatures and tube wall temperatures, each disk was instrumented for calculating film coefficients. A typical temperature profile is shown in Figure 3.

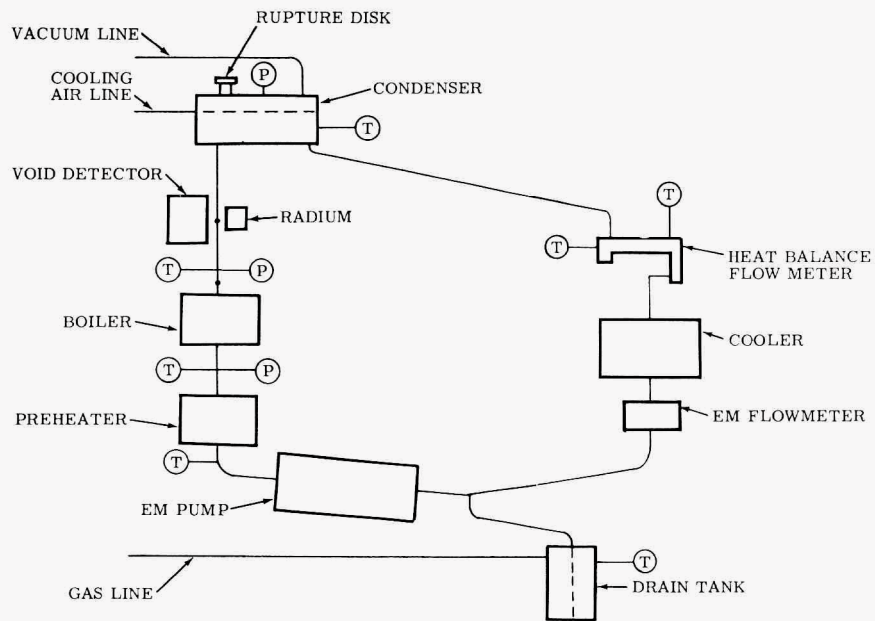


Figure 1. Schematic diagram for boiling liquid metal transfer loop.

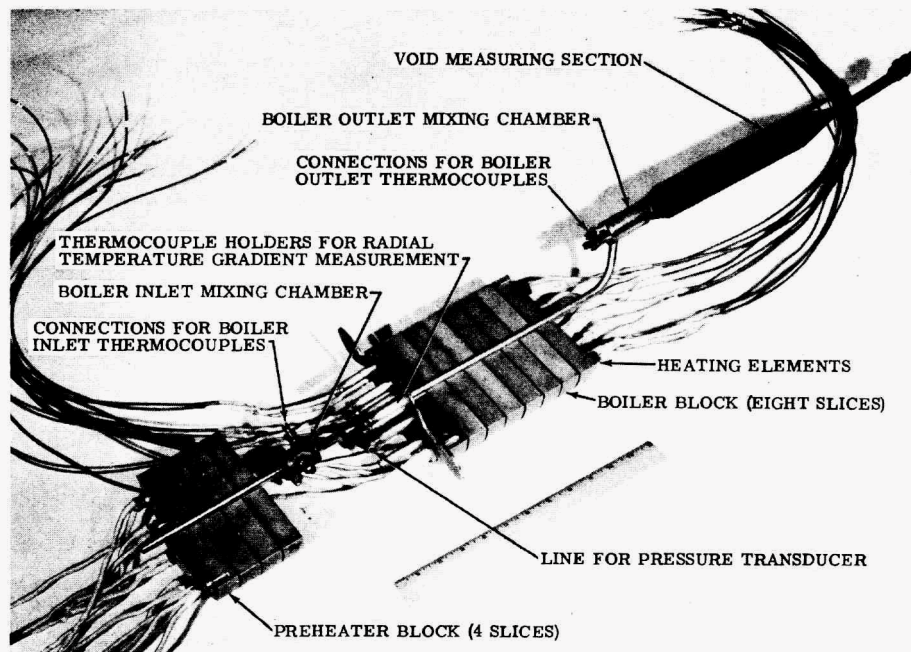


Figure 2. Cross section of the preheater and boiler test section.

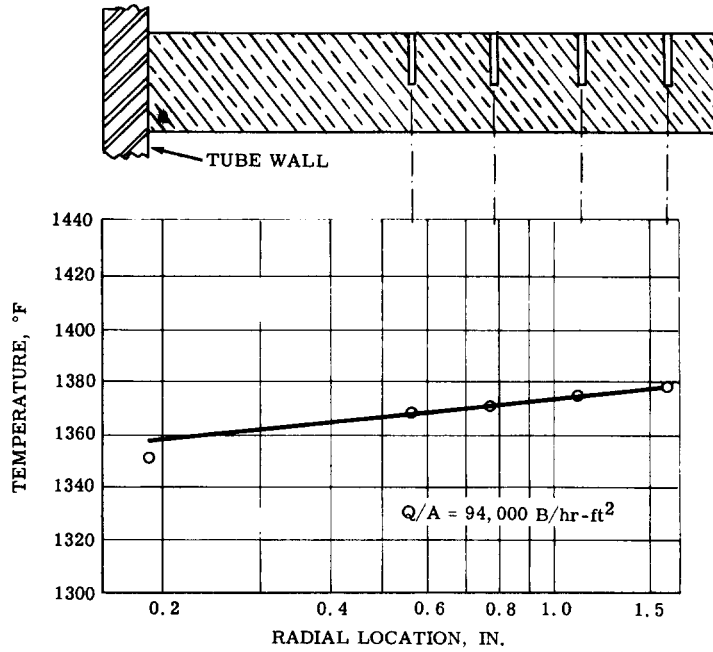


Figure 3. Radial copper block temperature profile.

During operation, net boiling was indicated by the void fraction detector reading. The incipience of net boiling was determined by the enthalpy change of the fluid and the saturation temperature corresponding to the pressure in the boiler. Since the fluid temperature at boiler inlet was below saturation temperature (100 to 300°F subcooled), a portion of the boiler was used to provide the sensible heat necessary to reach saturation. The incipience of surface boiling was assumed at the location where the inner tube wall exceeded the saturation temperature. The mean fluid temperature at each disk was calculated using a heat balance for the individual disk. The temperature difference between the heating surface and bulk fluid was used for the calculation of heat transfer coefficients. The wall superheat, ΔT , is defined as the difference between the boiler T_w and T_{sat} in both net and surface boiling conditions.

RESULTS AND DISCUSSIONS

Net Boiling Data

Values of heat flux density for the net boiling region of the test section are plotted in Figure 4 as a function of wall superheat. The results of both compositions (44.5% K and 14.7% K) are shown. Considerably higher wall superheat was required for the 14.7% K amalgams; this phenomenon tends to be similar to that experienced with pure mercury. The lines in Figure 4 represent the recommended correlations of (q/A) versus ΔT for these two compositions. As shown in Figure 4, more heat was transferred through the second disk than at any other location.

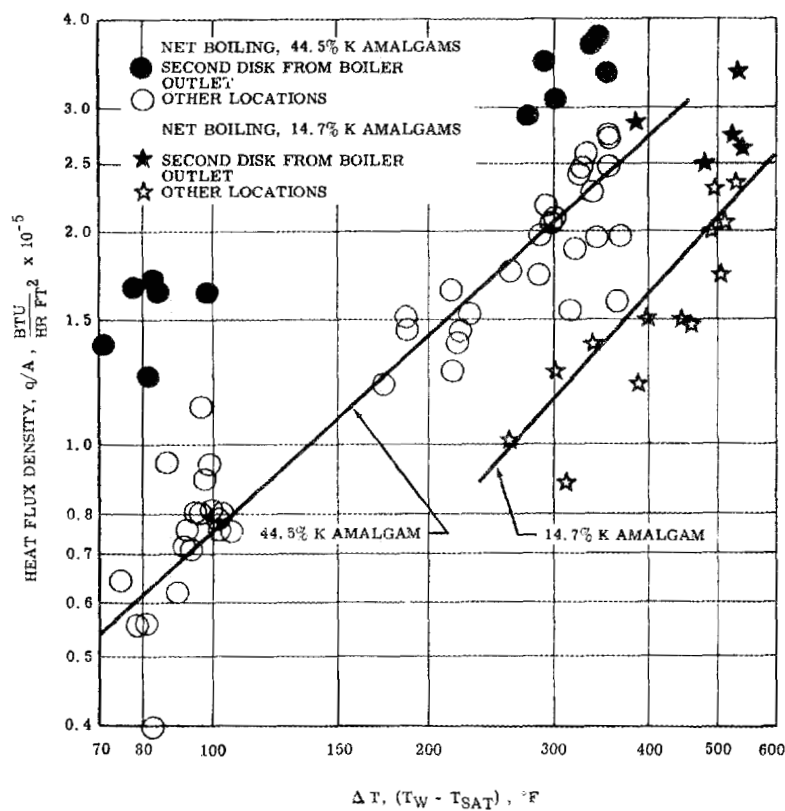


Figure 4. Net boiling heat transfer data for amalgams.

Surface Boiling Data

During the tests reported here, a major portion of the test section for all experiments experienced surface boiling where the heating surface temperature (inner tube wall) exceeded the fluid saturation temperature. The heat flux density (q/A) for surface boiling is again presented as a function of wall superheat for the 44.5% K amalgam in Figure 5. The data exhibit considerable scatter, and no single correlation can be drawn. As can be seen, the local heat flux densities are higher near the boiler entrance than near the net boiling region. This trend indicates that the vapor concentration near the surface influences the heat transfer; and the condition of critical flux for surface boiling is reached at locations near the net boiling region. It should be noted that the upper limits for surface boiling in Figure 5 (the maximum values of heat flux density obtainable in these experiments) are not more than twice those for net boiling. This is considerably different from results reported for surface boiling of water,⁸ indicating that the incipient boiling of amalgams requires high superheat; and the improvement of heat transfer with surface boiling of amalgams in tubes may be limited.

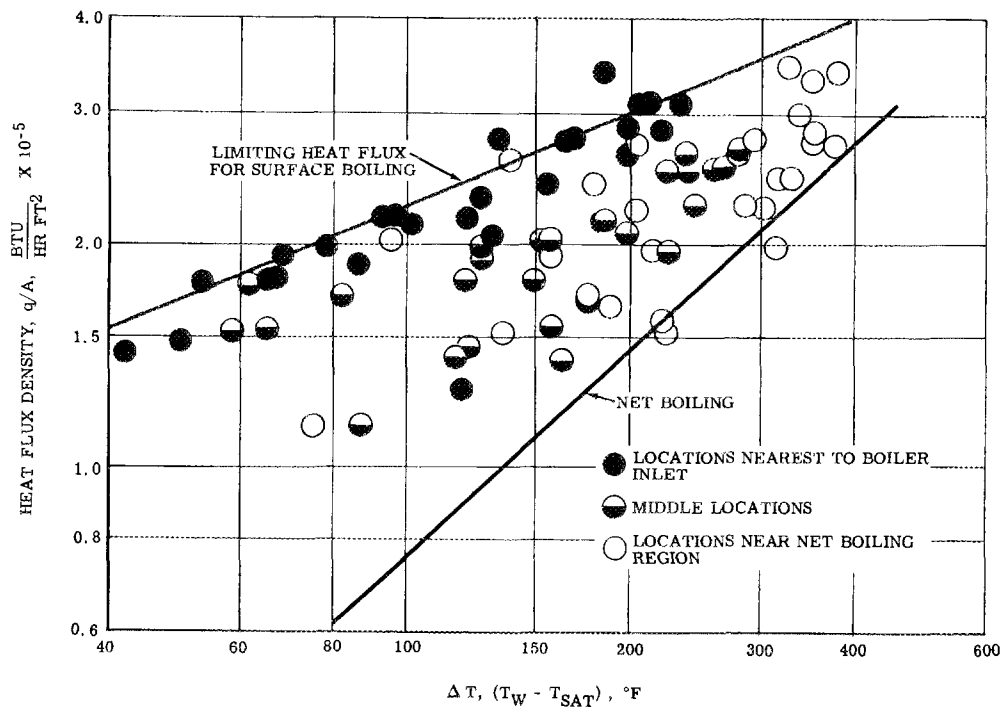


Figure 5. Surface boiling heat transfer data for 44.5% K amalgam.

Comparison of Present Results with Pure Component Data

The net boiling heat transfer data for potassium amalgams are compared with those for pure potassium^{9,10} and mercury¹¹ as reported in the literature (see Figure 6). The present data for amalgams are bracketed between the data for these pure components, as indicated, with boiling heat flux densities for the same ΔT increasing with increasing potassium content.

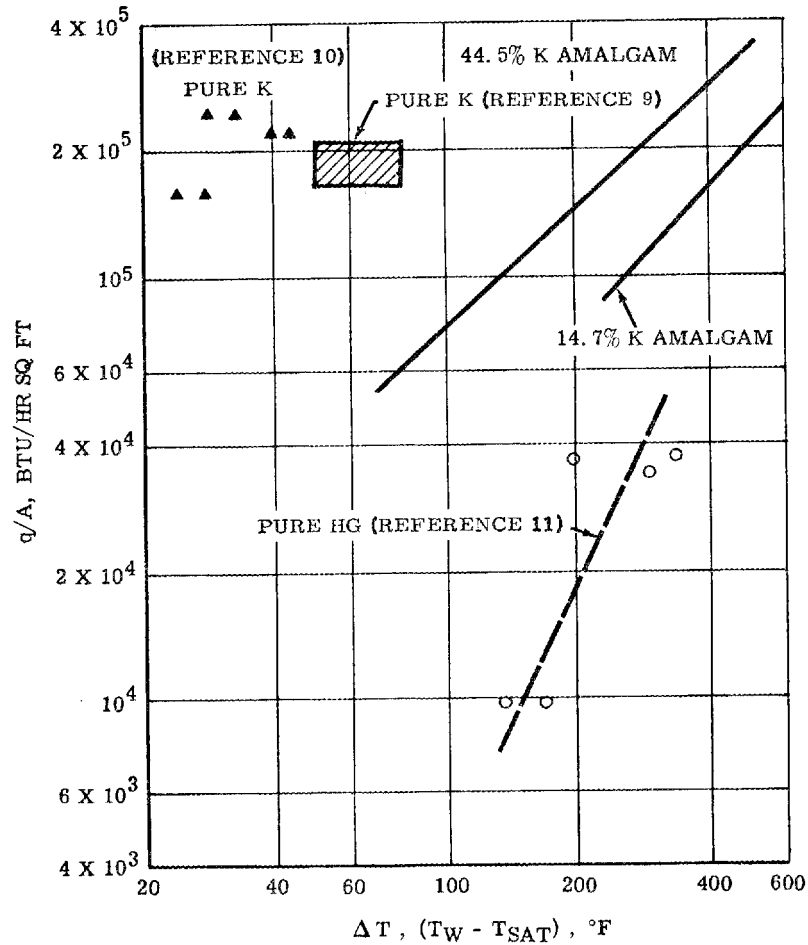


Figure 6. Boiling heat transfer data with mercury.

III. BINARY TWO-PHASE LIQUID METAL FLOW PHENOMENA

As demonstrated in the preceding section detailing with amalgam boiling heat transfer, two-phase flow phenomena are of importance in interpretation of heat transfer data for boiling liquid metals in tubes. In the analysis of two-phase flow, there is a choice of several parameters with which to correlate the characteristics of the system and experimental conditions. One such parameter is the slip velocity ratio, Φ , or the ratio of vapor velocity to liquid velocity in a two-phase system.

In the following equation,

$$\Phi = \frac{x}{1-x} \frac{1-\alpha}{\alpha} \frac{\rho'}{\rho''}$$

the slip velocity ratio is presented as a function of x , the quality of the two-phase stream, α , the vapor volume fraction or void fraction of the two-phase stream, and the ratio of liquid density to vapor density. In the present investigation, values of void fraction were obtained through experimental measurement, and values of two-phase quality were evaluated by means of a heat balance, flow rates, heat of vaporization, etc.

Initial results employing pure mercury during "shakedown" runs of the experimental apparatus have been previously reported in a paper presented at the Multiphase Flow and Heat Transfer Symposium, 55th Annual AIChE meeting.¹² Reported herein are the experimental results of two-phase program employing 44.5% K and 14.7% K (by weight) amalgam as the test fluid.

EXPERIMENTAL APPARATUS

The experimental liquid metal apparatus employed was that shown in Figure 1. The formation of two-phase conditions occurred in the instrumented test section shown in Figure 2. To measure void fractions resulting from the boiling of the amalgam, a void fraction detector was installed immediately above the boiling test section as shown in Figure 1. An Ohmart density gage with a 2-millicurie radium source was employed as the conventional gamma-ray attenuation technique. This approach was similar to the "single-shot" method described in an ANL report¹³ for similar measurement on steam-water systems.

As previously mentioned, earlier phases of the present study were conducted with the same experimental loop utilizing mercury as the working fluid. At that time, the Ohmart density gage was calibrated by mounting the meter and the test section in a horizontal position and filling the test section to a known level with mercury. As the meter is not linear, it was necessary to first set the end points using an empty and then a full test section. The meter output was then recorded for various known void fractions, and the curve shown in Figure 7 was established.

As the meter had already been calibrated, it was only necessary in the present study to reset the end points for the amalgam being studied and use the same characteristic curve. The latter was justified through mathematical analysis. This analysis showed the calibration method to be correct for homogeneous flow. Therefore, as the flow regime changes from homogeneous toward slug flow, an increasing error is introduced. On the basis of work conducted at ANL, the inaccuracies introduced by the "single-shot" method were found to be generally within 20% of the actual value for a tube size comparable with that used in this experiment.

With the aforementioned void fraction gage and the instrumented test section, data were recorded over a range of void fractions and two-phase qualities.

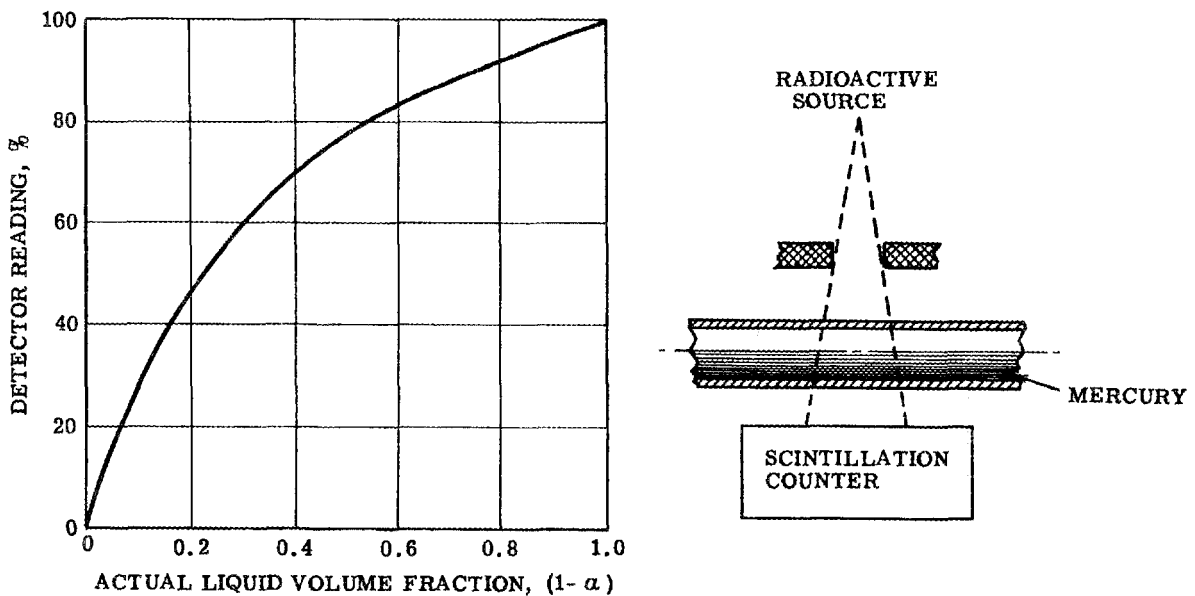


Figure 7. Calibration of void fraction detector.

RESULTS AND DISCUSSION

The only previous experimental results for liquid metal two-phase flow phenomena reported in the literature are for mercury-mercury vapor. Gremilov¹⁴ predicted the variation of void fraction with velocity ratio (i. e. , quality times density ratio) using the Froude number as a parameter. Here, the Froude number is a ratio of inertia forces to buoyancy forces. This correlation was substantiated for mercury-mercury vapor systems by the results of Siryi¹⁵ and Korneev.¹⁶ The mercury data obtained during the initial phase of the present investigation were correlated in a similar manner and are shown as the lower curve in Figure 8. This curve, based on the authors' data, indicates a similar trend with those of the Russian investigators. Inasmuch as the Froude number for the authors' data is in the order of 10^{-4} , it can be considered as a limiting case where the liquid velocity is approaching zero.

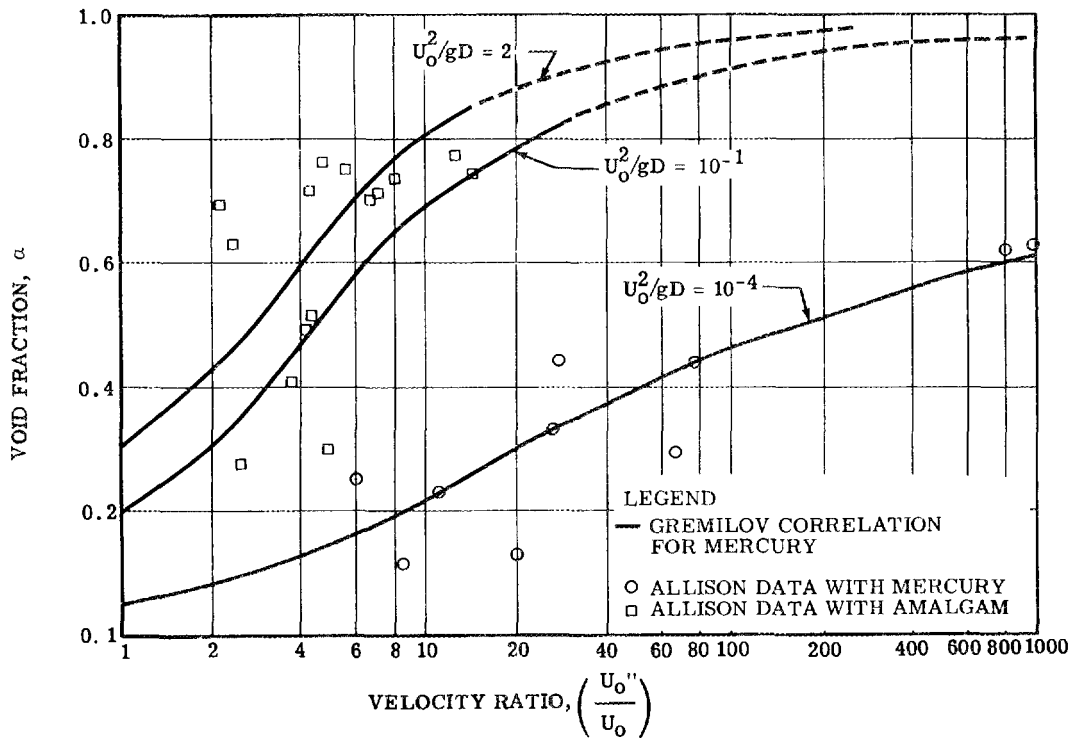


Figure 8. Correlation of void fraction with velocity ratio U_o''/U_o .

Also shown in Figure 8 are data from the amalgam portion of the present investigation. Because of the similarity in experimental apparatus and equipment, the Froude number was again very small (i. e., 10^{-3}). As can be seen from Figure 8, mercury-potassium amalgam experimental data could not be correlated with mercury-mercury vapor data in the manner used here. Because of the lack of amalgam data at other Froude numbers, a general statement regarding the correlation of amalgam data in the manner shown in Figure 8 can not be made. The results of void measurement in boiling amalgam systems and pure mercury systems are also shown in the Martinelli type correlation (Figure 9). This correlation was recently suggested by Baroczy for liquid metal two-phase systems.¹⁷ Due to the large flow cross section and small vapor qualities, almost all data lie in the turbulent-viscous two-phase flow regimes. Figure 9 indicates liquid fractions for these two different liquid metal systems are consistently higher than water-air or oil-air systems. No attempt was made, however, to apply a density ratio parameter as suggested in Baroczy's paper.

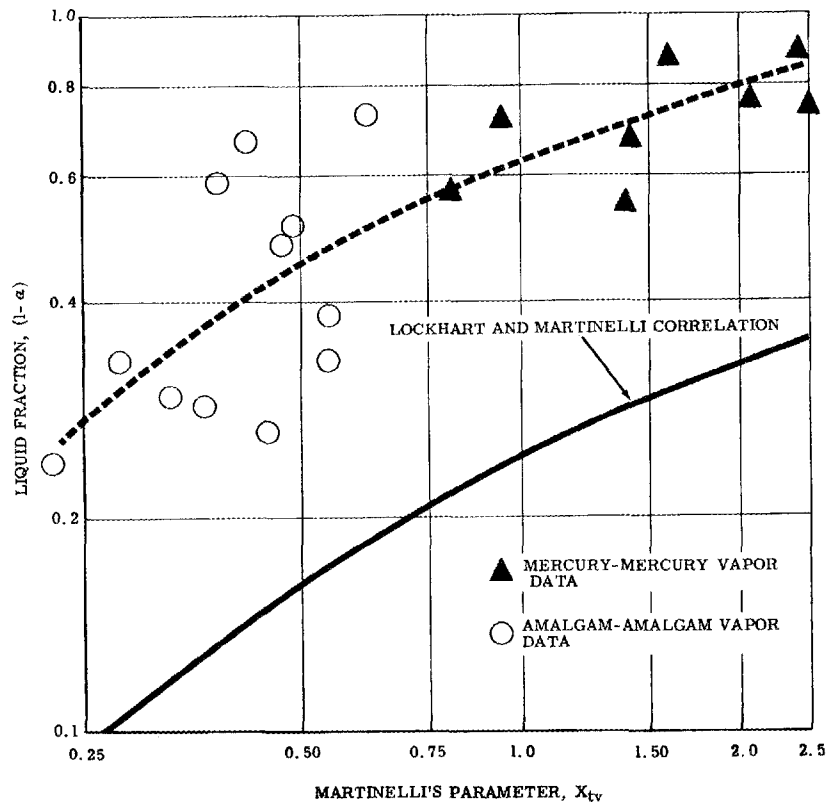


Figure 9. Comparison of Allison liquid metal data with Lockhart and Martinelli parameter.

IV. POTASSIUM AMALGAM BASIC PROPERTY EVALUATION

To carry out system analysis and component design of the Allison liquid metal cell, the thermo-physical properties of the amalgam were required. While a limited amount of such data is available in the literature, an extensive literature survey revealed a definite lack of required information. To compensate for this shortage, the Allison Research Department, in conjunction with Columbia University, is conducting a continuing program designed to provide the required data.

Specific areas of work already completed or currently being studied include the evaluation of the following properties:

1. Liquid-vapor phase equilibrium diagram
2. Thermal diffusivity
3. Vapor pressures
4. Surface tension
5. Latent heat of vaporization

LIQUID-VAPOR PHASE EQUILIBRIUM DIAGRAM

The design of the Allison liquid metal cell utilizing potassium and mercury requires a knowledge of the phase equilibrium diagram for potassium amalgams at 760-mm Hg pressure. A search of the literature, however, has yielded only partial data at low pressures.¹⁸ Therefore, an experimental program was conducted at Allison to establish the vapor-liquid equilibrium diagram for an amalgam system at 760-mm Hg pressure.

Upon considering the methods available for carrying out such a program, final selection was narrowed to two: the transpiration or dynamic method; and the direct sampling or static method. Because of required knowledge of partial pressures, molecular weights, masses of condensable and noncondensable vapors, and the complexity of experimental techniques, the direct sampling method was chosen.

Potassium amalgams of three different compositions (i. e. , 80, 60, and 47% potassium by mole fraction) were placed in individual evacuated apparatus similar to that shown in Figure 10. The apparatus were then placed in a furnace, brought up to the isothermal temperature corresponding to 760-mm Hg vapor pressure for each composition, and samples were removed into an evacuated trap.

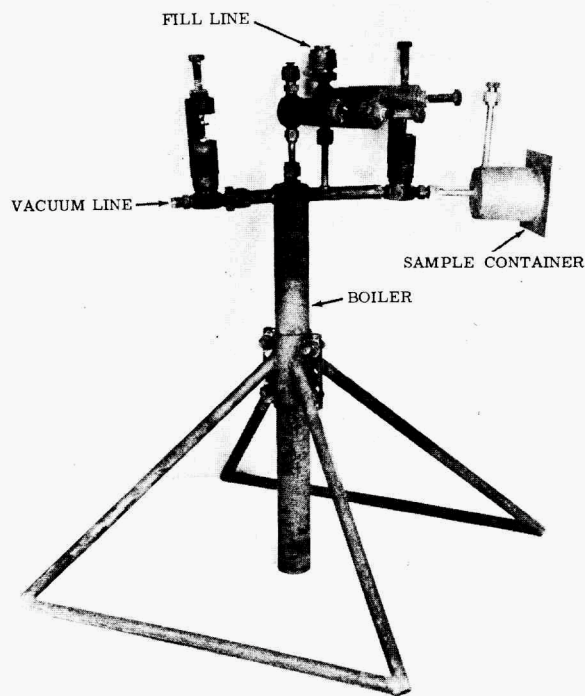


Figure 10. Direct sampling apparatus.

A total of 30 samples were obtained and analyzed. The resulting composition of the condensed vapors, plus a knowledge of the original liquid sample, permitted the establishment of a point of the liquid-vapor phase equilibrium diagram. The experimental results of this investigation are shown in Figure 11. Although the compositions studied cover only a relatively small range, the portion of the curve established was that of primary interest in the analysis of the liquid metal cell. This phase of the program was reported in greater detail in a paper presented at the Thermodynamics and Transport Properties Symposium, 1963 AIChE National Meeting, New Orleans.¹⁹

In conjunction with the forementioned experimental approach to evaluating the liquid-vapor phase diagram, work was carried out in an effort to theoretically predict such a diagram for the potassium amalgam system. By employing the method of Othmer, Ricciardi, and Thaker,²⁰

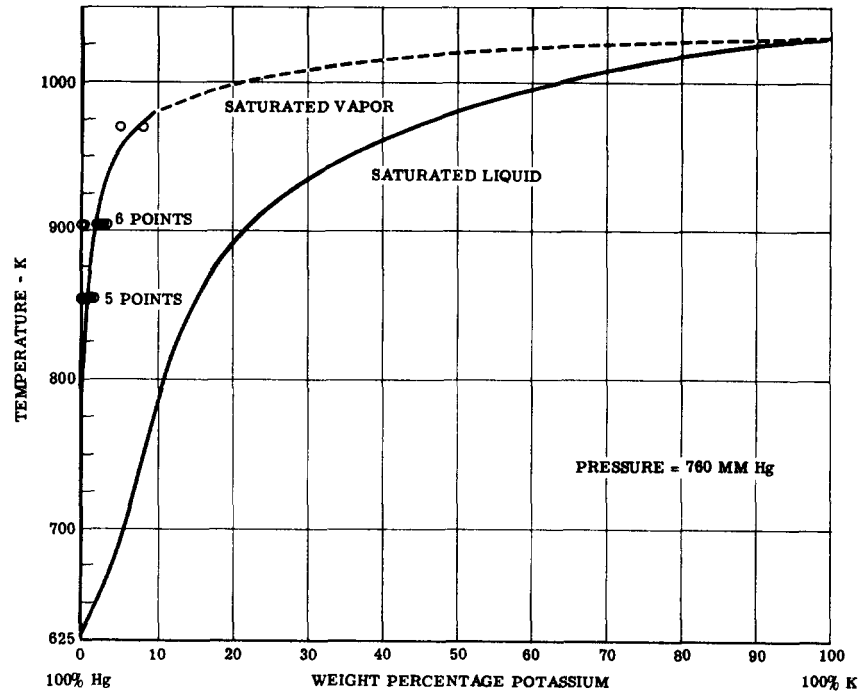


Figure 11. Liquid-vapor equilibrium diagram.

an equation relating the mol composition of mercury liquid and vapor, temperature, and the enthalpies of the components was developed. By assuming the vapor composition at a point very close to the pure potassium boundary (i. e., $X_K = 0.99$), the estimation of the vapor phase composition was carried out by stepwise integration of the relationship already mentioned. A comparison of the analytical and experimental data is shown in Figure 12. One can conclude that, on the basis of the good correlation shown here, the aforementioned theoretical approach is applicable.

THERMAL DIFFUSIVITY, VAPOR PRESSURE, SURFACE TENSION, AND LATENT HEAT OF VAPORIZATION

Physical property studies on thermal diffusivity, vapor pressure, surface tension and latent heat of vaporization have been carried out at Columbia University under the direction of Dr. Bonilla. The method of measuring the diffusivity begins with the addition of potassium to the

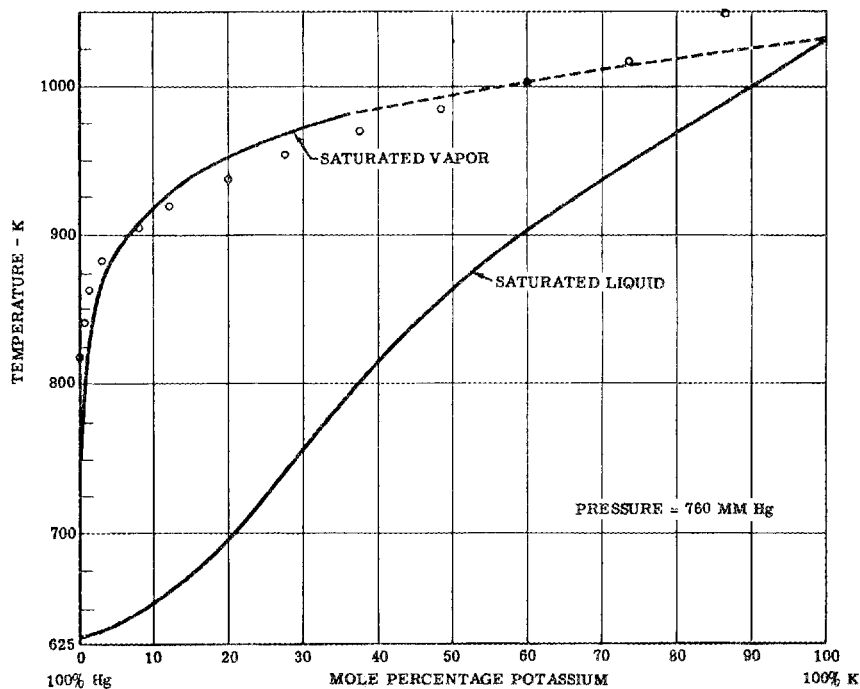


Figure 12. Comparison of analytical and experimental liquid-vapor phase equilibrium data.

top of a 2-in. deep layer of mercury in a vertical, cylindrical, thin-walled stainless steel cell in a vertical tube furnace. At successive time intervals, θ , direct current is passed axially along the cell, and the resistive voltage drops from the bottom of the cell to different heights, x , are measured by a high resistance device involving a Leeds and Northrup "microvolt amplifier" and a Sargent strip voltage recorder. The voltage at each x value is read with zero current and with the current in each direction. The resistivity data are then converted to amalgam compositions and the rate of diffusion can be determined. Results of the first few runs indicate that the diffusivity increases considerably with increasing potassium concentration.

Vapor pressure studies of the potassium-mercury system are being planned to permit the gathering of data with varying K-Hg compositions. Experiments are also being planned to carry out surface tension measurements on various compositions and temperatures.

V. BIBLIOGRAPHY

1. Henderson, R. E. and Agruss, B. Liquid Metal Electrochemical Cells. Paper presented in AIChE 49th National Meeting (March 1963).
2. Smith, C. R., Tang, Y. S., and Ross, P. T. Potassium-Mercury Amalgam Heat Transfer and Two-Phase Flow Investigation. Paper presented at Second Annual Meeting on High-Temperature Liquid Metal Heat Transfer Technology, Brookhaven National Laboratory (May 1962).
3. Benjamin, J. R. and Westwater, J. W. "Bubble Growth in Nucleate Boiling of a Binary Mixture." International Development in Heat Transfer, Part II. ASME (1961).
4. Bonilla, C. F. and Perry, C. W. "Heat Transmission to Boiling Binary Liquid Mixtures." Trans. AIChE (1942), pp 685-708.
5. Rose, W. J., Gilles, H. L., and Uhl, V. W. Subcooled Boiling Heat Transfer to Aqueous Binary Mixtures. AIChE Preprint No. 6, 5th National Heat Transfer Conference (1962).
6. Ross, P. T., Smith, C. R., and Tang, Y. S. Boiling Heat Transfer in a Potassium-Mercury System. Paper presented at 50th National Meeting, AIChE, Buffalo, New York (May 1963).
7. Tang, Y. S., Ross, P. T., Nicholson, R. C., and Smith, C. R. Forced Convection Boiling of Potassium-Mercury Systems. Paper to be presented in Liquid Metal Working Fluids for Space Power Application Session, 56th Annual Meeting, AIChE, Houston, Texas (December 1963).
8. Jiji, L. M. and Clark, J. A. Incipient Boiling in Forced-Convection Channel Flow. ASME Paper 62 WZ-202 (1962).
9. General Electric Company, Alkali Metals Boiling and Condensing Investigations. Contract No. NAS 3-2528, First Quarterly Report (July - September 1962).
10. Hoffman, H. W. and Krakoviak, A. I. "Forced-Convection Saturation Boiling of Potassium at Near-Atmospheric Pressure." Proceedings of 1962 High-Temperature Liquid Metal Heat Transfer Technology Meeting, Brookhaven National Laboratory (May 1962).

11. Kutateladze, S. S., et al. Liquid Metal Heat Transfer Media, Supplement No. 2. Translation, Consultants Bur. Inc., New York (1959), p 109.
12. Smith, C. R., Tang, Y. S., and Walker, C. L. Slip Velocity in Two-Phase Metallic Fluids. Paper presented at Multiphase Flow and Heat Transfer Symposium, 55th Annual AIChE Meeting, Chicago (December 1962).
13. Richardson, B. L. Some Problems in Horizontal Two-Phase Two-Component Flow. ANL Report 5949 (December 1958).
14. Gremilov, D. I. Combination Power Engines and Cycles (in Russian). Trudy TsKTI, Book 23, p 44, Mashgiz, Leningrad (1952).
15. Siryi, P. O., et al. in Sovetskoe Kotloturbostroenie, 8-9, 375 (1938) (in Russian).
16. Korneev, M. I. in Teploenergetika 4, 44 (1955) (in Russian).
17. Baroczy, C. J. Correlation of Liquid Fraction in Two-Phase Flow with Application to Liquid Metals. AIChE Preprint No. 26, presented at the 6th National Heat Transfer Conference, Boston, Massachusetts (August 1963).
18. Roeder, A. and Morawietz, W. in Zeit. für Elektrochemie. Vol 60 (1956), p 431.
19. Nicholson, R. C., Smith, C. R., and Walker, C. L. Liquid-Vapor Phase Equilibrium Diagram of Potassium-Mercury System. Paper presented at Thermodynamics and Transport Properties Symposium, 49th National Meeting, AIChE, New Orleans (March 1963).
20. Othmer, D. F., Ricciardi, C. G., and Thaker, M. S. Composition of Vapors From Boiling Binary Systems, Industrial and Engineering Chemistry. Vol 45 (August 1953) p 1815.

ADDENDUM

The Russian work in two-phase flow used for comparison purposes in the present paper appears in Reference 11 (i.e., Liquid Metal Heat Transfer Media, by Kutateladze). The works of Gremilov, Siryi, and Korneev (references 14, 15, and 16 respectively) are presented in graphical form (with appropriate references) by Kutateladze.

The authors attempted to obtain copies of the original Russian references cited by Kutateladze and were able to find only one (that of Korneev). This paper was irrelevant and did not contain the data attributed to it by Kutateladze.

DISCUSSION

MR. STEIN: Perhaps you mentioned this and I didn't hear it. How did you compute your saturation temperature for this amalgam?

MR. SMITH: We had three thermocouples located right at the boiler outlet. We assumed that the temperature indicated by these thermocouples, when our void fraction detector indicated net boiling existed, was the saturation temperature. This corresponded pretty closely to the value obtained from the vapor pressure curve using the pressure indicated by the pressure transmitter located at the boiler outlet. As it has already been pointed out, there is some problem with this type of transmitter; we did find, however, pretty good agreement between the temperatures recorded and the values calculated from the pressures.

MR. BONILLA: I don't recall now--I have seen some of this before--do you take into account the change in saturation temperature with quality which you would get in the two-component material?

MR. SMITH: Do you mean the fact that as you extrapolate down the boiler, the liquid head changes? You make a correction--

MR. BONILLA: No. The more you evaporate the mercury, the higher the boiling point is at a given pressure.

I might mention also that the slope of about 45-deg which you obtained may easily be due to that factor. In our own NaK boiling--though that was pool boiling--you would probably see a tilting over of the line, since the higher q/A , the greater the local change in phase composition must be. In other words, there are two effects. One is an axial change in saturation temperature, and the other is a radial change in composition, which is probably to be expected in a two-component mixture.

MR. SMITH: That's a good point.

MR. DWYER: In that connection, both the pure potassium line and the pure mercury line were parallel to that for the amalgam.

MR. BONILLA: That's true; yes.

MR. DWYER: That would tend to counteract Professor Bonilla's comment.

MR. BONILLA: No; it tends to bring in some more irrelevant points.

MR. CHEN: Are we talking about the slope of the boiling curve?

MR. SMITH: Yes; q/A versus ΔT .

MR. CHEN: If I may interject something which may be applicable in regard to the 45-deg slope. One of the slides I neglected to show did predict that in most regions with convective boiling the slope does drop; and, in fact, it is pretty hard to get away from 45-deg for convective boiling.

MR. BONILLA: For two components?

MR. CHEN: No; single component. The reason is that you get more of the macroconvective contribution--which gives a 45-deg slope.

MR. BONILLA: But most people don't report a 45-deg slope.

MR. CHEN: I noticed in your data, and in data presented earlier today (by Poppendiek, I believe), a slope of 45-deg.

MR. BONILLA: But with forced convection present. You have a boiling slope which is something above one and less than three; when you put in the convective component, you get a curve. It goes to zero, if it is saturated. So, there ought to be a curve.

MR. STEIN: I will make a comment--using my chairmanship as a prerogative--directed partially at Dick and perhaps also to the last few authors. I may ask the question as to whether we are clouding the issue somewhat by displaying and trying to correlate data for boiling as heat transfer coefficients. Maybe, Dick, you can answer it since I noted in your paper that the data were not presented as heat transfer coefficients although, with a similar system, it was possible to do this. I wonder how people feel about it.

MR. ROHSENOW: One vote in favor!

MR. KILLACKEY: What does Professor Rohsenow suggest we use?

MR. ROHSENOW: Pure grain ΔT !

MR. STEIN: Since you raise the point, maybe I can answer. There are implications that we can bring the data together, as we do in single-phase. What we are really interested in at this stage of the game--and this is the same stage as we originally were in in which we also tried to use heat transfer coefficients--is a display of the experimental data so we can study it and maybe get some ideas. So we want heat flux versus temperature for boiling systems. This is what we are really interested in, I think.

MR. BONILLA: My comment would be that the heat-transfer coefficient is more sensitive. For instance, it would be foolish not to use the friction factor in talking about the pressure drop for flow in tubes, since the pressure drop data for single-phase flow are so accurate that you can utilize this and get much more information out of it.

But the boiling data are probably not reliable enough to use heat transfer coefficients.

MR. GOLDMANN: I guess I got into that argument with supercritical water, too; and I feel very strongly that heat transfer coefficients are very useful as long as the coefficient is only flow or geometry dependent. But the moment the coefficient also becomes a function of the heat flux itself, then the coefficient is no longer a useful tool.

MR. BONILLA: But with fluid flow, the temperature drop can be temperature dependent; still the friction factor is the ideal way to correlate it.

MR. GOLDMANN: I agree with you. It is a flow phenomenon, and the heat transfer coefficient (expressed normally as the Nusselt number versus the Reynolds number) becomes a function of the geometry, flow conditions, and properties of the fluid, not just a function of the fluid.

MR. POPPENDIEK: Well, in fluid flow, the shear stress varies linearly from a maximum at the wall to zero at the center line. This is a simple flow situation. In convective heat transfer, without volumetric processes, there are analagous equations; and you can talk about a conductance which is analagous to something like friction. However, when you have additional

fluxes of some type in the volume, as you do in boiling, the coefficient, which is really the inverse of the heat-transfer resistance, tries to lump a number of things. I think it is better to separate these. Thus, at this stage of the game, I think, as Ralph says, an over-all temperature difference between a wall and a bulk of some sort and a flux is more meaningful.

MR. ROHSENOW: I will ask Carlos a question. What is the equation of that curve? It's $y=mx$, isn't it? You want to select the correct value of m for every x . If h is a function of ΔT , this is the same thing. Now, h can be a function of absolute temperature--this is legal--but when h is a function of ΔT , you don't want to use h . That's my point.

MR. BONILLA: You could say ΔT equals the function of velocity, and still it is helped by introducing the friction factor aspect.

MR. ROHSENOW: Yes. But there you can do this all as a small exponent; a small effect. The friction factor is a small effect.

MR. BONILLA: I think we all agree that we don't know enough about boiling to do it quantitatively, but eventually we probably will.

MR. STEIN: On that statement we will end this discussion.

HEAT TRANSFER DURING FILM CONDENSATION
OF A LIQUID METAL VAPOR

S. P. Sukhatme

W. M. Rohsenow

Massachusetts Institute of Technology
Cambridge 39, Massachusetts

I. INTRODUCTION

Developments in nuclear power technology and in other fields, in which liquid metal vapors are used as heat transfer fluids, have increased the need for a thorough understanding of the process of heat transfer during film condensation of liquid metals.

At the present moment, there exists considerable disagreement between theory and experiment for the case of film condensation of a liquid metal vapor. Experiments^(1,2) have consistently yielded heat transfer coefficients much lower than those expected from theory.

From a practical as well as a fundamental viewpoint, it would be useful to remove the present disagreement and to understand the reasons for its existence. This is the object of the research investigation being reported here.

II. GENERAL REVIEW OF LITERATURE

Development of the Theory. The specific problem under consideration is the case of film condensation of a stationary, pure, saturated vapor on an isothermal vertical surface. The first formulation of the problem is due to Nusselt⁽³⁾, who made the following assumptions:

- (i) The temperature of the liquid-vapor interface is the saturation temperature.
- (ii) The condensate flow is laminar.
- (iii) The fluid properties are constant.
- (iv) Subcooling of the condensate may be neglected.
- (v) Momentum changes through the condensate are negligible, i.e., there is essentially a static balance of forces.
- (vi) The stationary vapor exerts no drag on the downward movement of the condensate.
- (vii) The temperature distribution in the film is linear.

He derived the well known formula:

$$Nu = 0.943 \sqrt[4]{\frac{g \beta^2 L^3 \lambda}{\mu k (T_v - T_w)}} \quad \dots (1)$$

Seban⁽⁴⁾ has extended Nusselt's analysis for the case of higher Reynolds numbers by assuming a transition from laminar to turbulent flow at a Reynolds number of 1600 and a universal velocity distribution in the film. His results verify the qualitative expectation that heat transfer coefficients should increase for common fluids ($Pr \approx 0.5$ or greater) but should not for low Prandtl number fluids because of high values of thermal diffusivity as compared to the turbulent diffusion coefficient for heat.

Nusselt's analysis has been extended by Bromley⁽⁵⁾, who included effects of subcooling of the condensate, and by Rohsenow⁽⁶⁾, who allowed for non-linearities in the film temperature distribution. These refinements become

important only at high values of $C_p(T_v - T_w)/\lambda$. Actually in most applications, this parameter has a value between 0 and 0.2.

Sparrow and Gregg⁽⁷⁾ have solved the boundary layer equations for a laminar film through a similarity transformation, thus taking account of momentum changes. For common fluids, their results follow Nusselt's prediction closely, but for low Prandtl number fluids, the heat transfer coefficient drops below the Nusselt prediction with increasing $C_p(T_v - T_w)/\lambda$. Mabuchi⁽⁸⁾ has obtained substantially the same results by an integral method.

Recently Chen⁽⁹⁾, Koh, Sparrow and Hartnett⁽¹⁰⁾, and Koh⁽¹¹⁾ have almost simultaneously considered the effect of the vapor drag. Their results indicate little disagreement with Nusselt's theory for common fluids. For low Prandtl number fluids, however, the heat transfer is found to drop even below that determined by Sparrow and Gregg.

Thus the latest refinements to Nusselt's analysis have removed the restrictions of assumptions (iv), (v), (vi) and (vii). Figures 1 and 2 illustrate the results of the above investigators.

Experimental Investigation for Liquid Metals

Although experiments have substantially borne out the theoretical predictions for common liquids⁽¹²⁾ ($Pr \gg 0.5$), the same cannot be said for liquid metals. The only experimental data to date for the particular geometry of Nusselt's theory is that of Misra and Bonilla⁽¹⁾, who have used mercury and sodium. Their data (Figs. 1 and 2), which is quite scattered, falls very much below the theoretical predictions⁺. For sodium, the values seem to be even lower than those for mercury.

⁺It is worth mentioning that in a recent paper, Dukler⁽¹³⁾ has suggested a theory which seems at first glance to agree reasonably well with Misra and Bonilla's experiments. In the opinion of the present authors, however, this agreement can only be fortuitous. In the outer region of the film, Dukler has made the assumption that the molecular heat transport coefficient is negligible in comparison to the turbulent eddy coefficient (refer to Appendix of his paper). This assumption is reasonable for high Prandtl number fluids, but is totally unjustifiable for Prandtl numbers of the order of 0.01 particularly at the Reynolds numbers in Misra and Bonilla's experiments. Sample calculations have shown that by not making this assumption, Dukler's results would fall close to Nusselt's.

III. A MODIFIED THEORY OF FILM CONDENSATION

As has been stated earlier, the most recent modifications^(9,10,11) of Nusselt's theory have removed the restrictions of assumptions (iv), (v), (vi) and (vii). Assumptions (ii) and (iii) can always be satisfied within reason by controlling the rate of condensation and by choosing a suitable fluid. We wish to concentrate our attention now on examining the validity of assumption (i).

Schrage⁽¹⁴⁾ has studied the phenomenon of interphase mass transfer from the standpoint of kinetic theory. An equation derived by him for the case of condensation of a pure vapor can be expressed in the following more useful form (with the additional restriction that the vapor is saturated):

$$m = \left(\frac{\sigma}{2 - \sigma} \right) \left(\frac{2}{\pi} \right)^{1/2} \left(\frac{M}{\bar{R}} \right)^{3/2} \frac{P_v \lambda}{T_v^{5/2}} (T_v - T_s) \quad \dots (2)$$

Here m is the rate of condensation per unit area, σ is called the condensation coefficient (the ratio of molecules that strike the liquid surface and condense to the molecules which strike the surface), M is the molecular weight, \bar{R} is the universal gas constant, P_v and T_v are the saturation pressure and temperature, λ is the latent heat of vaporization and T_s is the liquid temperature at the liquid-vapor interface.

The Condensation Coefficient σ

The coefficient σ is believed to have a functional dependence upon the state of the surface and the kind of molecules involved. For water, many investigators have measured the value of σ to be around 0.04.

For mercury, measured values of σ have ranged from 0.0005 to 1, with 0.1 being the most consistently reported value. The value of 1 was measured by Knudsen⁽¹⁵⁾ when he took the greatest precautions to insure the purity of the mercury, while the value of 0.0005 was also measured by him when he took no particular precautions and could see a slight brownish scum

contaminating the surface. In any condensing system, although great purity cannot be obtained, it should be noted that a new vapor-liquid interface is being constantly created. Therefore, a value between the two extremes and of the order of 0.1 seems likely to be obtained.

Values of σ for other liquid metals are not known.

Estimating the Value of $(T_v - T_s)$

The rate of condensation per unit area at a distance z from the top of a vertical condenser is given by Nusselt's classical theory by the equation

$$m = \left(\frac{k^3 (T_v - T_w)^3}{\lambda^3} \cdot \frac{\rho^2 g}{4 \mu z} \right)^{1/4} \quad \dots (3)$$

Combining equations (2) and (3), we have

$$(T_v - T_s) = \frac{\pi^{1/2}}{2} \left(\frac{2 - \sigma}{\sigma} \right) \left(\frac{\bar{R}}{M} \right)^{3/2} \left(\frac{k^3 \rho^2 g}{\lambda^3 \mu} \right)^{1/4} \frac{T_v^{5/2}}{P_v} \frac{(T_v - T_w)^{3/4}}{z^{1/4}} \dots (4)$$

For any given fluid and a chosen set of conditions, equation (4) can be used for calculating the value of $(T_v - T_s)$. This has been done in the following table for three fluids -- water, mercury and sodium. In all instances, the saturation pressure P_v has been chosen to be atmospheric pressure.

$(T_v - T_s)$ in $^{\circ}\text{F}$:

	σ	$(T_v - T_w)=5^{\circ}\text{F}$		$(T_v - T_w)=50^{\circ}\text{F}$	
		$z = 3''$	$z = 6''$	$z = 3''$	$z = 6''$
Water	$\sigma = 0.04$	0.22	0.18	1.2	1.0
Mercury	$\sigma = 1.0$	0.37	0.31	2.1	1.7
	$\sigma = 0.1$	7.0	5.9	39.5	33.2
Sodium	$\sigma = 1.0$	0.52	0.44	2.9	2.5

It is seen that for water with $\sigma = 0.04$, $(T_v - T_s)$ is small compared to $(T_v - T_w)$; for mercury it is small if $\sigma = 1$, but of the same order of magnitude if $\sigma = 0.1$; while for sodium if σ is assumed to have the maximum possible value of unity, $(T_v - T_s)$ is small but not negligible compared to $(T_v - T_w)$. The fact that for some cases $(T_v - T_s)$ is calculated to be greater than $(T_v - T_w)$ is of no consequence.

We may conclude from the above calculations that under some circumstances, $(T_v - T_s)$ may not be negligible compared to $(T_v - T_w)$. Also, an examination of equation (4) reveals that these circumstances are more likely to occur with liquid metals because of their high thermal conductivities and higher saturation temperatures for the same pressure as compared to other fluids with higher Prandtl numbers.

A Modified Form of Nusselt's Theory taking Account of the Resistance at the Vapor-Liquid Interface.

A theory which relaxes the assumption that the vapor-liquid interface is at saturation temperature, can now be developed. It is formulated along exactly the same lines as Nusselt's classical theory. The sole modification consists in utilizing equation (2) to express the unknown temperature T_s in terms of the saturation temperature, T_v . The following differential equation is obtained:

$$\frac{d^2 \delta^+}{d z^{+2}} = \frac{\pi_I \pi_{III}}{\pi_{II}^2} \cdot \frac{1}{\delta^{+6}} - \frac{24}{5 \pi_{II}} \cdot \frac{1}{\delta^{+4}} \cdot \frac{d\delta^+}{dz^+} - \frac{\pi_{III}}{\pi_{II}} \cdot \frac{1}{\delta^{+3}} \frac{d\delta^+}{dz^+} - \frac{2}{\delta^+} \left(\frac{d\delta^+}{dz^+} \right)^2 \dots (5)$$

where

$$\delta^+ = \text{non-dimensional film thickness} = \delta/L$$

$$z^+ = \text{non-dimensional distance along condenser} = z/L$$

$$\pi_I = \frac{C_p (T_v - T_w)}{\lambda}$$

$$\pi_{II} = \frac{g \rho^2 L^3 C_p}{\mu k}$$

$$\pi_{III} = \frac{24}{5} \left(\frac{\sigma}{2 - \sigma} \right) \left(\frac{2}{\pi} \right)^{1/2} \left(\frac{M}{R} \right)^{3/2} \cdot \frac{\lambda^2 P_v}{T_v^{5/2}} \cdot \frac{L}{k}$$

π_I and π_{II} are familiar numbers from Nusselt's theory. π_{III} is a new non-dimensional number introduced because of the thermal resistance at the interface. The deviation of the present theory from Nusselt's classical theory depends upon the value of π_{III} . For high values of the order of 10^5 or more (which is the case for saturated steam at atmospheric pressure), the deviation is negligible. As π_{III} decreases, the deviation from the classical theory increases.

If we now define two Nusselt numbers based on the overall temperature drop ($T_v - T_w$) and on the temperature drop across the film ($T_s - T_w$) as follows:

$$Nu_1 = \frac{l}{k(T_v - T_w)} \int_0^L (q/A)_z \cdot dz \quad \dots (6)$$

$$Nu_2 = \frac{l}{k} \int_0^L \frac{(q/A)_z}{(T_s - T_w)} \cdot dz \quad \dots (7)$$

then we can state that

$$\left. \begin{array}{l} Nu_1 \\ Nu_2 \end{array} \right\} = f(\pi_I, \pi_{II}, \pi_{III}) \quad \dots (8)$$

In Nusselt's classical theory, since the resistance at the liquid-vapor interface is neglected, $Nu_1 = Nu_2$.

The differential equation (5) can be simplified for low values of π_{III} (up to about 10^2) by an order of magnitude analysis to yield the explicit solution

$$Nu_1 = \frac{5\pi_{III}}{8} \left\{ \frac{1}{3} - \frac{5\pi_{III}}{96} \left(\frac{5\pi_I \pi_{III}}{8\pi_{II}} \right)^{1/3} \right\}$$

$$Nu_2 = \frac{3}{2} \left(\frac{8\pi_{II}}{5\pi_I \pi_{III}} \right)^{1/3}$$

For higher values of π_{III} (between approximately 10^2 and 10^5) for which the solution has moved towards Nusselt's solution but has not merged with it, the differential equation can still be considerably simplified, but a numerical solution is necessary.

Fig. 3 shows the calculated variation of Nu_1 and Nu_2 with π_I . The parameter π_{III} has been varied by factors of 10 to obtain a set of curves, while the parameter π_{II} has been held fixed. The particular value (6.1×10^{10}) of π_{II} for which the curves are plotted, corresponds to the conditions of our experimental set-up (the case of mercury condensing on a vertical surface 6 in. long).

It is obvious that a comparison between any data point obtained from experiment and the present theory requires a knowledge of the value of π_{III} . This in turn requires the value of σ , which is in fact an unknown quantity. However, in any given system where condensation is continuously taking place, it seems reasonable to expect that σ attains a certain steady value. In our experiments, therefore, we intend to run a continuous series of tests varying the parameter π_I . It is hoped that the experimentally measured values of Nu_1 and Nu_2 will match the theoretical values for one particular value of σ .

In the following table, values of π_{III} have been calculated for mercury over a wide range of saturation pressures with $\sigma = 0.1$ and $L = 6$ in. These values in conjunction with Fig. 3 give an estimate of the Nusselt numbers expected in the experiments.

Saturation pressure P_v (in m.m.)	Non-dimensional parameter π_{III}
760	7570
400	4580
200	2640
100	1500
10	220

It may be mentioned that a more approximate theory which applies equation (2) in an overall fashion over the whole length of the condenser and utilizes Nusselt's solution for the film drop ($T_g - T_w$), yields results which are in close agreement with the above theory.

IV. EXPERIMENTAL PROGRAM

The apparatus, which will be used to test the theory, has just been assembled and operated. However, due to various difficulties, no quantitative data has been obtained as yet.

Basically the apparatus (Fig. 4) is a closed boiler-condenser system made of stainless steel 304. Mercury is being used as the working fluid. The condenser is a vertical nickel tube, 3/4 in. O.D., 6 in. long, on which the nature of the condensation is observed through vycor windows mounted in the walls of the test chamber. Water is the cooling liquid.

Determination of Nu_1

Of the quantities involved in the definition of Nu_1 (equation 6), $\int_0^L (q/A)_z \cdot dz$ is determined by measuring the flow rate of the cooling water and its rise of temperature. T_v is measured directly. T_w is determined from a precise measurement of the electrical resistance of a section of the nickel tube. This measurement yields the average temperature of the condenser tube. T_w can be calculated from this since the heat flux through the condenser tube is known.

Determination of Nu_2

Because of the high thermal conductivity of liquid metals, it is justifiable to assume that the temperature variation across the condensate film is linear. Equation (7) which defines Nu_2 , can therefore be put into the following form:

$$Nu_2 = \int_0^L \frac{1}{\delta} dz$$

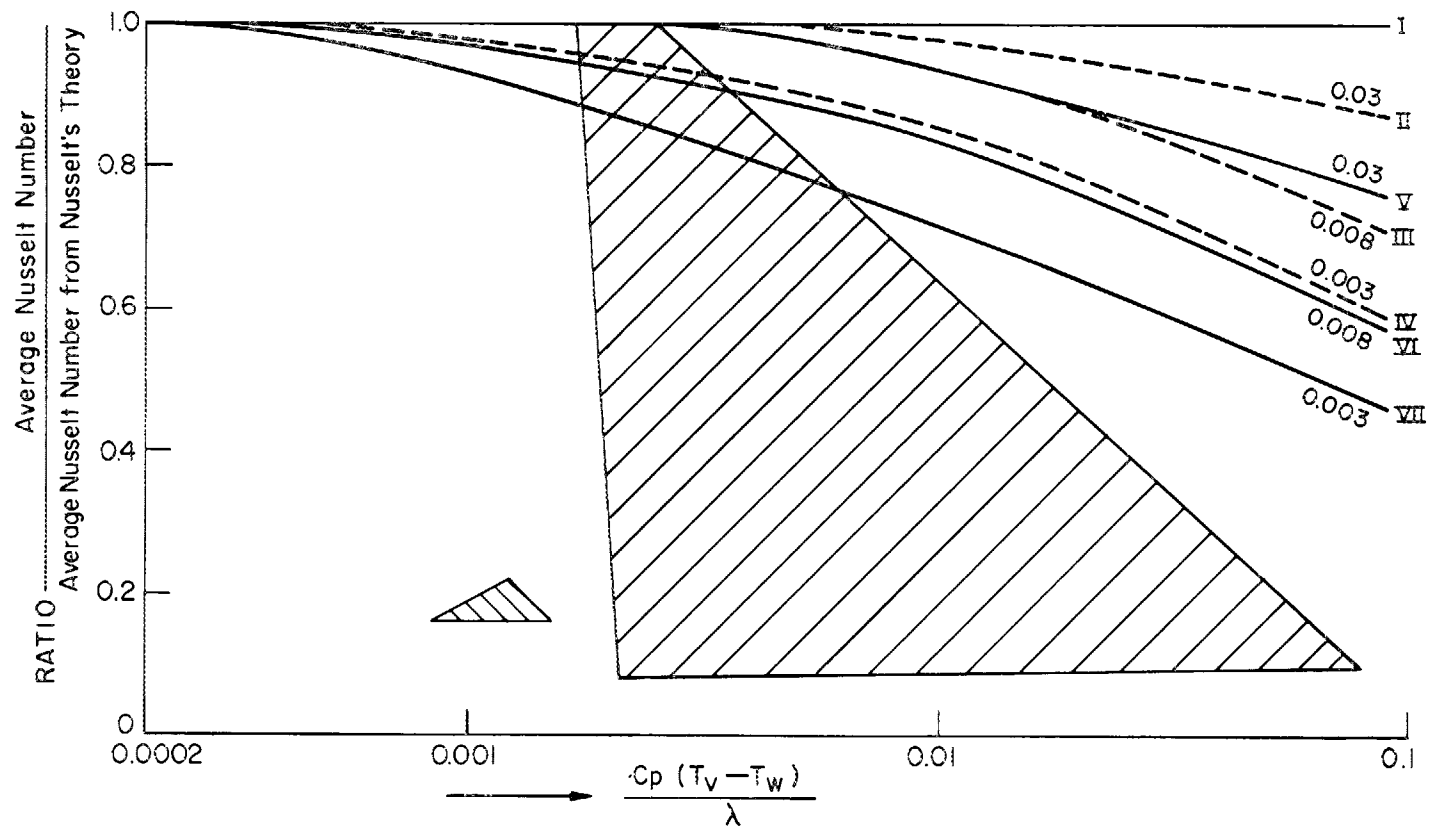
The film thickness δ is being measured by a gamma ray attenuation technique. The gamma rays are emitted by a 2 mc Co^{57} source. They pass through the walls of the test chamber, the mercury condensate film and the walls of the nickel tube before being picked up on the other side by a detector consisting of a NaI crystal and a photo-multiplier tube. The Co^{57} source and the detector can be traversed vertically, so that the film thickness along the length of the condenser tube can be measured. The technique is sensitive to variations of 0.001 in. in the mercury film thickness.

V. REFERENCES

1. Misra, B., and C. F. Bonilla, Chem. Eng. Progr. Symposium, Series No. 18, 52, 7, (1956).
2. "Alkali Metals Boiling and Condensing Investigations;" Qtr. Report 1 covering July 1, 1962 through Sept. 30, 1962, Ctr. NAS 3-2528, MSD, General Electric Co.
3. Nusselt, W., Zeitsch.d.Ver.deutsch Ing., 60, 541, (1916).
4. Seban, R. A., Trans. ASME, 76, 299, (1954).
5. Bromley, L. A., Ind. and Eng. Chem., 44, 2966, (1952).
6. Rohsenow, W. M., Trans. ASME, 78, 1645, (1956).
7. Sparrow, E. M., and J. L. Gregg, Trans. ASME, Series C, 81, 13, (1959).
8. Mabuchi, I., Trans. Japan Soc. Mech. Engrs., 26, 1134, (1960).
9. Chen, M. M., Trans. ASME, Series C, 83, 48, (1961).
10. Koh, C. Y., E. M. Sparrow and J. P. Hartnett, Int. Journal Heat and Mass Transfer, 2, 69, (1961).
11. Koh, C. Y., Trans. ASME, Series C, 83, 359, (1961).
12. McAdams, W. H., "Heat Transmission," McGraw-Hill.
13. Dukler, A. E., Chem. Eng. Progr. Symposium, Series No. 30, 56, 1, (1960).
14. Schrage, R. W., "A Theoretical Study of Interphase Mass Transfer;" Columbia University Press, New York, (1953).
15. Knudsen, M., Ann. Phys., Lpz., 47, 697, (1915).

VI. SYMBOLS

C_p	liquid specific heat
g	gravitational constant
k	liquid thermal conductivity
L	length of condenser
m	rate of condensation per unit area
M	molecular weight
Nu	Nusselt number from Nusselt's theory
Nu_1	Nusselt number based on overall drop ($T_v - T_w$)
Nu_2	Nusselt number based on drop across film ($T_s - T_w$)
P_v	pressure in vapor space
$(q/A)_z$	heat transfer rate per unit area at distance z
\bar{R}	universal gas constant
T_v	saturation temperature corresponding to P_v
T_w	wall temperature
T_s	temperature of liquid at liquid-vapor interface
z	distance along condenser
z^+	defined by z/L
δ	condensate film thickness
δ^+	defined by δ/L
ρ	liquid density
λ	latent heat of vaporization
μ	liquid viscosity
σ	condensation coefficient (fraction of molecules striking vapor-liquid interface and condensing).



Investigator	Curve No.	Investigator	Curve No.
Nusselt	I (for all Pr Numbers)	Chen	I (Pr > 0.5)
Rohsenow	I (" " " ")	Koh, Sparrow, Hartnett	V (Pr = 0.03)
Sparrow, Gregg	I (Pr > 0.5)	Koh	VI (Pr = 0.008)
Mabuchi	II (Pr = 0.03)		VII (Pr = 0.003)
	III (Pr = 0.008)	Misra, Bonilla	{
	IV (Pr = 0.003)		{ // Mercury data Pr ≈ 0.016
			{ // Sodium data Pr ≈ 0.005

FIGURE 1

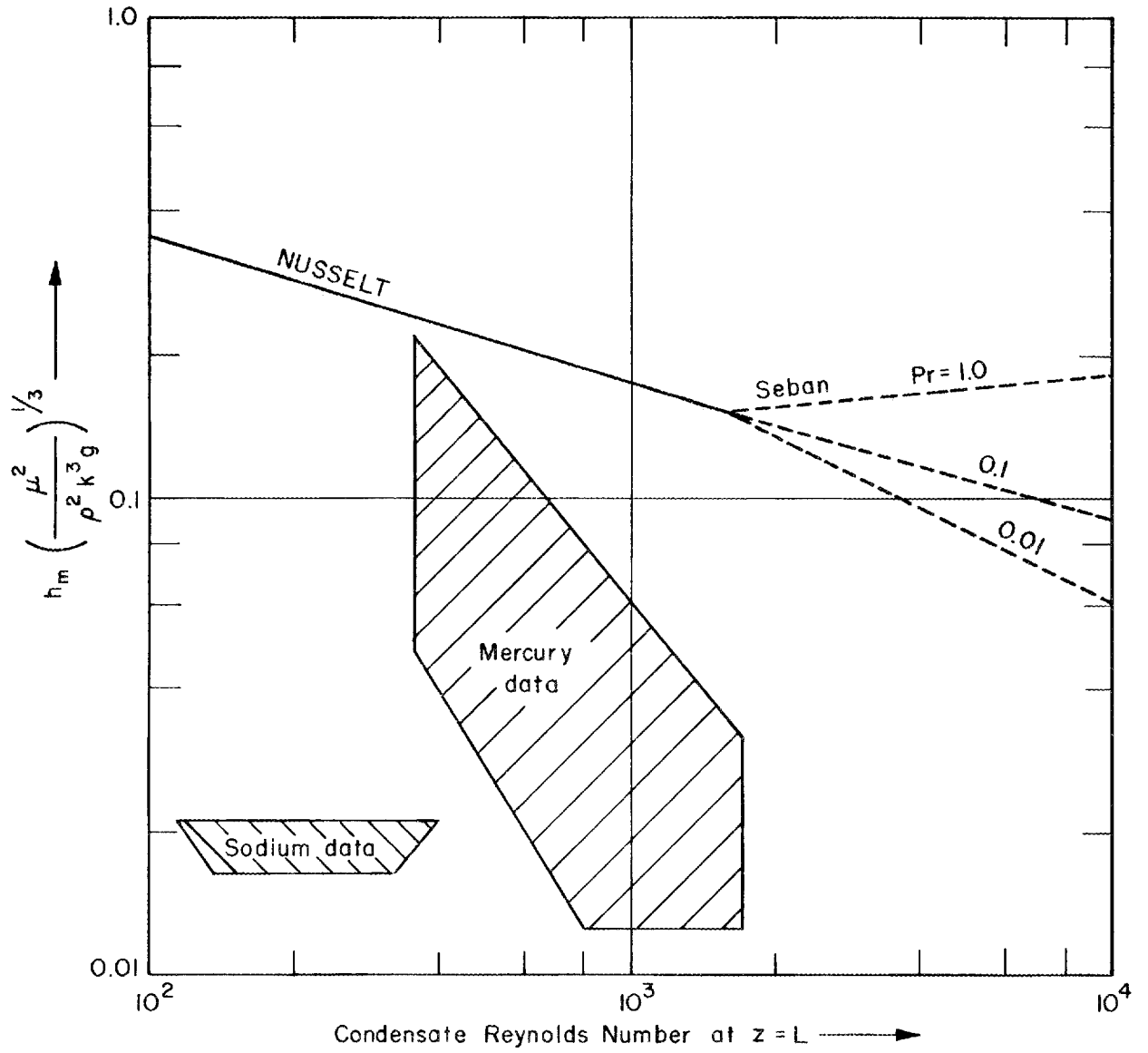


FIGURE 2

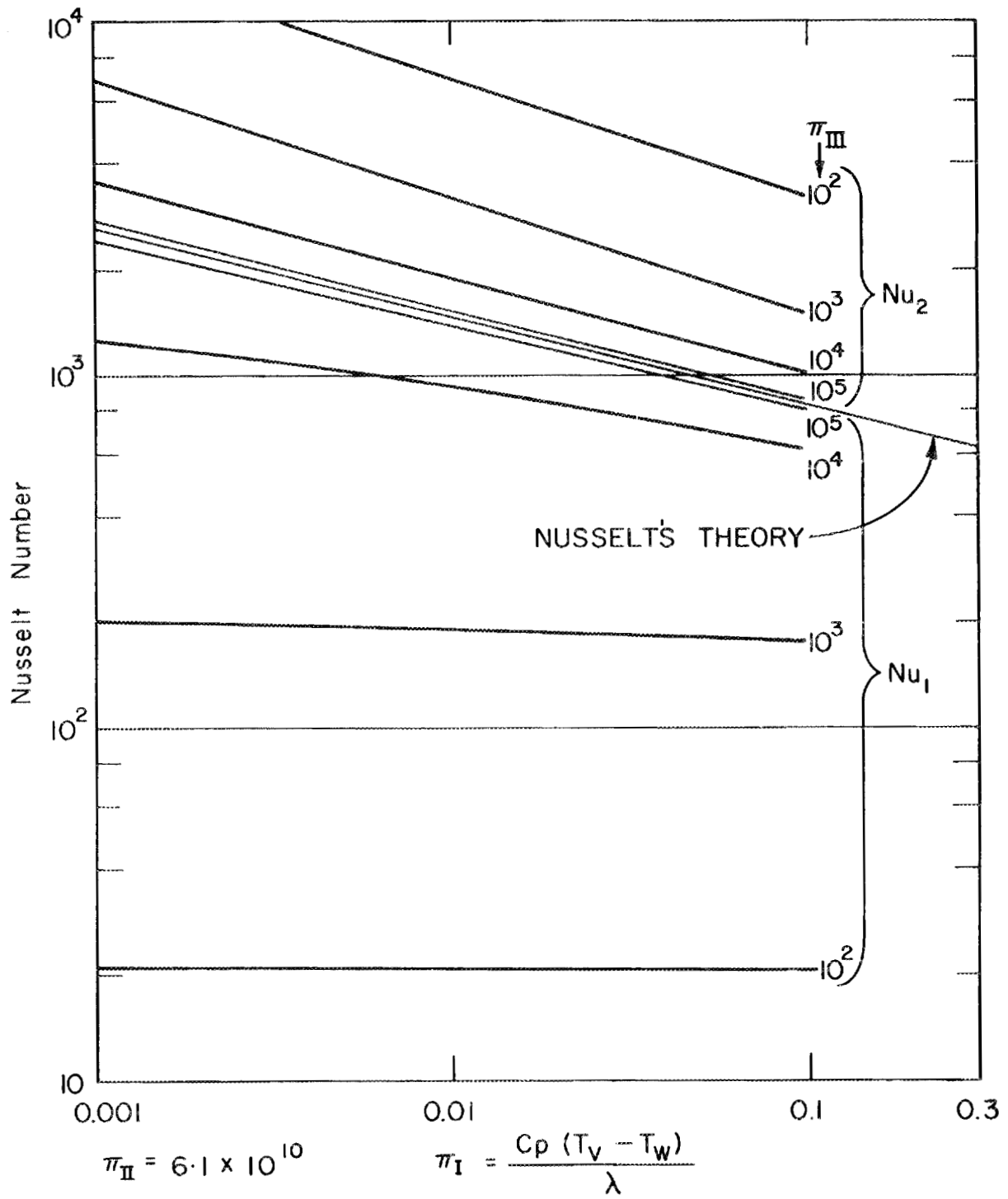


FIGURE 3

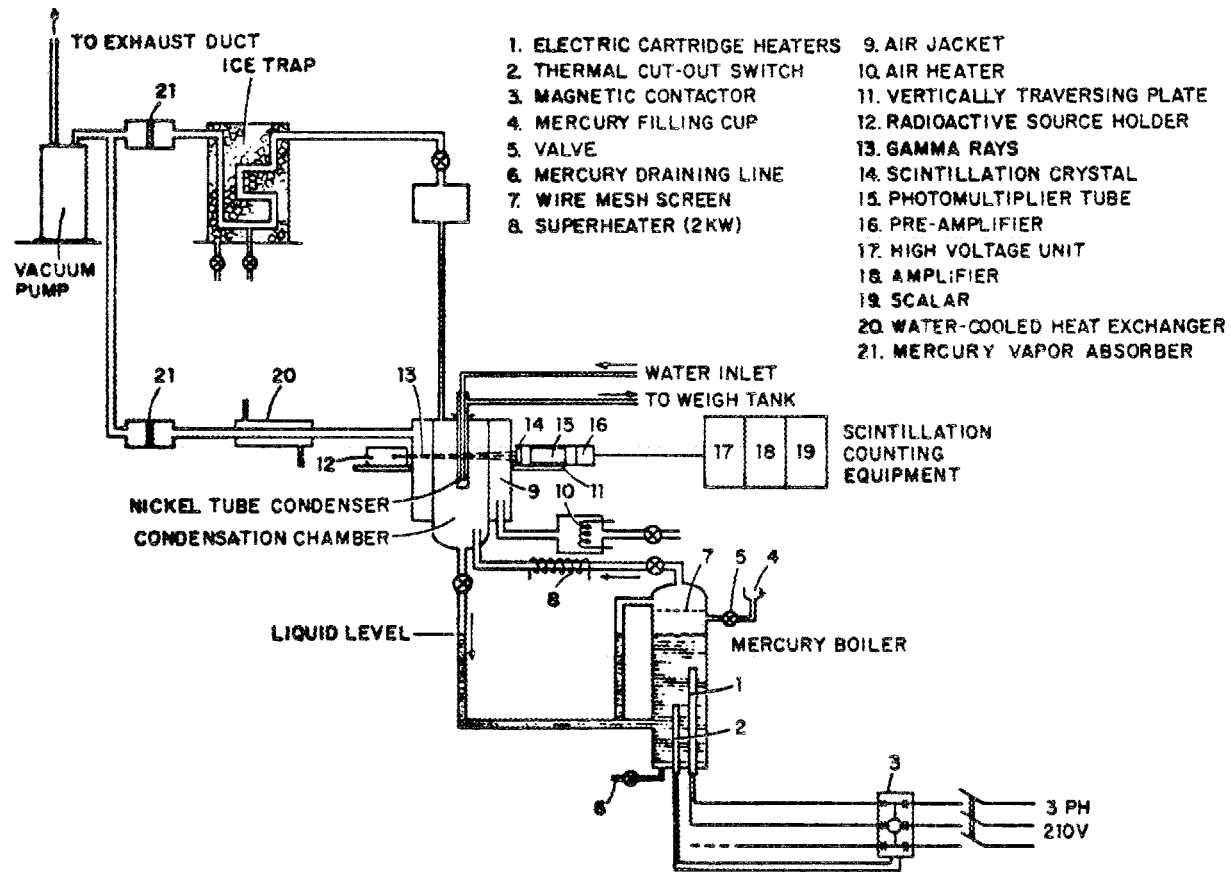


FIGURE 4 SCHEMATIC DIAGRAM OF APPARATUS

DISCUSSION

MR. BONILLA: I don't recall exactly what was in the paper; but if it isn't here, then it is in his full dissertation. We considered this effect, and we found that it helped at the lowest pressures.

We did not use a condensation coefficient other than 1 because - you have your arguments in the paper - it just didn't seem to us that it could possibly be below for the beautifully, self-cleaning surface that you would have to have there with no inert gas present. Well, it brought the low pressure data right up to the Nusselt theory, while the other data was hardly changed at all. In other words, if you got up to atmospheric pressure, it would have hardly any effect. The reason we didn't calculate a sigma for every point was that we were confident we would get a wide range, 10^{-6} maybe, for some of the points.

However, as I recall, that we did have this thought - that at a high rate of condensation, high q/A , you have quite a little torrent of condensate running down. You can assume then that the surface is completely covered with condensate; and, therefore, that some kind of condensation coefficient, presumably 1, would be applicable. But if you have a low rate of condensation, unless you had a wetted surface, there will be drop-wise condensation; and the phenomenon would be more complex.

MR. ROHSENOW: Is this a mixture of drop and film?

MR. BONILLA: Yes, it would be droplets running down. That's what I am sure you would get, unless it was stainless steel and mercury. With nickel we got nice, continuous drops.

MR. ROHSENOW: We are hoping nickel will be our salvation here. On page 11 of our paper we have a table showing the values for the influence of pressure on π_3 for a Σ of 0.1. It is quite significant.

MR. BERENSON: I would think that an annular flow vaporization, which is essentially the reverse of this process, would have the same kind of effect coming in. I guess this is what Kurt Goldman was alluding to earlier. Where you would have to have an excess of the interface temperature over the saturation temperature, in order to drive the vapor away from the interface. This also might be more important in liquid metals.

MR. ROHSENOW: This is possible. The condensation coefficient on evaporation is a little more difficult to see. Once you form vapor, how are you going to have an accommodation coefficient any more?

MR. BERENSON: In that case maybe the accommodation coefficient would be only 1. Knudson calculated vapor pressure in this way: By considering a vapor flowing toward the surface in balance with the molecules leaving the surface, and he found with mercury that many people's lives had been saved because the mercury surface was dirty.

MR. GOLDMAN: Since I am out in left field anyhow, let me go a little further and say that perhaps here, too, you get condensation starting in your vapor region, so that you actually start bunching molecules together and forming droplets in the region which you described as a falling-off temperature, between T/S and T/W , so that you have droplets falling onto that liquid film rather than just molecules getting there.

MR. ROHSENOW: It's possible.

MR. POPPENDIEK: Warren, someone told me the other day that Penner wrote a paper on prediction of accommodation coefficients for liquid systems, not for solid systems. And I think the outcome was that for most liquids, the value was very high. Very near unity. I was wondering if you had seen that paper on liquid. I haven't seen it myself.

MR. ROHSENOW: I haven't seen it; no.

MR. POPPENDIEK: He was going back to the old point that maybe not all liquid surfaces are dirty, and maybe they are higher than we think. But it may be something to look at.

MR. ROHSENOW: We will get after that and get ahold of it.

MR. SAMUEL: With respect to this condensation thing, has this particular condenser ever been pre-wetted with mercury?

MR. ROHSENOW: No. How do you do this?

MR. SAMUEL: The first time you put liquid metal through the pipes, if it is not wet, the pump is not pumping properly. Simply put an acetylene torch on the outside of that until it gets red hot. Once wetted it remains wetted from then on.

MR. ROHSENOW: Great. Thank you. We know that time in operation is supposed to cause the liquid to wet the surface, but if we can accelerate that process, that's fine.

MR. BONILLA: This π_3 , what is the significance to these numbers? Is it how much it deviates from ten times pressure?

MR. ROHSENOW: π_3 represents the influence of the interface resistance.

MR. BONILLA: From looking at this table, can you show a predicated significance?

MR. ROHSENOW: No. You have to go back to the results curve in a later figure. What we had on the curve were decades, and this goes through more than a decimal point.

What we are really saying here is that for liquid metals this effect is more pronounced at any accommodation coefficient than it is in non-liquid metals, and we believe it is worth studying. In any event, we are going to try to make some careful measurements, and maybe even gunk up the system intentionally to see what happens.

LIQUID METAL JET CONDENSERS

Lance Hays¹

An investigation of jet condensers using mercury as a working fluid was concluded. The application which motivated this work was the use of this component as a vapor condenser in space dynamic power systems. Advantageous features such as high condensation rates, positive vapor-liquid separation, simple start-up, and significant conversion of vapor thermal energy to condensate mechanical energy were demonstrated and are discussed herein. Simplified expressions for momentum exchange and heat transfer were obtained and are used to correlate experimental results obtained with mercury, and to indicate trends of performance available with variations in geometric and fluid parameters.

NOMENCLATURE

The following nomenclature is used in the paper:

- A = area, sq ft
 A_1^o = area ratio of injector to tube inlet
 A_2^o = area ratio of injector to throat
 A_{th}^o = area ratio of throat to tube inlet
 C_d = discharge coefficient
 C_p = specific heat of liquid, BTU/lb^oF
 d = diameter, ft
 g = constant = 32.2, (lbm/lbf)(ft/sec²)
 h_{fg} = heat of vaporization, BTU/lb
 H_j = jet condenser ideal power output, kw
 H'_j = $(1 - 1/\Delta P_\ell^o)(\Delta P_v^o/m_R)$
 K_d = diffuser loss coefficient
 L = length, ft, in
 \dot{m}^o = mass flow rate, lb/hr
 m_R^o = ratio of injected liquid mass flow to vapor mass flow (saturated vapor flow for quality less than unity)
 m_R^{*o} = mass flow ratio for $T_{\ell e} = T_{vo}$

¹Engineer, Electro-Optical Systems, Inc., Pasadena, California.

Presented at the Third Annual High Temperature Liquid Metal Heat Transfer Technology Conference, Oak Ridge, Tenn., 4 September 1963

- P = pressure, psi(a)
 ΔP_a = pressure rise from jet condenser inlet to outlet, psi(d)
 ΔP_i = pressure drop across injector, psi(d)
 $\Delta \beta_l$ = ratio of pressure rise, ΔP_a , to dynamic pressure of injected liquid
 $\Delta \beta_v$ = ratio of pressure rise, ΔP_a , to dynamic pressure of inlet vapor flow
 $\Delta \beta_{th_l}$ = ratio of pressure rise from inlet to throat to dynamic pressure of injected liquid
 $\Delta \beta_{th_v}$ = ratio of pressure rise from inlet to throat to dynamic pressure of inlet vapor flow
 Q_R = heat rejected to liquid jet from condensing vapor, BTU/hr
 r = radius, ft
 Re = Reynolds number
 T = temperature, time, °F, sec
 ΔT_{sc} = outlet subcooling = $T_{vo} - T_{le}$, °F
 ΔT_R = "radiator" temperature drop = $T_{le} - T_{lo}$, °F
 V = velocity, ft/sec
 \bar{V} = ratio of inlet vapor velocity to injected liquid velocity
 x = distance, ft, in
 x_{vo} = inlet vapor quality
 α = angle, thermal diffusivity, ($^\circ$), ft²/sec
 α_t = turbulent diffusivity for heat, ft²/sec
 μ = μ^{th} characteristic root of Bessel's Function, J_0
 η_a = ratio of measured to calculated pressure rise
 η_i = ratio of ideal to actual injector pressure
 ρ = density, lb/ft³
 $\bar{\rho}$ = ratio of liquid to vapor densities
 τ_w = wall shear stress, lb/ft²
 ϕ = stream potential, ft²/sec
 χ = jet utilization factor = $(T_{le} - T_{lo}) / (T_{vo} - T_{lo})$
 ψ = heat transfer parameter = $\chi V_{lo} / V_R$

Subscripts

o = inlet of jet condenser, station number
1 = throat of jet condenser, station number
2 = outlet of jet condenser, station number
b = bulk, boundary
c = condensation
(calc) = calculated
d = diffuser
e = Exit, outlet of jet condenser
i = injector
j = jet
l = liquid
m = mixed
R = Relative
s = saturated conditions
t = tube
v = vapor
w = wall

INTRODUCTION

The majority of dynamic space power systems currently under development utilize direct condenser-radiators as the heat rejection component. However, problems of startup, system ground testing, two phase flow in a zero-gravity environment, and multi-tube instability, have resulted in serious interest in the application of indirect condensers (1, 2)². Moreover, the role of indirect condensers in space will become much more prominent as power systems in the megawatt class are developed. For these large power levels, the problems associated with startup and stability of direct condenser-radiators

²Numbers in parentheses refer to the Bibliography at the end of the paper.

may become more severe. Also, preliminary analyses indicate significant weight savings are probable using an indirect condensing system (3 and 4).

In the indirect type of condenser, vapor is first condensed in a jet condenser or compact heat exchanger-condenser, and the heat released by condensation is subsequently rejected in an all-liquid radiator. A schematic of one type of indirect condensing system employing the jet condenser is shown in Figure 1.

In the jet condenser, subcooled liquid working fluid is injected into the vapor stream. Physical mixing of vapor and liquid, and subsequent condensation of the vapor occur within a relatively short distance downstream of the region of injection. The resulting condensate-liquid flow circulates through a liquid radiator where the heat absorbed by condensation is rejected. Part of the resulting subcooled liquid is bypassed and injected into the jet condenser. The remainder is returned to the boiler to complete the flow cycle.

The jet condenser component is very compact relative to a direct condenser-radiator or a heat exchanger condenser. Moreover, this unit may provide significant pressure augmentation to circulate the liquid in the liquid-radiator loop. In particular, for steady-state operation, if the pressure rise in the jet condenser ($\Delta P_a = P_a - P_v$) is equal to the sum of the injection pressure drop ($\Delta P_i = P_i - P_v$), the liquid radiator pressure drop ($\Delta P_{LR} = P_a - P_o$), and the total line-pressure drop ($\Delta P_t = P_o - P_i$), no external pressure boost would be required during steady-state operation to circulate the injected liquid flow.

Jet condensers have previously been used in small steam power plants, for boiler feed water circulation (in place of a rotating pump) and for several process applications (5, 6, 7). In addition, use has been made of the basic momentum exchange process for steam ejectors (7) and to provide thrust and control turbine back pressure in torpedo powerplants (8, 9). However, none of the above applications

has resulted in published information which is suitable to determine the required performance characteristics of jet condensers when used with liquid metals. As a consequence, the current investigation was initiated to determine jet condenser performance characteristics with a liquid metal, mercury, as a test fluid. The primary objective of the program was to obtain experimental data suitable for preliminary design of a jet condenser in a mercury Rankine cycle power system.

THEORETICAL FLOW AND ANALYSIS

Schematic illustrations of two types of jet condensers are presented in Fig. 2. Many possible variations of injector, mixing chamber, and throat geometry exist. However, this figure presents two simple geometries, constant area and variable area, similar to those investigated on this program.

Vapor flows from left to right and enters the condenser at Station 0. At that location subcooled liquid is also injected in the form of a central jet. Vapor and liquid flow concurrently through a mixing chamber with simultaneous mass transfer, heat transfer and momentum exchange occurring. Finally, with sufficient heat exchange between vapor and subcooled liquid, at some location within a throat (or the mixing chamber) complete condensation of the vapor will occur.

Condensation Mechanisms

The transport of vapor from the main flow stream to the subcooled liquid jet is primarily a result of the pressure difference from the main vapor stream to the subcooled liquid boundary. For a free boundary with no net mass transfer, the vapor pressure at the boundary must be in equilibrium with the saturation pressure of the liquid phase (neglecting surface tension effects). That is:

$$P_{vb} \approx P_{lb} \approx P_s(T_{lb}) \quad (1)$$

Very strong pressure gradients within the vapor are likely to occur at the initial location of injected liquid. Here, the liquid is at the lowest temperature in the mixing chamber and the

corresponding saturation pressure is lowest. Thus a rather strong interaction with the vapor flow and correspondingly, high initial condensation rates are possible. The maximum vapor flow rate which can be condensed on the jet at this point is determined by the jet area and the sonic velocity of the vapor (10). However, as vapor is condensed on the jet, the heat released by condensation results in raising the jet temperature and liquid saturation pressure. Hence the pressure difference between the main vapor stream and the liquid jet is reduced, and the flux of vapor to the jet decreases.

An increase in the temperature of the liquid jet at the surface (which tends to reduce the condensing vapor flux) will result as the bulk or mixed cup temperature of the jet increases due to heat addition from the condensing vapor. A temperature gradient within the jet is required to remove the heat of condensation released at the surface; thus the surface temperature will be greater than the bulk temperature for heat transfer into the jet.

These effects are illustrated in Fig. 3, an idealized representation of the vapor and liquid temperature gradients at different axial locations in the mixing chamber. The initial temperature field (at 0) consists of a large local temperature (and pressure) gradient in both the vapor and liquid near the interface. However, as heat is transferred, due to condensing vapor, the bulk temperature, T_j , is raised and the temperature gradient within the liquid phase decreases. The temperature at the jet surface, $T_{\ell b}$, is increased as the vapor temperature gradient decreases. Finally, as complete condensation of the vapor is approached, the bulk temperature of the fluid approaches its final value. The difference in free stream vapor pressure, P_{v0} , and the saturation pressure for the bulk temperature, $P_s(T_j)$, may still be a significant quantity. However, the surface temperature of the jet, $T_{\ell b}$, must be greater than the bulk temperature, T_j , to transfer heat to the interior. Therefore, the

local vapor pressure difference, $P_{vo} - P_s(T_{lb})$, may be very small with resulting low values of local condensation rate.

Pressure Distribution and Interface Formation

The condensation of vapor upon the liquid jet produces a sizeable conversion of thermal energy to mechanical energy (pressure or velocity head). This conversion process has been demonstrated both by analysis and experiments (9, 17). The question may then be raised as to what effect the addition of this mechanical energy has upon the shape and character of the injected liquid. Moreover, what force mechanisms are present to produce all-liquid flow at the outlet when stratified vapor-liquid flow occurs upstream?

Qualitative answers to both questions may be postulated by considering the momentum exchange process, previous work on the stability of jets, and previous internal measurements made across vapor-liquid interfaces.

For the case of a jet condenser with a central liquid jet, the following steps in the formation of the final interface are postulated and are illustrated by Fig. 4.

1. At the point of injection, rapid condensation upon the liquid jet occurs. This results in a negative radial liquid pressure gradient, which in turn results in a reduction in the jet radius and produces surface waves which may or may not be amplified by the interaction of the vapor stream with the surface (Station 1).

2. As condensation on the jet occurs, the jet temperature increases in the axial direction, suppressing condensation in the downstream regions.

3. As lower condensation rates occur, the liquid surface pressure is reduced to be more nearly equal to the vapor pressure, due to the decrease in the flux of vapor momentum received by the jet. This results in the establishment of a positive radial pressure gradient in the liquid (Station 2).

4. The positive radial pressure gradient in the liquid results in a radial flow component in the liquid which tends to reduce the vapor flow area and fill the condenser flow passage.

5. When the passage is filled, the walls result in the establishment of a uniform radial pressure profile within the liquid.

It should be noted that the jet profile sketched in Fig. 4 was taken from a single frame of Fastax motion pictures (8000 frames per second) taken of a jet condenser operating with mercury.

The high heat transfer rates and large pressure gradients (relative to condensation on a wall) occurring in jet condensers, result in a final separation of the vapor and liquid which is not strongly influenced by gravity body forces. This is particularly true if the final expansion of the jet required to fill the flow passage is small. The positive separation results in single phase flow out of the mixing section or throat. Therefore, effects of the increase in mechanical energy of the liquid can be treated in a conventional manner downstream of the interface.

Analysis of Heat Transfer into Jet

Several complex mechanisms occur during condensation of the vapor on a subcooled liquid jet. In order to provide a guide for testing and to obtain information on the important variables, an analysis was performed to identify the possible limiting resistance in the heat transfer process, i.e.: the conduction and convection, into the interior of the subcooled liquid phase, of the heat released at the liquid-vapor interface.

The model considered for analysis assumes the liquid phase exists as a solid cylinder with a constant radius, r_0 , which is injected into the vapor at a constant velocity $V_{\rho 0}$. The vapor temperature, (T_{v0}) , is assumed to remain constant throughout the mixing chamber. With these assumptions, it is then possible to write an expression for the rate of heat conduction and convection into the interior of the liquid. Details of this analysis are

summarized in Ref. 4. Equation 2 expresses the results:

$$\chi = \frac{T_{\ell e} - T_{\ell o}}{T_{vo} - T_{\ell o}} = \sum_{\mu=1}^{\mu=\infty} \frac{4}{\beta_{\mu}^2} \left[1 - \frac{1}{\beta_{\mu}^2} \frac{V_{\ell o} r_{\ell}^2}{L_c (\alpha + \alpha_t)} \right] \left[1 - \exp \left(- \frac{\beta_{\mu}^2 L_c (\alpha + \alpha_t)}{V_{\ell o} r_{\ell}^2} \right) \right] \quad (2)$$

In this expression, the temperature of the liquid at the exit, $T_{\ell e}$, is related to initial conditions of the jet and vapor ($T_{\ell o}$, T_{vo} , $V_{\ell o}$, r_{ℓ}), to the properties of the flow (α and α_t), and to the distance traversed by the jet (L_c).

Equation 2 is plotted in Fig. 5 as the residence time (of the liquid jet in vapor) required for heat transfer vs the jet utilization factor (or nondimensional temperature) of the liquid jet. Curves are presented for different values of the ratio of the total heat diffusivity to the square of the jet radius. Several interesting features may be determined by examining the curve.

1. Operation of the jet condenser with the final liquid temperature equal to vapor temperature would result in an infinite distance required for condensation of the vapor flow rate (for a finite liquid velocity).

2. Increasing contributions of eddy heat transfer to the total heat transfer result in much shorter condensation distances (or jet residence time) for a given value of jet utilization factor.

3. For a given value of jet utilization factor and total heat diffusivity, lower jet velocities result in shorter condensation lengths. Attempts to operate with extremely high jet velocities would result in longer condensation lengths.

4. Decreasing values of jet radius, for a constant value of total heat diffusivity, result in shorter condensation lengths (for a given value of jet velocity and jet utilization factor).

5. Relatively short lengths of times are required to attain given jet utilization factors for reasonable values of diffusivity factors. For example, for a diffusivity factor of 50, a jet utilization factor of .8 is obtained after about 0.02 seconds. Thus, for a jet velocity of 10 ft/sec a condensation distance of .2 ft would be required.

Figure 5 cannot be used directly to predict condensation length due to a lack of information upon the local variation of eddy diffusivity for heat, α_t , (cf EXPERIMENTAL RESULTS) and because the jet radius and vapor temperature at the jet surface are somewhat different than parameters assumed for the calculation. However, the results indicate the major trends of condensation length with jet utilization factor and also provide information of the important variables of the problem.

Constant Area Pressure Rise Analysis

The geometry of Fig. 2a was treated in an analysis which is summarized in Ref 17. The equation for conservation of momentum was applied to a control volume about the condenser. The analysis rests upon the following assumptions:

1. The radial pressure gradient at the inlet and outlet stations is zero.
2. Flow at the exit is homogeneous and in thermal equilibrium.
3. For an inlet vapor quality less than unity, no vapor-liquid slip exists in the entering flow.
4. Wall friction within the mixing chamber is negligible compared to the magnitude of the pressure rise.
5. An injector discharge coefficient of unity is assumed.

The final expressions of the analysis were further simplified by considering complete condensation of the inlet vapor flow and by assuming an inlet vapor quality of unity. For these assumptions, the following equations were derived:

$$\Delta P_v^0 = 2 \left[\left(\frac{m_R^0}{\rho} \right)^2 \frac{(1-A_2^0)^2}{A_2^0} + (1 - A_2^0) \right] - \frac{2(1-A_2^0)^2}{\rho} (m_R^0 + 1)^2 \quad (3)$$

$$\Delta P_\ell^0 = 2 \left[A_2^0 + \left(\frac{\rho}{m_R^0} \right)^2 \frac{A_2^0}{(1-A_2^0)} \right] - 2A_2^0 \left(1 + \frac{1}{m_R^0} \right)^2 \quad (4)$$

Equation 3 expresses the ratio of pressure rise to the vapor inlet dynamic pressure (ΔP_v^0) in terms of the mass flow ratio of liquid to vapor (m_R^0), the density ratio of liquid to vapor (ρ), and the area ratio of the injector to tube (A_2^0).

Equation 4, which gives the ratio of pressure rise to the injected liquid dynamic pressure (ΔP_ℓ^0), provides a significant measure of jet condenser performance from the standpoint of pumping requirements. For an optimum design injector with a discharge coefficient of unity, the latter parameter expresses the ratio of pressure rise to the pressure drop required to inject subcooled liquid into the mixing chamber. If ΔP_ℓ^0 were equal to unity, no net pumping power would be required to effect the injection of liquid into the jet condenser. The only power consumption would be that required to circulate the liquid through the lines and liquid radiator. Moreover, if values of ΔP_ℓ^0 higher than unity are obtained, the jet condenser can contribute to pumping the liquid through the radiator loop. These equations are plotted in Figs. 6 and 7 for a range of liquid-vapor mass flow ratios and injector to tube area ratios. Lines of constant vapor to liquid velocity ratio are presented for reference.

The curves were determined for a density ratio of liquid to vapor of 2620, which corresponds to that of mercury vapor at 700°F. From Fig. 6, the following conditions can be seen to favor a high

absolute value of pressure rise (for constant vapor inlet conditions):

a) a low ratio of injector to tube area; b) a high ratio of liquid to vapor flow rate.

For a given mass flow ratio, higher values of inlet vapor velocity result in a higher pressure rise. In addition, from Equation 3, high vapor densities (or a low ratio of liquid to vapor density) also result in high absolute values of pressure rise.

Examination of Fig. 7 reveals that opposite trends result in high values of ΔP_l^0 in some instances. That is, conditions favoring a high absolute magnitude of pressure rise may result in smaller values of the ratio of pressure rise to injection pressure drop. From Fig. 7, the following favor a high ratio of pressure rise to injected liquid dynamic pressure: a) a large ratio of injector to tube area; b) low ratios of liquid to vapor flow rate.

Also, from Equation 4, high values of liquid to vapor density ratio tend to increase ΔP_l^0 .

Relatively large numerical values of pressure rise coefficient can be obtained for some inlet conditions. For the values of mass flow ratio shown in Fig. 6, the pressure rise referred to vapor dynamic pressure attains values as high as 140; i.e., the pressure rise through the condenser would be 140 times that which would be obtained if the dynamic pressure of the vapor alone were recovered.

The main results of the analysis from the standpoint of design trends can be summarized as follows:

1. The non-dimensional parameters in the expressions for pressure rise for constant area jet condensers are: density ratio, mass flow ratio and the ratio of injector area to tube area.
2. High vapor densities and high absolute magnitudes of either inlet vapor velocity or inlet liquid velocity tend to favor high absolute magnitudes of pressure rise.
3. Values of liquid to vapor mass flow ratio and of the area ratio of injector to tube which favor high absolute

magnitudes of pressure rise may result in high pumping power requirements for a constant area jet condenser. If a large pressure rise relative to the pressure drop required for injection is desired, then higher ratios of injector to tube area and low values of liquid to vapor mass flow ratio should be used.

Variable Area Pressure Rise Analysis

Although the above analysis for constant area jet condensers is useful in evaluating experimental performance, the maximum pressure rise potential of jet condensers is not realized in this geometry. A geometry which should produce much higher values of vapor to liquid pressure rise is shown in Fig. 2-b. In this geometry the mixing chamber is contoured to effect condensation with little reduction in the jet velocity at the point of final condensation. Thus, the expansion losses of the constant area geometry are avoided. Moreover, if a diverging section is added for efficient diffusion, the pressure increment added to the vapor should be increased by a large amount over the constant area geometry.

Use of a converging-diverging geometry results in an additional complicating factor in the analysis of pressure rise. Since the mixing chamber geometry has an axial variation of flow area, the integral of the wall pressure must be evaluated in order to apply the conservation equation of momentum. Due to a lack of information for the internal pressure distribution in this region, the validity of the analysis must rest upon whatever assumptions are made as to pressure distribution.

In this section, the general equation for pressure rise is first derived. The case of inlet vapor pressure occurring at the mixing chamber wall is then treated.

In the derivation of the general equation, the following assumptions were made:

1. Liquid pressure equals vapor pressure at Station 0.
2. No heat loss from the condenser wall.

3. Entering vapor quality equals unity.
4. Homogeneous flow within each phase exists at the entrance and exit stations with complete condensation.
5. The radial pressure and velocity gradients at the inlet and outlet are zero.
6. Injector discharge coefficient equals unity.
7. Uniform flow (constant velocity profile) occurs at the entrance and exit.

With these assumptions, application of the conservation equations for momentum, mass and energy from Stations 0 to 2 results in the following expression for pressure rise (Ref. 17):

$$\begin{aligned}
 P_2 - P_0 = & P_0 \left(A_{t0} / A_{t1} - 1 \right) + \frac{\dot{m}_{v0}^2}{g \rho_v A_{t1} (A_{t0} - A_{l0})} + \frac{\dot{m}_{l0}^2}{g \rho_l A_{t1} A_{l0}} \\
 & - \frac{\dot{m}_T^2}{g \rho_l A_{t1}^2} + \frac{\dot{m}_T^2}{2 g \rho_l} \left[\frac{1 - K_d}{A_{t1}^2} - \frac{1}{A_{t0}^2} \right] \\
 & - \tau_w A_w (\cos \alpha) / A_{t1} - \frac{1}{A_{t1}} \int_0^{X_1} P_w \pi d_t \tan \alpha dx \quad (5)
 \end{aligned}$$

Equation (5) expresses the total pressure rise in terms of:

1. Geometry and inlet flow parameters.
2. Two unknown terms which contain properties of the boundary flow, i.e., the shear stress of the vapor on the wall and the internal pressure distribution at the wall.

In order to obtain numerical results, assumptions must be made of the values of the quantities of Item 2. In all cases it is felt that the friction term is small relative to the total pressure rise, (the extremely short condensation distance and high values of pressure rise measured during testing support this simplification). Another assumption which can be used to make Equation (5) more tractable is to use the inlet

vapor pressure as the pressure at the walls of the mixing chamber. This assumption appears to be reasonable in view of internal measurements made by other investigators (9) and because of the saturated state of the vapor.

Results of the analysis carried out for the constant inlet pressure model are presented in terms of the parameters discussed previously: the ratio of pressure rise to injected liquid dynamic pressure, ΔP_{ℓ}° , and the ratio of pressure rise to inlet vapor dynamic pressure, ΔP_v° . Substitution of $P_w = P_{vo}$ into the pressure integral term of Equation (5) and neglecting vapor friction ($\tau_w = 0$) and diffuser losses ($K_d = 0$) results in the following expressions for pressure rise:

$$\Delta P_{thv}^{\circ} = (P_1 - P_o) / \rho_v v_{vo}^2 / 2g = 2 \frac{(1 - \overset{\circ}{A}_2)}{\overset{\circ}{A}_{th}} \left[1 + \left(\frac{\overset{\circ}{m}_R^2}{\overset{\circ}{\rho}} \right) \frac{(1 - \overset{\circ}{A}_2)}{\overset{\circ}{A}_2} - \frac{(\overset{\circ}{m}_R + 1)^2 (1 - \overset{\circ}{A}_2)}{\overset{\circ}{\rho} \overset{\circ}{A}_{th}} \right] \quad (6)$$

$$\Delta P_{th\ell}^{\circ} = (P_1 - P_o) / \rho_{\ell} v_{\ell o}^2 / 2g = 2 \overset{\circ}{A}_1 \left[1 + \left(\frac{\overset{\circ}{\rho}}{\overset{\circ}{m}_R} \right) \frac{\overset{\circ}{A}_2}{1 - \overset{\circ}{A}_2} - \left(1 + \frac{1}{\overset{\circ}{m}_R} \right)^2 \overset{\circ}{A}_1 \right] \quad (7)$$

$$\Delta P_v^{\circ} = (P_2 - P_o) / \rho_v v_{vo}^2 / 2g = 2 \frac{(1 - \overset{\circ}{A}_2)}{\overset{\circ}{A}_{th}} \left[1 + \left(\frac{\overset{\circ}{m}_R^2}{\overset{\circ}{\rho}} \right) \frac{(1 - \overset{\circ}{A}_2)}{\overset{\circ}{A}_2} \right] - \frac{(\overset{\circ}{m}_R + 1)^2}{\overset{\circ}{\rho}} (1 - \overset{\circ}{A}_2) \left[\frac{1}{\overset{\circ}{A}_{th}^2} + 1 \right] \quad (8)$$

$$\Delta P_{\ell}^{\circ} = (P_2 - P_o) / \rho_{\ell} v_{\ell o}^2 / 2g = 2 \overset{\circ}{A}_1 \left[1 + \left(\frac{\overset{\circ}{\rho}}{\overset{\circ}{m}_R} \right) \frac{\overset{\circ}{A}_2}{(1 - \overset{\circ}{A}_2)} \right] - \left(1 + \frac{1}{\overset{\circ}{m}_R} \right)^2 (\overset{\circ}{A}_1^2 + \overset{\circ}{A}_2^2) \quad (9)$$

Equations (6) and (7) relate the pressure rise from the vapor to the liquid at the throat to the dynamic pressure terms. Equations (8) and (9) relate pressure rise from the vapor to liquid at the diffuser outlet to the dynamic pressure terms. The latter two equations are most suitable for design purposes and for evaluation of test data. However, the former expressions are also of interest in comparing the amount of pressure rise added by the diffuser to that resulting at the throat.

Also, operation of a jet condenser with the diffuser exit area less than the vapor inlet area will result in a pressure rise in between the limits supplied by these equations.

Numerical examples of interest for the above equations were computed and are presented in Figs. 8 through 11 in order to illustrate predicted performance of variable area jet condensers. Figure 8 presents the calculated throat and diffuser pressure rises (referred to injected liquid dynamic pressure) vs. the mass flow ratio of liquid to vapor for a given liquid to vapor density ratio and injector to tube inlet area ratio. Curves are presented to show the influence of different values of the ratio of injector to throat area.

As in the case of constant area jet condensers, low values of mass flow ratio result in higher calculated values of pressure rise referred to liquid dynamic pressure. For example, the curve for $\overset{\circ}{A}_1 = 0.895$ predicts a value of $\overset{\circ}{\Delta P}_\lambda = 4.7$ at a mass flow ratio of 10, while at a mass flow ratio of 100, a value of $\overset{\circ}{\Delta P}_\lambda = 1.0$ results. Also, use of throat areas more nearly equal to injector area results in higher values of predicted pressure rise.

Comparison of the curves for the pressure rise at the throat to the pressure rise at the exit of the diffuser provides some interesting conclusions. At a mass flow ratio of 10, the pressure rise at the throat is within 80 percent of the pressure rise at the diffuser exit ($\overset{\circ}{A}_1 = \text{unity}$). This implies that the contribution of the vapor to the total pressure rise is very high at lower values of liquid to vapor mass flow ratio; i.e., efficient recovery of the liquid dynamic pressure at the throat only increases the pressure rise by about 20 percent. However, as higher liquid flow rates are used the effect of the liquid head becomes more important than contributions from the vapor, and efficient recovery of the injected liquid velocity is required to achieve a high pressure rise.

The above value of $\overset{\circ}{\Delta P}_\lambda = 4.7$ means that for an injector discharge coefficient of unity, 3.7 times the dynamic pressure of the injected

liquid is available for circulation of the outlet liquid through the liquid radiator loop (cf. Fig. 1) back to the point of injection. For example, if a set of flow conditions were chosen such that the liquid dynamic pressure were 10 psi, a total of 37 psi would then be available as a pressure difference for circulation of the outlet liquid flow. This result, if verified by experiments, has profound significance in the use of a jet condenser in a Rankine cycle system. It means that a jet condenser could be used with little, if any, pumping power weight penalty (if other performance requirements such as stable operation are met).

An interesting observation can be made as to the source of the energy producing the jet condenser pressure rise by referring to Fig. 8. For the mass flow ratio of 10 and the densities and area ratio of this figure, the inlet vapor dynamic pressure is approximately 0.2 times the inlet liquid dynamic pressure. Thus, if both were recovered with no losses, a maximum value of ΔP_{ℓ}° of 1.2 could be obtained. The only other energy source which is available for the pressure rise through the condenser is the internal energy of the vapor, which manifests itself as random thermal energy. Thus, the results predicted by the analysis could only result if conversion of vapor thermal energy to a directed mechanical energy in the liquid were to occur.

Figure 9 presents the calculated values of pressure rise referred to inlet vapor dynamic pressure for the same geometric and flow variables. Once again, as in the case of the constant area jet condenser, increasing mass flow ratio has an opposite effect upon the magnitude of this pressure rise term from that of Fig. 8. That is, increasing mass flow ratio produces increasing values of ΔP_v° and decreasing values of ΔP_{ℓ}° . For example, increasing mass flow ratio from 10 to 100 produces an increase in ΔP_v° from 30 to 600 for an area ratio of 1.0. This can be contrasted to the behavior of ΔP_{ℓ}° from Fig. 8 where a decrease from 5.1 to 1.0 is experienced. The same general trends are exhibited for the predicted pressure rise at the throat, with the exception that

different area ratios have crossover points and the area ratio for $\overset{\circ}{A}_1 = 1.0$ falls off very sharply with increasing mass flow ratio.

In order to illustrate the effect of density ratio, Fig. 10 was computed for a given geometry ($\overset{\circ}{A}_1 = 0.90$ and $\overset{\circ}{A}_2 = 0.075$). As can be seen, higher values of liquid to vapor density ratio produce higher calculated values of ΔP_ℓ . For example, increasing density ratio from 2620 (700° F for mercury) to 14,500 (530° F for mercury) produces an increase in ΔP_ℓ from 1.85 to 6.0 (for a mass flow ratio of 20). For constant mass flow ratio, this decrease in density can be interpreted as an increase in vapor velocity. Thus, it appears the jet condenser becomes a more effective pressure recovery device (for given geometry and mass flow rates) as lower vapor pressures are utilized.

The effect of the ratio of injector to tube area is illustrated in Fig. 11 (for a given density ratio and injector to throat area ratio). Results are similar in trend to those obtained for the constant area jet condenser; that is, increasing values of $\overset{\circ}{A}_2$ result in increases in the non-dimensional pressure rise referred to injected liquid dynamic pressure, or an increase in the effectiveness of the jet condenser as a pumping device. On the other hand, the absolute magnitude of pressure rise is increased as lower injector to tube area ratios are used.

The above results are useful in expressing the values of pressure rise which may be possible using a jet condenser and to indicate major trends. However, it is also meaningful to examine the pumping characteristics of these devices.

The net power output (in kw) of a jet condenser which is available for circulation of the bypass liquid flow is given by:

$$H_j = \frac{(\Delta P_a - \Delta P_i) \dot{m}_{l0}}{738 \rho_\ell} \quad (10)$$

or

$$H_j = \frac{\left(1 - \frac{\Delta P_i}{\Delta P_a}\right) (\Delta P_a \dot{m}_{l0})}{738 \rho_\ell}$$

for a perfect injector ($c_d = 1.0$), $\frac{\Delta P_a}{\Delta P_i} = \Delta P_\ell^o$

Rearranging and substituting for ΔP_a and $\dot{m}_{\ell o}$ gives

$$H_j = \left(1 - \frac{1}{\Delta P_\ell^o}\right) (\Delta P_v^o \frac{m_R^o}{m_v^o}) \frac{\rho_v v_{vo}^2 / 2g}{738\rho_\ell} \dot{m}_{vo} \quad (11)$$

Thus, Equation (11) expresses the power output in terms of jet condenser operating parameters. It should be noted that all values of ΔP_ℓ^o less than unity produce a negative power output; i.e., pumping power is required by the condenser. For fixed inlet vapor conditions, the effect of mass flow ratio on power output can be illustrated by plotting the expression:

$$H_j^* = \left(1 - \frac{1}{\Delta P_\ell^o}\right) (\Delta P_v^o \frac{m_R^o}{m_v^o}) \quad (12)$$

This parameter, which is directly proportional to the useful power output, is plotted vs. mass flow ratio in Fig. 12 for three different area ratios (injector to total inlet). All three geometries exhibit maxima within the range of flow ratios considered. The smallest injector, while producing the highest calculated value of H_j^* , has the smallest range of operation; the useful power output going to zero at a mass flow ratio of 25. On the other hand, an injector to tube area ratio of 0.075 theoretically provides useful power over the entire range of mass flow ratios of the curve (0-100). The peak value of H_j^* for this geometry is 775 at a mass flow ratio of 60 vs. a peak of 1140 at a mass flow ratio of 13 for $\frac{A_2^o}{A_1^o} = 0.010$.

EXPERIMENTAL APPARATUS

Experimental investigations of jet condensers were performed during this program using a closed cycle mercury test loop (Ref. 15) as shown in Fig. 13. Mercury vapor was generated in a pool boiler, circulated through a baffle and superheater to obtain a controlled quality, and then delivered to the test section. Liquid mercury at nearly ambient

temperature was pressurized by a low speed gear pump, heated to the desired injection temperature, and subsequently was mixed with the vapor stream in the test section. The outlet flow of liquid from the test section was cooled to nearly ambient temperature and pressurized. Part of this flow was delivered to the test section (cf. below) and the remainder was returned to the boiler to complete the flow circuit.

Test Section Construction

The optimum test section geometry to insure both high pressure rise and high heat transfer rates consists of a properly designed converging section. However, initial tests were conducted on a constant area geometry to determine feasibility and heat transfer characteristics for central injectors. These data were used for sizing of variable area geometries.

The first test sections used had a vapor internal diameter of 0.19 inches. Results from these tests were used to scale condenser geometries to larger size units (vapor internal diameter of 0.75 inches). Finally a multiple unit test section was built which had a capacity equal to the single units with 0.75 inch internal diameter. Figure 14 is a photograph of one of the large diameter geometries.

The majority of test sections were constructed with transparent mixing sections in order to record condensation length and obtain high speed photographs of the internal flow. However, some units featured all-metal construction for tests where very high pressure rises (greater than 50 psid) were to be obtained. The transparent sections were constructed of quartz in order to maximize high temperature strength and minimize problems of thermal shock (as opposed to Pyrex). Sealing between the stainless steel and quartz was accomplished by compression of a high temperature gasket material at both ends.

Instrumentation and Experimental Error

Pressure, temperature, and flow instrumentation were calibrated over the range of operation for jet condenser tests. Calibrations varied somewhat but the differences were small ($\sim \pm 1/2$ percent) on all instrumentation with the exception of the electromagnetic flowmeters. These calibrations changed by approximately seven percent in six months due to decreases in the permanent magnet strength. A summary is given

below (Table 1) of the maximum probable error in measured parameters. This error estimate is based on the scatter encountered in calibrations, and on the least readings possible with the visual and electronic readout techniques used.

TABLE 1

Summary of Measurement Techniques and Maximum Probable Error:

<u>Measured Parameter</u>	<u>Instrumentation</u>	<u>Maximum Probable Error</u>
Pressure (absolute)	Bourden Tube Gage	± 1.0 psia
Pressure(differential)	Bellows Type Gage with Isolators	± 0.2 psid and ± 0.5 psid
Flow Rate	Electromagnetic Flowmeter	± 5 percent
Temperature	Stainless Steel Sheathed Chromel- Alumel Thermocouples	$\pm 2^{\circ}$ F
Condensation Distance	Visual	$\pm 1/16''$
	High Speed Camera	$\pm .01''$

Calibrations were conducted periodically on the gages (every 3 or 4 test days). The maximum deviation among calibrations was always less than the maximum error given in the table. The zero reading on the gages shifted slightly from "cold" to test conditions due to the change in ambient temperature inside the test enclosure. However, the zero values were recorded with no flow both before and after each test sequence and the average applied to the gage reading to determine the actual pressure rise.

Thermocouples and the associated readout equipment were calibrated using the melting points of tin, lead, and zinc (450° , 621° and 785° F respectively). Freezing curves were plotted on the recorder for all thermocouples and the melting point determined by the constant temperature portion of the curve. As indicated, the maximum deviation obtained of the readings from the above values was 2° F.

EXPERIMENTAL RESULTS

Condensing Length for Constant Area Condenser

Curves of condensation length vs. the jet utilization factor are shown in Fig. 15 for several average liquid-vapor mass flow ratios for a constant area condenser. Choice of a high jet utilization factor in a jet condensing system has the effect of reducing liquid radiator weight by increasing the average rejection temperature. However, high values of χ may result in excessive condensation lengths, unstable conditions, and poor pressure recovery characteristics. A correlation of the relation between condensation length and χ for variations in other flow parameters is therefore important for preliminary design purposes.

The value of χ at which the condensation length exhibits a rapid increase appears to be dependent upon the mass flow ratio of liquid to vapor. For example, the curve of $\dot{m}_R^0 = 66$ rises at a value of $\chi = 0.6$ while the curve for $\dot{m}_R^0 = 16$ rises at $\chi = 0.85$.

Flow parameters have a strong influence on condensation length for a given jet utilization factor. As the vapor velocity is increased with liquid injection flow rate held constant, shorter condensation lengths are obtained for the same value of utilization factor. For example, curves (1) and (3) correspond to the same liquid injected flow rate with different vapor flow rates. Curve (1), which has a vapor velocity of about 55 fps, shows a condensation length of 2-1/2 inches to occur at a value of $\chi = 0.7$. Curve (3), which is for a vapor velocity of about 130, gives a condensation length of only 3/8 inches for the same value of χ . A probable reason for this increase in heat transfer rate is the increase in heat transfer area caused by the greater breakup of the liquid jet due to higher values of vapor shear.

As the liquid injected flow rate is increased, with vapor flow rate held constant, longer condensation lengths occur for the same value of utilization factor. Curves (5) and (3) are for the same

vapor velocity with mass flow ratios of 13.5 and 30 respectively. Curve (5) shows a condensation length of 3/8 inches at $\chi = 0.8$, while Curve (3) gives a condensation length of 1 inch for the same value of χ . This variation is probably due to two effects:

1. Decreasing liquid velocity results in a larger value of the relative vapor velocity ($V_{v0} - V_{l0}$) which increases vapor-liquid shear and heat transfer area.
2. Decreasing liquid velocity increases the time a given particle of liquid spends in the vicinity of the vapor. Thus, it is able to absorb a greater amount of heat and condense more vapor in traversing a given distance.

Pressure Rise in Constant Area Condenser

The measured pressure rise appears to be closest to the calculated pressure rise for the test runs which had the highest ratio of liquid mass flow to vapor. This trend is shown in Fig. 16 which contains a plot of η_a , the ratio of actual to theoretical pressure rise, vs. the jet utilization factor, χ . Lines of constant mass flow ratio, $\frac{m}{m_R}^0$, are shown. The curve for $\frac{m}{m_R}^0 = 69$ exhibits peak values of η_a which are greater than 90 percent. However, the curve for the lowest mass flow ratios (13.5 - 16.0) has a maximum value of η_a of only about 75 percent. The increase in losses resulting from operation of this geometry at lower mass flow ratios may be due to increased frictional and mixing losses. For the constant area geometry, the main source of pressure rise appears to be the kinetic energy of the injected liquid. Operation at a lower mass flow ratio means the vapor flow is greater relative to a fixed injected liquid kinetic energy. Thus, frictional losses due to the vapor flow will be greater relative to the pressure rise resulting from the liquid, and η_a will be less than for a higher mass flow ratio.

This figure also illustrates the narrow range of operation for lower mass flow ratios. For example changing χ from 0.75 to 0.89 results in an increase in η_a from about 0.5 to 0.75. Further increases in χ from 0.89 to 0.90 result in a very steep drop in η_a from 0.75 to about 0.40. Comparison of this curve with the corresponding curve (No. 6) of Fig. 15 provides the possible explanation for this behavior. The region of χ for peak pressure rise appears to be the same region of χ in which

condensation distance is very sensitive to small changes in χ . Very small changes (e.g., from 0.89 to 0.90) result in very large changes in condensation distance (from about 1.0 to 4.5 inches) with corresponding greater increases in frictional losses. As indicated previously, operation of a jet condenser system at higher values of χ is desirable in order to achieve a higher average liquid radiator temperature. However, considerations of stability, range of operation, and pressure rise must also be weighed in the selection of operating conditions.

Heat Transfer in Variable Area Condensers

Results of testing variable area jet condensers are shown in Fig. 17. In this curve, the value of a correlating factor, $\Psi = \chi V_{l0}/V_R$ is plotted versus density ratio for all test runs where the interface was in the throat. The factor $\chi V_{l0}/V_R$ was determined by trial and error to provide the best correlation of test data. Increasing this factor resulted in moving the interface downstream of the throat while decreasing Ψ had the opposite effect.

The value of χ obtainable for a particular set of the other parameters is provided by the curves. As noted above, χ is the fraction of the heat absorbing capabilities of the jet which can be utilized for a given condensation distance. A value of χ equal to unity would result in the liquid radiator inlet temperature being equal to the vapor temperature. Thus, the radiator would operate at the highest possible temperature and would require the smallest size.

The effects of V_{l0} and V_R on Ψ are as follows: Higher values of liquid velocity, V_{l0} , result in a shorter residence time of liquid in vapor. The fraction of the heat absorbing capacity of the liquid which is utilized (χ) is therefore reduced. On the other hand, high values of vapor velocity relative to the liquid ($V_R = V_{vo} - V_{l0}$) produce higher shear forces and tend to promote physical mixing, increasing the heat absorbed by the jet in a given distance. The vapor density has an important effect upon the jet. Increasing values of vapor density, (decreasing values of δ) produce a higher flux of vapor molecules upon the jet. Thus, for constant values of V_{l0} and V_R , decreasing δ results in increases in χ .

The figure shown illustrates these trends. For example, from Fig. 17 the value of $\chi V_{\ell 0}/V_R$ which produces an interface at one inch (large diameter test unit) decreases from about 0.10 at $\beta = 2000$ to about 0.045 at $\beta = 6000$. Further increases in β above about 10,000 appear to effect a very rapid decrease in the value of Ψ which can be achieved with the interface at the throat location. The reason for the strong change in trend around $\beta = 10,000$ is probably that as the vapor becomes more rarified the limiting resistance in the heat transfer process becomes the vapor flux attainable at the jet surface rather than the internal liquid heat transfer.

Information on the importance of conduction relative to turbulent heat exchange within the liquid jet can be obtained for this larger geometry. Calculation of the ratio α/r_{ℓ}^2 for mercury at $\sim 400^{\circ}\text{F}$ and a jet radius of 0.103" gives a value of approximately 1 ft²/sec. However if the experimental values of x_c , L_c and V_{ℓ} are plotted on Fig. 5 the test points fall on values of $\frac{\alpha + \alpha_t}{r_{\ell}^2} \approx 100 - 300$. Therefore the turbulent mode is dominant and conduction accounts for less than 1 % of the total heat transfer.

Pressure Rise in Variable Area Jet Condensers

The pressure rise divided by liquid dynamic pressure is plotted versus mass flow ratio for the two larger diameter jet condensers in Figs. 18 and 19. Values of ΔP_{ℓ}^0 were obtained which are as much as eight times the values which could be achieved if the vapor and liquid dynamic pressure were the only sources of pressure rise. For example, in Fig. 18, the maximum value of ΔP_{ℓ}^0 obtained is about 12. That is, the measured pressure rise through the jet condenser (ΔP_a) is 12 times the dynamic pressure of the injected liquid ($\rho_{\ell} V_{\ell 0}^2/2g$). For this particular test run the dynamic pressure of the inlet vapor ($\rho_v V_{v0}^2/2g$) was only about 0.4 times the liquid dynamic pressure. Thus, the ratio of measured pressure rise to the sum of the dynamic pressure terms is 8.7. In order for this result to occur, conversion of vapor thermal energy to liquid mechanical energy must occur in the jet condenser. This experimental result supports the analytical conclusions reached previously. As a

consequence a very large source of energy is made available for liquid circulation in a Rankine cycle system.

The curves of ΔP_{ℓ}° versus m_R° show the trends predicted by analysis; i.e.,

1. Decreasing mass flow ratio produces an increase in the ratio of pressure rise to injected liquid dynamic pressure.
2. Increasing density ratio (decreasing vapor density) usually effects an increase in ΔP_{ℓ}° .

Figures 18 and 19 include calculated curves for the maximum density ratio of the test runs for reference. As can be seen, the trend of the analysis is followed relatively closely over the range of ΔP_{ℓ}° (1.7-12.0) and mass flow ratio (13-66) for these curves.

The lowest value of ΔP_{ℓ}° obtained for steady-state operation with the interface in the throat location was 1.25 with the majority of the test data falling above 1.5. Thus, for these operating variables and for a perfect injector (discharge coefficient of unity), the pressure increment added to the vapor would always be greater than that required to inject the liquid. For a mercury Rankine cycle system the operating parameters for a jet condenser would probably include a vapor temperature of 600-700° F and a mass flow ratio of 20-40. For these conditions, the large diameter jet condensers tested had a range of ΔP_{ℓ}° of about 1.25 to 2.0. However, if the geometric trends of the analysis are followed (as were those for flow variables) higher values of ΔP_{ℓ}° should be obtainable for these conditions by use of a larger area ratio of the injector to tube inlet.

In order to enable more general use of the test results, experimental performance can be compared to that predicted by analysis by using the model which incorporated the assumption that the mixing chamber wall pressure was equal to the inlet vapor pressure. The results are shown in Fig. 20 which plots measured pressure rise versus calculated rise. The average deviation appears to be about + 30 percent and - 25 percent of measured from calculated. Considering the simplifying assumptions

of the analysis, possible uncertainties in the values of density ratio used in the analysis, and the possibility of off-design operation, the agreement shown is considered to be reasonably good. Thus, the calculation method used for prediction of pressure rise appears to be useful for preliminary design purposes. The results suggest that the calculated values would probably provide a low estimate of the pressure rise in jet condensers, especially if vapor friction and diffuser losses were included in the calculated values.

CONCLUDING REMARKS

The present investigation has provided performance characteristics of jet condensers using a liquid metal working fluid (mercury). Design relations have been prepared for a specific geometry for preliminary design of jet condensers for space power systems operating on the Rankine cycle with mercury as the working fluid (17).

The most significant result of this program was demonstration of the high values of pressure rise possible in convergent-divergent jet condensers. Absolute values of pressure rise as high as 62 psid were obtained. Values of the ratio of pressure rise to the dynamic pressure of injected liquid ranged up to 12.2. The latter result was obtained through the conversion of vapor thermal energy to mechanical energy in the outlet liquid. Thus, the jet condensers tested performed both as condensers and as vapor driven circulation pumps. The experimental values of pressure rise for larger geometries agree to within about + 30 percent and - 25 percent with values predicted by the analysis. The recommended equation for predicted pressure rise is:

$$\Delta P_t^o = 2A_1^o \left[1 + \left(\frac{\rho^o}{\rho_m^o} \right) \frac{A_2^o}{1-A_2^o} \right] - \left[A_1^{o2} + A_2^{o2} \right] \left[1 + \frac{1}{\rho_m^o} \right]^2$$

Scaling relations were applied to test results obtained for small diameter units (0.19 inches i.d.) to design larger (0.75 inches i.d.) jet condenser geometries. These larger units performed with all-liquid flow at the outlet and fluctuations of pressures, flows and temperatures which were less than 1-2 percent of the average values. Simple startup techniques were possible and no gravity effects on the final interface were observed.

Performance of jet condensers with other geometric variables and other liquid metals can be estimated using the results of the pressure rise and heat transfer analyses reported. However, experimental

verification should be obtained before these estimates are used as the basis for preliminary design.

Surface tension forces in jet condensers are very small (<1 percent) compared with the large liquid and vapor inertial forces occurring. Therefore, whether the fluid is nonwetting or wetting should not have an important influence upon stability and/or pressure rise. Some results from investigations using mercury as a working fluid may therefore be applicable to other liquid metals such as potassium or rubidium. However, experimental investigations with these fluids should be initiated if preliminary design data is to be available for second-generation space power systems.

ACKNOWLEDGMENT

This work was sponsored by the National Aeronautics and Space Administration. Overall administration was provided by Mr. W. Scott of the NASA Washington Office. NASA technical direction was provided by Mr. S. Lieblein of the Lewis Research Center. The author is very grateful to Mr. Lieblein and Dr. J. Neustein of Electro-Optical Systems for their guidance and numerous helpful suggestions during this investigation.

BIBLIOGRAPHY

1. "SNAP-8 Radiator Topical Report", J. Payne, Aerojet General Nucleonics Report No. AN-551, June 1962
2. "Sunflower Power Conversion System Quarterly Report", Tapco Report No. ER-4608, June - August 1961
3. "Space Radiator Study", R. Denington, et al., Tapco Report No. ER-4544, ASD Technical Report No. 61-697, April 1962
4. "Condenser Space Heat Rejection Systems", L. Hays, Electro-Optical Systems, Report No. 500-Final. Prepared for Army Ballistic Missile Agency under Contract DA-04-495-506-ORD-2007, December 1960
5. "Chemical Engineer's Handbook," J. Perry, McGraw-Hill, 1950
6. Penberthy Manufacturing Company, Prophetstown, Illinois, Commercial Literature
7. Schutte and Koerting Col, Cornwells Heights, Pa., Commercial Literature
8. "Condensuctor for Deep Running Torpedoes", J. Kaye, et al., Joseph Kaye and Co., Report No. N-2, Contract N298-(122)11039, October 1956
9. "The Mixing of Vapor and Liquid Jets", Aerojet-General Corp., Report No. 1344(Final), Contract Nonr 869(00) Task NR 062-157, October 1957
10. "To the Problem on Heat Transfer from Condensing Steam to a Turbulent Water Jet", V. Konovalov, Izvestia Vyshikh Uchebnych Zavedeniy, 1958, (Electro-Optical Systems Internal Translation No. 2)
11. "Investigation of Spray-Type Condensers with Mercury and Water", L. Hays, J. Collins, J. Neustein, Proceedings of the 1961 Heat Transfer and Fluid Mechanics Institute, 1961
12. "Temperature and Velocity Distribution and Transfer of Heat in a Liquid Metal", H. Brown, et al., Transactions of the American Society of Mechanical Engineers, 1957

BIBLIOGRAPHY (cont)

13. "On Sprays and Spraying", W. Ranz, Engineering Research Bulletin B-65 of Pennsylvania State University, March 1956
14. "Spray Formation and Breakup, and Spray Combustion", A. Fuhs, Sunstrand Turbo Report-AMF/TD No. 1199, February 1958
15. "Investigation of Condensers Applicable to Space Power Systems, Part I - Direct Condensers", L. Hays, Electro-Optical Systems Report No. 1588-Final. Prepared for the National Aeronautics and Space Administration under Contract NAS 7-11, September 1962
16. "Fluid Mechanics", R. Daugherty and A. Ingersoll, McGraw-Hill, 1954
17. "Investigation of Condensers Applicable to Space Power Systems, Part II - Jet Condensers", L. Hays, Electro-Optical Systems Report No. 1588-Final, Prepared for the National Aeronautics and Space Administration under Contract NAS 7-11, November 1962

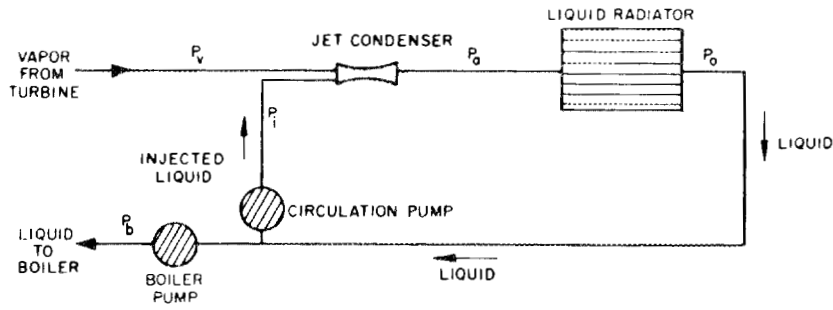
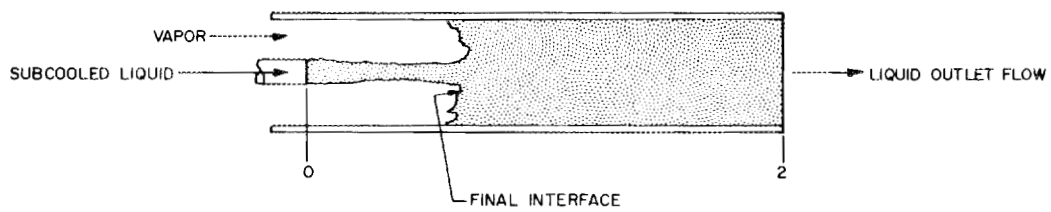
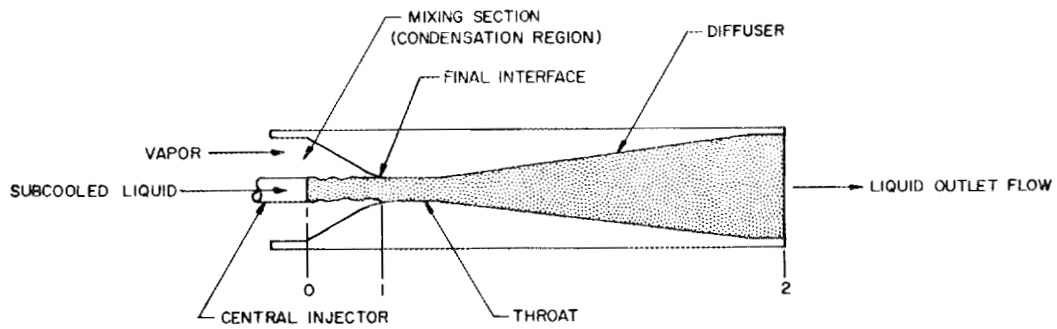


FIG. 1 SCHEMATIC OF INDIRECT CONDENSER SYSTEM USING A JET CONDENSER



2a. CONSTANT AREA JET CONDENSER



2b. VARIABLE AREA (CONVERGING DIVERGING) JET CONDENSER

FIG. 2 SCHEMATIC OF JET CONDENSER GEOMETRIES

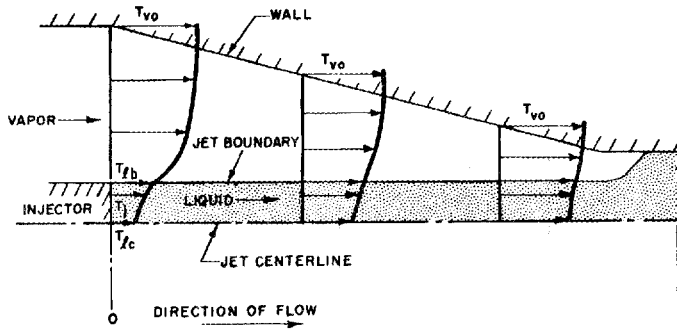


FIG. 3
IDEALIZED TEMPERATURE PROFILES
IN JET CONDENSER (CONSTANT
VAPOR TEMPERATURE AT WALL)

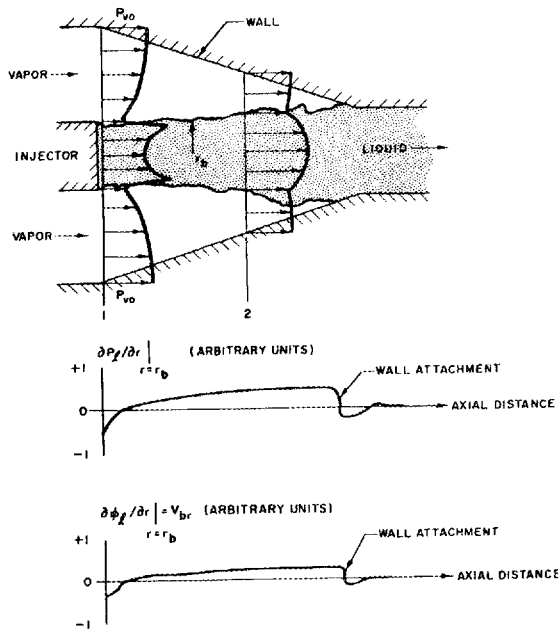


FIG. 4
DEVELOPMENT OF RADIAL PRESSURE
GRADIENT AND FLOW IN JET CON-
DENSER FOR HIGHER LIQUID FLOW
VELOCITY

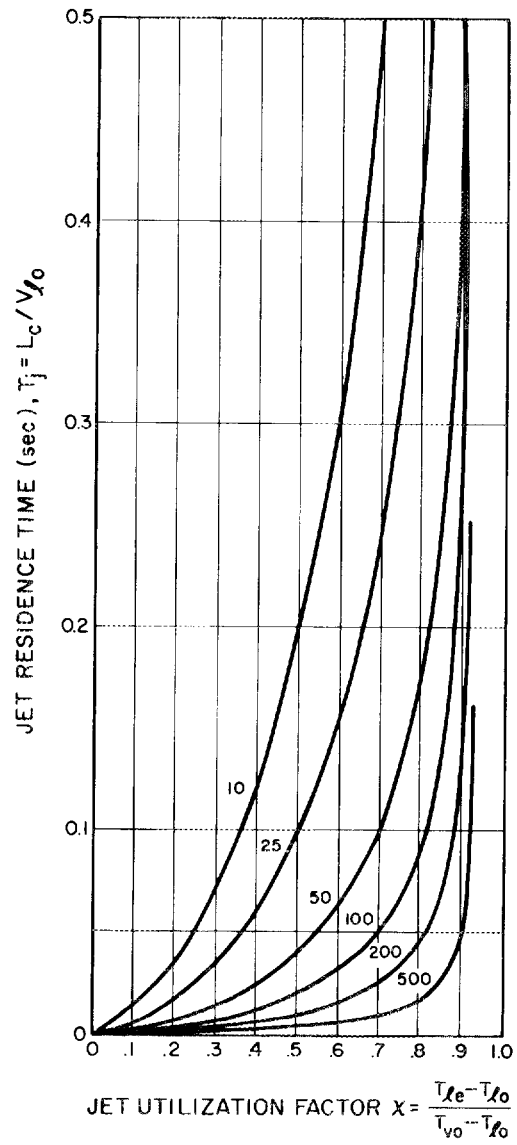


FIG. 5 CALCULATED JET RESIDENCE TIME VERSUS JET UTILIZATION FACTOR $\left(\text{LINES OF CONSTANT } \frac{\alpha + \alpha_t}{r_l^2} \right)$

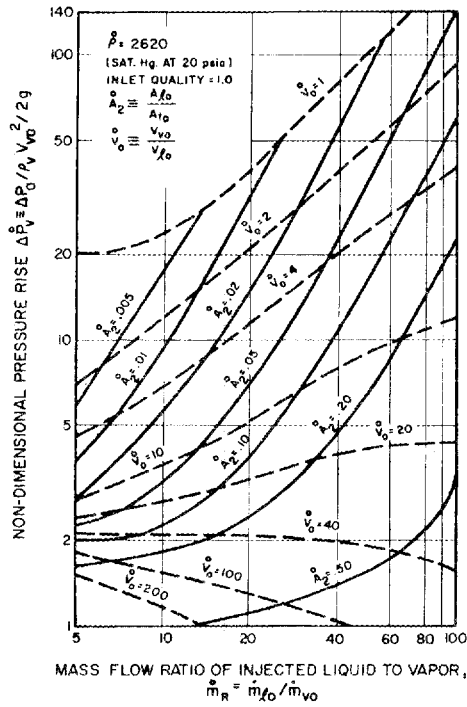


FIG. 6
CALCULATED PRESSURE RISE FOR
CONSTANT AREA JET CONDENSER
(REFERRED TO VAPOR DYNAMIC
PRESSURE)

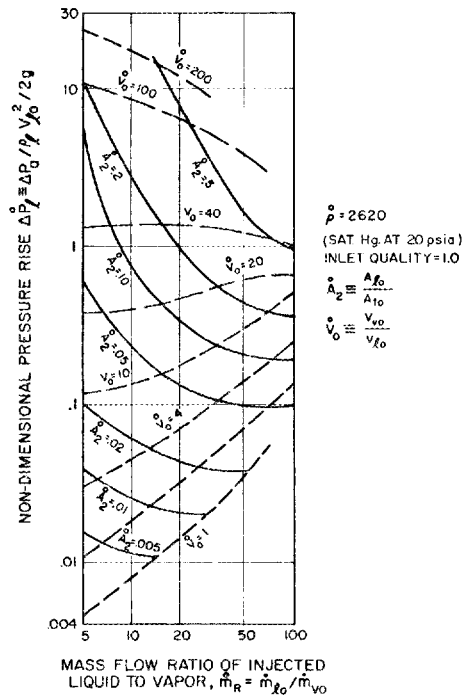


FIG. 7
CALCULATED PRESSURE RISE FOR
CONSTANT AREA JET CONDENSER
(REFERRED TO LIQUID DYNAMIC
PRESSURE)

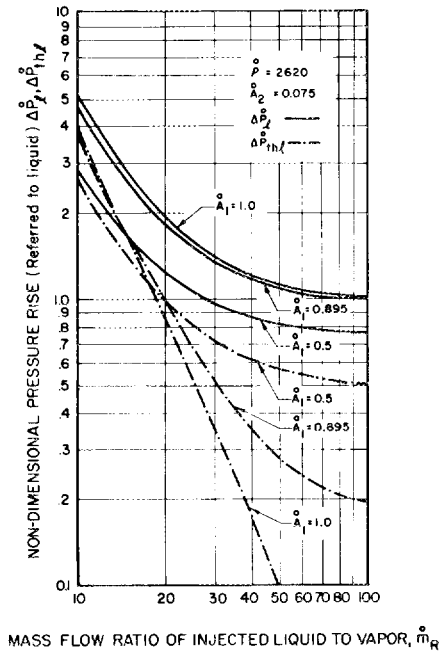


FIG. 8
CALCULATED PRESSURE RISE (REFERRED TO LIQUID) FOR VARIABLE AREA JET CONDENSER, EFFECT OF INJECTOR-THROAT AREA RATIO

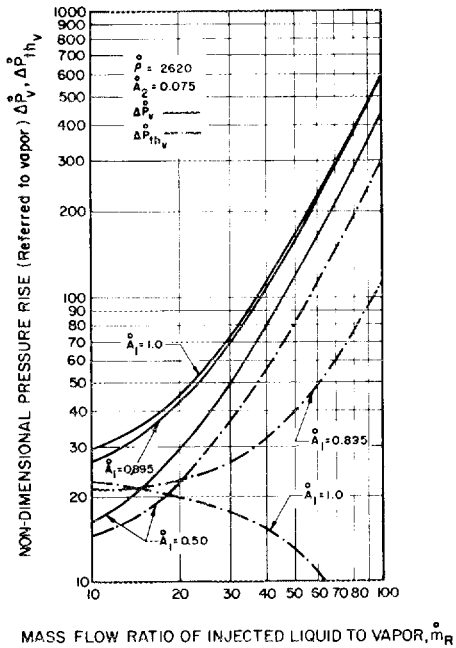


FIG. 9
CALCULATED PRESSURE RISE (REFERRED TO VAPOR) FOR VARIABLE AREA JET CONDENSER, EFFECT OF INJECTOR-THROAT AREA RATIO

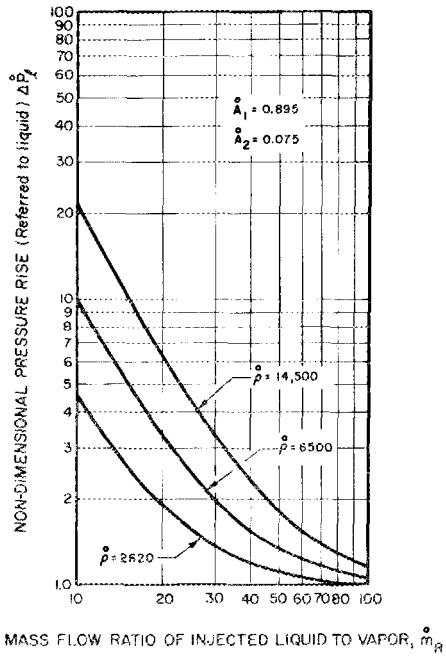


FIG. 10
CALCULATED PRESSURE RISE (REFERRED TO LIQUID)
FOR VARIABLE AREA JET CONDENSER, EFFECT OF
LIQUID-VAPOR DENSITY RATIO

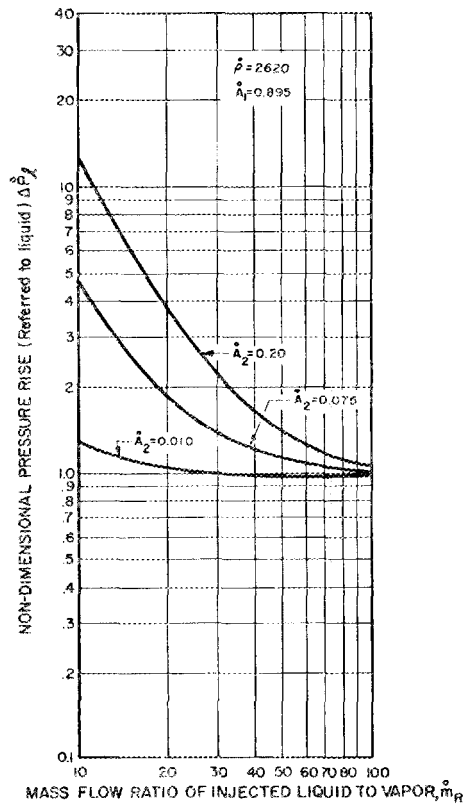


FIG. 11
CALCULATED PRESSURE RISE (REFERRED TO LIQUID)
FOR VARIABLE AREA JET CONDENSER, EFFECT OF
THE RATIO OF THE INJECTOR AREA TO TOTAL INLET
AREA

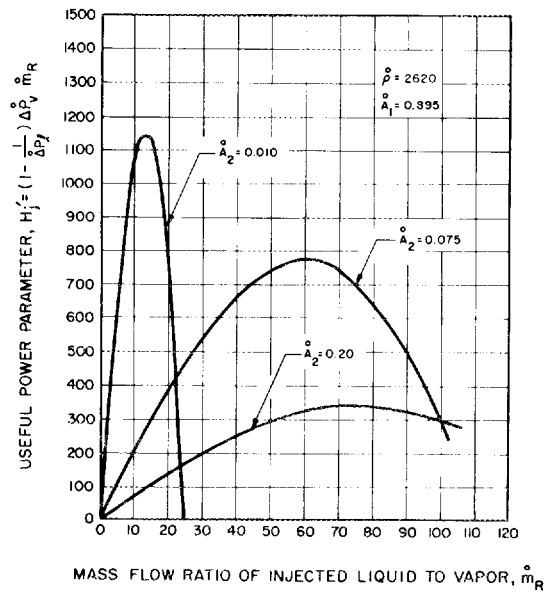


FIG. 12
USEFUL POWER PARAMETER
(CALCULATED) FOR VARIABLE
AREA JET CONDENSER VS
MASS FLOW RATIO

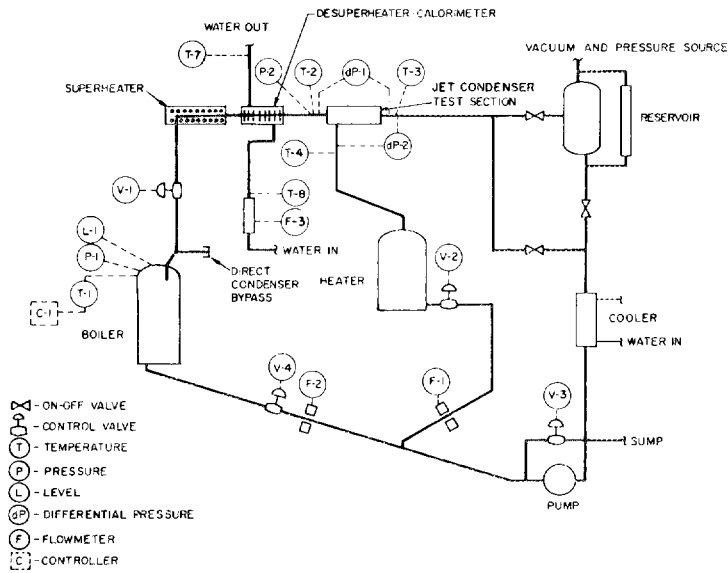


FIG. 13
10 kw TEST LOOP
SCHEMATIC

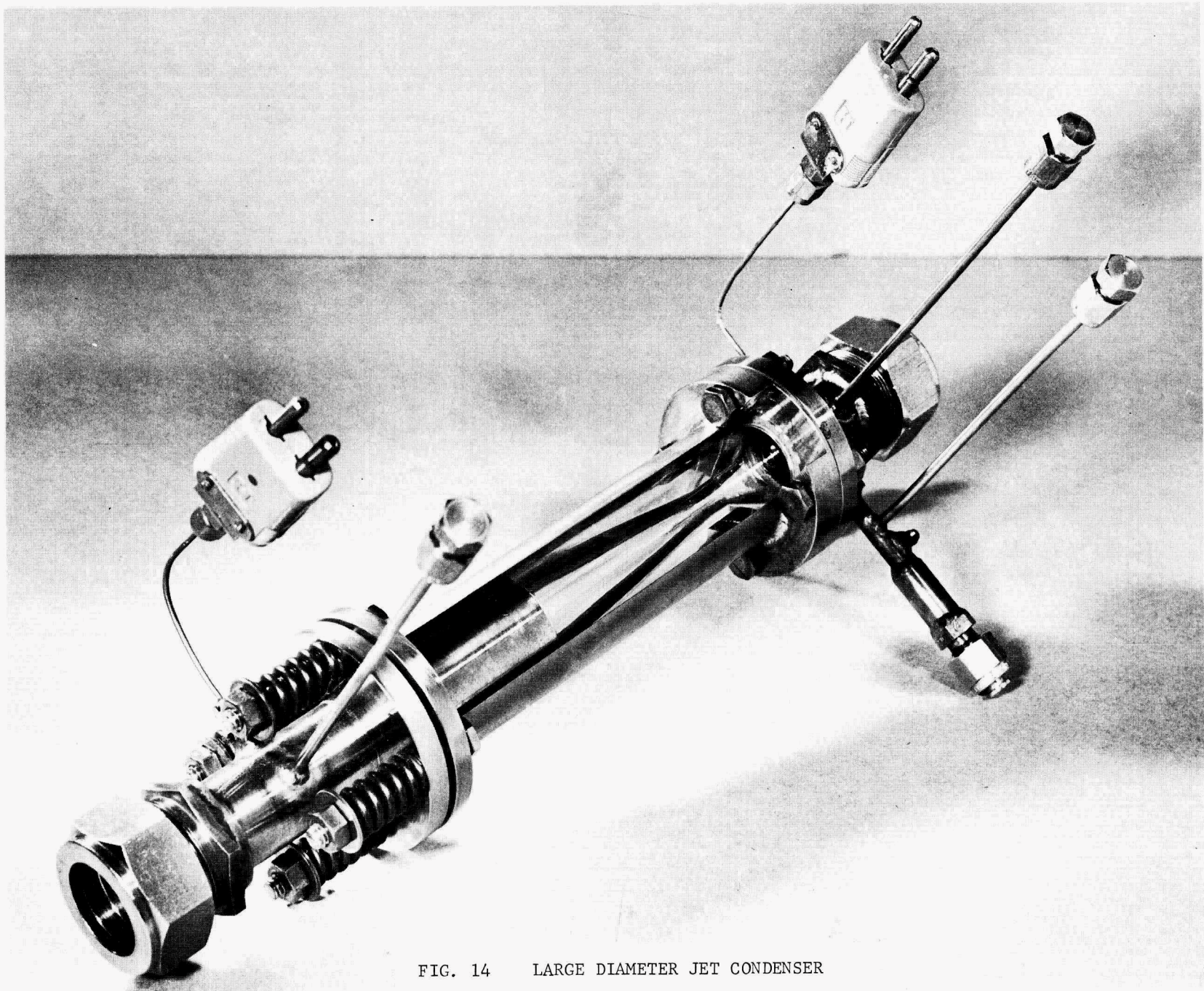


FIG. 14 LARGE DIAMETER JET CONDENSER

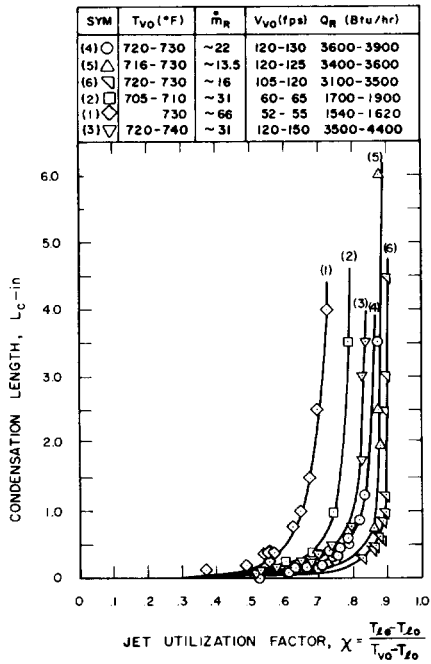


FIG. 15
CONDENSATION LENGTH VERSUS JET UTILIZATION FACTOR FOR CONSTANT AREA JET CONDENSER

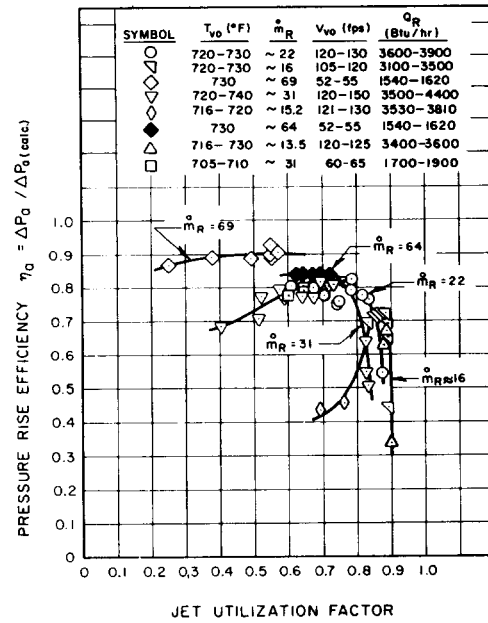


FIG. 16
RATIO OF ACTUAL TO CALCULATED PRESSURE RISE VERSUS JET UTILIZATION FACTOR FOR CONSTANT AREA JET CONDENSER

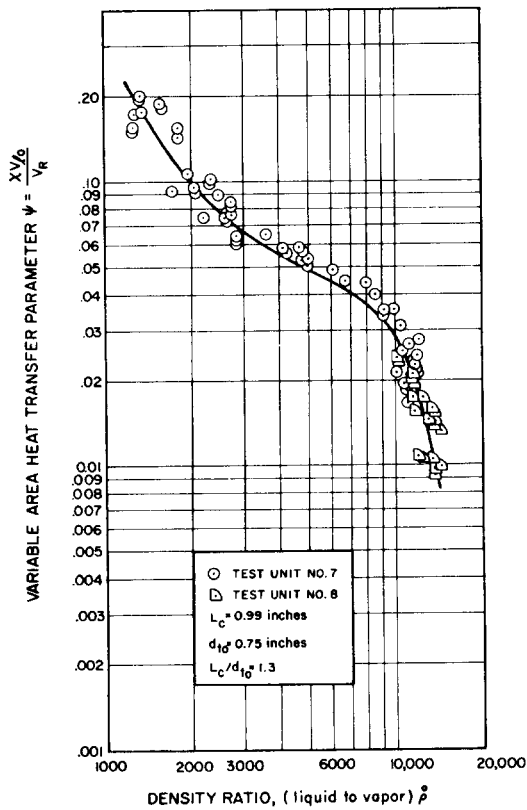


FIG. 17
VARIABLE AREA HEAT TRANSFER PARAMETER VERSUS LIQUID TO VAPOR DENSITY RATIO FOR LARGE DIAMETER JET CONDENSERS

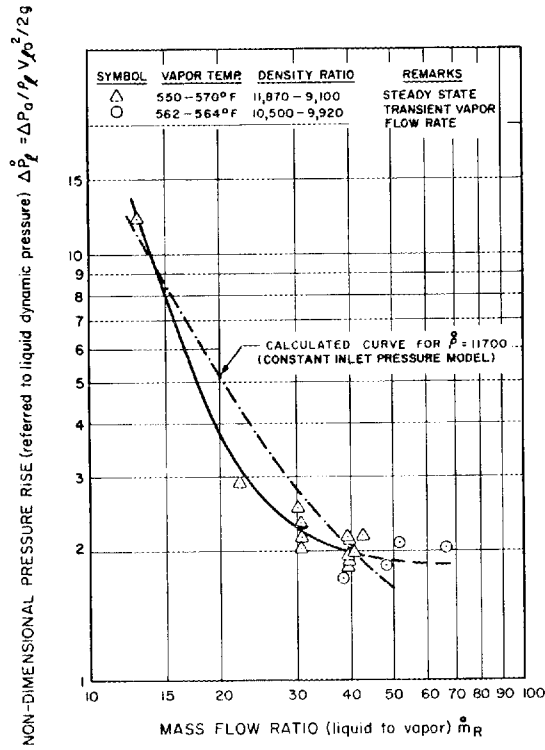


FIG. 18
NON-DIMENSIONAL PRESSURE RISE (REFERRED TO LIQUID DYNAMIC PRESSURE) FOR LARGE DIAMETER JET CONDENSER (TEST SEC. No. 7) VERSUS MASS FLOW RATIO OF LIQUID TO VAPOR

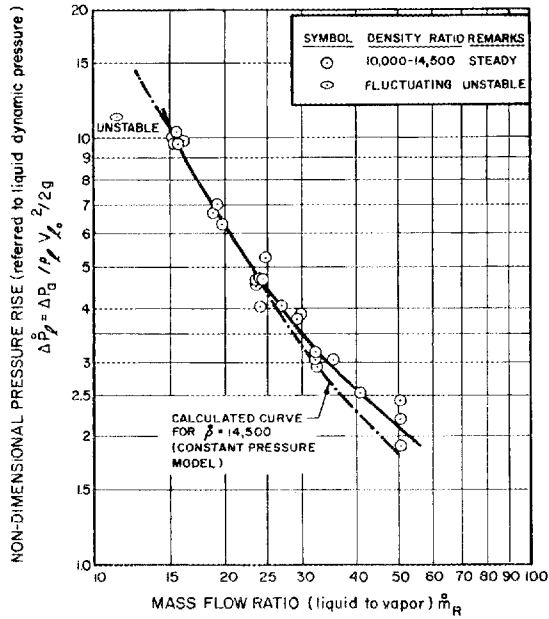


FIG. 19
NON-DIMENSIONAL PRESSURE RISE (REFERRED TO LIQUID DYNAMIC PRESSURE) FOR LARGE DIAMETER JET CONDENSER (TEST SEC. No. 8) VERSUS MASS FLOW RATIO OF LIQUID TO VAPOR

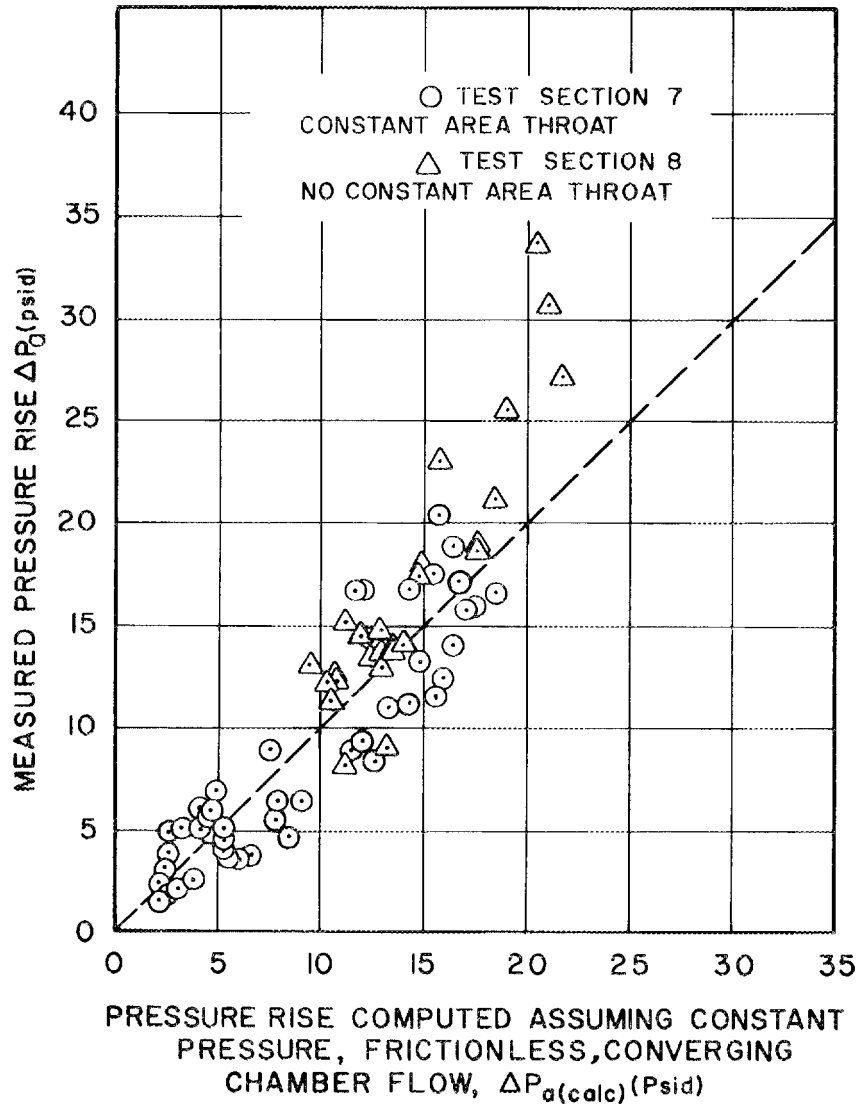


FIG. 20 COMPARISON OF MEASURED PRESSURE RISE IN LARGE DIAMETER JET CONDENSERS (FOR ALL TEST RUNS WITH INTERFACE IN THROAT AND STEADY STATE CONDITIONS) WITH CALCULATED VALUES

DISCUSSION

MR. DWYER: Did you notice, in the throat of your condenser, whether you had a liquid phase that was a continuous phase? Is there a tendency for cavitation?

MR. HAYS: No. The entire test section was transparent. We would observe, at higher liquid injection rates, when the heat balance was upset the interface would start to move downstream, and under these conditions, the first indication of movement would be the appearance of small vapor bubbles on the inside surface of the test section. These are the only bubbles which could be seen, since the fluid was opaque. With further deviation from the heat balance the entire interface would move downstream.

MR. DWYER: They would collapse, wouldn't they, at some point; which would tend to form cavitation?

MR. HAYS: That is correct. However, under conditions where the interface was right at the throat, this occurrence was not noticeable. Incidentally, when the interface moved downstream the pressure rise would drop off very sharply.

MR. BONILLA: I still don't understand exactly the mechanism whereby you figure that the enthalpy of the vapor accelerated the liquid jet.

MR. HAYS: Well, the jet receives a very high condensation flux since the liquid is sub-cooled. The pressure in the vapor has to be equal to the saturation pressure of the liquid phases at the surface. However, this is very much below the saturation pressure of the vapor as it enters.

MR. KRAKOVIAK: How did you find your heat flux area?

MR. HAYS: The heat flux area was based on the average jet area. As you saw, surface waves were present which increased the area. The conditions chosen for the area calculations were mass flow ratios on the order of 30 to 40. At these points the jet had a nearly constant diameter.

MR. GOLDMAN: How much sub-cooling did you have in your jet as it entered, and what was the sub-cooling at the throat?

MR. HAYS: The sub-cooling ranged from as much as 500°F (for vapor temperatures of 600-700°F) to around 100° at the inlet.

The outlet temperature of the liquid ranged from about 100° below the vapor temperature, to within about 7 to 8°F.

MR. DWYER: I have another question. Did I understand you to say that when you used mercury as the working fluid here you broke even on your weight, on your specific weights?

MR. HAYS: For SNAP-8 system parameters.

MR. DWYER: I assume you suffered there, because you had to have the high liquid flow rate, didn't you? You get a lot of liquid mercury here sending your weight up.

MR. HAYS: Yes. The inventory with the mercury is a major problem.

MR. DWYER: When you switch over to alkali metal you don't have this penalty, so it would show to a much greater value.

MR. HAYS: That is correct. This result is consistent with an analysis we did earlier for alkali metals. A particular analysis we did resulted in a plot of specific weight (pounds per kilowatt versus kilowatt) for sodium. For a direct condenser versus power level, we would get a curve like this. The jet condenser starts out higher, at lower power levels but soon crosses over to show a lower specific weight.

MR. SILL: This break-even weight, was that with the direct condenser, or indirect?

MR. HAYS: Three cases were considered in this study: direct, a heat exchanger condenser, and a jet condenser. The break-even point for the heat exchanger condenser was always at a somewhat higher power level than the jet condenser. For this curve the point around a thousand kilowatt thermal, for the heat exchanger condenser while it was 300 kilowatt thermal for the jet condenser. The jet condenser always has the advantage over the heat exchanger condenser if redundant sections in the radiator aren't considered, being a much more compact device, and also providing its own pumping power for the recirculation flow.

MR. LEIGHTON: When you talk about a break-even point, are you talking about a component break-even or system break-even?

MR. HAYS: A component break-even point.

MR. LEIGHTON: Isn't this a little bit meaningless?

MR. HAYS: I don't think so; if the identical inlet conditions and input parameters are used for system operation.

MR. LEIGHTON: The jet pump is going to require a heck of a lot more pumping power.

MR. HAYS: It provides its own pumping power. This is demonstrated experimentally. The main problem that might be present in actual system is one of stability. However, this probably is not a problem. You can always provide a fix on the system.

Fog-Flow Mercury Condensing Pressure Drop Correlation

By A. Koestel, Thompson Ramo Wooldridge Inc.

M. Gutstein - NASA-Lewis Research Center

R. T. Wainwright - NASA-Lewis Research Center

A B S T R A C T

A theory is presented to predict the local pressure drops of mercury vapor flowing and condensing inside tubes. The theory is based on the assumption that condensation takes place at the tube wall and, subsequently, drops are entrained into the vapor as a fine dispersion or fog. A relationship between $\phi^2 X^{3/4}$ and the Weber number is derived from the analysis, where ϕ^2 is the two-phase frictional pressure gradient ratio and X is the quality. Experimental data from several sources were examined and are shown to correlate well with the theory.

Fog-Flow Mercury Condensing Pressure Drop Correlation

By A. Koestel, Thompson Ramo Wooldridge
 M. Gutstein, NASA-Lewis Research Center
 R. Wainwright, NASA-Lewis Research Center

INTRODUCTION

Rankine Cycle powerplants utilizing mercury as a working fluid have been considered for space applications. Inherent in the performance of such plants is the need to condense the effluent of the turbine, that is, the mercury vapor. In a powerplant for space, this process might occur inside tubes and the heat of condensation would be dissipated by radiation. To specify the dimensions of the tubes, their diameter, length, taper, etc., requires an accurate prediction of the pressure drops associated with mercury condensing at low heat fluxes. Recognizing that such was not available, the Lewis Research Center of N.A.S.A. sponsored a program at Thompson Ramo Wooldridge Inc. to measure the local static pressures along tubes of constant and varying diameter in both the wetting and non-wetting regimes. A parallel effort of analyzing the fluid mechanics of condensing mercury was included to develop a means to predict the pressure drops. A portion of the results of this program is presented below.

The static pressure difference which might be measured between two horizontal points of a tube in which condensation occurs is given by the expression:

$$dP_{\text{measured}} = dP_{\text{two phase frictional}} + dP_{\text{momentum}} \quad \text{Equation (1)}$$

where $dP_{\text{two phase frictional}}$ is the pressure difference required to overcome the frictional resistance to flow, and dP_{momentum} is the pressure difference due to net momentum changes in the fluid.

The above expression may be expanded to the form shown in Reference 1:

$$dP_{\text{measured}} = dP_{\text{TPF}} + \frac{G_T^2}{g} \left[d \left(\frac{(1-X)^2}{\rho_f R_f} \right) + d \left(\frac{X^2}{\rho_v R_v} \right) \right] \quad \text{Equation (2)}$$

where G_T is the total mass velocity and R_f , R_v are the liquid and vapor volume fractions

Equation 2 indicates that the frictional component of the measured static pressure difference can be obtained only when the volume fractions (or local slip ratio, U_f/U_v *) are known. For mercury condensing, this information is

*The slip ratio is related to the volume fraction by

$$R_v = 1 - R_f = \frac{1}{\left(\frac{1-X}{X} \right) \left(\frac{\rho_v}{\rho_f} \right) \frac{U_v}{U_f} + 1}$$

presently unavailable and must be assumed. Thus, Reference 3 reports frictional pressure gradients for mercury condensing for two limiting cases, those of a slip ratio of zero and one. Reference 3 further recommends a slip of zero based on photographic observation and the general agreement of their data with the Martinelli correlation. However, deviations from the correlation were noted, particularly at low heat fluxes, which were attributed to the presence of fog flow (i.e., slip ratios of approximately one).

Baroczy, Reference 4, presents a correlation of mercury liquid volume fractions based on adiabatic measurements with nitrogen-mercury. This correlation is believed to be inapplicable to the case of mercury condensing for reasons which are discussed in the Appendix.

The authors have employed a slip ratio of one to reduce measured pressure differences to frictional pressure drops since they observed that fine drops dispersed in the vapor was the predominant flow pattern for low heat flux mercury condensation. The fact that these frictional pressure gradients tended to correlate with a fog-flow analysis justified this assumption. A derivation of the liquid volume fraction for fog-flow mercury condensing is described in the Appendix.

A veritable literature exists today which describes, predicts and correlates two-phase frictional pressure gradients. For condensation, however, and for mercury condensation in particular, the correlation of Lockhart-Martinelli, Reference 2, and its refinement, the correlation of Baroczy and Sanders, Reference 5, are of most significance. The Lockhart-Martinelli approach consists of equating the pressure gradients obtained from isothermal, two component flows to the case of condensation at the equivalent superficial liquid to vapor pressure gradient ratios. The total frictional pressure difference across the tube is then obtained by integration of the local gradients. The work of Baroczy and Sanders constitutes an improvement to the basic isothermal correlation by accounting for a vapor Reynolds Number effect.

Reference 3 applied these correlations to mercury condensation data and found general agreement to within about ± 25 percent. As previously noted, however, at low heat rejection rates or low qualities (low vapor Reynolds Numbers), no agreement of the test results with these correlations was apparent. This was attributed to fog flow, a flow pattern to which, the authors of this Reference believed, the Martinelli Correlation did not apply.

Reference 6 presents a comparison of two-phase, mercury-nitrogen pressure differences with the Martinelli curve. It likewise compares over-all pressure differences of mercury condensation in horizontal tubes with the same correlation. In both cases, agreement is good. However, condensation inside horizontal tapered tubes and inside inclined tubes of constant diameter showed considerable deviation. Thus, it appears that the Lockhart-Martinelli correlation does not satisfactorily predict the pressure gradients of mercury condensation at low vapor velocities and low heat fluxes, or those for unusual geometries and orientations.

The analysis of two-phase pressure losses for condensing mercury, performed under the Thompson Ramo Wooldridge program previously mentioned, assumed

the fog flow regime based on the following observation. During all the experiments which were conducted, including the wetting runs, tiny drops were seen dispersed in the flowing vapor. The analysis and its corroboration are presented below along with a comparison of its ability to predict pressure gradients with that of the Lockhart-Martinelli correlation. A more complete discussion of the fog-flow model is presented in Reference 1.

DESCRIPTION OF THE FLOW REGIME

Fundamental to the prediction of two-phase pressure drop or heat transfer is a knowledge of the existing flow regime. For the case of condensation occurring inside tubes, wetting fluids generally form a thin, annular layer at the heat transfer surface. In all likelihood, drops are sometimes broken from this film and are entrained in the vapor core. For mercury condensation, however, a continuous liquid film is difficult to obtain even when the mercury wets its container. More typically, a layer of drops is formed at the tube wall. The greater portion of the condensate is then transported to the tube exit by the entrainment of these drops into the vapor stream. At relatively high vapor velocities, this two-phase flow has been described as a "fog" flow (Reference 7). Even at lower vapor flow rates, the "fog" regime is present although gravity effects, such as large agglomerated drops, do appear. A more detailed picture of the fog flow regime of mercury condensation is offered below for the purpose of deriving a two-phase frictional pressure drop prediction. Figure 2a is a sketch of the configuration of the flow which is envisioned to exist.

The authors postulate that the drops which are entrained into the vapor stream are extremely small (of the order of 0.001 to 0.010 inches diameter) and are rapidly accelerated to very nearly the local vapor velocity. The drops are further conceived to respond to the turbulent fluctuations of the vapor phase and are dispersed so that the effects of concentration gradients are negligible. In effect, the drops travel with and become a part of the vapor stream: the two phase mixture is thus assumed to behave as a single phase fluid.

This liquid-vapor fog flows through the duct formed by the drops which are attached to the tube wall. The duct, however, is essentially hydraulically smooth due to the close packing of the drops on the wall. (Experimental confirmation of the existence of such a characteristic is presented in Figure 1 which was obtained from Reference 10. This Figure is a plot of the friction factor as a function of roughness density of spheres glued to a tube wall.) It is further assumed that increasing the packing of the drops at the wall by raising the heat flux would have little or no effect on the friction factor. The diameter of the duct through which the fog-like mixture flows is $D_T - 2\delta_D$, where δ_D is the effective thickness of the drop layer at a particular location.

In a previous study performed by the senior author, Reference 8, it was shown that the diameter of mercury drops which were entrained into a flowing nitrogen stream was related to the velocity of the gas. It is suggested that such a relationship also exists for mercury condensing: a drop grows to a particular size, called the critical drop diameter (defined by the velocity of the vapor), and is then entrained into the vapor core. The effective thickness of the drop layer on the wall at a particular position,

d_D , was therefore taken as equal to the critical drop diameter at that position. Thus, the vapor velocity (here, the velocity of the fog) determines the thickness of the condensate layer at the wall and is, in turn, dependent on this thickness by continuity. The prediction of the frictional pressure gradients for condensing mercury based on the above considerations is derived below.

DERIVATION OF THE FOG MODEL

A. Critical Drop Size

Reference 8 presents a detailed experimental and theoretical analysis of the entrainment of mercury drops. A brief review of this work as it applies to mercury condensation is presented below, since the mechanics of this process forms an important part of the fog-flow model.

As a drop forms and grows on a tube surface, forces are produced which tend either to make the drop move or to oppose its movement. These forces consist of the drag caused by the flowing vapor, the gravity force and the interfacial force between the drop and the wall arising from the deformation of the drop by either of the two previous forces. At a particular drop size, the critical drop diameter (d_c), these forces are no longer balanced and the drop is displaced. Thus, at incipient movement, the following force balance must be applicable: (Drag Force) \pm (Gravity Force) - (Interfacial Force) = 0

$$\text{or } \frac{\pi d_c^2}{4} \frac{C_{d_f} \rho_v U_v^2}{2g_c} \pm n \sin \theta \rho_f \frac{\pi d_c^3}{6} - \pi d_c \sigma E_\sigma = 0 \quad \text{Equation (3)}$$

where C_{d_f} is the drag coefficient for the drop

n is the ratio g/g_c

σ is the surface tension

and E_σ is a constant which accounts for the effects of drop deformation, contact angle and surface condition. E_σ has a value less than one.

The coefficient of drag for drops, C_{d_f} , is also dependent on the deformation. In general, the coefficients for deformable bodies (bubbles, drops, etc.) are greater than for solid spheres and have values very nearly one (see Figure 3). For simplicity, the coefficients may be assumed equal to one and the value of E_σ can be made to accommodate the deformation effect. Thus, in horizontal tubes or in the absence of a gravitational field, the critical drop size is related to the vapor velocity as follows:

$$\frac{d_c \rho_v U_v^2}{2g_c \sigma} = 4 E_\sigma \quad \text{Equation (4)}$$

The term on the left side of equation 4 is the Weber Number for the drop.

Experiments were conducted, both in tubes and with inclined flat plates, which permitted the evaluation of E_{σ} . E_{σ} was found to have the value of 0.0464. For a more detailed discussion of these experiments and their analysis Reference 8 should be consulted.

B. Derivation of the Fog-Flow Model

If the discussion of the previous sections truly describes the flow regime for mercury condensing inside tubes, then the frictional component of the static pressure drop of Equation 1 may be written as a single equation for both phases as follows:

$$\left(\frac{dP}{dl}\right)_{\text{TFE}} = \frac{f_m W_m^2}{2g_c D_m \rho_m \left(\frac{\pi D_m^2}{4}\right)^2} \quad \text{Equation (5)}$$

where f_m is the friction factor for the fog mixture

and D_m is the diameter of the flow passage formed by the drops on the wall through which the fog flows.

The frictional pressure drop which would result if the vapor portion of the fog were to flow through the bare pipe is:

$$\left(\frac{dP}{dl}\right)_v = \frac{f_v (X W_m)^2}{2g_c D_T \rho_v \left(\frac{\pi D_T^2}{4}\right)^2} \quad \text{Equation (6)}$$

The Lockhart-Martinelli modulus, Φ_v^2 , defined as the ratio of the two gradients, is therefore:

$$\Phi_v^2 = \frac{(dP/dl)_{\text{TFE}}}{(dP/dl)_v} = \frac{f_m}{f_v} \frac{1}{X^2} \frac{\rho_v}{\rho_m} \left(\frac{D_T}{D_m}\right)^5 \quad \text{Equation (7)}$$

The friction factor for turbulent flow in smooth passages is given by:

$$f_m = \frac{0.316}{(N_{Re,m})^{1/4}} = \frac{0.316}{\left(\frac{D_m G_m}{\mu_m}\right)^{1/4}} \quad \text{Equation (8)}$$

and

$$f_v = \frac{0.316}{(N_{Re,v})^{1/4}} = \frac{0.316}{\left(\frac{D_T G_m X}{\mu_v}\right)^{1/4}} \quad \text{Equation (9)}$$

The viscosities, μ_m and μ_v , are transport properties and are more dependent on the volume fraction of the two phases than on the weight fraction. Since the volume fraction of the flowing liquid is much less than one, it can be assumed that

$$u_m = u_v \quad \text{Equation (10)}$$

Therefore,
$$\frac{f_m}{f_v} = \left(\frac{D_m X}{D_T} \right)^{1/4} \quad \text{Equation (11)}$$

The density ratio may be considered to be weight fraction dependent. Thus:

$$\frac{\rho_v}{\rho_m} = X \quad \text{Equation (12)}$$

Combining equations 7, 11 and 12 gives:

$$\phi_v^2 = \frac{1}{X^{3/4}} \left(\frac{D_T}{D_m} \right)^{4.75} \quad \text{Equation (13)}$$

A relationship between D_T/D_m and the Weber Number may be derived as follows. From Equation 4 the Weber Number based on the tube diameter may be obtained:

$$\frac{D_T \rho_v u_m^2}{2g_c \sigma} = \frac{4 E_\sigma D_T}{\sigma_c} \quad \text{Equation (14)}$$

Note that the vapor density is employed rather than the mixture density since only the vapor conditions influence the entrainment.

From continuity,

$$\frac{\pi D_T^2}{4} \rho_v u_v = \frac{\pi D_m^2}{4} \rho_v u_m \quad \text{Equation (15)}$$

where u_v represents the velocity of the vapor in a bare tube with all the liquid removed. Therefore,

$$\left(\frac{D_T}{D_m} \right)^2 u_v = u_m \quad \text{Equation (16)}$$

Substituting into equation 14:

$$\frac{D_T \rho_v \left(\frac{D_T}{D_m} \right)^4 u_v^2}{2g_c \sigma} = \frac{4 E_\sigma D_T}{\sigma_c} \quad \text{Equation (17)}$$

Utilizing the assumption that, at a particular point in the tube, the critical drop diameter corresponds to the effective thickness of the drop layer:

$$D_T - 2\sigma_c = D_m \quad \text{Equation (18)}$$

or

$$\frac{D_T}{\sigma_c} = \frac{2}{\left(1 - \frac{D_m}{D_T} \right)} \quad \text{Equation (19)}$$

Substituting into Equation 17:

$$\frac{D_T \rho_v U_v^2}{2 g_c \sigma} = \frac{4 E_\sigma}{\left(\frac{D_T}{D_m}\right)^4} \left[\frac{2}{1 - \frac{D_m}{D_T}} \right] \quad \text{Equation (20)}$$

or

$$\frac{D_T \rho_v U_v^2}{2 g_c \sigma} = \frac{8 E_\sigma}{\left(\frac{D_T}{D_m}\right)^4 - \left(\frac{D_T}{D_m}\right)^3} \quad \text{Equation (21)}$$

Thus from equations 13 and 21, a relationship has been shown to exist between the Lockhart-Martinelli modulus, Φ_v^2 , and the Weber Number such that:

$$\Phi_v^2 \times^{3/4} = f\left(\frac{D_T \rho_v U_v^2}{2 g_c \sigma}\right) \quad \text{Equation (22)}$$

By assuming values of the ratio, D_T/D_m , the relationship between the Weber Number and $\Phi_v^2 \times^{3/4}$ may be obtained. This is shown as a line in Figures 5 through 11. In addition, experimental values of $\Phi_v^2 \times^{3/4}$ and the Weber Number are plotted for confirmation of the fog-flow theory. A discussion of these figures is presented below.

CONFIRMATION OF THE FOG-FLOW MODEL

An experimental program to measure local pressure drops for mercury condensation was recently conducted at Thompson Ramo Wooldridge Inc. (herein designated TRW), Reference 1, and the results were utilized to corroborate the fog-flow model. Moreover, data reported in the literature of local and over-all mercury condensing pressure drops have been used as a further check of the theory. Brief descriptions of these experiments and the comparisons of their results with the fog model are presented below.

A. TRW Experiments

Local pressure drops were obtained on a rig shown schematically in Figure 4. This rig consisted of a pot boiler immersed in an electrically heated salt bath, a pre-heat section for slightly superheating the mercury vapor, an air cooled condensing test section, a flow meter and the return line to the boiler. Pressures within the condenser tubes were measured using mercury manometers at taps spaced every 14 or 18 inches. The features of the flow regime were observable at any point in the condenser with a combination X-ray and fluoroscopic screen.

The condenser test sections consisted either of constant diameter or tapered tubes of about 8 feet in length. However, the point at which complete condensation occurred was varied from about 4 feet to the total tube length. Table I lists the various tube sizes and the ranges of the variables which were employed.

Figures 5, 6 and 7 present the comparison of the fog-flow theory with the experimental data obtained from Series A, E and F respectively. From observation of the interface, it was determined that the mercury was in the nonwetting condition for these Series. These Figures show that at Weber Numbers greater than about 10, the experimental values of $\Phi_v^2 \times^{3/4}$ seem to be equal to the value of one and are independent of the Weber Number. At lower Weber Numbers, $\Phi_v^2 \times^{3/4}$ becomes greater than one and dependent

on the Weber Number. Although considerable scatter is present, the fog-flow theory predicted this trend of the data. The greater scatter of the data for Series E is attributed to the larger tube diameter and the consequent difficulty in measuring the smaller frictional pressure drops.

The results of Series W and G are shown in Figures 8 and 9. Series W were experiments conducted with the stainless steel tube of Series A but which the mercury eventually wetted. Series G were tests in which magnesium and titanium were added to the mercury for the express purpose of creating wetting. The wetting condition of both these Series was characterized by a greatly elongated interface whereas the nonwetting interface was more or less vertical as shown in Figure 12. That the fog-flow model also predicts the pressure drop trends for the wetting condensation is probably explained by one of the following two possibilities. The degree of wetting may have been limited and the condensation may still have been essentially dropwise. On the other hand, wetting may actually have been the mode of condensation. If this were true, then the results of Figures 8 and 9 would indicate that the fog regime was still present and that the film behaved very much like the drop layer (i.e., thickness, formation of drops, diameter of drops, etc.) A sketch of the wetting flow pattern which might account for its similarity to the nonwetting regime is presented in Figure 2b.

Preliminary results of the nonwetting tapered tube experiments are shown in Figure 10. Additional experimental data are available but await reduction to the parameters shown in this graph.

B. EOS Experiments

The frictional pressure drops associated with condensing mercury were obtained in a series of experiments conducted by the Electro-Optical Systems, Inc., Reference 3. Briefly, these tests consisted of condensing inside air-cooled glass and metal tubes of relatively small diameter and short length. Both complete and partial condensation within these tubes were explored. A comparison of the range of variables of the EOS experiments is shown in Table II.

Figure 11 presents the results plotted against the relationship predicted for fog flow. Once again, corroboration of the predicted trends is afforded by these data.

C. Previous TRW Experiments

References 6 and 9 report the results of mercury condensing completely in horizontal tubes, in tubes inclined upwards at 15 degrees, and in horizontal tubes under approximately zero gravity conditions. Table III lists the range of variables of these data. Only over-all rather than local pressure measurements were obtained in these experiments. It was therefore necessary to integrate the relationships of equations 5 and 6 over the total tube length in order to compare the data with the fog-flow model. The integration was performed as follows:

$$\frac{\Delta P_{TPF}}{\Delta P_V} = \frac{\int_0^{L_T} \left(\frac{dP}{dL}\right)_{TPF} dL}{\int_0^{L_T} \left(\frac{dP}{dL}\right)_V dL} \quad \text{Equation (23)}$$

$$= \frac{\int_0^{L_T} \frac{f_m M_m^2 dL}{D_m \rho_m 2g_c \left(\frac{\pi D_m^2}{4}\right)^2}}{\int_0^{L_T} \frac{f_v X^2 M_m^2 dL}{D_T \rho_v 2g_c \left(\frac{\pi D_T^2}{4}\right)^2}} \quad \text{Equation (24)}$$

Since the heat fluxes for these experiments were essentially constant, the quality may be written as:

$$X = 1 - \frac{L}{L_T} \quad \text{Equation (25)}$$

and

$$dX = - \frac{dL}{L_T} \quad \text{Equation (26)}$$

Substituting into Equation 24 gives:

$$\frac{\Delta P_{TPF}}{\Delta P_V} = \frac{\int_1^0 \frac{f_m dX}{D_m^5 \rho_m}}{\int_1^0 \frac{f_v X^2 dX}{D_T^5 \rho_v}} \quad \text{Equation (27)}$$

For fog flow with small liquid volume fraction, Equation 12 is employed, or:

$$\frac{\Delta P_{TPF}}{\Delta P_V} = \frac{\int_0^1 \frac{f_m X dX}{D_m^5}}{\int_0^1 \frac{f_v X^2 dX}{D_T^5}} \quad \text{Equation (28)}$$

Since the Weber Number will be evaluated at average conditions for the tube (i.e., at a quality of 0.5) and the ratio D_T/D_m is a function of this number (Equation 21), then D_m will be evaluated for average conditions. Therefore:

$$\frac{\Delta P_{TPF}}{\Delta P_V} = \left(\frac{D_T}{D_m}\right)^5 \frac{\int_0^1 f_m X dX}{\int_0^1 f_v X^2 dX} \quad \text{Equation (29)}$$

Substituting the turbulent friction factors of Equations 8 and 9 gives:

$$\frac{\Delta P_{TPF}}{\Delta P_V} = \left(\frac{D_T}{D_m}\right)^{4.75} \frac{\int_0^1 X dX}{\int_0^1 X^{7/4} dX} \quad \text{Equation (30)}$$

$$= \frac{11}{8} \left(\frac{D_T}{D_m} \right)^{4.75} \quad \text{Equation (31)}$$

or

$$\frac{8}{11} \left(\frac{\Delta P_{TPF}}{\Delta P_v} \right) = \left(\frac{D_T}{D_m} \right)^{4.75} \quad \text{Equation (32)}$$

For laminar flow, the following friction factors are employed

$$f_m = \left(\frac{64}{\frac{4 M_m}{\pi D_m \mu_m}} \right) \quad \text{Equation (33)}$$

and

$$f_v = \left(\frac{64}{\frac{4 X M_m}{\pi D_T \mu_v}} \right) \quad \text{Equation (34)}$$

which results in the relationship

$$\frac{\Delta P_{TPF}}{\Delta P_v} = \left(\frac{D_T}{D_m} \right)^4 \quad \text{Equation (35)}$$

Figure 13 illustrates the relationships between the Weber Number and the ratio,

$$\left(\frac{8}{11} \right) \left(\frac{\Delta P_{TPF}}{\Delta P_v} \right), \quad \text{for turbulent and laminar fog flow. The}$$

experimental data which were described above are likewise plotted on this graph. It is concluded that these data lend further support to the existence over a wide range of conditions of a fog regime in mercury condensation.

COMPARISON WITH THE LOCKHART-MARTINELLI CORRELATION

The frictional pressure drop data for a nonwetting and a wetting test series are plotted in Figures 14 and 15 respectively. The correlation of Lockhart-Martinelli is also plotted on these graphs. Different symbols have been used to distinguish the three flow regimes suggested by the correlation which were present in the experiments.

Examination of Figures 14 and 15 shows that the data exhibit no particular trend with regard to flow regimes and that the Martinelli correlation generally predicts the condensing pressure gradients at the high quality, high vapor Reynolds Number region (i.e., low values of the Martinelli parameter, X). At low qualities and low vapor Reynolds Numbers, however, a large deviation from the correlation is present. Reference 3 reported a comparable deviation of their data from the Martinelli correlation under similar conditions (qualities less than 50 percent). When the measured pressure drops used in these graphs were converted to frictional

pressure drops by a momentum correction based on a significant liquid holdup, holdup, the deviations were even greater. Thus momentum effects did not account for this discrepancy. Baroczy and Sanders, Reference 5, modified the Martinelli correlation for the effect of a vapor Reynolds number. Plotting the data of Figures 14 and 15 on this correlation produced an identical divergence. Thus, the possibility that the vapor Reynolds Number explains the difference between the data and the correlation was discounted.

Figures 14 and 15 again point up the similarity between the wetting and the nonwetting mercury condensing pressure drops as obtained from the experiments at TRW.

CONCLUSIONS AND RECOMMENDATIONS

A fog-flow theory has been presented to predict the frictional pressure gradients of mercury condensing inside tubes at low heat fluxes. This theory is based on the observation that condensation occurs at a tube surface and drops are subsequently entrained into the flowing vapor stream. The theory proposes that the critical drop Weber Number which correlates the entrainment of mercury drops, equation 4, may be coupled with the force balance used to predict the frictional pressure gradients of a fog mixture, equation 5. A comparison of condensing mercury data reported by several investigators with the resultant fog-flow relationships shows that the theory satisfactorily predicts the trends of this data over a wide range of variables, Figures 5 through 11, and Figure 13.

The authors recommend that future studies of mercury condensation determine the limits of the fog-flow theory. The application of the theory to condensing at higher heat fluxes, greater tube inclinations, etc., is as yet uncertain. Finally, future investigations should include a study of the flow regimes encountered and a careful determination of the liquid volume fractions, both of which are essential to a complete understanding of the physics of condensation.

Acknowledgments

The authors wish to thank R. Gido and T. Jaenke who performed the condensing experiments and P. Lawlor who helped in the preparation of this paper.

TABLE I

RANGE OF VARIABLES FOR MERCURY CONDENSING EXPERIMENTS PERFORMED AT TRW (REFERENCE 1)

<u>Variable</u>	<u>Series A</u>	<u>Series F</u>	<u>Series E</u>	<u>Series W</u>	<u>Series G</u>	<u>Tapered Tube</u>
Condensing Length (inches)	94	53-94	48-95	94	53-94	48-82
Tube Diameter (inches)	0.319	0.319	0.397	0.319	0.319	0.4x0.2
Tube Material	316 SS	Haynes 25	Haynes 25	316 SS	Haynes 25	Haynes 25
Vapor Inlet Pressure (psia)	8.0-30.2	12.1-30.4	11.4-30.4	19.6-20.2	10.6-30.5	14.9-30.1
Vapor Inlet Quality	1.0	1.0	1.0	1.0	1.0	1.0
Vapor Inlet Velocity (ft/sec)	114-278	82-302	50.238	152-200	74-291	86-195
Vapor Inlet Reynolds Number	477-50,000	833-43,159	706-36,096	700-36,000	808-40,000	1670-39,200
Mass Flow Rate (lb/min)	1.09-3.12	1.18-2.36	1.12-2.40	1.64-2.14	1.05-2.36	1.41-2.91
Heat Rejection Rate Per Unit Area x 10 ⁻⁴ (BTU/hr ft ²)	1.26-3.59	1.36-3.47	1.04-3.22	1.89-2.46	1.21-2.80	2.00-4.14
Outlet Quality	0.0	0.0	0.0	0.0	0.0	0.0
Remarks	Nonwetting	Nonwetting	Nonwetting	Wetting	Wetting	Nonwetting

TABLE II
 RANGE OF VARIABLES FOR MERCURY CONDENSING
 EXPERIMENTS PERFORMED AT EOS (REFERENCE 3)

<u>Variable</u>	<u>Section 1</u>	<u>Section 2</u>	<u>Section 3</u>
Tube Length (inches)	20.0	20.0	16.25
Tube Diameter (inches)	0.072	0.150	0.157
Tube Material	Pyrex	Pyrex	316 SS
Vapor Inlet Temp. (°F)	718-740	712-722	675-685
Vapor Inlet Quality	0.11-0.51	0.18-0.55	0.57-1.0
Vapor Inlet Velocity (ft/sec)	40-280	18-91	18-195
Vapor Inlet Reynolds Number	2300-16,200	2000-10,200	1700-18,400
Mass Flow Rate (lb/min)	0.258-0.450	0.305-0.482	0.076-0.472
Heat Rejection Rate Per Unit Area x 10 ⁻⁴ (BTU/hr ft ²)	7.40-11.0	1.30-3.80	0.17-2.80
Outlet Quality	0.0	0.0	0.05-1.0

TABLE III

RANGE OF VARIABLES FOR MERCURY CONDENSING
EXPERIMENTS PERFORMED AT TRW (REFERENCES 6 AND 9)

<u>Variable</u>	<u>Inclined 15°</u>	<u>Horizontal</u>	<u>Zero Gravity</u>
Tube Length (inches)	7.5-34	22-72	19.8
Tube Diameter (inches)	0.157	0.145-0.150	0.133-0.1385
Tube Material	Glass	Glass	Glass
Vapor Inlet Pressure (PSIA)	2.5-4.6	2.1-9.0	2.0-11.0
Vapor Inlet Quality	1.0	1.0	1.0
Vapor Inlet Velocity (ft/sec)	28.4-151		60-230
Vapor Inlet Reynolds Number	324-1600	1230-6000	1300-3000
Mass Flow Rate (lb/min)	.0135-.0648	4.2×10^{-4} -.249	.3-.55
Outlet Quality	0.0	0.0	0.0

NOMENCLATURE

- C_{d_f} - Drag coefficient for mercury drops, dimensionless
 D - Diameter, feet
 E_σ - Constant of equation 3, dimensionless
 G - Mass velocity, pounds per hour per square feet
 L - Length, feet
 N_{Re} - Reynolds Number, dimensionless
 R - Volume fraction, dimensionless
 U - Average velocity, feet per second
 W - Mass flow rate, pounds per second
 dP - Increment of pressure
 f - Friction factor, dimensionless
 g - Local gravitational acceleration
 g_c - $32.174 \frac{\text{lb. m} - \text{ft}}{\text{lb. f.} - \text{sec}^2}$ conversion factor
 m - Mass flow rate, pounds per second (Figure 16)
 η - Ratio, g/gc
 x - Quality, dimensionless
 f - Function of
 $t-t$ - Lockhart-Martinelli turbulent liquid-turbulent gas flow regime
 $t-v$ - As above for turbulent liquid-viscous gas flow regime
 $v-t$ - As above for viscous liquid-turbulent gas flow regime
 Δ - Finite difference
 Φ - Lockhart-Martinelli parameter
 X - Lockhart-Martinelli parameter
 d - Drop diameter, feet
 θ - Angle of inclination
 μ - Viscosity
 ρ - Density, lbs mass per cubic foot

σ - Surface tension

Subscripts

f - Liquid

m - Fog mixture

T - Total

TPF - Two phase frictional

v - Vapor

REFERENCES

1. Koestel, A., et al, "Mercury Wetting and Nonwetting Condensing Research," TRW contract NAS 3-2159, Final Report to be published.
2. Lockhart, R. W., and Martinelli, R. C., "Proposed Correlation of Data for Isothermal Two-Phase, Two-Component Flow in Pipes," Chemical Engineering Progress, Vol. 45, No. 1, page 39, 1949.
3. Hays, L., "Investigation of Condensers Applicable to Space Power Systems, Part I, Direct Condensers," Electro Optical Systems, Inc. Contract NAS 7-11, Final Report 1588, September 10, 1962.
4. Baroczy, C. J., "Correlation of Liquid Fraction in Two-Phase Flow With Application to Liquid Metals," Atomics International Contract AT(11-1)-GEN-8, Special Report NAA-SR-8171, April 15, 1963.
5. Baroczy, C. J., and Sanders, V. D., "Pressure Drop for Flowing Vapors Condensing in a Straight Horizontal Tube," Atomics International Contract AT(11-1)-GEN-8, Special Report NAA-SR-6333, June 1, 1961.
6. Kiraly, R., and Koestel, A., "The SNAP 2 Power Conversion System Topical Report No. 8, Condenser Development and Design Study," TRW Report No. ER-4104, June 30, 1960.
7. Gido, R. G., and Koestel, A., "Mercury Wetting and Nonwetting Condensing Research," TRW Contract NAS 3-2159, Progress Report ER-5214, January 1963.
8. Koestel, A., et al., "Space Radiator Study," TRW Contract AF 33(616)-7368, Technical Report ER-4544, April 30, 1962.
9. Jaenke, C. T., Koestel, A., and Reitz, J. G., "The SNAP 2 Power Conversion System Topical Report No. 13, Orbital Force Field Boiling and Condensing Experiment (OFFFACE)," TRW Report No. ER-4670, October 1962.
10. Schlichting, H., "Experimental Investigations of the Problem of Surface Roughness," NASA Technical Memo No. 823.
11. Hughes, R. R., and Gilliland, E. R., "The Mechanics of Drops," Chemical Engineering Progress, 48, No. 10, 497, October 1952.

APPENDIX

The correlation of liquid volume fraction presented by Baroczy is considered not applicable to the case of condensing for the following reasons. The correlation is based on the adiabatic, two component data of Reference 8. These liquid volume fractions were obtained by trapping and weighing the mercury which was entrained in a flowing nitrogen stream. The mercury was introduced into the nitrogen with a spray nozzle, a device which forms drops considerably larger than those formed during condensation. Moreover, in condensation, it is believed that drops grow at sites which are distributed more or less uniformly over the entire interior surface of the tube. The adiabatic tests captured only those drops at the tube wall which managed to stick as a result of a collision. Gravity forces and perhaps turbulence cause these drops to collide with the wall, mechanisms which are different from those present in condensation. Finally, the adiabatic holdup data may be shown to be very sensitive to the design of the equipment used in their measurement (i.e., the length of pipe between the spray nozzle and the test section and even the test section length itself). A more detailed discussion of these points may be found in Reference 1.

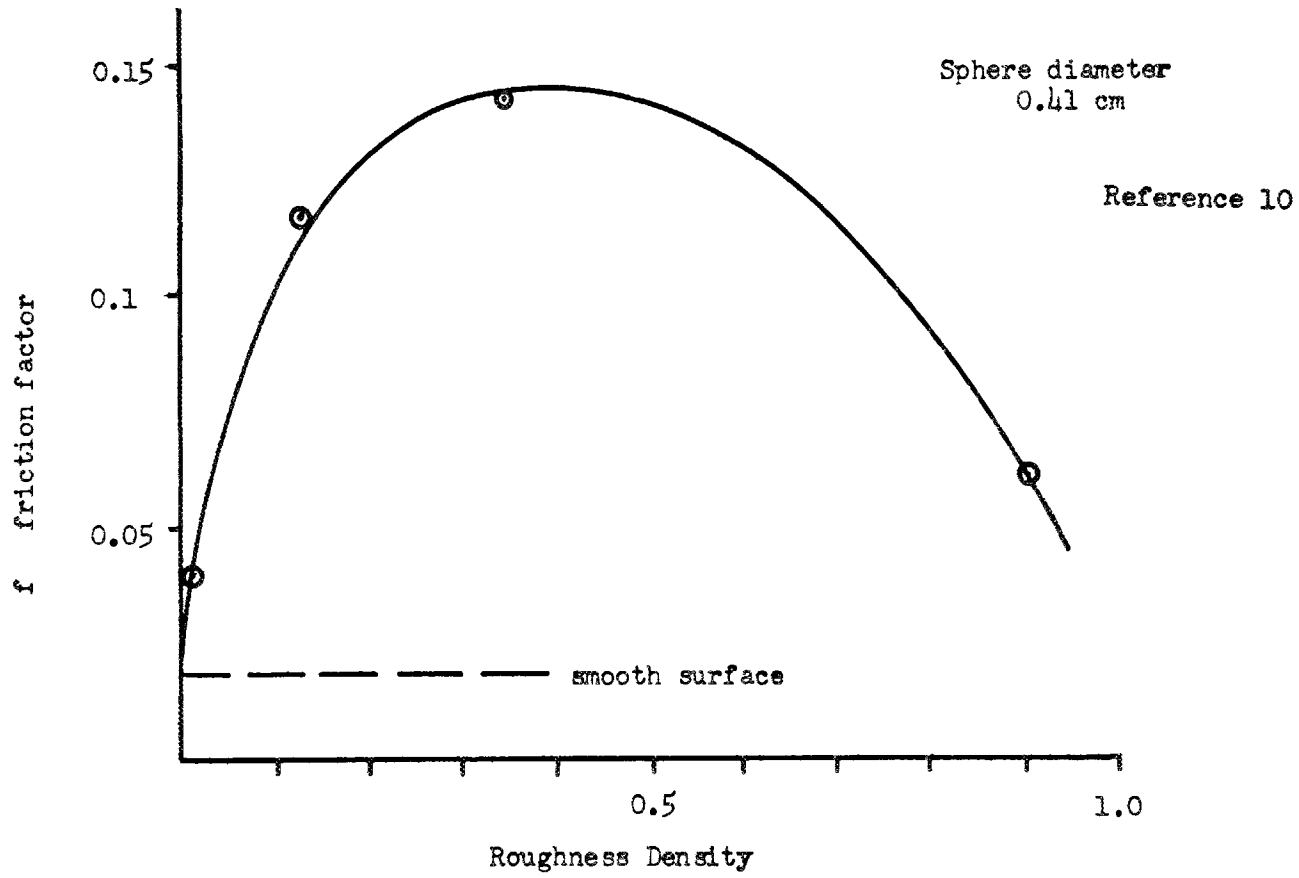
A comparison of the adiabatic holdup data* employed by Baroczy with the liquid volume fractions predicted by the fog-flow and the homogeneous models for the same diameter tube is presented in Figure 16. Both the experimental data and the fog-flow predictions are shown for several constant mass flow rates of vapor.**

The deviations between the data and the fog-flow theory are shown in Figure 16 to be considerable. The reliance to be placed on the liquid fractions predicted by the fog theory remains to be determined by experiment but the significance of the graph lies in its word of caution to those who would apply adiabatic, two component data to the case of condensation.

The lines of liquid volume fraction, R_f , shown in Figure 16 were obtained from the fog-flow theory as follows. In the fog core, the volume fractions predicted by the homogeneous model were assumed. At the wall, an annular layer of liquid was assumed to exist and its thickness was taken equal to the local critical drop size, δ_c . The cross-sectional areas occupied by the liquid in the core and at the wall divided by the total cross-sectional area of the tube thus determined the values of R_f for fog-flow.

- - - - -
 * For purposes of comparison, the gas flow rates of this data have been increased to reflect the greater density of mercury vapor.

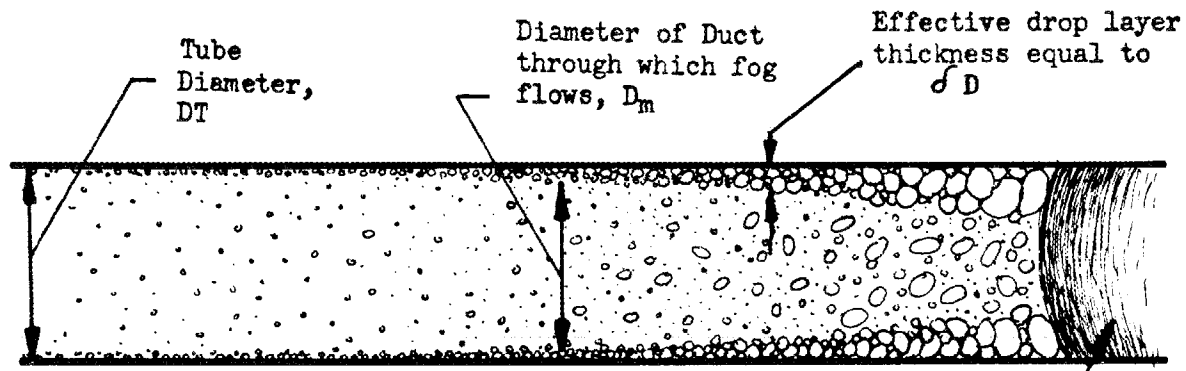
** Note that for a condenser, the mass flow rate of vapor continuously changes. Thus, the liquid fractions would trace out paths like the one shown by the curve in the upper right hand corner of Figure 16. This curve represents the liquid fractions predicted by the fog model for an inlet saturated vapor flow of 0.038 pounds per second to a condenser uniformly dissipating heat.



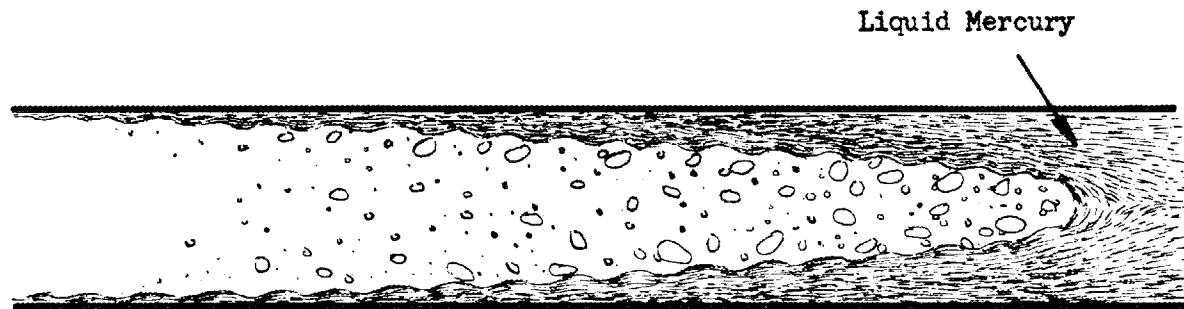
(Projection of spheres on plane normal to direction of flow divided by plate area)

Friction Factor as a Function of Roughness Density of Spheres Glued to a Tube Wall

FIGURE 1



(a) non-wetting condensing



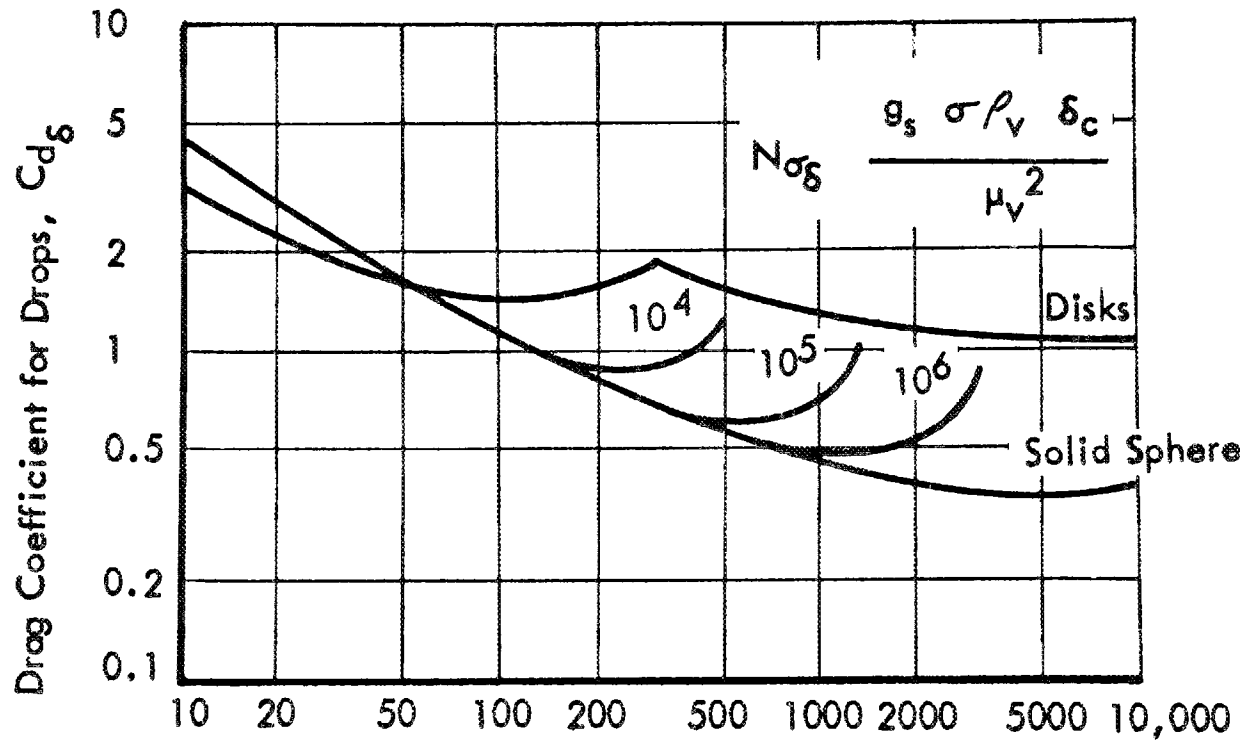
(b) wetting condensing

Similarity Between Wetting and Non-Wetting Flow
Patterns

FIGURE 2

DRAG COEFFICIENTS FOR SPHERES, DISKS AND DROPS

Reference 11



$$N_{R\delta} = \frac{\delta u \rho_v}{\mu_v}$$

FIGURE 3

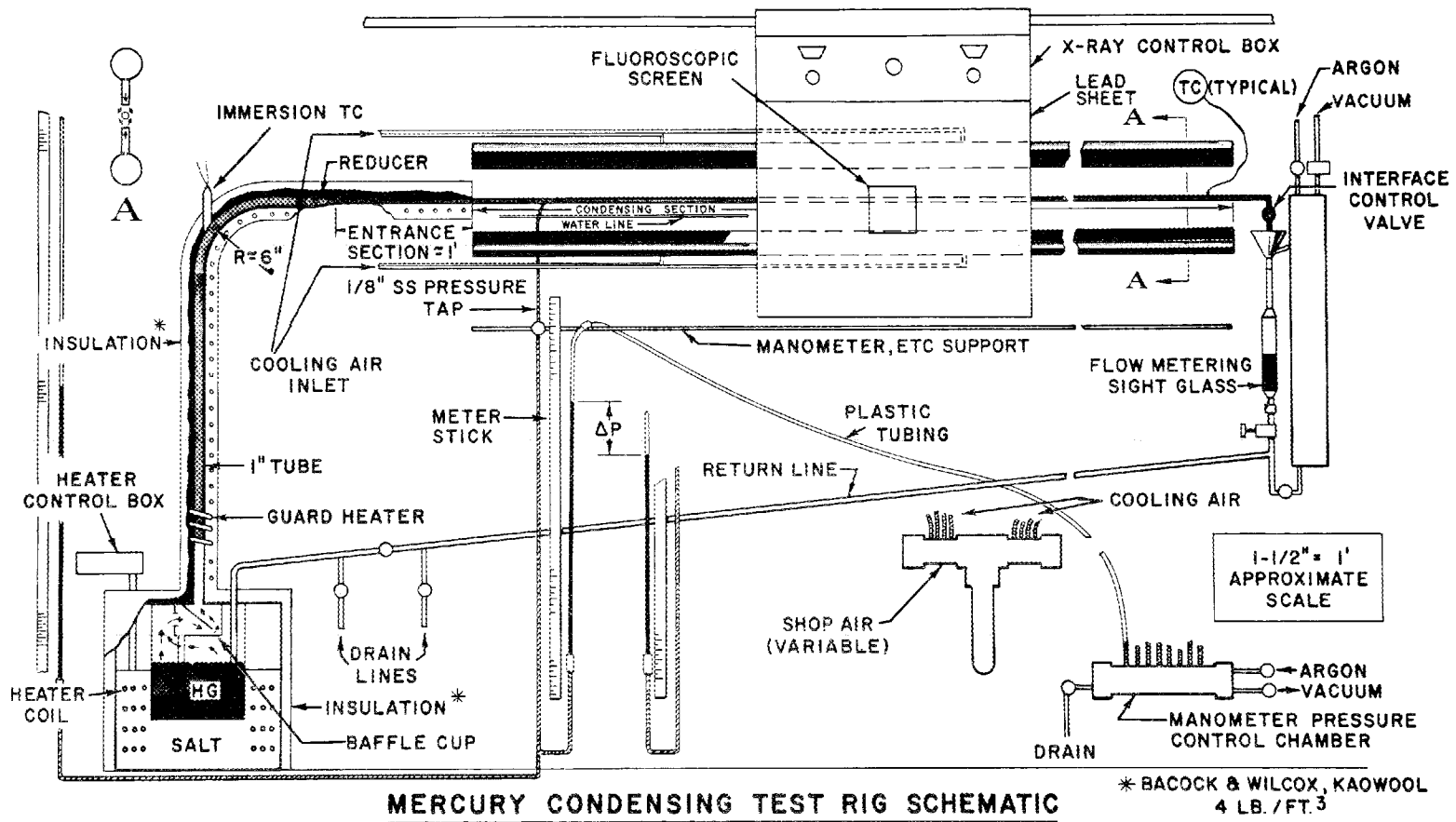


FIGURE 4

Comparison of TRM Series A Data
With Fog-Flow Prediction

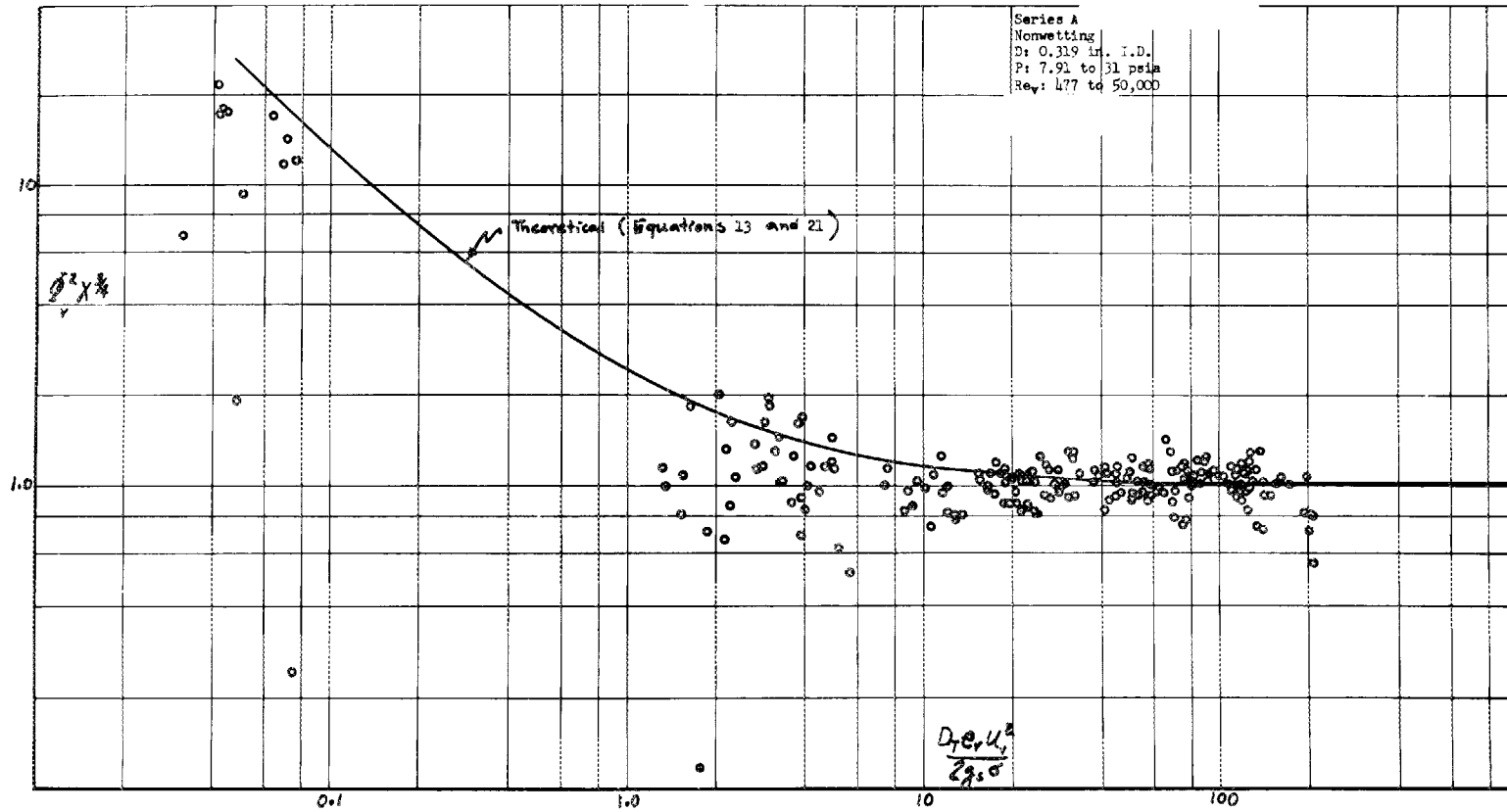


FIGURE 5

Comparison of TRW Series E Data
With Fog-Flow Prediction

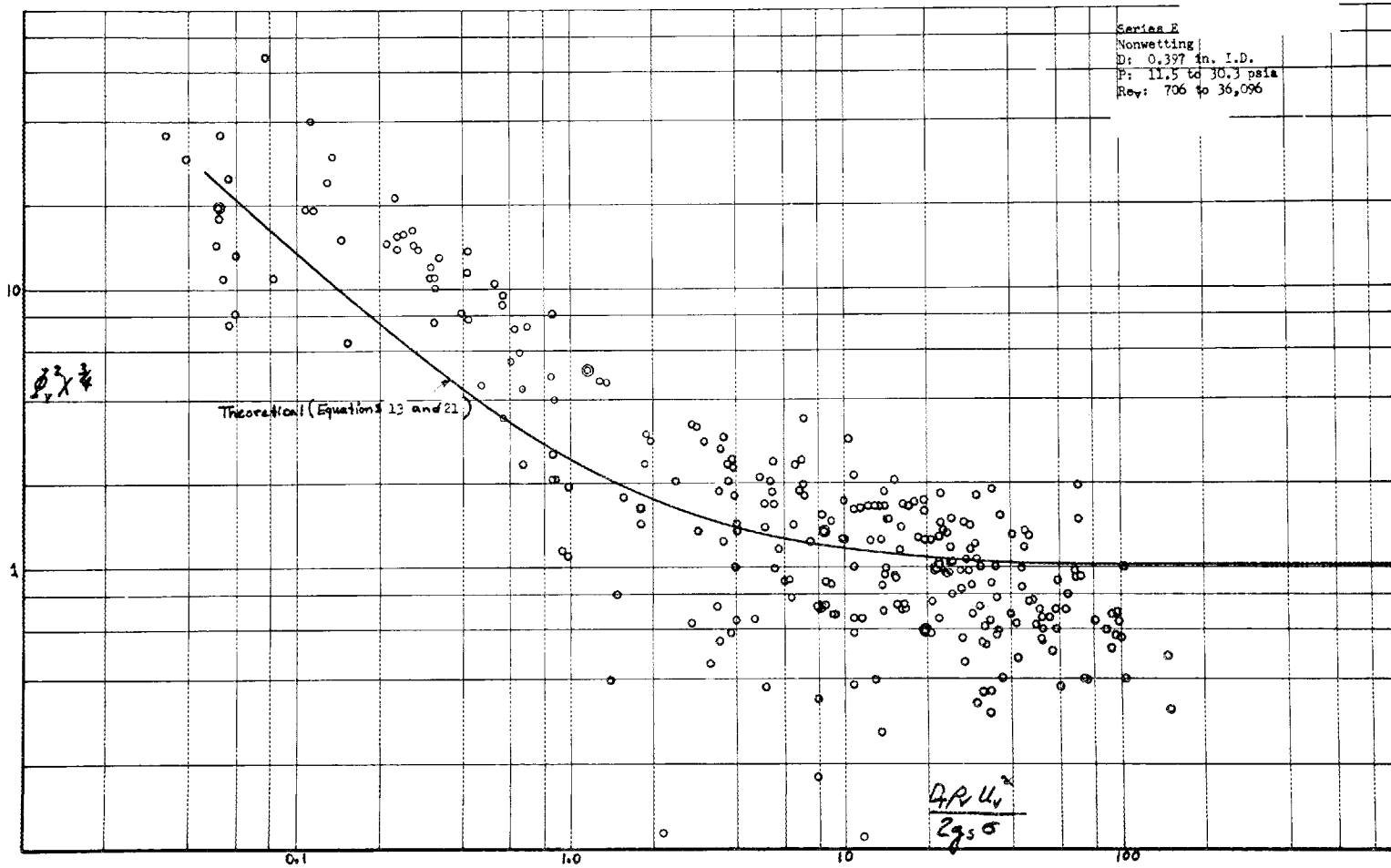


FIGURE 6

Comparison of TRW Series F Data
With Fog-Flow Prediction

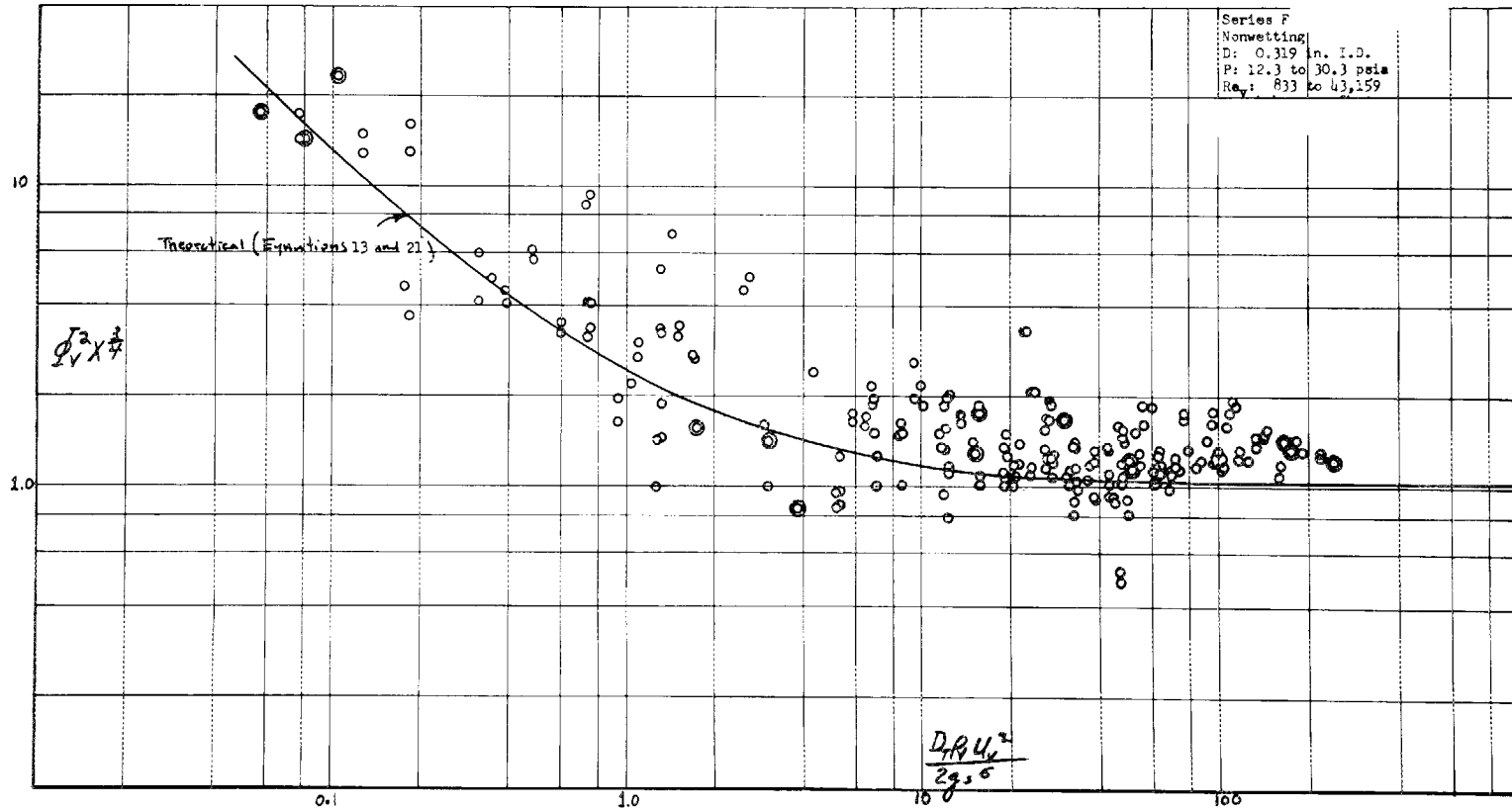


FIGURE 7

Comparison of TRW Series W Data
With Fog-Flow Prediction

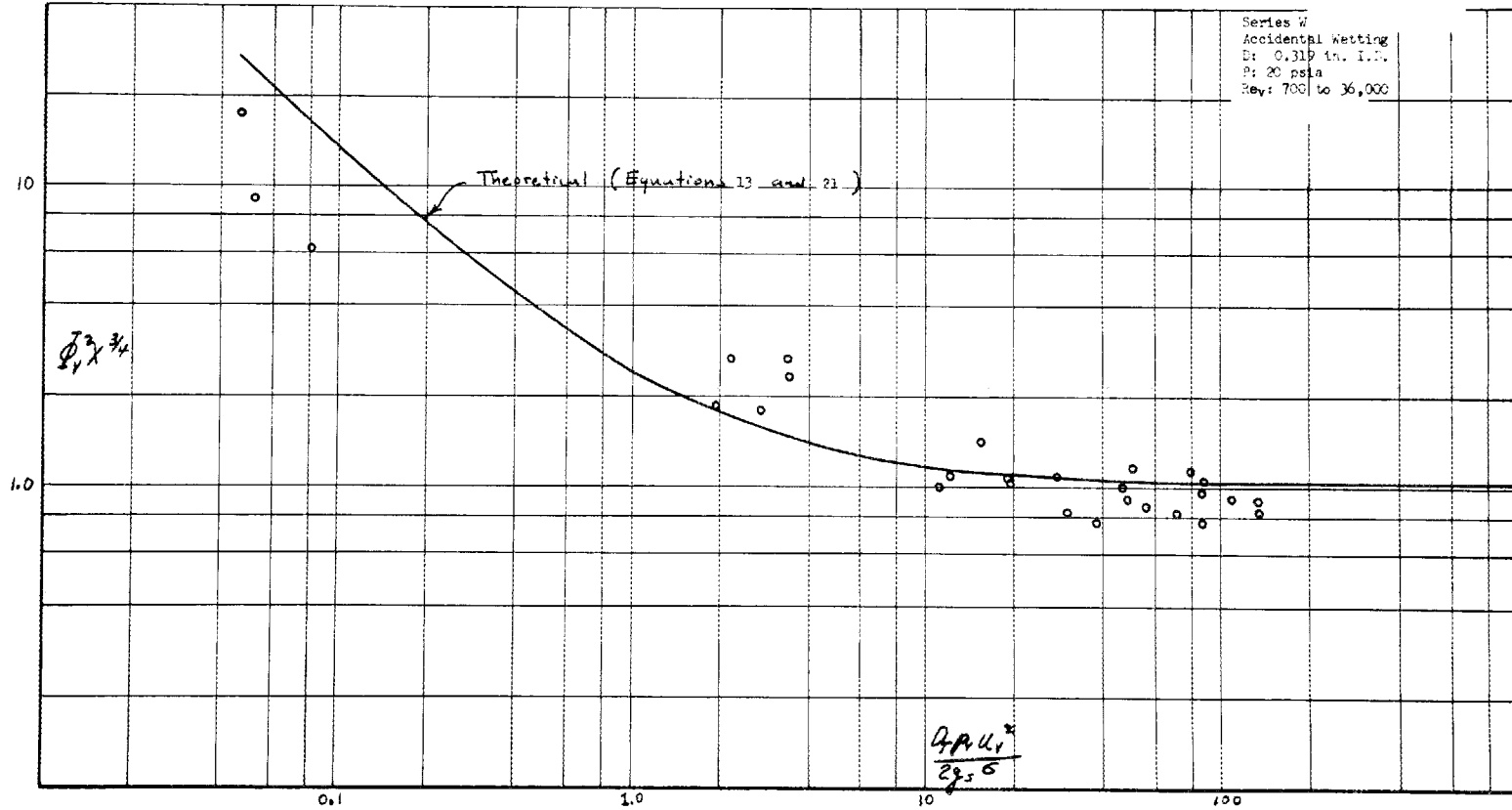


FIGURE 8

Comparison of TRW Series G Data
With Fog-Flow Prediction

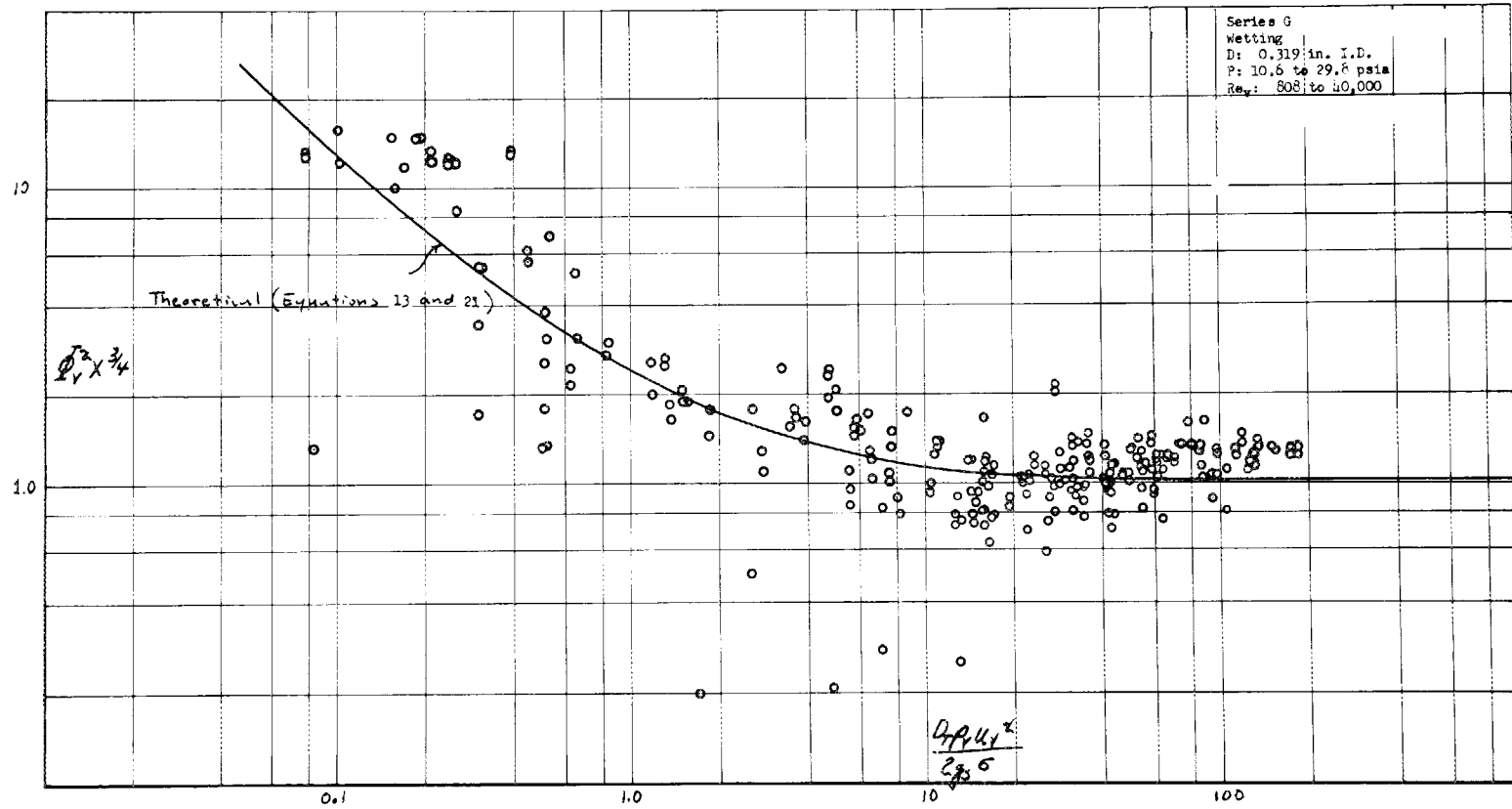


FIGURE 9

Comparison of THW Tapered Tube Data
With Fog-Flow Prediction

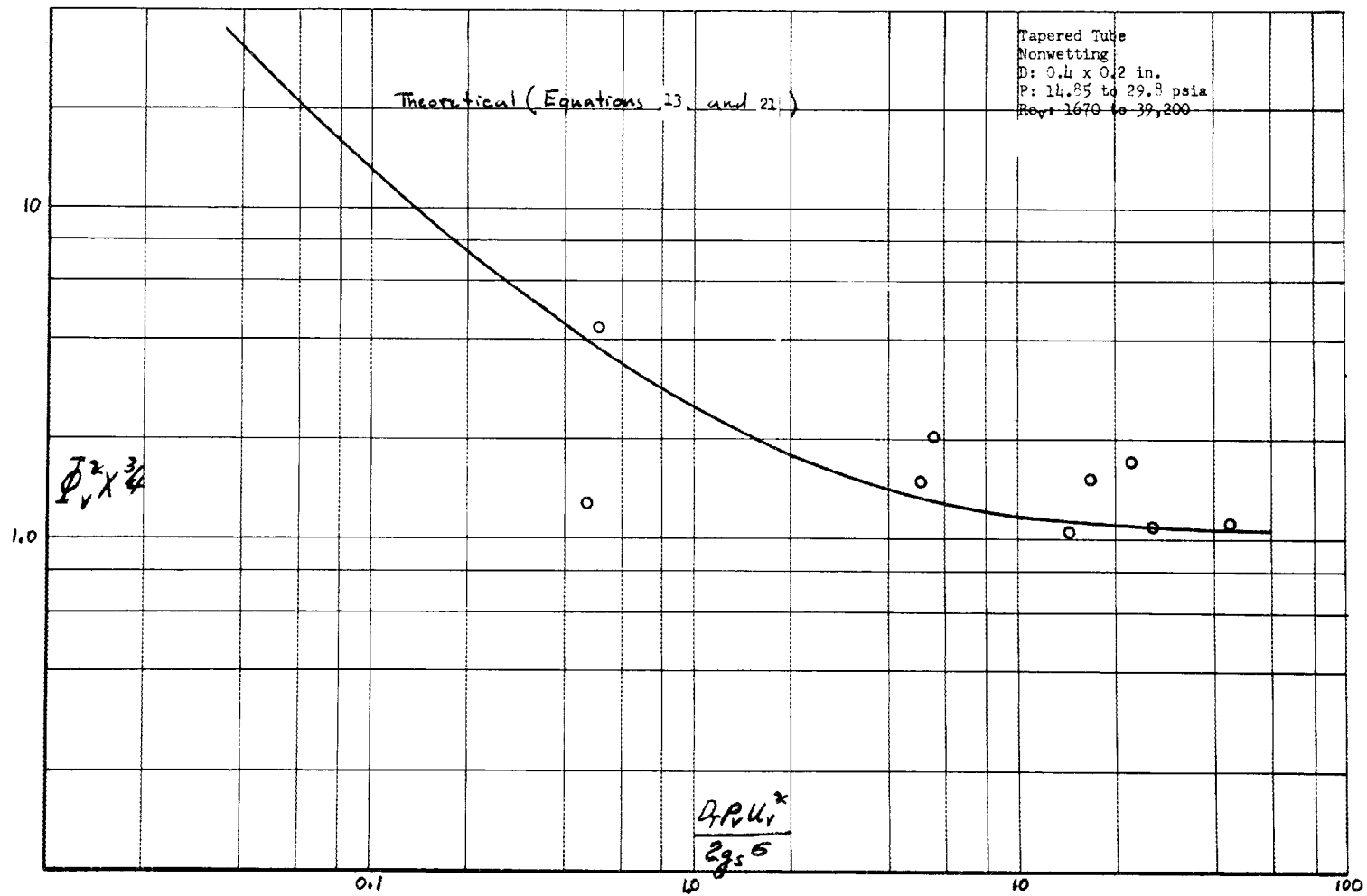


FIGURE 10

Comparison of ECS Data
With
Fog-Flow Prediction

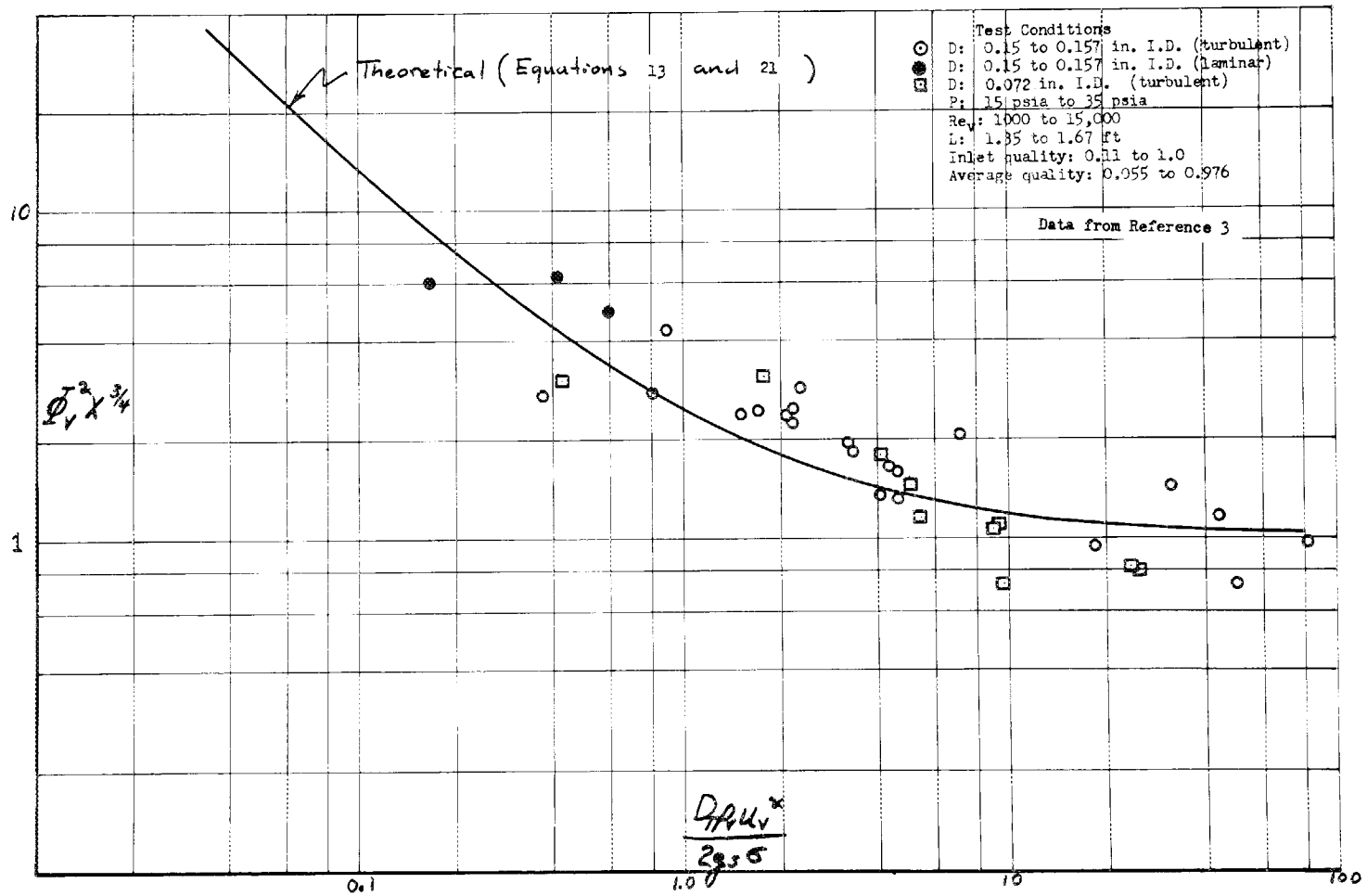


FIGURE 11

SKETCHES OF FLUOROSCOPIC OBSERVATIONS DURING CONDENSATION OF MERCURY
IN A HORIZONTAL 316 STAINLESS STEEL TUBE

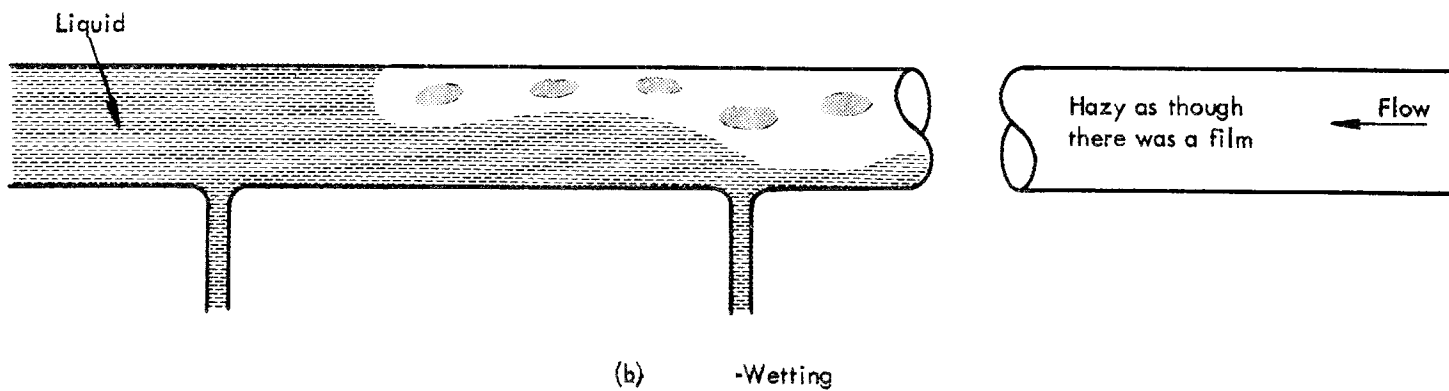
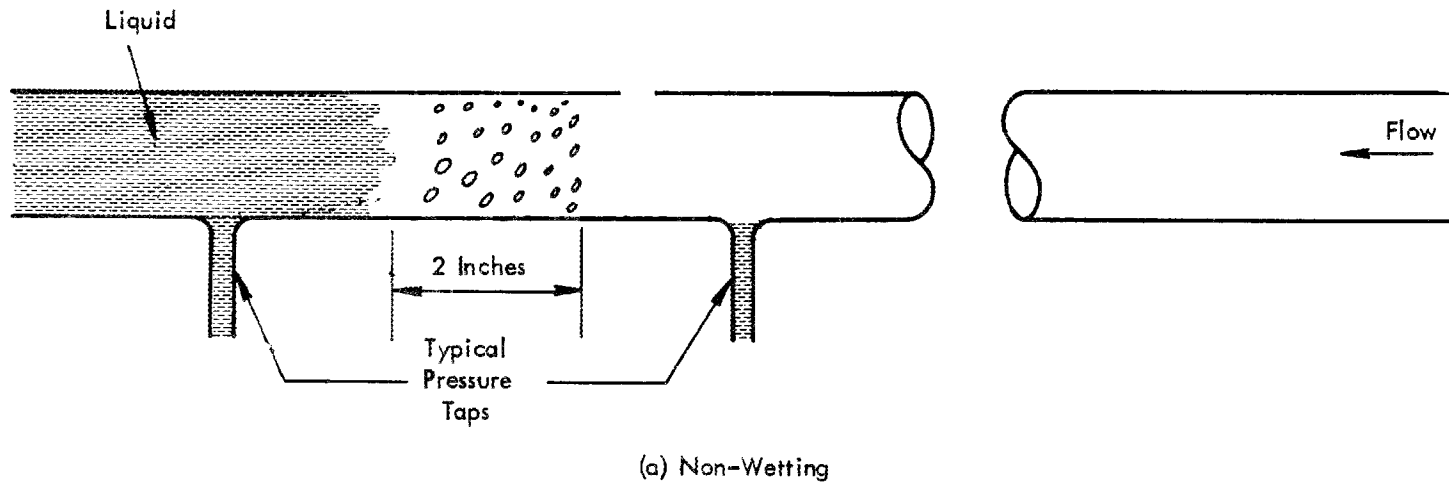


FIGURE 12

Comparison of TFM Data for Complete Condensing in
 Horizontal Tubes, in Tubes Inclined at 15°
 and
 in Tubes at Zero Gravity With Fog-Flow Prediction

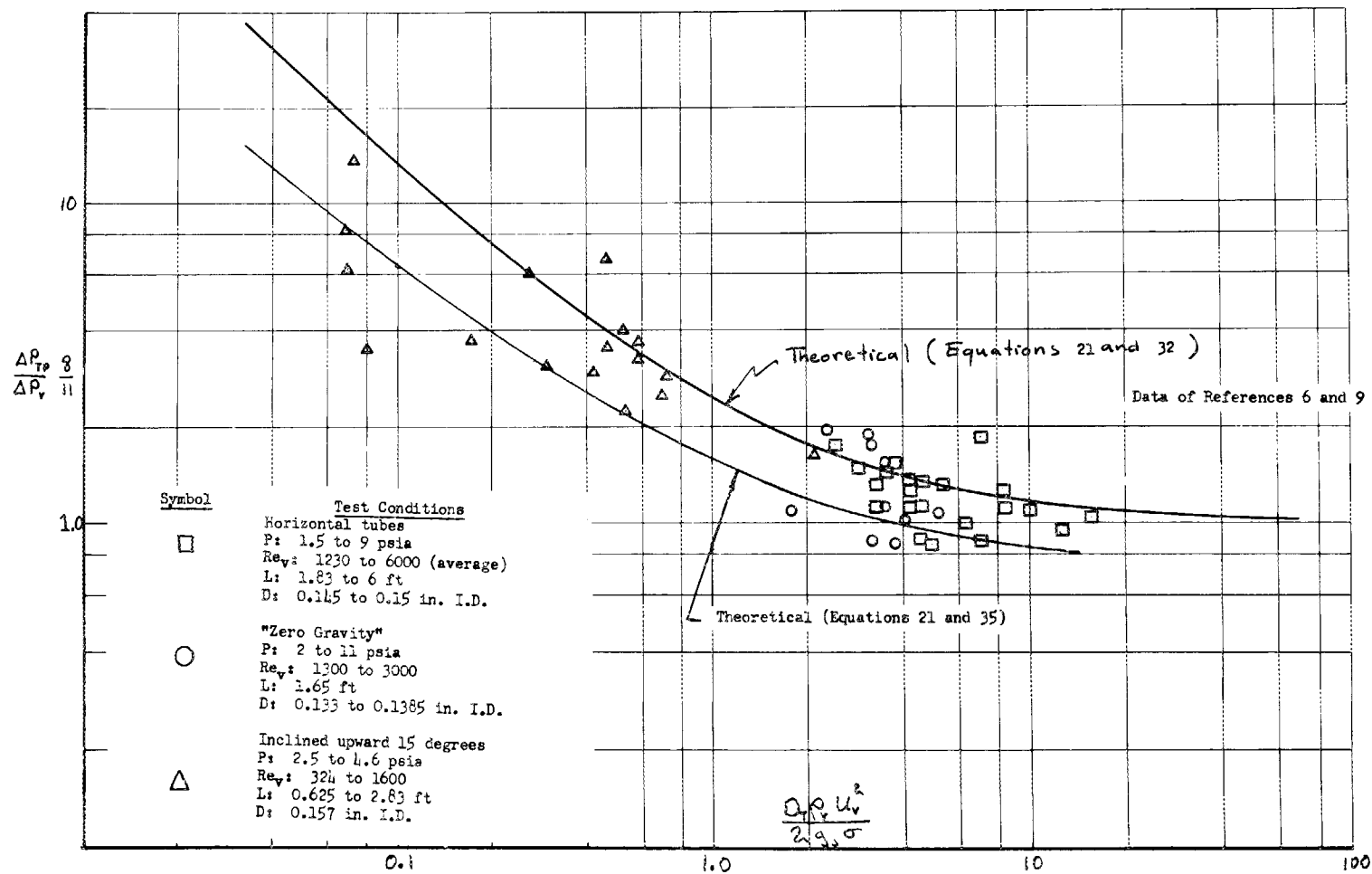


FIGURE 13

Comparison of THW Non-Wetting Data
With Lockhart-Martinelli Correlation

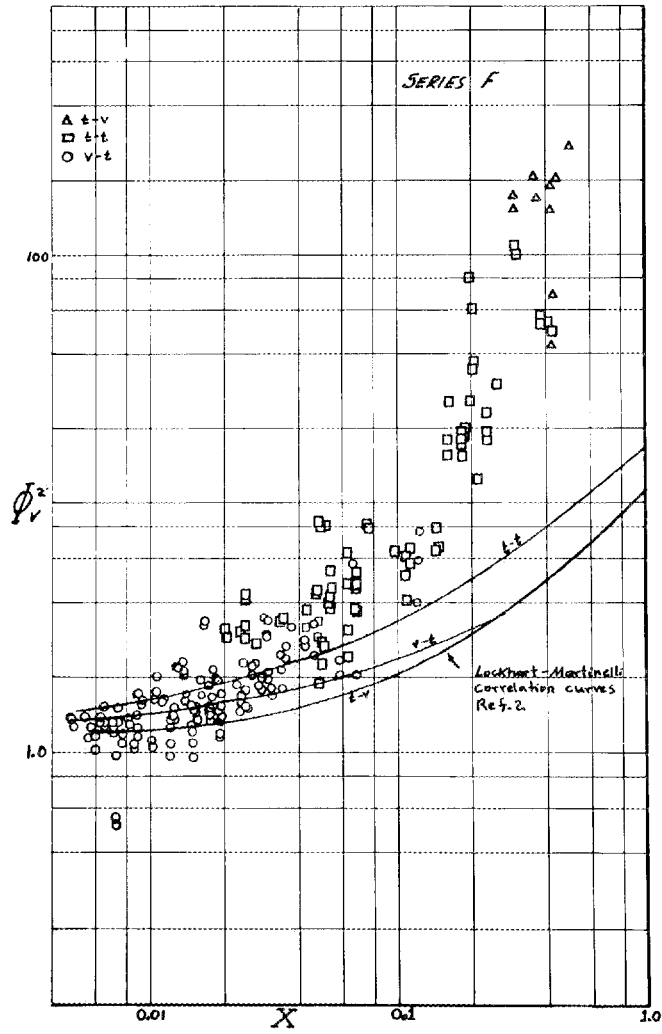


FIGURE 14

Comparison of TBM Waiting Data
With Lockhart-Martirelli Correlation

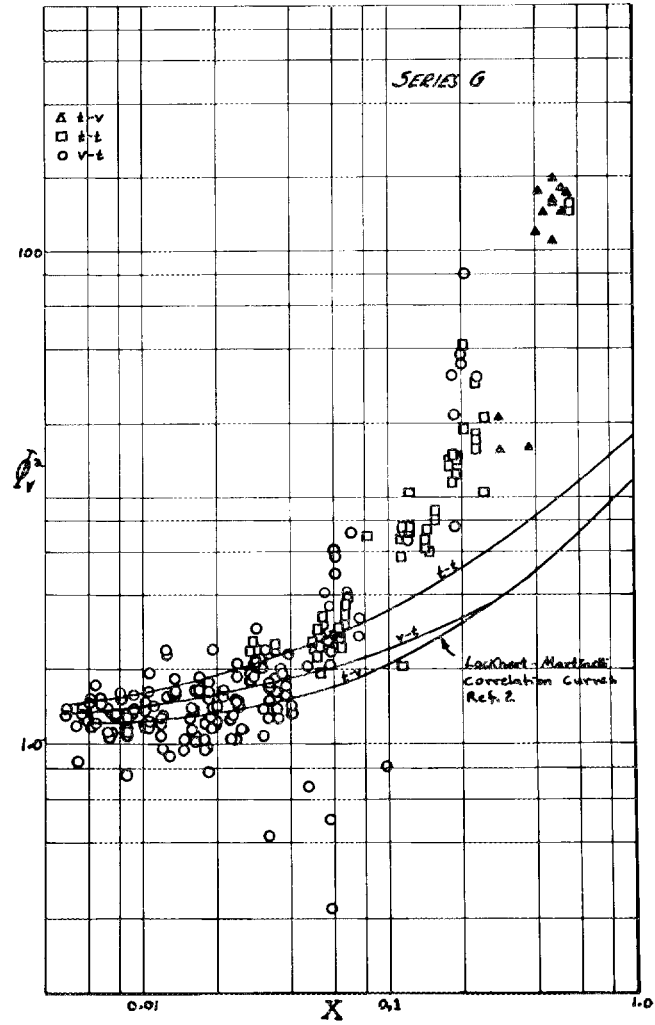
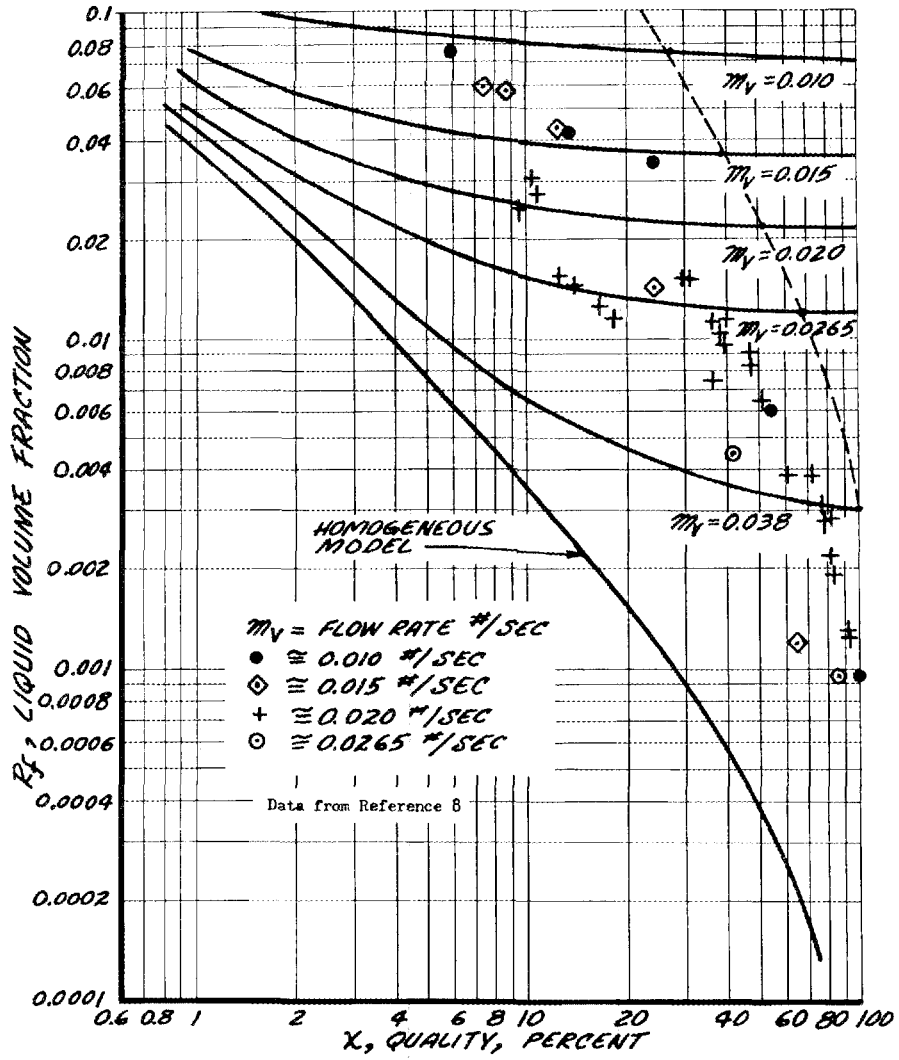


FIGURE 15



PROPOSED CORRELATION OF LIQUID VOLUME FRACTION FOR LOW HEAT FLUX CONDENSING MERCURY

FIGURE 16

DISCUSSION

MR. DAVIS: I don't quite understand the lack of inclusion of the decelerating--

MR. GUTSTEIN: The momentum terms were taken out of the experimental data by assuming the slip ratio was 1. I forgot to mention that. We corrected, in essence, the measured static pressure drop with a momentum term based on a slip ratio of 1. This is because we feel the drops travel at the same speed as the vapor.

MR. DAVIS: Which slip ratio of 1, both the vapor and droplets are accelerating as the vapor continually condenses?

MR. GUTSTEIN: Right. This was taken into account.

MR. HAYS: I notice on some of the figures ϕ_v^2 is the ratio of two-phase to the single-phase pressure drop. I notice some of the points were as low as 1/2. Is there a significance to this?

MR. GUTSTEIN: I don't know why there are these values that are that low. This is one of those mysteries. There were some really far-out points. I don't know why.

MR. STEIN: Perhaps we can answer why. He has to subtract the momentum pressure drop, and, secondly, these are experimental measurements. The theory certainly didn't go down below 1. So this is a kind of an inaccuracy you might expect.

MR. GUTSTEIN: Yes, but he is talking about the way out ones, where there were really low values.

MR. STEIN: I don't know if this is true in Marty's results, but in certain regions the frictional pressure drop component is pretty small, and when you subtract out the momentum you are left with a very inaccurate result. I don't know if that is true in yours.

MR. GUTSTEIN: That is true in the low Weber number region. This is where you get very low pressure drops, and you would expect to be very inaccurate in that area.

MR. STEIN: And your way-out points were in that low area.

MR. GUTSTEIN: For the most part, yes. There were very low pressure drops in that region.

MR. ROHSENOW: I missed the point. What is it you are measuring here? This was not isothermal, was it?

MR. GUTSTEIN: No. The static pressure difference was measured every foot in an eight-foot tube.

MR. ROHSENOW: And you assume no slip. You calculated the quality?

MR. GUTSTEIN: This was an air-cooled condenser, and the controlling heat transfer is the air coefficient, and we assumed this was practically constant over the whole tube, and therefore the $\frac{Q}{A}$ was practically constant. So you know the quality as a function of distance.

MR. ROHSENOW: No slip in the quality?

MR. GUTSTEIN: Right.

MR. STEIN: Just to clarify it in my mind: The empirical factors in this analysis are the customary friction factor relationships. These are the customary ones you used.

MR. GUTSTEIN: Right.

MR. STEIN: So that leaves your E_0 .

MR. GUTSTEIN: E_σ .

MR. STEIN: How were the values of E_σ obtained?

MR. GUTSTEIN: From separate measurements.

MR. STEIN: They are from entirely different measurements.

MR. GUTSTEIN: Yes.

MR. STEIN: So your theory, then, is something which is not an empirical relationship, really, for the pressure-drop measurements themselves? That is, you didn't take constants that appear in the analysis and evaluate these constants with the pressure-drop data?

MR. GUTSTEIN: No, we didn't; actually at Weber numbers above 10, the constants become unimportant. But what you have said is correct.

MR. KEYES: In your Eq. (4), which relates the Weber number to the ratio of 4 times E_{σ} , you indicate measured values of E_{σ} of .0464 which gives a critical Weber number of about .2. This seems unusually low. Is there a difference between mercury and other fluids in that analysis?

MR. GUTSTEIN: There is an Eq. (4) in the paper which gives the critical drop size times the velocity of the vapor squared over the surface tension, in other words, the Weber number for the critical drop size, equal to 4 times E_{σ} , and the question is that if you plug in the value of E_{σ} , you get a very low critical drop Weber number. Is this peculiar to mercury? And I think the answer is yes. But here I--I just know that, for example, for spraying, forming drops by spraying, you get a higher value of the Weber number.

I think for condensing, the Weber number is lower, characteristically.

I don't know if this helps you as an answer.

MR. STEIN: Are you saying that the Weber number is low for mercury, or do you really mean for this particular kind of a thing that's going on? This drop-wise condensing? If it were some other liquid metal, would you expect it to be the same?

MR. GUTSTEIN: It's a function of the surface tension. It is one over the surface tension.

MR. STEIN: That's in the Weber number.

MR. GUTSTEIN: I would rather say this is for mercury. I don't really know, frankly.

HEAT TRANSFER FROM A HOT SODIUM
SPRAY IMPINGING ON A VERTICAL PLATE¹

W. H. Nurick², J. D. Seader³ and T. A. Coultas⁴

Rocketdyne

A Division of North American Aviation

Canoga Park, California

¹ This study was conducted by the Combustion, Heat Transfer and Fluid Dynamics Group of the Research Center at Santa Susana, California

² Research Engineer, Heat Transfer and Fluid Dynamics Unit

³ Principal Scientist, Heat Transfer and Fluid Dynamics Unit

⁴ Group Scientist, Combustion, Heat Transfer and Fluid Dynamics Group

INTRODUCTION

In virtually all practical pyrotechnic ignition systems for solid propellant rocket engines, hot particles play a significant part in the transmission of thermal energy to a solid propellant surface. The objective of this program is to develop empirical correlations for determining heat transfer by this mode. Some examples of hot particles are aluminum and zirconium oxides and potassium chloride. While the effects of the various parameters important to heat transfer must ultimately be determined for these materials, the initial experimental studies reported here were conducted at lower temperatures where more convenient measurement techniques could be used. Sodium was used because it is easily handled and exists in the liquid state over a wide range of temperature. Once the correlation is established with sodium, tests using other materials such as potassium chloride should be conducted to ascertain any physical property effects.

The major variables are droplet size, angle of impingement, physical properties, flowrate per unit area and impingement velocity. An outline of the means of obtaining data for each variable is discussed below. Results from experiments with liquid sodium at temperatures of approximately 1100°F indicate that the heat transfer coefficient varied from about 360 to 530 $\text{Btu/hr-ft}^2\text{-F}$ when the sodium driving pressure was varied from 300 to 900 psig. This corresponded to a variation in flowrate per unit area of about 0.68 to 4.90 lb/sec-ft^2 .

EXPERIMENTAL APPARATUS

A schematic flow diagram of the test apparatus is shown in Figure 1. A photograph of the test chamber is shown in Figure 2. A 2-inch by 0.5-inch wide molybdenum - 0.5% titanium plate was used as the test strip. It was 0.010-inch thick to minimize conduction effects. Provisions were made for electrically heating the strip to a temperature above the freezing point of sodium. This was accomplished by silver soldering the ends of the test strip to copper bus bars. A bank of dc motor-generator sets provided the heating power. The test strip was mounted vertically in the test chamber and was instrumented with four thermocouples on the back side as shown in Figure 3. The two couples on either side of the center were Pt/Pt-10% Rh of 0.001-inch wire diameter, and the other two couples were Iron-constantan of 0.01-inch wire diameter.

All recording of temperatures as a function of time was made on a Consolidated Electrodynamics Company recording oscillograph at a film rate of 12.8 inches/second. Voltage and current measurements for the electrical pre-heating of the strip were recorded on conventional Brown Electronik recorders. Test chamber pressure was measured with a Bordon type vacuum-pressure gage. All tank and valve pressures were adjusted by standard hand loaders and various sodium feed line temperatures were monitored by Sim-Pyl-Trol gages.

Hot liquid sodium was sprayed onto the test strip by an injector directed at and located about two-inches from the center of the test strip. A study conducted by Burge (Ref. 1) indicated that single-hole jets are not practical to adequately distribute alkali metals. His study showed that the hole size would have to be about 0.001-inch in diameter, and two holes would be required to adequately spray a square inch of surface area. Further, the high surface tension of the liquid metal would result in a requirement for high starting pressure in order to force the liquid sodium through the small holes. He solved the problem by utilizing impinging jets, in doublet fashion, to form spray fans which covered large areas. This arrangement was utilized in this study. To date only a flat-face plate injector with two 0.0135-inch holes impinging at an included angle of 30 degrees was tested. Inserted in the manifold of the injector was a shielded Chromel-Alumel thermocouple to measure the sodium injection temperature.

EXPERIMENTAL PROCEDURE

Prior to the start of a series of tests, the sodium, sodium tank, lead lines and manifold were pre-heated to a selected temperature (usually between 900 and 1100°F). Because of the incompatibility of sodium with air, the test chamber was evacuated by means of a vacuum pump; then Argon was bled into the chamber and a desired pressure level was established. Argon was also used to pressure-feed the liquid sodium from the tank through the injector. Prior to sodium injection, the sodium

tank pressure was pre-set and the test strip was pre-heated to a temperature above the freezing point of sodium. The strip was heated in order to insure that the sodium would not freeze and adhere to the test strip during the run. The oscillograph was then turned on and approximately two seconds later (this time varied) the power to the strip was turned off and simultaneously the sodium valve was opened, which allowed sodium to be sprayed on the test strip. After about a 4 second run duration, the sodium flow was terminated. A typical temperature-time plot for the two Pt/Pt-10% Rh thermocouples is shown in Figure 4. The slight temperature decrease seen initially is due to plate cooling after shutoff of the electrical heating power. As seen, a reasonably steady-state condition was reached in less than 0.5 seconds.

The amount of sodium impinging on a selected area of the plate was measured in separate tests by means of a pre-weighed catch tank. The placement of the catch tank in the chamber was such that its center coincided with the center of the molybdenum strip. Two thermocouples were placed at different locations on the catch tank, and were connected to a recording oscillograph. The sodium at a pre-selected tank pressure, and heated to the desired temperature, was then sprayed in the same manner as in previous runs. The catch tank was then removed and reweighed. The change in weight divided by the average time indicated by the thermocouples gave the average flow rate impinging on the area of interest.

METHOD OF ANALYSIS

A heat balance on the central portion of the test strip during the transient period yields the following relationship:

$$m C_p (dT/d\theta) = hA (T_{Na} - T) - q_{cr} \quad (1)$$

where:

- m = test strip mass corresponding to spray area, lb_m
- C_p = test strip specific heat, Btu/lb_m-F
- T = temperature, F
- θ = time, hr
- h = heat transfer coefficient, $Btu/hr-ft^2-F$
- A = spray area, ft^2
- T_{Na} = sodium injection temperature, F
- q_{cr} = convection and radiation losses from back of strip, Btu/hr

Equation (1) is valid only if the Biot number, (ht/k) , is less than about 0.01 and if conduction from the center outward towards the bus bar connections is negligible. Based on the tests reported below, Biot numbers were typically less than 0.01. The determination of the possible error introduced by neglecting conduction along the length of the test strip was determined from the experiments. This was accomplished by placing thermocouples at two other locations near one end of the length of the strip as shown in Figure 3. In general, calculations based on the measured temperature profiles indicated that the conduction loss was probably no greater than 10 percent during the initial portion of the transient period. The 0.01 inch thick molybdenum strip was, therefore,

adequate for the approximation involved in applying Equation 1. A calibration of the test strip under conditions of no sodium spray indicated that q_{cr} was negligible. The solution for the heat transfer coefficient then becomes simply:

$$h = \rho t c_p \left(\frac{dT}{d\theta} \right) / (T_{Na} - T) \quad (2)$$

where:

$$\rho = \text{test strip density, lb/ft}^3$$

$$t = \text{test strip thickness, ft.}$$

Values of $dT/d\theta$ are determined at different points on the temperature-time response curve. The sodium temperature, T_{Na} , was assumed to be that measured at the injector or in the sodium tank. These two temperatures were maintained approximately equal by heating of the line from the tank to the injector.

TEST RESULTS

Four tests were performed at the following conditions:

<u>Run</u>	<u>Sodium Tank Pressure, psig</u>	<u>Chamber Pressure, in Hg</u>	<u>Sodium Temperature, °F</u>
1	500	15	1130
2	900	15	1030
3	700	15	1030
4	300	15	930

For each run, heat transfer coefficients were calculated as a function of time for the initial portion of the transient period from Equation (2) using the respective transient temperature response curves. As noted above, a typical response curve for Run 3 is shown in Figure 4. As seen, the centrally located thermocouples 3 and 4 measured approximately the same values. Typical calculated heat transfer coefficients are plotted in Figure 5.

As seen in Figure 5, heat transfer coefficients on the order of 400 to 500 Btu/hr-ft²-°F were measured. These coefficients appeared to decrease with increasing time. More refined measurements will be required to ascertain this.

Measurements of the sodium flow rate were not entirely satisfactory due to some lack of reproducibility of the spray characteristics with sodium. From the data obtained, sodium flow rates of about 0.68 to 4.90 lb/sec-ft² corresponded to the driving pressure range of 300 to 900 psig. Check flow rate measurements with water, however, gave consistent values and indicated that about one-half of the total injector flow rate impinged on the 0.25 square inch central section of the test strip.

CONCLUSIONS

The results reported here are only preliminary and do not begin to adequately describe the effects of all the variables. More data must be obtained even for the parameters already tested. The

other parameters such as droplet diameter and impinging angle must then be tested. Once these variables are studied an explicit expression must then be determined which describes the effects. When this is accomplished the phase of the program using sodium will be terminated. The correlation should then be tested with higher temperature materials to check its validity.

The data reported above also indicate that a more refined measurement technique is desirable to obtain a more detailed temperature profile. In addition, an improved test strip geometry appears to be necessary.

In order to determine the variables such as impact velocity, droplet diameter, and droplet breakup characteristics, various high-speed photographic methods should be employed.

REFERENCE

1. Burge, H. L., "A Fundamental Study of Spray Cooling Processes," Rocketdyne Report R-3746.

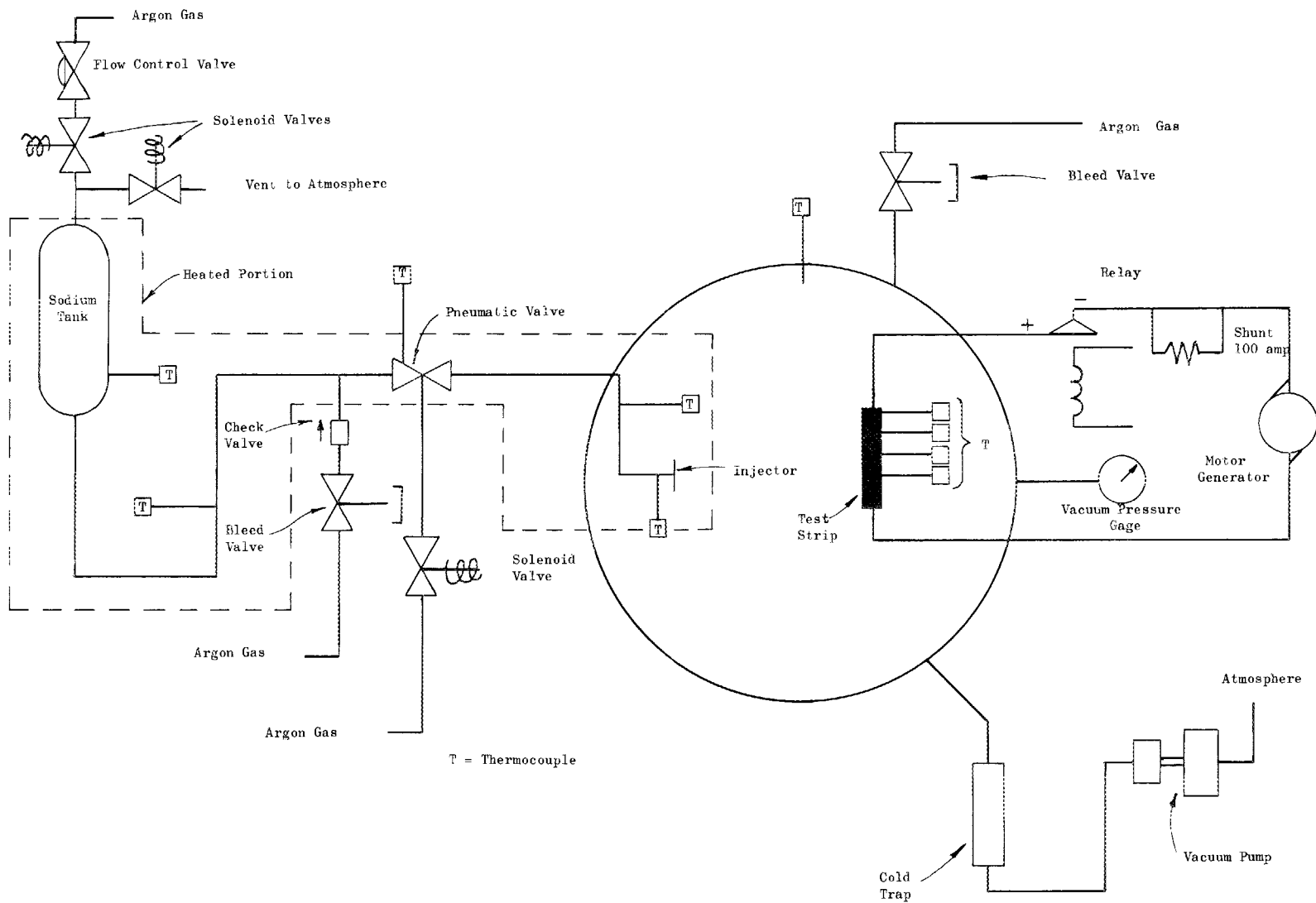
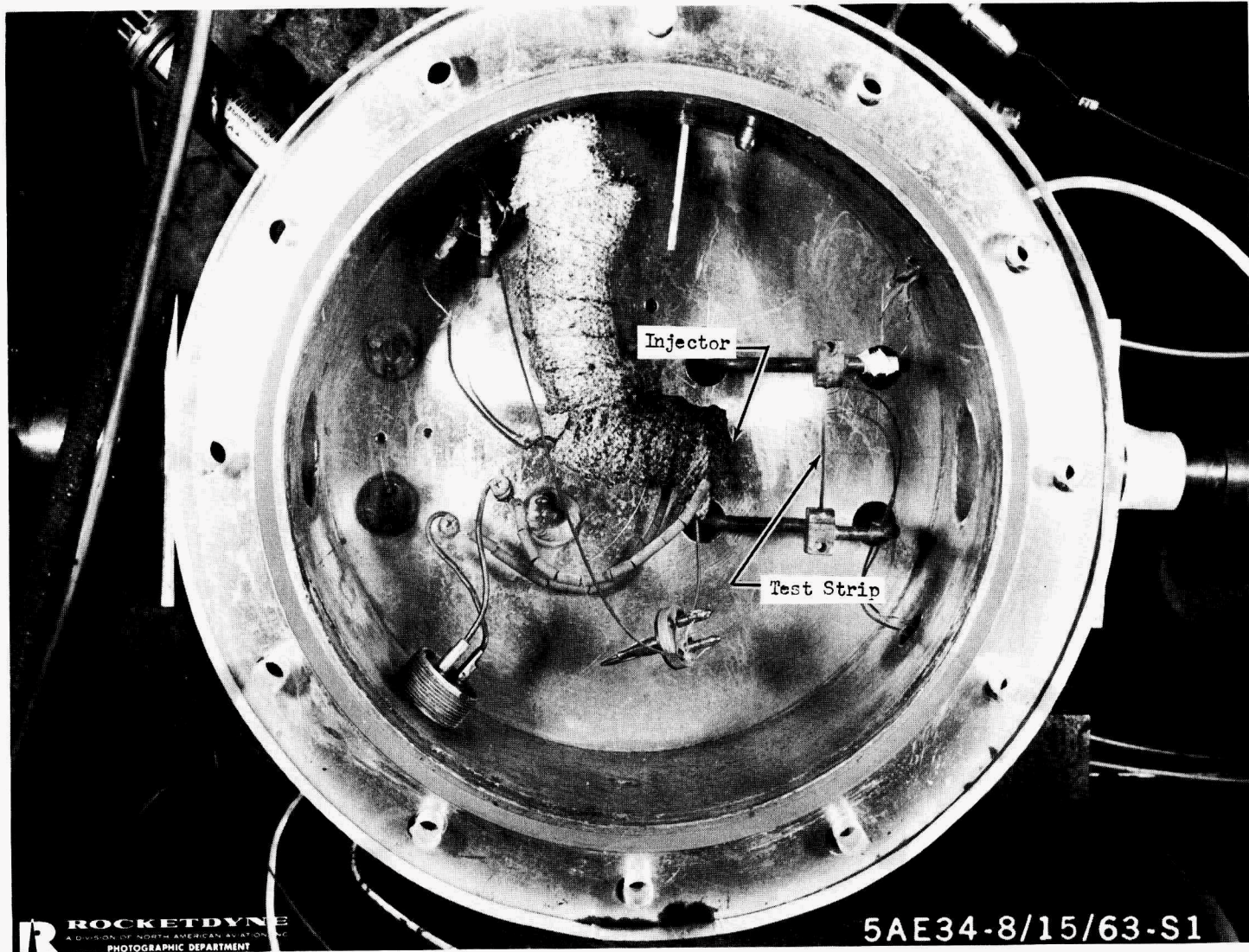


Figure 1. Schematic Flow Diagram of Test Apparatus

Figure 2. Photograph of Test Chamber



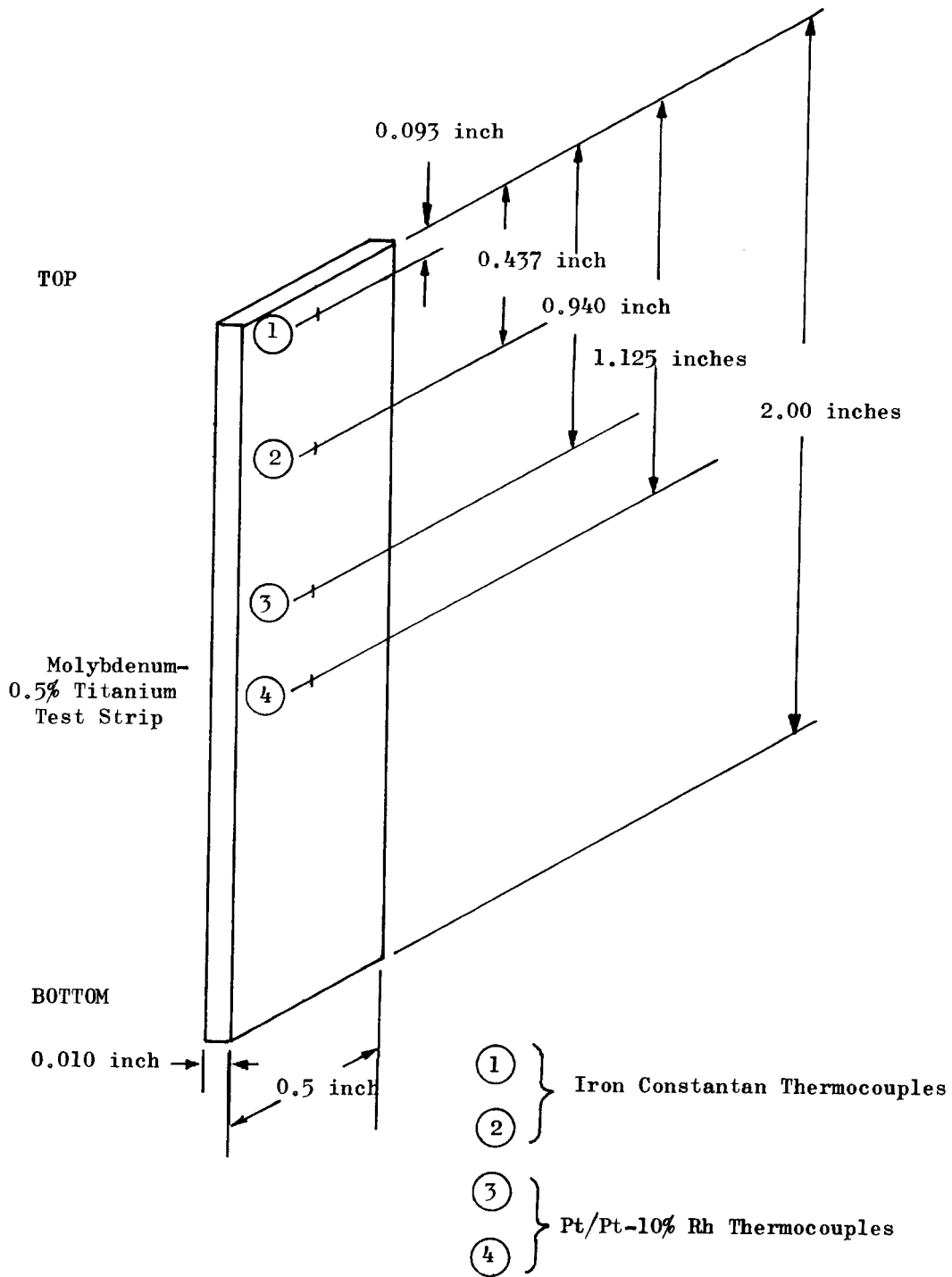


Figure 3. Test Strip Thermocouple Placement

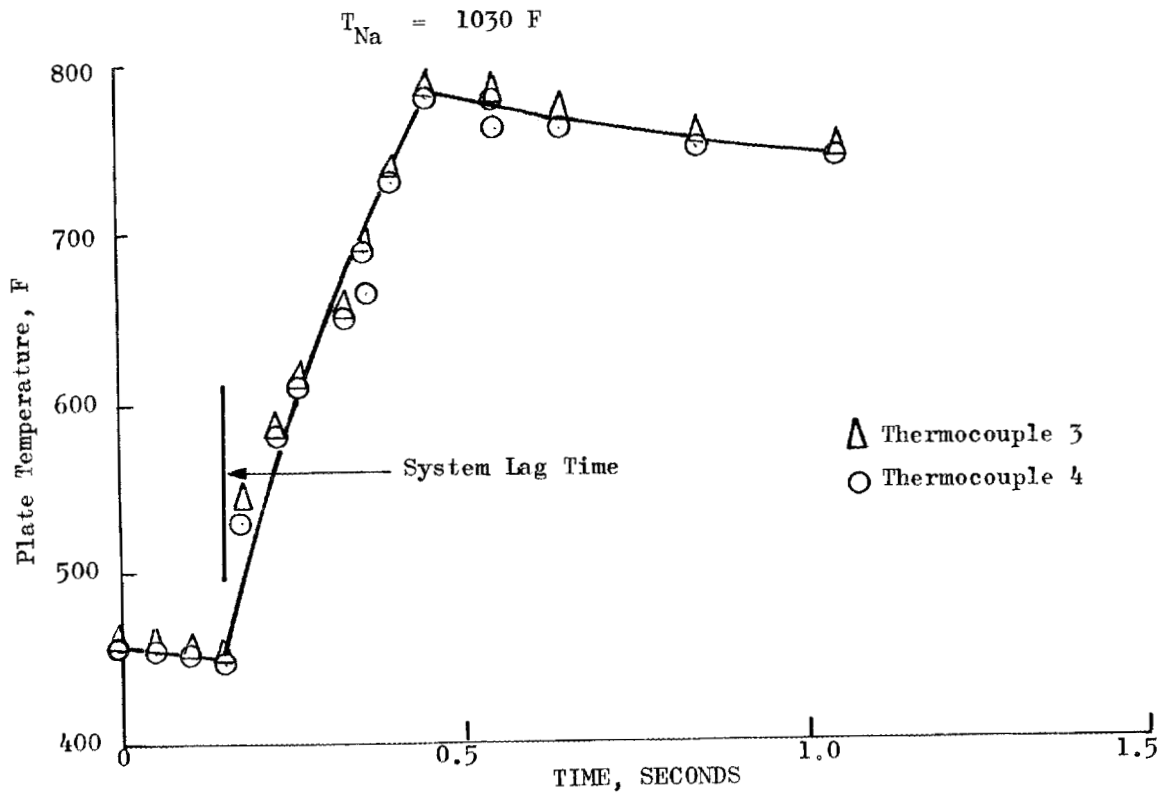


Figure 4. Typical Transient Temperature Response Curve, Run No. 3

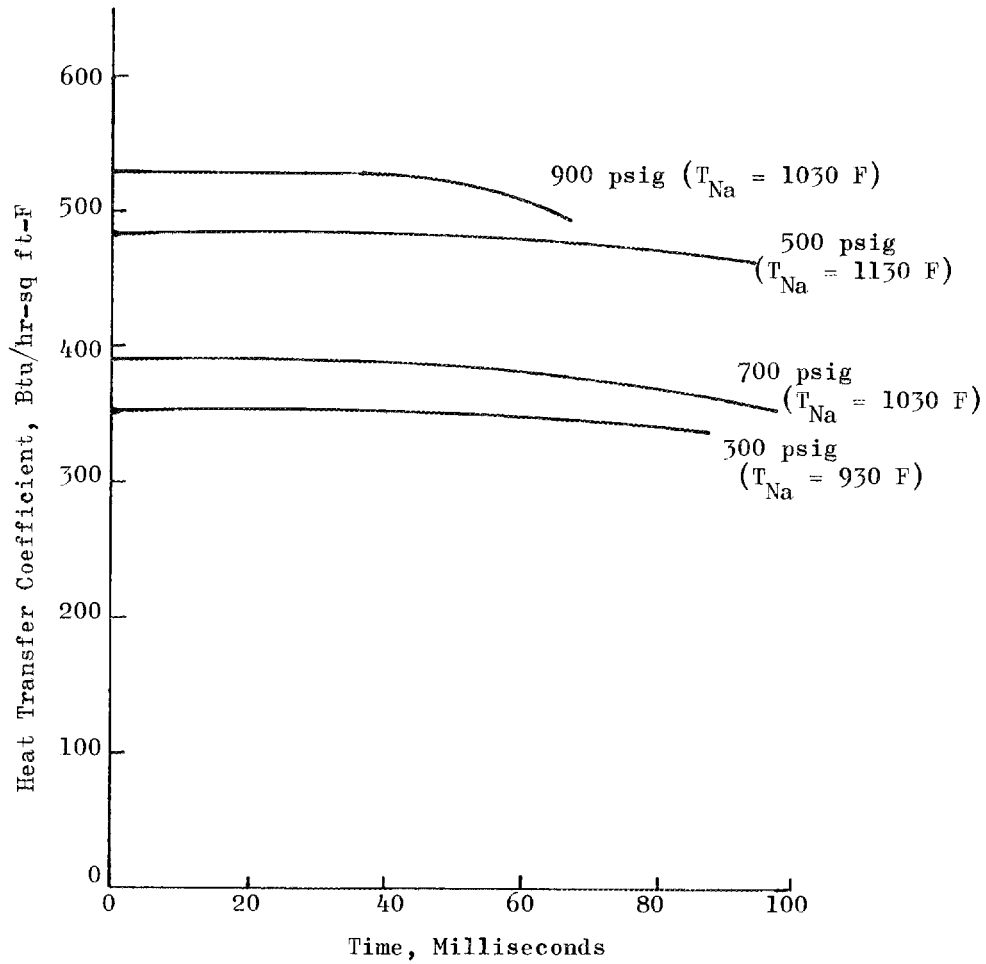


Figure 5. Heat Transfer Coefficient vs Time

DISCUSSION

MR. LYON: As I understand it, you measured the flow rate per unit area by catching the flow in a bucket, and you were attempting to measure the velocity of the particals by--

MR. NURICK: No, we haven't measured the velocity yet.

MR. LYON: I see. But you intend to.

MR. NURICK: Yes.

MR. LYON: It occurs to me this would have a very pronounced effect on heat transfer, wouldn't it?

MR. NURICK: I would say it has a very great effect.

MR. LYON: I was wondering whether you could do this by either impulse--perhaps by an impulse impinging on a small section.

MR. NURICK: Our flow rates are so low that I think the accuracy that is involved here would be deleterious to us.

MEASUREMENT OF THE PRESSURE DROP OF SUPERHEATED CESIUM VAPOR ACROSS A LAMINAR FLOW DEVICE

By

William A. Samuel
MSA Research Corporation
Callery, Pennsylvania

INTRODUCTION

The work described herein was included in a study sponsored by the National Aeronautics and Space Administration, the objective of which was to obtain design information for a zero-gravity mass flowmeter for cesium in the milligram per second range. In this paper, only those facets of the study which are pertinent to liquid metals per se will be discussed.

The problem of how to demonstrate feasibility of an approach seemed to have one best answer: build and operate a prototype system. Although the zero-gravity effects could not be duplicated, the questions of corrosion, mass transfer, and general soundness of principle could at least be partly resolved by such a demonstration. The program was directed toward the assembly of a system in which the flow rate of superheated cesium vapor would be metered by measuring the pressure drop across a laminar flow device. An apparatus was built in which cesium was boiled and the vapor subsequently superheated. The pressure drop created by the passage of this vapor through a capillary was measured at various flow rates by means of an attitude insensitive device designed and built at MSAR. The problem of determining the vapor throughput was resolved by actually condensing the cesium and measuring its volume.

Throughout this study the emphasis was placed on establishing the feasibility of this approach. Great pains to refine measurements therefore were not warranted; the main effort was expended rather to obtain a workable integrated system. The experimental equipment included the boiler, superheater, control panel, collection apparatus, capillary, differential pressure device and electronic components to read out the position of the differential pressure device. A plot was made of flow rate vs. differential pressure, and this was compared with the theoretical value. The agreement was quite good and indicated how this principle might be used as a means of measuring the viscosity of superheated vapors.

APPARATUS

Boiler and Superheater

The dimensions and details of the boiler are shown in Fig. 1. Based upon MSAR's past experience, Type 316 stainless steel was chosen for the principal material of construction. The maximum level of cesium

was limited to two inches below the demister, which was added as a precaution against liquid droplets being entrained to the superheater. The full length of the boiler was heated by a 1600 watt electric furnace.

During the design stage it was arbitrarily assumed that the boiler would produce vapor of approximately 90% quality at 1000 F. The duty of the superheater would have been to heat this material to 1200 F. As it developed, however, during operation the upper portion of the boiler reached temperatures of 1200 to 1400 F, thus obviating the need for the superheater. The vapor was superheated by the demister and the top of the boiler. Heat losses from the cesium stream were virtually eliminated through the use of trace heaters all along the vapor lines.

Condensate Collector

For the measurement of the cesium flow rate, the most direct approach was taken - that of collecting the material as condensate in a calibrated glass receiver. Because the tendency for cesium to wet glass would soon obscure the entry side of the tube, the collection receiver was made with two legs, as shown in Fig. 2. Although this resulted in some inaccuracy, it was negligible for the application involved. A connection was provided leading to a trap, bubbler and vacuum pump to maintain a collection pressure of essentially 40 mm. For reasons of safety, the tube was placed inside a Pyrex cylinder, and a blast shield was placed in front of the glassware assembly when it was operated under vacuum. During operation with cesium, the cylinder was heated with a nichrome trace heater to insure that the cesium remain molten.

Capillary Sizing

From the Hagen-Poiseuille law for loss of head with laminar flow, it was calculated that a six inch capillary one millimeter in diameter would produce a pressure drop of about 1 psi for the desired flow rate of 25 cc/sec of cesium vapor at 1200 F and 3 psia. The equation used was:

$$q_c = \frac{\pi g D^4}{128 \mu L} \Delta P \quad (1)$$

For a given capillary at constant temperature, this can be reduced to:

$$q_c = K \Delta P \quad (1a)$$

where K is a constant since viscosity does not vary with small changes in pressure. (It can be seen here that if q_c and ΔP are both measured, the viscosity can be calculated if the dimensions of the capillary are known.) Since q_c is a volumetric quantity, to get a mass flow it must be multiplied by a density factor. Since density at

the midpoint of the capillary varies with changes in differential pressure, it is more convenient to compute the mass rate at the entrance. For this, the volumetric rate must be determined at the device inlet, and the mass rate will be:

$$M = q_i d_i \quad (2)$$

By assuming that the pressure drop from the boiler to the capillary inlet is negligible and that Boyle's Law applies,

$$q_i = q_c \left(\frac{P_c}{P_i} \right) = K \Delta P \left(\frac{P_B - \frac{\Delta P}{2}}{P_B} \right) = K \left(\Delta P - \frac{\Delta P^2}{2 P_B} \right) \quad (3)$$

For the stainless steel capillary used in this study, with the boiler at 1000 F and the superheater at 1200 F, the mass flow equation becomes:

$$M = 0.64 \left(\Delta P - \frac{\Delta P^2}{183} \right) \quad (2a)$$

where M is in mg/sec and ΔP is in inches of water. A plot of this equation is shown as the theoretical curve of Fig. 10.

Differential Pressure Gage

The purpose of this transducer system was to demonstrate feasibility of principle at minimum cost. No effort was expended, therefore, to make the unit compact or light in weight. The device was designed for operation at 1200 F over a differential range of 1 psi and for an accuracy of 5%, using principles that would be suitable for zero-gravity operation. Fig. 3 shows a schematic of the apparatus. For low flow rates, as in this study, a single capillary tube would be used as the pressure drop element, while for high rates a multi-channel laminar flow element would be employed.

In operation, the large bellows tends to be displaced to the right by an increase in differential pressure. The two smaller bellows permit motion and allow access for the control and corrective forces. When the large bellows is slightly displaced from the null position, the differential transformer sends a proportionate signal to the amplifier. The amplifier output operates the servo motor to displace the Bellofram (a commercial item) in a corrective direction. For an increase in differential pressure, the Bellofram rises and compresses the inert gas to counteract the displacement. When the core of the differential transformer returns to the null position, the system will be in balance and motion will cease. The pressure on the indicating gage is proportional to the pressure differential across the main bellows. To insure that the differential transformer was at null during the tests, an oscilloscope was connected in parallel with the amplifier

output to verify null polarity. Although in this prototype a direct-reading bourdon tube gage was used to measure the balancing pressure, in a space application a transducer with electrical output would be provided.

In constructing the apparatus, all parts which were to be exposed to hot cesium were made of 300 series stainless steel. These various components were then assembled into the system shown in Fig. 4. Prior to operation with cesium, calibration tests were made on the differential pressure transducer using argon gas. Tests were run both at room temperature and at 1200 F. The calibration of this gage is shown as a plot relating the readout signal of balance pressure vs. the differential pressure in inches of water as measured on a manometer (Fig. 5). It is seen that the room temperature points fall within a fairly narrow band, approximately +5%. When the differential pressure gage was heated to approximately 1200 F, however, a calibration check produced the widely deviating points shown as squares in the figure. It was determined that this was due to temperature transients and gradients, and since the gage was merely a prototype for principle and not a model, it was thought that rectifying these problems was not justified in view of the program schedule. Although it was realized that this calibration shift would tend to cause poor reproducibility, it was expected that operation at a given setting could still give good data for a particular run.

EXPERIMENTAL PROCEDURE

Operation

After outgassing the system at the maximum expected operating temperatures, the vacuum was broken with argon, and MSAR cesium of 99.9% purity was charged to the boiler. Prior to operation, while the system was still at room temperature, the apparatus was evacuated to remove most of the argon. The equipment was then brought up to operating temperature, the boiler being heated last to eliminate any tendency to condense cesium in those parts of the system where only vapor should be present. All parts of the system other than the boiler were heated to 1200 F, and the boiler was then brought to a temperature of 1000 F. The autotransformers which supplied power to the boiler were so adjusted that heat losses were nearly equal to the heat input, thus requiring minimum controller action. The early tests revealed that the ΔP apparatus was sensitive to temperature fluctuations and that the device responded slowly to control valve changes because of its relatively large volume. The tip of the control valve, a standard 1/4 in. bellows sealed model, was not a true needle, but a parabolic plug. This configuration, plus the possibility of traces of condensate in the valve, caused poor control characteristics. At the higher flows this posed little problem; at lower rates it was more pronounced.

For the purpose of establishing the feasibility of the differential pressure device, these limitations were acceptable. They did, however, make it undesirable to alter the control valve position unless a major deviation from the desired setting occurred. In the runs, the valve was adjusted to give approximately the chosen balancing pressure setting. During the operation the oscilloscope was checked to insure that the ΔP gage was at null when readings were taken. Measurements were recorded of the condensate volume, boiler temperature, balance pressure and system pressure every two to five minutes during most runs. Other readings were taken approximately two or three times per hour.

Results and Discussion

The key data are summarized in Figs. 6, 7 and 8, which are plots of the cumulative condensate volume vs. the elapsed time for each of three runs. Although it was intended that each experiment would be carried out at a constant flow rate, the poor characteristics described earlier made it more feasible to permit the balancing pressure to drift somewhat rather than to attempt to adjust it by operating the control valve. In this manner, operation at fairly constant differential pressures was maintained.

It developed, however, that there appeared to be a definite point after which the average balancing pressure was somewhat lower than it had been previously. As would be expected, this produced a lower average flow rate over that portion. These breaks were the basis for the designations A and B of each run. This cannot be interpreted as merely a calibration drift, because the flow rate still corresponded to the differential pressure.

A plausible explanation would be that a slight heat leak permitted a small amount of condensation upstream of the valve. When this condensate coalesced and moved near the valve seat, it could act as a restriction and a partial throttle on the flow. When the flow rate was sufficiently high, a dynamic equilibrium would be reached whereby the effluent vapors would evaporate condensate at the same rate at which it was formed. If the flow was too low, eventually a liquid slug would completely block the channel. This latter case is believed to be the reason for the inability to maintain very low flow rates.

In the runs shown, the breaks in the condensate curves are well marked, and the best straight lines were drawn by sight through the two portions of each curve. For the purposes of this study, in consideration of the relatively crude controls and measurement means, statistical determination of the best lines was not justified. In order to provide better visualization of the overall results, Run Summary Charts were plotted. One of these is shown as Fig. 9. A phantom line showing the average flow rate, as determined from the condensate accumulation plots, is included so that the relationship between the other variables and the throughput can be examined. This rate was calculated using a value of 1.8 for the specific gravity of

the liquid cesium. The representative summary chart shows that temperature control was quite good, but that the total system pressure tended to drop slightly.

From this chart, it is seen that the drop in condensate rate coincides well with the drop in balance pressure. A visual averaging of the balance pressure for Part A gives a BP of about 8 psig; for Part B, 6.2 psig appears about right. Similar procedures were followed for the other runs, and these data are listed in Table 1 along with the correlation of balance pressure to differential pressure in inches of water as taken from Fig. 5. Comparison of these data points with the theoretical curve for this capillary, Fig. 10, shows quite good agreement, and it confirms the validity of using differential pressure measurement across the capillary to measure flow rate in a cesium vapor system under these conditions. The maximum deviations are within 15% of the theoretical line.

Examination of Components After Study

Upon completion of the experimental work, the apparatus was examined for evidence of corrosion, erosion, and metal transport, with special attention being given to the capillary and the control valve. Prior to dismantling and washing the apparatus, x-ray photographs were made of both the capillary and the control valve. Neither item showed any indication whatever of any change in diameter or any evidence of build-up of material due to metal transport. The valve was later sectioned, and although the tip showed a slight scoring due to over-tightening, all other edges were perfectly sharp with no evidence whatever of deterioration. It is realized that this was a very short test, totalling less than 200 hours at temperature, even allowing some acceleration for the two dozen or so heating-cooling cycles. It is indicative, however, that containment should not be a major problem.

CONCLUSIONS

This study verified the feasibility of a vapor system for metering cesium in the milligram per second range. It also demonstrated an approach for measuring the viscosity of alkali metal vapors.

SYMBOLS

mg	-	milligrams
q	-	volumetric flow - ft^3/sec
D	-	inside diameter, ft
g	-	gravity constant, $32.2 \text{ ft}/\text{sec}^2$
μ	-	viscosity, $\text{lb}_m/\text{ft}\cdot\text{sec}$
ΔP	-	pressure drop, lb_f/ft^2
L	-	capillary length, ft
M	-	mass flow rate, mg/sec
K	-	arbitrary constant
d	-	vapor density, lb_m/ft^3
T	-	absolute temperature, $^\circ\text{R}$
P	-	pressure, lb_f/ft^2

Subscripts

B	-	boiler conditions
i	-	capillary inlet conditions
c	-	capillary midpoint conditions
o	-	base conditions for calculations
α, β	-	range over which a variable was evaluated

TABLE 1 - EXPERIMENTAL POINTS, FLOW RATE VS. ΔP

<u>Run No.</u>	<u>Flow mg/sec</u>	<u>BP psig</u>	<u>ΔP in. H₂O</u>
4B	2.23	2.75	3.4
4A	2.69	3.0	3.9
2B	5.4	6.2	9.0
2A	8.0	8.0	12.0
3B	11.3	13.8	21.4
3A	13.2	14.3	22.2

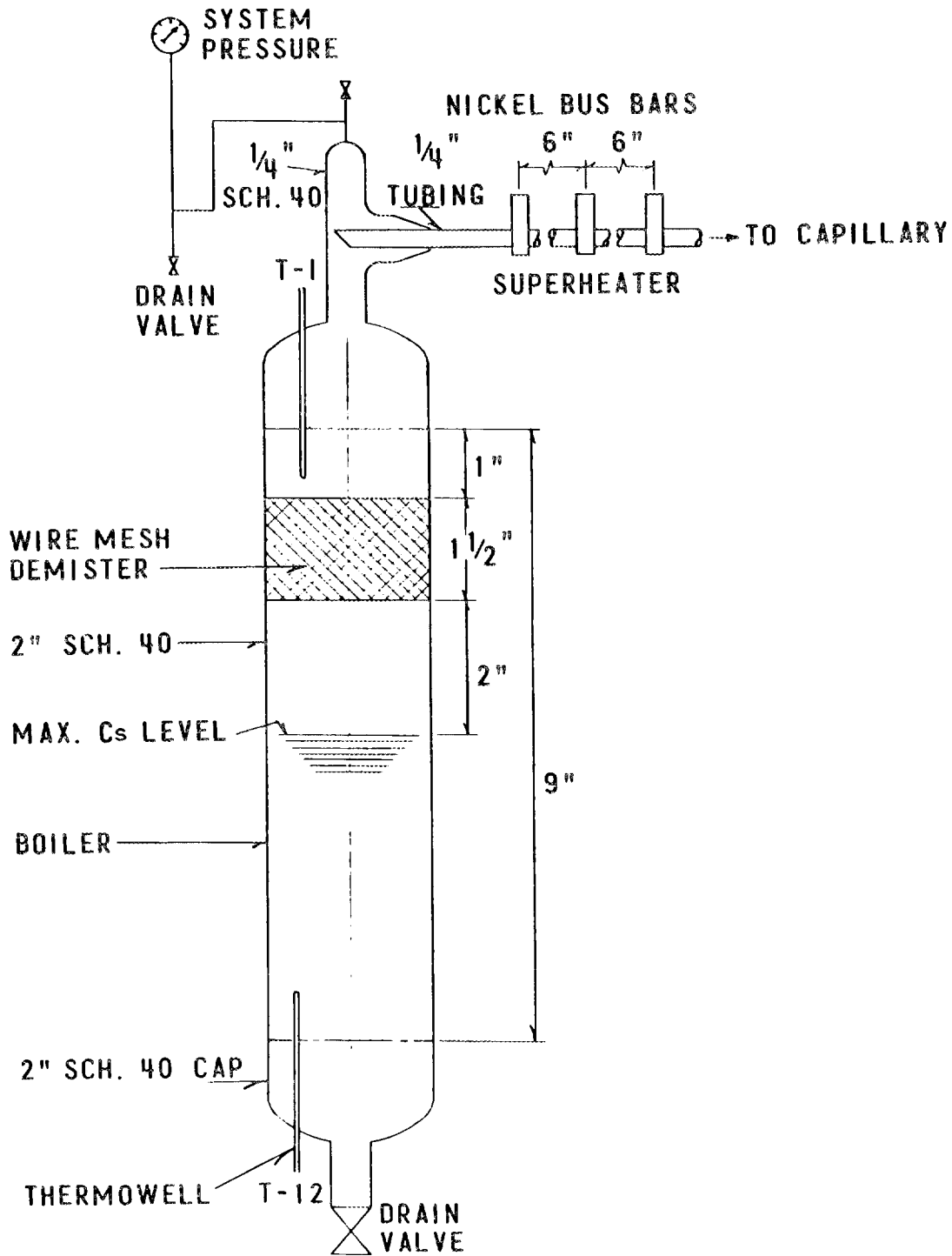


FIG. 1 - BOILER AND SUPERHEATER DETAILS

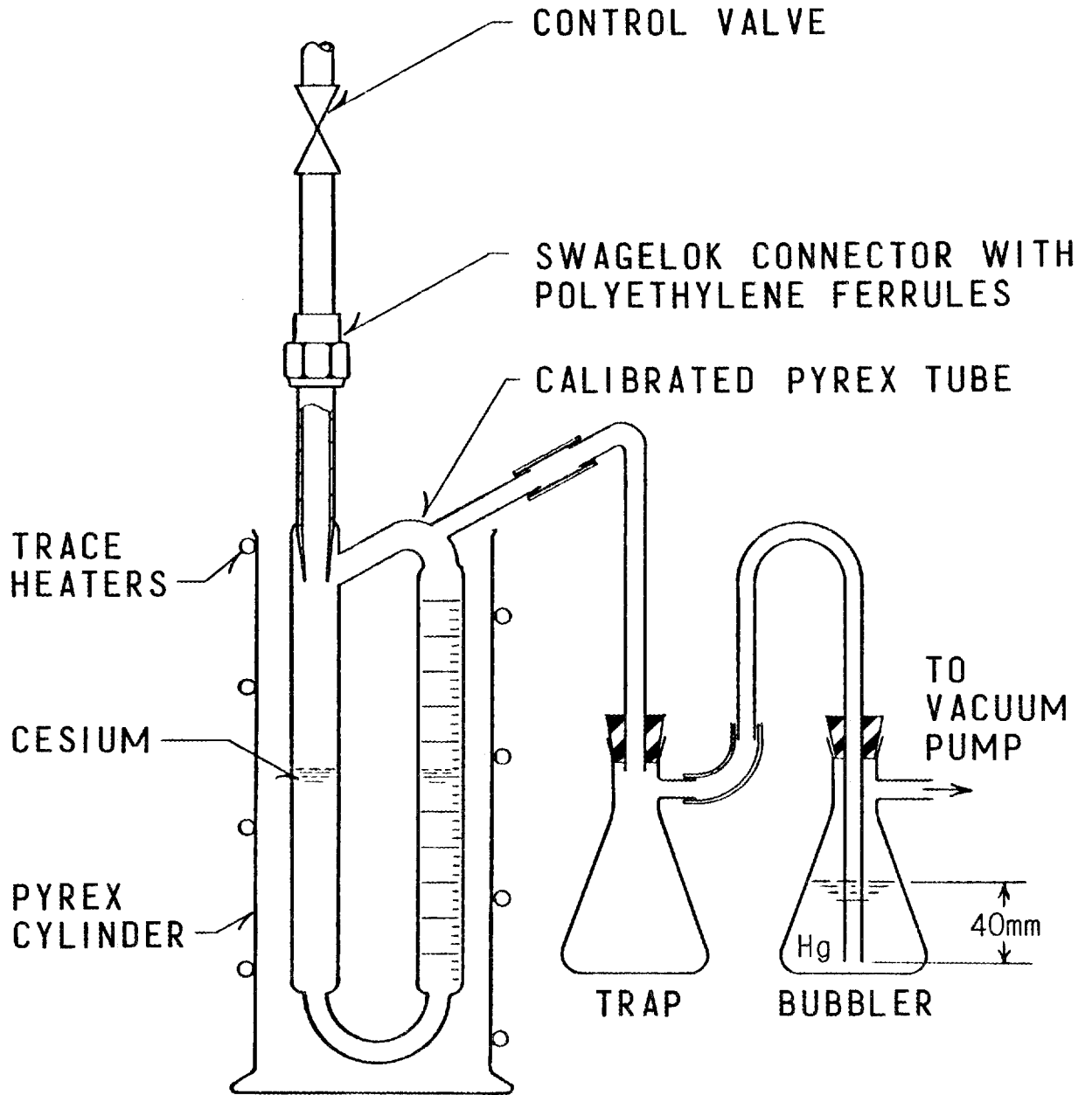


FIG. 2 - CONDENSATE COLLECTOR APPARATUS

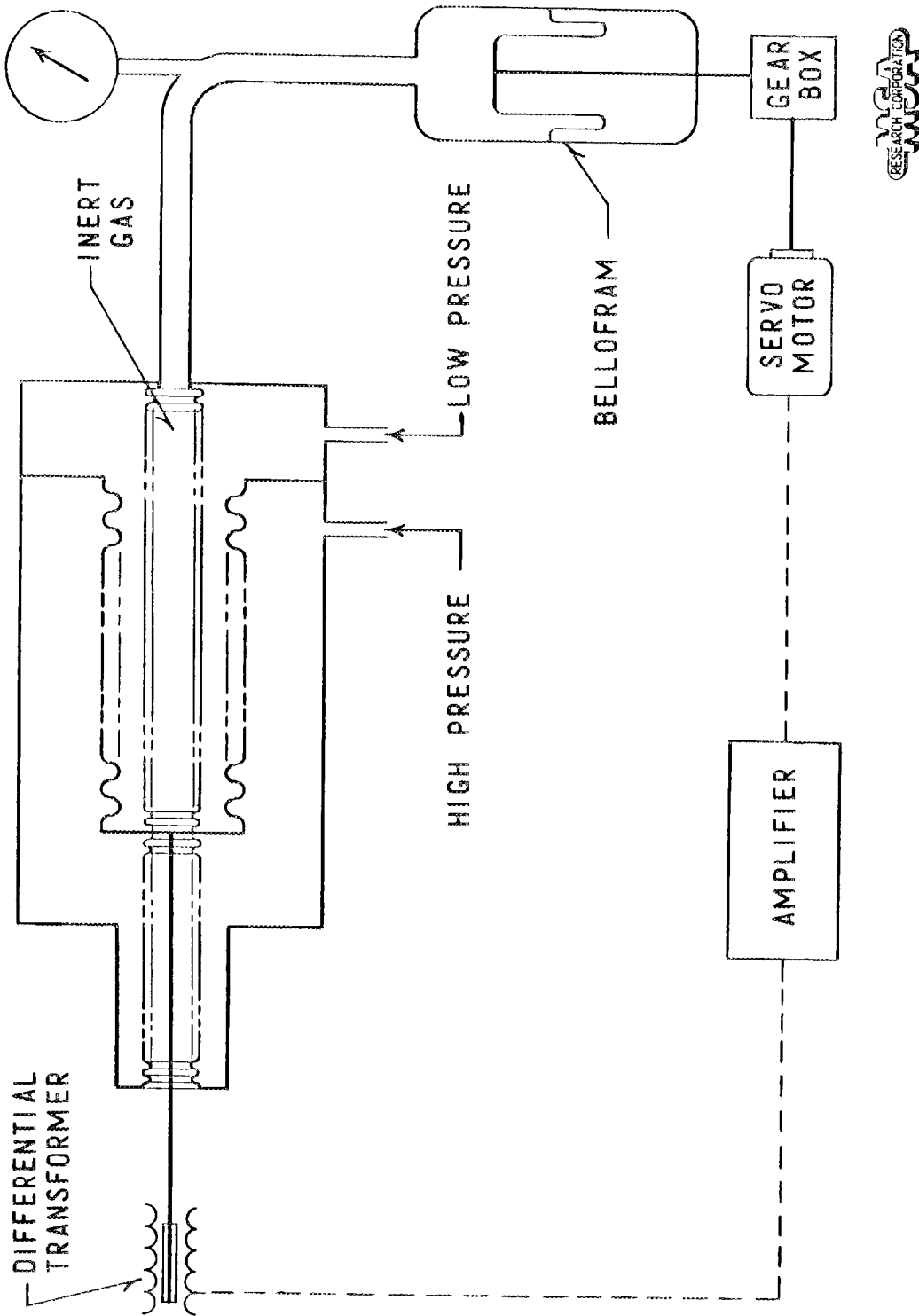


FIG. 3 - DIFFERENTIAL PRESSURE TRANSDUCER



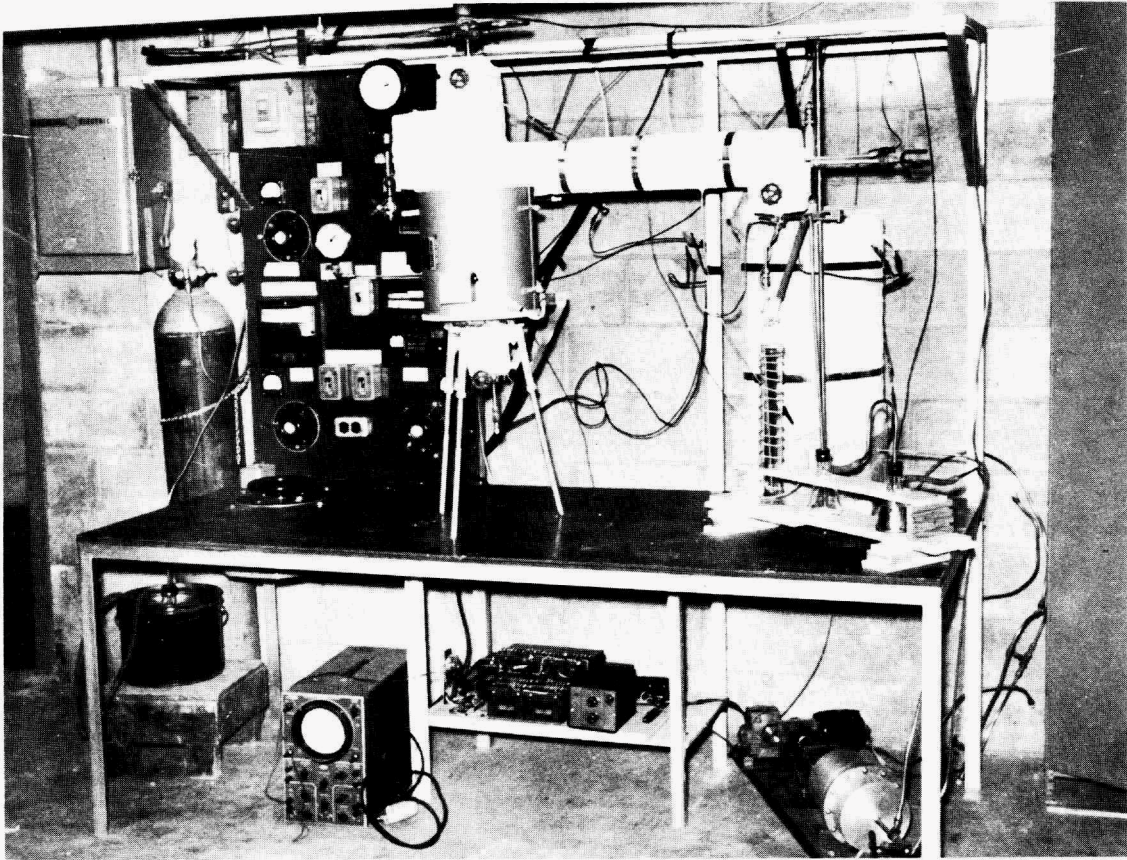


FIG. 4 - COMPLETE TEST APPARATUS

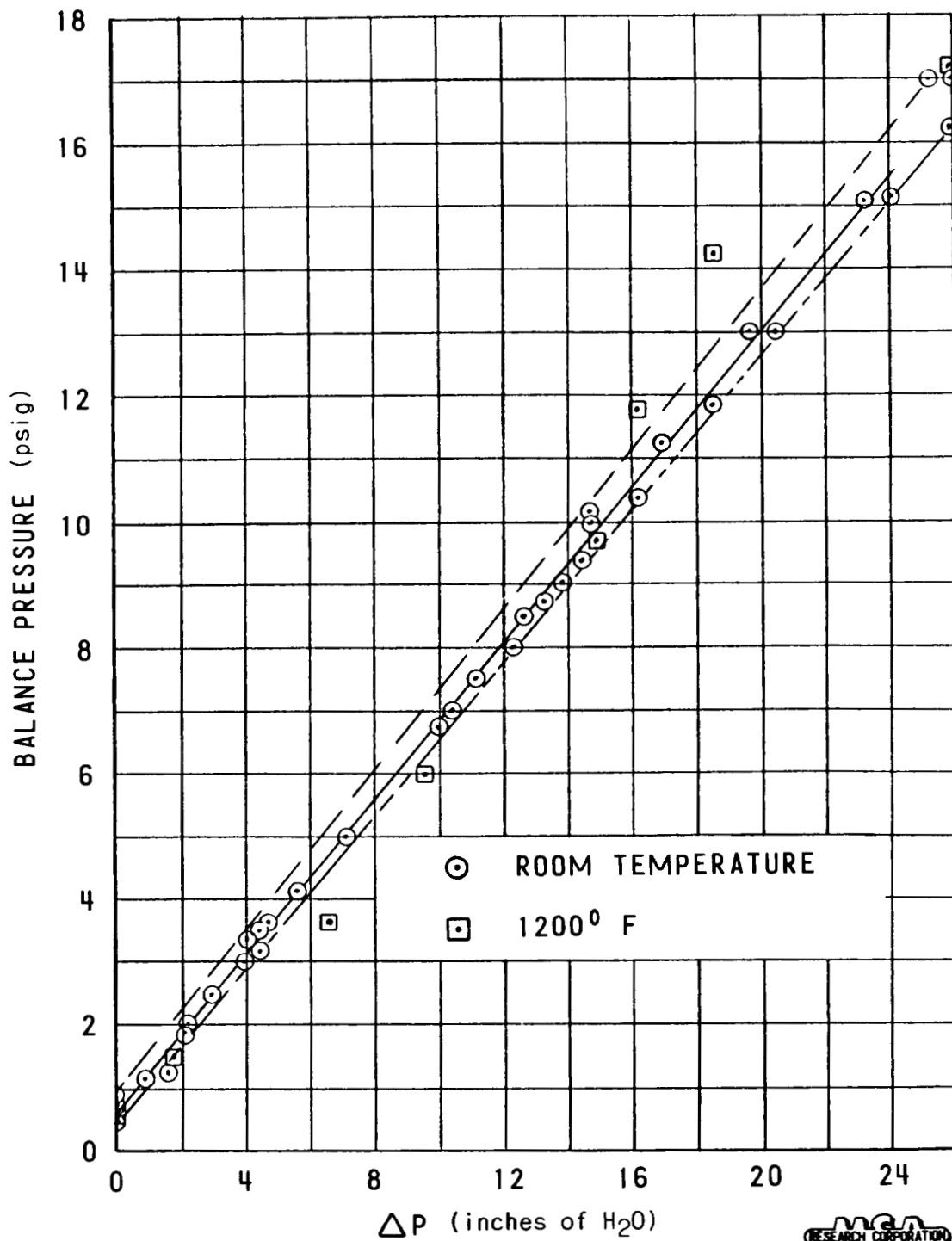


FIG. 5 - ΔP TRANSDUCER CALIBRATION

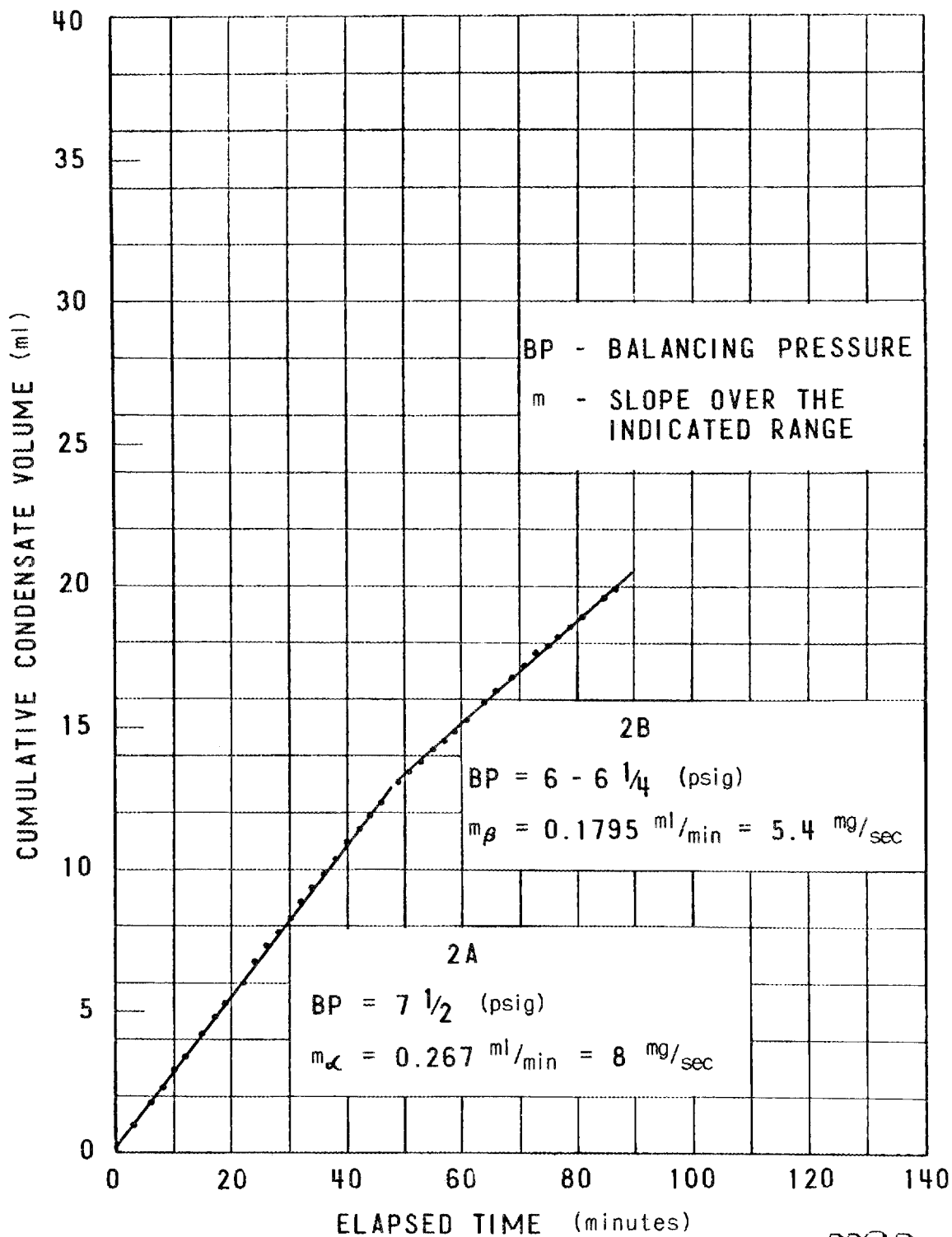


FIG. 6 - CONDENSATE vs TIME (RUN 2)

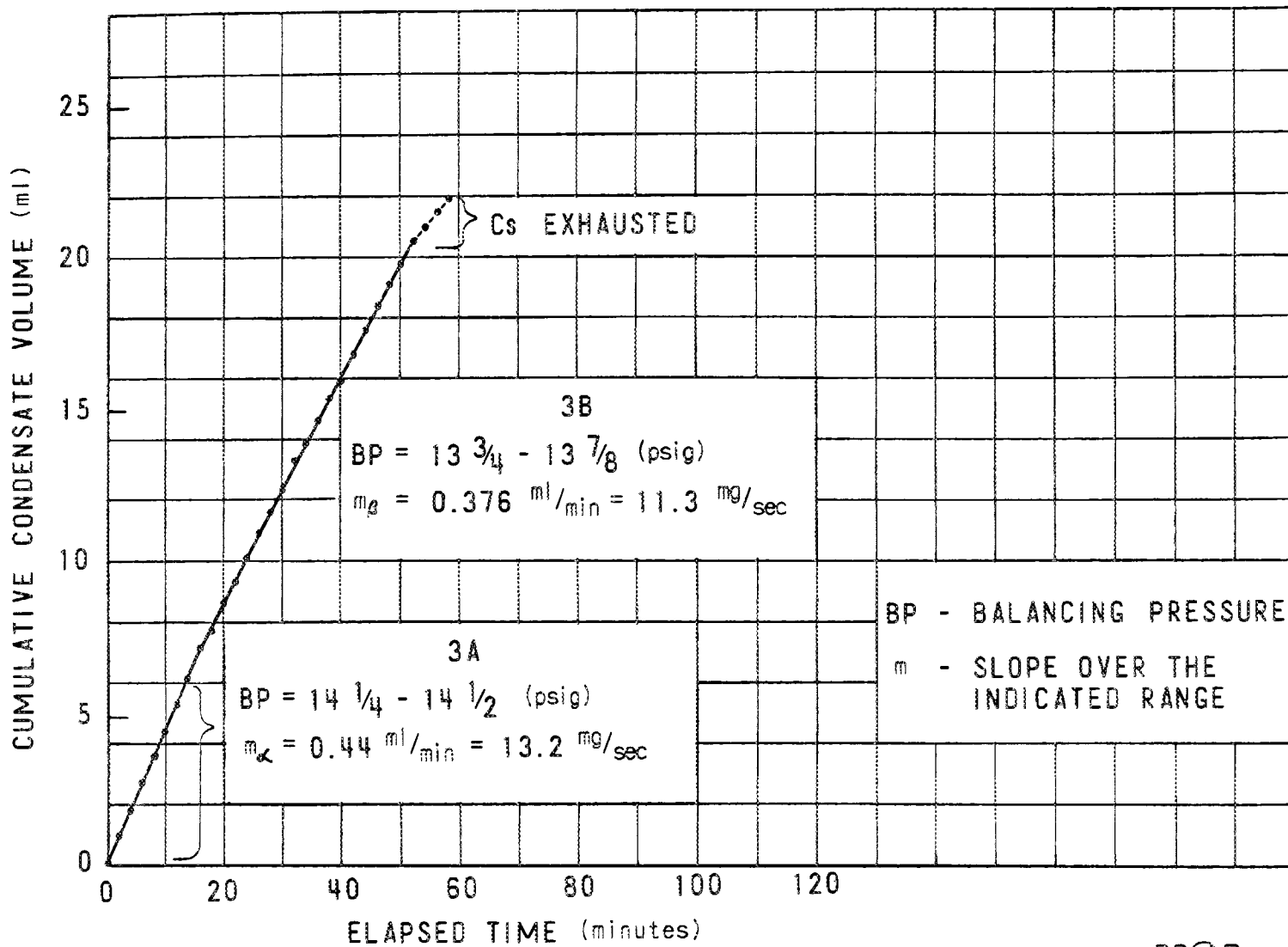


FIG. 7 - CONDENSATE vs TIME (RUN 3)



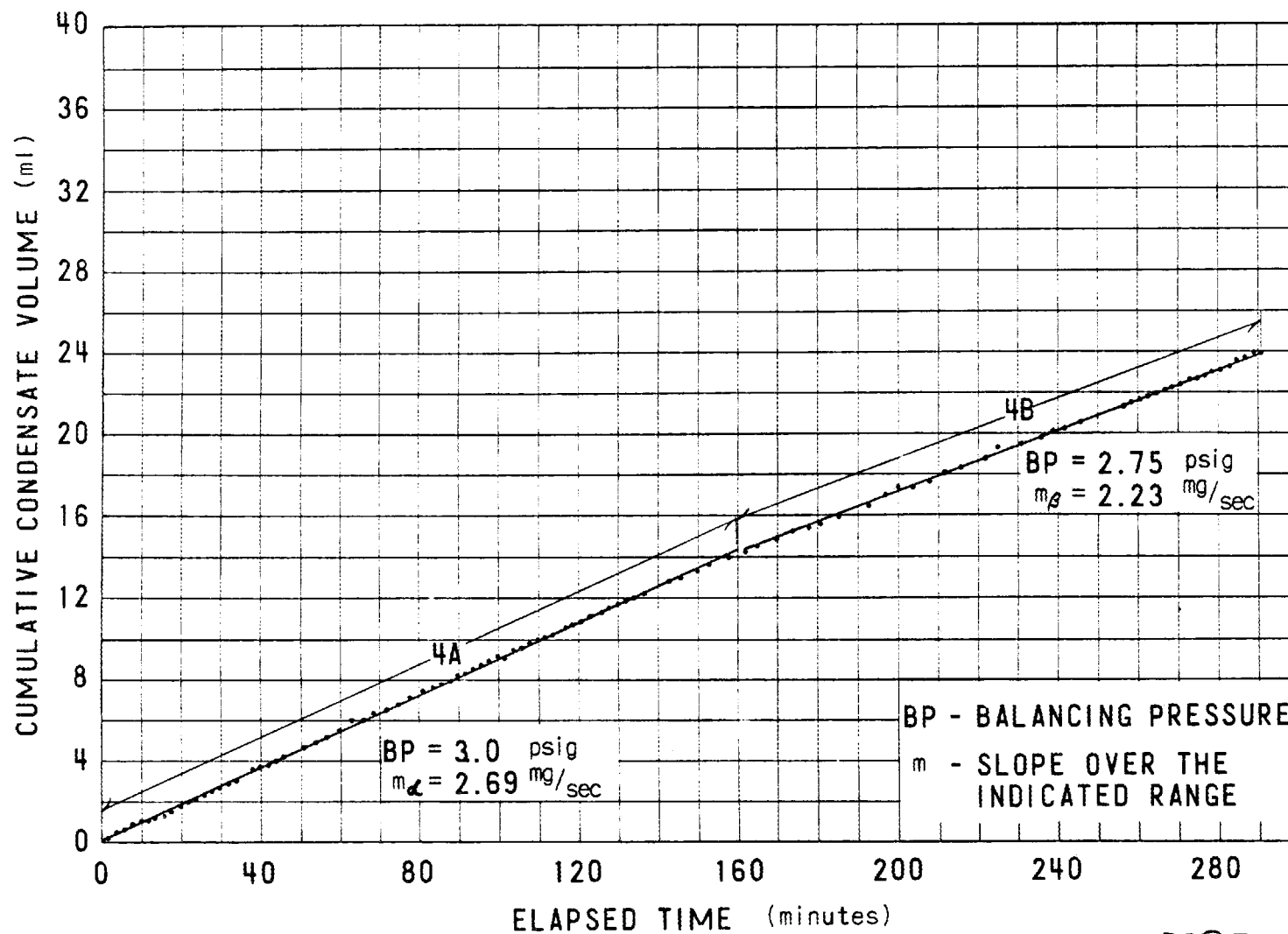


FIG. 8 - CONDENSATE vs TIME (RUN 4)

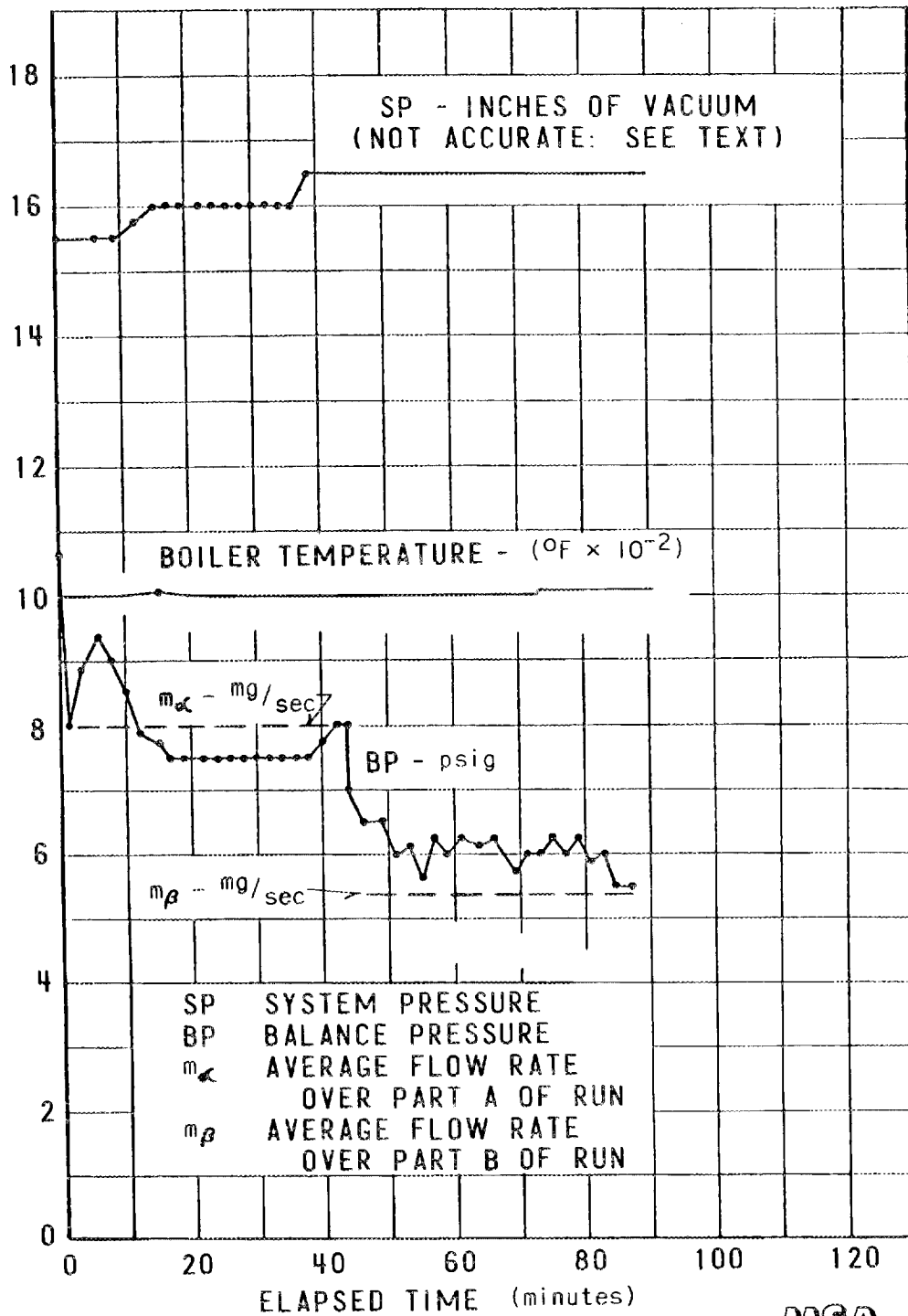


FIG. 9 - RUN SUMMARY CHART (RUN 2)

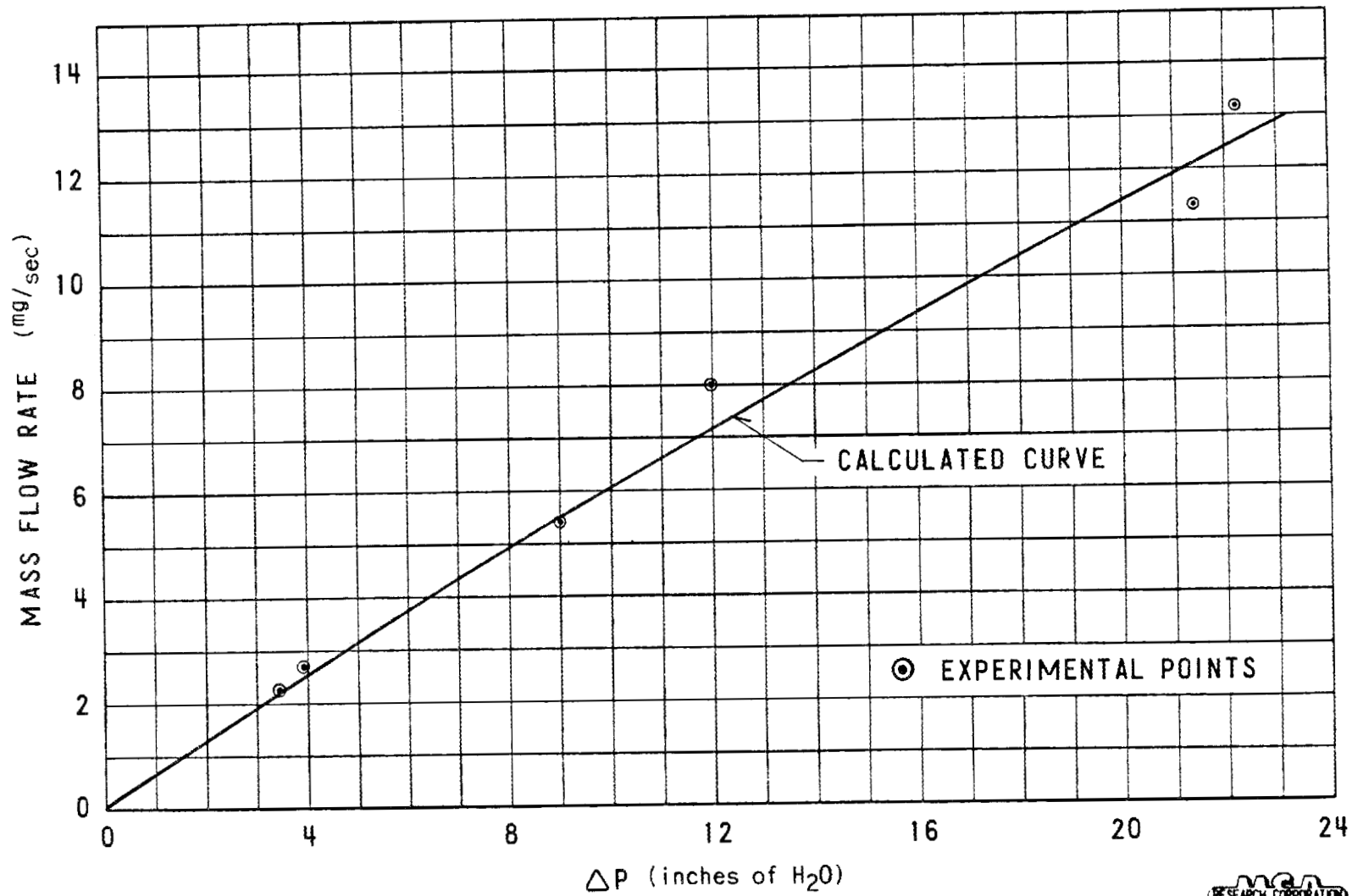


FIG. 10 - MASS FLOW RATE vs ΔP



DISCUSSION

MR. ROHSENOW: You used a density ratio being proportional to the pressure ratio. This assumes constant temperature. What was the difference between the temperature at the inlet and outlet of the capillary? In the isotropic flow if there weren't a capillary, you would have a pressure ratio of K^{-1} to K . Complete capillary, with slug flow, you would probably have isothermal.

MR. SAMUEL: We are very, very close, we think, to isothermal flow. The points read 1200 F; as I have pointed out, refinement of measurement is not our particular objective at this time. We wanted to find out if this thing would work, and as far as I could see, we feel that the capillary was at constant temperature throughout.

MR. ROHSENOW: This might be worth checking. Such as changing that exponent of ΔP^2 , putting a different number on it.

MR. SAMUEL: It is something to look at.

MR. LYON: What was the logarithmic decrease in pressure, which would give an indication, perhaps, of what the change in ΔT would be?

MR. SAMUEL: The logarithmic decrease in pressure at which point?

MR. LYON: What was the ratio of the drop to the pressure of the system?

MR. SAMUEL: Somewhere around 30%. The maximum differential pressure at which we operated was 1 pound. Therefore, it would be one-third at the most. In most cases it was not this high.

MR. LYON: The other question that I had: You mentioned that you found the stainless steel, 300-series stainless steel, works well with cesium up to 1200. Do you have evidence that above 1200 it doesn't work well?

MR. SAMUEL: No, we do not.

MR. BONILLA: Did you merely use the mean pressure, as indicated on the slide, and pressure difference, in calculating--well, in the operation of the viscometer? I have mentioned it because we have already worked out

and published the correct equation, and in view of what Dick says there, or you pointed out, with that large a ratio of pressure drop to absolute pressure, there is a very large correction, due to the change in density as you go along the capillary.

MR. SAMUEL: Are you referring to the change in density caused by the acceleration of the gas in the capillary?

MR. BONILLA: That's merely a correction. It's a change in velocity in the capillary due to the change of pressure in the capillary.

MR. SAMUEL: The Q_c in our equation was the volumetric rate at the center point of the capillary, and in the preprint we discussed that we had corrected that volume back to the inlet volume, where we know the pressure. In other words, we say that the volume here is so much. We can apply the ideal gas law which we feel that we can do under these circumstances, and compute the volume then on the basis of the inlet volume, because of the change in densities.

MR. BONILLA: Yes. I will send you a reprint, anyway. It has been studied over years, and it is very well established, the right way to handle the data. You may have done it that way, or you may have overlooked it.

MR. SAMUEL: Thank you.

SELECTED PARAMETERS
FOR
TWO-PHASE FLOW OF SODIUM

By

Kurt Goldmann

August 16, 1963

Prepared for presentation at the
Third Annual High-Temperature
Liquid-Metal Heat-Transfer Technology Conference
Oak Ridge National Laboratory
September 4-6, 1963

UNITED NUCLEAR CORPORATION
Development Division
5 New Street
White Plains, New York

INTRODUCTION

In spite of the considerable interest in boiling and condensing of liquid metals which has developed in recent years, there are still very little data available for the determination of two-phase flow characteristics for liquid metals. The present paper presents selected two-phase flow parameters for sodium systems. They are based on analytic techniques which previously have proven useful for water systems. Thus, flow pattern charts are developed similar to those given for water in Reference 1, and two-phase pressure drop and vapor-volume fraction data are presented following an approach used for water in References 2 and 3. As with the results for water, experimental data are required to verify the predictions, but judging by the agreement found for water, one should be able to use the results presented in this paper for the scoping design of sodium systems with reasonable confidence.

TWO-PHASE FLOW PATTERNS

Fig. 1 shows predicted two-phase flow patterns as a function of quality and total mass velocity for several pressures. The flow patterns, as shown, are based on a generalized chart by Baker⁴ and the following properties for sodium:

Table 1 — Sodium Properties

Pressure, psia	14.7	100	240
Saturation Temperature, °F	1612	2080	2372
Vapor Density, lbm/ft ³	0.016	0.081	0.242
Liquid Density, lbm/ft ³	46.6	42.8	39.3
Liquid Surface Tension, dyne/cm	113	92	72
Liquid Viscosity, centipoise	0.170	0.153	0.148

For high performance systems, which are probably of greatest interest, mass velocities are usually higher than 200,000 lbm/hr-ft². It is seen from Fig. 1 that for such systems, the fluid will take on a dispersed (fog) flow appearance for any vapor quality larger than a few percent. This is not surprising in view of the relatively large vapor volumes corresponding to these qualities at the selected pressures. At mass velocities between 50,000 and 200,000 lbm/hr-ft², annular flow obtains depending somewhat on vapor quality and pressure. Although a distinction is made here between dispersed and annular flow, one should expect thin liquid films to exist on adiabatic walls exposed to dispersed flow.

It may be concluded from Fig. 1 that other flow patterns such as bubble flow are almost nonexistent, and slug flow will occur only at very low qualities and low mass velocities of sodium liquid-vapor mixtures.

TWO-PHASE PRESSURE DROP

1. Friction

The pressure losses resulting from frictional resistance for two-phase sodium flow have been obtained by extending the methods of Martinelli

and Nelson.³ This involves use of the Lockhart and Martinelli parameter χ_{tt} ,² which is a function of quality and physical properties of the fluid, and a correlating graph relating this parameter to the ratio of the local two-phase pressure gradient to the all-liquid pressure gradient. This graph was established originally from data obtained for two-phase mixtures at atmospheric pressure. The graph was extended for water by Martinelli and Nelson to cover pressures up to the critical pressure by forcing a fit with additional experimental data obtained for two-phase water flow at higher pressures. A graph with pressure as a parameter resulted, and was used here to generate a dependence of local two-phase pressure gradient with quality for sodium as shown in Fig. 2.

The curves of Fig. 2 were then integrated to obtain the overall ratio of two-phase pressure drop to all-liquid pressure drop for a heated duct. It was assumed that the heat flux at the wall and, therefore, the quality gradient along the duct are constant. The resultant curve for sodium is compared with that of water at 14.7 psia in Fig. 3. Additional curves of the overall two-phase frictional pressure drop factors for sodium flowing through heated ducts at other pressures are given in Fig. 4. While the curves represent integrations from zero quality at the inlet to any quality at the outlet of a heated duct, the results may be applied to any quality at the duct inlet by appropriate subtractions. Of course, they also may be applied to cooling cases. By extrapolating to the critical pressure, taken as 5032 psia from Reference 5, and cross plotting, Fig. 5, corresponding to Fig. 4 of Reference 3, is obtained.

2. Acceleration

As the sodium evaporates while flowing through a heated duct, it accelerates, i.e., its velocity and momentum increase at the expense of pressure losses which have to be added to the friction losses to obtain the total pressure drop.

If it is assumed that the liquid and vapor phases flow at the same velocity (no slip) at any given cross section, then the acceleration pressure drop can be calculated from

$$\Delta P_a = \frac{G^2}{g} \left[(1-x) + x \frac{v_g}{v_\ell} - 1 \right] v_\ell = \frac{G^2}{g} \cdot r_1 \quad (1)^*$$

where G is the total mass velocity in lbm/hr-ft^2 , x is the vapor quality, v is the specific volume in ft^3/lbm and subscripts g and ℓ refer to vapor and liquid conditions, respectively.

The multiplier r_1 has been plotted for sodium in Fig. 6. A similar relation can be derived for flow with slip between the liquid and vapor phases.

$$\Delta P_a = \frac{G^2}{g} \left[\frac{(1-x)^2}{1-R_g} + \frac{x^2}{R_g} \frac{v_g}{v_\ell} - 1 \right] v_\ell = \frac{G^2}{g} \cdot r_2 \quad (2)$$

The multiplier r_2 has been plotted for sodium in Fig. 7, using vapor-volume fraction (R_g) data given below.

*The form of Eq. 1 has been chosen to be comparable with Eq. 2.

As with the friction loss factors, Figs. 6 and 7 may be used for quality inlet conditions and condensing by suitable, simple manipulations.

VAPOR-VOLUME FRACTION

The methods outlined in References 2 and 3 have been utilized to calculate vapor volume fractions for sodium flows. The results are given in Fig. 8. The slip ratio may be calculated from Fig. 8 using

$$S = \frac{V_g}{V_l} = \frac{x}{1-x} \frac{(1-R_g) \rho_l}{R_g \rho_g} \quad (3)$$

where V is the velocity, and R_g is the fraction of cross section of a duct filled with the vapor phase.

CONCLUSIONS

Selected two-phase flow parameters for sodium are presented in Figs. 1 through 8 for ready use in the scoping designs of two-phase sodium systems.

ACKNOWLEDGMENTS

This work was carried out at United Nuclear Corporation under Contract AT(30-1)-2303 (XIII) for the United States Atomic Energy Commission. The calculations were performed by F. Beers.

REFERENCES

1. K. Goldmann et al., Burnout in Turbulent Flow – A Droplet Diffusion Model, Trans. ASME, J. Heat Trans. Vol. 83, Series C, No. 2 (May 1961).
2. R. W. Lockhart and R. C. Martinelli, Proposed Correlation of Data for Isothermal Two-Phase, Two-Component Flow in Pipes, Chem. Engr. Prog., Vol. 45, No. 1 (Jan. 1949).
3. R. C. Martinelli and D. B. Nelson, Prediction of Pressure Drop During Forced-Circulation Boiling of Water, Trans. ASME, Vol. 70 (Aug. 1948).
4. O. Baker, Simultaneous Flow of Oil and Gas, Oil and Gas Journal, Vol. 53 (July 26, 1954).
5. E. L. Dunning, The Thermodynamic and Transport Properties of Sodium and Sodium Vapor, ANL-6246 (Oct. 1960).

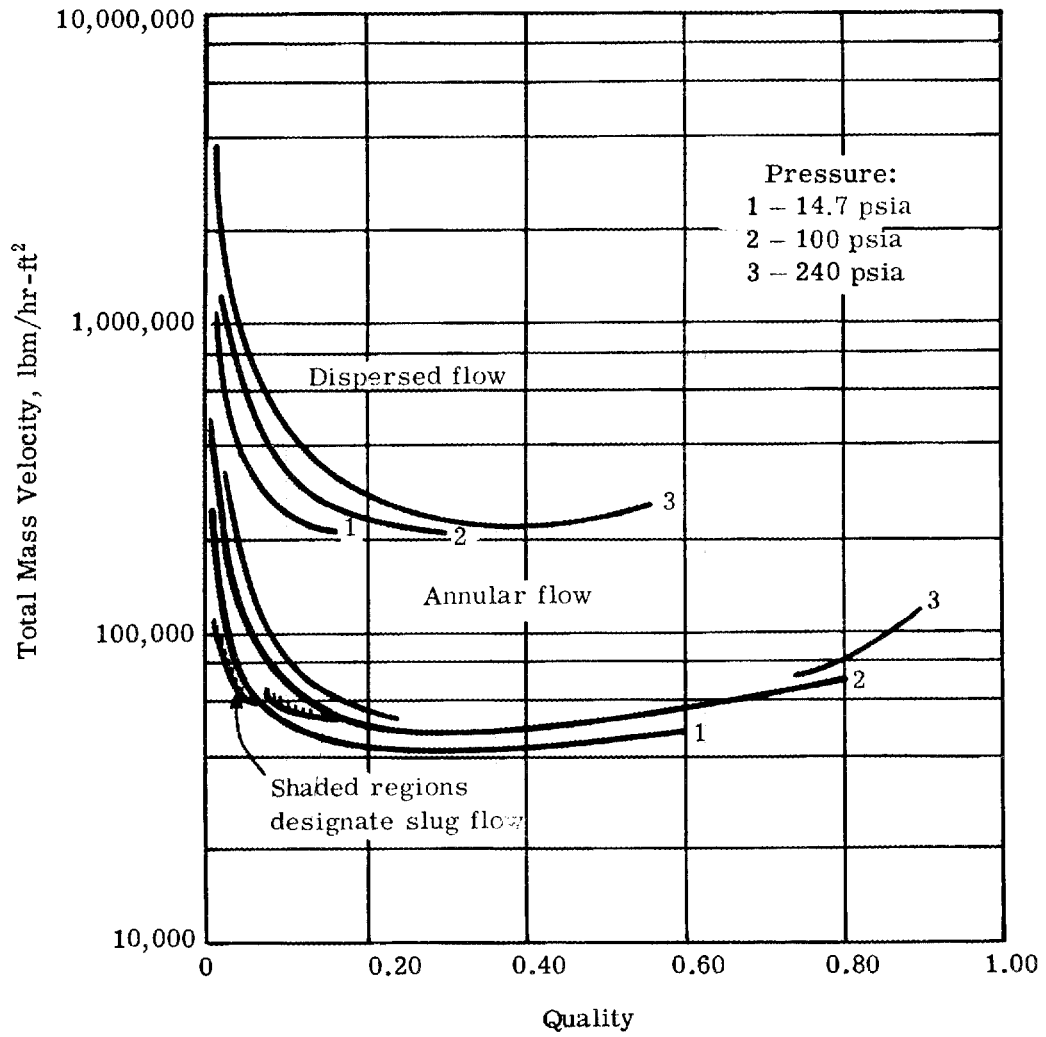


Fig. 1 — Sodium two-phase flow pattern chart

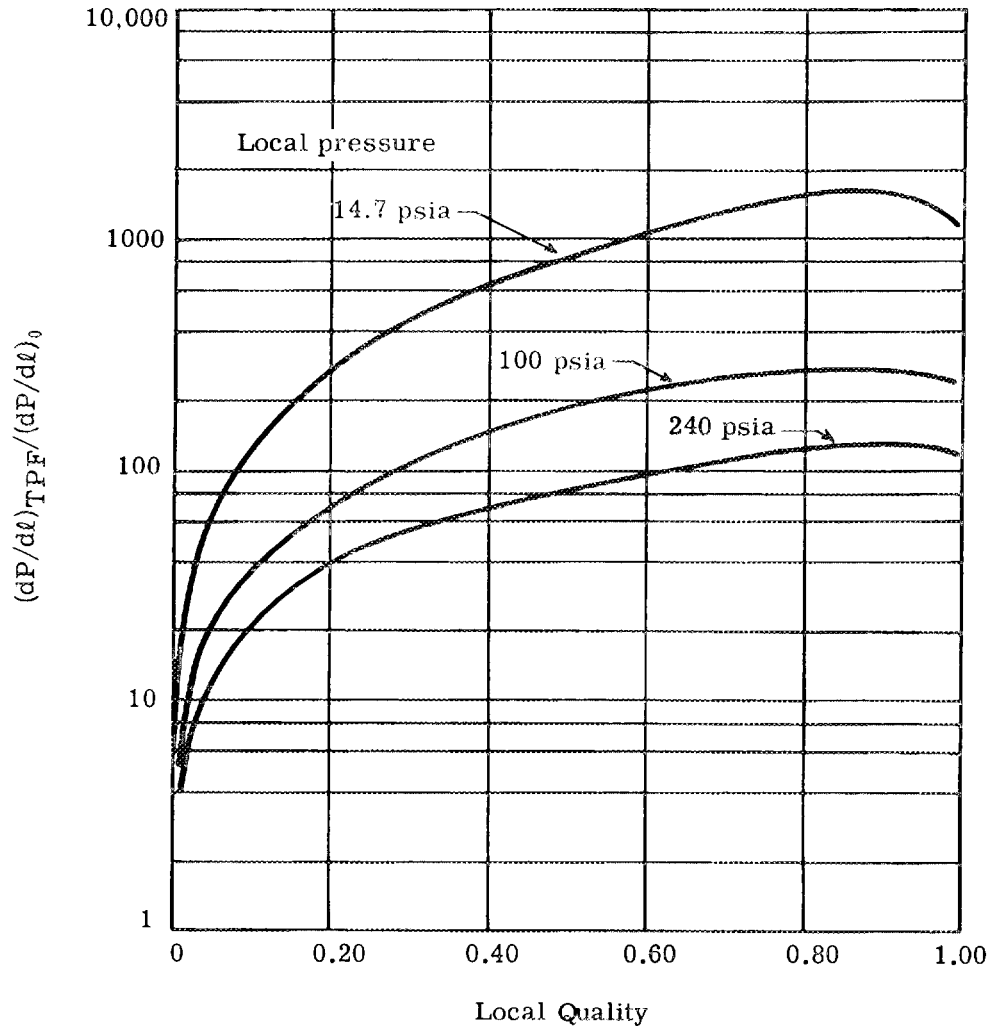


Fig. 2 — Ratio of local two-phase frictional pressure gradient to pressure gradient for all liquid flow for sodium vs local quality

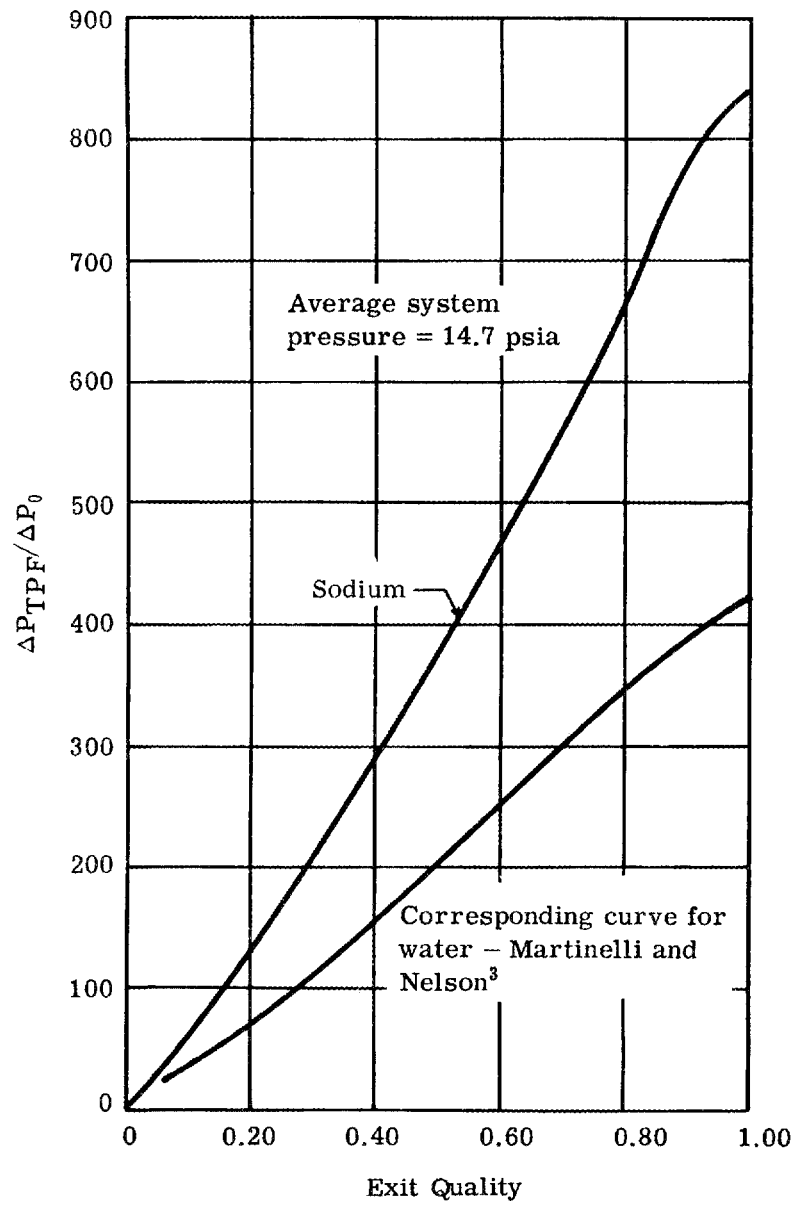


Fig. 3 — Ratio of overall two-phase frictional pressure drop to pressure drop for all liquid flow vs exit quality — comparison of sodium with water

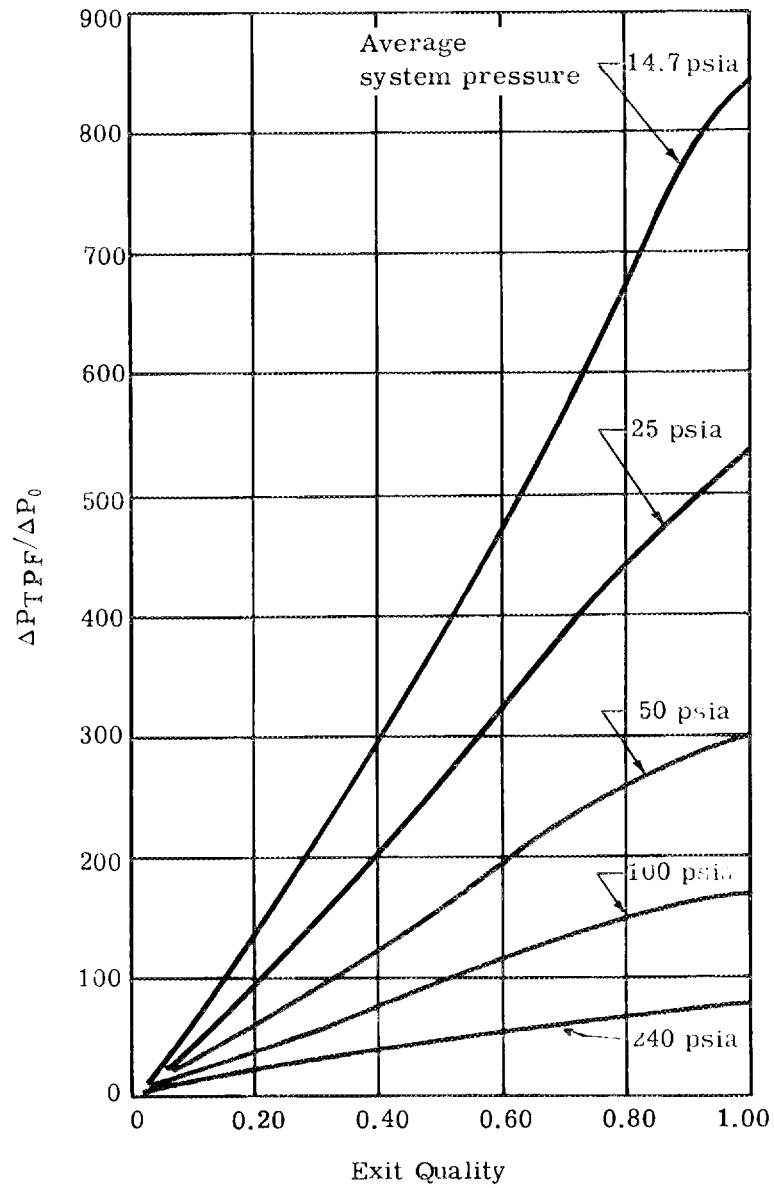


Fig. 4 — Ratio of overall two-phase frictional pressure drop to pressure drop for all liquid flow for sodium vs exit quality

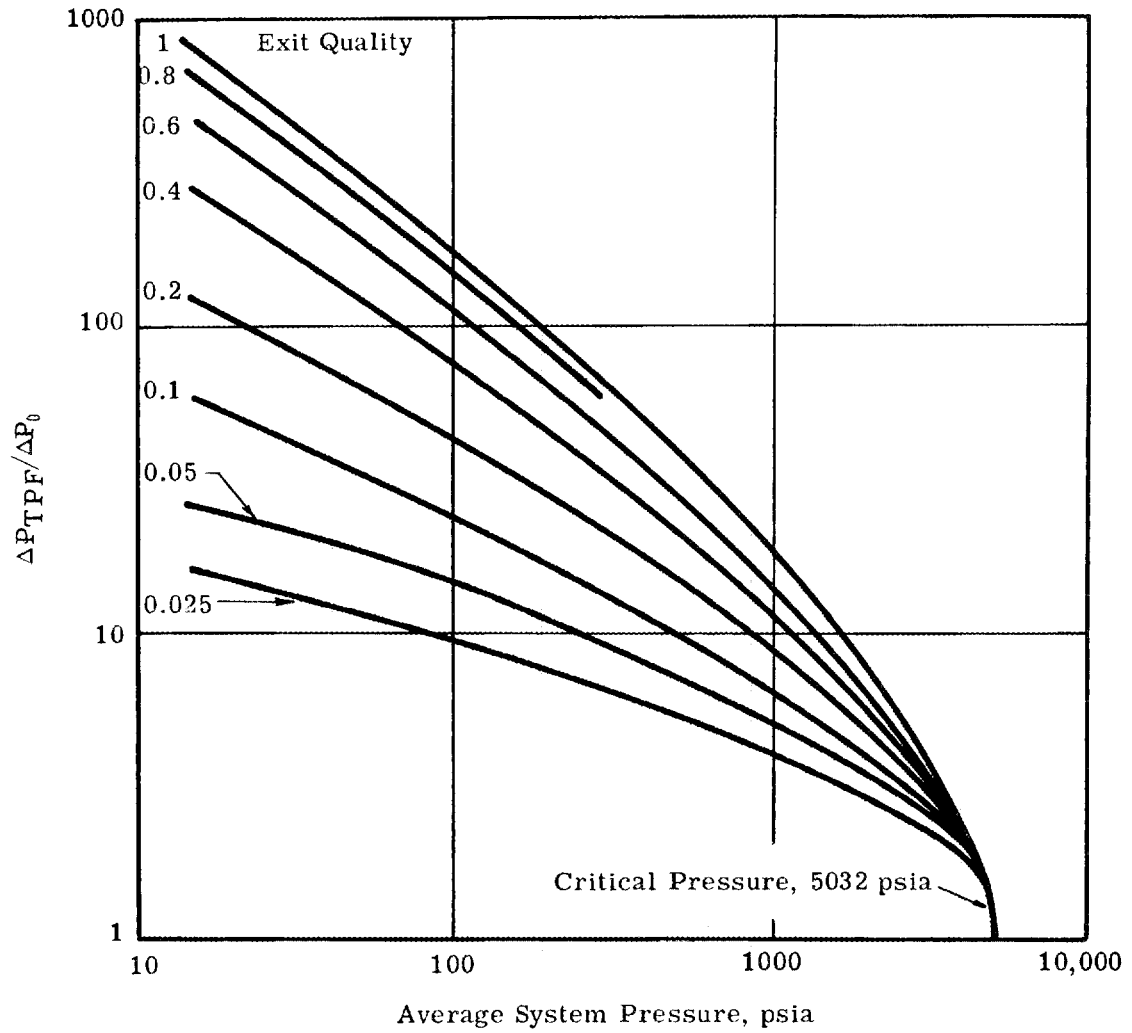


Fig. 5 — Ratio of overall two-phase frictional pressure drop to pressure drop for all liquid flow for sodium vs average system pressure

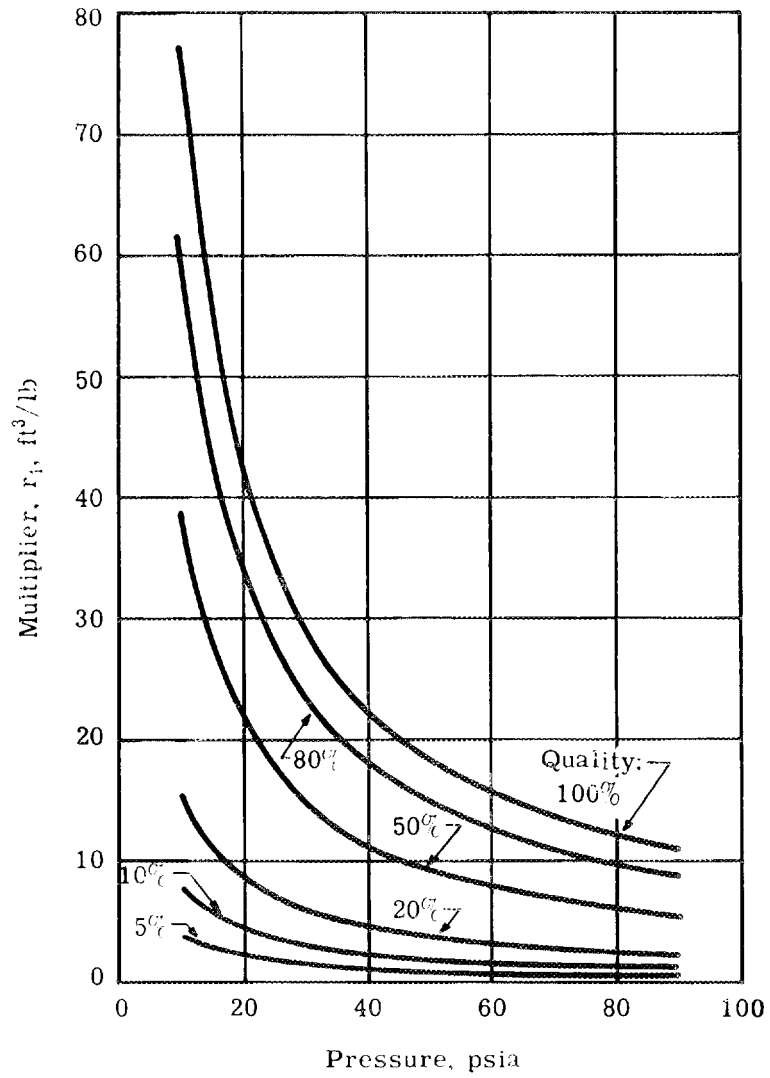


Fig. 6 — Acceleration pressure drop multiplier for dispersed two-phase sodium flow. $\Delta P_a = G^2/g \cdot r_1$

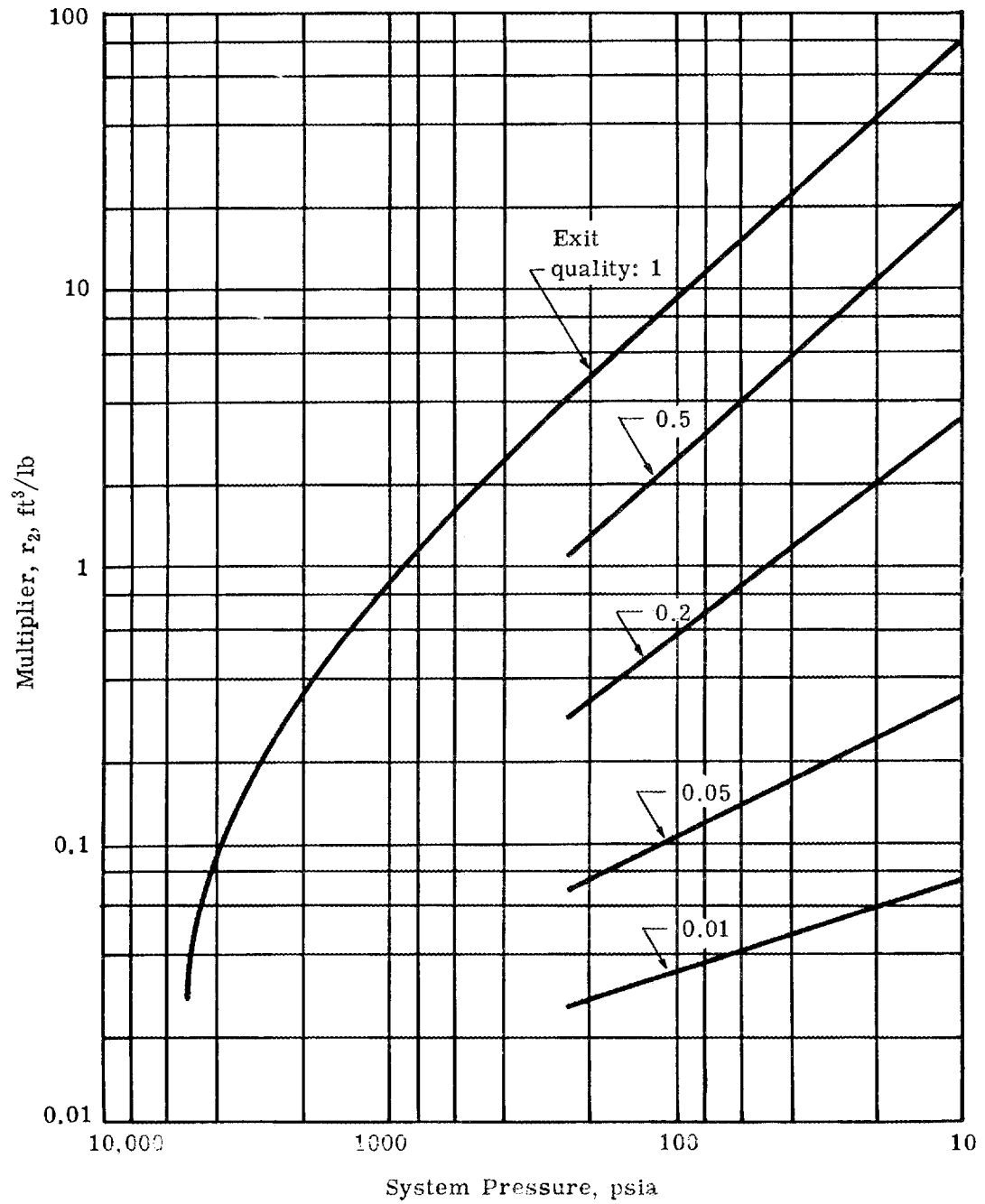


Fig. 7 — Acceleration pressure drop multiplier for separated two-phase sodium flow (predicted). $\Delta P_a = G^2/g \cdot r_2$

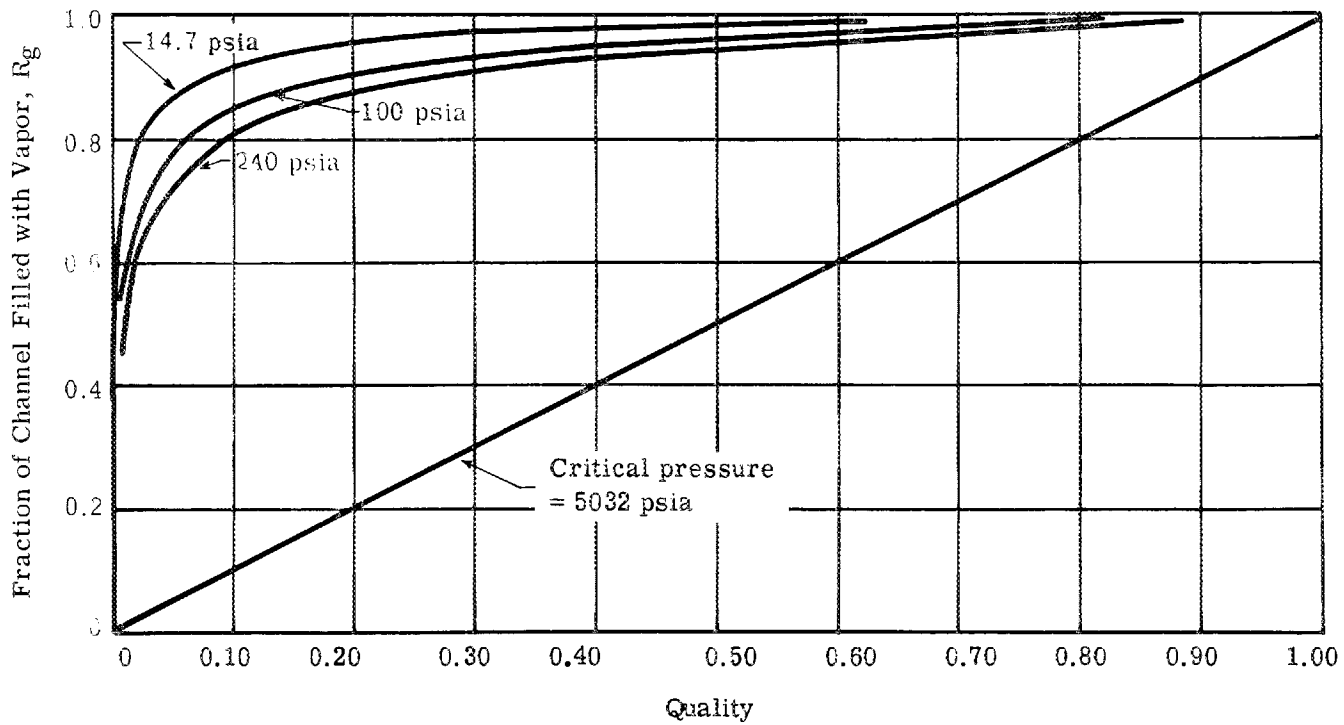


Fig. 8 — Fraction of channel filled with vapor vs quality for two-phase sodium flows

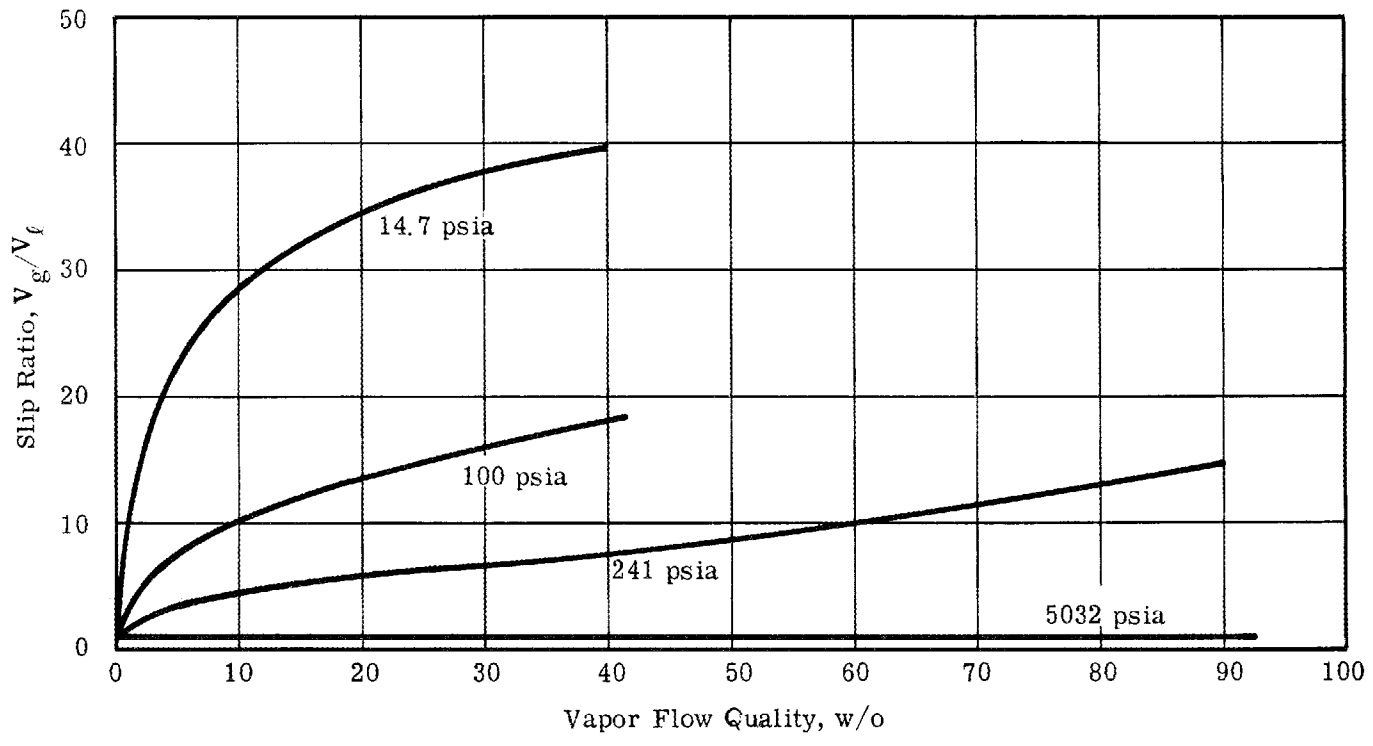


Fig. 9 — Slip ratio for sodium flow

DISCUSSION

MR. ROHSENOW: Kurt, this is all based on data which are a pretty far extrapolation from it, but I wonder how these two-phase flow regimes compare with some of the other flow regime maps of Peter Griffith, and a Russian map, and somebody else's?

MR. GOLDMAN: The maps really aren't too far different, at least the ones that had come out until about two years ago; and at that time when we looked over various maps, we sort of thought that Baker's map was probably the most representative one. Of course it allows a very ready extrapolation to any fluid, because he presents the data in terms of certain normalized parameters.

Admittedly, there is no data for sodium, for instance.

MR. ROHSENOW: Another thing we might do here, and it would take just a minute to try to get a handle on Herb Hoffman's data. From your knowledge of properties of potassium, how would the curves change for potassium?

MR. GOLDMAN: Not very much. As a matter of fact they didn't even change much from water, because the principal parameters are viscosity, and the surface tension, and specific volume.

MR. ROHSENOW: Don't these dispersed flow curves move off to the right with water?

MR. GOLDMAN: No, they look just about like that, for water.

MR. ROHSENOW: What we are trying to get at, here, is Herb's mass velocities are down in the range of annular flow on this map. They suggest they go off to higher qualities. That you don't get the dispersed flow, but you get annular flow. And Herb's data show the burn-out, the critical heat flux, and increasing mass flow rate, rather than decreasing out of the high-quality zone, and I wonder if this is the reason? That with liquid metals you always have annular flow, and with water it tends to tear those films off.

MR. GOLDMAN: Well, of course we are now making assumptions as to what kind of flow you have with heat flux, and I tried to be careful, but perhaps wasn't careful enough, in pointing out that these flow charts, if

they are true at all, are certainly true only for adiabatic conditions. The moment you have heat flux at the wall, then all bets are off! I think, in general, the lines move to the left. That is, you are getting into dispersed flow, or annular flow, out of bubble flow, earlier, and at lower qualities than what is indicated here.

Now the argument as to whether or not Herb has films on the wall or doesn't have films on the wall: I think that is an entirely separate argument; and he doesn't, I think, know whether or not he has films on the wall.

MR. HAYS: Can you tell me concerning the Martinelli original paper? Do you believe it to be valid for cases of dispersed flow? It seems to me the implicit assumption in his derivation is there is a continuous liquid phase and continuous vapor phase.

MR. GOLDMAN: Yes, the derivation is based on continuous phases, but I believe that the results are applicable to dispersed flow. An obvious weakness--and Martinelli was the first one to point it out--is that the derivation does not take account of flow patterns. Another weakness is that the pressure drop factors are not a function of mass velocity. I think one should expect, at otherwise the same conditions, that the pressure-drop ratio should change with mass velocity.

Now the Martinelli-Nelson approach does not account for this.

A number of years ago Isbin, and I forget the reference now,* published a paper showing the effect of mass velocity on the two-phase pressure-drop factors, and in effect it showed that at lower velocities, he gets higher factors than Martinelli-Nelson; and at higher mass velocities, he gets lower factors.

Now perhaps one explanation for this is that at the lower mass velocities you have more of a chugging kind of a flow, and therefore get more pressure loss, whereas at the higher mass velocities you have a more dispersed and more uniform kind of a flow, and therefore the pressure-drop factor should be lower.

*Isbin, H. S., Moen, R. H., Wickey, R. O., Mosher, D. R. and Larson, R. C., Two-Phase Steam-Water Pressure Drops, Chem. Eng. Prog. Symp. Ser., Vol. 55, No. 23, 1959.

But it turns out that, at least of all the data that he collected, which was sort of in the range that one might be interested in, that Martinelli-Nelson fell right in the middle of the data.

MR. BERENSON: I always felt a little uncomfortable using the Martinelli-Nelson paper for moderately high qualities, because they base their two-phase pressure drop on the liquid pressure drop, so you are using pressure factors that are anywhere from ten to even more than a thousand.

What we did, in analyzing our two-phase data, which made me a little happier, was to switch from basing the two-phase pressure drop on the liquid pressure drop when the ratio of the liquid to the vapor passed through 1, and in doing this, the Martinelli multiplier was never greater than 4.2. And it turned out that we were basing the two-phase pressure drop on the vapor pressure drop above a quality of 2% over almost the entire range we were multiplying our vapor pressure drop rather than the liquid pressure drop. This multiplier was generally very small. We were happier doing that than multiplying by thousands.

MR. GOLDMAN: I am not so sure that I would agree with you, Paul. I believe that the accuracy is the same, that is multiplying by a factor of a thousand can be made with the same number of significant figures as that of 1, if you like.

If you talk about a different model for the derivation, then the reason why I think that Martinelli-Nelson has a better approach is that on the wall, where you really have the friction, you have liquid flow, and it is the shear in the liquid which is going to make the major contribution to what the friction pressure drop is. So I am not so sure that you inherently ought to get better results by starting off with vapor, because it is the shear on the wall, or near the wall, which is all liquid. As long as we are talking about adiabatic walls, I think.

A question was asked from the floor regarding the adequacy of the homogeneous model coupled with a statement that it gave results within 20% of Martinelli-Nelson.

MR. GOLDMAN: I believe there are some regions in which the discrepancy between homogeneous and Martinelli-Nelson is more than 20%.

MR. DAVIS: Excluding the low-pressure data.

MR. GOLDMAN: There undoubtedly are many regions where the homogeneous model gives you about the same results. I believe there is some Argonne data--is anybody here from Argonne who remembers this? They have some data that showed a large difference between the homogeneous model predictions and the Martinelli-Nelson predictions.

MR. POPPENDIEK: I thought when Martinelli derived the expression in normalizing the final, two-phase flow pressure drop, he used a denominator if only a liquid flow was flowing and if only a gas was flowing, and I remember the final answer is exactly the same. There is no difference.

MR. GOLDMAN: What Martinelli-Nelson did, it comes out to be exactly the same. I wasn't sure whether Paul was not talking about a different model. Their model assumed there was liquid film at the wall, and that makes some difference.

MR. POPPENDIEK: I think there was one point he pointed out, and I think that's what you were referring to, but I wasn't quite clear. That is, in the original derivation, when he talks about the two pressure-drop terms, he recognizes there is a difference in velocity between the two phases, and he doesn't account for that, and so that finally is determined empirically by the constants α and β , when he makes a final fitting of these data. But I think this is the major weakness which he recognized and couldn't do anything about. Only if you have separated the flows, do you know the relative difference exactly, or at least ideally.

MR. GOLDMAN: Well, that is one weakness. I think perhaps the major weakness is that the whole result is completely independent of mass velocity and, therefore, flow regimes, and you just intuitively expect two-phase pressure drop factors are to be a function of mass velocity.

MR. BROOKS: In most systems it is quite easy to measure the liquid pressure drop of a particular system in which you are measuring two-phase drops. So this is a reference data as to correlation.

MR. ROHSENOW: I think we can settle this, because for any given flow rate, at a given quality, the ΔP of the liquid, ΔP of the vapor, in the Martinelli correlation are fixed numbers; very definite numbers; and the two-phase flow ΔP divided by either one of them has the same percentage of error in it, whether you multiply by a thousand, or 4. There is the same percentage of error.

MR. GOLDMAN: I agree. On the other hand, I wasn't sure, perhaps, what Paul was referring to. I thought he was turning the model inside out, so to speak, assuming that he has liquid slugs flowing through the center of the pipe, and vapor flowing along the outside of the pipe. You could make such a model, which you might want to call a Martinelli-Nelson vapor versus liquid, and if he had done that, then--

MR. BERENSON: I was referring to the standard position.

MR. BONILLA: Since this is such a hot topic, I don't think we ought to let Paul down. I mean, after all, there is the work that is included in the Martinelli-Nelson, and other papers, but then there is also the fact that the pressure drops with single phases are much more accurately predictable than with two phases, and I tend to side with Paul there; that you can predict the pressure drop for the vapor alone with considerable accuracy, and if the liquid is small in amount, it is merely a perturbation, so to speak, on that pressure drop, and I would much prefer to base a calculation of the perturbation, we will say, on the data that are more accurate for the main component.

MR. STEIN: Same answer, either way.

MR. BONILLA: No, you would not get the same answer. You would only get the same answer if the Martinelli-Nelson correlation happened to be a hundred per cent accurate, which I don't see how it could possibly be a hundred per cent accurate over a full quality range.

MR. LYON: During the last few days we have had a number of data presented on pressure drop, and it is my impression that most of those gave lower pressure drops than were predicted by the Martinelli correlations, with, I think, the exception of Randall, who had a higher pressure drop. Would you care to comment on that?

MR. GOLDMAN: I am starting to stick my neck out again! I suspect that some of those data were taken at fairly high velocities. These were condensing data. And when you condense at high velocities you really ought to write more equations than the equations which are written by Martinelli-Nelson, and an important equation or result of the equation is that when you have a compressible fluid cooled while it is flowing at a high velocity, you can actually get a gain in stagnation pressure, because you are cooling the compressible fluid at a high rate while it was flowing at a high velocity.

Now I wouldn't be surprised but, as I say, I am sticking my neck way out, that if the data were looked at carefully, that perhaps this might explain some of the low pressure losses.

MR. HAYS: The thought had also occurred previously that there might be some kind of an effect which was analagous to two-phase boundary layer, and a mass affected by condensation by fluxes, that this might be analagous to reducing the frictional pressure.

MR. GOLDMAN: I don't think this is an assumption as such. It was Shapiro and Hawthorne who first discovered that when you cool a high-velocity, compressible flow stream, that you get a gain in stagnation pressure, and I think this is exactly what you would get when you cool.

On the other hand, when you heat a fluid, a compressible fluid, at high velocities, you get a loss in stagnation pressure.

So you should take that into consideration if the velocities are high. This just comes out of all the equations. Intuitively one cannot explain it.

MR. STEIN: Trying to judge the reasons why the Martinelli-type approach or predictions fits or doesn't fit data, or is higher or lower, it seems to me is another one of these situations in which there is confusion because of trying to connect empiricism with theoretical approach.

Certainly the equations that are used are one-dimensional equations, which are reasonable with respect to a physical picture. Only when you have two extreme situations, when you have a perfectly homogeneous flow, or when you have a perfectly stratified flow.

Further, there are computations that--I believe I remember this correctly, and check me on it--that I think is overlooked sometimes. In the approach that is used we correlate a frictional pressure drop ratio and a vapor volume fraction with an empirical-correlating factor, this X_{tt} of Martinelli and Lockhart. There was some physical picture associated with this X_{tt} used by Martinelli and Lockhart which concerns itself with a stratified flow and with an adiabatic system.

This required, if I remember correctly, making a statement about equality of pressure drop and, very important to the treatment, was that the pressure drop only occurred because of the friction, and nothing else.

As a result, one might question the use of this X_{tt} for the situation where you have, say, momentum changes.

MR. GOLDMAN: Well, this is certainly another contribution as to why you really shouldn't expect the results to be absolutely accurate. And there are the others we mentioned before, as well. They all contribute to some expected, as one should expect, scatter in the data. (There was some further discussion on slip ratios and Mr. Goldman drew a curve on the blackboard which is reproduced here as Fig. 9.)

Stability
of
Parallel-Path
Two-Phase
Flow

by

Thomas J. Vild (1)

Donald E. Sill (2)

(1) Senior Research Engineer, Tapco Group, A Division of Thompson
Ramo Wooldridge

(2) Research Engineer, Tapco Group, A Division of Thompson Ramo
Wooldridge

ABSTRACT

The requirements for stable operation of a parallel-tube mercury condenser capable of flowing in opposition to 1 "g" were investigated analytically and experimentally. Included in the analyses were the effect of geometric and thermodynamic unbalances between tubes, header pressure loss, magnitude and direction of the gravity vector, and fluid/wall contact angle. The analytical conclusions were verified by experiment on a small scale condensing apparatus and applied to a full scale prototype condenser. The results of the analyses, the small scale tests, and the testing of the full scale prototype are presented.

Nomenclature

C_D	- Drag coefficient
D	- Diameter
F	- Force
G	- Weight flow per unit area
L	- Length
Re	- Reynolds number
Fr	- Froude number
P	- Pressure
ΔP	- Pressure drop
R	- Radius
V	- Velocity
W	- Weight
X	- Flowing quality
d	- Diameter
f_v	- Vapor friction factor
h_{fg}	- Heat of vaporization
\dot{m}	- Mass flow rate
g	- Gravitational constant
g_c	- Local gravitational constant
q_r	- Heat rejected per unit length and time
r	- Radius
x	- Weight
x	- Distance
x	- Distance
α	- Angle or deviation from design quality
θ	- Contact angle (liquid-solid)
δ	- Deviation from design heat rejection
δ	- Deviation from design diameter
ϕ	- Angle
σ	- Surface tension, liquid-solid
τ	- Interfacial shear
ρ	- Weight density
μ	- Absolute viscosity
Φ	- $\Delta P_{TF} / \Delta P_V$

Subscripts

O	- Initial or inlet
C	- Condensing, condensate
D	- Design, drop, drag
e	- Exit
INT	- Integrated
H	- Header
i	- Interfacial
l	- Liquid, local
m	- Momentum, mean
s	- Static or local
T	- Total or tube
v	- Vapor
ST	- Surface tension

INTRODUCTION

In the operation of any fluid system, stability is often of prime consideration. Generally in single passage, single phase, incompressible flow, this stability is easily achieved. However, difficulty is encountered when considering two-phase or parallel tube flow. Even more troublesome is a combination of the above with flow against an external body force. These were the requirements of the condenser for the Sunflower I* space power conversion system employing mercury as the working fluid in a Rankine cycle. A further characteristic, the high density of the liquid condensate, also contributed to the difficulty of defining a stable design.

With this combination of adverse requirements, it was felt that extensive fluid dynamic analyses verified by experiment were necessary prior to embarking on the design of a full scale condenser.

This paper describes these analytical and experimental investigations and their application to prototype hardware.

SINGLE TUBE STABILITY

Analyses were conducted to evaluate the restrictions imposed on the condenser design as a result of the requirement that operation be sustained with a 0 to 1 g body force in any direction. Initially analyzed were the requirements for stability in a single tube under the various gravity orientations in which the Sunflower condenser is to operate. The following analysis, which assumes dropwise condensation and no agglomeration, will investigate the effect of vapor velocity on drop size, drop acceleration and drop velocity.

Consider the mercury drop of Figure 1 hanging on a wall under the influence of gravity and surface tension. At incipient movement the weight and surface tension forces can be expressed as follows:

$$F_w = n \sin \alpha \frac{\rho \pi R^3}{3} \left\{ 4 - [1 - \sin(\beta_m - 90)]^2 [2 + \sin(\beta_m - 90)] \right\} \quad (1)$$

and:

$$dF_{ST} \approx r_c d\theta \sigma \cos \theta \left\{ [-\cos(\beta_m + \Delta\beta)] - [-\cos(\beta_m - \Delta\beta)] \right\}$$

integrating:

$$F_{ST} = 4 \sigma R \cos(\beta_m - 90) \sin \beta_m \sin \Delta\beta \quad (2)$$

* Contract NAS 5-462 held by Thompson Ramo Wooldridge Inc. with NASA

Equating equations (1) and (2) yields the force balance at incipient movement

$$\rho_l \sin \alpha \frac{\rho_l \pi R^3}{3} \left\{ 4 [1 - \sin(\beta_m - 90)]^2 [2 + \sin(\beta_m - 90)] \right\} = 4 R \sigma \cos(\beta_m - 90) \sin \beta_m \sin \Delta \beta \quad (3)$$

Reynolds in Reference 1 showed experimentally that the distortion of the contact angle with a mercury droplet on a glass plate was $\pm 10^\circ$ at incipient movement as the plate was tilted. Using:

$$\beta_m = 141^\circ \text{ (mercury-glass; approximately the same for mercury-steel)}$$

$$\Delta \beta = 10^\circ \text{ (from Reference 1)}$$

$$\sigma = .0326 \frac{\text{lb}}{\text{ft}} \text{ (mercury-glass surface tension force)}$$

$$\rho_l = 800 \frac{\text{lb}}{\text{ft}^3} \text{ (liquid mercury density at } 600^\circ\text{F)}$$

and plotting R versus $\sin \alpha$ yields the curve of Figure 2. Also plotted is the experimental data of Reference 2 which is in good agreement with equation (3). Although the temperatures during the experiments of reference 2 were ambient, it is believed that β_m and α are fairly insensitive to temperature.

Drop Model

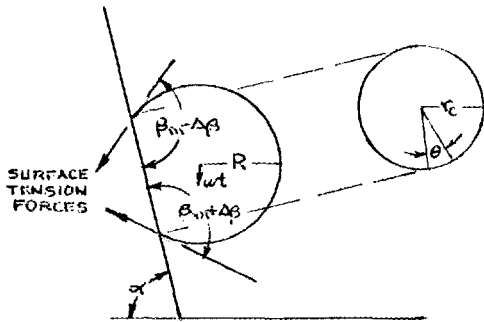


Figure 1

Drop Radius at Incipient Movement

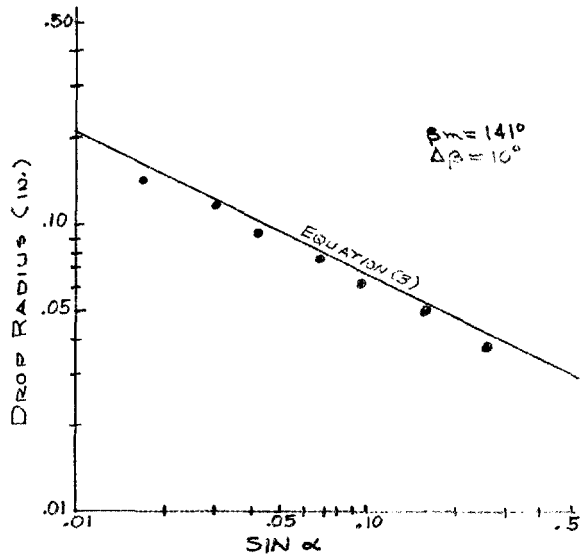


Figure 2

Next, the drag of the vapor on the condensing drop as it occurs in an actual condenser will be considered. This term in the force balance can be expressed as:

$$F_D = \frac{\rho_v V_v^2 C_D}{2g_c} R^2 \left[\frac{\pi R_m}{180} + \sin(\beta_m - 90) \cos(\beta_m - 90) \right] \quad (4)$$

where the bracketed term is an expression for the projected area, (β_m in degrees)

Here the value of C_D must be evaluated. Reference 2 suggests that based on values of C_D for spheres, drops, and freely rising vapor bubbles, an average value of 1.0 may be used, especially in the range of drop Reynolds numbers expected in the Sunflower application (100 - 200).

The general equation, then, of a drop in a mercury condenser, about to be swept or fall off a tube wall may be written:

Drag + weight component \pm surface tension resultant = 0

$$\frac{\rho_v V_v^2 C_D}{2g_c} R^2 \left[\frac{\pi R_m}{180} + \sin(\beta_m - 90) \cos(\beta_m - 90) \right] + \sin \alpha \frac{\rho_l \pi R^3}{3} \left\{ 4 - [1 - \sin(\beta_m - 90)]^2 [2 + \sin(\beta_m - 90)] \right\} - 4\pi R \cos(\beta_m - 90) \sin \beta_m \sin \Delta \beta = 0$$

To evaluate the drop diameters at the extreme conditions, four cases will

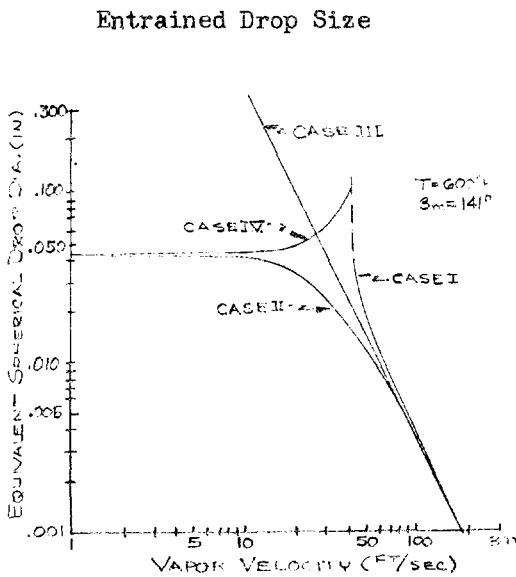


Figure 3

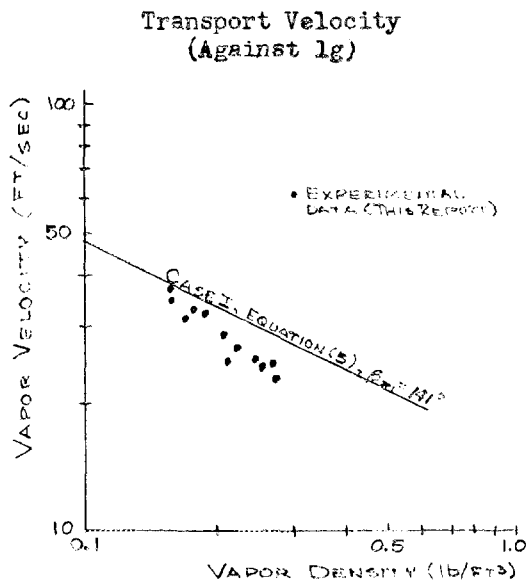


Figure 4

be assumed as follows: Case I, where flow is in opposition to gravity and the drop is about to be torn off the wall by the vapor. Case II, where flow is in the direction of gravity. Case III, 0 "g" and case IV where flow is in opposition to gravity and the drop is about to fall off the wall back toward the condenser inlet. Case IV is the unstable case. Using the Sunflower I operating level, plots of the diameter of equivalent spherical drops versus vapor velocity for the four cases are shown in Figure 3.

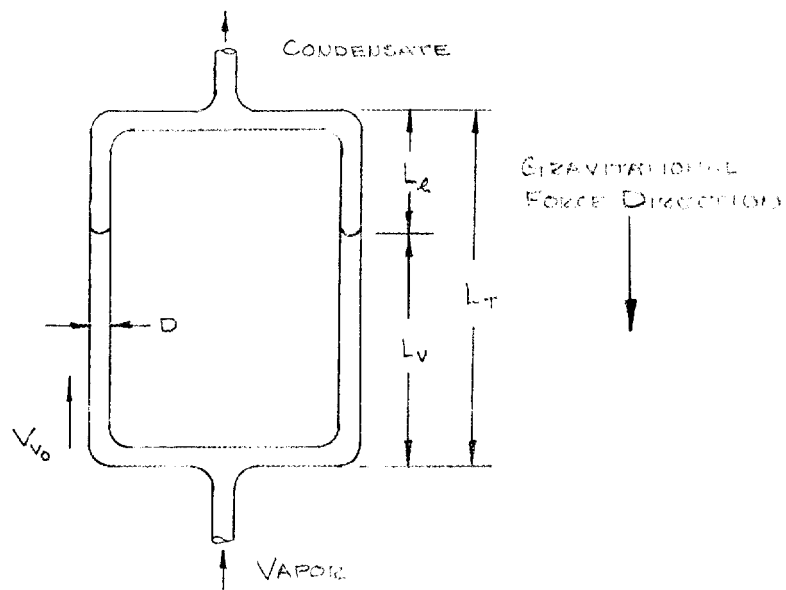
From the figure, it is evident that Cases I and IV are the most sensitive to vapor velocity, i.e., a vapor velocity of at least 45 ft/sec is needed throughout the condenser to assure that all the condensate will be delivered to the interface when flow is against gravity. Verification of this velocity requirement was obtained experimentally with a glass condensing apparatus approximating the prototype tube geometry. The data obtained from this rig (vapor velocity required to transport all condensate against gravity as a function of vapor density) is plotted in Figure 4 with Case I of equation (5).

PARALLEL TUBE STABILITY

With the characteristics of a single tube condenser defined it is then necessary to investigate parallel tube interaction.

Maintenance of a stable liquid vapor interface in a parallel tube condenser under the Sunflower I system acceleration requirement posed several problems.

As an example, assume the following condenser:



$$\Delta P_s = \Phi_{int} f' \frac{L_v}{D} \frac{\rho_v V_v^2}{2g_c} - \frac{\rho_v V_v^2}{g_c} + L_e \rho_e \mu$$

also: $q L_v = \dot{m}_v h_{fg} = \frac{\pi D^2}{4} G_o h_{fg}$

where: q = heat rejection per unit length

Combining equations results in:

$$\Delta P_s = \Phi f' \frac{\pi D G_o^3 h_{fg}}{8g_c \rho_v} - \frac{G_o^2}{\rho_v g_c} + \left(L_T - \frac{\pi D^2}{4} \frac{G_o h_{fg}}{q} \right) \rho_e \mu$$

differentiating:

$$\frac{d\Delta P_s}{dG_o} = \Phi f' \frac{\pi D h_{fg} 3G_o^2}{8g_c \rho_v} - \frac{2G_o}{\rho_v g_c} + \left(- \frac{\pi D^2 h_{fg} \rho_e \mu}{4q} \right)$$

substituting:

$$\frac{\pi D^2}{4} \frac{h_{fg}}{q} = \frac{L_v}{G_o}$$

results in:

$$\frac{d(\Delta P_s)}{dG_o} = \left(\frac{\Phi f' L_v}{D} - \frac{4}{3} - \frac{2L_v \rho_e \mu g_c \rho_v}{3G_o^2} \right) \frac{3G_o}{2g_c \rho_v}$$

From reference (3), a necessary and sufficient condition for stability is that $d(\Delta P_s)/dG_o$ is positive. This requires that:

$$\frac{\Phi f' L_v}{D} > \frac{4}{3} + \frac{2L_v \rho_e \mu g_c \rho_v}{3G_o^2} \quad (6)$$

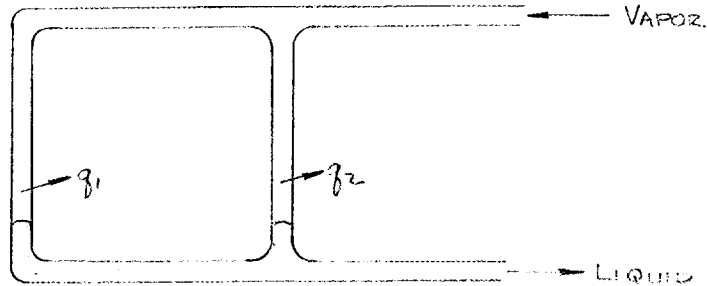
Substituting values from the Sunflower condenser into Equation (6) results in:

$$2.70 < 4/3 + 66.7$$

or the condenser would not be stable. Any attempt to satisfy the stability criterion would result in a higher pressure drop which cannot be tolerated. The single exception is a decrease in the local gravitation. The equation indicates stability at "g" levels below .02. This, however, is not consistent with the system acceleration specification.

Furthermore, in parallel tube condensers designed for zero or micro-gravity environments, the liquid vapor interface(s) may be held in each individual tube. Consequently, unbalances can be compensated for by shifting the interface positions in the tube as shown by the following analysis.

Consider the two-tube condenser below operating in zero or micro-gravity:



If, for instance, the heat rejection capability per unit length of tube #1 becomes greater than tube #2:

$$q_1 > q_2$$

and:

$$\dot{m}_{v1} > \dot{m}_{v2}$$

(vapor mass flow rates)

This means that the pressure drops are unequal:

$$\Delta P_1 > \Delta P_2$$

However, since the tube inlet pressures are equal (assuming negligible header pressure drop) the interface pressures are unequal, which is not a stable condition. Therefore the unbalance is compensated for by adjustment of the interface location until

$$\Delta P_1 = \Delta P_2 \quad \text{at which point } l_{c2} > l_{c1} \text{ and } \dot{m}_{v1} > \dot{m}_{v2}$$

where l_c is the respective condensing length

However, for the Sunflower condenser designed for a lg body force in any direction, the interface cannot be held in the tubes (as previously shown) and thermal and geometric unbalances can be compensated for only by changes in exit quality with the interface being maintained in a single location downstream of the parallel tube array. Obviously the design exit quality must be of sufficient magnitude to compensate for the unbalances without allowing the vapor velocity to drop below that value required for drop transport. Nor does one want to have too high an outlet quality because of the weight penalty involved. The minimum exit quality to meet the above requirements can be approximated by knowing the geometric and thermal unbalances.

Assuming a tapered condenser tube with a constant vapor velocity and neglecting the momentum pressure recovery, the following investigates the necessary outlet quality (based on 100% inlet quality) for parallel tube stability.

Friction:

$$dP_s = - \Phi f \frac{(GX)^2}{\rho v^2 g_c} \frac{dL}{D} \quad (7)$$

Thermal Balance:

$$dL = - \frac{G h_{fg}}{q} \frac{\pi D^2}{4} dx \quad (8)$$

combining equations 7 and 8

$$dP = - \Phi f \frac{(GX)^2}{\rho v^2 g_c} \left(- \frac{G h_{fg} \pi D^2}{4 D q} \right) dx$$

$$dP = C_1 \frac{G^3 x^2 D}{q} dx \quad (9)$$

where:

$$C_1 = \frac{\Phi f \pi h_{fg}}{8 \rho v^2 g_c}$$

The assumption that Φ and f are constant will not affect the answer greatly since two condensing tubes will be compared and these values will change very little from tube to tube over the quality ranges to be examined. The use of an average D rather than an integrated one should also have little affect since it is intended that the pressure drop of one tube be compared to another rather than the absolute value obtained.

Integrating equation (9)

$$\int_{P_1}^{P_2} dP = C_1 \frac{G^3 D_{ave}}{q} \int_{x_0=1}^{x_e} x^2 dx$$

$$P_1 - P_2 = C_1 \frac{G^3 D_{ave}}{q} \left[\frac{1 - x_e^3}{3} \right] \quad (10)$$

where C_1 is previously defined

Integrating equation (8) and solving for G

$$\int_0^L dL = - \frac{G h_{fg} \pi D_{ave}^2}{4g} \int_{x_0=1}^{x_e} dx$$

$$L = \frac{G h_{fg} \pi D_{ave}^2}{4g} [x_e - 1]$$

$$G = \frac{4Lg}{\pi D_{ave}^2 h_{fg} [1 - x_e]} \quad (11)$$

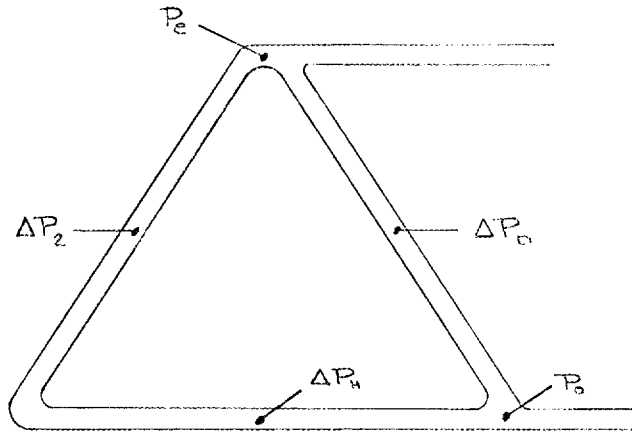
combining equations (10) and (11)

$$P_1 - P_e = C_2 \frac{g^2 [1 - x_e^3]}{D_{ave} [1 - x_e]^3} \quad (12)$$

where

$$C_2 \equiv C_1 \frac{1}{3} \left[\frac{4L}{\pi h_{fg}} \right]^3$$

Equation (12) provides an expression for tube exit quality as a function of tube geometric and thermal characteristics. This can now be applied to two parallel operating tubes as shown below.



it can be seen that:

$$\Delta P_2 + \Delta P_H = \Delta P_D \quad (13)$$

where ΔP_H is the header friction loss

Allow tube D to operate at design conditions and tube 2 deviate from design to the extent that:

$$\begin{aligned} g_2 &\equiv \epsilon_g g_D \\ D_{2,ave} &\equiv D_{D,ave} / \epsilon_D \\ X_{e2} &\equiv \alpha X_{eD} \end{aligned} \quad (14)$$

where ϵ_g and ϵ_D are > 1.0 , $\alpha < 1.0$, and X_e is the outlet quality of each tube (all deviations in accumulative direction)

Then, combining equations (12), (13) and (14) and cancelling:

$$\frac{\Delta P_D - \Delta P_H}{\Delta P_D} = \frac{[1 - (\alpha X_{eD})^3][1 - X_{eD}]^3 \epsilon_g^2 \epsilon_D^5}{[1 - \alpha X_{eD}]^3 [1 - X_{eD}]^3} \quad (15)$$

Equation 15 then, expresses the effect of pressure drop, thermal, geometric, and fluid dynamic unbalances between tubes on the design outlet quality necessary to maintain the vapor velocity greater or equal to α times the design exit vapor velocity.

A qualitative verification of this approach was obtained with the glass-tube mercury-condensing apparatus of Figure 5. All tests were conducted with the multiple tube flow vertically upward. The condensing tubes were step-tapered to maintain vapor velocity for operation in opposition to 1 g.

To operate, the glass tubes were preheated and the boiler heated at atmospheric pressure until boiling started. The system was then evacuated, increasing the boiling rate and initiating vapor flow through the condenser. The flow control valve was then shut and the interface allowed to proceed upstream in the interface tube. As this occurred, the quality at the exit of the multiple tubes decreased by the shift in relative condensing heat transfer area upstream and downstream of this junction.

Stability tests were performed by permitting the parallel tube exit velocity and quality to steadily decrease until slugging and unstable flow occurred. Interface location at this event then indicates the stability limit. Six of these runs were performed with an interface tube diameter of 6 mm. This tube was then replaced with a 10 mm tube and the tests repeated four times. Comparison of the results of these tests can thus yield a check on the heat transfer calculations employed to arrive at the quality and velocity conclusions.

MULTIPLE TUBE BREADBOARD

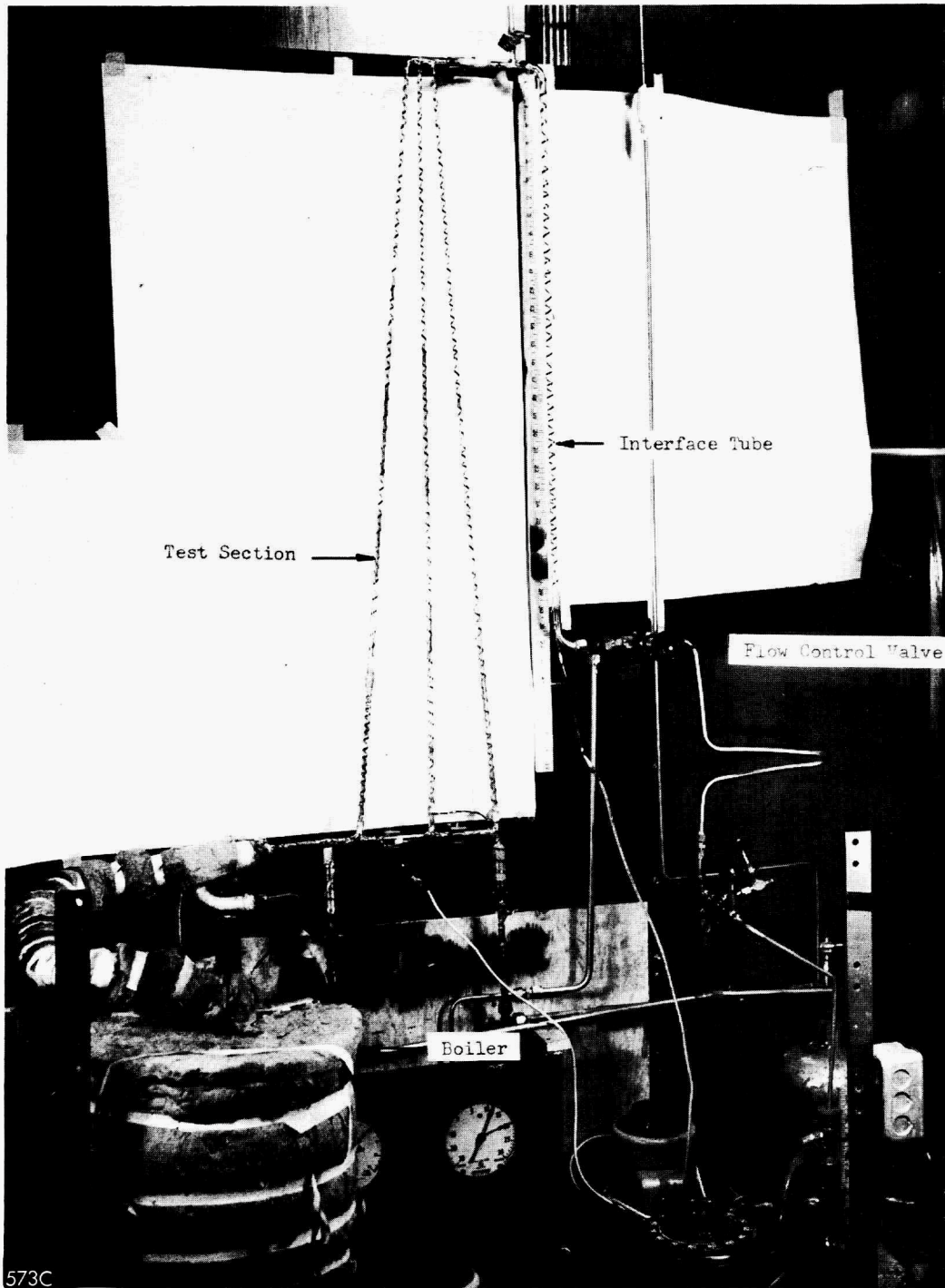


FIGURE 5

Repeatability of the stability point was demonstrated with this apparatus.

The qualitative results of this testing, however, were of limited value due to the difficulty in measuring tube geometric and thermal unbalances and in obtaining a range of the independent parameters with free convection heat rejection. The test did, however, demonstrate that the outlet vapor velocity of the parallel tube test section was the significant parameter in determining stability.

PROTOTYPE DESIGN AND TESTING

The values of the independent parameters of equation 15 expected in the Sunflower design are:

$$\Delta P_H = 0.1 \quad \Delta P_D = 2.0$$

$$\epsilon_g = 1.05$$

$$\epsilon_D = 1.01$$

Using these inputs and the fact that:

$$\frac{X_{L2}}{X_{L0}} = \frac{V_{L2}}{V_{L0}} = \alpha$$

results in the plot of Figure 6. This curve expresses (with the unbalances

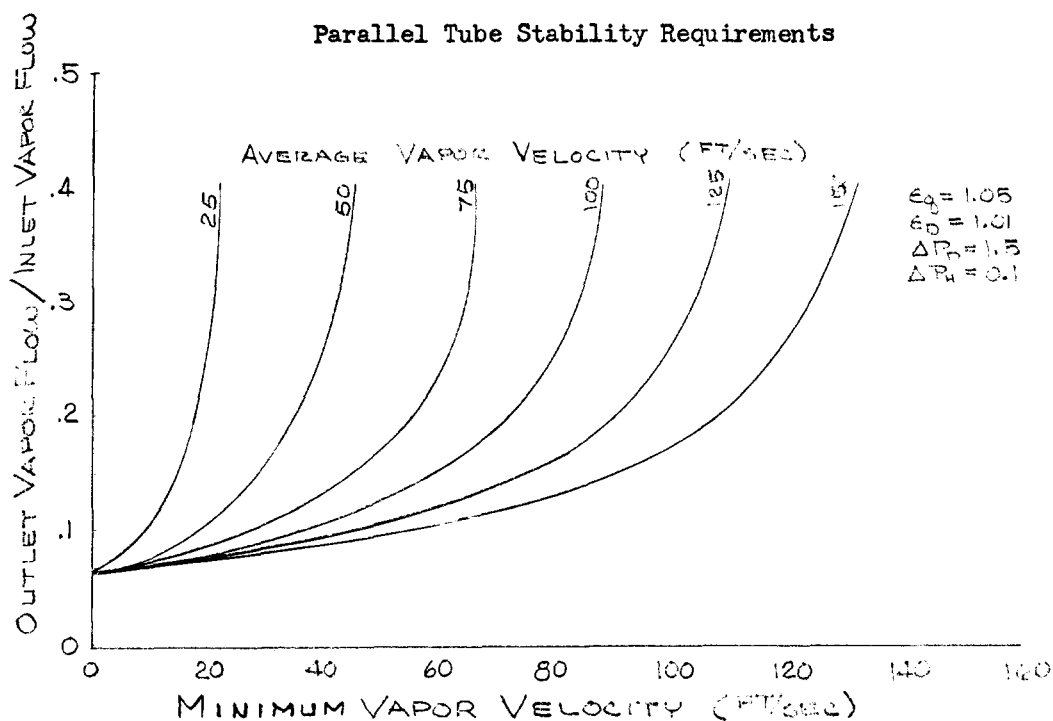


Figure 6

listed above) the average velocity that must be designed into the condenser to assure a "worst" tube minimum velocity above the single tube minimum. From this curve a design velocity of 90 ft/sec with an outlet vapor flow of 12% of the inlet vapor flow was chosen to provide the minimum of 45 ft/sec (from the single tube analysis) in the "worst" tube.

To summarize, with a .1 psi header pressure drop, 2.0 psi condensing tube drop, unbalances in q and D less than or equal to 5% and 1% respectively, and a 90 ft/sec design vapor velocity, the outlet velocity in the unbalanced tube will not drop below 45 ft/sec if the design outlet vapor flow is 12% of the inlet vapor flow.

The problem arises, of course, as to what to do with the vapor flow from the parallel tube condenser. This vapor is condensed in a single tube which, although inefficient, is immune to parallel tube instability. The complete condenser, then is composed of two parts, the primary, or parallel-tube condenser, and secondary, or single-tube condenser.

A photograph of the Sunflower I condenser installed in the test booth is shown in Figure 7. The primary and secondary condensers are clearly shown.

Successful operation of each portion as well as the complete condenser was achieved during the component test. Operation was sustained over a wide range in weight flow and inlet quality as well as during various transients. In all cases the incoming mixture was delivered to the interface as condensate and liquid hold-up did not accumulate.

Before experimental verification of the parallel tube stability analysis could be obtained, however, a deterioration in condenser performance was detected. This deterioration took the form of an inability to operate the condenser without experiencing slugging at a velocity level which did not previously incite slugging. A graphical presentation of this deterioration is shown in Figure 8. In this figure the minimum average velocity of the vapor (necessary to avoid slugging) leaving the primary condenser is plotted as a function of operating time. (Although the minimum velocity experienced on this curve, 45 ft/sec, is an apparent contradiction of the single tube and parallel tube analysis presented herein, due to an off-design in heat rejection at design flow, this curve is for a higher temperature and consequently a higher vapor density than the earlier curves.)

The cause of this deterioration in performance was laid to a progressive "wetting" or increase in contact angle between the mercury droplets and condenser tube walls.

Using the single tube analysis the effect of the contact angle on condenser stability can be investigated. Allowing β_m to vary in Equation 5, (σ is kept constant since Reynolds, in reference 1, postulates that surface tension is fairly constant even under changing contact angles) the curves of Figure 9 are generated for Case I operation.

SUNFLOWER I CONDENSER

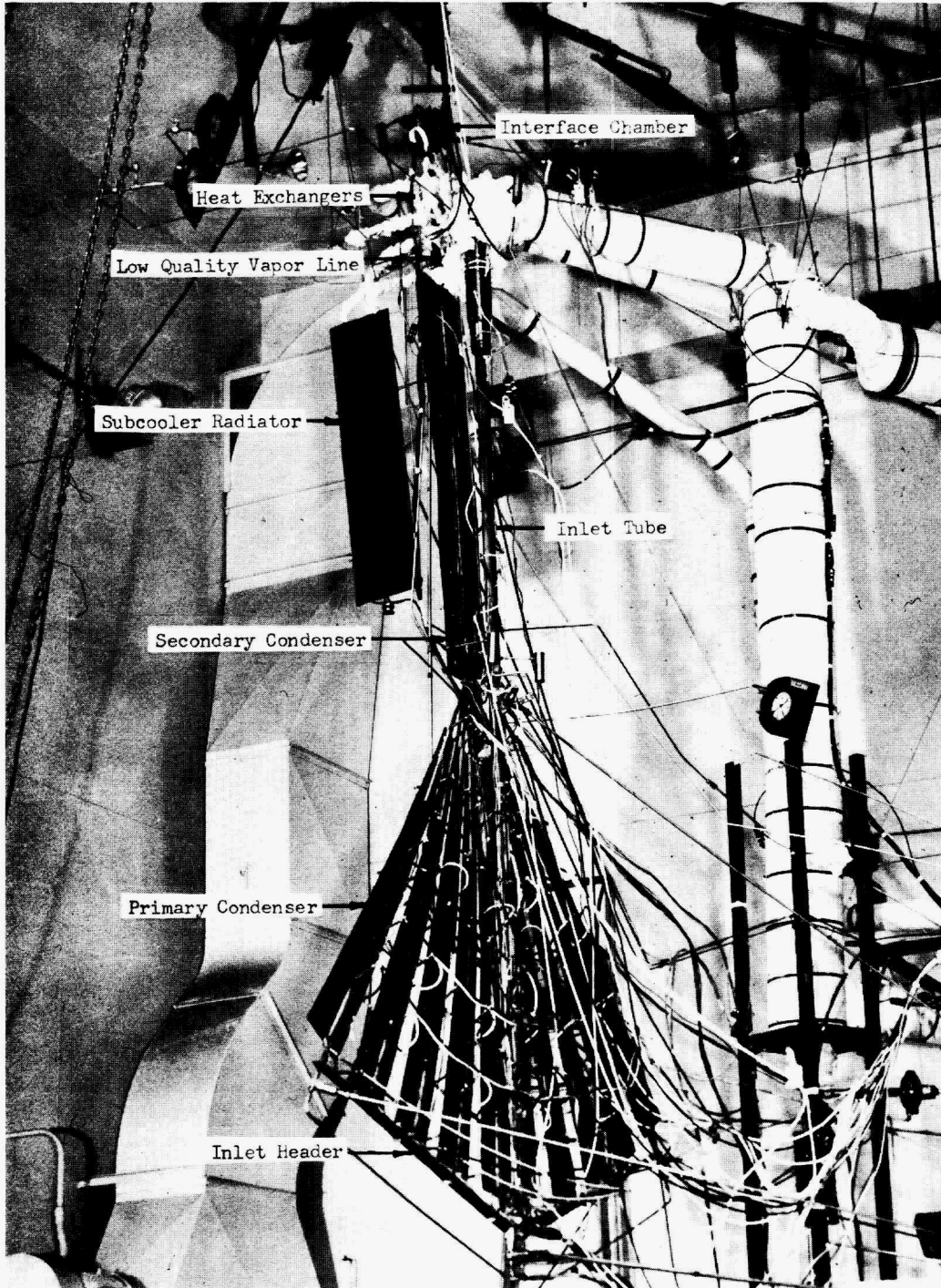


FIGURE 7

Performance Deterioration

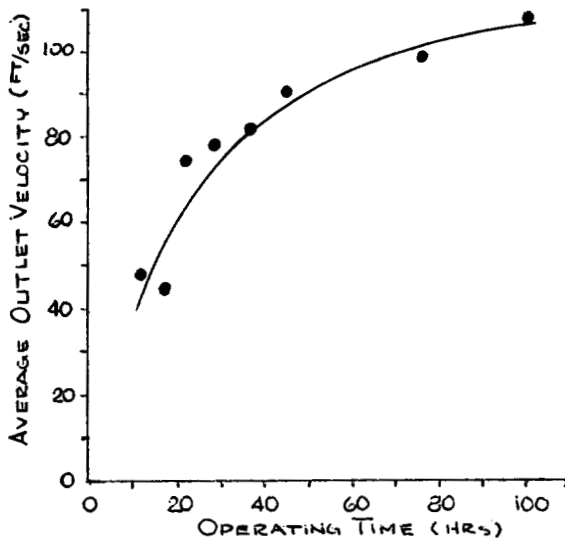


Figure 8

Effect of Contact Angle on Maximum Drop Size

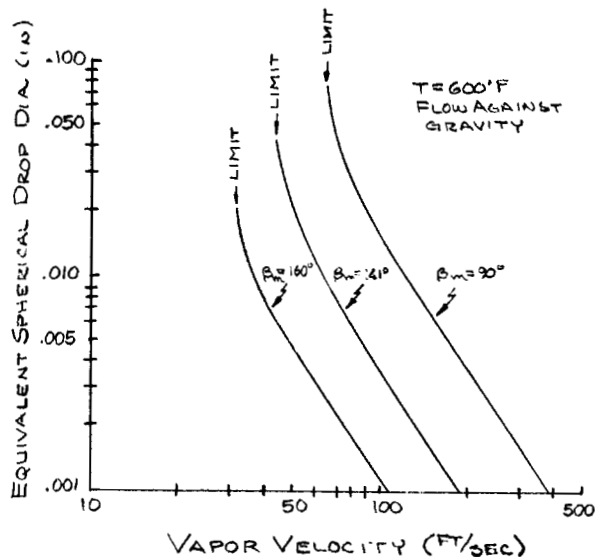
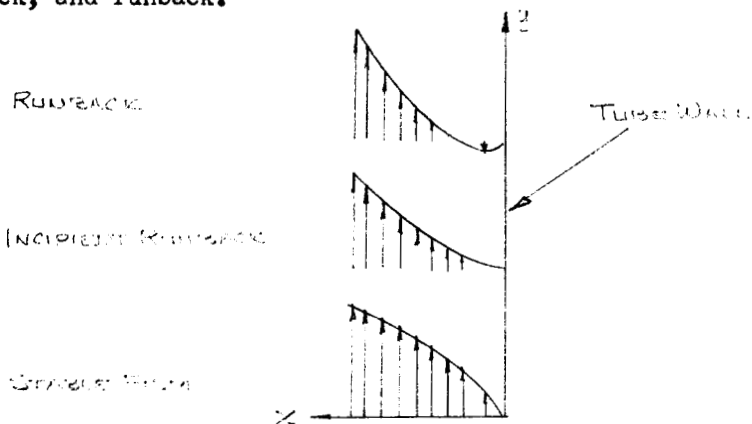


Figure 9

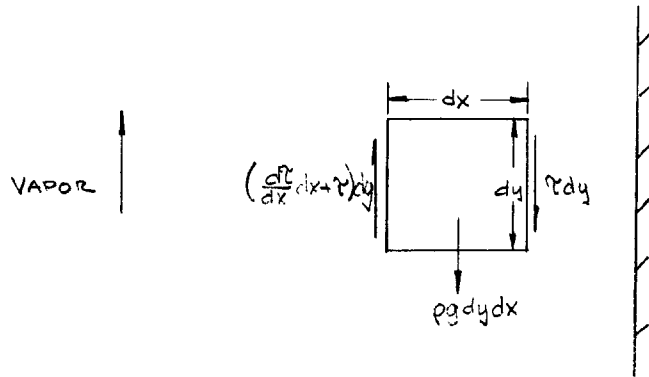
As can be seen, the minimum velocity required to experience Case I operation and avoid Case IV operation increases with decreasing contact angle (tendency toward wetting).

Although it is not known whether the tendency toward wetting would progress to a degree where film condensation would occur with mercury, this limiting situation can be investigated to determine the limiting stability condition (that condition being the minimum vapor velocity necessary to transport a liquid film without runback in opposition to 1 g). The first step is to analyze the conditions at the incipient runback point to differentiate between negligible and predominant factors. Reference 4 gives the following film velocity profiles for conditions of a stable film, incipient runback, and runback.



At the incipient runback point it can be seen that the velocity gradient at the wall is zero and the wall shear stress is therefore zero. It will also be assumed that there is no velocity in the X-direction and that the change in velocity in the Y-direction is negligible.

This latter assumption is pessimistic since it neglects the effect of the liquid momentum gain due to the effect of decreasing liquid velocity as the incipient runback point is reached. The last assumption is that the (vapor) pressure gradient is negligible which is also pessimistic since the pressure gradient would tend to support the film. Consider an incremental area within the liquid film:



Balancing the forces yields:

$$\left(\frac{d\tau}{dx} dx + \tau\right) dy = \mu \rho g_c dy dx + \tau dy \quad (16)$$

but

$$\tau = \mu \frac{dV_y}{dx}$$

and

$$\frac{d\tau}{dx} = \mu \frac{d^2 V_y}{dx^2}$$

which on substitution into equation 16 yields:

$$\frac{d^2 V_y}{dx^2} = \frac{\mu \rho g_c}{\mu}$$

integrating

$$\frac{dV_y}{dx} = \frac{\mu \rho g_c x}{\mu} + C_1$$

but since the limit for stability is $\frac{dV_y}{dx} = 0$ at $x=0$ and $C_1 = 0$.

Therefore

$$V_y = \frac{\mu x^2 \rho g_c}{2\mu} + C_2$$

but

$$C_2 = 0 \text{ at } x=0, V_y=0$$

and finally:

$$V_y = \frac{\mu x^2 \rho g_c}{2\mu}$$

and at $x = \delta$, $V_y = V_i$ (17)

$$\frac{\mu \rho g_c}{2} \frac{\delta^2}{2} = V_i \quad \text{where } \delta = \text{film thickness}$$

since the velocity profile is parabolic the average velocity is $1/3$ of the interfacial velocity (V_i) and from continuity:

$$\frac{V_i}{3} \rho \delta \pi d = \dot{m}_l \quad (18)$$

substituting equation 17 into equation 18 yields:

$$\frac{\mu \rho g_c \delta^3 \pi d}{6\mu} = \dot{m}_l$$

but

$$\tau_i = \mu \delta \rho g_c$$

and finally:

$$\tau_i = \mu \left(\frac{6 \mu \dot{m}_l \rho g_c}{\pi d g_c} \right)^{\frac{1}{3}} \quad (19)$$

which gives the expression for the interfacial shear at the runback point. However, the net interfacial shear is made up of two components; the frictional shear τ_f , and the momentum shear τ_m , where:

$$\tau_i = \tau_f + \tau_m$$

$$\tau_f = \frac{f}{4} \rho_v \frac{V_v^2}{2g_c} \quad (20)$$

$$\tau_m = \frac{\Delta \dot{m}_v V_v}{\pi d \Delta L g_c} \quad \text{where } \Delta \dot{m}_v = \text{vapor condensed.} \quad (21)$$

Equating equations 19, 20 and 21 yields:

$$\mu \left(\frac{6 \mu \dot{m}_l \rho g_c}{\pi d g_c} \right)^{\frac{1}{3}} = \frac{f}{4} \rho_v \frac{V_v^2}{2g_c} + \frac{\Delta \dot{m}_v V_v}{\pi d \Delta L g_c} \quad (22)$$

Since the slugging first occurred in the small diameter section of the Sunflower I condenser, equation 22 will be evaluated at this point.

$$N_{Re_0} = 5950$$

$$f = .036 \quad (23)$$

based on the condenser design conditions, equation 22 and 23 yield:

$$u(.650) = 1.68 \times 10^{-5} V_v^2 + 1.09 \times 10^{-3} V_v$$

Solving for V_v yields a minimum vapor velocity of 165 ft/sec for film condensation. This minimum vapor velocity could be lower, not only for the reasons previously mentioned, but also because the friction factor is based on a smooth surface between the vapor and liquid. With a turbulent vapor core this may not be the case; however, the effect of the boundary would have to be investigated experimentally to accurately determine the vapor-liquid friction factor.

An x-ray of the condenser showed the drop/wall contact angle to be approximately 90° after 100 hours of running. Referring to Figure 9, the adverse effect on condenser performance is evident. With a 90° contact angle, the minimum velocity necessary for anti-gravity operation is 64 ft/sec. Referring to Figure 6, it can be seen that with this actual velocity requirement and an outlet vapor flow of 12% inlet vapor, an average vapor velocity of ≈ 135 ft/sec is required. This compares with the experienced velocity requirement of 110 ft/sec (again at a higher-than-design pressure) during the prototype test after 100 hours of operation.

CONCLUSIONS AND RECOMMENDATIONS

Parallel tube stability with two-phase mercury condensing flow in opposition to gravity is possible without using the normal pressure drop producing methods of stabilization. This stability can be achieved by maintaining a high vapor velocity throughout the condensing section. The magnitude of this velocity is a function of tube geometric and thermal unbalances, header frictional pressure drop, vapor density, and drop contact angle.

Maintenance of this velocity requires the use of tapered condensing tubes. In addition, since a multiple tube array with flow against gravity is statically and dynamically unstable if multiple interfaces are held in the tubes (unless a high frictional pressure drop is experienced) this configuration is eliminated. Maintenance of an interface in a single position downstream of the multiple tubes is one possible approach. In this configuration the outlet quality of the parallel tubes is finite and a single tube condenser is used to reject the remaining latent heat.

The deterioration in performance noted during the condenser component test (higher vapor velocity required for non-slugging operation as a function of operating time) has been attributed to some form of wetting of the tube walls by the mercury. In this case a pseudo-wetting of mercuric oxide to tube material oxide probably occurred rather than an

intimate mercury-stainless steel wetting. This problem appears to be of serious consequence in condensers flowing against gravity, since the greater degree of wetting, the greater the design compromise to insure stability. The effect is problematical to a lesser degree in condensers designed to operate in only zero or micro-gravity.

Determine experimentally the effect of tendency toward wetting on mercury condenser performance. If serious design compromises are indicated, investigate methods of promoting or maintaining non-wetting operation. If non-wetting cannot be insured for mission times, determine analytically and experimentally the requirements for wetting film stability.

In space condensers where parallel tube stability is a problem due to shifting interface positions, low frictional pressure drops, and/or system internal (flow) and external (vibration) disturbances, maintenance of a single interface downstream of the parallel tube array as in the Sunflower I condenser should be considered. The advantages over a conventional multiple interface-in-condenser tube approach are: less sensitivity to system acceleration or vibration, less liquid hold-up, less sensitivity to inventory shifts due to possible boiler oscillations, capability of predicting the location of and bleeding off non-condensibles, and capability of operating with flow against gravity with reasonable pressure drop.

References

1. Reynolds, W. C. Hydrodynamic Considerations for the Design of Systems for Very Low Gravity Environments Technical Report number LG-1, Department of Mechanical Engineering, Stanford University, September, 1961
2. Koestel, A., Reinmann, J. J., Mercury Condenser Research and Development, Thompson Ramo Wooldridge report number ER-4410, April, 1961, or Government-Industry Conference on Mercury Condensing, NASA TN D-1188, February, 1963
3. Griffith, P., Kulinski, E. S., Water Condensing Tests, Thompson Ramo Wooldridge report number ER-4200
4. Dennington, R. J., Koestel, A., Saule, A. V., Shure, L. I., Stevens, G. T., Taylor, R. B., Space Radiator Study, Thompson Ramo Wooldridge report number ER-4544

DISCUSSION

MR. KEYES: I just wanted to emphasize that I think you have to be careful, in using this criterion, in explaining what you mean by stability. Actually you have to use the transient energy equation, and I think that what you are really defining here is a criterion for excursion or transition from one stable condition to another, rather than instability which one normally thinks of as oscillatory, or at least fluctuating, phenomena. I think a paper by Quandt a few years back brought this point out very clearly. I just wanted to say that this criterion of positive slope is not necessarily a sufficient criterion.

MR. VILD: You say the paper was by whom?

MR. KEYES: Quandt, Westinghouse. At a Buffalo conference, several years ago.

MR. VILD: Does it differ very much from this?

MR. KEYES: Oh, yes; there is no comparison. Because he starts out with a transient time-dependent equation and uses perturbation theory. You start out with more or less steady-state equations. I feel that what you are developing is a transition from one steady-state to another; this is what you are interested in, I realize. I just wanted to point out you have to be careful in using this criterion.

MR. VILD: Well, I am sure what you are saying is right. But I want to make one point: This analysis really wasn't pertinent--well, it was pertinent, though it really wasn't a sensitive input into the condenser design--because you can almost intuitively say, unless you are going to use a very high pressure drop, that an inverted mercury condenser with multiple interfaces will not work. I used that as an example to prove it in numbers.

MR. LYON: I am not sure I understood your last comment. Perhaps that answers my question. You considered, in your drag considerations only one drop and not the influence of an adjacent drop; is that correct?

MR. VILD: That's right. Each drop singly traveling from the tube wall, all the way through the tube without collision.

MR. LYON: There are several cases in the literature, and also some work we have been doing on the movement of particles on the bottom of a horizontal tube, which indicate that there is quite a lot of interaction between adjacent particles, in some cases tending to lump them together in clumps, which might be beneficial in your case by making larger drops.

MR. VILD: Well, I think, as you say, this might happen more with the body force in this direction - with the flow horizontal. Of course, the requirement of transporting the drops at the interfaces, you could do it with a very low velocity if you are not worried too much about hold-up. So it really does help you, because the body force tends to gather the drops at the bottom of the tube, whereas when flowing against gravity this is not true.

MR. KILLACKEY: Does this requirement for 1 gee in any direction still hold for the SNAP-8 condenser or for the Sunflower?

MR. VILD: Well, as well as any requirement holds. The only activity on the program, now, is the rotating unit that has been going for a few thousand hours.

Incidentally, I might mention we did integrate this condenser with a system that employed a rotating unit with a turbine, pump, and alternator on one shaft, and a boiler heat storage component. It ran fairly stably. We had some problems with it, of course. We didn't have a collector. We used an electric heat input for the boiler.

But as far as any requirement exists on the program, it still does; yes.

THE APPLICATION OF ALKALI METAL VAPOR SYSTEMS
TO MHD SPACE POWER GENERATORS*

by

Bernard Hoffman and Frederick Shair

Space Sciences Laboratory
Missile and Space Division
General Electric Company
King of Prussia, Penna.

ABSTRACT

This report describes a theoretical and applied research program directed toward prolonging the lifetime of magnetohydrodynamic (MHD) energy converters by reducing the necessary operating temperatures to the range 1000° - 2000° k. The process of interest is the use of the magnetically induced electric field in the MHD generator for electrical breakdown of appropriate working fluids. Work was directed toward the use of alkali metals for Rankine (vapor) cycles (although the results are applicable to Brayton cycles with certain nuclear reactors) and alkali metal seeded nosle gases for studying the basic parameters of the breakdown.

*The work covered by this report was sponsored by the Aero Propulsion Laboratory of the Air Force Aeronatical Systems Division under Contract AF 33(657)-8298.

1.0 GENERAL INTRODUCTION

As our nation's space program progresses, the electric power requirements for both auxiliary systems and propulsion spacecraft will continually increase. A promising power generation technique for future application to manned-planetary missions demanding hundreds of kilowatts to megawatts of electricity for periods of the order of one year or longer is the direct conversion magnetohydrodynamic (MHD) power generator.

MHD generators do not fit into schemes like the fuel cell, which converts chemical energy directly into electricity, nor thermionic or thermoelectric devices, which convert heat directly into electricity. Rather, the MHD generator serves the combined function of the turbine and alternator in either the conventional Brayton (gas) cycle or Rankine (vapor) cycle system.

The basic concept of MHD power generation can be seen from Figure 1. In this representation, when a conductor passes perpendicularly through a magnetic field of strength B at a velocity v , a voltage will be induced in the conductor orthogonal to the magnetic and velocity vectors. This voltage results from the Lorentz force acting on the free electrons in the conductor; and, if the conductor is any closed configuration (such as a wire loop), a current will flow. Extension of this single conductor model to many conductors repeatedly cutting the magnetic field yields a direct current Faraday generator. Furthermore, it is logical to progress to a conducting fluid conveyed in a duct between the poles of a magnet. In this case, by placing electrodes in the top and bottom duct walls and connecting the electrodes to the external load, a current will flow through the conducting fluid. Basically, then, the MHD generator is a variation of the Faraday generator. The primary difference between them is that in the MHD generator system the working fluid is itself an electrical conductor and forces itself through a magnetic field delivering power directly; while, if the conversion machine is a turbine, the working fluid causes a turbine wheel to move and thereby forces a length of conducting wire through a magnetic field.

For the most part, current development programs leading to mission capability in the tens of kilowatts range utilize the Rankine cycle to convert

nuclear heat to electrical power via conventional turbogenerators. To minimize the radiator area (and, hence, weight of the system) working fluids which condense at high temperatures are indicated. The alkali metals meet this criteria and are attractive working fluids because of their heat-removal properties, thermodynamic properties, and stability in the nuclear and thermal environment. Unfortunately, higher condensing temperatures imply higher maximum cycle temperatures.

Although the basic design technology for turboelectric systems is well established, the use of rotating machinery in high temperature alkali metal systems has the following basic limitations:

- 1) The reduced creep strength of existing construction materials at high temperatures and the deleterious effect of the slight change in dimensions in the turbine inlet limit the growth potential of the turbo-machinery.
- 2) The attack on known alternator winding insulations by the alkali metal working fluid is another serious problem area.
- 3) Since hermetically sealed packages are necessary for space applications, the required liquid metal-lubricated bearings are a challenge.

Since it can be completely non-rotating, the utilization of an MHD generator in place of the turbo-generator eliminates the above three problem areas; and, unlike the turbo-generator system the MHD vapor cycle has growth potential to higher temperatures and powers with a corresponding reduction in specific weight and increase in efficiency.

By utilizing non-thermal ionization techniques, it may be possible to operate the MHD generator under boiling and condensing temperatures almost identical to the turboelectric alkali metal vapor cycle. With the use of a superconducting magnet coil, the weight of a $1 \text{ mw}_{(e)}$ MHD power generator utilizing potassium boiling at 2000°F has been estimated at about 1200 pounds contrasted to an estimated weight of 5300 pounds for a $1 \text{ mw}_{(e)}$ turboelectric rotating package. In addition, the equivalent overall turbogenerator

cycle efficiency of the MHD vapor cycle is estimated to be of the same order as that of the turboelectric rotating package: 13 percent compared to 16 percent.

The MHD package is at the disadvantage for lacking the design experience of a turboelectric system. In comparison to the wire-wound generator, the MHD generator is more complex to analyze because the electrical conductivity and working fluid velocity are variable properties and the plasma is not constrained to move in any precise path. In comparison to the analysis of compressible flow in a duct, the flow in the MHD generator is also more complex because the Lorentz force and ohmic heating vary over a cross-section.

For practical MHD power generation (that is, power densities from 0.1 to 1 kw/cm³) electrical conductivities in excess of 100 mhos/meter are required for generator channels of reasonable length. This may be seen from an approximate momentum equation for a constant velocity MHD generator¹:

$$\frac{dp}{dx} = \vec{j} \times \vec{B} = \sigma (1 - K) u B^2 \quad (1.1)$$

which may be integrated to yield the generator length L:

$$L = \frac{P_1 \left(1 - \frac{P_2}{P_1} \right)}{\sigma (1-K) u B^2} \quad (1.2)$$

where

P_1 = inlet static pressure

P_2 = exit pressure

σ = effective electrical conductivity (assumed constant)

u = gas velocity

B = magnetic field

K = ratio of load voltage to open circuit voltage

From the energy equation, the temperature ratio is given by:

$$\frac{T_2}{T_1} = \left(\frac{P_2}{P_1} \right)^{\frac{K(\gamma - 1)}{\gamma}} \quad (1.3)$$

Since it is desirable to maximize the energy extracted per unit mass of working fluid, given by $C_p (T_1 - T_2)$, the temperature ratio T_2/T_1 should be made as small as possible. For $P_2/P_1 < 1$, this requires K to be close to unity. Selecting $K = 0.8$, $\sigma = 100$ mhos/meter, $P_1 = 1$ atmosphere, $P_2/P_1 \ll 1$, $u = 10^3$ meters/second, and $B = 40$ kilogauss, then

$$L = 0.33 \text{ meters}$$

which is reasonable.

The corresponding power density is

$$\frac{P}{V} = \underline{j} \cdot \underline{E} = \sigma (k) (1-k) n^2 B^2 = 0.26 \text{ kw/cm}^3$$

which falls in the required range.

It is quite evident that the key to achieving good power densities is the electrical conductivity; that is, the higher the conductivity the greater the power density for a given plasma state. As currently envisioned, the working fluid must be contained by ordinary physical walls and, hence, the total temperature of the working fluid cannot exceed about 2000°K (3560°F)*. At the same time, most MHD generator designs indicate the necessity for operation at pressures not too far from atmospheric. With this combination of pressures and temperatures, the working fluid (gas or vapor) would be essentially electrically non-conducting. The reason is simply that at these conditions the working fluid will be essentially unionized; that is, insufficient free electrons will be present in the plasma to carry a current. It is, therefore, apparent that some "non-thermal" path for achieving appreciable ionization of the working fluid must be followed if successful closed-cycle, nuclear-MHD power generation is to be achieved.

*Even with cooled walls, this temperature probably represents an upper limit. Presumably the heat source for such a system will be a nuclear fission reactor and even advanced reactor technology does not envision higher coolant outlet temperatures.

Appreciable non-thermal electrical conductivities in the working fluid under conditions (impurity level, temperature, pressure, selection of working fluid, etc.) that are reasonably compatible with foreseeable reactor technology can be achieved by supplying electrical fields. Of course, from a practical standpoint, the electrical energy used to create the non-thermal condition must be less than the electrical energy generated in the MHD generator. Several methods have been proposed for attaining the non-thermal ionization with less power than is generated: 1) magnetically induced ionization whereby the induced Faraday and Hall electric fields in the MHD generator are used to increase the thermal energy of the working fluid, which should then ionize a constituent of a carrier fluid having a low ionization potential or the working fluid itself; and 2) ionization of the working fluid by particulate or electromagnetic radiation. The first approach is most appealing from the point of simplicity since no external electron guns, beam penetrations, or fixing of irradiation devices along the channel are required. Furthermore, theory indicates that such a system should be feasible.

2.0 MAGNETICALLY INDUCED NON-EQUILIBRIUM IONIZATION

Magnetic field ionization refers to the method whereby the Faraday and Hall electric fields induced by the magnetic field in an MHD generator are used to increase the thermal energy of a gas or vapor. The theoretical basis is that the magnetic field causes the electrons to drift transverse to the flow and subsequent collisions with the heavy particles in the flow increase the electron temperature and decrease the gas temperature.

According to the kinetic theory for electrons, the energy received from the electric field is the scalar product of the electron current and the electric field in coordinates moving with the mass average velocity. In these coordinates, energy fed to the electrons from the electric field E^* is lost to the heavy particles during elastic collisions with them. In an elastic collision, the energy loss is the product of twice the electron to atom mass ratio and the energy difference between the electron and the heavy particle. To convert to a volume basis, this must be multiplied by the electron density and the electron collision frequency. Thus, neglecting net radiation losses and electron-electron collisions, the energy balance for the electrons is:²

$$\vec{j}_e \cdot \vec{E}^* = \sum_{i \neq e} (n_e \nu_{ei}) \left(\frac{2m_e \delta_i}{M_i} \right) \left(\frac{3}{2} k T_e - \frac{3}{2} k T_i \right) \quad (2.1)$$

where

$$\vec{j}_e = \text{electron current} = \frac{\sigma}{1 + \omega_e^2 / \nu_e^2} \vec{E}^* - \frac{\omega_e}{\nu_e} \vec{E}^* \times \vec{B} \quad (\text{assuming } \vec{E}^* \cdot \vec{B} = 0)$$

$$\sigma = \text{scalar electrical conductivity} = n_e e^2 / m_e \nu_e$$

$$\vec{E}^* = \text{moving electric field} = \vec{E} + \vec{u} \times \vec{B}$$

$$\vec{u} = \text{gas velocity}$$

$$\vec{E} = \text{static electric field}$$

$$\vec{B} = \text{magnetic field induction}$$

$$n_e = \text{number density of electrons}$$

$$m_e = \text{electron mass}$$

$$M_i = \text{mass of heavy particle of } i^{\text{th}} \text{ species}$$

$$\omega_e = \text{electron cyclotron frequency} = eB/m_e$$

$$\nu_{ei} = \text{the electron collision frequency with the } i^{\text{th}} \text{ species} = n_i Q_{ei} \langle c \rangle_e$$

$$\langle c \rangle_e = \text{mean thermal electron speed} = \sqrt{8kT_e / \pi m_e}$$

$$\nu_e = \sum_{i \neq e} \nu_{ei}$$

$$k = \text{Boltzmann's constant}$$

$$Q_{ei} = \text{elastic electron - } i^{\text{th}} \text{ particle collision cross section}$$

$$T_e = \text{electron temperature} = \frac{m_e}{3k} \langle c \rangle_e^2$$

$$T_i = \text{temperature of heavy particles of } i^{\text{th}} \text{ species}$$

$$\delta_i = \text{correction factor to account for inelastic collisions with } i^{\text{th}} \text{ species}$$

Since $\vec{j}_e \cdot \vec{E}^*$ is always positive¹, the electron temperature exceeds the gas temperature and if the ionization follows the electron temperature extremely high electrical conductivities may be obtained. To solve Equation 2.1 for the ratio of electron temperature to gas temperature, the relationship between \vec{j}_e and \vec{E}^* (which is dependent on generator geometry and loading) must be specified.

The three basic linear generator configurations having rectangular cross-sections are the continuous electrode, segmented electrode and Hall generator loading configurations (see Figure 2). Comparison of these configurations by Sutton¹ has shown that in a linear generator the segmented electrode geometry yields the highest power density for any given efficiency.

In the segmented electrode arrangement, the current flow is essentially transverse to the gas flow and no net Hall current exists in the downstream direction. With the Hall current equal to zero, an electric field will develop in the axial direction (in the absence of ion slip) according to:

$$E_x = \frac{\omega_e}{\nu_e} (Ey - UB) \quad (2.2)$$

and the current will be

$$j_y = \sigma (ey - UB) \quad (2.3)$$

The open circuit voltage corresponding to $j_x = 0$ is UB . It is common to express the electric field under load as some fraction K of the open circuit field. Thus for the segmented electrode geometry:

$$K = \frac{Ey}{UB} \quad (2.4)$$

where for generation of electrical power, $0 < K < 1$.* Substitution of Equation 2.4 in Equation 2.2 yields

$$E_x = - (1-K) \frac{\omega_e}{\nu_e} UB \quad (2.5)$$

Since

$$E^* = \vec{E} + \vec{U} \times \vec{B} \quad (2.6)$$

$$E_y^* = -(1-K) UB \quad (2.7)$$

$$E_x^* = E_x = - (1-K) \frac{\omega_e}{\nu_e} UB$$

*Note that j_y is always negative for electrical power generation and hence the Lorentz force $\vec{j} \times \vec{B}$ acts in the negative flow direction and tends to retard the flow. On the other hand, if $K > 1$ (corresponding to the electrodes being attached to a voltage source), j_y is positive and the Lorentz force accelerates the flow.

Thus from Equations 2.3 and 2.7

$$j_e \cdot E^* = (1-K)^2 \sigma U_B^2 \quad (2.8)$$

Thus the energy balance equation (2.1) yields the following temperature ratio for the segmented electrode geometry:

$$\frac{T_e}{T_o} = \frac{1 + \frac{\gamma}{3} (\omega \tau)^2 \bar{M}^2 \bar{\delta}^{-1} (1-K)^2}{1 + \frac{1}{2} (\gamma - 1) \bar{M}^2} \quad (2.9)$$

where

T_e = electron temperature

T_o = total temperature = $T_i (1 + \frac{\gamma-1}{2} \bar{M}^2)$

\bar{M} = weighted average Mach Number = u/a

a = speed of sound = $(\frac{\gamma P}{\rho})^{1/2}$

P = pressure = $\sum_i n_i k T_i \approx n k T_o$

n = total number of particles

ρ = mass density = $\sum_i n_i m_i$

γ = ratio of specific heats

τ = average time between electron-ion-electron collisions = ν_e^{-1}

$\bar{\delta}$ = weighted average correction factor¹ =

$$\frac{\sum_{i \neq e} \frac{\chi_i \delta_{ei} Q_{ei}}{m_i} \cdot \sum_{i \neq e} \chi_i m_i}{\sum_{i \neq e} \chi_i Q_{ei}}$$

χ_i = number density of i^{th} heavy particle

Based upon this theory, calculations³ (procedure for which is outlined in reference 4) were carried out to determine the relative performance of MHD generators utilizing magnetically induced non-equilibrium ionization in all the pure alkali metal vapors, in helium seeded with lithium, and in system of hydrogen, argon, and mercury seeded with cesium. The influence of the total temperature, total pressure, Mach number, ionization potential,

atomic weight, elastic electron collision cross-section, and magnetic field strength upon electron temperature, plasma conductivity, and power density were determined. Due to much smaller elastic electron collision cross-sections in hydrogen, helium, argon and mercury, as compared to that of the alkali metals, the electron temperatures, plasma conductivities and power densities are generally higher in the former group as compared to the equivalent systems of the latter group. The loss factor (δ) was taken as unity in all systems except hydrogen, in which case $\delta = 10$.

Typical results for the argon, hydrogen, mercury and helium systems are presented in Table I. A comparison of pure alkali metal vapor systems is presented in Figure 3. For alkali metal vapors, the decrease in ionization potential of the heavier elements (Cesium at 3.87 e.v. contrasted to Lithium at 5.363 e.v.) is greatly overshadowed by the increase in atomic weight and especially by the increase in electron-neutral collision cross-section. Lithium is undesirable because of the high operating temperatures required due to its low vapor pressure. Rubidium and cesium are undesirable because of their high atomic weights and large electron-neutral collision cross-sections. Either potassium or sodium would be acceptable working fluids; however, the amount of equilibrium dimer in the vapor is much greater in sodium than in potassium (see Figure 4). Consequently, potassium appears the best choice among the alkali metals as an MHD working fluid.

Predicted power densities in a potassium vapor MHD generator are displayed in Figure 5. A comparison between the results for equivalent potassium and seeded inert gas systems strikingly displays the higher magnetic field requirements of the pure vapor system; however, at magnetic field intensities and total temperatures which are currently attainable, power densities in the range 0.1 to 1.0 kw/cm³ can still be realized by drastically reducing the total pressure (see Figure 6).

TABLE I

<u>SYSTEM</u>	<u>TOTAL TEMPERATURE</u>	<u>TOTAL PRESSURE</u>	<u>MACH NUMBER</u>	<u>MOLE FRACTION OF SEED</u>	<u>MAGNETIC FIELD</u>	<u>POWER DENSITY</u>
ARGON-CESIUM	1600°K	50 psia 20 psia	0.6	5×10^{-4}	20,000 gauss	0.5 kw/cm ³ 1.0 kw/cm ³
HYDROGEN-CESIUM	2000°K	20 psia	1.5 0.8	10^{-4}	19,000 gauss	1.0 kw/cm ³ 1.0 kw/cm ³
MERCURY-CESIUM	2000°K	20 psia	1.5	10^{-4}	41,000 gauss	1.0 kw/cm ³
HELIUM-LITHIUM	1000°K	20 psia	0.6 1.0 1.5	5×10^{-3}	42,000 gauss 23,000 gauss 13,500 gauss	1.0 kw/cm ³

3.0 EXPERIMENTAL PROGRAM

While theoretical analysis indicated that low temperature conductivity could be achieved via magnetically induced ionization, the phenomenon remained to be experimentally verified. Since the possibility of obtaining a highly conducting plasma at low temperatures would lead to highly efficient and compact MHD generators for space power applications, a theoretical and applied research program was undertaken in this area of non-equilibrium ionization of plasmas in the temperature range 1000°K to 2000°K .

In the following sections, several items of work being carried out under the program are described: seeded inert gas system (M-4), short term potassium vapor blowdown studies (M-5), and a closed cycle potassium system (M-6).

The M-4 MHD Generator

Although the superiority of the Rankine (vapor) cycle over the Brayton (gas) cycle for MHD space power generation can be demonstrated as the basis of relative radiator weights (see reference 5 for a detailed analysis of various MHD power cycles), the alkali metal-seeded noble gas system is being used for basic research purposes.

The M-4 MHD generator is powered by a high pressure manifold containing twenty-two argon gas cylinders. Test times, with argon flow rates near 0.15 pounds per second, run near 60 minutes. The basic equipment is shown in Figures 7 and 8.

The argon flow, monitored by means of a rotameter, is heated to temperatures around 1200°K by means of a molybdenum mesh heater suspended by a molybdenum coil which is tightly packed into dense alumina tubes through which the argon is forced to flow. This design provides approximately six times the heat transfer area per unit length and twice the heat transfer coefficient as compared to a conventional resistance heater. Furthermore, the design has avoided thermal shock damage during heater start-up. Power input to the heater is accurately controlled by means of a saturable core reactor feeding a step-down transformer giving low-voltage, high current power to the heater.

After the gas leaves the heater, it passes into a plenum where cesium is injected by a motor-driven syringe (see Figure 9). All cesium lines are heat traced to prevent cesium solidification. The dry box is under continuous argon purge. The seeded gas passes from the plenum chamber through a molybdenum screen to a nozzle for isentropic expansion into the MHD channel. The test section is formed from 99.7% alumina blocks contained in a rectangular cross-section stainless steel shroud.

A typical segmented electrode MHD test section is shown in Figure 10. In this particular test section, grooves were cut perpendicular to a 1 x 3 cm constant area channel. The electrode probes are positioned in these grooves and brought out of the channel shroud through Conax pressure glands. Three electrodes are instrumented with Pt/Pt- 10% Rh thermocouples for measurement of the temperature at the surface of the cathodes. Ten mil thick tungsten, molybdenum, tantalum and molybdenum-rhenium electrodes have been spot welded to the electrode probes.

In Figure 10, three groups of electrodes can be distinguished; the first four electrodes can be used to pass high voltage currents through the plasma immediately prior to entering the magnetic field region; the next seventeen electrodes are the power electrodes within the magnetic field region; and the last four electrodes are available for low voltage current input in order to measure de-ionization rates downstream of the magnetic field region.

The magnet provides a 2-inch gap between 6" x 13" pole faces in which the test section is suspended. The copper core magnet is water cooled and will operate continuously at a field strength of 25 kilogauss.

Current experiments include parametric studies of magnetically induced non-equilibrium ionization and determination of ionization and de-ionization rates. Future experiments will incorporate an electron beam in conjunction with metastable gas mixtures to increase the electron temperature above that of the neutral particles.

The M-5 MHD Generator

To demonstrate magnetically induced non-equilibrium ionization in alkali metal vapors, a potassium vapor blowdown experiment was conceived. Based on the theoretical MHD generator calculations presented in reference 4, magnetically induced non-equilibrium ionization should be detectable in a potassium vapor system at a total gas pressure of 10 psia and a total gas temperature of 800°C at a Mach Number of only 0.5 in the generator channel. With such operating parameters in mind, the following criteria were applied to the design of a blowdown experiment:

- (a) The vapor temperature must not fall below the potassium vapor pressure line during expansion into the generator channel in order to prevent agglomeration or condensation of potassium in the generator.
- (b) From the standpoint of materials availability and ease of fabrication, the blowdown tank would be fabricated from 316 stainless steel. This would limit the maximum operating temperature to somewhat below 900°C .
- (c) Without continuous injection of potassium into the heater tank, the upstream temperature and pressure of the potassium vapor will continuously decrease with duration of blowdown; therefore, the volume of the blowdown tank should be sufficiently large to maintain relatively constant upstream conditions for several seconds.
- (d) To enhance the safety aspects of the operation, the total potassium change should be small.

A system characterized by the operating line shown on Figure 11 meets these requirements. If 37.5 grams of potassium are introduced into an evacuated 4 ft^3 vessel and heated, the pressure-temperature operating line will follow the vapor pressure line until the last of the potassium is vaporized.

As the temperature is further increased to superheat the vapor to 900°C , the operating line follows the ideal gas line until a pressure of 517 mm Hg (10 psia) is reached. An isentropic expansion of the vapor through a Mach 0.5 nozzle will reduce the pressure and temperature to 8.19 psia and 810°C , respectively. As can be seen from Figure 11, the vapor temperature after expansion is still about 100°C above the vapor pressure line; consequently, no agglomeration or condensation will occur at the entrance to the MHD channel. Furthermore, assuming the potassium to be an ideal gas undergoing an adiabatic-isentropic expansion, it can be shown that during the initial 1/2-second blowdown period the total pressure has dropped to about 80% of its initial value and still exceeds the vapor pressure.

A system capable of achieving the indicated operating conditions and meeting the functional requirements of the experiment was designed on the basis of simplicity, high reliability of operation and use of the best readily available materials of construction. The system consists essentially of a heated blowdown tank, a thimble incorporating the nozzle-MHD generator channel assembly and a condenser arranged as shown in Figures 12 and 13.

The thimble arrangement (Figure 14) consists of two sub-assemblies: The nozzle section and the MHD channel section. The nozzle section combines a pipe-to-nozzle transition joint and a nozzle housing in a single stainless steel unit. The design of the nozzle housing permits adjustment of flow characteristics (developed Mach Number) by simple replacement of inserts. The sub-assembly is coupled to the blow-down line and the MHD channel section by flanges. The MHD channel assembly consists of a high density alumina generator channel blocks (Figure 15) arranged within a square cross-section stainless steel shroud. This sub-assembly is flanged for coupling to the nozzle section and the condenser section.

Although the M-5 facility, unlike the M-4 Experiment, has not yet attained operational status, a more complex alkali metal vapor facility has already been designed and fabrication will be started in the very near future.

The M-6 MHD Generator

To demonstrate continuous Rankine cycle magneto-hydrodynamic power generators utilizing non-equilibrium ionization, a prototype closed-cycle alkali metal vapor system has been designed. The design of the facility emphasizes long life, reliability and flexibility of the prototype. Fabrication will carry out these design criteria using the best available materials and techniques for construction under strict quality control. Operation and evaluation of the system will be directed towards the development of high power Rankine cycle MHD power generators for space application.

The operating lines superimposed on the temperature-entropy diagram shown in Figure 16 depict the alkali metal vapor cycle. From this diagram it is readily seen that inappropriate selection of the vaporization pressure (line 2-3-4-5 is an isobar) in combination with expansion to too high a Mach Number (line 5-6) can result in an MHD generator condition (point 6) lying below the potassium vapor pressure line. To determine the possible operating limits, screening calculations of anticipated MHD generator performance were prepared. For example, a vaporizing 1 gram/sec of potassium at 0.5 psia, superheating of the vapor to 2500°R and isentropic expansion to Mach 1.7, the MHD channel pressure will drop to 0.09 psia which is above the condensation pressure. At these conditions, a plasma conductivity of 380 mhos/meter could be achieved in a magnetic field of about 12 kilogauss and the resultant power density, $W(1-K)/K$, would be approximately 0.2 KW/cm³. On the other hand, on vaporizing 15 grams/sec at 6.1 psia, superheating to 2500°R and expansion at $M = 1.5$, the static pressure will drop to 1.5 psia (incipient condensation). At these conditions (and assuming that the vapor does not actually condense), a plasma conductivity of 35 mhos/meter could be achieved in a magnetic field of about 30 kilogauss. The resultant power density would be about 0.1 KW/cm³. Operation at higher vaporization pressures or higher Mach Numbers (or combinations of the two) would certainly result in vapor condensation. Since the operation of a wet potassium vapor generator is not a priori in conflict with the

magnetically induced non-equilibrium ionization, an experimental system capable of operating in either dry or wet regimes was designed while a theoretical study of the effect of wet potassium vapor (droplets) on non-equilibrium electron heating (and, generator performance) was undertaken.

The M-6 facility will be capable of generating as much as 2 pounds/minute of saturated potassium vapor at temperatures ranging from approximately 1200°R to 2000°R (0.1 to 29 psia). After superheating to a maximum of 2500°R , the vapor will be expanded through a nozzle to attain supersonic velocities at the entrance to the MHD generator. The vapor discharge from the generator channel will be de-superheated and condensed in nitrogen and air-cooled units, respectively, and the condensate returned to the boiler by means of an electromagnetic pump. Auxiliary systems include a by-pass purification system capable of 10 loop volume throughputs per hour, a potassium transfer system, and vacuum and cover gas systems. The system is fully instrumented for both steady-state and transient operation with minimum operator coverage. A flow and instrumentated schematic is presented in Figure 17.

To date, detailed construction drawings covering all system components have been prepared. The system will be arranged as shown in Figure 18 and positioned in a vapor container 10' x 16' x 8' (not shown). Electric power diagrams and instrumentation, alarm and control wiring schematics have already been prepared. Installation of this facility is scheduled to begin on or about October 1, 1963.

REFERENCES

1. Sutton, G. W., "The Theory of Magnetohydrodynamic Power Generation," G.E. Report R62SD990, December 1962.
2. Hurwitz, Jr., H., Sutton, G. W., and Tamor, S., "Electron Heating in Magnetohydrodynamic Power Generators," ARS Journal, August 1962.
3. Shair, F. H., "Theoretical Performance of MHD Generators Utilizing Magnetically Induced Non-Equilibrium Ionization in Pure Alkali Metal Vapors and in Seeded Gas Systems Presentation at 4th Symposium on the Engineering Aspects of Magnetohydrodynamics, Berkeley, Calif., April 1963.
4. Shair, F. H., and Cristinzio, F., "Theoretical Performance for MHD Generators Utilizing Non-Equilibrium Ionization in Pure Alkali Metal Vapor Systems" G.E. Report R62SD94, January 1963.
5. Freedman, S. I., "Thermodynamic Consideration for MHD Space Power Systems," G.E. Report R62SD83, September 1962.

SCHEMATIC DIAGRAM-FARADAY GENERATOR

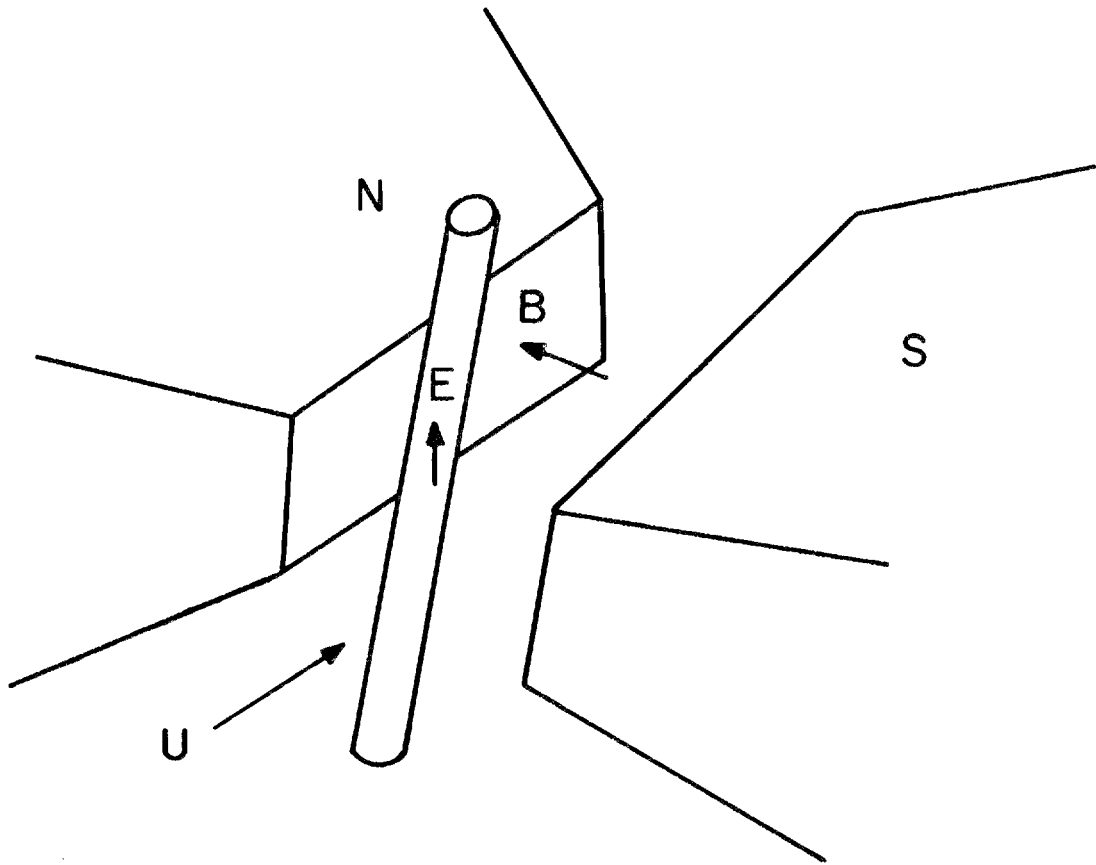
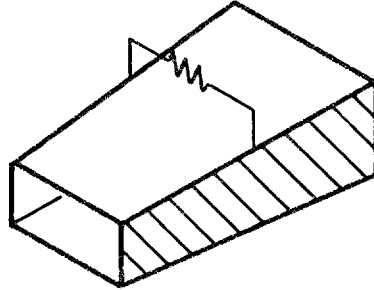
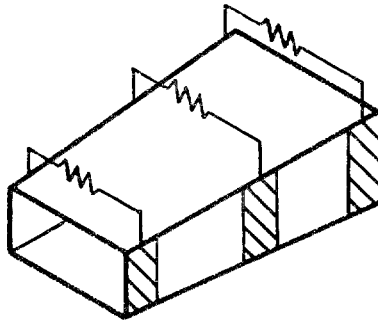


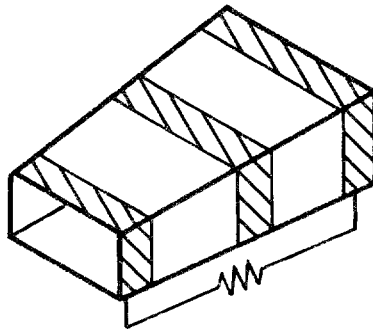
Figure 1



CONTINUOUS ELECTRODES



SEGMENTED ELECTRODES



HALL GENERATOR

Figure 2. Linear Generator Geometries Having Rectangular Cross Sections

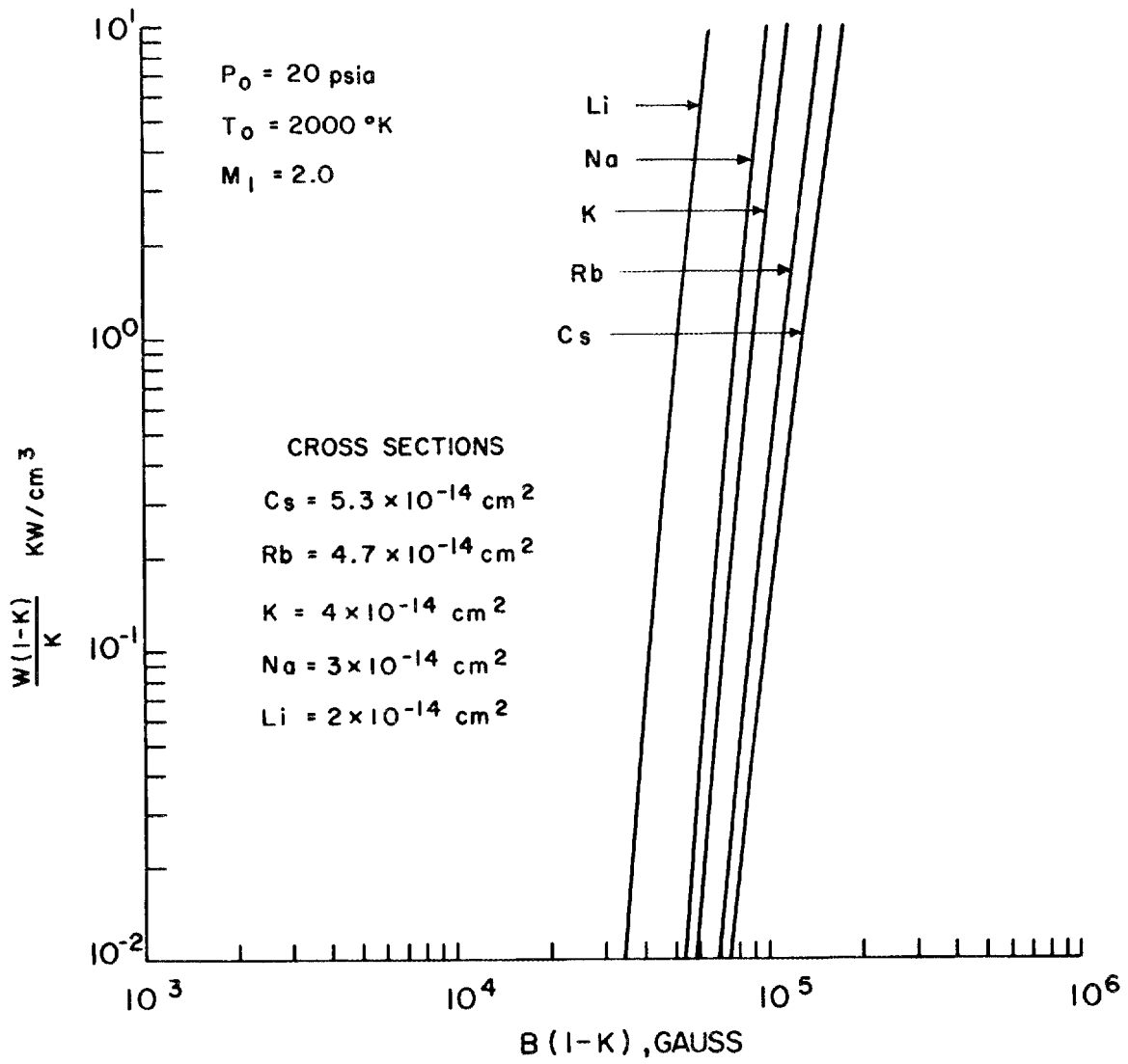


Figure 3. Comparison of Power Densities for Pure Alkali Metal Vapor Systems

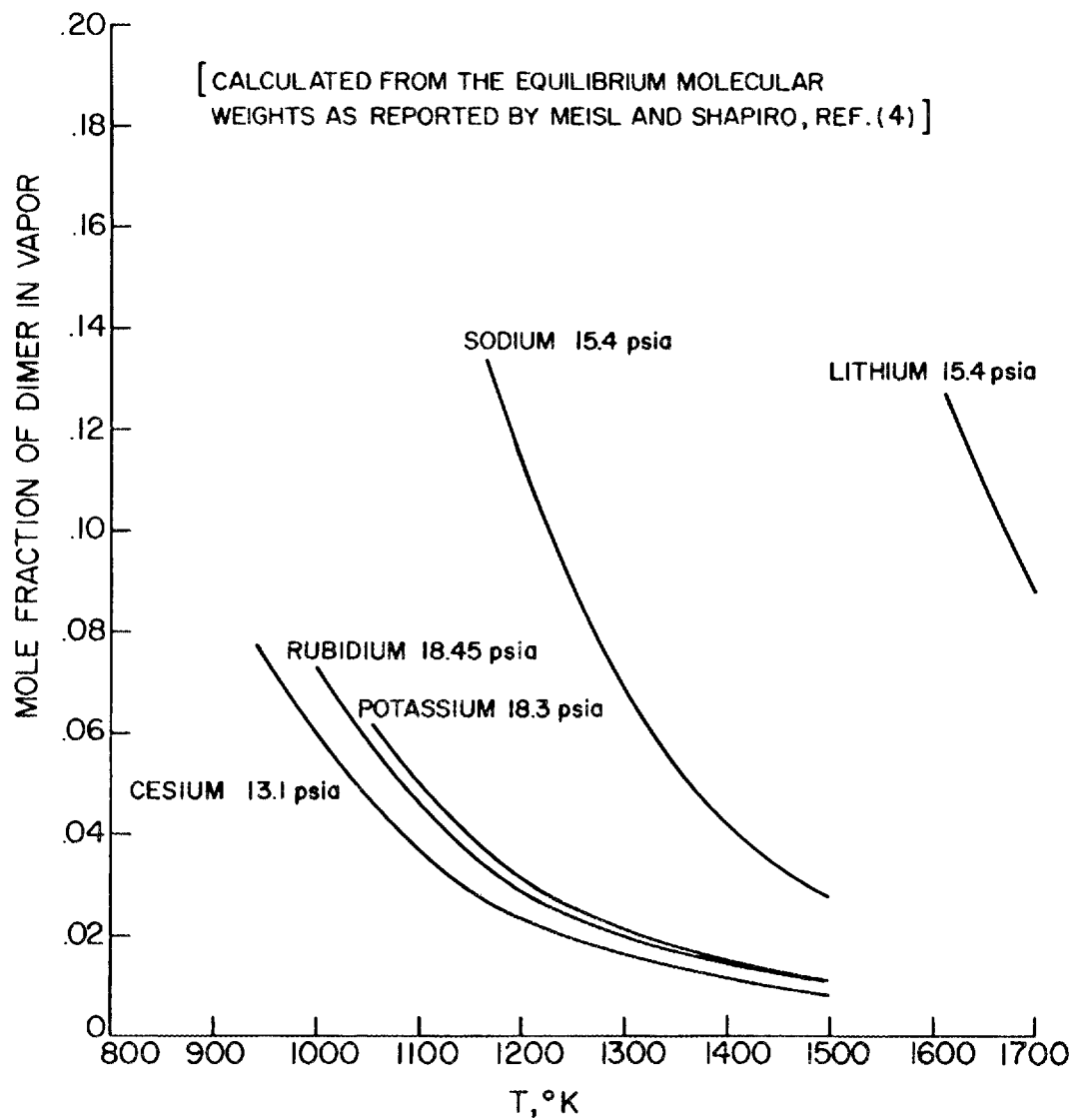


Figure 4. Equilibrium Dimer Concentration in Pure Alkali Metal Vapors Near Atmospheric Pressure

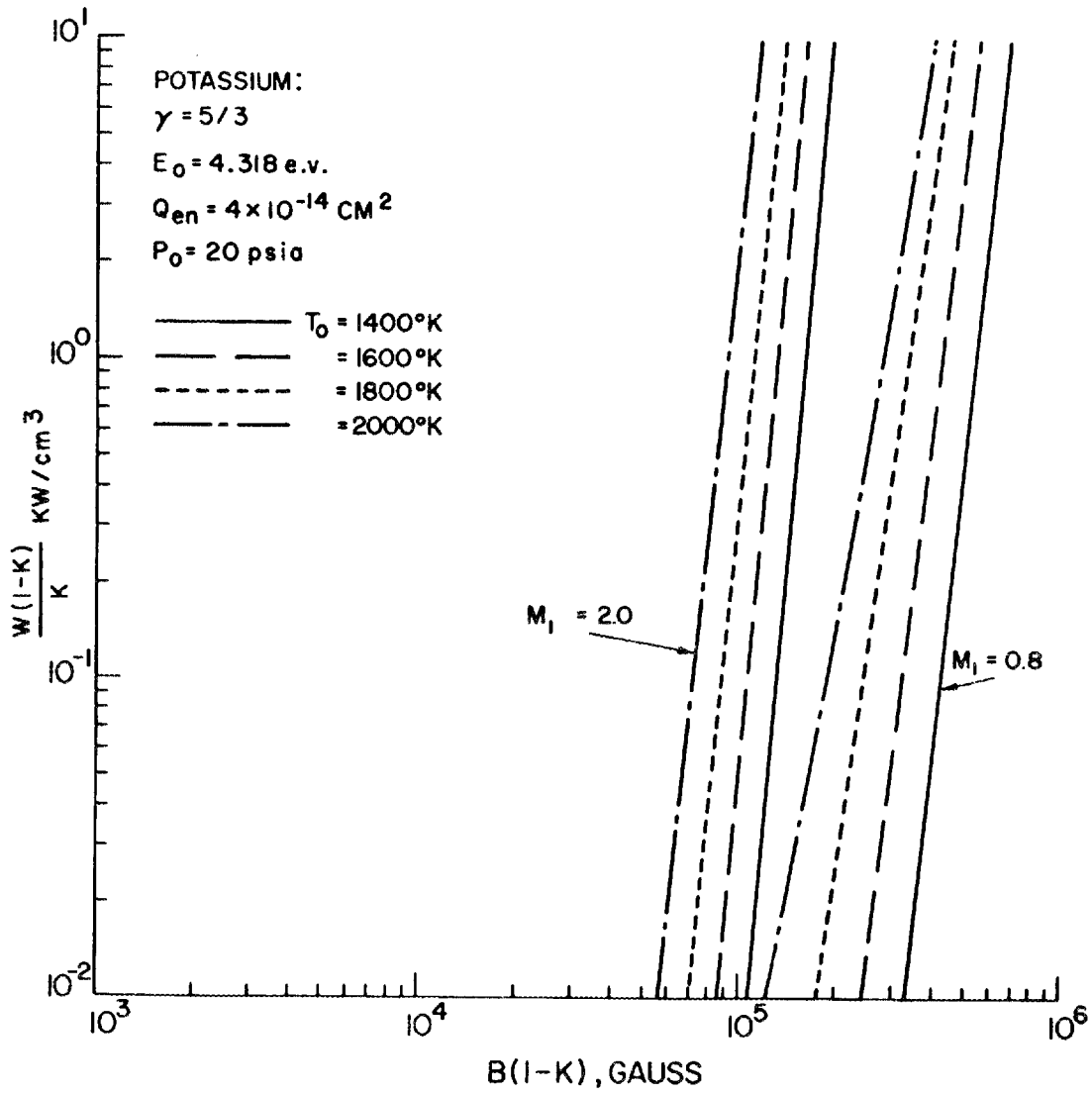


Figure 5. Power Density for Potassium Vapor, $Q_{en} = 4 \times 10^{-14} \text{ cm}^2$

POWER DENSITY FOR POTASSIUM VAPOR

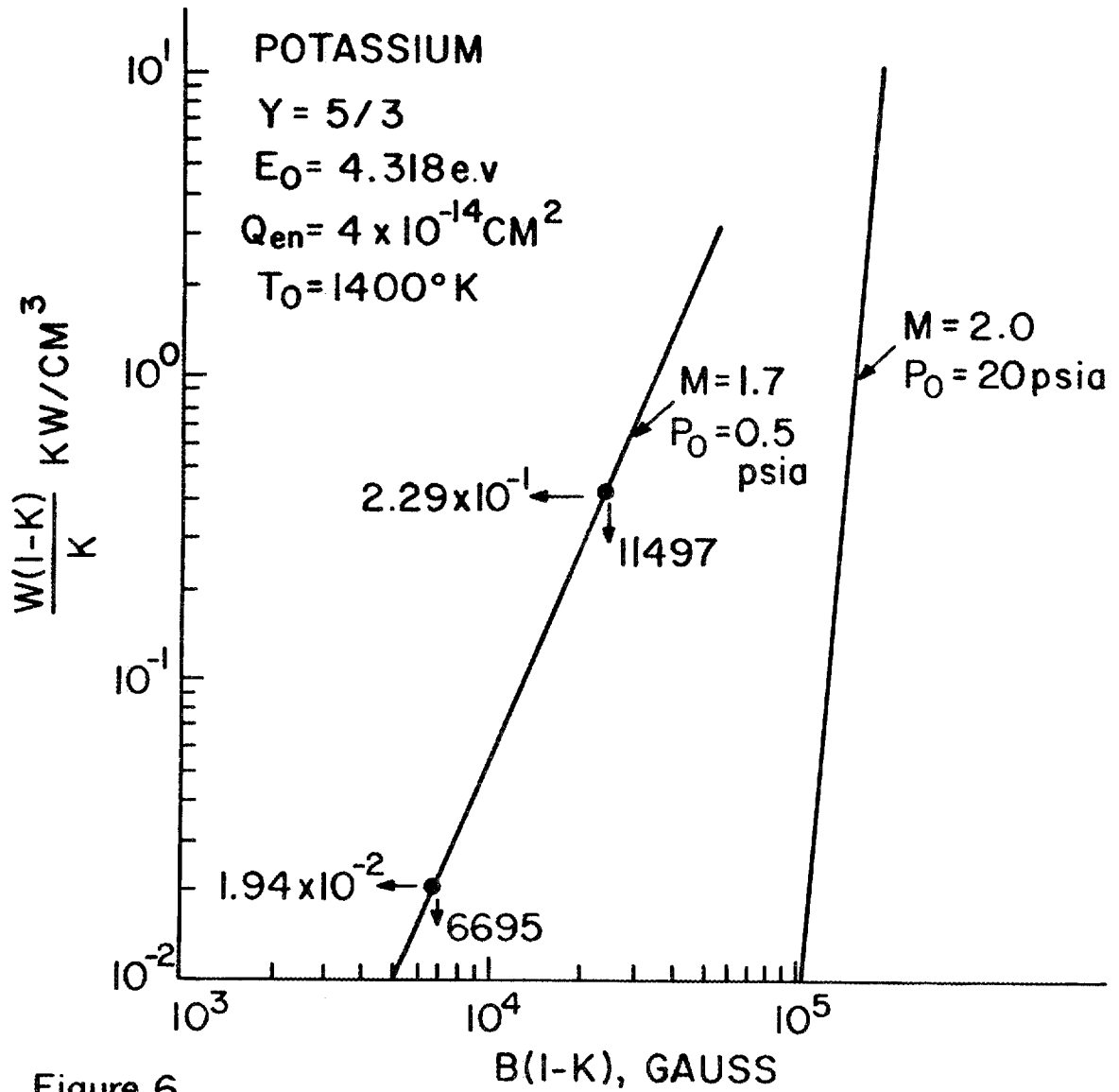


Figure 6

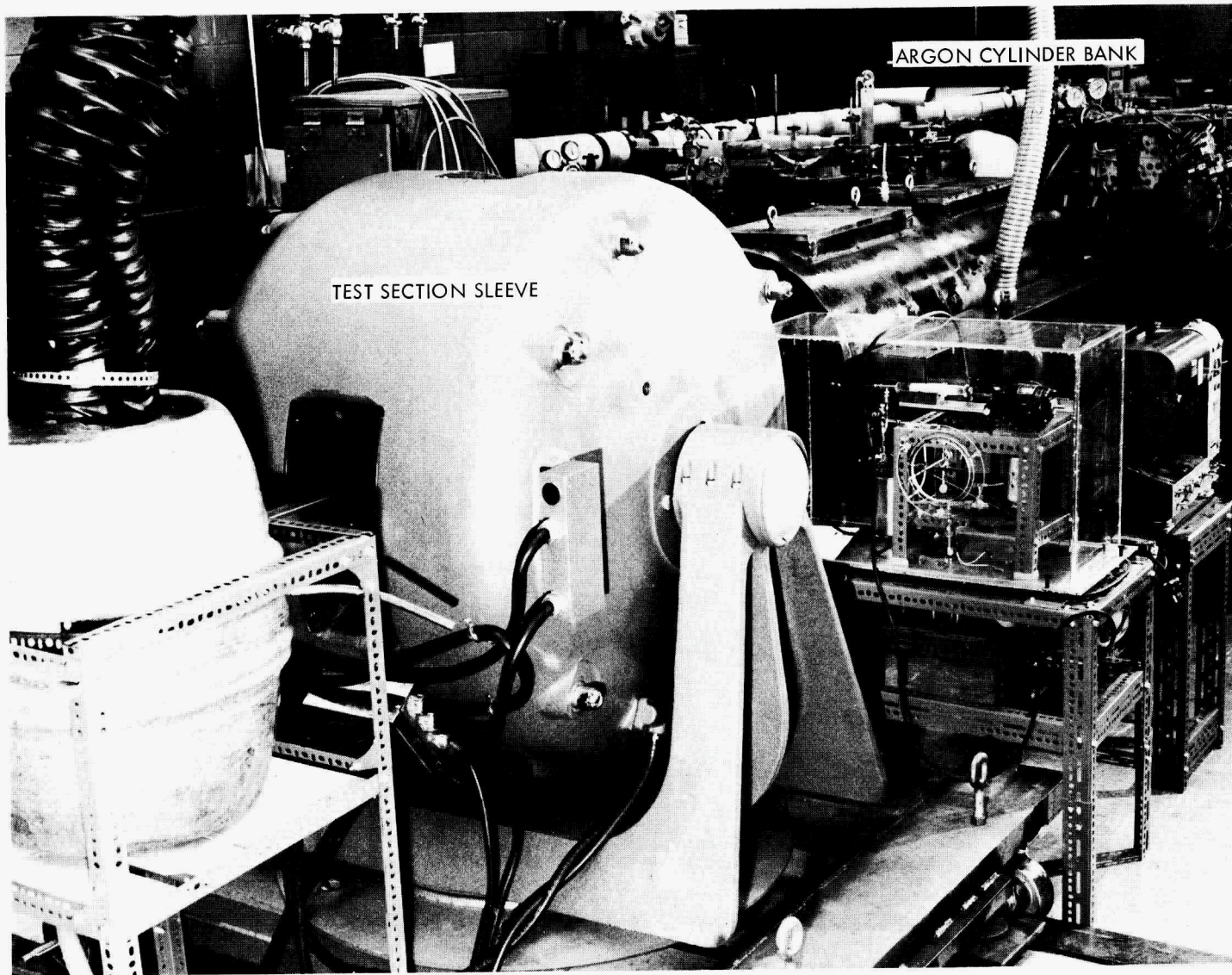


Figure 7

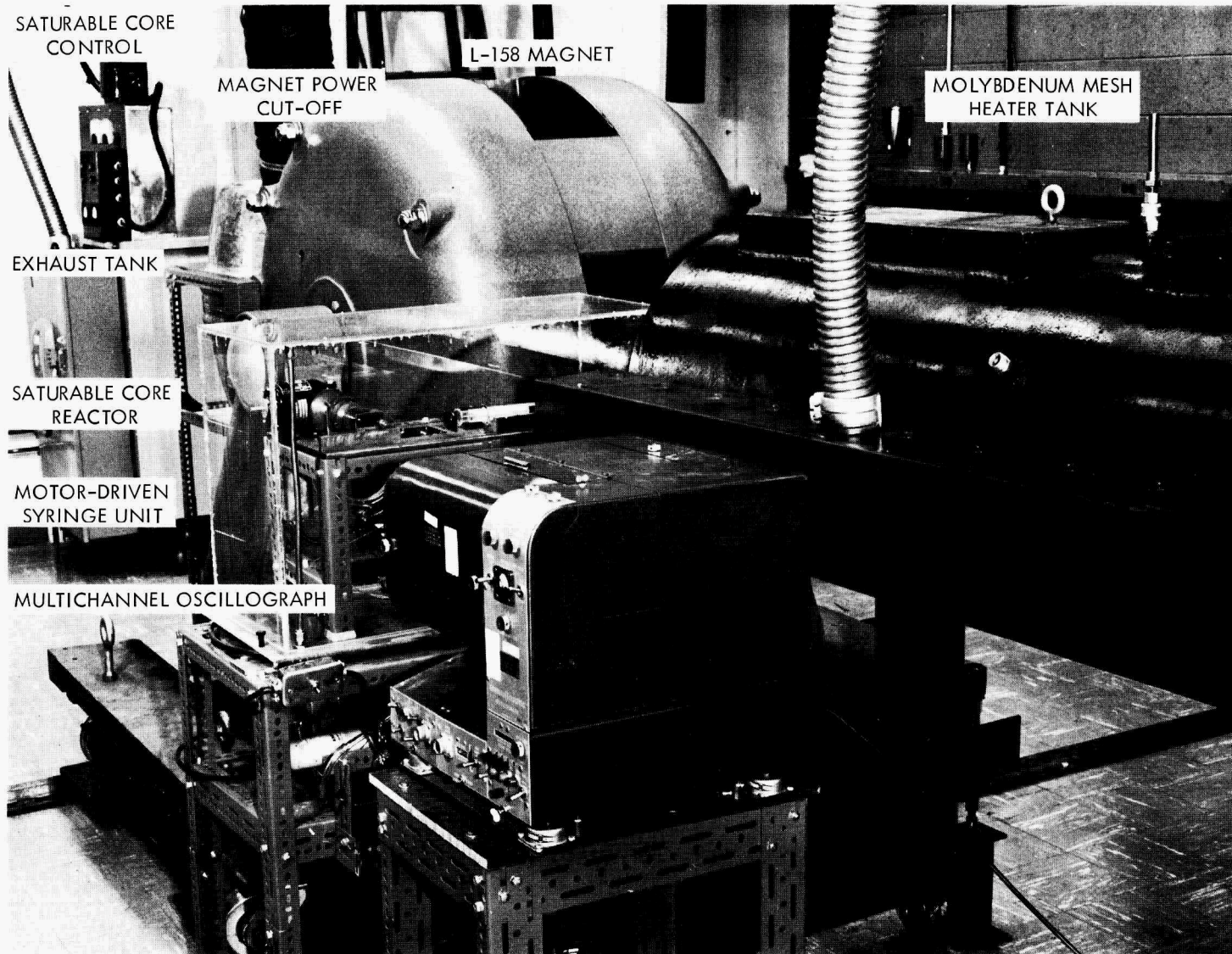


Figure 8

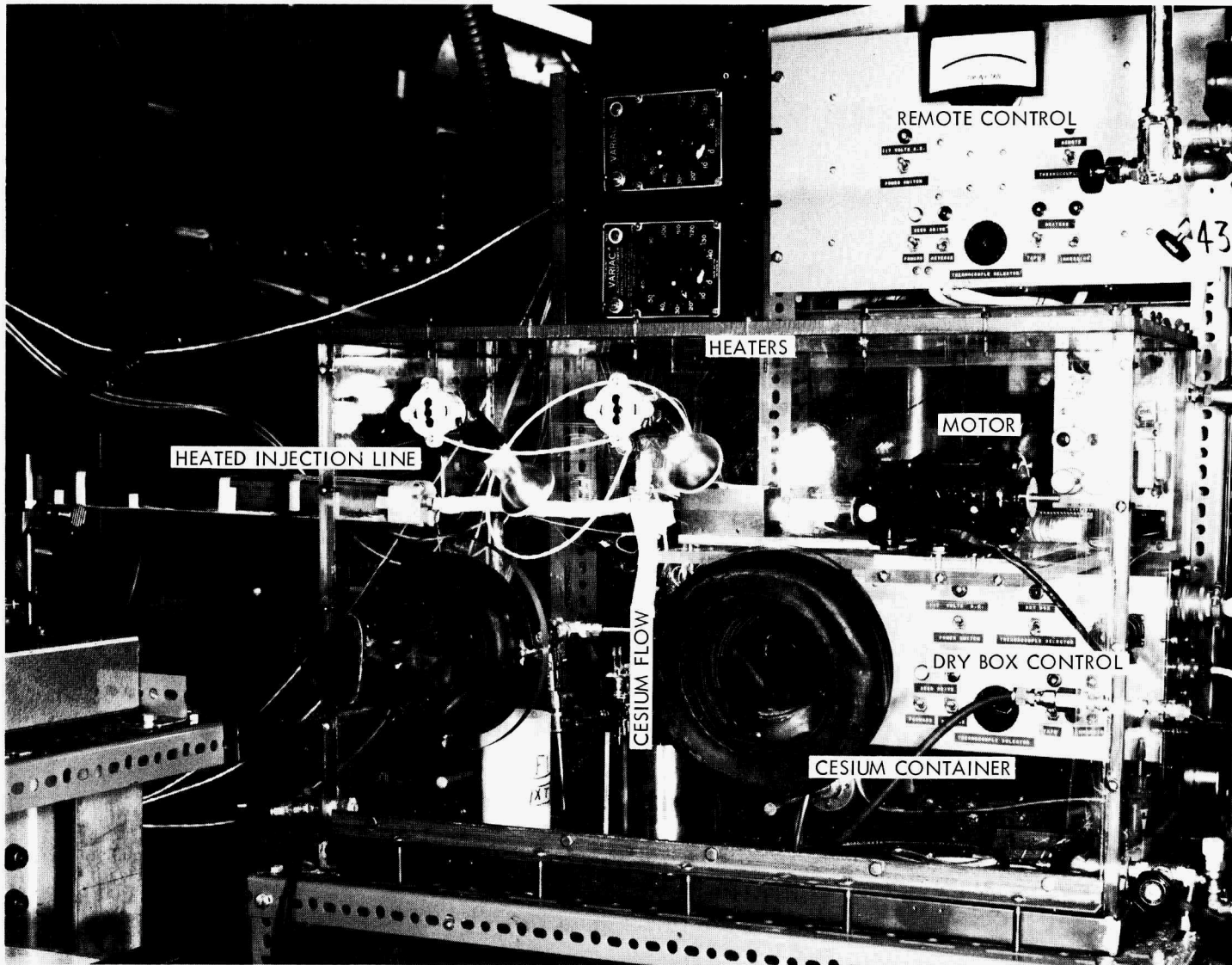


Figure 9

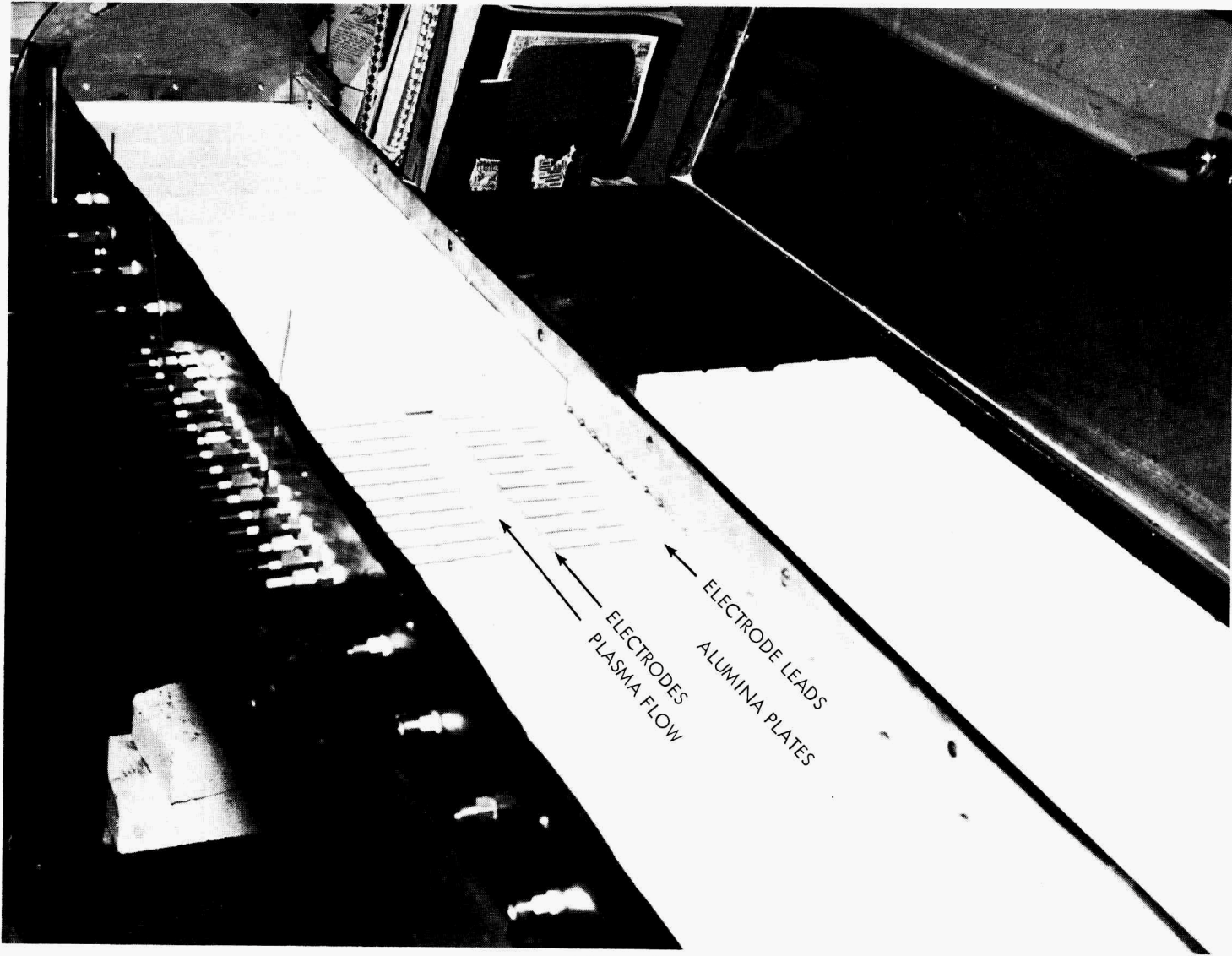
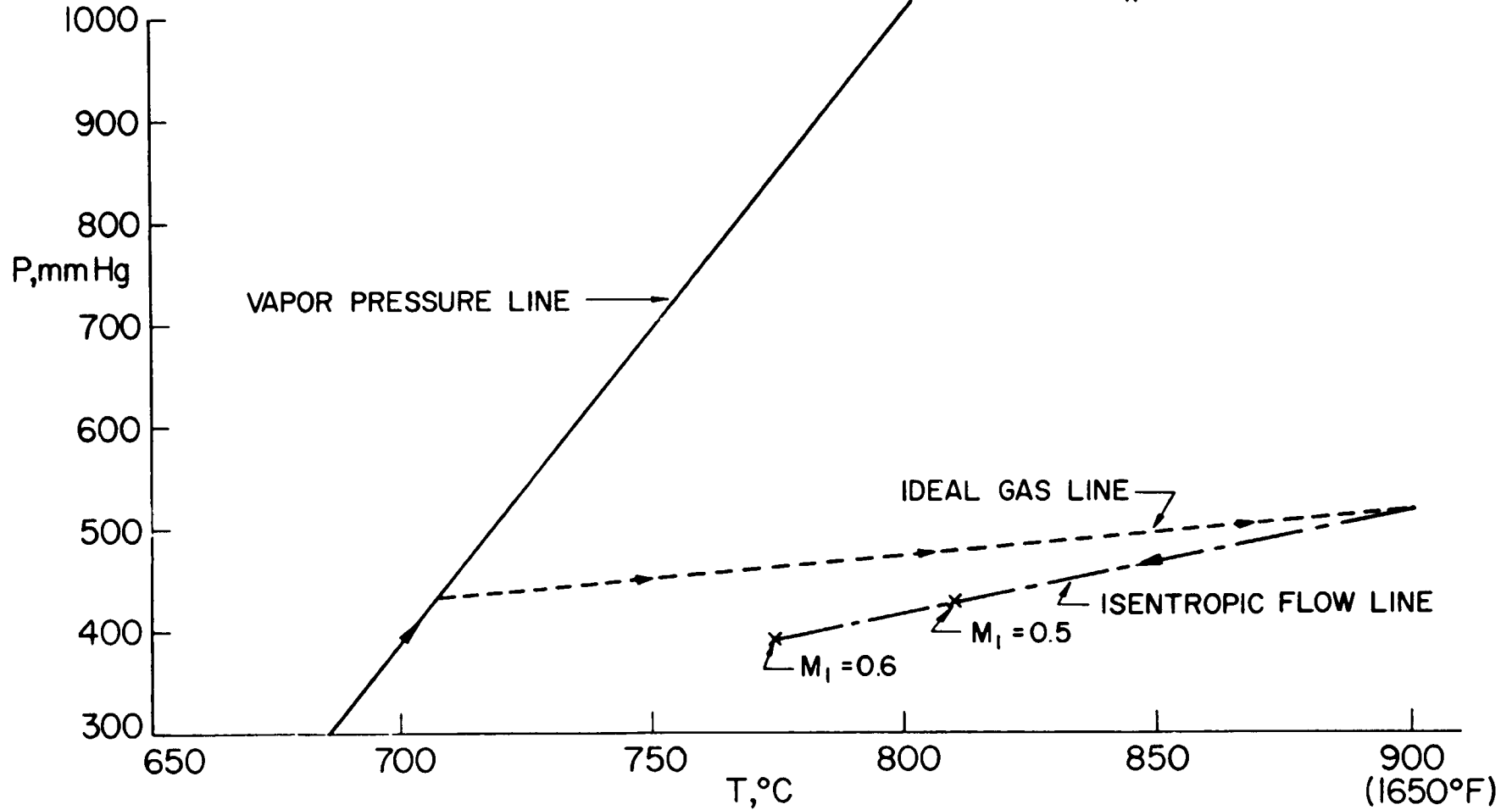


Figure 10

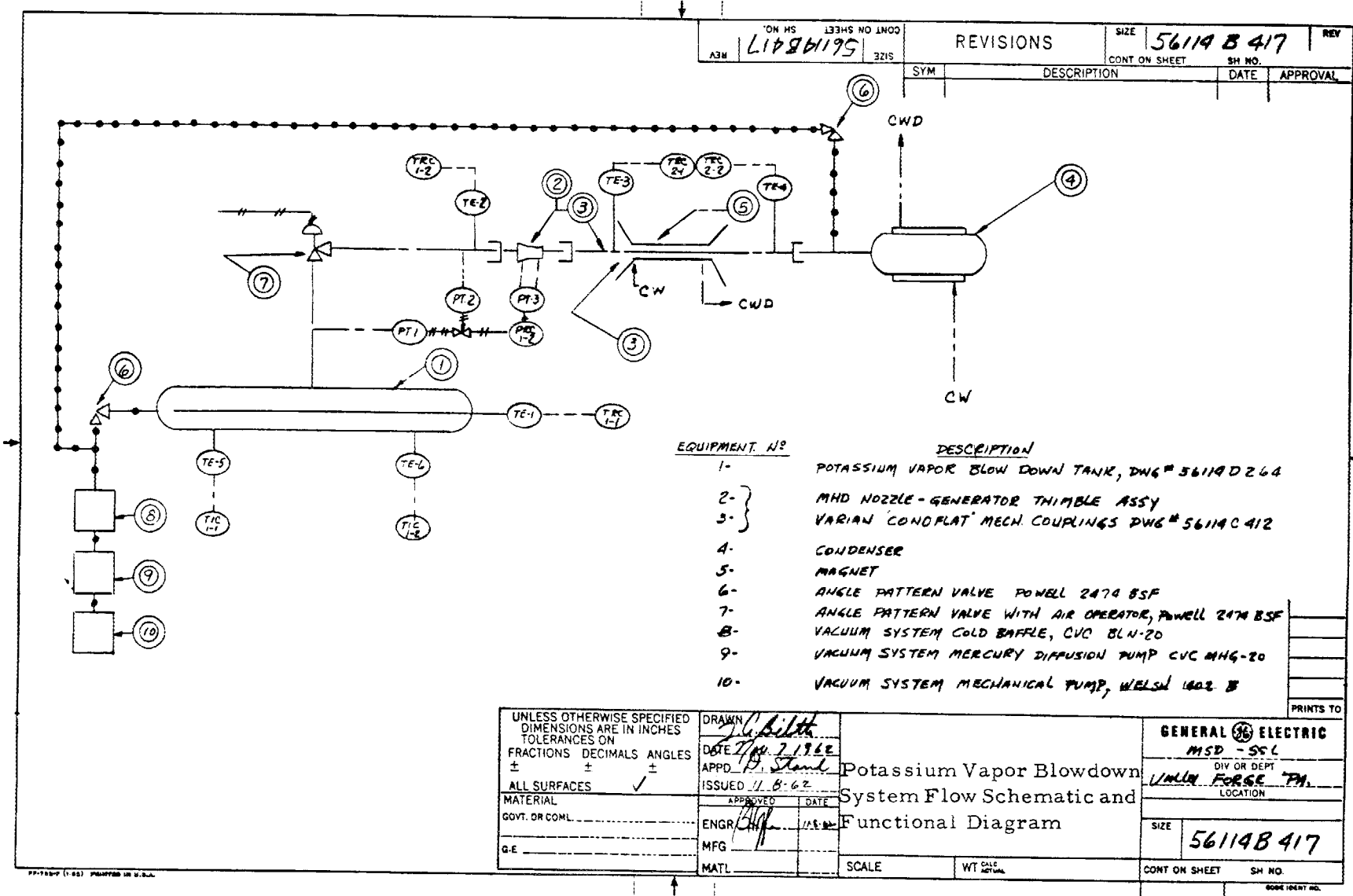
OPERATING LINE FOR MHD POTASSIUM EXPERIMENT

VOL. = 33 GALLONS
 $n = 37.5$ GRAMS



344

Figure 11. Operating Line for MHD Potassium Experiment



REV	56114B417	SIZE	56114B417	CONT ON SHEET	SH NO.
REVISIONS	SYM		DESCRIPTION	DATE	APPROVAL

EQUIPMENT. NO	DESCRIPTION
1-	POTASSIUM VAPOR BLOW DOWN TANK, DWG # 56114D264
2- }	MHD NOZZLE-GENERATOR THIMBLE ASSY
3- }	VARIAN CONOFLAT MECH. COUPLINGS DWG # 56114C412
4-	CONDENSER
5-	MAGNET
6-	ANGLE PATTERN VALVE POWELL 2474 BSF
7-	ANGLE PATTERN VALVE WITH AIR OPERATOR, POWELL 2474 BSF
8-	VACUUM SYSTEM COLD Baffle, CVC BLN-20
9-	VACUUM SYSTEM MERCURY DIFFUSION PUMP CVC MHG-20
10-	VACUUM SYSTEM MECHANICAL PUMP, WELSH 1602 B

UNLESS OTHERWISE SPECIFIED DIMENSIONS ARE IN INCHES TOLERANCES ON FRACTIONS DECIMALS ANGLES \pm \pm \pm ALL SURFACES \checkmark MATERIAL _____ GOVT. OR COM. _____ G.E. _____	DRAWN <i>J. G. Belitt</i> DATE <i>2/19/62</i> APPD. <i>B. Stand</i> ISSUED <i>1.8.62</i>	Potassium Vapor Blowdown System Flow Schematic and Functional Diagram	GENERAL ELECTRIC MSD - SCL DIV OR DEPT VACUUM FORGE PA. LOCATION
	APPROVED _____ DATE _____ ENGR. <i>[Signature]</i> DATE _____ MFG _____ MATL _____		SCALE _____ WT. CHG. _____ CONT ON SHEET SH NO.
	SIZE 56114B417		PRINTS TO
	GORE IDENT. NO.		

Figure 12

345

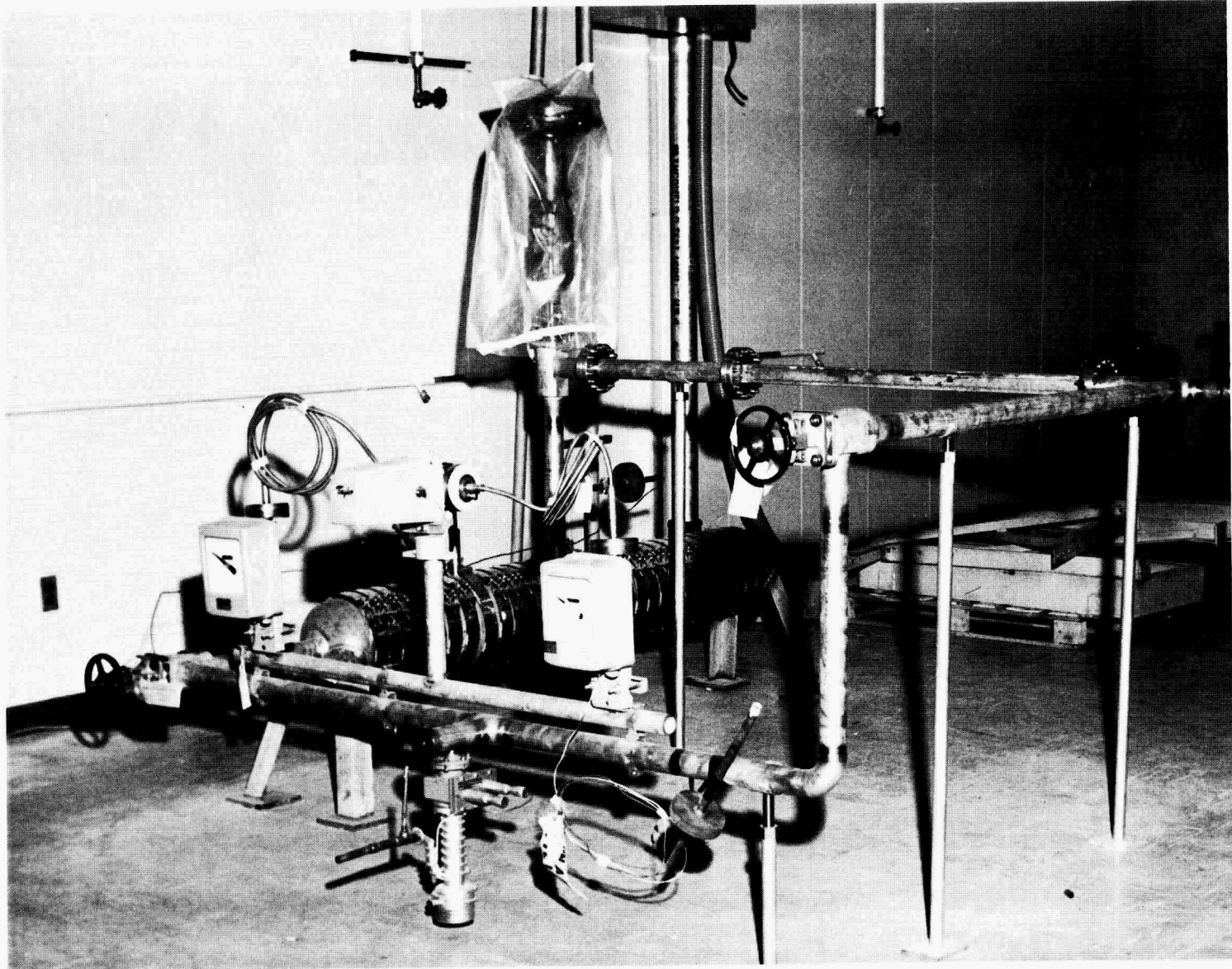
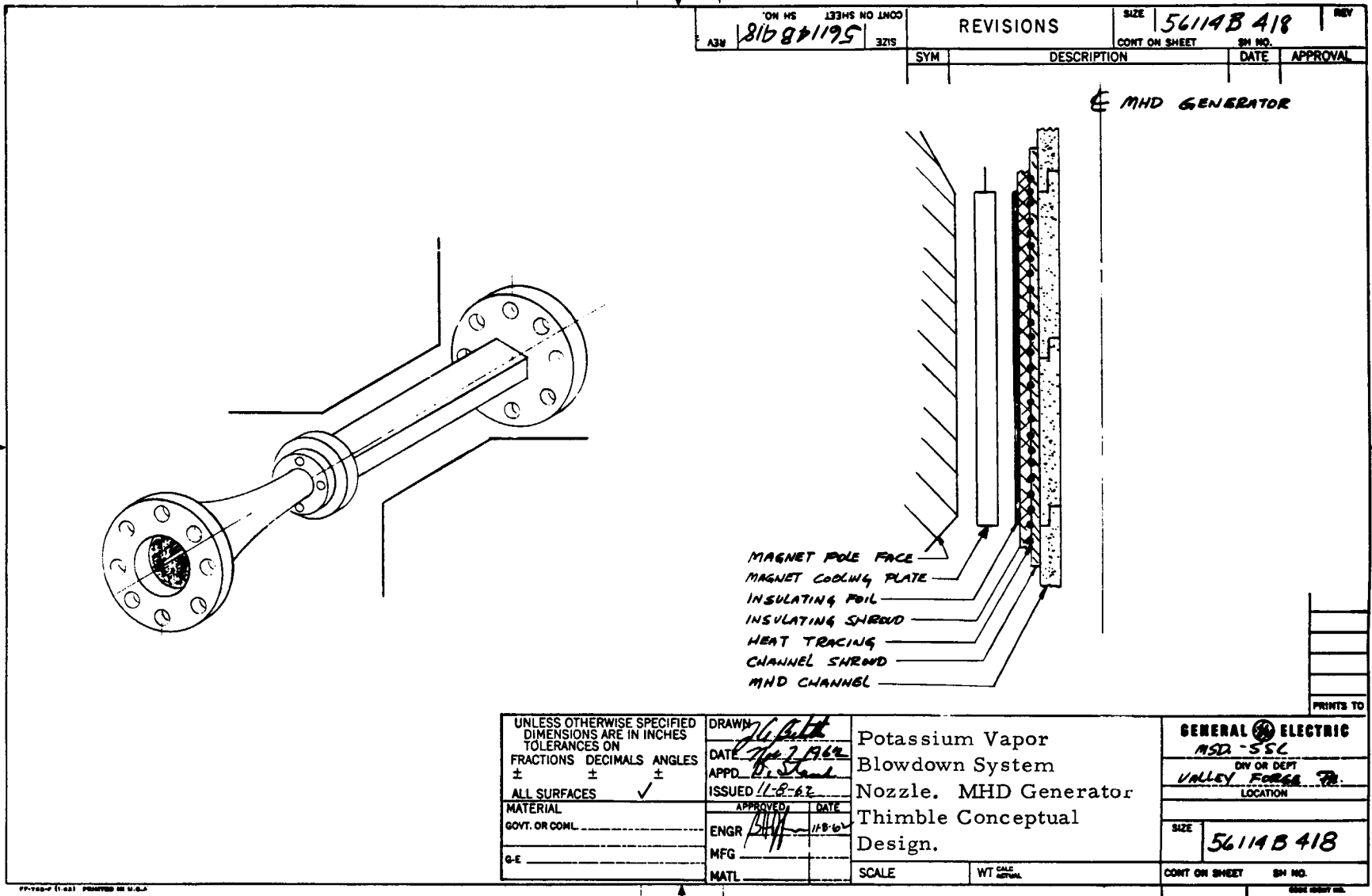


Figure 13.



347

Figure 14

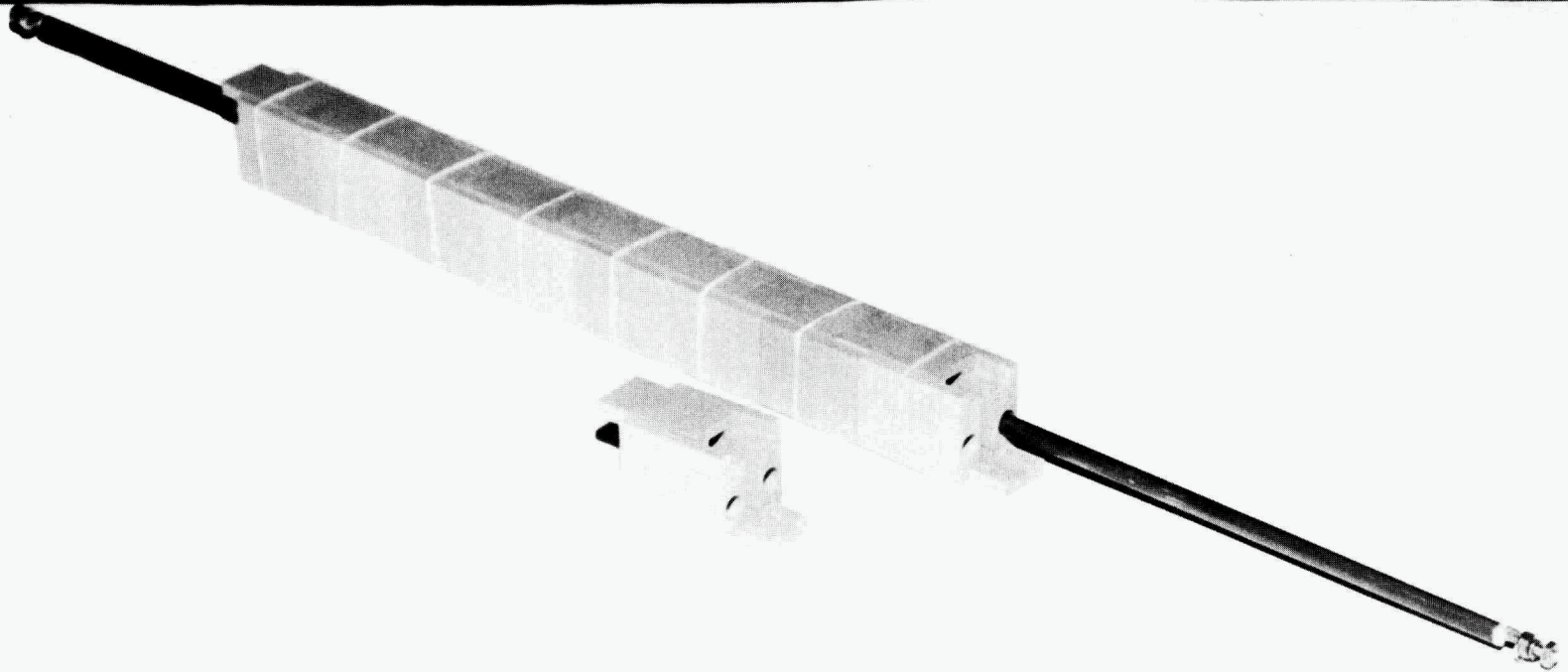
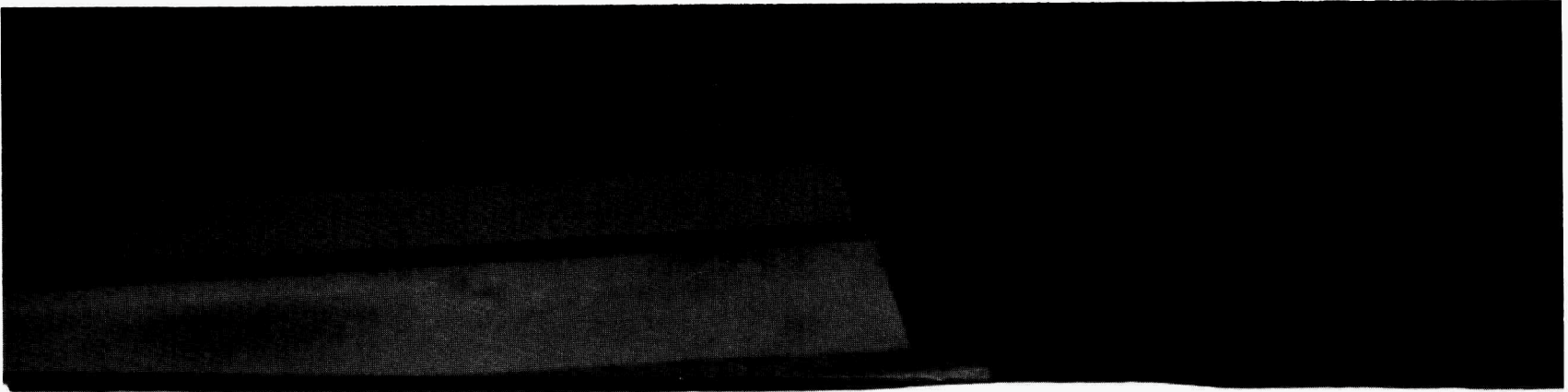
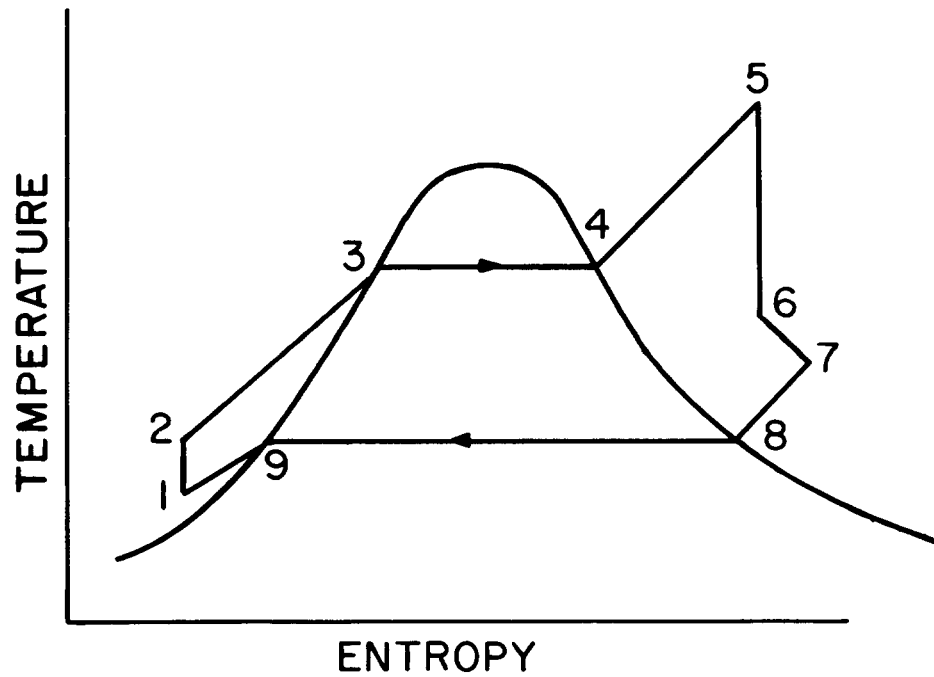


Figure 15



ALKALI METAL VAPOR LOOP-RANKINE CYCLE

- 1-2 : PUMP
- 2-3 : HEATER
- 3-4 : BOILER
- 4-5 : SUPERHEATER
- 5-6 : ISENTROPIC EXPANSION
- 6-7 : GENERATOR
- 7-8 : DE-SUPERHEATER
- 8-9 : CONDENSER
- 9-1 : COOLER

Figure 16

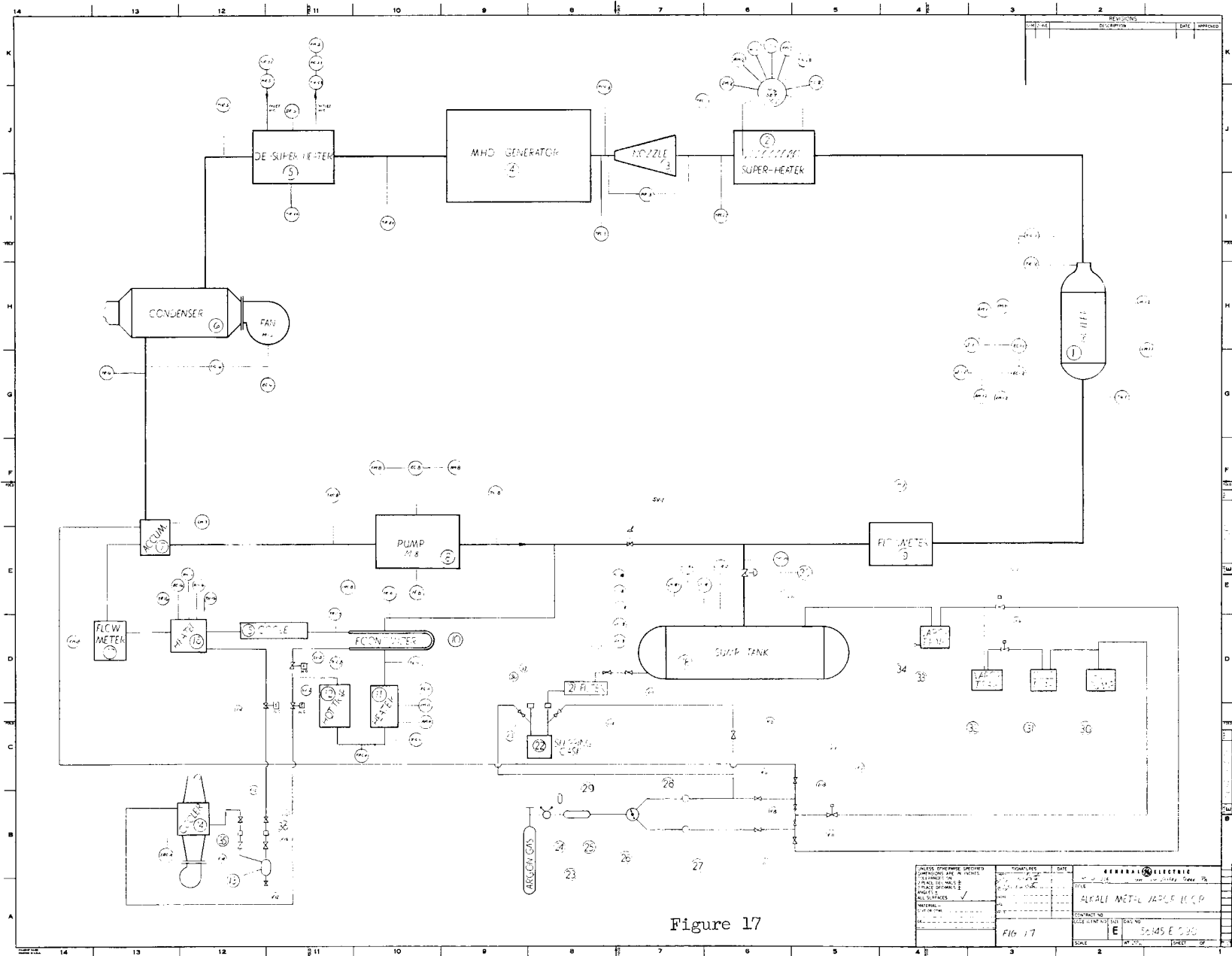


Figure 17

DESIGN APPROVED	DATE	GENERAL ELECTRIC
DESIGNED BY		ALBANY METAL WORKS CO.
CHECKED BY		
DATE		
CONTRACT NO.		
SCALE		

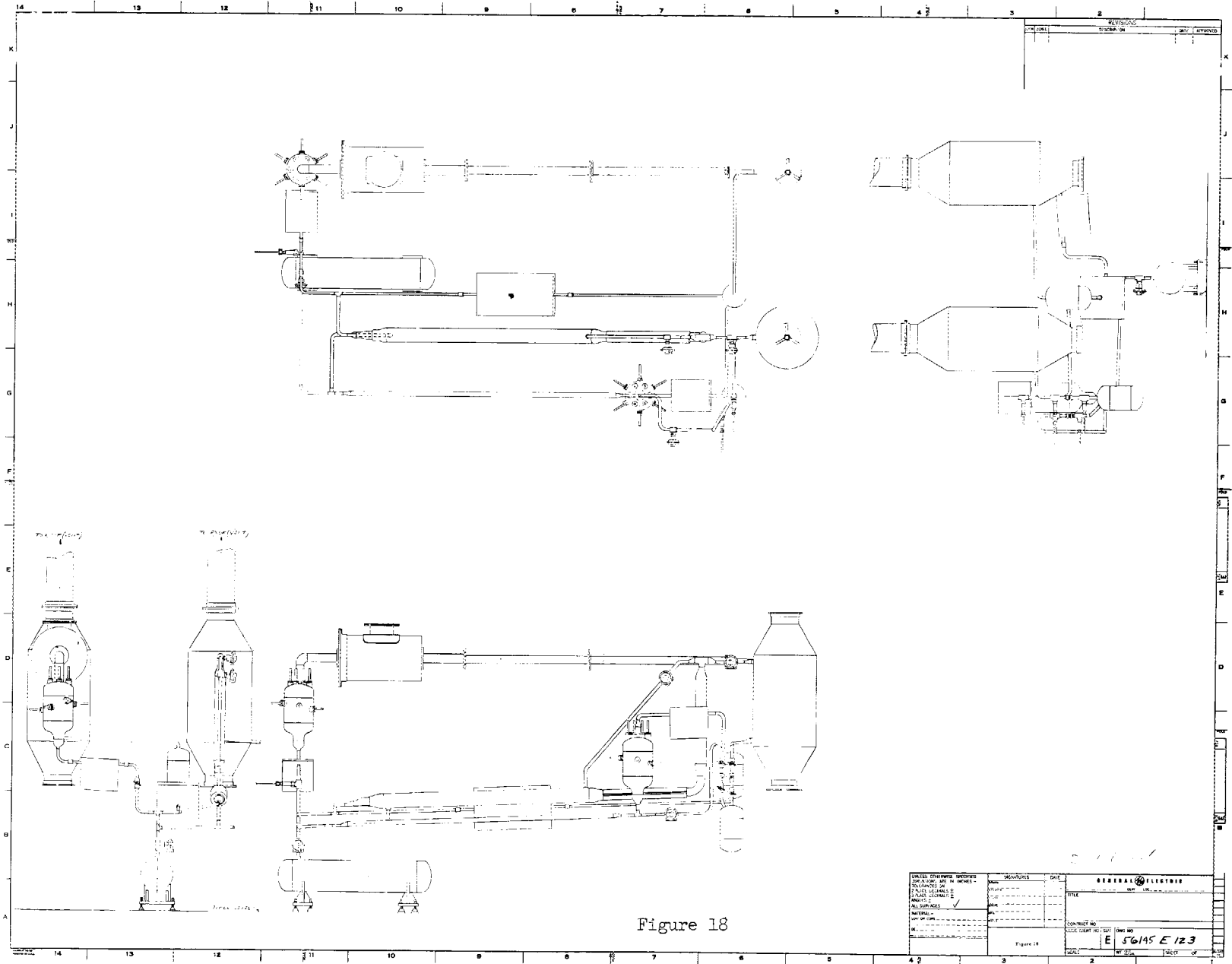


Figure 18

DESIGN ENGINEER	DATE	GENERAL ELECTRIC
DESIGNED BY		
PLANT DESIGNER		
PROJECT MANAGER		
MATERIALS		
CONTRACT NO.		
FIGURE NO.		
SCALE		

Figure 18

E 56145 E 123

DISCUSSION

MR. BERENSON: What are the irreversibilities in MHD generators?

MR. HOFFMAN: There are a couple. Of course it depends on where you operate. In reading through this paper you probably noticed that the MHD generator operates in a range between 0 and 1 for K . This is for power generation.

Now if K is greater than 1, you have to add power to the system, and it acts as an accelerator. Indeed, you can reverse the electro-leads and get K less than 1; and then it is just a brake. The Lorentz force holds you back. Of course, if what you are talking about is, "What can I get out of this thing?" it certainly isn't a perpetual-motion machine. You have to continue to feed heat to it. This is the whole point. The heat, of course, would depend upon somebody else's supply from the reactor. The idea being if somebody can build a reactor to give the right temperature, then material problems don't exist in MHD generators; because they have already been solved.

MR. BERENSON: What I actually had in mind would cause the entropy increase.

MR. HOFFMAN: Could I discuss this with you? I think it would take a little too much time to put things on the board. It is due to the fact that in this particular geometry, there is no net Hall current which is allowed to flow in the system. I will be happy to discuss it with you.

ANALYSIS OF THE ACCELERATION OF
LITHIUM IN A TWO-PHASE NOZZLE¹

David G. Elliott²

Jet Propulsion Laboratory
Pasadena, California

Abstract

To generate electric power magnetohydrodynamically from a liquid metal in a closed cycle, the metal must first be accelerated to several hundred feet per second in a two-phase nozzle. This paper presents results of calculations on the acceleration of lithium by cesium vapor in a two-phase nozzle. The calculations indicate that 85% to 90% of isentropic velocity can readily be attained, and this conclusion is supported by experiments on the acceleration of water by nitrogen and by Freon.

¹This paper presents the results of one phase of research carried out at the Jet Propulsion Laboratory under contract NAS 7-100, sponsored by the National Aeronautics and Space Administration.

²Engineering Group Supervisor, Advanced Propulsion Engineering Section.

Introduction

The long lifetimes required of space powerplants make nonrotating powerplant cycles attractive. A nonrotating power conversion cycle under investigation at JPL is the liquid magnetohydrodynamic system shown schematically in Fig. 1. In this system a fluid, such as cesium, circulates in the vapor loop and causes a liquid metal, such as lithium, to circulate through an MHD generator in the liquid loop.

In operation, the cesium leaves the radiator as condensate, flows through an EM pump to the mixer, vaporizes on contact with the lithium, atomizes and accelerates the lithium in the nozzle, separates from the lithium in the separator, and returns to the radiator. The lithium leaves the separator at high velocity (typically 500 ft/sec), decelerates through the production of electric power in the MHD generator, and leaves the generator with sufficient velocity (typically 300 ft/sec) to return through a diffuser to the nuclear reactor where the lithium is reheated. Presently estimated flow rates for 300 kw electric output, with 2000^oF nozzle inlet temperature and 1400^oF radiator temperature, are 20 lb/sec of cesium and 120 lb/sec of lithium.

An analysis of the liquid MHD system is given in Ref. 1, and initial test results with water and nitrogen are presented in JPL Space Programs Summary Numbers 37-17 and 37-21, Volume IV.

Single-component cycles (for example, liquid potassium accelerated by its own vapor) are possible, but preliminary analysis indicates that fluid-friction losses in the separator and generator would be higher than with the two-component cycle. With the latter, potassium or rubidium are possible alternatives to cesium as the driving vapor, but solubility is presently known only for cesium (Ref. 2).

A key problem in the cesium-lithium cycle is the efficient acceleration of

the lithium by the cesium in the two-phase nozzle. It is necessary, first, for the lithium to vaporize the cesium at the inlet of the nozzle, then for the lithium to be atomized by the cesium vapor, and finally for the lithium to be accelerated by the cesium while transferring heat to the cesium vapor to maintain its temperature. The analysis to be presented here indicates that these processes can be accomplished sufficiently well in a nozzle of reasonable length to yield an exit velocity between 85% and 90% of isentropic. It will be shown that the analysis correctly predicts exit velocities for water accelerated by nitrogen and by Freon 1301, the latter vaporized by the water at the nozzle entrance.

Analysis

Nomenclature and Assumptions

Fig. 2 shows the parameters which describe the two-phase nozzle flow. At axial distance x from the entrance the gas has flow rate \dot{m}_g , velocity V_g , temperature T_g , density ρ_g , specific heat c_g , viscosity μ_g , and thermal conductivity k_g . The liquid, assumed to be in the form of spherical droplets all of diameter D , has flow rate \dot{m}_l , velocity V_l , temperature T_l , density ρ_l , specific heat c_l , and surface tension σ . The pressure is p and the flow area is A .

The main idealization in this model is the assumption of equal droplet diameters. Partial justification is the fact, discussed later, that large droplets break up and narrow the drop-size distribution, but the main justification is the good agreement of the model with experiment. Other idealizing assumptions are that the flow is one-dimensional and that there is no friction or heat transfer at the wall.

Continuity

The nozzle flow area is equal to the gas flow area, $\dot{m}_g / \rho_g V_g$, plus the liquid flow area, $\dot{m}_l / \rho_l V_l$:

$$A = \dot{m}_g \left(\frac{1}{\rho_g V_g} + \frac{r}{\rho_1 V_1} \right) \quad (1)$$

where r is the mixture ratio \dot{m}_1/\dot{m}_g .

Momentum

The momentum flux of the mixture is

$$\dot{M} = \dot{m}_g V_g + \dot{m}_1 V_1 \quad (2)$$

If the nozzle were cut off at the station in question and the mixture allowed to attain equilibrium with no change in pressure, the velocities would equalize while maintaining the same momentum flux. The resulting equilibrium or "mean" velocity of the mixture, designated by \bar{V} , is, therefore, given by

$$\dot{m}_g V_g + \dot{m}_1 V_1 = (\dot{m}_g + \dot{m}_1) \bar{V} \quad (3)$$

or,

$$\bar{V} = \frac{V_g + rV_1}{1 + r} \quad (4)$$

The momentum flux in terms of \bar{V} is

$$\dot{M} = (\dot{m}_g + \dot{m}_1) \bar{V} \quad (5)$$

Since the sum of \dot{m}_g and \dot{m}_1 is a constant, regardless of any mass transfer between phases, the momentum-flux gradient is

$$\begin{aligned} \frac{d\dot{M}}{dx} &= (\dot{m}_g + \dot{m}_1) \frac{d\bar{V}}{dx} \\ &= \dot{m}_g (1 + r) \frac{d\bar{V}}{dx} \end{aligned} \quad (6)$$

In the absence of wall friction, the momentum flux gradient is equal to minus the pressure gradient acting over the flow area. Thus,

$$\dot{m}_g (1 + r) \frac{d\bar{V}}{dx} = -A \frac{dp}{dx} \quad (7)$$

Substituting the value of A from Eq. (1), the momentum equation becomes

$$\frac{d\bar{V}}{dx} = -\frac{1}{1+r} \left(\frac{1}{\rho_g V_g} + \frac{r}{\rho_1 V_1} \right) \frac{dp}{dx} \quad (8)$$

The ratio of relative to mean velocity will be called the slip, s . Thus,

$$s = \frac{V_g - V_1}{\bar{V}} \quad (9)$$

From Eqs. (4) and (9) it can be shown that

$$V_g = \left(1 + \frac{rs}{1+r} \right) \bar{V} \quad (10)$$

and

$$V_1 = \left(1 - \frac{s}{1+r} \right) \bar{V} \quad (11)$$

Substituting Eqs. (10) and (11) into Eq. (8), and noting that $2\bar{V}d\bar{V} = d\bar{V}^2$, the final form of the momentum equation is

$$\frac{d\bar{V}^2}{dx} = -\frac{2}{1+r} \left[\frac{1}{\left(1 + \frac{rs}{1+r}\right) \rho_g} + \frac{r}{\left(1 - \frac{s}{1+r}\right) \rho_1} \right] \frac{dp}{dx} \quad (12)$$

In the limit as the slip approaches zero the flow becomes isentropic. From Eq. (12) the isentropic-velocity gradient is

$$\frac{dV_1^2}{dx} = -\frac{2}{1+r} \left(\frac{1}{\rho_g} + \frac{r}{\rho_1} \right) \frac{dp}{dx} \quad (13)$$

Slip Gradient

The accelerating drag force on each liquid droplet of diameter D is

$$F_d = C_D \left(\frac{\rho_g s^2 \bar{V}^2}{2} \right) \left(\frac{\pi D^2}{4} \right) \quad (14)$$

The accelerating buoyancy force is

$$F_b = -\frac{\pi D^3}{6} \frac{dp}{dx} \quad (15)$$

The sum of these two forces equals the product of mass and acceleration of the droplet. Thus,

$$F_d + F_b = \left(\frac{\pi D^3 \rho_1}{6} \right) \left(V_1 \frac{dV_1}{dx} \right) \quad (16)$$

Combining Eqs. (14), (15), and (16), the liquid velocity gradient is

$$\frac{dV_1}{dx} = \frac{3\rho_g s^2 \bar{V}^2 C_D}{4\rho_1 V_1 D} - \frac{1}{\rho_1 V_1} \frac{dp}{dx} \quad (17)$$

From Eq. (11), dV_1/dx can also be written

$$\frac{dV_1}{dx} = \left(1 - \frac{s}{1+r}\right) \frac{d\bar{V}}{dx} + \frac{\bar{V}}{1+r} \left(\frac{s}{1+r} \frac{dr}{dx} - \frac{ds}{dx}\right) \quad (18)$$

Solving Eq. (18) for ds/dx and evaluating dV_1/dx from Eq. (17) the slip gradient is

$$\frac{ds}{dx} = \frac{\left(1 - \frac{s}{1+r}\right) (1+r)}{\bar{V}} \frac{d\bar{V}}{dx} + \frac{s}{1+r} \frac{dr}{dx} + \frac{1+r}{\rho_1 V_1 \bar{V}} \frac{dp}{dx} - \frac{3\rho_g s^2 \bar{V} C_D (1+r)}{4\rho_1 V_1 D} \quad (19)$$

The drag coefficient can be conveniently evaluated from Stonecypher's least-squares fit (Ref. 3, page 3) to Perry's tabulation (Ref. 4, p. 1018):

$$\ln C_D = 3.271 - 0.8893 (\ln Re) + 0.03417 (\ln Re)^2 + 0.001443 (\ln Re)^3 \quad 0.1 < Re < 2 \times 10^4 \quad (20)$$

where the Reynolds number is based on relative velocity:

$$Re = \frac{\rho_g s \bar{V} D}{\mu_g} \quad (21)$$

For small Reynolds numbers Stokes' law holds:

$$C_D = \frac{24}{Re} \quad Re \leq 0.1 \quad (22)$$

For large Reynolds numbers, up to the largest encountered in practical nozzles, C_D can be taken as constant at 0.457, the value given by Eq. 20 for $Re = 2 \times 10^4$.

Energy

With no heat transfer at the wall, the total enthalpy flux of the mixture remains constant. Thus

$$\frac{d\dot{H}}{dx} = 0 = \dot{m}_g \left(c_g \frac{dT_g}{dx} + \frac{1}{2} \frac{dV_g^2}{dx} \right) + \dot{m}_l \left(c_l \frac{dT_l}{dx} + \frac{1}{\rho_l} \frac{dp}{dx} + \frac{1}{2} \frac{dV_l^2}{dx} \right) \quad (23)$$

Heat Transfer

The rate of convective heat-transfer from the liquid droplets to the gas is

$$\frac{dQ}{dt} = \pi D^2 \dot{N} h (T_l - T_g) \quad (24)$$

where h is the heat-transfer coefficient and \dot{N} is the number flow rate of droplets, the latter given by

$$\dot{N} = \frac{6 \dot{m}_l}{\pi D^3 \rho_l} \quad (25)$$

Due to circulation within the droplets their internal temperature is uniform so that

$$\frac{dQ}{dt} = -\dot{m}_l c_l \frac{dT_l}{dt} \quad (26)$$

Combining Eqs. (24), (25), and (26) and noting that $dx/dt = V_l$, the liquid-temperature gradient is

$$\frac{dT_l}{dx} = \frac{6h (T_g - T_l)}{D \rho_l c_l V_l} \quad (27)$$

Eqs. (23) and (27) neglect cooling effects due to formation of additional vapor during expansion, but such cooling has little effect on velocity since it mainly affects the liquid temperature which decreases little during expansion.

The heat-transfer coefficient can be evaluated from the following relations (Ref. 5, p. 379):

$$h = \frac{2 k_g}{D} \quad \text{Re} \leq 1.0 \quad (28)$$

$$h = c_g \rho_g s \bar{V} \left(\frac{2.2}{\text{Re}} + \frac{0.48}{\sqrt{\text{Re}}} \right) \quad 1 < \text{Re} \leq 25 \quad (29)$$

$$h = \frac{0.37 k_g \text{Re}^{0.6}}{D} \quad \text{Re} > 25 \quad (30)$$

Droplet Breakup

The ratio of drag to surface-tension forces for a liquid droplet is proportional to the Weber number defined by

$$We = \frac{\rho_g D s^2 \bar{V}^2}{2\sigma} \quad (31)$$

Various analyses and experiments indicate (Ref. 6, page 3) that a droplet moving relative to a gas stream will break up if the Weber number exceeds 6, provided the time of exposure to the velocity differential is at least as great as the natural period of oscillation of the droplet, $\frac{\pi}{4} \sqrt{\rho_l D^3 / \sigma}$. The latter condition is met in two-phase nozzles of interest here. Hence, the maximum, or critical, droplet diameter is

$$D_{\max} = \frac{12\sigma}{\rho_g s^2 \bar{V}^2} \quad (32)$$

The droplets are assumed to break up to D_{\max} whenever D_{\max} falls below the current diameter D .

Comparison with Experiment

The preceding equations were used to calculate the theoretical performance of an experimental two-phase nozzle employing nitrogen gas to accelerate water. Fig. 3 is a photograph of the nozzle in operation.

The nozzle has an entrance diameter of 14 in., a throat diameter of 3.18 in., an exit diameter of 5.2 in., and a length of 50 in. The convergent half-angle is 20 deg, and the divergent half-angle is 2.5 deg. The area change in the throat region is very gradual so as to limit the slip, s , to about 0.5. The injector employs 1656 pairs of nitrogen and water jets impinging at right angles, the former 0.005 in. x 0.13 in., and the latter 0.040 in. x 0.13 in.

The nozzle was tested over a range of mixture ratios from $r = 15$ ($\dot{m}_g = 6.1$ lb/sec, $\dot{m}_l = 92$ lb/sec) to $r = 70$ ($\dot{m}_g = 2.6$ lb/sec, $\dot{m}_l = 182$ lb/sec). The

nozzle inlet pressure was held at 150 psia, and the pressure differentials across the injection orifices ranged from 170 psi to 30 psi for the nitrogen and from 14 psi to 38 psi for the water. The mean exit velocity, \bar{V} , was determined by dividing the nozzle thrust by the total flow rate.

Theoretical computations were made for initial droplet diameters ranging from 0.002 in. to 0.050 in. It was found that exit velocities remained constant for initial diameters greater than 0.010, because of the breakup criterion, Eq. (32), which caused larger droplets to break up to that size within 16 in. of the entrance.

Fig. 4 compares the experimental and theoretical exit velocities, the latter computed for "large", i.e., greater than 0.010 in., initial droplet diameter. Also shown is the isentropic velocity, corresponding to zero droplet diameter. The experimental and theoretical velocities agree closely and are 85% of the isentropic velocity.

The same nozzle was tested with Freon 1301 (CBrF_3) and water. The Freon was injected as a liquid at -70°F and the mixture ratio was varied from 4 to 14 with the nozzle inlet pressure held at 150 psia. The water, initially at 60°F , was cooled 5 to 20°F by the vaporization of the Freon, and the resulting Freon vapor had 0 to 15°F superheat.

Fig. 5 compares the theoretical and experimental exit velocities with the Freon. The experimental values are slightly below theoretical, but close enough to show that substantially all the Freon must have vaporized near the nozzle entrance. The experimental exit velocities are 91% of isentropic, higher than with nitrogen because of the higher density of Freon vapor.

The good performance obtained with Freon and water is evidence that lithium would efficiently vaporize cesium (or potassium or rubidium) in a similar nozzle, since the heat-transfer properties of the latter systems are at least as favorable as those of the Freon-water system.

Theoretical Cesium-Lithium Performance

Fig. 6 shows the theoretical exit velocity for a cesium-lithium mixture expanding from 202 psi and 2000^oF to 20 psi, based on the property values of Ref. 7. The concentration of cesium dissolved in the lithium was assumed to be 6% by weight at the nozzle entrance (the lower of the two values reported in Ref. 2) and to decrease in proportion to the cesium pressure. The lithium vapor pressure was assumed constant at 2 psi. A source of uncertainty was the lithium surface tension which was taken as 230 dyne/cm based on extrapolation to 2000^oF using the Eötvös Rule.

Initial droplet diameter was taken as 0.050 in., exit velocity being found constant with droplet diameter beyond 0.020 in. The nozzle contour assumed was that of the experimental nozzle of Fig. 3 doubled in length to 100 in. Computations were made for exit mixture ratios from 3.85 (inlet $r = 5$) to 14.5 (inlet $r = 100$). Fig. 6 shows that the corresponding theoretical exit velocities range from 816 ft/sec to 454 ft/sec, values which are 88% of isentropic.

The variations of area, droplet diameter, velocity, and temperature with axial distance for an exit mixture ratio of 6.3 are presented in Figs. 7, 8, and 9. Changes in flow conditions are small for the first 20 in. of the nozzle, this section being an essentially constant-pressure transition duct required by the large diameter of the injector. Beyond 20 in. the droplets break up within an additional 10 in. distance and velocities rise steadily to their exit values. The gas temperature drops to 1760^oF at the exit, reflecting the heat transfer from the lithium without which the cesium temperature would follow the adiabatic curve, shown, to 1320^oF. The lithium temperature drops by 8^oF due to heat transfer to the cesium vapor (or by 21^oF when cooling due to additional cesium and lithium vaporization within the nozzle are included).

Conclusions

1. Based on the Freon-water results, vaporization of cesium (or potassium or rubidium) by lithium at the entrance of a two-phase nozzle appears feasible.
2. Based on the analysis, and its good agreement with experiment, it is concluded that lithium can be accelerated to within 85 to 90% of isentropic velocity in a nozzle of reasonable length.

References

1. Elliott, D. G., "Two-Fluid Magnetohydrodynamic Cycle for Nuclear-Electric Power Conversion," ARS Journal, Vol. 32, No. 6, June 1962, pp. 924-928.
2. Cuerou, T. R., and Tepper, F., Solubility of Cesium in Lithium at Elevated Temperatures, ARS Space Power Systems Conference, Santa Monica, California, ARS Preprint 2537-62, September 25-28, 1962.
3. Stonecypher, T. E., "Quarterly Progress Report on Engineering Research", Report No. P-60-17, Rohm and Haas Company, Huntsville, Alabama, December 27, 1960.
4. Perry, J. H., ed., Chemical Engineers Handbook, 3rd Edition, McGraw-Hill, New York, 1950.
5. Krieth, F., Principles of Heat Transfer, International Textbook Co., Scranton, Pennsylvania, 1960.
6. Morrell, G., Critical Conditions for Drop and Jet Shattering, NASA TN D-677, February, 1961.
7. Weatherford, W. D., Jr., Tyler, J. C., and Ku, P. M., Properties of Inorganic Energy-Conversion and Heat-Transfer Fluids for Space Applications, WADD Technical Report 61-96, November 1961.

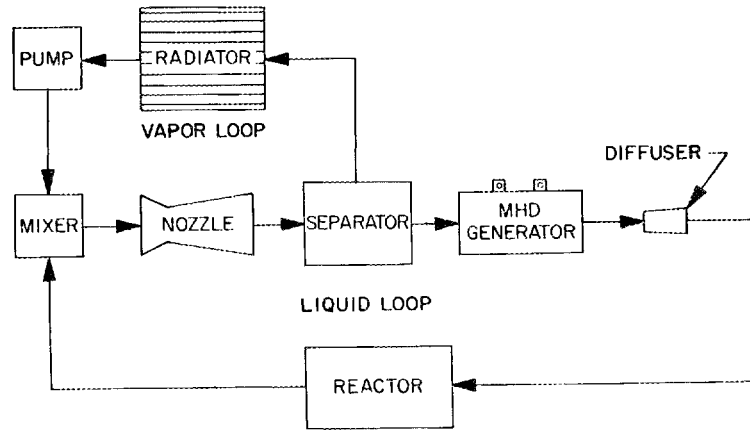


Fig. 1 Liquid MHD Cycle

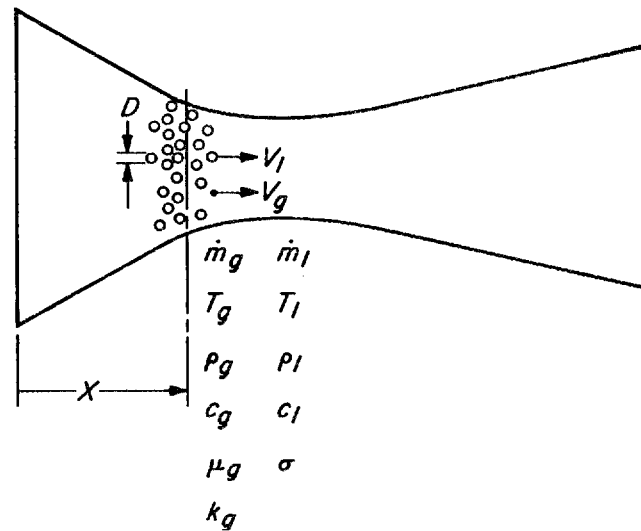


Fig. 2 Two-phase nozzle nomenclature

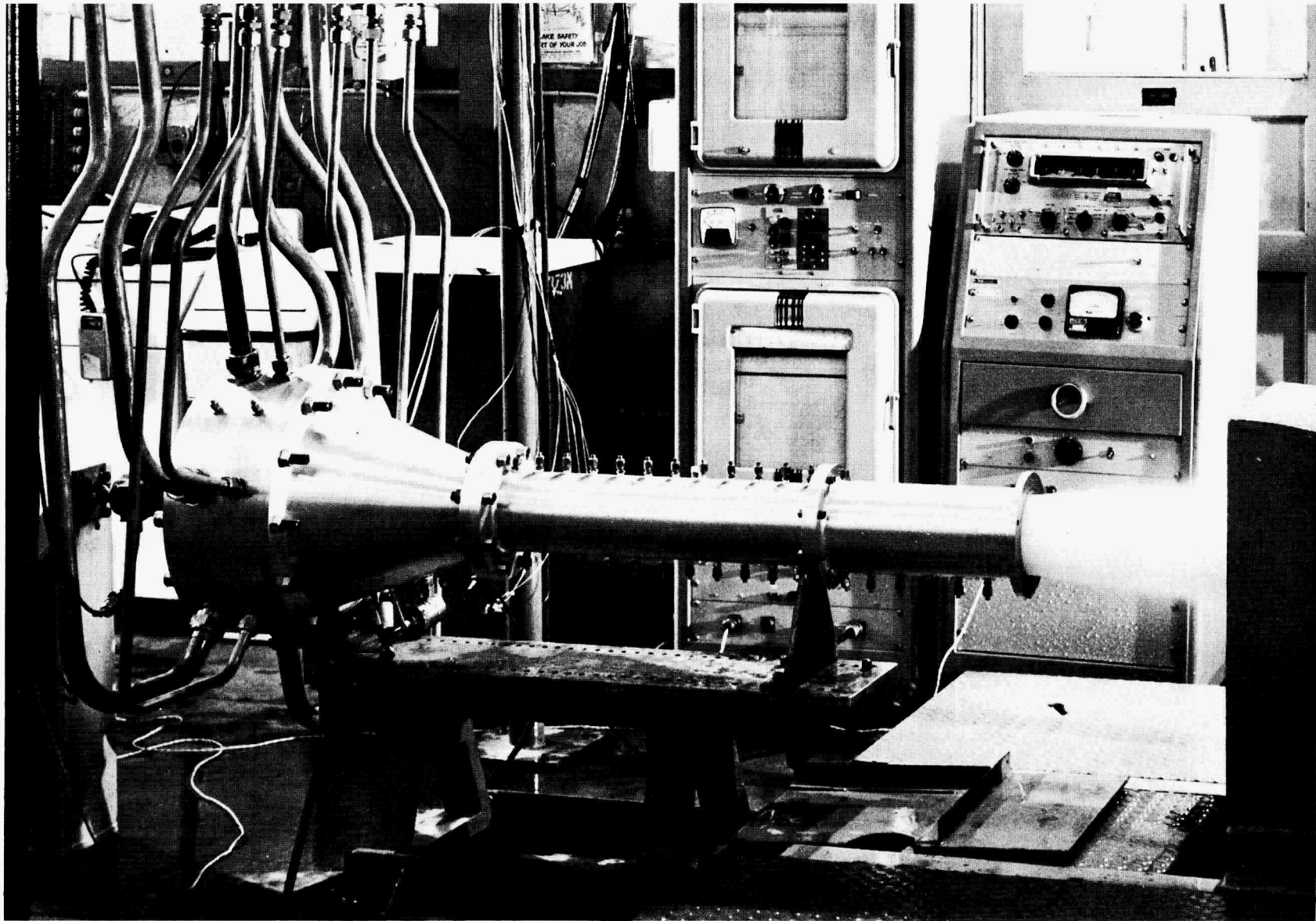


Fig. 3 Experimental two-phase nozzle in operation.

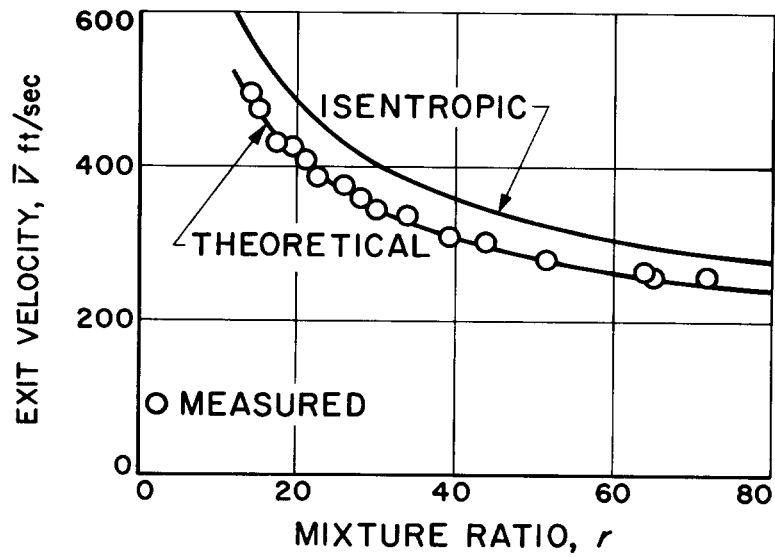


Fig. 4 Comparison of theoretical and experimental exit velocities for nitrogen and water with 150 psia inlet pressure and 14 psia exit pressure.

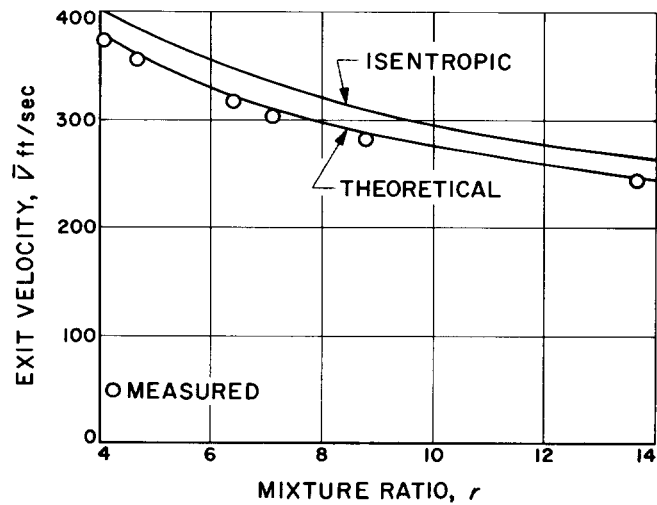


Fig. 5 Comparison of theoretical and experimental exit velocities for Freon 1301 and water with 150 psia inlet pressure and 14 psia exit pressure.

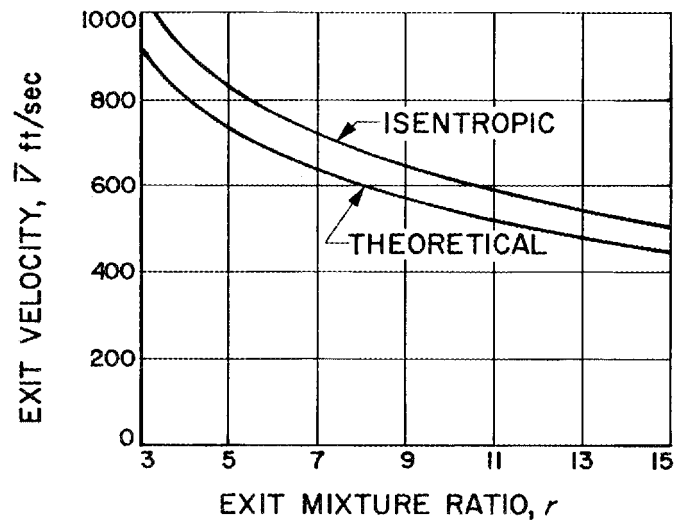


Fig. 6 Theoretical exit velocity for cesium and lithium with 202 psia inlet pressure, 2000°F inlet temperature, and 20 psia exit pressure.

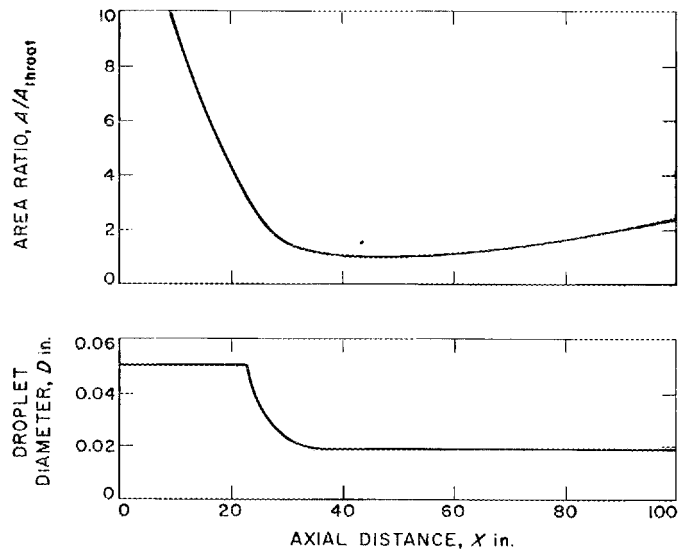


Fig. 7 Variation of area and droplet diameter with distance for cesium-lithium nozzle.

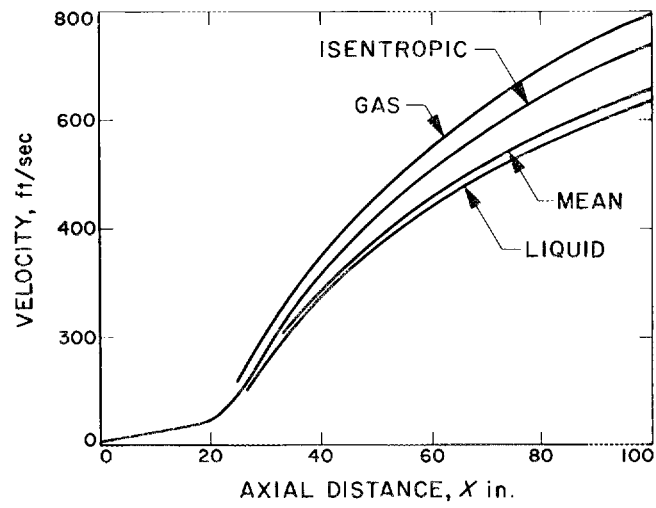


Fig. 8 Variation of velocity with distance for cesium-lithium nozzle.

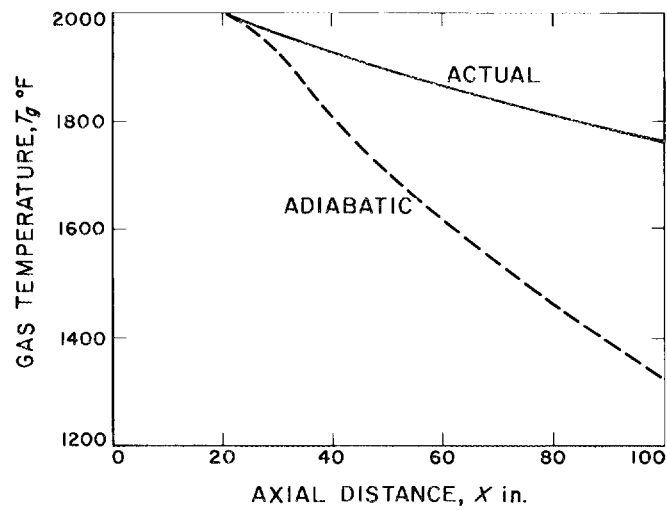


Fig. 9 Variation of gas temperature with distance for cesium-lithium nozzle.

DISCUSSION

MR. DWYER: What flow rates and velocities would go with your proposed NaK conversion system?

DR. ELLIOTT: About 150 or 200 pounds a second of NaK would be circulating in the NaK loop, and the velocity entering the generator would be about 300 feet per second, coming out at about 200.

MR. DWYER: How about vibration problems?

DR. ELLIOTT: With the water tests we have not observed any vibration. The operation is very smooth, like liquid flow, essentially. Slow oscillation due to systems instabilities are, of course, possible.

MR. KEYES: Although the exit velocity is not sensitive to droplet size, I would think the overall performance would be, including the separation phase, and also the drop size distribution probably includes a wide range of drop sizes. Was that taken into account?

DR. ELLIOTT: In regard to the effect on separator performance, it turns out that the drop sizes given by the Weber number = 6 rule are about ten to a hundred times larger than a drop which would be able to appreciably deflect before it hits the separator. That is, it would be necessary to go down to drop sizes of less than a mill in order for them to deviate, say, a quarter of an inch as they approach the separator. So it may be fortunate that you do not get small droplet sizes from the nozzle. The sizes we do get just go straight to the separator with hardly any deviation.

As to the drop-size distribution: due to the breaking up of large droplets you continually narrow the drop-size spectrum from the top, so that you end up with a fairly narrow range of droplet sizes. The fact that the separator separates as well as it does is proof that there cannot be a very large mass fraction of liquid tied up in droplets smaller than 1 mill, say. Those droplets are the ones that constitute the half per cent which is lost.

MR. BALZHISER: I recall on one plot you had nozzle exit velocity versus the ratio of liquid to vapor which decreased continually and leveled off to the right. I think I recall hearing some reports that critical

velocity in two-phase mixtures frequently has a minimum perhaps much lower than the values you showed.

DR. ELLIOTT: Yes, you are thinking of sonic velocities. This is a supersonic nozzle. The sonic velocity is very low, like a hundred feet per second. So the Mach number, based on that sonic velocity, is about 3 leaving the nozzle. Mach numbers are even higher leaving the separator. There is about a one-to-one volume ratio of gas mixed with liquid coming out of the separators to the generator. The Mach number there runs about 4 or 5.

MR. BALZHISER: Could you comment briefly on what experience you might have had with sonic velocity and two-phase mixture?

DR. ELLIOTT: Yes. We have some rather interesting work going on that I haven't gone into. There is a Cal-Tech student doing a thesis on supersonic two-phase flow, for example, measuring the pressure ratio across normal shocks and comparing the pressure rises with the theory. You can definitely see all of the supersonic flow phenomenon in these two-phase mixtures.

For instance, in our diffuser you cannot have a contraction ratio between the diffuser inlet and throat greater than a certain amount, or it won't start. There will be a shock at the inlet.

MR. STEIN: Do I understand correctly that in the analysis you did which seemed to work so well, that you included drag between droplets and vapor, but none between the fluid and the nozzle wall?

DR. ELLIOTT: Yes. In that analysis, the wall friction was neglected. A rough estimate shows it is perhaps a per cent or two of the thrust.

MEETING SUMMATION

R. N. Lyon

Oak Ridge National Laboratory

MR. LYON: I wondered why I was getting such a wonderful introduction, and he finally pointed out why!

Also, I thought perhaps he was going to say that the position of the last speaker who presents the summation is more difficult than the rest, because you don't know what it is you are going to summarize until the last, previous speaker has finished. Mr. Elliott presented a number of interesting points which were not included in his paper, so I will try to fit them in, but I may not get to them.

I am going to try to do this job in about 15 or 20 minutes. Since there were 33 technical papers, this means about 30 seconds apiece. So if I appear to slight you, it is merely because of the pressure of time.

One of the things that interested me in this whole discussion was that although most of us think of the current applications of nuclear energy for space power, there were a number of other applications being approached.

In the case of space power, of course, we have a simple Rankine cycle, using a reactor. There was one paper which described experiments aimed at developing solar energy systems. The last two papers discussed application in MHD generators.

Aside from space power we had a discussion of the problem of cooling rocket nozzles. We had a discussion--one I would never have guessed we would have--on the problem of igniting rocket fuels. And we had one paper which was related to reactors, but was involved in part with the problem of preventing boiling, or the problems that one might get into with boiling in a system which normally should operate in a nonboiling condition.

I divided the discussion into several parts, more or less along the lines of the breakdown in the program. You will remember that on Wednesday the first series of papers was on physical properties, and I have passed out a sheet in which I have listed most of the physical properties

which were discussed, and an indication of the approximate maximum temperatures to which the physical properties have been determined.

Now I think it is a very impressive list, of course lithium and sodium, there has already been a great deal of work done on. The fact it is blank doesn't mean the data are not available. But in potassium, rubidium and cesium, the other remaining common liquid metals--alkali metals--the list is almost complete, if one includes these values, these properties which I have checked. The check mark is intended to indicate that work is now in progress to the extent of having equipment designed or in construction.

In a number of cases I have indicated question marks. These are areas in which the speaker indicated they were approaching the problem, but the design was not complete, and perhaps in some cases the actual techniques which would be used, have not been decided upon.

The little superscripts, of course, refer to the various speakers who discussed their work. The last three columns refer to electrical resistivity, thermoelectric power, and chemical analysis.

Also, in the course of the program, there were a number of interesting little side points not directly related to heat transfer, such as some comments on corrosion and some comments on components.

For example, Professor Bonilla mentioned that he had had difficulty with A-nickel in potassium at elevated temperatures, that it became porous. And that with high-purity, low-carbon nickel, he developed a worm hole. Later Gene Hoffman suggested this might have been due to nucleation in the bottom of the hole, which would have increased mass transfer.

For very high temperatures, of course, everybody thinks largely of columbium 1-zirconium. There was some mention of molybdenum-1/2 titanium. Both of these require protection from the atmosphere, and there was discussion of the problems of protecting these somewhat reactive metals from the atmosphere.

Davis from JPL gave probably the most complete discussion of work on wrapping the system with layers of titanium, or tantalum, or zirconium, or molybdenum. From his paper I conclude that he has decided that a layer of

Physical Properties Reported at This Meeting
(Temperature in °F)

	C_f	C_g	h_{sf}	h_{fg}	k_f	k_g	ρ_f	(PVT)		P_{sat}	σ	Elec. Res.	Therm. Elec. Power	Chem. Anal.
								ρ_g	μ_f					
Li					1450 ⁶ 2000 ⁶ (✓)									
Na													1250 ⁸	C ⁵ 10 ppm
K	2000 ⁷	2100 ⁷	m.p. ⁷	2100 ^{7*}	1400 ⁷			2100 ⁷	1250 ⁷		2100 ⁷	1350 ⁶	2100 ⁷	1600 ⁸
Rb	1650 ⁴ 2000 ⁵	(?) ⁵	m.p. ⁵	1800 ⁴	(?) ⁵	(?) ⁵	1670 ⁴ 2000 ⁵	1900 ⁵	(✓) ⁵	(✓) ⁵	2000 ⁴ 2000 ⁵		2000 ⁵	1250 ⁸ C ⁵ (✓) O ⁵ (✓)
Cs	1650 ⁴ 500 ⁹ 600 ⁵ (1900) ⁵	(?) ⁵		1600 ⁴	(?) ⁵	(?) ⁵	1670 ⁴ 708 ⁵ 2000 ⁵ (✓)	(✓) ⁵	(✓) ⁵	(✓) ⁵	2000 ⁴ 1940 ⁵		1100 ⁸	C ⁵ (✓) O ⁵ (✓)

*Calc. from Clapyron Eq. using measured ρ_g .

⁴AGN (Achener)

⁵MSA (Tepper)

⁶ORNL (Cooke)

⁷EMI (Lemmon)

⁸CU (Bonilla)

⁹Anon.

zirconium on the outside of two layers of tantalum would probably be best. In his discussion he also mentioned that they might use molybdenum on the outside, because of its very rapid scavenging ability, but that the molybdenum would have to be at a lower temperature because of the volatility of molybdenum oxide, and the tendency for the columbium to remove the oxygen from the molybdenum.

Another comment that was passed on was by Lewis from NASA who said that his welders, in monitoring the cover gas in welding, preferred to use stainless steel above anything else, because of its very rapid and apparent darkening at extremely low concentrations of oxygen.

There were several other discussions of corrosion.

Kelly of Pratt and Whitney described a number of components which have been constructed of columbium 1-zirconium, which demonstrates that almost any component can be made of columbium 1-zirconium. It is expensive, but it can be done.

Finally, in the line of components, Samuel, from Mine Safety, described vapor velocity detection, or measurement equipment, using a capillary tube which he explained this morning could also be used as a vapor viscometer.

In the area of pressure drop, first of all in single-phase flow, Lewis of NASA discussed vapor expansion in nozzles. He has data for sodium, and he plans to go on and get data with potassium. He will extend this work very shortly to the test of complete turbines for SNAP systems.

He also is developing pumps for liquid condensate at temperatures near the boiling point, and in connection with that work he has found that they do get some cavitation, and plans to study various materials for resistance to cavitation corrosion.

The field of two-phase flow was discussed by a number of people. In general it appeared that the Martinelli correlations gave high values. Randall of Pratt and Whitney found, however, the reverse was true. And of course this morning you heard Dr. Goldman give a summation in the form of graphs which will make it easier to predict the pressure drop on the basis of the Martinelli-Nelson approach.

Flow stability is also a problem in any kind of multiple-tube system, and you heard Mr. Vild this morning, from Thompson-Ramo-Wooldridge describe a method which apparently enables one to predict what flow conditions and what degrees of quality are required, in order to have a condenser operating upside down in a lg system.

The last speaker, of course, discussed the problem of two-phase jets and had remarkable agreement between his theoretical prediction and the experimental data which he obtained.

I might say in passing that it is always very satisfactory when one works out a theory, and has to make a point, that the line that is drawn is a theoretical line, not the experimental line. This isn't an experience that happens to us very often.

There were several sets of data which described pressure drops in twisted tapes with two-phase flow.

Berenson raised an interesting question of whether, in the Martinelli correlation, if you have a rough pipe, the smooth pipe friction factor should not be used, and I will qualify this in view of Dr. Goldman's comments and say perhaps this should only apply if we have adiabatic wall conditions, the argument being that the liquid film which tends to develop along the wall, tends to smooth out the roughnesses.

In heat transfer in single-phase, Stein presented a very interesting new approach to the problem of turbulent-flow heat transfer with varying wall conditions, which appears to explain some of the anomalies that are now in published liquid metal heat transfer data. It is most easily applied at the present time to co-current heat exchange conditions, but he feels it may be capable of extension to counter-current systems.

Desmond, of Hercules, gave data on natural circulation in liquid tin and found that the Eckert relationship applied even up to accelerations of 20g, and in spite of an appreciable incline in the tube. It might be pointed out that this paper really fits the title of this whole meeting, which of course, is High Temperature Liquid Metal Heat Transfer. Mr. Desmond was talking in terms of temperatures of up to 2800° centigrade,

whereas most of the rest of the speakers were down in the range of 2,000° Fahrenheit or below.

Nurick of Rocketdyne presented preliminary data on the problem of heating a vertical surface by spraying hot sodium metal on it.

In condensing, Rohsenow of MIT described experiments planned to determine the validity of the usual assumption that the condensing surface temperature is at the saturation temperature. It is going to be very interesting to see how that turns out--whether the accommodation factor really exists--whether it is due to some impurities on the surface, and so on.

Hays of Electro-Optical presented results along with an interesting short movie strip showing the behavior of a mercury jet condenser as a function of the mass flow ratio, the ratio between the mass flow of liquid and vapor.

Heat fluxes of the order of 10^7 or higher were obtained in this system and it was noticed that there was an appreciable pressure rise as the jet was operated, which varied with the mass flow ratio. It was suggested that perhaps this device, in addition to being a condenser, might be used either for an auxiliary pump or for the main pump in the space system, eliminating the necessity for a mechanical pump.

Brooks, of G.E., gave some potassium data on condensation which were roughly in the area predicted by Seban's correlation.

Gutstein, of NASA presented a drop-growth annular-flow theory of drop-wise mercury condensation, which appeared to be corroborated by the experiments. This consisted of the drops building up on the walls, the drops themselves growing, and at the same time the annular condensate ring increasing in size until it approached an actual interface between the vapor and the liquid, across the whole tube diameter.

In the field of pool boiling, studies were described by Rohsenow of MIT which appear to confirm an equation relating the size of solid-surface depressions or holes to the superheat required for maintaining the activity of that hole as a bubble nucleation site.

Bonilla of Columbia presented preliminary pool data with potassium, using equipment which had been used previously, with sodium, and he plans to continue that work with new equipment which is now under construction.

Balzhiser of Michigan described pool boiling in which, under some circumstances, he actually got indications of film boiling as well. He made measurements in the pool, also, which indicated some interesting temperature variations axially up and down the pool. He plans at the present time to extend the work into fully-film boiling.

Noyes of AI showed recordings of the surface temperature fluctuations in pool boiling, and he noticed that there was one particular frequency which seemed to be a resonant frequency at about 2.4 cycles per second. There was no attempt made to indicate whether this was a general phenomenon for other equipment. But it was interesting, with a very sharp peak, regardless of the heat flux which occurred at about 2.4 cycles per second. He also presented burn-out heat fluxes and actual measured surface superheats.

In forced convection boiling Berenson, AiResearch, presented data on potassium forced convection up to about 65% exit quality.

Brooks, in discussing G.E.'s potassium data, commented on a hump which occurred in the axial temperature measurements along the boiler wall, this hump occurring just at the point where the entering potassium reached the saturation temperature. This was consistent for a variety of fluxes and inlet temperatures, so that this hump always occurred at that point on the liquid temperature scale, rather than at some particular point in the tube, and therefore was not, apparently, an experimental difficulty with a bum thermocouple.

Randall of Pratt and Whitney described results of tests on various configurations of small tubes: tubes which were pushed in in various spots, tubes which were in a sine wave shape, and so on. His method of heating was interesting. He heated his tubes by condensing potassium on the outside. This enabled him to get all the way up to 100% quality without any danger of burn-out, since the wall temperature was limited by the saturation temperature of the condensing potassium on the outside.

He actually used this in a subsequent, similar device in the same loop for producing superheat.

Hoffman of ORNL presented the most recent data on burn-out and heat transfer of boiling potassium that have been obtained here.

Noyes of AI presented sub-cooled boiling sodium results, and also net boiling results with qualities up to about 30%.

Fisher of Aerojet described forced convection results with rubidium with outlet qualities up to about 80%.

In the preliminary, non-boiling tests there was a rather unusual spread in his heat transfer data, and Poppendiek of Geoscience was reminded of similar results which were obtained here about ten years ago by Bill Harrison in sodium, with very short heated lengths of tubes, and indicated perhaps this was not just an experimental difficulty, but might actually be a real effect. You will remember that in Fisher's apparatus the heater consisted of a number of relatively short lengths of heaters, rather than one continuous one, with nonheated gaps in between.

Smith of Allison gave results of forced convection boiling of potassium-mercury amalgams. He got ΔT 's up as high as 600°, which led him to believe that perhaps he was in the film-boiling region.

After that paper there was an interesting discussion on the relative merits of presented boiling data in terms of h as opposed to presenting them as a plot of $\frac{Q}{A}$ versus ΔT .

Poppendiek and Greene of Geoscience presented a theory of dry-wall fog-flow evaporation and experimental data which fell fairly close, about 20% below, in a system containing a spiral flow.

Davis of JPL later commented he believes boiling should be carried on on the outside of heated tube banks in order to encourage the impingement of droplets in the fog which develops in the boiling process.

Krakoviak of ORNL described a model which predicted very high superheats obtainable in liquid metals containing no vapor, and proposed that no nucleation at smooth metal walls occurs in liquid alkali metals, heat

instead being conducted from the smooth wall out through the liquid metal to a liquid interface in the interior of the evaporating fluid. Some discussion followed that paper.

Chen of Brookhaven proposed a model by means of which two interacting heat-transfer mechanisms operated parallel in forced convection systems. A macro- or forced-convection agitation system, and a micro- or bubble-growth agitation mechanism. Using this model he was able to predict the coefficients close to those obtained by ORNL with potassium, and those obtained with sodium at G.E.

In looking over the whole program, and in listening to the papers, I had several reactions. One was that it seems to me we need more analyses of the type given by Poppendiek and by Chen and by Stein and by Elliott, where we are really trying--either to see what is going on, or at least to get a handle on predicting the situation, perhaps at the expense of some experimental work. There were a great many experimental data presented, and I recognize that we are all engineers and we are aimed at pieces of hardware. If we have a piece of equipment and we have to run a test on it, of course we have to run a test on it, and we might as well publish the data. But with the data we have now, it occurs to me that it is time to sit down and attempt to examine what is actually going on, and in what directions we have to go to develop further understanding.

You will remember that Nick Grossman, in his introduction, pointed out that liquid metals are difficult, because you can't see them, and you can't tell whether you are in turbulent or laminar flow, even though the Reynolds number says perhaps you are in turbulent flow. This, of course, is even more important in the light of questions Dr. Goldman has raised as to whether or not there is a film on an evaporating wall, the degree to which there is fog flow as opposed to annular flow, and so on. He has emphasized this over and over again, and while sometimes the discussion became lively, I am sure we all agree that what we need to do is to find some way of looking inside, theoretically or experimentally, to determine what the situation is inside of this opaque material.

Finally, I would like to comment that although I once was quite active in the liquid-metal field, I haven't been very active personally for some time. I have found it stimulating to come back, as it were, and listen to these papers which were, without exception, well presented, and well thought out. What was even more stimulating to me, was the fact that everybody who was presenting a paper, and everyone who was discussing a paper, seemed to have a real enthusiasm for the field and to be earnestly interested in pushing forward our knowledge of high temperature liquid metal heat transfer.

LIST OF ATTENDEES

Achener, P. Y. - Aerojet-General Nucleonics
Berenson, P. J. - AiResearch Mfg. Co.
Berkowitz, L. - United Nuclear Corp.
Balzhiser, R. E. - University of Michigan
Bleckermann, S. S. - Pratt & Whitney Aircraft Co.
Bonilla, C. F. - Columbia University
Brooks, R. D. - General Electric Co.
Carlino, Justino - Sunstrand Aviation Corp.
Chen, J. C. - Brookhaven National Lab.
Conrad, R. R. - Sunstrand Aviation Corp.
Cooke, J. W. - Oak Ridge National Lab.
Cunningham, C. W. - Oak Ridge National Lab.
Davis, J. P. - Jet Propulsion Lab.
Delaney, C. L. - USAF, Aero Propulsion Lab.
Desmon, L. G. - Hercules Powder Co.
DeVan, J. H. - Oak Ridge National Lab.
Dwyer, O. E. - Brookhaven National Lab.
Egli, Richard - AEC (Canel)
Elliott, D. G. - Jet Propulsion Lab.
Fisher, C. R. - Aerojet-General Nucleonics
Fraas, A. P. - Oak Ridge National Lab.
Gambill, W. R. - Oak Ridge National Lab.
Goldberg, G. - Oak Ridge National Lab.
Goldmann, K. - United Nuclear Corp.
Greene, N. D. - Geoscience Ltd.
Grindell, A. G. - Oak Ridge National Lab.
Grossman, Nicholas - USAEC (Washington)
Gutstein, M. - NASA, Lewis Res. Center
Hays, Lance - Electro Optical Systems
Heineman, J. B. - Argonne National Lab.
Hoffman, Bernard - General Electric Co.
Hoffman, E. E. - Oak Ridge National Lab.
Hoffman, H. W. - Oak Ridge National Lab.

Horan, J. J. - Pratt & Whitney Aircraft Co.
Kelly, Robert W. - Pratt & Whitney Aircraft Co.
Keyes, J. J., Jr. - Oak Ridge National Lab.
Kidd, G. J., Jr. - Oak Ridge National Lab.
Killackey, J. J. - AiResearch Mfg. Co.
Krakoviak, A. I. - Oak Ridge National Lab.
Leighton, G. A. - USAEC (Washington)
Lemmon, A. W., Jr. - Batelle Memorial Inst.
Lewis, J. P. - NASA, Lewis Res. Center
Lloyd, D. B. - Oak Ridge National Lab.
Lyon, R. N. - Oak Ridge National Lab.
Miller, A. J. - Oak Ridge National Lab.
MacPherson, H. G. - Oak Ridge National Lab.
MacPherson, R. E. - Oak Ridge National Lab.
Noyes, R. C. - Atomics International
Nurick, W. H. - Rocketdyne
Parker, K. O. - Garrett Corp.
Phillippone, R. L. - USAEC (Oak Ridge)
Pidkowicz, Joseph - USAEC (Oak Ridge)
Poppendiek, H. F. - Geoscience Ltd.
Randall, D. G. - Pratt & Whitney Aircraft Co.
Rohsenow, Warren M. - Mass. Inst. Technology
Samuel, W. A. - MSA Research Corp.
Savage, H. W. - Oak Ridge National Lab.
Self, Randall J. - USAF, Aero Propulsion Lab.
Sill, D. E. - Thompson-Ramo-Wooldridge, Inc.
Simons, E. M. - Batelle Memorial Inst.
Smith, C. R. - Allison Div. of GMC
Stein, Ralph P. - Argonne National Lab.
Tepper, Fred - MSA Research Corp.
Thurber, W. G. - Oak Ridge National Lab.
Vild, T. J. - Thompson-Ramo-Wooldridge, Inc.
Walker, C. L. - Allison Div., GMC
Weinberg, A. M. - Oak Ridge National Lab.
Yarosh, M. M. - Oak Ridge National Lab.

ORNL-3605
 UC-33 -- Propulsion Systems and
 Energy Conversion
 TID-4500 (34th ed.)

INTERNAL DISTRIBUTION

- | | |
|-------------------------|--|
| 1. L. G. Alexander | 24. H. G. MacPherson |
| 2. R. A. Armistead, Jr. | 25. R. E. MacPherson |
| 3. S. E. Beall | 26. M. W. Rosenthal |
| 4. C. A. Brandon | 27. G. Samuels |
| 5. R. B. Briggs | 28. W. K. Sartory |
| 6. R. D. Bundy | 29. H. W. Savage |
| 7. J. W. Cooke | 30. M. J. Skinner |
| 8. C. W. Cunningham | 31. I. Spiewak |
| 9. J. H. DeVan | 32. J. A. Swartout |
| 10. A. P. Fraas | 33. D. G. Thomas |
| 11. W. R. Gambill | 34. W. C. Thurber |
| 12. G. Goldberg | 35. A. M. Weinberg |
| 13. A. G. Grindell | 36. R. P. Wichner |
| 14-16. H. W. Hoffman | 37. M. M. Yarosh |
| 17. J. J. Keyes, Jr. | 38. Gale Young |
| 18. G. J. Kidd, Jr. | 39-41. Central Research Library |
| 19. A. I. Krakoviak | 42-43. ORNL - Y-12 Technical Library
Document Reference Section |
| 20. C. E. Larson | 44-73. Laboratory Records Department |
| 21. D. B. Lloyd | 74. Laboratory Records, ORNL R.C. |
| 22. R. N. Lyon | 75. Reactor Division Library |
| 23. A. J. Miller | |

EXTERNAL DISTRIBUTION

76. P. Y. Achemer, Aerojet-General Nucleonics, P.O. Box 77, San Ramon, California 94583
77. C. H. Armbruster, USAF, Aero Propulsion Laboratory (ASRPP-10), Wright-Patterson AFB, Ohio
78. R. E. Balzhiser, Department of Chemical and Metallurgical Engineering, University of Michigan, Ann Arbor, Michigan
79. J. Batch, General Electric Company, Hanford Atomic Products Operation, Richland, Washington
80. P. G. Berenson, AiResearch Manufacturing Company, 9851-9951 Sepulveda, Los Angeles 9, California
81. L. Berkowitz, United Nuclear Corporation, 5 New Street, White Plains, New York 10601
82. H. Bilfinger, c/o Professor C. F. Bonilla, Columbia University, Department of Chemical Engineering, New York 27, New York
83. S. S. Bleckermann, Pratt and Whitney Aircraft Company, CANEL, Middletown, Connecticut
84. C. F. Bonilla, Columbia University, Department of Chemical Engineering, New York 27, New York
85. A. F. Brinsmade, Allegany Ballistics Laboratory, P.O. Box 210, Cumberland, Maryland

86. R. D. Brooks, General Electric Company, Space Power and Propulsion Section, Cincinnati, Ohio
87. M. W. Carbon, University of Wisconsin, College of Engineering, 1513 University Avenue, Madison, Wisconsin
88. J. Carlino, Sunstrand Aviation Corporation, 2480 W. 70th Avenue, Denver, Colorado
89. J. C. Chen, Brookhaven National Laboratory, Building 815, Upton, Long Island, New York
90. R. R. Conrad, Sunstrand Aviation Corporation, 2480 W. 70th Avenue, Denver, Colorado
91. T. A. Coultas, Rocketdyne, 6633 Canoga Avenue, Canoga Park, California
92. J. P. Davis, Jet Propulsion Laboratory, 4800 Oak Grove Drive, Pasadena, California
93. H. W. Deem, Battelle Memorial Institute, 505 King Avenue, Columbus, Ohio
94. C. L. Delaney, USAF, Aero Propulsion Laboratory (ASRDP-10), Wright-Patterson AFB, Ohio
95. L. G. Desmon, Allegany Ballistics Laboratory, P. O. Box 210, Cumberland, Maryland
96. H. T. Drue, c/o Professor C. F. Bonilla, Columbia University, Department of Chemical Engineering, New York, New York
97. J. E. Duval, Chief, Nuclear Power Division, Headquarters USAF (AFRNE-B), Washington, D.C.
98. O. E. Dwyer, Brookhaven National Laboratory, Building 815, Upton, Long Island, New York
99. J. A. Edwards, North Carolina State College, Engineering Mechanics Department, Raleigh, North Carolina
100. R. Egli, USAEC, CANEL Office, Middletown, Connecticut
101. D. G. Elliott, Jet Propulsion Laboratory, 4800 Oak Grove Drive, Pasadena, California
102. C. T. Ewing, U.S. Naval Research Laboratory, Chemistry Division, Code 6130, Washington, D.C.
103. H. B. Finger, NASA, Director Office of Nuclear Systems, Washington, D.C.
104. C. R. Fisher, Aerojet-General Nucleonics, P. O. Box 77, San Ramon, California 94583
105. D. V. Foster, Westinghouse Astronuclear, Pittsburgh, Pennsylvania
106. K. Goldmann, United Nuclear Corporation, 5 New Street, White Plains, New York 10601
107. N. D. Greene, Geoscience Ltd., 410 S. Cedros Avenue, Solana Beach, California 92075
- 108-109. N. Grossman, USAEC, Division of Reactor Development, Engineering Development Branch, Washington, D.C.
110. M. Gutstein, NASA, Lewis Research Center (SEPO 86-5), 21000 Brookpark Road, Cleveland, Ohio
111. J. B. Heineman, Argonne National Laboratory, 9700 South Cass Avenue, Argonne, Illinois 60440
112. E. B. Hall, Battelle Memorial Institute, 505 King Avenue, Columbus, Ohio

113. B. Hoffman, General Electric Company, Missile and Space Division, P. O. Box 8555, Philadelphia, Pennsylvania
114. E. E. Hoffman, General Electric Company, Space Power and Propulsion Section, Cincinnati, Ohio
115. P. Holstead, USAEC, Richland Operations Office, Richland, Washington
116. J. J. Horan, Pratt and Whitney Aircraft Company, CANEL, Middletown, Connecticut
117. W. Jens, Atomic Power Development Associates, Detroit, Michigan
118. J. C. Jones, Deputy for Development, Office of the Assistant Secretary of the Air Force for Research and Development, Department of Defense, Washington, D.C.
119. R. W. Kelly, Pratt and Whitney Aircraft Company, CANEL, Middletown, Connecticut
120. G. M. Kikin, Jet Propulsion Laboratory, 4800 Oak Grove Drive, Pasadena, California
121. A. Koestal, Thompson Ramo Wooldridge, Inc., 7209 Platt Avenue, Cleveland, Ohio
122. R. R. Kyi, c/o Professor C. F. Bonilla, Columbia University, Department of Chemical Engineering, New York, New York
123. Lamprey Program, Director, Los Alamos Scientific Laboratory, Los Alamos, New Mexico
124. D-I. Lee, c/o Professor C. F. Bonilla, Columbia University, Department of Chemical Engineering, New York, New York
125. G. S. Leighton, USAEC, SNAP 50/SPUR Office, Washington, D.C.
126. A. W. Lemmon, Jr., Battelle Memorial Institute, 505 King Avenue, Columbus, Ohio
127. S. Levy, General Electric Company, Atomic Power Equipment Department, San Jose, California
128. J. P. Lewis, NASA, Lewis Research Center, 21000 Brookpark Road, Cleveland, Ohio
129. S. Lieblein, NASA, Lewis Research Center, 21000 Brookpark Road, Cleveland, Ohio
130. J. Longo, Jr., General Electric Company, Space Power and Propulsion Section, Cincinnati, Ohio
131. W. H. Lowdermilk, NASA, Lewis Research Center, 21000 Brookpark Road, Cleveland, Ohio
132. B. Lubarsky, NASA, Lewis Research Center, 21000 Brookpark Road, Cleveland, Ohio
- 133-134. J. J. Lynch, NASA, Office of Nuclear Systems, Washington, D.C.
135. G. Malmstrom, USAEC, Canoga Park Area Office, Canoga Park, California
136. P. J. Marto, c/o Professor W. M. Rohsenow, Department of Mechanical Engineering, Massachusetts Institute of Technology, Cambridge, Massachusetts
137. G. Mattingley, USAEC, Chicago Operation Office, Argonne, Illinois
138. T. C. Min, Department of Engineering Mechanics, University of Tennessee, Knoxville, Tennessee
139. A. Murchison, MSA Research Corporation, Callery, Pennsylvania 16024
140. S. G. Nordlinger, USAEC Scientific Representative, United States Embassy, London, England

141. R. C. Noyes, Atomics International, P. O. Box 309, Canoga Park, California
142. W. H. Nurick, Rocketdyne, 6633 Canoga Avenue, Canoga Park, California
143. K. O. Parker, AiResearch Manufacturing Company, 9851-9951 Sepulveda, Los Angeles, California
144. R. L. Phillipone, USAEC, Oak Ridge Operations Office, Oak Ridge, Tennessee
145. W. M. Phillips, Jet Propulsion Laboratory, 4800 Oak Grove Drive, Pasadena, California
146. J. Pidkowicz, USAEC, Oak Ridge Operations Office, Oak Ridge, Tennessee
147. H. F. Poppendiek, Geoscience Ltd., 410 S. Cedros Avenue, Solana Beach, California 92075
148. J. Radcliff, USAEC, San Francisco Operations Office, Berkeley, California
149. D. G. Randall, Pratt and Whitney Aircraft Company, CANEL, Middletown, Connecticut
150. F. Roehlich, MSA Research Corporation, Callery, Pennsylvania 16024
151. W. M. Rohsenow, Department of Mechanical Engineering, Massachusetts Institute of Technology, Cambridge, Massachusetts
152. L. Rosenblum, NASA, Lewis Research Center, 21000 Brookpark Road, Cleveland, Ohio
153. P. T. Rose, Allison Division of General Motors Corporation, P. O. Box 894, Indianapolis, Indiana
154. E. W. Salmi, Los Alamos Scientific Laboratory, Los Alamos, New Mexico
155. W. A. Samuel, MSA Research Corporation, Callery, Pennsylvania 16024
- 156-157. R. M. Scroggins, USAEC, Division of Reactor Development, Engineering Development Branch, Washington, D.C.
158. J. D. Seador, Rocketdyne, 6633 Canoga Avenue, Canoga Park, California
159. R. J. Self, USAF, Aero Propulsion Laboratory (ASRPP-10), Wright-Patterson AFB, Ohio
160. F. Shair, General Electric Company, Missile and Space Division, P. O. Box 8555, Philadelphia, Pennsylvania
161. D. E. Sill, Thompson Ramo Wooldridge, Inc., 7209 Platt Avenue, Cleveland, Ohio
162. E. M. Simons, Battelle Memorial Institute, 505 King Avenue, Columbus, Ohio
163. H. O. Sloan, NASA, Lewis Research Center (SEPO), 21000 Brookpark Road, Cleveland, Ohio
164. C. R. Smith, Allison Division of General Motors Corporation, P. O. Box 894, Indianapolis, Indiana
165. F. W. Staub, General Electric Company, Advanced Technology Laboratory, Schenectady, New York
166. R. P. Stein, Argonne National Laboratory, 9700 South Cass Avenue, Argonne, Illinois 60440
167. B. Sternlicht, Mechanical Technology, Inc., Latham, New York

168. D. H. Stewart, USAEC, Division of Reactor Development, Program Evaluations, Washington, D.C.
169. S. P. Sukhatme, c/o Professor W. M. Rohsenow, Department of Mechanical Engineering, Massachusetts Institute of Technology, Cambridge, Massachusetts
170. H. Swenson, Babcock and Wilcox Company, Alliance Research Center, Alliance, Ohio
171. Y. S. Tang, Allison Division of General Motors Corporation, P. O. Box 894, Indianapolis, Indiana
172. F. Tepper, MSA Research Corporation, Callery, Pennsylvania 16024
173. D. T. Traitel, Electro-Optical Systems, Inc., 300 N. Halstead Street, Pasadena, California
- 174-175. U.S. Atomic Energy Commission, Reactor Division, Oak Ridge Operations Office, Oak Ridge, Tennessee
176. U.S. Atomic Energy Commission, Research and Development Division, Oak Ridge Operations Office, Oak Ridge, Tennessee
177. U.S. Atomic Energy Commission, Technical Evaluations Branch, Office of Army Reactors, DRD, Washington, D.C.
178. U.S. Atomic Energy Commission, Reports and Statistics Branch, DRD, Washington, D.C.
179. U.S. Atomic Energy Commission, Reactor Experiments Branch, DRD, Washington, D.C.
180. U.S. Atomic Energy Commission, Space Nuclear Power Office, DRD, Washington, D.C.
181. U.S. Atomic Energy Commission, Military Compact Reactors Branch, Office of Army Reactors, DRD, Washington, D.C.
182. U.S. Atomic Energy Commission, Liquid Metal Reactors Branch, DRD, Washington, D.C.
183. U.S. Atomic Energy Commission, SNAP Reactors Branch, DRD, Washington, D.C.
184. U.S. Atomic Energy Commission, Director, Division of Intelligence, Washington, D.C.
185. U.S. Atomic Energy Commission, Division of Technical Information, Washington, D.C.
186. T. J. Vild, Thompson Ramo Wooldridge, Inc., 7209 Platt Avenue, Cleveland, Ohio
187. R. T. Wainwright, NASA, Lewis Research Center (SEPO 86-5), 21000 Brookpark Road, Cleveland, Ohio
188. C. L. Walker, Allison Division of General Motors Corporation, P. O. Box 894, Indianapolis, Indiana
189. J. F. Walling, Battelle Memorial Institute, 505 King Avenue, Columbus, Ohio
- 190-191. R. Weltmann, NASA, Lewis Research Center (SEPO), 21000 Brookpark Road, Cleveland, Ohio
192. M. M. Wiener, c/o Professor C. F. Bonilla, Department of Chemical Engineering, Columbia University, New York, New York
193. L. S. Wolfson, Jet Propulsion Laboratory, 4800 Oak Grove Drive, Pasadena, California
194. J. Zelenak, MSA Research Corporation, Callery, Pennsylvania 16024

- 195-196. N. Zuber, General Electric Company, Advanced Technology Laboratory, Schenectady, New York
- 197-820. Given distribution as shown in TID-4500 (34th ed.) under Propulsion Systems and Energy Conversion category (75 copies - CFSTI)